Iron-Catalysed Reactions of Alkenes and Allenes : Isomerisation, Polymerisation and Hydrofunctionalisation

A thesis submitted for the degree of Doctor of Philosophy

Woof, Callum

Award date:
2021

Awarding institution:
University of Bath

Iron-Catalysed Reactions of Alkenes and Allenes : Isomerisation, Polymerisation and Hydrofunctionalisation

Callum R. Woof

A thesis submitted for the degree of Doctor of Philosophy

University of Bath

Department of Chemistry

June 2021

Copyright Notice

Use of this thesis

Candidate signature :

Declaration of any previous submission of the work

The material presented here for examination for the award of a higher degree by research has not been incorporated into a submission for another degree.

Candidate signature :

Declaration of authorship

I am the author of this thesis, and the work described therein was carried out by myself personally, with the exceptions below. In Sections 2.7 and 5.4, electron paramagnetic spectroscopy data interpretation and simulation was performed by Dr Emma Richards, Cardiff University (data collection was performed by the author). In Section 2.8, single crystal X-ray diffraction and analysis was performed by Dr Nathan Coles, University of Bath. In Sections 2.9 and 3.2, density functional theory studies were performed by Derek Durand, University of Bristol. In Section 3.3, wide-angle x-ray diffraction studies were performed and analysed by Dr Adam Squires, University of Bath.

Candidate signature :

Table of Contents

Acknowledgements

When it came to writing these acknowledgements (and this thesis), I started to reflect just how *long* I have been associated with the University of Bath. A back of envelope calculation suggests I have spent 93% of my time as an adult associated with the place. And I started so long ago that back then the biggest threat to world peace and stability was that Mitt Romney might win the upcoming presidential election. And I have to say I have enjoyed the last (nearly) nine years — the city, the campus, and the department (barring a succession of avaricious vice-chancellors, endless queuing for buses and exorbitant rent for damp old houses).

Right, actual acknowledgement time — it goes without saying that I would not have been able to start, finish, and do most of the middle of this thesis without Ruth's supervision. She has put an absolute ton of her time and effort into generating ideas, suggestions, solutions and advice over the last 3 ½ years and been an extremely supportive mentor (Like, if Tripadvisor ratings were used in reviewing supervisors she'd be straight five out of fives). As well as that, nothing in life gives me quite the same mixture of feelings of intrigue and trepidation as receiving an email notification leading with "Ruth Webster : (no subject)" — it could be an experiment suggestion, or a Netflix recommendation, or anything in between.

Having rocked up in the group as a Masters student in 2015 and gone through nearly one-and-a-half turnovers in group members it feels strange to be done with it all now. I have been lucky to have a range of colleagues who have been supreme in their support, helpfulness, and dedication to fostering a good working environment, and only once in my PhD have I been worried about the lab being blown to smithereens. Dr Nathan Coles, Dr Cei Provis-Evans, Dr Dani Gasperini, Adam Barrett, Tom Linford-Wood, Dr Samantha Lau, Emily Pocock and Mirela Johnson have all been great sources of advice, resolve and entertainment, and any other research group in the building who think they are working in a better squad is empirically wrong (On the other hand, having a workspace with an external window somewhere is definitely on my future career aims). I've also had two sincere and hardworking MChem students over the course of my PhD, Dave Pilley and Jonny Nevett, who understood that the best project students are the ones that supply the most chocolate/beer.

This thesis is a collaborative effort brought to you by the Centre for Doctoral Training in Catalysis, and I am grateful for them for funding myself and my research. The skills and techniques in this project would not have been brought about without collaboration, and my co-supervisors Dr Natalie Fey, Dr Emma Richards and Prof Craig Butts have been superb in offering ideas, direction and insight in some aspects of the research. As well as them, Derek Durand (University of Bristol) has performed seemingly endless Density Functional Theory studies to support the work in Chapters 2 and 3.

I'm grateful to work in a department where advice, support and help is available, and I've realised I have chased down an awful lot of people in the department to use their equipment, steal— I mean, borrow— their chemicals or straight up try to get them to solve all my problems. This includes (in a rough order of where it comes up through this thesis) — Dr Maialen Espinal-Viguri, Dr Anne-Fred Pecharman, Connie Isaac, Dr John Lowe, Dr Catherine Lyall, Jack Stewart, Prof Frank Marken, Dr Josh Tibbetts, Dr Rémi Castaing, Dr Martin Levere, Dr Thom McGuire, Pollyanna Payne, Aneesa Al-Ani, Dr Adam Squires and Thomas Horsley Downie, as well as the technical and support staff in Bath who I have desperately tried to get on the good side of over the years. And thanks to all those other people (AA, Yozza, Alex Jr, Scottish Laura, Oil, Ferry, 'Ambulance' Alison, Shifty Andy *et.al.*) who have made the last 3 ½ years significantly brighter and enabled me to get to the top of the departmental gossip tree.

I think my family has eventually got the gist of what a Chemistry PhD entails, and I'm in a permanent state of gratitude to them for putting up with my sass over Skype/alcohol and their eternal support to me to follow my dreams or whatever you're meant to put at this juncture. I did a PhD to do some exciting science, learn a bit more about the world and put off all major life decisions for half a decade, and… well, the latter I definitely did. If I had any regrets, it would be getting a few more reactions right first time, not slicing my finger (sometimes Suba-Seals just won't fit…) and, most importantly, improving my below-par 'blue roll challenge' time.

Stay cool,

Callum

16th June 2021

Abstract

Using iron complexes as homogeneous catalysts for bond forming and functionalisation reactions is both highly desirable and a research field of growing interest. In this thesis, iron complexes are used as catalysts for a range of transformations, and the transformations themselves are investigated for reactivity, scope, and mechanistic insight. A range of approaches to understanding catalysis are used in order to gain a more complete picture of chemical behaviour.

Following a general introduction, literature review and discussion in Chapter 1, Chapter 2 builds on previously reported alkene functionalisation reports to study the isomerisation of alkenes catalysed by iron complexes. Following examination of conditions and substrate scope, mechanistic studies attempt to prove, and subsequently disprove, an initially proposed catalytic cycle. Using a multifaceted approach including density functional theory, electron paramagnetic resonance spectroscopy, cyclic voltammetry and deuteration studies a second catalytic cycle can be proposed which can more fully account for all observations.

Chapter 3 shifts the choice of substrate from alkenes to allenes. Using the same conditions generates divergent reactivity — rather than isomerisation, polymerisation is instead the primary reaction observed. The resulting poly(phenylallene) is relatively unusual, and the structural properties of the polymers are investigated. Through mechanistic investigation it is clear that this process has some mechanistic similarities with the findings in Chapter 2, and some attempts to perform and study [2+2] cycloaddition reactions are also reported.

Allenes are then used as substrates in hydrophosphination chemistry in Chapter 4, merging previously reported hydrophosphination studies with some of the findings observed in Chapters 2 and 3. This generates novel phosphorus compounds and interesting regioselectivity findings, and the tolerance of the reaction to various allenes and phosphines is studied. Again the mechanism is studied, and a catalytic cycle proposed, although this has some significant differences to the previous studies.

In Chapter 5 the focus shifts away from using organic substrates to coupling phosphorus compounds, and investigating a route to phosphorus–phosphorus bonds using phosphines and chlorophosphines as reagents. Dehydrochlorination of a secondary phosphine and chlorophosphine generates a diphosphine, and the effects of substituent and conditions are investigated, as well as the effects when using primary phosphines as substrates. Although this reaction requires a catalytic amount of an iron complex, it has some marked difference in mechanism and reactivity compared to the previous chapters which are examined.

Abbreviations

Ad - adamantyl

AIBN - azobisisobutyronitrile

Ar - aryl

br - broad

cod - cyclooctadiene

Cy - cyclohexyl

d - doublet

Dba - dibenzylideneacetone

DCM - dichloromethane

DHC - dehydrocoupling

DP - degree of polymerisation

dppf - 1,1'-bis(diphenylphosphino)ferrocene

DSC - differential scanning calorimetry

EtMgBr - ethylmagnesium bromide

EtOH - ethanol

EPR - electron paramagnetic resonance (spectroscopy)

eq. - equivalents

GC - gas chromatography

GPC - gel permeation chromatography

h - hour(s)

HAT - hydrogen atom transfer

HBpin - pinacolborane

HMDS - hexamethyldisiliazide

HMPA - hexamethylphosphoramide

MALDI - matrix-assisted laser desorption/ionisation

Mes - mesityl

M_n - number average molecular mass

M_w - weight average molecular mass

MS - molecular sieves

NEt_3BzCl - benzyltriethylammonium chloride

NMR - nuclear magnetic resonance (spectroscopy)

PCC - pyridinium chlorochromate

Ph - phenyl

pin - pinacol

RT - room temperature

s - singlet

SET - single electron transfer

t - triplet

T_g - glassy transition temperature

THF - tetrahydrofuran

TMEDA – tetramethylethylenediamine

TON – turnover number

TsOH - tosylic acid

TEMPO - (2,2,6,6-Tetramethylpiperidin-1-yl)oxyl

VT - variable temperature

WAXS/WAXD - wide angle X-ray scattering / diffraction

Chapter 1 - Introduction

In this chapter a range of chemistry relevant to the studies of this thesis is reviewed and discussed. Initially both the use of both iron and β-diketiminate complexes in catalysis are introduced, with notable previous reports highlighted. Following this, the four primary catalytic transformations investigated in this thesis are reviewed, along with further relevant literature.

1.1 Iron as a Catalyst

Catalysis and transition metals

The synthesis of new chemical structures and compounds is an essential part of both the natural and industrial world, and catalyst-mediated reactions are a crucial part of both life's natural processes and in 90% of synthetic reactions and transformations. Without catalysis many processes would not be feasible, non-selective or be extremely energy intensive, and developing catalytic methods further is crucial to decrease the energy demands, toxicity, and inefficiency of many current processes.

Catalysis can be distinguished by form, as well as by composition. While heterogeneous chemistry is dominant in terms of industrial scale, and biocatalytic and enzymatic reactions underpin life-mediated chemistry, this study focuses on the third major class — homogeneous systems. The main advantages homogeneous catalysts have over the alternatives are their selectivity, variability and ease of study compared to other systems. The importance of homogeneous catalysis can be shown by the number of Nobel Prizes being awarded in this field, including for enantioselective hydrogenation and oxidation (Knowles, Noyori and Sharpless, 2001), olefin metathesis (Chauvin, Grubbs and Schrock, 2005) and palladium cross-coupling reactions (Heck, Negishi and Suzuki, 2010). [1]

Virtually all stable elements have been reported to perform some form of catalytic activity. Despite recent advances in main group, f-block and organocatalysis, transition metal systems arguably still have the greatest diversity and application of catalytic behaviour across the periodic table. [2] This can be attributed to several factors. Firstly, the majority of transition metals can access multiple oxidation states with relative ease. For example, manganese can be found in the (II) through (IV), (VI) and (VII) oxidation states, while iridium commonly exists in the (I) and (III) states. This inherent reactivity allows oxidation and reduction of metal species to frequently be facile. In catalysis, organic molecules that cannot perform redox activity readily on their own can bind to metal centres and take part in redox-active behaviour. Secondly, transition metals can adopt a range of coordination structures and bind well to a range of ligands. While f-block metal complexes are typically dominated by ligand sterics alone, the more directional nature of d-electron orbitals enables more defined and directional structures in many cases for transition metal complexes. Thirdly, the electronics and reactivity of metal centres can be altered to a strong degree by the ligand environment it exists in, permitting diversity in chemical behaviour.

While not universally consistent, the first row (3d) transition metals typically have distinct behaviour compared to the second and third rows (4d and 5d) directly beneath them, which have similar chemical properties to each other. This is especially true of the later transition metals,

where, for example, the properties of palladium and platinum have similarities between them compared to nickel (e.g. in terms of air stability, oxidation states and compound structures). The platinum group metals have been of particular focus for investigation and development in catalysis and continue to be studied. They offer a wide range of beneficial properties, in particular being highly active, readily tuned with ligands and stable for long periods of time, and as a result are easy to store, use, and lead to high levels of turnover. Perhaps the most renowned homogeneous catalytic process using these metals is the Suzuki-Miyaura reaction, enabling aryl C–C bond formation that was previously exceptionally difficult to perform (Scheme 1).

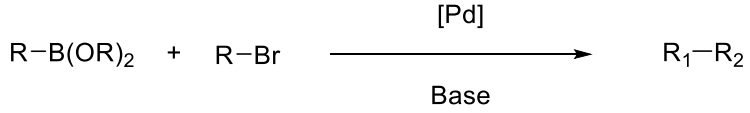

Scheme 1 – Generalised scheme for the Suzuki-Miyaura reaction, an effective route to form new C–C bonds and arguably one of the most important chemical transformations in use today. The reaction requires a palladium complex as a catalyst to proceed.

Using Iron in Catalysis

The platinum group metals are to some extent synonymous with the precious metals, and the naming is somewhat warranted. A combination of low universal abundance, high density and complicated extraction means all of them are scarce, and difficult to extract where they are present. Iridium, for example, is the rarest primordial metal in the Earth's crust. Precious metals are often found in the same ores, and because of their similar chemical properties, extraction and purification of them is energetically demanding and wasteful. These ores are found in some of the most remote corners of the Earth, [3] increasing the cost of extraction and intensifying the environmental damage of both extraction and purification. Cost and availability of such metals have become pegged to factors that can easily fluctuate, including climate change, tariffs, and economic uncertainty.

Aside from these issues, precious metals have further concerns. The majority of them are cytotoxic as both salts in solution or airborne particulates, and this toxicity is a hazard even at parts per billion levels. As they are not particularly abundant in nature, they are not readily metabolised and can accumulate in soils or biomass. Because of this, any substrates synthesised using these metals as catalysts that end up in humans directly (such as pharmaceuticals) or indirectly (such as pesticides or fertilizers for crops) must be purified extensively. This again increases the cost of production and the volume of waste produced. [4]

Because of these reasons, there is increased demand and interest in using non-precious metals in catalysis. The first-row transition metals are generally more abundant (often considerably so) than the metals directly beneath them, decreasing extraction difficulty and cost, which can be demonstrated by their wider application on much larges scales (*e.g.* copper in electronics, titanium in paint). In terms of toxicity almost all of them are still relatively toxic compared to, for example, the alkali metals, and some such as chromium and manganese have caused considerable environmental damage in their usage. A notable exception to this trend is iron — most transition metals have toxicity concerns at 10 ppm or less, but iron is benign up to 1300 ppm. [5] Iron is also the most abundant of all the transition metals — one estimate puts it as three and a half million times more abundant than palladium in the Earth's crust [6] — and because of this extraction is

focused on the richest and most accessible ores, somewhat mitigating the waste and energy required to extract it.

Iron in Homogeneous Catalysis

Iron has been utilised by human hands for at least five and a half thousand years, initially harvested from meteorites, and through refining, forging, and alloying since at least 1500 BC. As a material iron has a huge number of desirable properties — malleability, strength, conductivity — and can be alloyed to attain further characteristics. Iron compounds have further applications in water purification, fortification of foodstuffs and pyrotechnics. [7] Most importantly to this study, iron has been developed as a catalyst.

Iron is the primary component of catalysts used in the Haber-Bosch process, underpinning the majority of the world's food supply, as well as potent in the Fischer-Tropsch process. Biologically, iron is fundamental in allowing aerobic transport and respiration to occur in vertebrates, as well as being present in many metalloproteins — blood is red because of the abundance of haemoglobin, an iron-centred metalloprotein. Because it is located in virtually the centre of the d-block, it can in the right conditions behave as both an 'early' transition metal and a 'late' transition metal. For example, it can form strongly-Lewis acidic salts like many early transition (or s-block) metals, but it also binds well to phosphine and carbene ligands, like many late transition metals.

Iron has some significant disadvantages to large scale uptake in homogeneous catalysis. Although most simple salts are affordable, the ligands required to form complexes that perform catalysis effectively are often more costly. Many polydentate ligands are challenging to synthesise, and complex phosphorus ligands can be expensive to prepare and environmentally damaging if not disposed of correctly.

Elemental iron is more reactive than most precious metals, as practically evidenced by its tendency to rust. Some organometallic complexes containing iron are bench stable, particularly those with 18 electrons, but low coordinate, low-oxidation state complexes are typically air sensitive. An alternative approach is to start with a simple air-stable salt (*e.g.* iron chlorides or acetates) and form an active species *in situ* using a ligand and reducing agent (typically a Grignard reagent or alkali metal base) — however, the reaction itself must still be conducted under a relatively inert atmosphere, and this also generates waste and introduces mechanistic complexity from the reducing agent.

Iron complexes have been shown to be effective catalysts in a broad range of transformations from fundamental diversification of feedstocks [8] to late stage C–H functionalisation. [9] C–H activation and C–C cross-coupling, two of the most challenging transformations in modern chemistry, have seen a huge range of development with iron catalysts in the last ten years; this has been extensively reviewed by Rana and Maiti. [10] This is partly due to the significant amount of focus on mimicking well-known palladium cross-coupling reactions with iron, in particular Kumada and Negishi couplings. [11] Of particular relevance to this study is alkene functionalisation using iron catalysts — for example hydrogenation, where in particular reports from Milstein and Morris have shown a wide range of iron complexes are adept at this transformation for a broad range of substrates. [12] These fields use radically different complexes and reaction approaches to undertake these transformations, demonstrating both the variability and changeable nature of catalytic behaviour.

The majority of iron species investigated in this study, as well as reviewed in the introduction, are low-valent and low-coordinate organometallic complexes. A seminal example of the preparation and use of well-defined bulky iron complexes was reported by Power, where a terphenyl iron(I) complex can be oxidised to the extremely unusual Fe(V) oxidation state through reaction with azidoadamantane. [13]

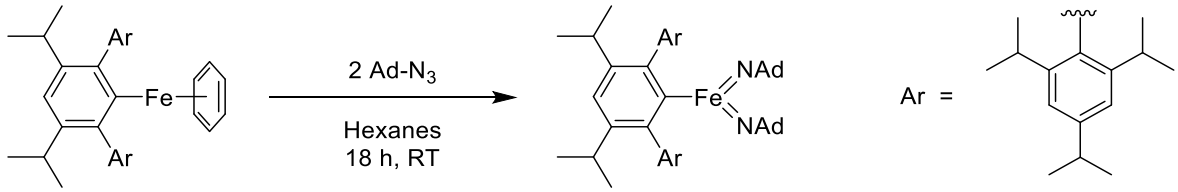

Scheme 2 – Power's work has shown that very bulky, low-coordinate iron complexes can perform surprising reactivity and form stable compounds containing iron in unusual oxidation states and structures. [14]

Studying Mechanisms of Iron Catalysis

Palladium metal complexes generally exist in the Pd(0) and Pd(II) oxidation states, and palladium-mediated catalysis can often be broken down into two electron oxidation/reduction steps (*e.g.* oxidative addition, reductive elimination) and neutral processes (*e.g.* transmetallation). Iron-mediated catalysis can perform two electron (or redox neutral) steps, but they are generally disfavoured over single electron transfer (SET) mechanisms and pathways. Although ligand environment plays an important role, iron centres are generally high spin, whereas 4d and 5d metals are generally low spin. The crystal field splitting energy difference is relatively small for first row transition metals compared to their heavier counterparts, favouring unpaired electrons in high spin states. Spin interconversion between high and intermediate spin states can often occur, further complicating the behaviour of iron centres. To perform 'palladium-like' transformations, it is desirable for an iron complex to behave more like a lower transition metal, for example by being amenable to two electron redox processes, possessing vacant 3d orbitals, and having a rationalizable ligand environment. However, to 'behave' like a precious metal, iron requires distinct metal-ligand cooperative behaviour, necessitating specific ligands as already discussed. [15] Furthermore, it is desirable to have some understanding of the catalytic mechanism.

Mechanistic studies of iron-catalysed reactions are challenging for a range of reasons, compared to main group and even other transition metal-mediated systems. Firstly, there is a range of redox couples possible in both two- and one-electron processes. Iron complexes can normally exist in any of the states from Fe(0) to Fe(III), although higher and lower states are further known and postulated. This means a large number of redox (and non-redox) pathways are at least plausible under most reaction conditions, resulting in iron exhibiting frequently capricious reactivity. Secondly, iron systems have practical challenges. Iron is paramagnetic due to its unpaired electrons, which leads to broadening and unusual chemical shifts in NMR spectroscopy. Paramagnetic effects on NMR chemical shift can border on the inscrutable and depend upon both structure geometry and electron density, and it can often be challenging to assign *in situ* iron intermediates from NMR spectroscopy alone.

Because of the unpaired electrons present, EPR spectroscopy can be utilised as an alternative technique. EPR is several orders of magnitude more sensitive than NMR, and can be used to determine spin and oxidation states present. However, not all iron species with unpaired electrons

are EPR active, and whether electronic transitions are active or forbidden is governed by complex selection rules. [16] A relatively robust rule of thumb is structures with an even number of d electrons give weak or even no signals in standard experimental setup, whereas odd numbered systems give relatively intense signals. For iron, Fe(0) and Fe(II) are d8 and d6, whereas Fe(I) and Fe(III) are d7 and d5, leading to the latter giving more intense EPR signals compared to the former. Spin state is also an important consideration – high spin states (S = 5/2) are often only observed at liquid helium temperatures owing to their rapid relaxation, whereas low spin complexes (S = ½) are observed at liquid nitrogen or room temperature. Despite these obstacles, EPR spectroscopy can provide valuable insight into the behaviour of iron centres in reactions (This is demonstrated in Chapters 2 and 5).

Several more specific techniques offer further insight into the mechanism, although they are considerably less widespread in research facilities. Magnetic Circular Dichroism (MCD) enables unambiguous spin state determination, as well as further insight to metal-ligand bonding. Unlike EPR, all paramagnetic species have allowed transitions. [17] The ^{57}Fe isotope is well suited to analysis through Mössbauer spectroscopy, where the 'recoil' effect of nuclei subject to gamma ray exposure is measured. This technique is both sensitive and offers insight into three distinct properties: the isomer shift (a measure of oxidation state and electronic behaviour of the metal centre), quadrupole splitting (indicating both spin and ligand symmetry) and magnetic hyperfine splitting (further coupling with adjacent nuclei). [18] Because of these, Mössbauer analysis can offer a large amount of insight into metal complex behaviour — recent studies by Neidig [19] and Ackermann [20] showcase its utility. X-ray techniques such as X-ray absorption near-edge spectroscopy (XANES) and extended X-ray absorption fine structure (EXAFS) can also be used to study electronic structure which in turn can determine oxidation state and ligand environment. [21, 22]

Combining some of these techniques along with other experimental information, such as isolated crystallographic data, theoretical calculations and synthetic experiments can lead to a large amount of information about a catalytic system being ascertained. Even with this information, there is still a relative degree of uncertainty — the reaction pathway studied may be off-cycle, alternative pathways may simultaneously be feasible and competitive, and even elementary steps may have unidentified complexity. [23] Despite this, efforts and understanding into iron-catalysed mechanisms have grown rapidly in recent years and discovery and study continue to offer further insight into chemical behaviour.

1.2 β-Diketiminate ligands and Catalytic Applications

Homogeneous catalysis drives demand for new ligands and complexes to be synthesised and evaluated for potential. Iron and other early first row transition metals bind particularly strongly to N- and O-based ligands; one of the simplest of these is acetylacetonate (termed 'acac'), which can form both Fe(II) and Fe(III) complexes (although iron, like many late transition metals, also binds readily to phosphine and carbene ligands). Iron acetylacetonate complexes are established pre-catalysts in their own right and are utilised in Chapter 5.

Synthetically, it is relatively easy to synthesise nitrogen analogues of these proligands through condensation between a diketone and two equivalents of an amine. These can also be ligated to

metal complexes, with the additional 'R' group conveying greater steric bulk to the ligand. Although there is some variance, they are generally considered to form strong metal-ligand bonds. Depending on the source, these are termed Nacnac or β-diketiminate ligands; they are referred to as the latter throughout this thesis. These have been known for over 60 years, [24] but have only relatively recently been investigated for catalytic applications.

As stated, these ligands are relatively easy to synthesise through condensation reactions of diketones and anilines (Scheme 3). Deprotonation in the presence of a metal salt then generates the complex. Both of the starting reagents have a range of commercially available substrates and are relatively easy to synthesise in turn, so a range of proligands can be easily made. Some proligands give NMR data that indicate the nitrogens have distinct amine and imine environments, while others show that the system is in resonance and both are equivalent — this depends on their bulk and electronics.

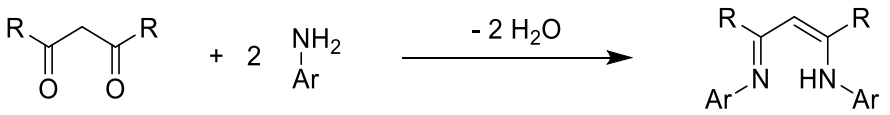

Scheme 3 – Generic synthetic route to β-diketiminate proligands through a condensation reaction of diketones and anilines. The 'R' and 'Ar' groups have been varied greatly to achieve ligands with a diverse range of steric and electronic properties.

Complexes with these ligands typically exist in either monomeric or dimeric forms. In dimeric forms these ligands can stabilise unusual element bonds, or be bridged by a ligand. This includes classically poor ligands such as dinitrogen, as well as unconventional ligands such as P_4, small organic molecules and dioxygen. [25] Monomeric complexes tend to have one or two additional halide or organic ligands bound to the metal centre — in catalytic processes, these are typically eliminated or substituted to generate the active species.

β-Diketiminate ligands and complexes have been regularly compared with pincer ligands and complexes, as they are both bulky ligands that bind strongly, stabilise a range of metal centres and are frequently encountered in catalysis (it should be said that there are a range of other ligand classes – adamantyl, PyBOX and PDI, for example – that this is equally true for). Both have been proposed to behave as spectator ligands, but also as non-innocent ligands which are intimately involved in reactivity. [26, 27] The majority of pincer ligands contain phosphorus centres, which increase cost and complicate disposal, whereas β-diketiminate complexes generally only contain carbon, nitrogen and hydrogen. Furthermore, while in some cases reactivity is complimentary, in many cases the difference in ligand choice results in very different reactivity and chemoselectivity.

It has been known for some time that low-coordinate first row transition metals display unusual properties compared to more saturated analogues, for example, in 1987 reports by Tilley and Rheingold showed the unusual behaviour of bulky iron silyl complexes. [28] Whilst transition metals, at least classically, seek to attain 18 electrons to achieve stability, the large bulk of the ligand prevents this from happening in the case of β-diketiminate complexes. Where these have further organic ligands or substrates bound, the bulk of the ligands often further prevents agostic interactions with organic ligands, further stabilising the system and preserving low coordination. Nitrogenase enzymes proceed through low-coordinate iron centres, and as such these complexes

have attracted interest for nitrogen fixation and reduction in the hope of repeating this chemistry. [29]

The earliest iron β-diketiminate complexes were Fe(II) complexes synthesised by Holland — these are prepared as halides from an initial salt precursor, but can be transformed into organometallic complexes through straightforward transformations (Scheme 4). [30] Other early reports of these class of complexes include **1**, which is used extensively in this study, and **2**, which has an alkoxide ligand (Figure 1).

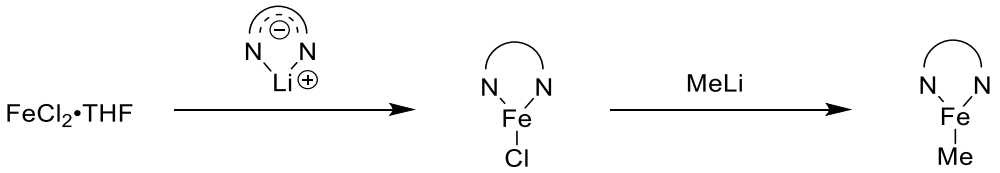

Scheme 4 – Generalised synthesis of β-diketiminate complexes as reported by Holland. [30] By reacting an iron halide salt with a lithiated proligand an initial chloride complex is formed, which can be further reacted through salt metathesis. Identical reactivity is observed with cobalt, while nickel complexes form solvent adducts.

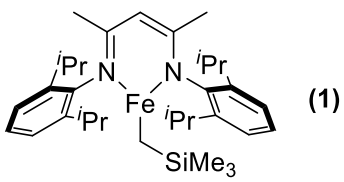

(1)

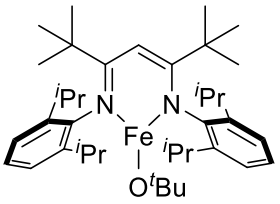

(2)

Hessen, *Inorganic Chimica Acta*, 2006

Gibson, *Dalton Trans*., 2002

Figure 1 – Further β-diketiminate iron complexes reported by Hessen [31] and Gibson. [32]

All these complexes possess iron centres in the Fe(II) oxidation state, and this remains the most common oxidation state attained in these complexes. These generally exist as three-coordinate iron centres with a conformation somewhat more linear and bent out of plane than a true trigonal planar structure. If a neutral ligand, such as dinitrogen or an alkene is bound instead of an alkyl ligand, then an Fe(I) species is instead formed. Stable complexes in the Fe(0) and Fe(III) states have also been prepared; some examples are shown in Figure 2. [33] In some cases the oxidation state is not clear cut — there is debate whether dimeric species with a bridging dinitrogen can be considered as Fe(I) or Fe(II) centres, depending on if the dinitrogen is treated as neutral N_2 or an $(N=N)^{2-}$ species.

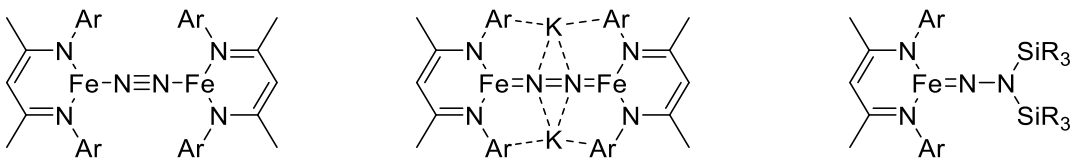

Figure 2 – The oxidation state of iron β-diketiminate complexes can vary depending on the ligand and how it binds to the metal centre, as shown by a range of iron-nitrogen complexes prepared by Holland. Note that Ar = 2,6-diisopropylaniline in all complexes. [33]

Isolation of dimeric species in the solid state are common with complexes with small molecules or ligands bound to them. Common species include dinitrogen or bridging chlorides, hydrides or cyanides, although a range of more exotic bridging species have also been reported, including nitric oxide [34] and phosphorus radicals. [35] However, this sometimes simplifies a more complex existence in the solution phase, where a monomeric species may or may not be preferred in terms of formation.

Iron β-diketiminate complexes in catalysis

A huge range of metal β-Diketiminate complexes have been used in catalysis, from titanium [36] to zinc. [37] An area of particularly keen interest in these complexes across a range of metals is polymerisation, particularly with lactide and other oxygen-containing monomers. The complex reported by Gibson above was utilised for this purpose; a recent example of this behaviour is shown with rare-earth metals by Robinson for β-butyrolactone polymerisation. [38]

There has also been increased focus on bond-forming reactions. Several of these are discussed in further detail in other parts of this study, and it should be appreciated that a wide range of new bonds can be catalytically formed using these low-valent complexes. A relatively early report of bond forming catalysis was the hydrodefluorination of aromatic systems by Holland using **3**. More than three catalytic turnovers are only observed with a few strongly electron withdrawing systems, but this is suggested to arise from the stability of the C–F bond rather than weakness in the catalyst design.

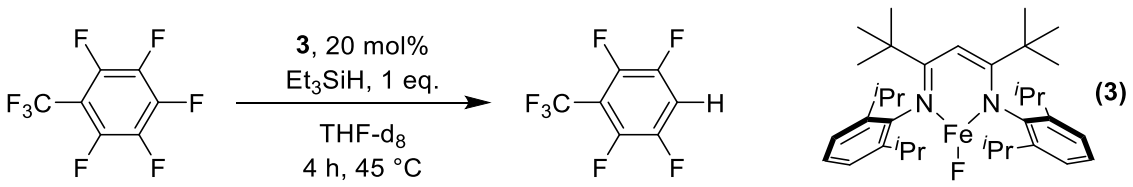

Scheme 5 – Hydrodefluorination of fluorobenzenes reported by Holland. [39]

Mechanistically, the active species is believed to be an iron(II) hydride species – a hypothesis that is found in numerous catalytic reactions. The hydride is formed upon reaction of the pre-catalyst with triethylsilane, being driven by the strong Si–F bond being formed. The hydride is then added over the C–F bond with consequent elimination of an iron fluoride.

A more common reaction has been the formation of carbon-heteroatom bonds by adding a H–X moiety over an alkene. Catalytic hydroamination is known for various metals but still remains a chemical challenge. [40] Hannedouche developed an intramolecular hydroamination process using complex **4**. Unlike complexes **1** through **3** this is formally four coordinate, although the THF molecule likely disassociates readily. [41] As well as being solely an intramolecular process, the system is limited to forming five-membered cycles, as well as requiring primary amines.

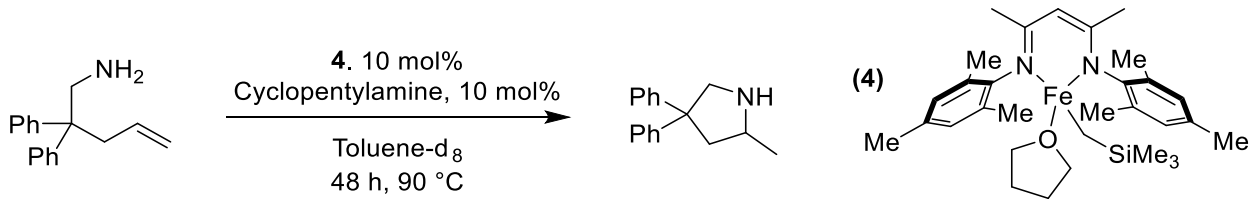

Scheme 6 – Iron-catalysed hydroamination of alkenes reported by Hannedouche. [41]

Mechanistically the amine is proposed to displace the tetramethylsilane ligand (generating $SiMe_4$), from which the tethered alkene can also interact with the metal centre. Adding the iron-nitrogen bond over the alkene then generates the new C–N bond. This intermediate generates the desired product through reaction with a further molecule of substrate or cyclopentylamine, forming a further iron-nitrogen species and the product. Under certain conditions, it can alternatively undergo β-hydride elimination (Scheme 7). Further investigations into this transformation have also been reported. [42, 43] These primary steps — pre-catalyst activation, addition across a double bond, β-hydride elimination and protonation/substitution are commonplace for a range of hydrofunctionalisation reactions.

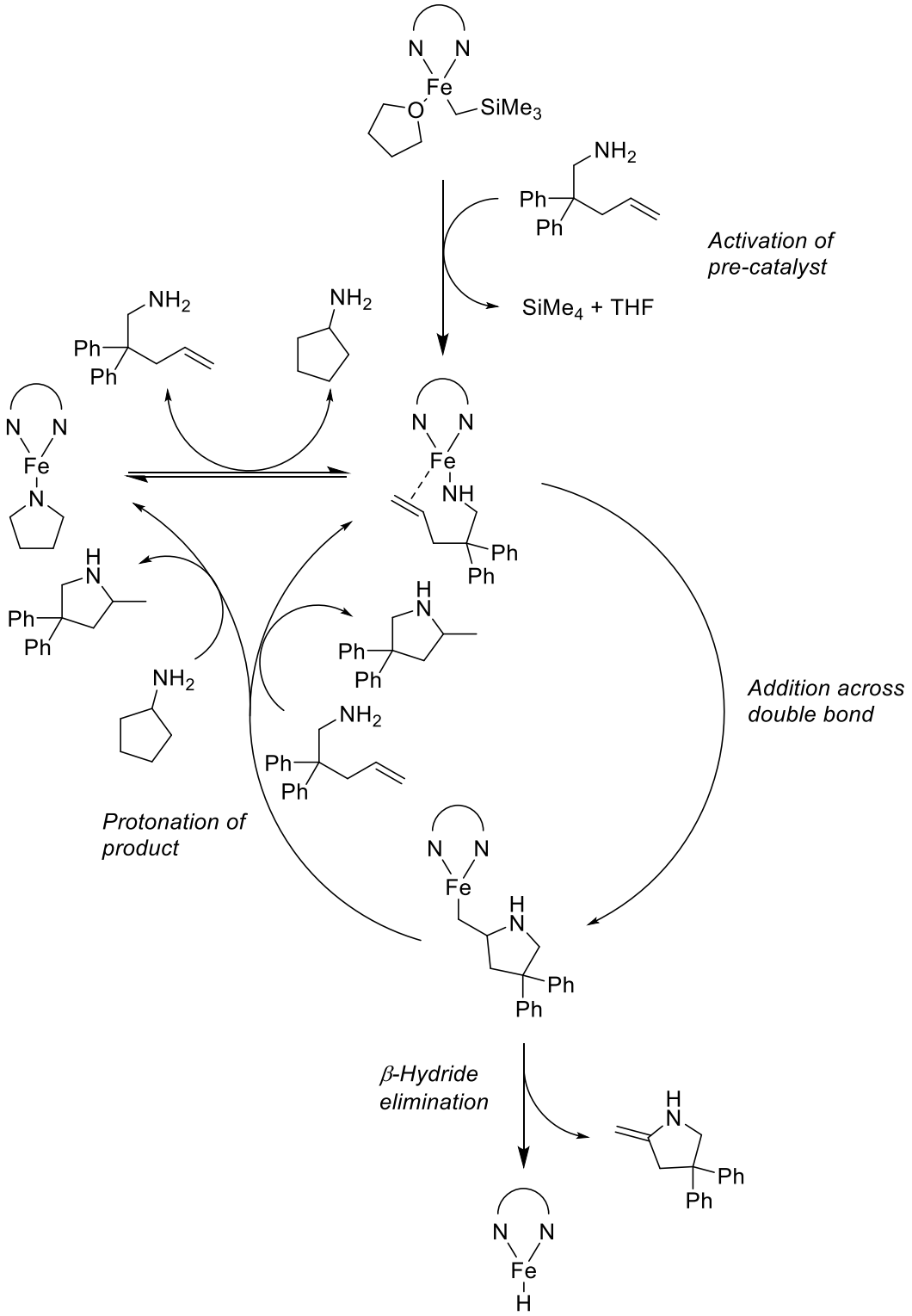

Scheme 7 – Proposed mechanism for the catalytic hydroamination of alkenes. [41] The additional amine acts as a resting state and as an alternative route to generating the product, while a small amount of the dehydrogenated product (and iron hydride complex) is also observed.

Other bond forming reactions include hydroboration and hydrophosphination, with **1** being used as a pre-catalyst. These reactions and some mechanistic aspects are discussed in further detail in Sections 2.1 and Chapter 4 respectively. Hydrophosphination has been shown to be both

intramolecular and intermolecular — for intramolecular hydrophosphination, the Markovnikov selectivity observed is similar to the previous hydroamination study (Scheme 8). [44]

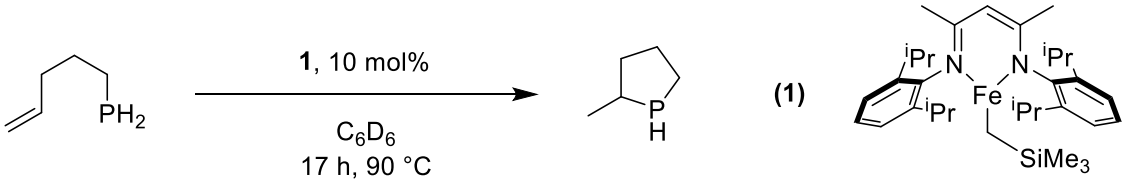

Scheme 8 – Intramolecular hydrophosphination reaction catalysed by β-diketiminate complexes reported by Webster. [44] Further intermolecular reactions catalysed by **1** are discussed elsewhere in this thesis.

By combining both these protic and hydridic bond activation pathways, it is also possible to perform transfer hydrogenation of alkenes, and because of the strong regioselectivity in both these processes, selective protonation-deuteration reactions can be performed. Again, this reaction is discussed further in Section 2.1. Further studies by Webster have shown that these complexes are also competent as catalysts in a range of dehydrocoupling reactions, including with phosphines [45] (see Section 1.7), silanes [46] and amine borane [47] substrates. There have also been recent notable developments in dinitrogen activation [48] and Suzuki couplings [49] using these iron complexes. Although β-diketiminate iron complexes offer reactivity that is both extended and different from simple iron salts and complexes, it does not mean they offer improved catalytic performance for all reactions. For example, the β-diketiminate complex shown in Scheme 9 is considerably poorer as a catalyst for the reaction shown than either $Fe(acac)_2$ or $Fe(acac)_3$. [50]

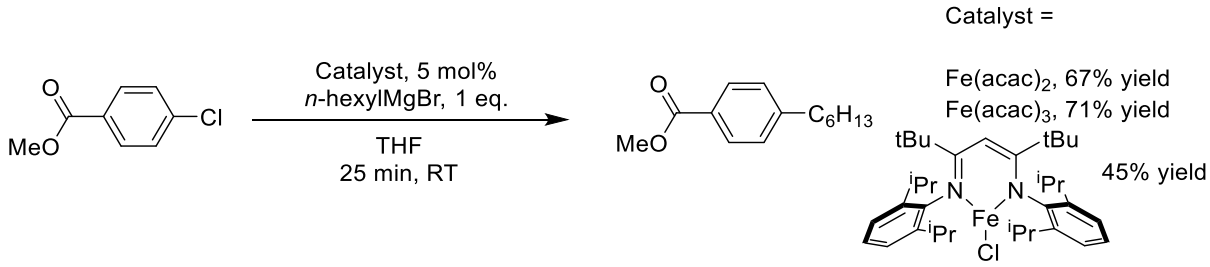

Scheme 9 – In this cross-coupling reaction reported by Holland, the β-diketiminate complex is noticeably poorer as a catalyst than either of the simpler iron acetylacetonate complexes. [50]

The majority of catalytically competent iron complexes are iron(II), and proceed in redox neutral processes like the hydroamination shown in Scheme 7. There are a handful of examples of iron(I) complexes being used as catalysts, for example in nitrene transfer as reported by Holland using **5** (Scheme 10). [51] Cobalt(I) β-diketiminate complexes have also been utilised in catalysis. [52]

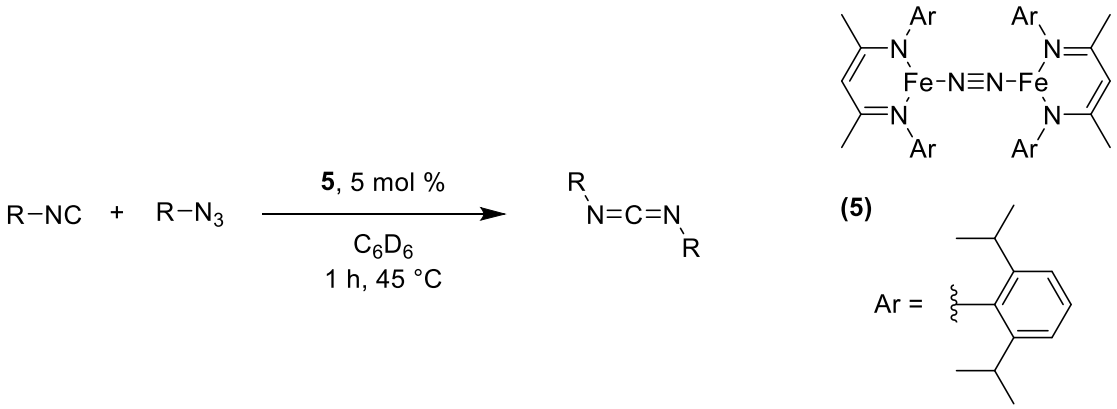

Scheme 10 – Although most catalysis with β-diketiminate iron complexes uses iron(II) pre-catalysts, there are some catalytic transformations using iron(I) pre-catalysts, such as carbodiimide formation reported by Holland. [51]

1.3 Alkene Isomerisation – Catalysts, Mechanisms and Challenges

Much of the world's demand for energy and materials is met from crude oil, and the aliphatic hydrocarbon chains it consists of. Through cracking of longer chains, a huge quantity of alkenes are produced, and these represent the simplest way to both introduce functionality into hydrocarbons, as well as functionalise them further. Alkenes are useful reagents as they are unsaturated, so new bonds and functional groups can be added to a molecule with a reasonable degree of regiocontrol, and these transformations are high in atom efficiency. These range from simple processes such as hydrogenation to more complex transformations, such as hydrofunctionalisation, selective oxidation and polymerisation.

Almost all alkenes have a range of structural isomers, and many also have stereoisomers. Alkenes are, as far as functional groups go, exceptionally amenable to isomerisation reactions, as the carbon-carbon double bond is reactive enough to break, but stable enough to be reformed. The most common forms of isomerisation are *cis-trans* isomerisation, where the *cis-trans* configuration of an alkene is inverted, and chain walking isomerisation, where protons or in rare cases other functional groups are shuttled along a carbon chain — in a skeletal structure the double bond appears to 'walk' along the chain, hence the name (it can also be considered as a tautomerisation). Simple schemes of both are shown in Figure 3.

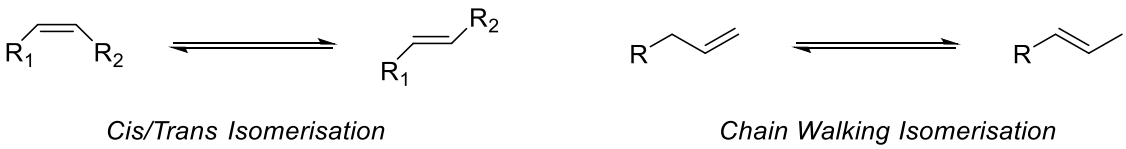

Figure 3 – A comparison of *cis*/*trans* isomerisation and chain walking isomerisation.

Where alkenes are not in a fully conjugated system (such as an aromatic ring), alkene isomerisation is generally not spontaneous, and molecules that do perform this, such as bullvalene, are unusual. [53] This means that alkene isomers are usually chemically distinct and can be prepared and utilised in isolation from one another (Figure 4).

Not Spontaneous
Isomers Chemically Distinct
Common

Spontaneous
Isomers interconvert
Uncommon

Figure 4 – Most non-aryl alkenes do not isomerise spontaneously, so individual isomers can be prepared and have distinct chemical properties (but-1-ene and but-2-ene shown). Compounds that do isomerise spontaneously such as bullvalene (owing to the ease of a Cope rearrangement) are unusual.

Where a range of regioisomers are possible, it is generally easier to synthesise terminal alkenes over internal ones. Large scale cracking, as well as many other well-known laboratory preparations generally lead to terminal alkenes, whilst routes to internal alkenes (such as alkyne reduction or E2 elimination routes) are more involved processes or require more expensive starting materials. To avoid these procedures it can be easier to prepare terminal isomers and access internal products through a further isomerisation step.

More substituted alkenes are generally more thermodynamically stable compared to less substituted (*i.e.* terminal) structures, except in cases where they disrupt conjugation or induce greater steric strain on the molecule. Because of these two considerations, it is both feasible and somewhat desirable to isomerise terminal alkenes to more substituted internal ones. However, it is also possible to form less substituted alkenes as the kinetic product, and many reported methods rely on maximising selectivity towards either the thermodynamic or kinetic product.

Catalytic Approaches to Alkene Isomerisation

For reasons of practicality, ease of reaction and reduction of the amount of waste produced, it is desirable to use catalysts to achieve this transformation. The two principal challenges to performing this reaction are the activity and selectivity — in that a reaction methodology must be able to activate the double bond, and thence isomerise the double bond to an alternative position, ideally with a significant degree of regio- and stereocontrol. A wide range of catalytic approaches to this process have been developed over the past seventy years, and it is performed on a very large scale in many current industrial processes. A broad range of heterogeneous [54, 55] and enzymatic catalysts [56] have been developed, although in this case homogenous processes are more relevant. Base-mediated transformations were first discovered by Prosser, [57] and studies by Cram showed there is a general mechanistic pathway where a proton is abstracted and released by the base (Scheme 11). [58]

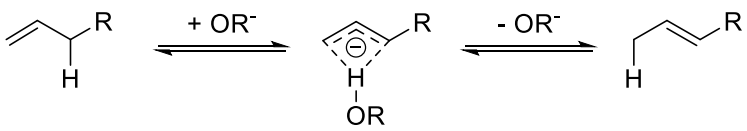

Scheme 11 – General base-catalysed isomerisation mechanism proposed by Cram. [58]

Base-catalysed routes are straightforward to perform, and the catalysts needed are generally not complex or expensive molecules. However they lack any real control over selectivity, and normally require a high loading of base to proceed (although the transformation is still catalytic in nature).

Generally relatively strong bases are required – potassium *tert*-butoxide, [57] *n*-butyl lithium [59] and superbases [60] have all been reported. These bases are frequently incompatible with a range of functional groups. In theory proton transfer is intramolecular as shown in the mechanism shown in Scheme 11, although competing side-reactions can lead to the formation of conjugate acids resulting in intermolecular proton transfer.

By utilising transition metal catalysts, there is potential for greater control over selectivity, as well as improved functional group tolerance and lower catalyst loading. Transition metals generally bind well to alkenes, weakening the π bond so activation is more facile. In classical transition metal catalysis, β-hydride elimination is considered undesirable, but in this case oxidative functionalisation of the adjacent C–H bond leads to a metal-allyl species being formed. From here, performing a reductive elimination step on the less substituted carbon leads to a second alkenyl complex, with the double bond on the more substituted position . This is an allyl mechanism, containing a formal oxidation of the metal centre and reduction of the allyl fragment, with proton transfer being a 1,3-hydride shift. This is similar in some respects to the base-catalysed mechanism, in that an allyl species is formed and proton transfer is intramolecular.

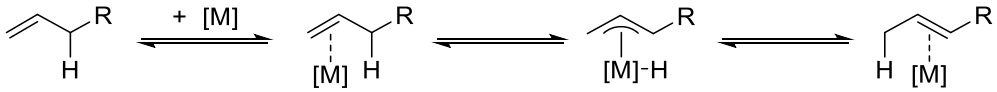

Scheme 12 – Generalised allyl mechanism for a metal-catalysed isomerisation reaction.

An alternative mechanism exists if a metal hydride (or non-metal hydride) is instead the active catalyst. Here, the metal-hydrogen bond can in effect be added over the alkene, generating a metal-carbon σ bond. β-hydride elimination from the more substituted position then forms the more substituted alkene. As the hydride on the metal is added to the molecule and a different proton regenerates the metal hydride, this mechanism is intermolecular, and the overall process is a 1,2-hydride shift. The range of metal complexes for which this mechanism has been investigated has been reviewed by Mazet. [61]

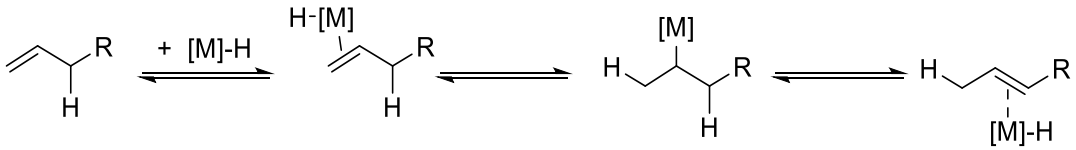

Scheme 13 – Generalised alkyl mechanism for a metal hydride-catalysed isomerisation reaction.

Discerning between these two mechanisms experimentally was first investigated by Sen, [62] and is discussed in Section 2.4. Both mechanisms have been proposed in a range of transformations, as seen in various examples below. From a metal-centric perspective, the allyl mechanism is a redox active route whereas the alkyl mechanism is redox neutral. It should be noted that this distinction is not always clear cut, and alternatively these two routes can be considered as extremes of a range of organometallic interactions.

A third alternative mechanism which is increasingly investigated is a hydrogen atom transfer (HAT) mechanism. HAT chemistry is an extremely broad field, and both first-row transition metals and light mediated processes are of key interest from both sustainability and mechanistic perspectives. [63] In the context of alkene isomerisation, a HAT mechanism proceeds through a pair of radicals,

one substrate centred, one metal centred. Crucially, the catalyst does not have a role in the rearrangement step, which is radically facilitated by the substrate itself (Scheme 14). HAT transfer can be identified through strong preference for the thermodynamic product, presence of both intramolecular 1,2 and intermolecular 1,3 hydride shift, and the presence of 'free' organic radicals in the reaction medium (although these frequently exist in close proximity to metal-centred radicals). [64]

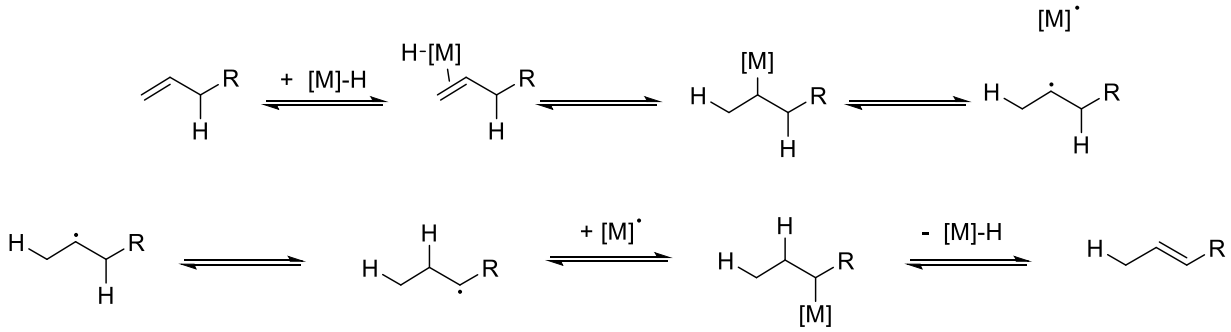

Scheme 14 – Generalised scheme for a metal-catalysed HAT process. Note that the isomerisation step occurs from the radical organic species rather than through a direct metal-mediated process.

Although previous examples were extant, [65, 66] the first example of a transition-metal catalysed process with a strong degree of stereocontrol was reported by Felkin in 1978. [67] Compared to previous reports, this reaction was both facile and had a strong preference towards formation of the *trans* product. This selectivity was justified by sterics around the allyl intermediate. Miyaura subsequently showed that allyl silyl ethers display similar reactivity and selectivity with iridium catalysts. [68]

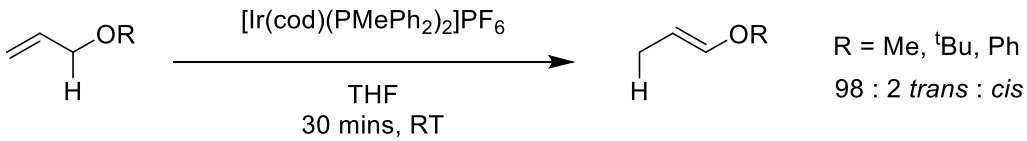

Scheme 15 – Iridium catalysed isomerisation of allyl alcohols reported by Felkin. [67] This procedure is strongly selective towards the *trans* isomer.

Further catalysts have been developed using ruthenium and rhodium complexes, which are generally proposed to proceed through an allyl mechanism. [69] Grubbs-type catalysts are well known for olefin metathesis, but Donohoe has shown that with the correct conditions and substrates they are also adept at isomerising terminal alkenes. [70] Generally the *trans* product is produced in high selectivity. The majority of transformations are from a primary to a secondary alkene, or between secondary alkene isomers, although Zhao has shown that some substrates can generate tertiary alkenes through a combination of catalyst design and less facile conditions (Scheme 16). [71]

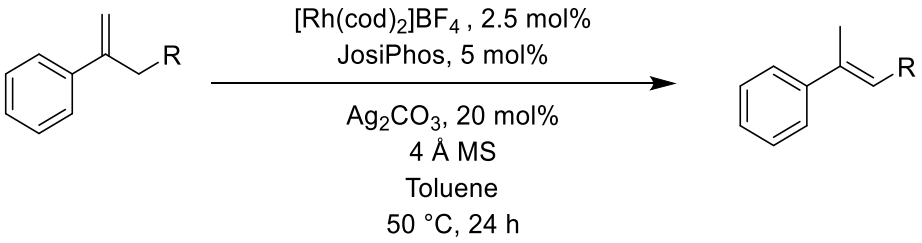

Scheme 16 – Formation of tertiary alkenes from primary alkenyl substrates, as reported by Zhao. [71]

Palladium-based systems have also been widely known and applied to this form of catalysis. [72] Chain-walking isomerisation by palladium salts was first reported by Davies, [73] and a range of complexes and substrates have been shown to be effective in isomerisation. By careful choice of ligands and conditions, selectivity can be enforced to some degree, although there are limited reports of strongly *cis*-selective isomerisation and highly regioselective isomerisation of linear alkenes.

Generally palladium systems follow an allyl pathway, and palladium hydrides do not play active roles in catalysis (a notable exception is discussed below). In some cases palladium systems can be influenced and directed by neighbouring functional groups on the substrate to a strong degree, as Wang has investigated. [74] Brookhart and Daugulis have shown that functional groups such as silyl enol ethers can direct a strong degree of selectivity. [75, 76] Several studies have further shown that palladium catalysts can isomerise other unsaturated systems, such as alkynes into dienes. [77]

Danishefsky has demonstrated numerous examples using palladium-catalysed isomerisation as part of total syntheses [78-80] — an example, where an initial isomerisation step is utilised as part of a synthesis towards quinocarcinol methyl ester, is shown in Scheme 17.

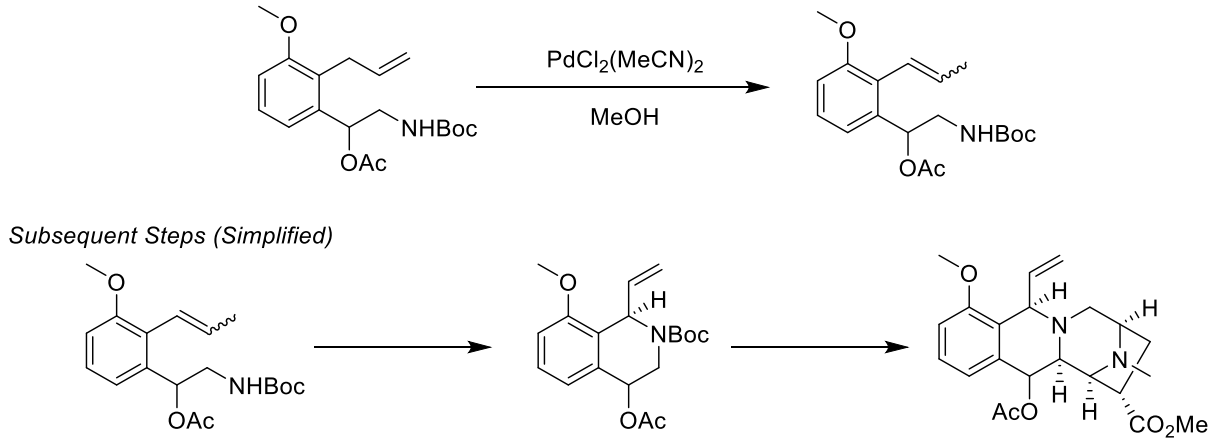

Scheme 17 – Danishefsky reported a synthetic route to quinocarcinol methyl ester. [79] The first step in this synthesis is a palladium-catalysed alkene isomerisation reaction.

Lindhardt and Skrydstrup have developed further palladium-based catalysis. Recent studies have showcased how bulky ligands (in this case, a phosphine) and an additive can lead to high conversions even with very low loading of catalyst. [81] In substrates with *Z*-alkenes that cannot chain-walk this generates the corresponding *E*-isomers; whilst for substrates that can undergo structural isomerism high conversions are observed for both relatively active substrates such as allylbenzenes, as well as more challenging substrates such as alkyl alcohols and amines.

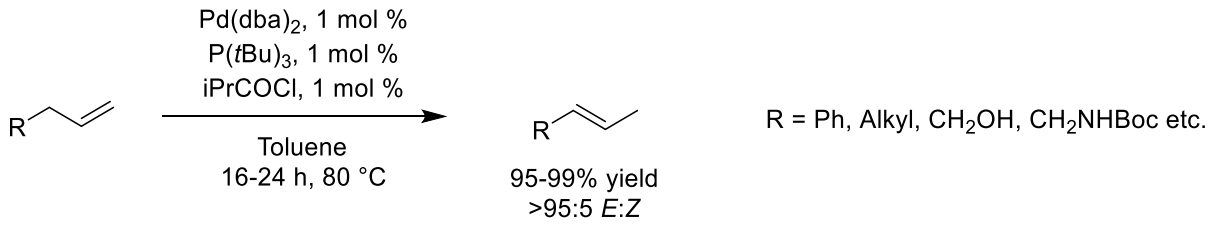

Scheme 18 – The catalysts used by Lindhardt and Skrydstrup can functionalise a large range of alkenes selectively towards secondary alkenes. [81]

Some investigation of the mechanism (and why bulky ligands have a beneficial effect) was also undertaken. It is postulated that the bulk of these ligands stabilises a palladium(II) hydride species that is formed, and can be observed through ^{31}P NMR spectroscopy *in situ*. This is then expected to perform a hydropalladation step and isomerisation proceeds through an alkyl mechanism, although there are some complexities in reaction behaviour that are not fully explained. This pathway is unusual as most other palladium-catalysed systems are postulated to go through an allyl pathway.

Hartwig reported an unusual isomerisation-hydrofunctionalisation-defunctionalisation reaction, leading to the thermodynamically disfavoured alkene being formed. [82] Following an initial palladium-catalysed isomerisation and hydrosilylation, the silane is eliminated to reform an alkene (Scheme 19). Although the overall transformation is isomerisation, it is not fully catalytic owing to the eliminated silane.

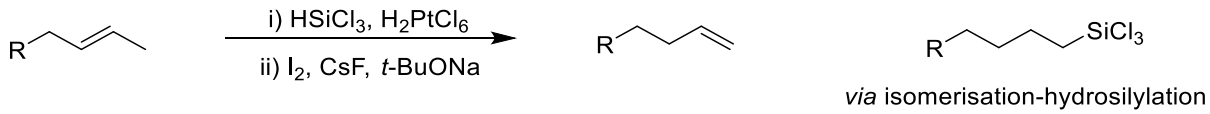

Scheme 19 – By proceeding *via* isomerisation-hydrosilylation, Hartwig reported the synthesis of the less favoured terminal alkene from a more substituted one. [82]

As well as a fundamental transformation, isomerisation can proceed in tandem with other chemical transformations. These include C–C bond breaking steps [83], Claisen [84] and Cope [85] rearrangements and carbonyl allylation [86] — select examples are shown in Scheme 20. Furthermore unsaturated molecules with alcohols can also be isomerised into carbonyls, as shown by Grotjahn. [87] These sequential or tandem methods are an efficient and elegant strategy to perform some complex molecular rearrangements, although many are somewhat limited in scope and application.

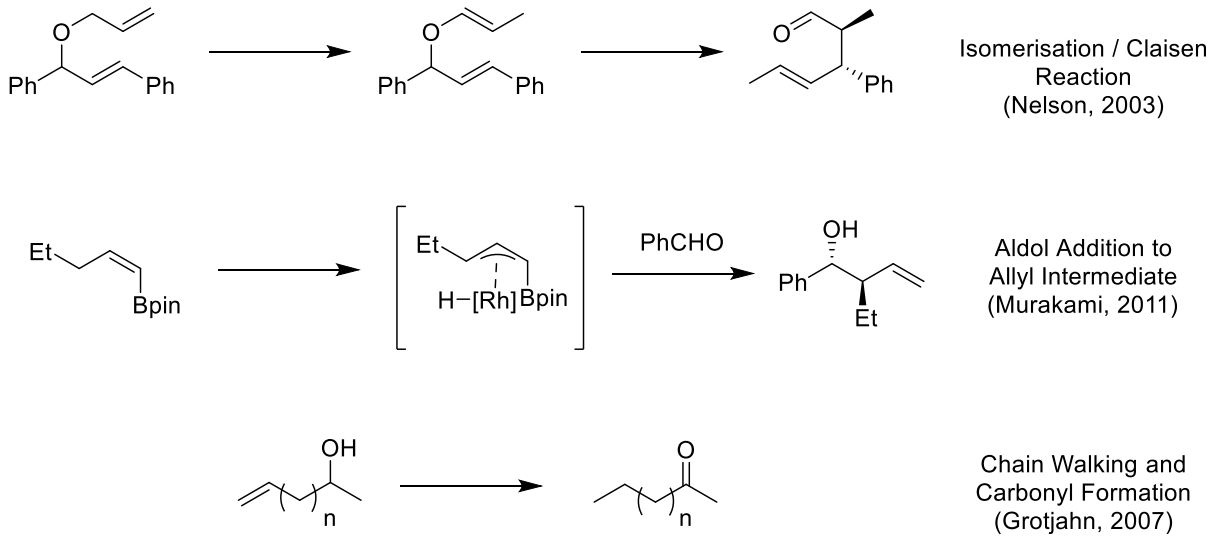

Scheme 20 – Some examples of isomerisation reactions in tandem reactions or secondary processes to perform more diverse molecular transformations. All three of these are postulated to proceed through allyl-like intermediates.

First Row Transition Metal-Catalysed Isomerisation

As discussed in Section 1.1, there are clear advantages to using abundant first-row transition metals as catalysts, in particular iron, and using them is of increased research interest. This sub-section reviews relevant reports of both iron- and cobalt-catalysed olefin isomerisation. In terms of isomerisation chemistry, studies involving iron, although somewhat limited, have a long history. Stoichiometric reactions between alkenes and iron carbonyls have been known since 1930, and have attracted interest due to their ease of synthesis and amenability to study through FTIR spectroscopy, [88] and there have been numerous reports of iron carbonyl complexes being used as catalysts. [89] With regards to catalytic isomerisation, among the earliest reports was the isomerisation of fatty esters by Frankel, Enkel and Davison, [90] although more relevant to this study are the findings by Hess and Waegell in the 1980s. Hess showed that linear alkenes such as pentene can be isomerised at low temperatures using iron carbonyls activated with cyclooctane to form **6**. [91] Here the major product is *trans*-2-pentene, with a small amount of *cis*-2-pentene also formed (Scheme 21). Waegell subsequently showed that selectivity is improved if a conjugated system is formed in the product(s). [92] There have been numerous reports of isomerisation of allyl alcohols to carbonyls, most notably by Grée. [93, 94]

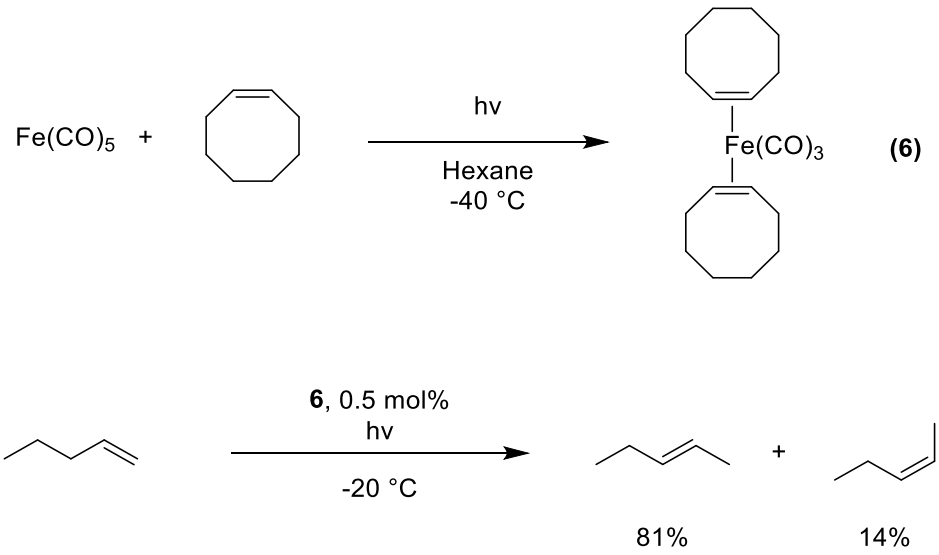

Scheme 21 – Formation of **6** and consequent use in alkene isomerisation as reported by Hess. [91]

Harris has subsequently investigated similar catalytic systems to a deeper degree, particularly through time-resolved IR spectroscopy. [95] By using these studies, as well as DFT calculations, it is postulated that these reactions proceed through an allyl intermediate (Scheme 22), although this intermediate was too short lived to be identified on the timescale of the experiment (70 ns). This mechanistic pathway has previously been proposed by Casey. [96]

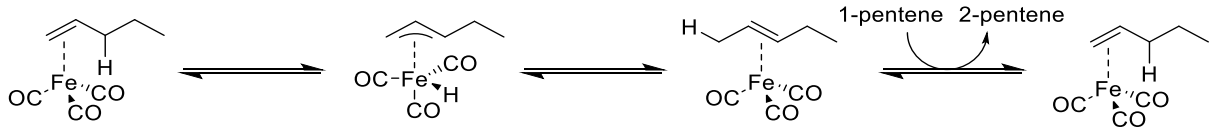

Scheme 22 – The allyl mechanism proposed by Harris, showing the isomerisation of 1-pentene to 2-pentene using an iron carbonyl pre-catalyst. [95]

Although this is the most common postulated mechanism for iron carbonyl catalysts, several others have been proposed — most notably by Crivello, who has proposed that in the presence of a strong base the active species is instead the $[Fe_2(CO)_7]^{2-}$ dianion as opposed to a neutral species. [97]

Subsequent studies by Hesse have demonstrated further scope and applications for iron carbonyl-catalysed systems, for example, forming enamides from allyl amides. [98] Furthermore, mechanism and rate have been shown to be strongly solvent dependent by Laperle, with strongly coordinating solvents slowing down the rate of reaction and resulting in alternative reaction intermediates forming. [99] Beller has additionally shown that a variety of neutral and anionic iron carbonyl complexes have varying activities, but broadly consistent selectivities. [100] Iron carbonyls easily activate alkenes, and proceed with rapid catalytic turnover. Disadvantages to their use are that they are generally toxic due to their volatility (although less so than $Ni(CO)_4$), and their lability and flexible denticity means it is difficult to control the metal environment. Because of this, amongst other reasons, ligands offering greater electronic and steric control and tuneability have been developed in many catalytic fields. The most recent and pertinent studies for catalytic isomerisation are discussed below.

There have been a range of studies with cobalt-based catalysts, and reactivity has been shown to be broad and divergent in some cases. Holland reported in 2014 isomerisation catalysis using **7** that is selective, somewhat unusually, towards the *cis* isomer (Scheme 23). [101] Furthermore, this catalytic system has significant regiocontrol, forming 2-hexene rather than chain-walking further to the 3-hexene isomer.

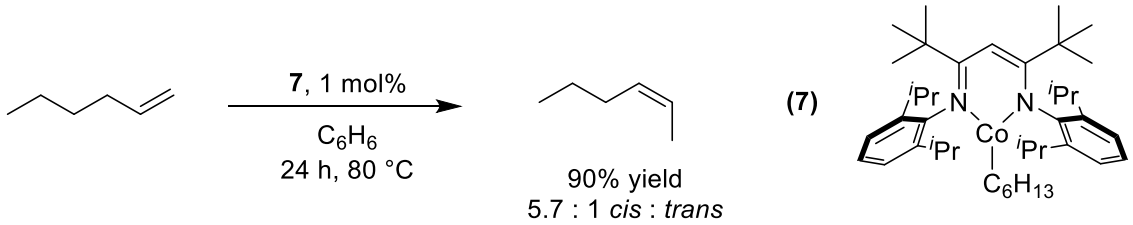

Scheme 23 – Cobalt-catalysed isomerisation of alkenes reported by Holland, using a bulky β-diketiminate pre-catalyst. The process was also applied to fifteen additional substrates. [101]

Mechanistically this is proposed to proceed through an alkyl mechanism, where the pre-catalyst undergoes β-hydride elimination to form a cobalt(II) hydride, with subsequent insertion, chain walking and β-hydride elimination to form the product. A steric model is proposed which determines that the large steric bulk of the ligand forces the transition state to adopt the *Z*-selective conformation. This also prevents the 2-hexene product from being isomerised further. Further studies showed that *cis-trans* isomerism is also present in the process (and somewhat reduces stereoselectivity).

Subsequently Hilt has shown alternative ligand motifs can also lead to the *Z*-isomer being preferentially synthesised. [102] These catalytic systems require activation of **8** through reaction with diphenylphosphine, and by using $DPPh_2$ it can be seen there is significant H/D scrambling between the activating reagent and the substrate (Scheme 24). Compared to Holland's system, this catalyst is somewhat less selective (typical selectivities are 6:1 *Z*:*E*). The reason that the reaction requires both zinc metal and halide salts is not fully discerned, although they are both essential to achieve a reasonable yield.

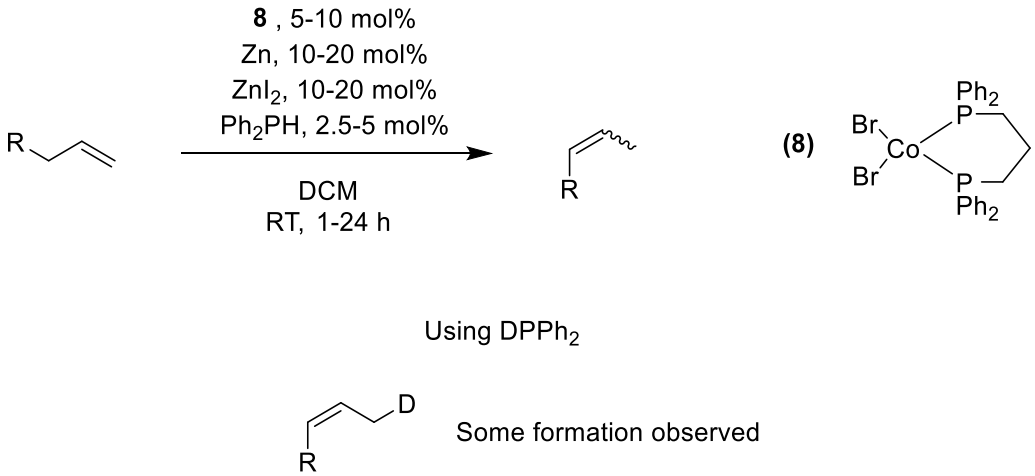

Scheme 24 – Studies by Hilt also predominantly form the *Z*-isomer using a cobalt catalyst. For some substrates dppp is replaced by alternative phosphine ligands, and loadings are also varied. Deuteration studies show that there is hydride exchange between the phosphine co-reagent and the resulting product. [102]

E-selective studies have also been reported. The earliest examples include radical HAT processes reported initially by Shenvi, [103] and later cycloisomerisation transformations by Norton. [104] Further studies have been reported by Liu using cobalt pincer complex **9**. Here catalyst activation occurs through addition of ammonia borane, which has similarities with the chemistry reported in Chapter 2. [105] Terminal alkenes can be converted readily to internal systems, and the *cis* product is favoured, with the additional thermodynamic preference of reduced ring strain. Again, this reaction is mechanistically postulated to proceed through an alkyl mechanism similar to that proposed by Holland, although in this case the ligand structures generally favour the *E* isomer. Again the mono-isomerised secondary alkene is selectively formed over more substituted isomers, and when an asymmetric structure is used (R ≠ H) the regioselectivity is controlled.

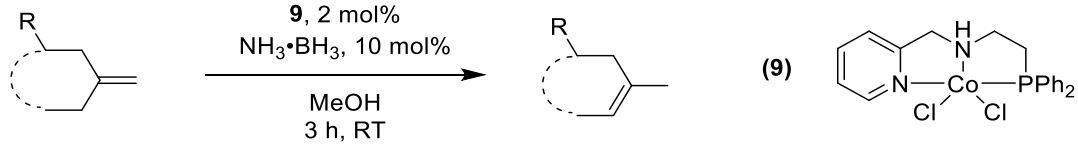

Scheme 25 – Regioselective isomerisation of terminal alkenes in cyclic molecules reported by Liu. [105]

Recent research by Findlater also utilised cobalt complexes activated by ammonia borane and a base. [106] The base is required to active proligand **10**, whilst ammonia borane is again postulated to allow a cobalt(II) hydride to form (Scheme 26). Kinetic isotope effect experiments indicate that the metal hydride insertion over the alkene is rate determining, and the π-stacking of the R groups with the side pyridine on the ligand are essential to allow the reaction to proceed.

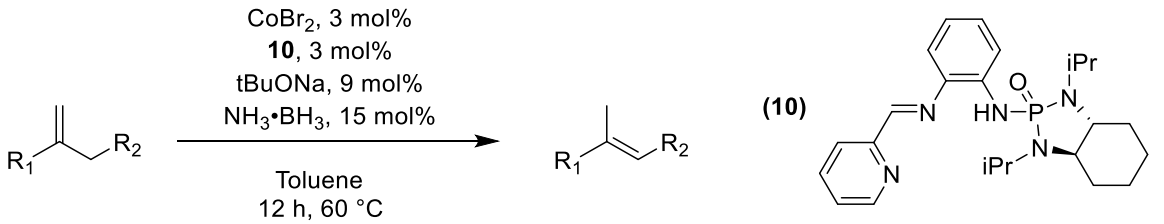

Scheme 26 – Isomerisation of terminal alkenes reported by Findlater, using a cobalt salt, proligand **10**, base and ammonia borane. As in Liu's report, ammonia borane is proposed to facilitate the formation of a cobalt hydride. [106]

As a final cobalt-based report, Xia has shown that minor ligand and substrate changes can exhibit large variation in chemical behaviour. When using a *cis* alkene adjacent to an aromatic ring *cis-trans* isomerisation is observed, [107] whereas if the substrate is a terminal alkene (with certain structural requirements) then chain-walking double bond isomerisation is observed instead (Scheme 27). [108] In both cases, the postulated mechanism is through formation of a cobalt hydride and subsequent proton addition/elimination.

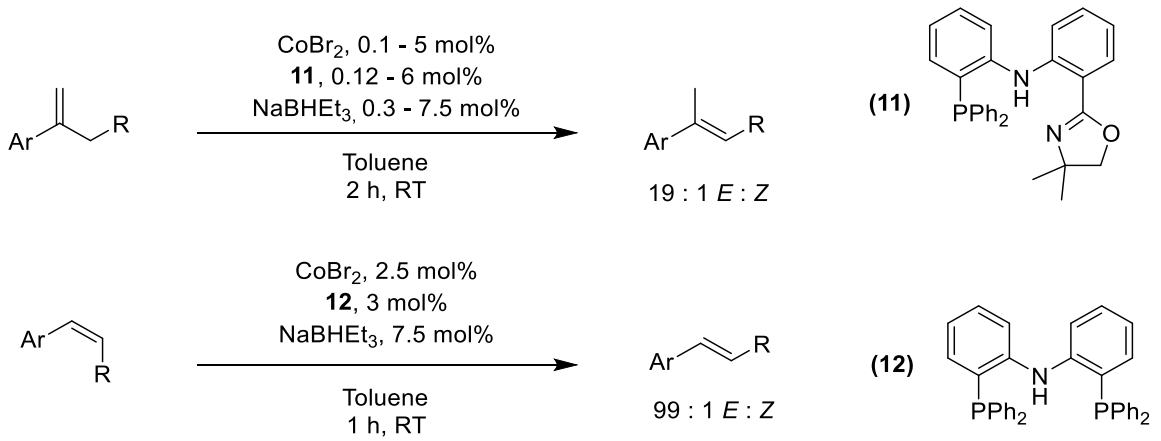

Scheme 27 – Xia has reported that, by varying ligands, divergent *cis-trans* isomerisation and chain walking isomerisation can occur, although both are substrate specific. [107]

Compared to cobalt, there are significantly less catalytic processes using iron complexes (aside from the aforementioned iron carbonyl reports). Many iron-catalysed systems are activated by a reducing agent to produce the active species. This approach has been investigated in isomerisation by von Wangelin, primarily using phenylmagnesium bromide and $Fe(acac)_3$ complexes. [109] This has been shown to work for a broad range of alkenes, and in certain cases perform *cis-trans* isomerisation where chain walking reactions are not possible (Scheme 28).

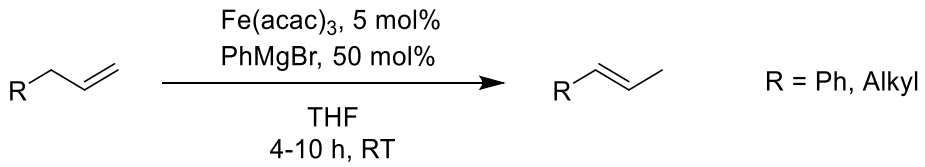

Scheme 28 – Iron-catalysed isomerisation of alkenes reported by von Wangelin. [109]

Some mechanistic studies have been undertaken, but an overarching catalytic cycle and active species are not proposed. Previous studies by Fürstner have suggested that similar reactions form 'inorganic Grignard' reagents with formal iron-alkali metal bonds, [110] although their fundamental characteristics, such as oxidation state, is not discussed in this reaction. There is also the possibility the active species could be nanoparticles as opposed to defined complexes.

There are additionally several reports of iron-catalysed allylalkene to carbonyl isomerisation, for example the base-catalysed system reported by Gaillard and Renaud (Scheme 29). [111] In this case, the presence of the adjacent strongly electron-withdrawing trifluoromethyl group is proposed to enhance reactivity of the double bond. Similar transformations have also been reported by Fan [112] and de Vries, [113] and an air-stable catalyst and methodology has been developed by Morrill. [114]

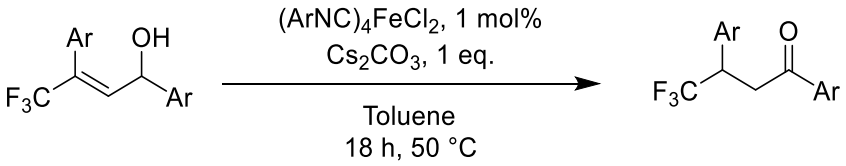

Scheme 29 – Isomerisation of allyl alcohols to ketones reported by Gaillard and Renaud. A stoichiometric equivalent of base (in this case, Cs_2CO_3) is necessary for a reasonable conversion. [111]

Generally, when carbonyl ligands are not present, catalytic isomerisation with iron complexes are proposed to proceed through an alkyl mechanism, and often through formation of a metal hydride. An exception to this is the recent study by Werncke, where *cis-trans* isomerisation proceeds with an Fe(I) HMDS cation (Scheme 30). [115] This can be considered as an unusual case, primarily as the substrate (dppe) can bind well and be isolated from the mixture as a coordinated ligand. To underline this rarity, such behaviour is not observed with other phosphine-containing compounds.

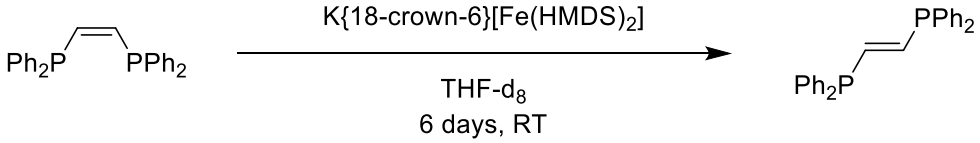

Scheme 30 – Werncke observed *cis-trans* isomerisation of dppe using an iron-HMDS anion. [115] Mechanistically this appears distinct from a simple alkyl or allyl pathway, which may be linked to the substrates secondary role as a ligand.

As well as solely isomeric transformations, there are a range of studies where isomerisation is catalytically performed in tandem with further alkene functionalisation. This gives the reaction a greater thermodynamic driving force through the forming of a new bond as well as more diverse structures. A relatively early example of this approach is from Darcel, [116] where an initial isomerisation reaction forms a carbonyl, followed by condensation, and then a further catalysed hydrogenation step to yield the amine product (Scheme 31).

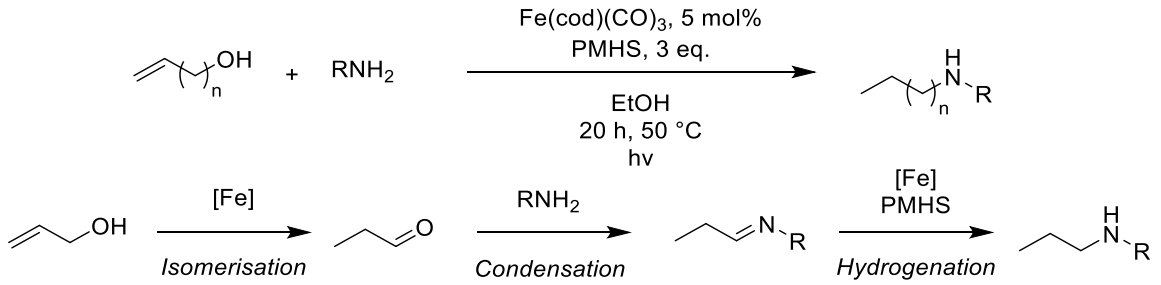

Scheme 31 – Isomerisation/functionalisation reaction reported by Darcel. [116] The reaction is proposed to proceed through isomerisation, condensation, and hydrogenation reactions in succession.

Tandem isomerisation-hydroboration has been reported in a reasonable number of cases with precious metals, including rhodium (Srebnik [117] and Crudden [118]) and iridium (Miyaura [119]), as well as part of more complex 'one-pot' synthesis as developed by Crudden. [120] In most cases these reactions are reported to only tolerate a few substrates or generate them as undesired side-products. Chirik first reported a cobalt-catalysed strategy in 2013, using an oxidative work up to

form terminal alcohols from internal alkenes, *via* hydroboration. [121] Base metal methodologies have been developed by Stradiotto and Turculet in several studies. Initial results reported that internal linear alkenes (such as octene) are chain walked then hydroborated to give terminal organoboranes (Scheme 32). [122] Through a combination of experimental study and theoretical modelling, this could later be applied to first row metals (manganese through nickel, including iron), and ligand and catalyst behaviour were studied and optimised for both the isomerisation and hydroboration components of the process. [123]

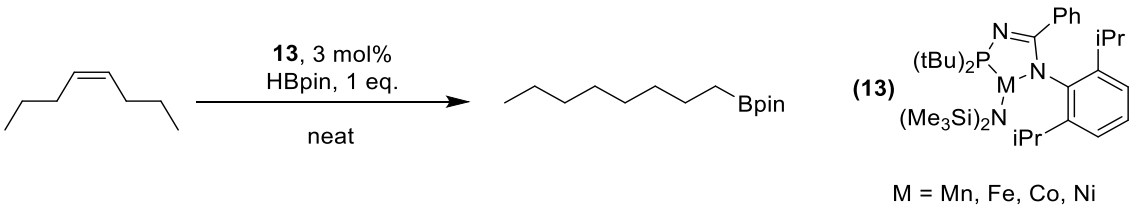

Scheme 32 – Tandem isomerisation-hydroboration of linear alkenes (in this case, octene) as reported by Stradiotto and Turculet. [123]

Again, the mechanism is reported to proceed through hydride formation, 1,2-insertion to an alkyl intermediate and isomerisation. From here, rather than β-hydride elimination (which would generate a terminal, less-stable alkene compared to the initial substrate) a borylation step occurs, where the metal-carbon bond is cleaved by a molecule of pinacolborane (Scheme 33). Because of this, there is proton transfer from pinacolborane to the product rather than hydride shift from the substrate. The previous mechanistic study by Chirik postulated a practically identical reaction pathway.

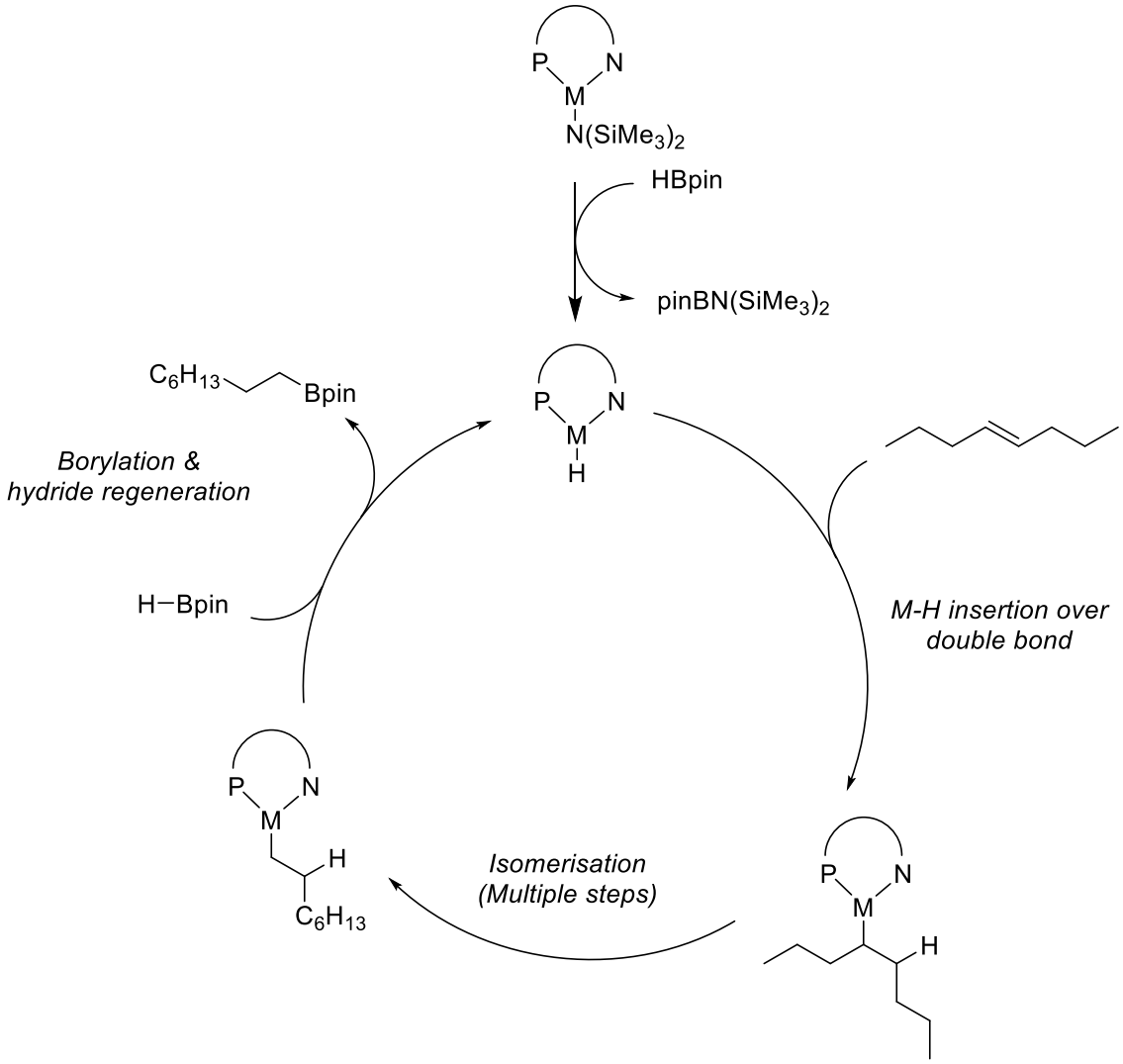

Scheme 33 – Proposed mechanism for catalytic isomerisation-hydroboration reactions (M = Mn, Fe, Co or Ni). The PN ligand is shown in Scheme 32.

In this case, isomerisation progresses towards the terminal position before undergoing functionalisation. Lu has developed a complementary transformation where the double bond is isomerised to the more favoured position adjacent to a π system (in the substrates evaluated, there is no feasible terminal product). [124] The alkene regioisomers can be observed forming *in situ*, indicating that the reaction is not concerted, but the hydroboration reaction only occurs in the α-position adjacent to the aromatic ring (Scheme 34). Although no additional activating reagent is required, the excess of pinacolborane needed to attain high conversion suggests that the pre-catalyst is activated upon a reaction with pinacolborane.

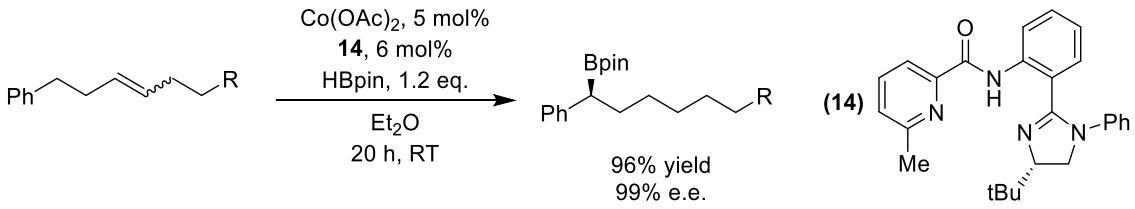

Scheme 34 – Isomerisation-hydroboration reaction reported by Lu. [124] Terminal organoboranes cannot be accessed; instead, hydroboration occurs adjacent to the aromatic ring.

Koh has also reported an iron-catalysed isomerisation-hydroboration process using **15**, [125] although it has significant setup and mechanistic differences. In this case an equivalent of base is required to enable the reaction to proceed (Scheme 35), and hydroboration is limited to β-positions adjacent to aryl groups.

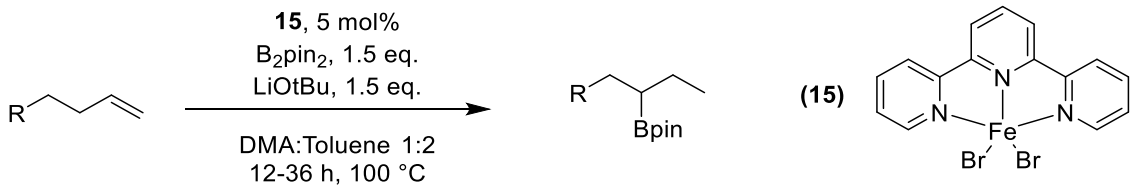

Scheme 35 – Isomerisation-hydroboration reaction reported by Koh, where R is an aryl group. [125]

The isomerisation and hydroboration steps are reported to proceed through entirely different active species, the former through an iron hydride, and the latter through iron-boryl and iron alkoxide species. These are formed as part of the catalyst activation — the hydride from the formation of the terminal regioisomer — and the more substituted alkene exists as a free species rather than an intermediary (Scheme 36). The additional proton on the product is shown from isotope labelling to come from the solvent reacting with lithium *tert*-butoxide, with this route of slow formation postulated to enable the substrate to undergo isomerisation first.

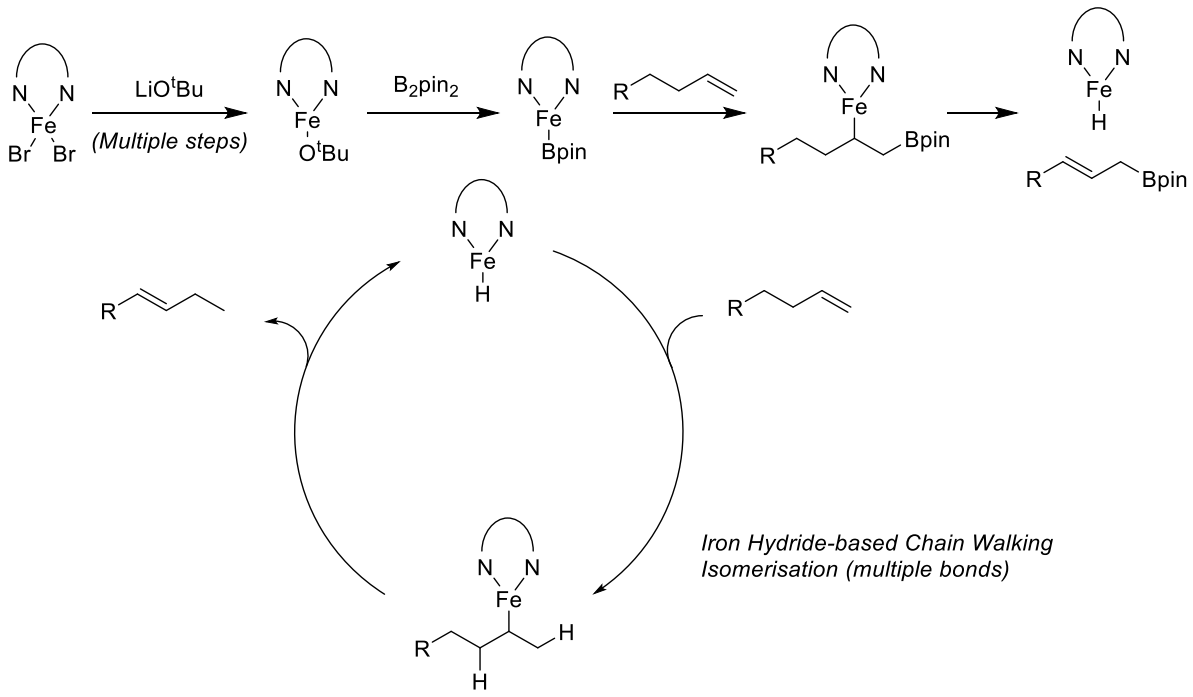

Scheme 36 – The proposed catalyst activation pathway and isomerisation catalytic cycles. The subsequent hydroboration step is a separate boryl/alkoxide based pathway.

Although this review is not universal, several major conclusions can be drawn from current transition metal catalysis. The key mechanistic difference between first row and second and third-row systems is that first-row systems are generally (but not always) proposed to proceed through a metal hydride and an alkyl mechanism, whereas second and third-row metals can proceed through alkyl or allyl pathways, the latter involving a redox-active process rather than a redox-neutral one. The metal hydride can be prepared from a pre-catalyst through a range of reagents, but it is generally not isolated from the reaction, and it is formed *in situ* rather than used as a pre-catalyst itself. It must also be noted that in many studies, particularly less recent reports, relatively little mechanistic study is undertaken.

1.4 Allenes and routes to Polyallenes

Introduction to Allenes

Compared to alkenes, allenes are less common in nature, less studied in research, and used less as synthetic building blocks, although in the case of the latter two, this has increased greatly in recent years. Allenes are the simplest form of cumulene, a class of molecule containing multiple adjacent carbon-carbon double bonds. [126] This leads to the relatively unusual molecular structure (Figure 5) containing two adjacent double bonds perpendicular to each other. Tetra-substituted allenes have the unusual property of possessing chirality despite containing no sp^3 carbon centres. This property has been increasingly used to synthesise complex molecular materials. [127]

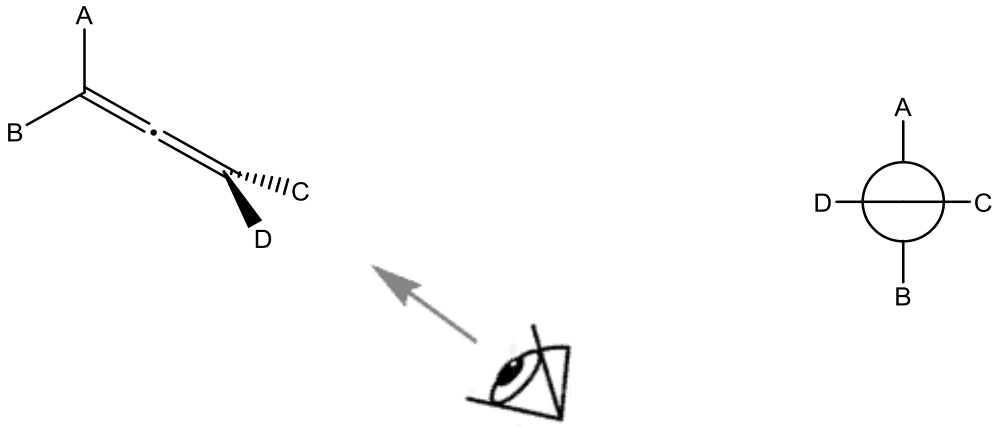

Figure 5 – The structure of allenes. Note the positions of the functional groups arising from the perpendicular nature of the two double bonds.

Allenes are considerably less abundant in nature than alkenes. Nevertheless, they are found in over 150 natural products, [128] some examples are shown in Figure 6. Allenes can also be prepared from a variety of synthetic routes, depending on both the scale and the functionalities required - typically they are synthesised from alkenes, alkynes, enynes or cyclopropane rings (Synthesis from the latter is discussed in Chapter 3). [129] It must be noted that some allenic structures remain challenging targets in organic synthesis.

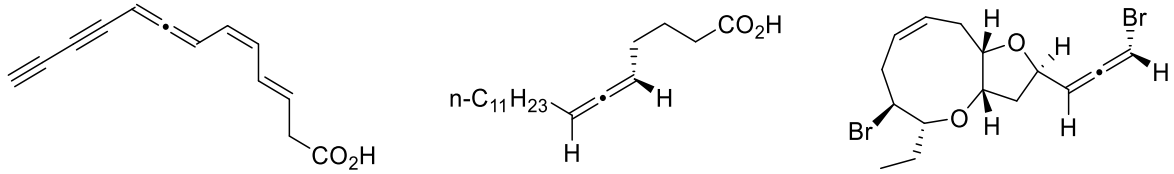

Mycomycin Laballenic Acid Isolaurallene

Figure 6 – Some examples of natural products containing allenes – mycomycin, a fungal metabolite, laballenic acid, found in various seed oils and isolaurallene, produced by certain species of red algae.

The most common functionalisation of allene substrates are addition reactions. [130] In terms of reactivity, they can generally be considered somewhere between alkynes and alkenes. [131] This trend can also be seen in many transition metal-catalysed reactions, for example, cycloaddition chemistry as reported by Wender and Houk. [132] This means most common reactions of alkenes and alkynes are feasible for allenes, including addition over bonds, cycloadditions, and binding to transition metals. Hydrofunctionalisation reactions are reviewed further in Section 1.5.

Furthermore, owing to their unsaturated nature, allenes are amenable to polymerisation reactions. [133] Unlike most polymers, including those derived from alkenes, polyallenes possess an sp^2 carbon in the backbone of the main chain (Figure 7). This leads to a chain conformation very different from alkene polymers such as polystyrene, for example well-defined helical polymers can be prepared. [134, 135] Furthermore, as one of the double bonds is left unreacted, the resulting polymer is amenable to further functionalisation.

Figure 7 – Comparison of polyalkenes and polyallenes. Polyalkenes generally have a fully saturated backbone, while polyallenes possess an sp^2 carbon centre on the backbone of the repeating unit.

Because of their structure, repeating units of polyallenes can have various structural isomers. In a monosubstituted allene, as examined in the results and discussion, there are two structural isomers (1,2- and 2,3-). Furthermore, 1,2-polymers can adopt various tacticities, the simplest ordered ones being isotactic and syndiotactic (Figure 8). If polymerisation is generally non-selective, a mixture of these structures is possible. Furthermore, if both double bonds on the same repeating unit react, crosslinking and cyclisation can be observed as significant side and terminating steps.

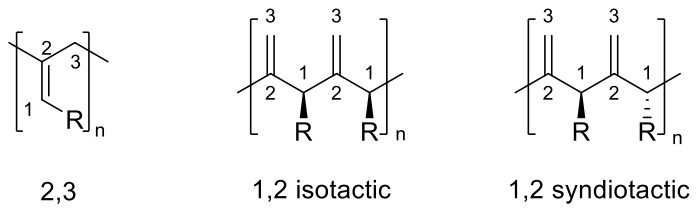

Figure 8 – Possible microstructures of allene-based polymers.

Polymerisation of propadiene (the simplest allene) was first reported by Baker, initiated by aluminium salts. [136] This generated a range of polymeric structures as well as lower molecular weight species. Because propadiene and other simple allenes are challenging to handle given their gaseous form, increased focus has gone into functionalised allenes with much higher boiling points. In particular substrates such as cyclohexylallene and phenylallene have attracted interest.

Polymerisation of phenylallene was first reported by Anderson in 1977. [137] Radical, emulsion and metal catalyst initiators were shown to have some degree of activity, although reported conversions are generally low (one of the highest-yielding reactions is shown in Scheme 37). Consistently the 2,3-configuration is favoured over the 1,2.

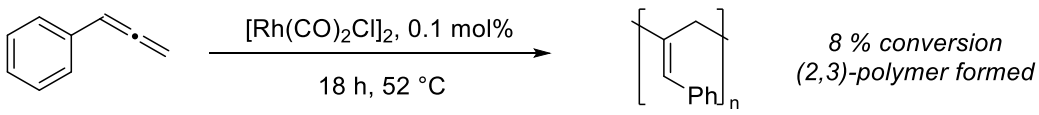

Scheme 37 – Polymerisation of phenylallene reported by Anderson. [137] Note the low conversion under these conditions.

More thorough investigations into this polymerisation were reported by Endo. [138] A range of radical initiators were tested, leading to conversions of 30–50 % and number average molar masses (M_n) of 2000–2500 Da. Polydispersities were reported to be in the range of Đ = 1.95–2.45, which is to be expected in a radical polymerisation, and it was demonstrated that copolymerisation with various other monomers was possible. More recently, metal complexes have been shown to initiate polymerisations of considerably longer molecular weight. Much of this has been reported by Endo and Tomita, who have shown that a range of nickel complexes can perform living polymerisation (An example using **16** is shown in Scheme 38). [139]

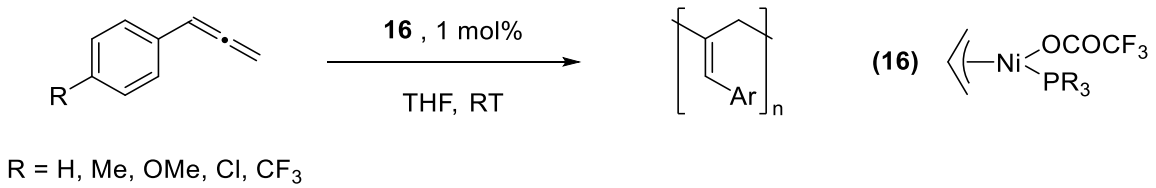

Scheme 38 – Living polymerisation reported by Endo, resulting in higher molecular weight and reduced polydispersity. [139]

Under these conditions, reported M_n values are increased (8000–9000 Da) and polydispersity is reduced (Đ = 1.05–1.15). The proposed mechanism is shown in Scheme 39. The same authors have developed modifications to this setup to vary the outcome, such as developing microspheres, [140] block copolymerisation with vinyl monomers [141] and multi-component coupling polymerisations to form higher-order structures with chirality. [142]

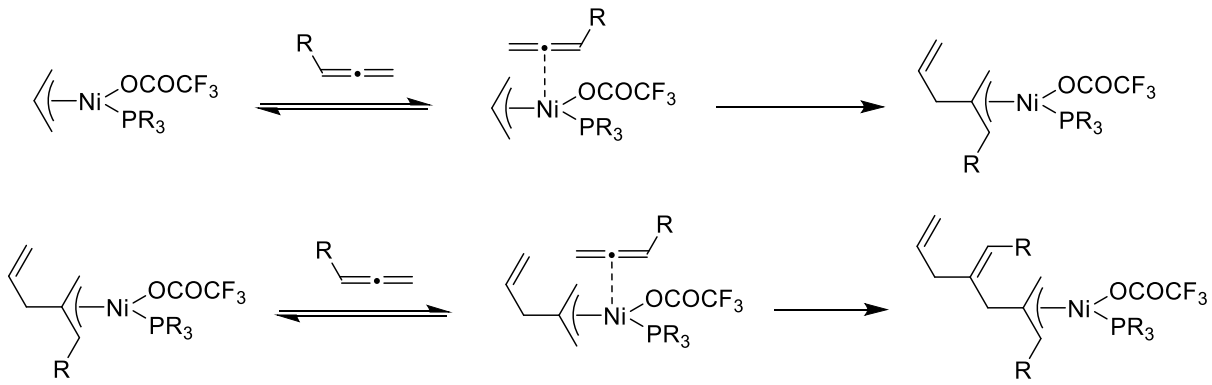

Scheme 39 – Mechanism of living allene polymerisation proposed by Endo. [143] The first two steps are shown.

As well as these studies, Cui has reported polymerisation of phenylallene with various lanthanide metal complexes derived from **17** (Scheme 40). [144] Using these complexes polymers with M_n of up to 25 kDa can be produced, although the PDI (Đ = 1.65) is significantly higher than the nickel living-polymerisation examples.

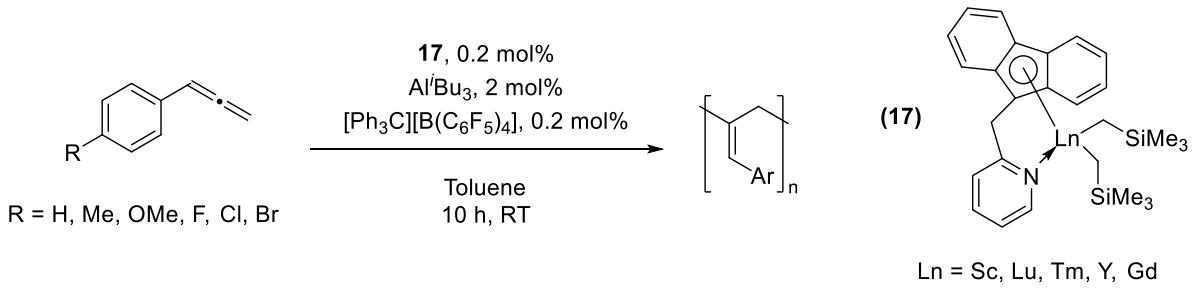

Scheme 40 – Polymerisation of phenylallene using rare-earth metal complexes, as reported by Cui. [144] In some cases, the metal complex **17** has an additional THF coordinated.

Barrett has shown that precious metals complexes can also be competent in allene polymerisation, but only for a limited range of substrates. [145] For example, whilst Grubbs catalyst **18** is generally adept at metathesis reactions for allenes, in the cases of phenylallene and para-tolyl-phenylallene polymerisation is instead observed (Scheme 41).

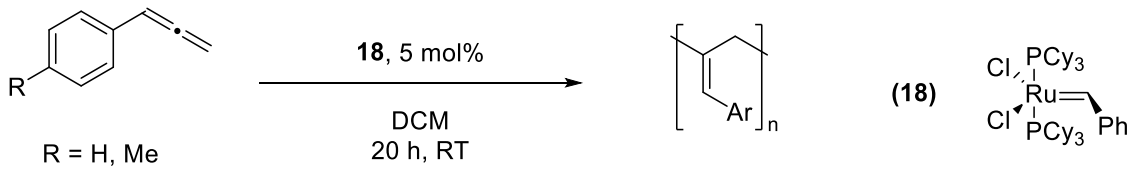

Scheme 41 – Polymerisation of phenylallene observed by Barrett. [145]

With the same substrates, Yamamoto has reported polymerisation with both rhodium complexes and cobalt complex **19** (Scheme 42), with long, polydisperse polymers formed (regioselectivity was not extensively investigated). [146] To our knowledge, this is the only first-row transition metal complex that has been used as a catalyst in this process.

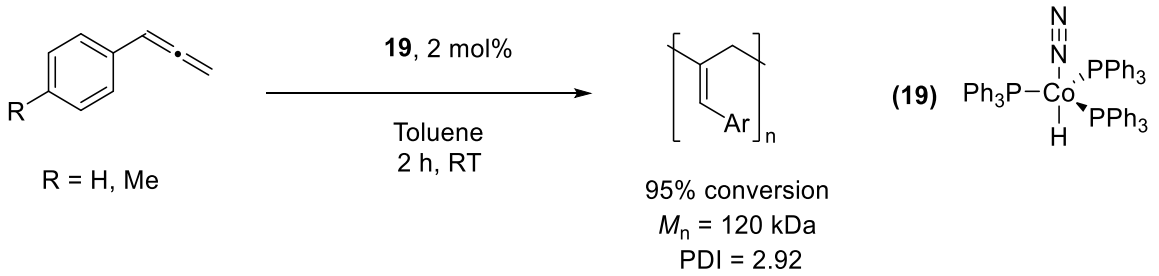

Scheme 42 – Polymerisation of phenylallene using a cobalt(I) species reported by Yamamoto. [146] This generates long polymers with a high polydispersity.

As shown, polymerisation of phenylallene can be performed by a relatively broad range of metal catalysts, and in some cases conditions are reasonably facile. However, there is little demonstration of control of molecular weight or dispersity. Furthermore, barring some of the living polymerisation investigations, there is little study into the mechanism of the reaction, and in many cases even the basic properties of the polymer (mass, dispersity or material) are not investigated.

1.5 Catalytic Hydrofunctionalisation of Allenes

Just as hydrofunctionalisation reactions are possible over alkenes, so are analogous addition reactions possible with allenes. Compared to alkenes, allenes have various advantages and disadvantages as substrates. As they are generally more reactive, reactions can be more facile. Much like polyallenes, monofunctionalised products contain a double bond, and this unsaturated nature means products are amenable to further functionalisation. Potential disadvantages are that regioselectivity becomes more challenging — classic alkene addition reactions can form only the Markovnikov and anti-Markovnikov products, whereas allenyl substrates can produce various regioisomeric products (Figure 9). Furthermore, as discussed in Section 1.4, allenes are generally considered more challenging substrates to synthesise. Finally, the bifunctional nature of allenes means that methods have to selectively monofunctionalise (or difunctionalise) the substrate. [147]

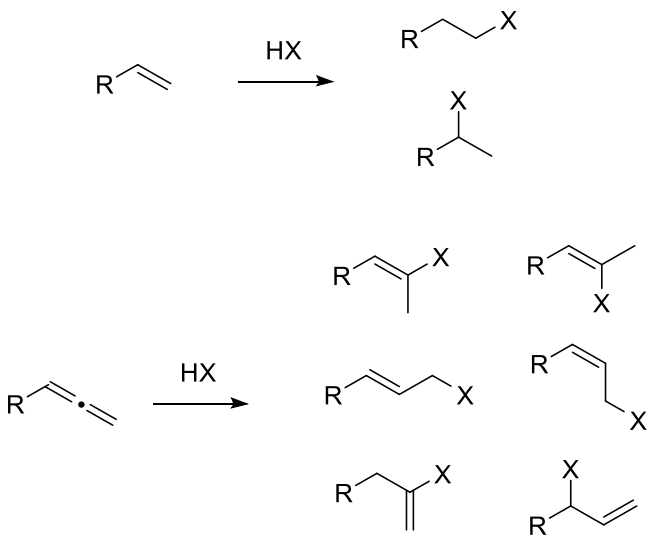

Figure 9 – The number of structural isomers possible when adding 'HX' over an allene are considerably greater than the comparable addition over an alkene.

Nevertheless, hydrofunctionalisation of allenes have been well-studied in recent years, in particular as substrates for C–N and C–B bond formation. Use of transition metal complexes as catalysts has enabled reasonable regioselectivity (and in some cases stereoselectivity) to be achieved. For hydroamination, a range of pre-catalysts have been shown to be adept with allenyl substrates, including precious metals, [148] group(IV) metals [149] and a limited number of other first row transition metals. Generally the terminal, rather than branched product is formed, and of the two terminal regioisomers the *E*-isomer is preferred over the *Z*. A recent copper-catalysed example reported by Taillefer and Monnier is shown in Scheme 43. [150] These conditions have also been shown to work for a range of other allenyl substrates. [151]

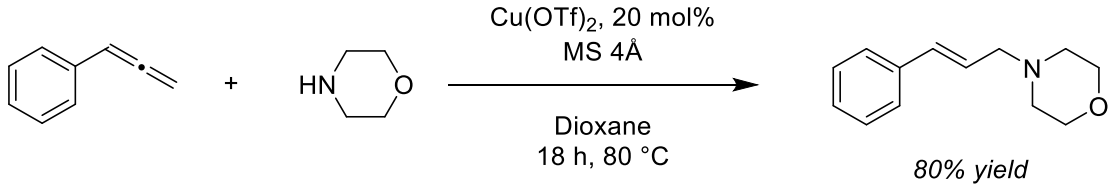

Scheme 43 – Terminal hydroamination of allenes using a copper catalyst reported by Taillefer and Monnier. [150]

Accessing the branched product is considered more challenging, despite this Breit has reported a rhodium-catalysed methodology using Josiphos-based ligand **20** (Scheme 44). [152]

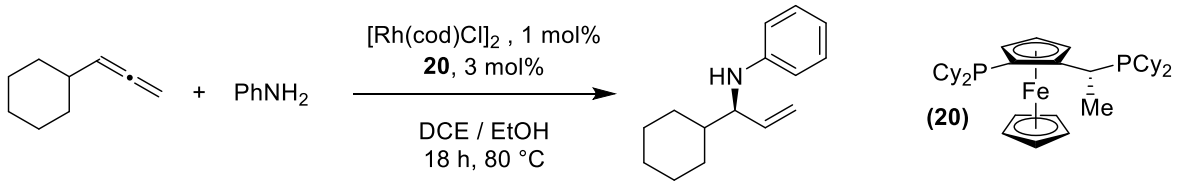

Scheme 44 – Branch selective hydroamination of allenes reported by Breit. [152]

Reactions involving hydroboration of allenes do not always require a catalyst to proceed, highlighting their more reactive nature compared to alkenes. In 1979 Brown reported the

hydroboration of various linear allenes with 9-BBN, [153] and Devaprabhakara had previously shown analogous reactivity with cyclic allenes. [154] For terminal hydroboration of allenes, the terminal *E* product is thermodynamically favoured and normally observed as the major product. Roush has shown the kinetic terminal *Z* product can also be synthesised under the correct conditions and reagents (Scheme 45), [155] and more recently Chida has shown that selectivity can be controlled solely by the borylating reagent. [156] It should be noted that for many boranes, including pinacolborane, the reaction does not proceed without a catalyst in the reported conditions. [157]

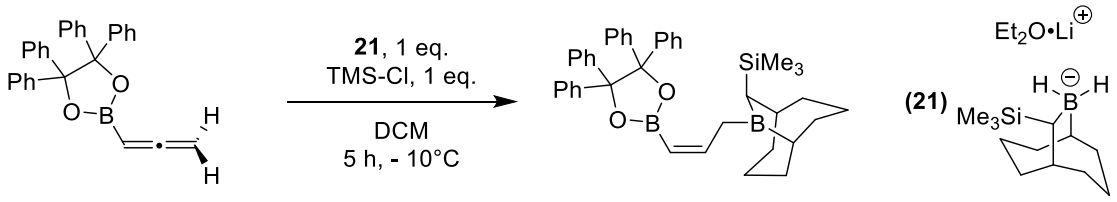

Scheme 45 – Hydroboration of allenes forming the kinetically favoured *Z*-product of a terminal allene substrate, as reported by Roush [155]. The majority of other reports form the thermodynamic terminal *E* product.

There are considerably fewer studies into analogous bond forming reactions with the heavier p-block elements, although catalytic hydrosilylation of allenes has received some interest in recent years. [158-160] In particular, there has been relatively few investigations into hydrophosphination of allenes.

Hydrophosphination of allenes – Precedent and potential

Phosphorus compounds have a wide range of chemical merits and applications, and one of the key current developments in phosphorus chemistry is the expansion of the synthetic toolkit in order to synthesise increasingly complex and varied molecules containing phosphorus centres. Complex phosphorus-containing compounds have found a range of applications including agrochemicals [161] and pharmaceuticals. [162]

While in some ways organophosphorus chemistry is a very established field — classic synthetic methods such as the Michaelis-Arbuzov reaction have been known since the nineteenth century — there are still key challenges. In particular (and of relevance to this study) is the desire to install C–P bonds in different ways and different locations, and developing new, less wasteful alternatives to current C–P bond forming routes. Since metal-catalysed hydrophosphination was first reported by Pringle in 1990, [163] it has been investigated and developed as a facile and efficient route to forming new phosphorus containing-compounds, and has been extensively discussed and reviewed. [164-166]

There has been some degree of interest in allenyl phosphines, that is, compounds containing allenes directly bound to phosphorus centres. Research, in particular by Swarmy, has shown these are competent in a range of reactions; [167] some examples are shown in Figure 10. Given the structural similarity, alkenyl phosphines produced by allene hydrophosphination could potentially also perform a range of reactions to form varied and complex compounds.

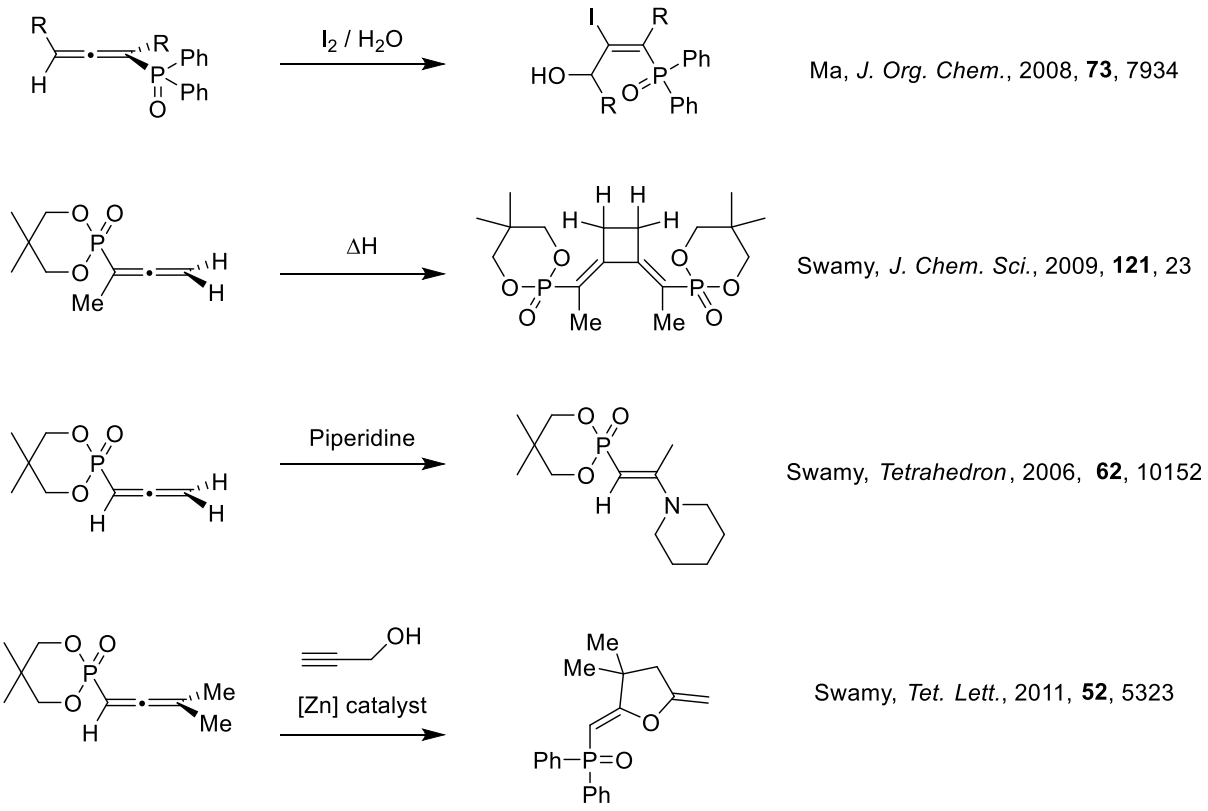

Figure 10 – Some examples of reactions involving allenyl phosphines, including iodohydroxylation, [168] cycloaddition, [169] nucleophilic attack [170] and cyclisation. [171]

Stoichiometric synthetic routes to terminal allylic phosphines are generally performed through salt metathesis through the lithiation of phosphine precursors (a range have recently been synthesised for further applications by Blair [172]). Catalytic cross-coupling reactions are challenging, due to potential β-hydride elimination and competing hydrogenative and Arbuzov-like reaction pathways. Montchamp has reported a successful cross-coupling with a P(V) centre; this requires a sacrificial silane, a specific phosphorus source and demanding conditions to proceed. [173]

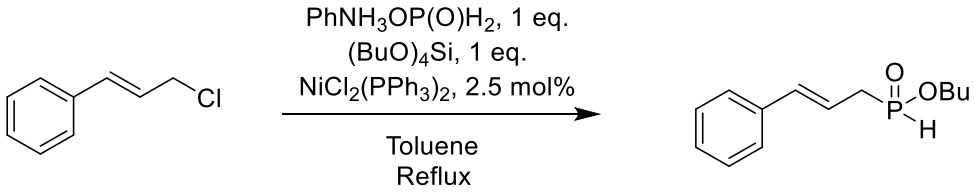

Scheme 46 – A cross-coupling reaction to form an alkenyl phosphine reported by Montchamp. [173]

The same researchers have also reported a catalytic condensation reaction using hypophosphorous acid as a source of phosphorus, again this generates a P(V) product. [174]

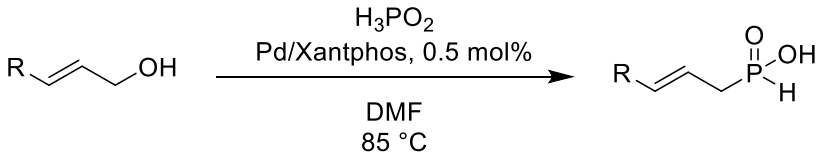

Scheme 47 – A route to similar compounds proceeding *via* condensation with hypophosphorus acid, again reported by Montchamp. [174]

A more desirable route would be the hydrophosphination of the allene with a simple phosphorus compound. Not only would this provide a more general route to these structures, but it would also be highly atom efficient, and, using the correct catalyst, ideally proceed in a facile manner and without sacrificial reagents.

Mitchell initially demonstrated a range of allenes that could be subject to hydrophosphination through radical methodology (Scheme 48). [175] This leads to high conversions (95%) but little control over selectivity — as in the case of some of the previous hydroamination and hydroboration reactions, the terminal-*E* product is formed in the highest yield. This study is revisited in Chapter 5.

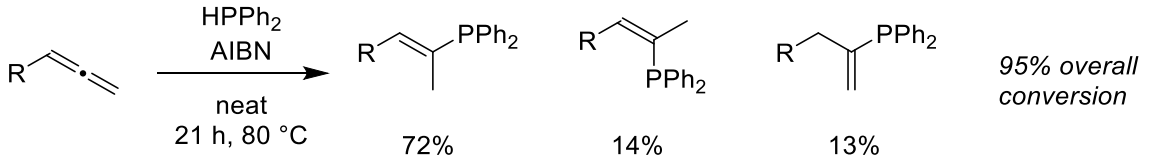

Scheme 48 – Radical hydrophosphination of allenes reported by Mitchell. [175] Conditions reported are for where R = Ph. The percentages below the products correspond to the relative distribution of isomers.

More recently, metal-catalysed routes have been developed. The first reported hydrophosphination of an allene using a metal catalyst was by Takaki, who reported a ytterbium-catalysed process using **22** (Scheme 49). [176] The reaction conditions are more facile than Scheme 48, but it has arguably poorer selectivity. Mechanistically, this reaction is reported to proceed *via* a ytterbium phosphide intermediate followed by addition over the double bond, although kinetic analysis has shown a number of intricacies are present in the catalytic pathway.

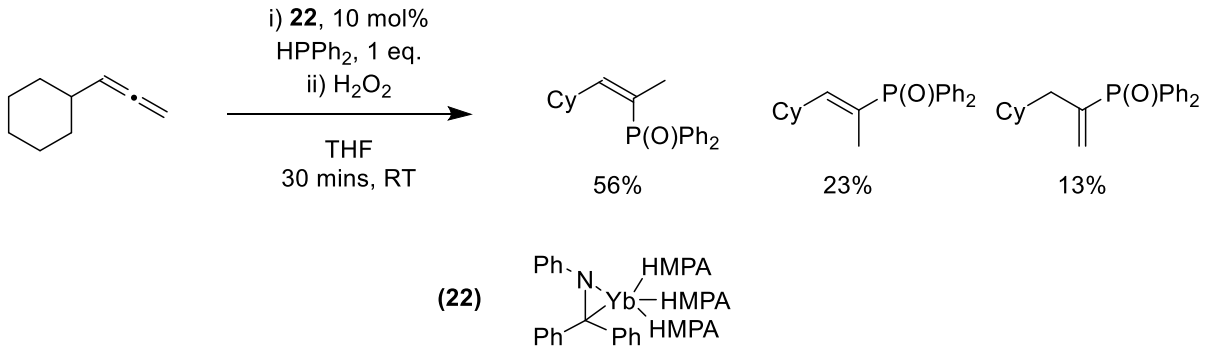

Scheme 49 – Ytterbium-catalysed hydrophosphination of cyclohexylallene reported by Takaki. [176]

A different approach has been taken by Busacca, who has shown that phosphino-boranes can also function as a phosphine source. [177] When using allenyl phosphine oxides this can lead to a bisphosphine product with two different phosphorus environments. The phosphino-borane can be deprotected with relative ease to yield the tertiary phosphine (PR_2).

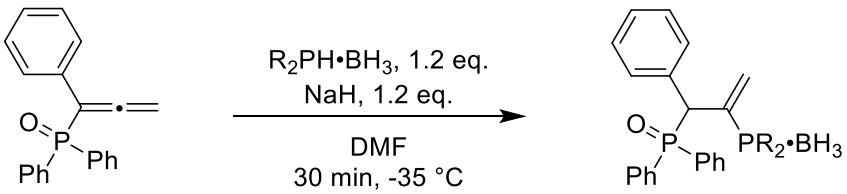

Scheme 50 – Synthesis of bisphosphines *via* hydrophosphination of an allenyl phosphine oxide with phosphine boranes, as reported by Busacca. [177]

A diverse range of P(V) compounds have been used as phosphorus sources. In addition to the reports above, Montchamp has developed a hydrophosphinylation methodology where hypophosphorous acid is used as a reagent (Scheme 51). [178] Interestingly, here the C–P bond is formed on the terminal carbon atom rather than the central carbon atom, but the product stereoselectivity appears to be very dependent on the substrate used. Similar reactivity is also reported when using $NiCl_2$ as a catalyst. [179]

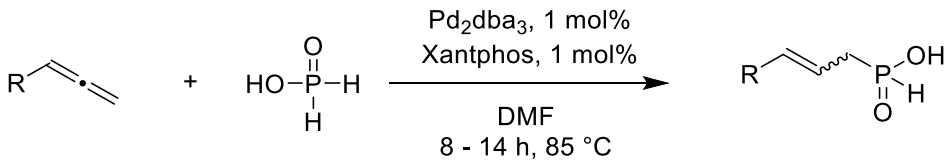

Scheme 51 – Palladium-catalysed hydrophosphinylation of allenes reported by Montchamp. [178]

In a similar fashion, Tanaka has utilised pinacol phosphonate as a P(V) source for allene hydrophosphorylation, thereby forming allyl phosphonates. [180] Again the terminal product is formed with a very strong preference for the *E* isomer where there are differing *E*/*Z* products.

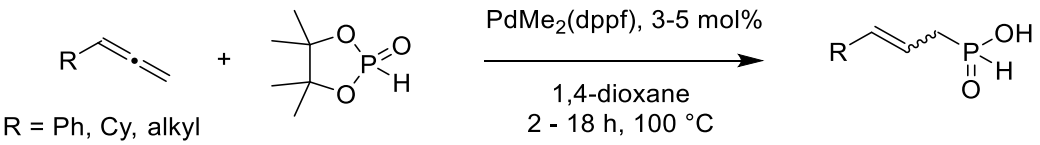

Scheme 52 – Tanaka's report of a hydrophosphorylation using pinacol phosphonate as a P(V) source. [180]

A further example of direct allene hydrophosphination has been reported by Leung. [181] In this case the substrate is fully difunctionalised, and the resulting diphosphine is coordinated to palladium (Scheme 53). Using the correct ligand enables this reaction to be stereospecific, with the isomer determined by X-ray crystallography. To obtain the doubly hydrophosphinated product a very electron-rich allenyl substrate is required.

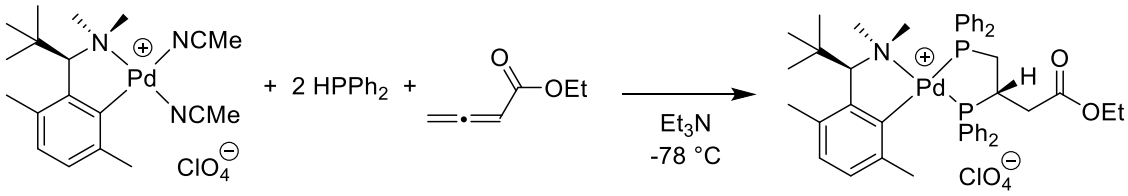

Scheme 53 – Preparation of diphosphines from allenes reported by Leung. [181]

Finally, there are some reports of using functionalised allenes to attain more complex products through P–C bond forming processes. A recent example by Xu and Gao uses allenic alcohols to

generate 2-phosphinoyl-1,3-butadienes using *H*-phosphonates as phosphorus reagents (Scheme 54). [182] Other reactions of this type include substrates such as β-allenic amines [183] and 2,3-allenols. [184]

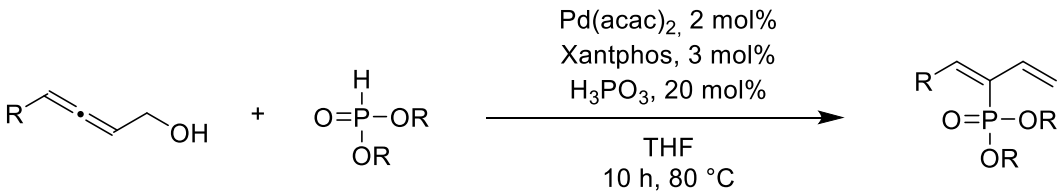

Scheme 54 – Use of allenic alcohols can generate phosphorus compounds with a 1,3-butadiene functionality as reported by Xu and Gao. Note that secondary and tertiary alcohols could also be utilised. [182]

As can be seen, there are various examples of C–P functionalisation of allenes, although most are limited in scope and functionality, and compared to hydroamination and hydroboration, there are considerably fewer methodologies to synthesise phosphine-containing products. Furthermore, there are challenges of controlling the selectivity of the reaction. Of particular importance to the studies in Chapter 4 is that the majority of reported catalytic transformation use palladium as a catalyst, and there is a noticeable absence of using more affordable and sustainable metals, such as iron.

1.6 Phosphorus and diphosphines – preparation and properties

In 1667 phosphorus was the first element to be discovered since ancient times, and its unique behaviour has continued to be developed and applied into the 21st century. Phosphorus is reasonably abundant in terrestrial terms, although these resources are under increasing pressure by large and growing demand for them. 95% of phosphorus obtained from abstraction is utilised in fertilizers, while the remaining 5% is typically converted into white phosphorus, which serves as the fundamental building block for all further organophosphorus compounds. [185] Aside from fertilizers, the principle uses of phosphorus compounds are as pesticides or other agrochemical uses, additives in materials as stabilisers, lubricants or surfactants, flame-retardants, medical applications, ligands in catalysis and as synthetic chemical reagents. [186] The latter two applications are of particular focus and relevance to the studies in Chapters 4 and 5.

Many phosphorus reagent-based methodologies were developed to displace previous sulfur-based reactions, or to utilise phosphorus's unique chemical behaviour — two of the most well-known are shown in Figure 11. While classic Appel chemistry has been largely displaced by less environmentally damaging approaches, the Wittig reaction remains a key tool in alkene synthesis. Unlike nitrogen, phosphorus can exist in the +5 oxidation state with relative ease, and the redox potential between the P(III) and P(V) states is reasonably accessible with chemical means. [187] Partly because of this, some recent studies are moving towards using phosphorus as a catalytic, rather than stoichiometric, reagent. [188, 189]

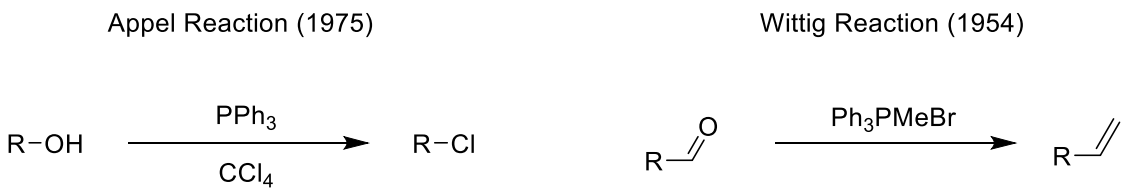

Figure 11 – The Appel and Wittig reactions both use phosphorous containing reagents in stoichiometric amounts. Contemporary Appel-type reactions use alternatives to CCl_4, while Wittig chemistry similar to above remains a key synthetic transformation.

From an organometallic perspective, phosphorus is ubiquitous for its role in ligands. Phosphines are generally good σ donors and reasonable π acceptor ligands, but, crucially, both of these can be controlled depending on the 'R' groups on the phosphorus centre itself. Furthermore, steric size can also be altered depending on the nature of these pendant groups. These properties can to some extent be predicted and applied to improve or alter catalyst performance. [190]

Use of phosphorus for both synthetic and catalytic purposes requires a range of approaches to forming phosphorus-heteroatom (or phosphorus-phosphorus) bonds. By doing this a wide range of substituents can be affixed to phosphorus centres. As discussed in Section 1.6, new routes to forming P–C bonds and consequent compounds are highly desirable. Further diversity of heteroatoms can lead to an even greater breadth of compounds, as well as further alterations of the chemical behaviour at phosphorus. Last but not least, improved formation of P–P bonds enables the synthesis of more complex ligands and flexibility of structure at the phosphorus centre (or centres).

Phosphorus-phosphorus bonds are, of course, found in elemental phosphorus and there are a range of phosphorus allotropes with P–P bonds in varying molecular structures. Compounds containing P–P bonds are generally unstable in air and as such are not found naturally, but this has not prevented a wide range of them being isolated and studied for over seventy years. P–P bonds are weaker than most first row homoelement bonds primarily due to poorer orbital overlap, and P–O and P–C bonds are generally stronger, hence their air instability. Despite this they are considerably more stable than lower-main group element homologous bonds, again for reasons of orbital overlap and bond strength.

One of the simplest structures containing a P–P bond is the 'R_4P_2' structure, where each phosphorus centre is bound to each other and two organic groups. Routes towards synthesis of symmetric 'R_4P_2' complexes are somewhat limited, and methods of preparing asymmetric '$R_2P–PR'_2$' are more unusual still. Part of the challenge of the latter is the potential of P–P bonds to exchange to attain a thermodynamic equilibrium. Asymmetric diphosphines with differing electronics can easily exchange as the bond polarity eases cleavage. [191] This was initially reported by McFarlane, who showed that a mixture of tetraphenyldiphosphine and tetramethyldiphosphine will form new diphosphine compounds *in situ* (Scheme 55). [192]

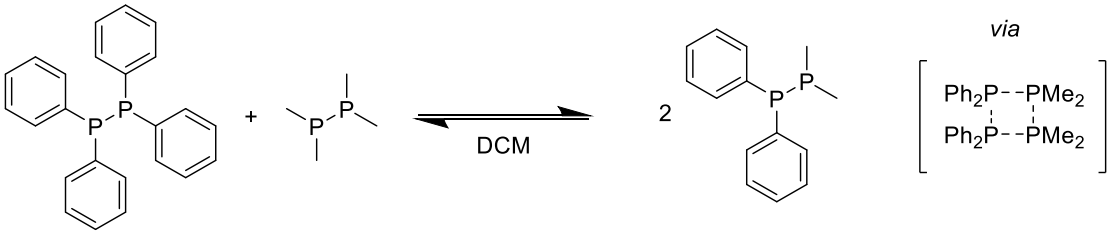

Scheme 55 – McFarlane showed that diphosphines can equilibrate to form mixtures. This process was proposed to proceed through a four-membered phosphacycle intermediate. [193]

Harris has later demonstrated that tetramethyldiphosphine and tetra(trifluoromethyl)diphosphine also exchange rapidly to form asymmetric diphosphines. [193] This was initially proposed as a spontaneous rearrangement through a four-coordinate intermediate (as in Scheme 55), however more recent theoretical studies have indicated that this mechanism is not energetically feasible and most likely arises from impurities present. [194] Grubba has prepared a range of asymmetric phosphines that can be isolated cleanly, and further shown that a variety of reagents (including chlorophosphines and lithiated phosphines) can catalyse P–P bond metathesis. [195] Recent studies by Pringle suggest that phosphorus exchange can proceed through formation of $R_2P\cdot$ radicals. [196]

The most studied catalytic route to P–P bond formation is through dehydrocoupling reactions, where a diphosphine and hydrogen are generated from the reaction of two molecules of precursor phosphines. Dehydrocoupling has numerous advantages as a methodology, primarily that atom efficiency is very high, and the release of dihydrogen provides an entropic driving force. For phosphines a wide range of catalysts have been reported, including precious metals (for example, Brookhart [197]), early transition metals (Stephan [198]) and main group systems (Wright [199]). Furthermore, base-metal catalysed dehydrocoupling has also been reported, for example using β-diketiminate complexes as shown by Webster. [45] Iron pre-catalysts are not only competitive with precious metal alternatives in terms of performance in dehydrocoupling, but they also offer catalysts that are cheaper and have less issues with recycling and waste. The study in Scheme 56 is further elaborated on in Chapter 5.

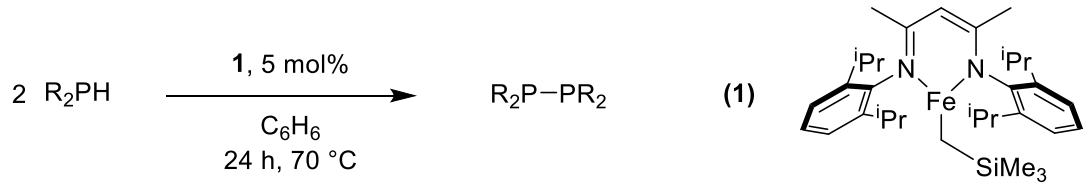

Scheme 56 – Dehydrocoupling of phosphines using **1** as a pre-catalyst. [45]

Typically phosphines are formed from either PH_3 or PCl_3 (which in turn are produced from white phosphorus). Phosphine is preferred on an industrial scale, although phosphorus trichloride is considerably easier (and safer) to handle in most smaller scale laboratory preparations. Additionally, chlorophosphines are generally less reactive to air and moisture and cheaper than the corresponding phosphines. For these reasons, in a range of cases it is desirable to use chlorophosphines as building blocks in phosphorus synthesis. Synthesising diphosphines through homocoupling of chlorophosphines is thermodynamically unfeasible directly, as the Cl_2 molecule formed is not a sufficient driving force, although it can be performed *via* an *in situ* reduction to the

corresponding phosphine. [200] Alternatively, a halohydrin elimination where HCl is formed is at the very least possible, as HCl formation is a sufficient driving force.

There are numerous synthetic pathways to interconvert phosphines and chlorophosphines between each other. From chlorophosphines to phosphines, preparation typically involves reaction of a chlorophosphine with a reducing agent such as lithium aluminium hydride. One of the earliest known and most commonplace reactions involving the reverse route is the Atherton-Todd reaction (Scheme 57), as part of a methodology to prepare phosphoramidates. [201]

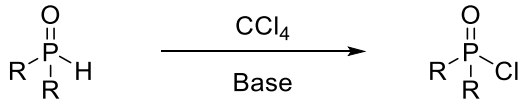

Scheme 57 – Generalised Atherton-Todd reaction to form new P-Cl bonds. The base deprotonates the phosphine which subsequently abstracts a chlorine from tetrachloromethane. More benign halide sources have also been developed and used.

There are less examples of synthesis of asymmetric diphosphines through dehydrochlorination, and the challenge is increased because of the ease of P–P metathesis reactions. Normally it is limited to where one or both reagents are specifically functionalised, such as the report by Cavell that requires a silylaminophosphine. [202] One of the most straightforward routes has been reported by Pringle. [203] Here the initial phosphine is lithiated, and the new P–P bond formed through a consequent salt metathesis with a chlorophosphine. This reaction tolerates a range of functional groups and limits competing homocoupling processes, although consumes a full equivalent of base to proceed.

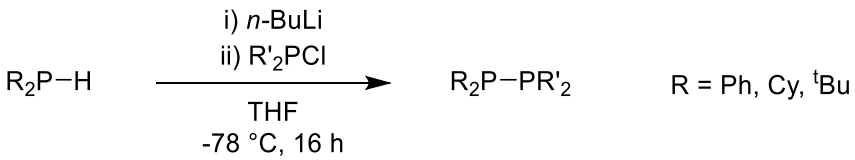

Scheme 58 – Salt metathesis route to diphosphines reported by Pringle, utilising a phosphine and a chlorophosphine. Specific reaction conditions depend on the substrate used. [203]

Diphosphines have a range of synthetic applications, with reactions generally proceeding through cleavage of the P–P bond. Aside from fairly straightforward oxidation and sulfonation routes to P(V) centres, the P–P bond can also be radically cleaved and added over unsaturated bonds. [191] This can be performed by formation of a diphosphine *in situ* as reported by Oshima, [204] or by reaction of a diphosphine and an alkyne under UV light, generating a 1,2-diphosphine product, as shown by Ogawa (Scheme 59). [205]

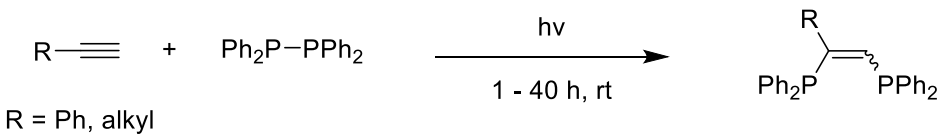

Scheme 59 – Ogawa reported the addition of tetraphenyldiphosphine over alkynes upon irradiation with UV light. [205]

Hirano and Miura have shown that by switching to a base-mediated reaction rather than photolytic, the *E*/*Z* selectivity can be controlled to a much greater extent, forming the *E*-isomer. [206] In this

case the corresponding phosphorus(V) sulfide was isolated as opposed to the P(III) phosphine (Scheme 60).

Scheme 60 – Base-mediated double hydrophosphination of alkynes using diphosphines reported by Hirano and Miura [206]

Double hydrophosphination of dienes has also been reported with tetraphenyldiphosphine, [207] and this molecule has seen other uses, such as an initiator in styrene polymerisation. [208] The monoxide $Ph_2P(=O)PPh_2$ has also been shown to display similar reactivity. [209] Kelemen and Pietschnig have reported reactions of diphosphines with oxygen, sulfur and selenium-containing species leading to mixed P(V)/P(III) species that preserve the P–P bond, whereas reactions with elemental tellurium lead to insertion across the former. [210]

The coordination chemistry of diphosphines has received limited attention. Initial reports from Issleib and Schwager demonstrated that there are two modes of bonding possible with transition metal halides. [211] Tetraphenyldiphosphine typically binds in a monodentate fashion, whereas tetracyclohexyldiphosphine adopts a bidentate 'side-on' structure (Figure 12). In some cases, the P–P bond can be fully broken on coordination with a metal centre, for example the reaction reported by Hey-Hawkins and Wolf. [212]

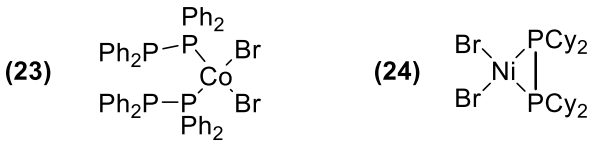

Figure 12 – Issleib and Schwager demonstrated the functional group on the phosphine affects the bonding mode when reacted with metal halides. [211] Ph_4P_2 bonds in a linear fashion as observed in **23** whereas Cy_4P_2 adopts a 'side-on' conformation as observed in **24**.

In both cases, the bite angle of the ligand is exceptionally small for bidentate ligands. The bite angle of a complex has considerable consequences for both catalytic performance and selectivity. [213] Where narrow bite-angle phosphine ligands have been used in catalysis, they have been shown to be potent and give unusual selectivity in a range of transformations. [214-216] Because of this, diphosphines have the potential to be used as ligands in catalytic reactions as well as synthetic reagents.

Chapter 2 – Redox Active Iron-catalysed Isomerisation of Alkenes

In Chapter 1 (in particular Sections 1.2 and 1.3), it was shown that iron complexes are competent catalysts for a range of organic transformations. In this chapter, the catalytic isomerisation of alkenes using β-diketiminate iron complexes is investigated. Although initial findings and literature precedence suggest catalysis proceeds through a redox-neutral process, detailed investigation shows that instead the reaction proceeds through a reductive activation of the pre-catalyst followed by an iron (I/III) oxidative addition / reductive elimination cycle. A range of synthetic and mechanistic aspects of this process are also studied.

This chapter has been adapted and accepted for publication as *Iron Catalyzed Double Bond Isomerization: Evidence for an Fe^{I}/Fe^{III} Catalytic Cycle* C. R. Woof, D. J. Durand, N. Fey, E. Richards, R. L. Webster, Chem. Eur. J., **2021**, 27, 5972.

2.1 From Hydroboration and Transfer Hydrogenation to Isomerisation

As described in Section 1.2, iron β-diketiminate complexes have a range of applications in catalysis, with one of the most studied complexes being **1**. Of particular importance to the chemistry in this chapter is the catalytic hydroboration of alkenes. As previously reported, this occurs in a facile manner over a wide range of alkenes (Scheme 61). [217]

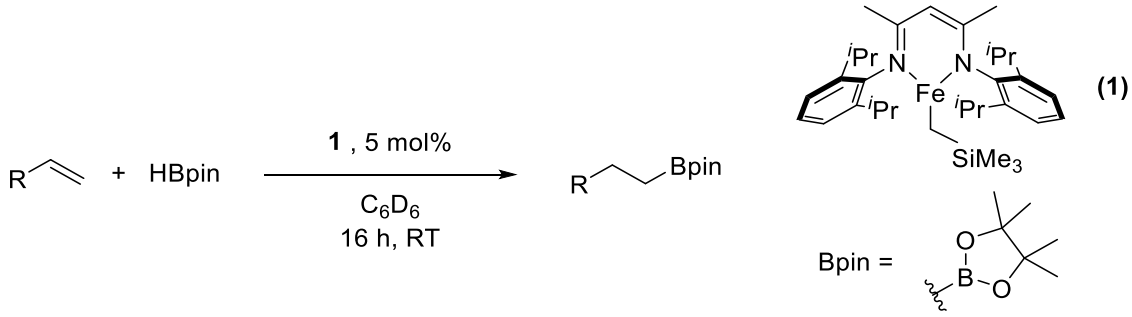

Scheme 61 – Previously reported hydroboration of alkenes. [217]

Mechanistically, this pathway is proposed to proceed by initially forming an iron hydride, followed by an addition of the 'Fe–H' moiety over the double bond and subsequent σ-bond metathesis. In each of these steps the iron centre remains formally Fe(II), and consequently no oxidation state change occurs in the reaction (Figure 13). The pinacolborane performs two roles in the process — it activates the pre-catalyst by providing a hydride, generating a boryl-silane adduct as a side product, and then subsequently cleaves the iron-carbon bond to regenerate the hydride and form the desired product.

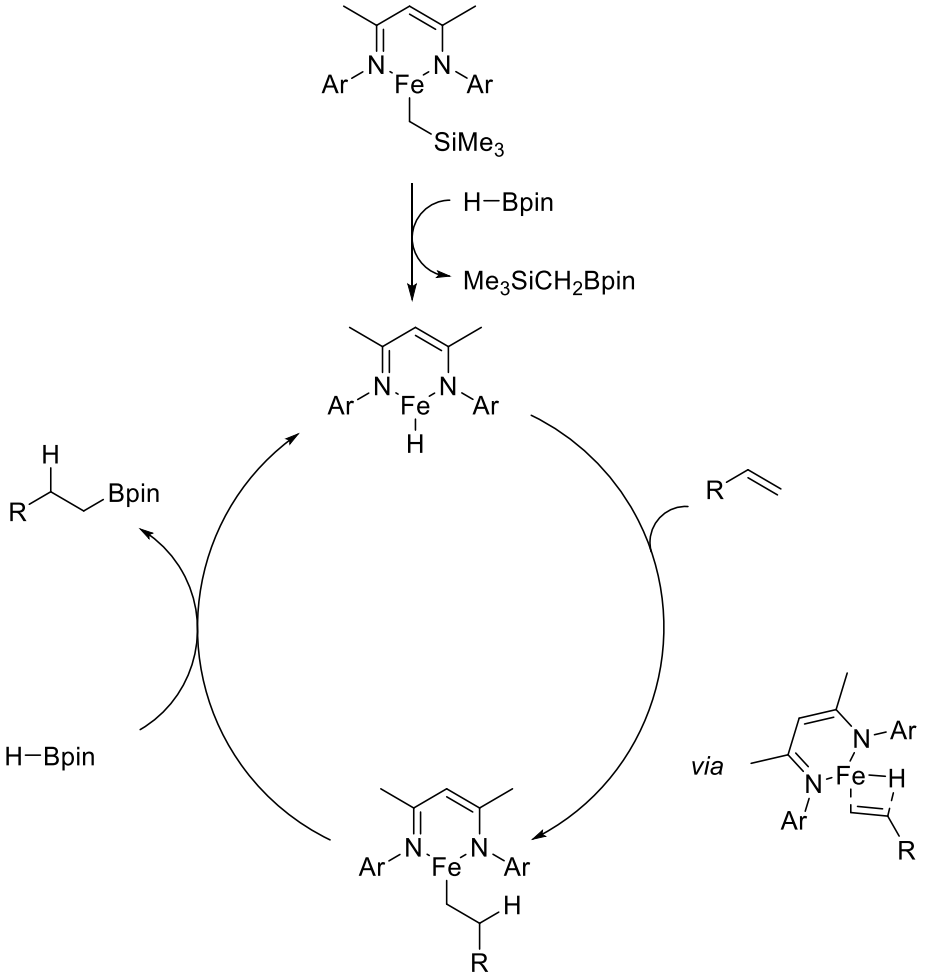

Figure 13 – Catalytic cycle for hydroboration of alkenes previously reported. [217]

This chemistry has subsequently been developed further to perform transfer hydrogenation catalysis. [218] By adding a source of protons (such as a primary amine), the iron-carbon bond is instead cleaved to generate a new C–H bond (Scheme 62). The selective nature of proton/hydride transfer can be shown by isotopic labelling. Alternative reagents, such as alcohols, can also react in the same manner. [219]

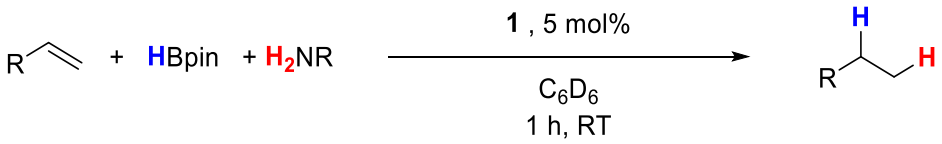

Scheme 62 – Previously reported hydrogenation of alkenes using the same iron pre-catalyst. [218] The hydrogens identified in **blue** and **red** are selectively added to the positions indicated in the product.

In both cases there are some indications that there are secondary C=C bond isomerisation reactions occurring. In the case of hydroboration, when using *trans*-β-methylstyrene the C–B bond is not added across the double bond, but instead in the terminal position. In the case of hydrogenation, when performing selective deuteration of 2-allylphenol there is significant H/D scrambling — when using deuterated aniline only 52% is formed on the expected terminal position (Scheme 63).

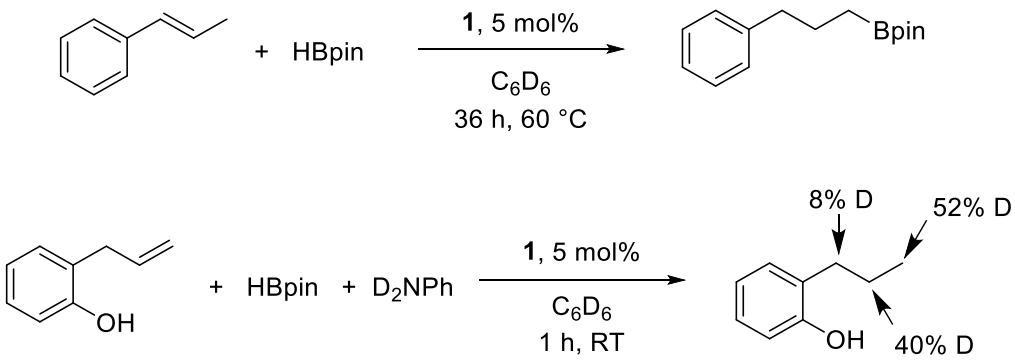

Scheme 63 – In some examples of both hydroboration and transfer hydrogenation reactions an underlying isomerisation is observed.

Studies were conducted to see if isomerisation could be performed independently of these functionalisation processes. The model substrate used in the initial reaction was allylbenzene. As detailed in Sections 1.3 and 1.4, this can be isomerised to methyl styrene products with a range of catalysts, and there is reasonable thermodynamic favourability towards the more substituted and conjugated methylstyrene products. There are also significant experimental benefits — there are only two feasible products (*cis*- and *trans*-β-methylstyrene), and they can be easily identified and differentiated by their alkenyl peaks in ^{1}H NMR.

Initially the amount of pinacolborane was reduced from 1 equivalent to various sub-stoichiometric levels. As can be seen in Table 1, this alters the chemoselectivity of the reaction.

Table 1 – Variation of the loading of pinacolborane and its effect on reaction chemoselectivity.

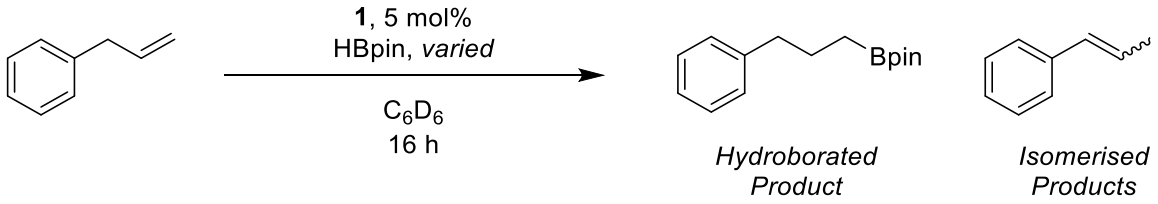

Entry	Loading of HBpin (mol%)	Temperature / °C	Hydroboration Conversion / %	Isomerisation Conversion / %
1	100	RT	65	-
2	50	RT	39	6
3	10	RT	2	44
4	10	60	1	96
5	5	60	Trace	68

Conditions : 600 µL C_6D_6, 0.5 mmol allylbenzene, 0.025 mmol (5 mol%) **1**. Pinacolborane loading with respect to allylbenzene. Conversions and reaction selectivity determined by ^{1}H NMR spectroscopy.

At a large loading of pinacolborane, hydroboration is facile and leads to reasonable conversions (Entries 1 & 2). When it is reduced, isomerised products begin to represent the majority of the conversion, although only through raising the temperature are high yields loading obtained (Entries 3 & 4). Reducing the amount of pinacolborane further does reduce conversion, suggesting a small excess of pinacolborane with respect to the catalyst is beneficial if not essential for catalysis. It is

also experimentally easier and reduces measuring errors to add a slightly larger volume of pinacolborane.

We can rationalise this change in chemoselectivity by theorising that as the concentration of pinacolborane becomes lower, it becomes less easy to perform the final [Fe]–C elimination to generate the hydroborated product, which requires a free molecule of pinacolborane to proceed. Consequently, an alternative β-hydride elimination step is performed to regenerate the iron catalyst and produce an unsaturated product (Figure 14). Further discussion and investigations into the mechanism are given in Section 2.4 onwards.

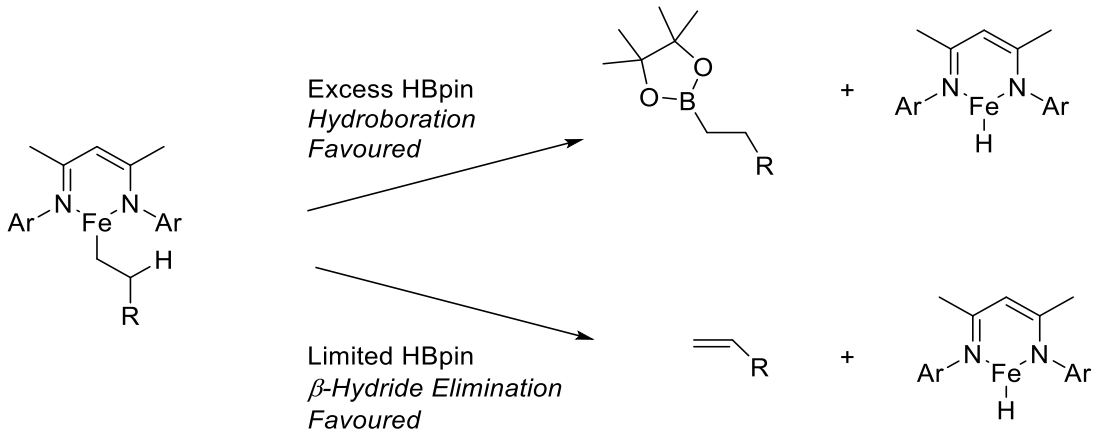

Figure 14 – We can rationalise the change in mechanism by considering the iron-carbon elimination step. When the concentration of pinacolborane is low, the hydroboration pathway becomes disfavoured, and the alternative elimination route dominates the catalytic cycle.

From this an initial reaction was developed that can isomerise allylbenzene in the presence of the iron catalyst and pinacolborane (Scheme 64). In terms of selectivity, the reaction favours the *trans* product over the *cis* in a ratio of 7.6:1. This equates to 82% conversion to the *trans* product and 11% conversion to the *cis* product under the conditions in Scheme 64. As previously discussed in Section 1.3, the *trans* product is thermodynamically favoured due to steric strain, and many (but not all) similar isomerisation reactions generate it as the sole or primary product, so this is somewhat expected.

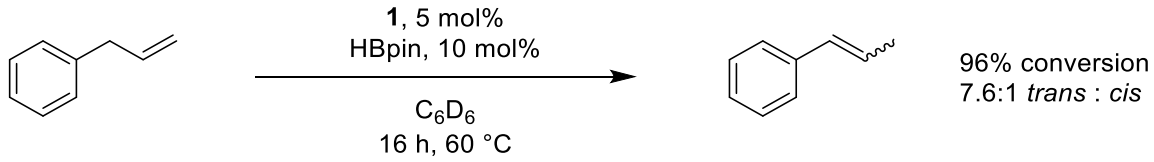

Scheme 64 – Conditions for isomerisation of allylbenzene using **1** and pinacolborane in a catalytic amount.

Both the *cis* and *trans* isomers can be clearly identified in the ^{1}H NMR spectrum, as they are both distinct from each other and the starting material. Both are well known; the NMR signals of both products and the starting material, as well as an *in-situ* NMR spectrum from the reaction identifying all three are shown in Figure 15.

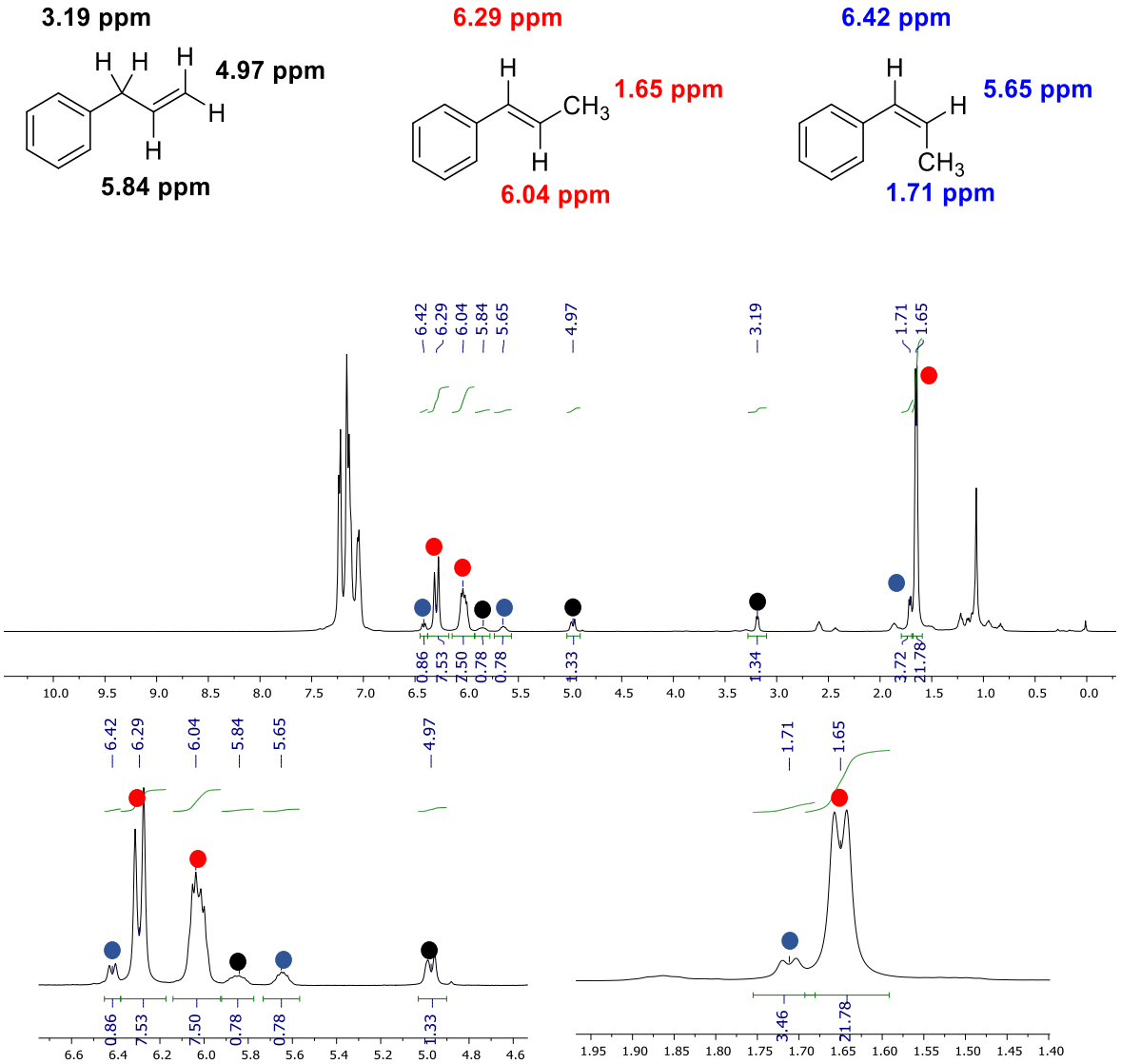

Figure 15 – Non-aryl ^{1}H NMR data for allylbenzene and the *cis* and *trans* isomerised products, and an *in-situ* ^{1}H NMR spectrum of the reaction mixture — signals belonging to allylbenzene are denoted with **black** ●, trans-β-methylstyrene with **red** ●, and cis-β-methylstyrene with **blue** ●. The peak at δ = 1.07 ppm corresponds to the methyl protons on pinacolborane (500 MHz, C_6D_6).

Through ^{1}H NMR reaction monitoring, it appears that the *cis* and *trans* isomers form in broadly the same ratio throughout the progression of the reaction. This appears to rule out the possibility of quenching the reaction at an earlier point in order to obtain a different reaction selectivity. Without pinacolborane, no conversion is observed, and likewise no reaction is observed when reacting pinacolborane and allylbenzene without a catalyst present. This confirms both the pre-catalyst and pinacolborane are instrumental for isomerisation to occur.

2.2 Variation and Optimisation of Reaction

Variation of hydride source and solvent

In our initial hypothesis, the only role the pinacolborane provides in catalytic isomerisation is the activation of the pre-catalyst to form an iron hydride in the same manner that it does in

hydroboration catalysis (Figure 13); beyond this all steps are undertaken on the metal centre. Because of this pinacolborane is referred to as the hydride source in this study, although this role is investigated further in Section 2.4 onwards. It seems reasonable to postulate that the hydride source in catalysis can be varied and is non-specific to pinacolborane, as various other compounds should be able to form an iron hydride upon reacting with the pre-catalyst.

To this purpose, various additional boranes and silanes were tested. Both boron and silicon have lower Pauling electronegativities than hydrogen, so the hydrogens bound to them can be considered hydridic (these contrast to nitrogen, oxygen, and halide bonds with hydrogen, which are generally considered protic). A summary of their reactivity is shown in Table 2. Two of the tested amine boranes are not commercially available, but can be prepared from the general route shown in Scheme 65; their preparation is reported in the Section 7.1.

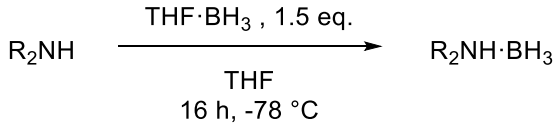

Scheme 65 – Route of synthesis for functionalised amine boranes.

Table 2 – Variation of boranes and silanes tested as hydride sources for catalytic isomerisation of allylbenzene.

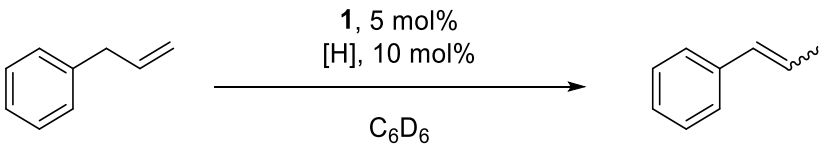

Entry	Additive 'H'	Conditions	Conversion /% (*Trans* : *Cis* selectivity)
1	HBpin	16 h, 60 °C	93 (7.6 : 1)
2	HBcat	16 h, 60 °C	-
3	HBcat	48 h, 80 °C	21 (9.6 : 1)
4	$NH_3{\cdot}BH_3$	16 h, RT	12 (8 : 1)
5	$NH_3{\cdot}BH_3$	16 h, 60 °C	99 (25 : 1)
6	$NMe_2H{\cdot}BH_3$	16 h, 60 °C	99 (31 : 1)
7	$TMP{\cdot}BH_3$	16 h, 60°C	8 (2.8 : 1)
8	$TMP{\cdot}BH_3$	48 h, 80°C	73 (3.6 : 1)
9	$PhNH_2{\cdot}BH_3$	16 h, 60°C	44 (2.9 : 1)
10	$HSiPh_3$	16 h, 60 °C	-
11	$H_2SiMePh$	16 h, 60 °C	2 (*not determined*)
12	$H_2SiMePh$	48 h, 80 °C	15 (4.1 : 1)

Conditions : 0.5 mmol of allylbenzene, 600 µL C_6D_6, 0.025 mmol (5 mol%) **1**. Reaction conversions and selectivity determined by *in situ* ^{1}H NMR spectroscopy.

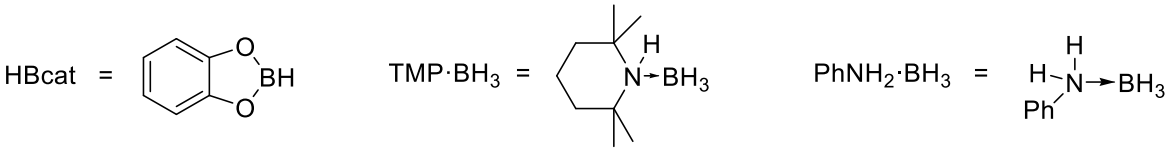

Several observations can be drawn from the data. Catecholborane, which is structurally similar to pinacolborane, gives a considerably poorer conversion even at higher temperatures — similar to the outcome observed in previous hydroboration studies (Entries 1-3). Presumably this arises from the differing sterics and Lewis acidity in catecholborane compared to pinacolborane, which has been previously noted. [220] Using ammonia borane or dimethylamine borane gives a higher conversion than pinacolborane, although a raised temperature is still required (Entries 1, 4-6). Furthermore, there is a significant change in selectivity, as the preponderance of the *trans* product is greatly increased (25 : 1 vs 7.6 : 1, Entry 5 vs 1).

Tetramethylpiperidine borane ($TMP{\cdot}BH_3$) and phenylamine borane ($PhNH_2{\cdot}BH_3$) give considerably lower conversions than either of these, even when applying more demanding reaction conditions (Entries 7-9), and are considerably less selective towards the *trans* product. The most selective borane towards the *cis* product is $TMP{\cdot}BH_3$, where the selectivity is approximately 3:1 *trans* : *cis*. Both are considerably bulkier than the simpler amine boranes, which is the most likely reason behind their lower conversions – the bulk hinders their ability to react with the iron complex easily. The differences in selectivity are less easily rationalised with the postulated cycle, a further attempt at explaining this is given in Section 2.8.

When switching to silanes catalytic activity is generally poorer; no reactivity was observed with triphenylsilane, and when using methylphenylsilane the conversion is low (Entries 10-12). The standard bond enthalpy of Si–H silane bonds is generally considered to be less than that of borane B–H bonds; [221] with these reagents it appears that the sterics and Lewis acidity of the hydride source are more important in activity rather than the strength of the bond.

Clearly pinacolborane and ammonia borane are the most active reagents for the isomerisation process. Interestingly, there is a clear difference in *cis*-*trans* selectivity when using different reagents, as well as some difference in conversion. This implies that the choice of hydride source has some effect on the mechanism as well as catalyst activation.

Some studies were performed to examine if choice of solvent had any effect on the reaction conversion and selectivity. Given their differences in conversion and selectivity, both HBpin and $NH_3{\cdot}BH_3$ were tested under the conditions reported in Table 3.

Table 3 – Comparison of different solvents in catalytic isomerisation, using both pinacolborane and ammonia borane.

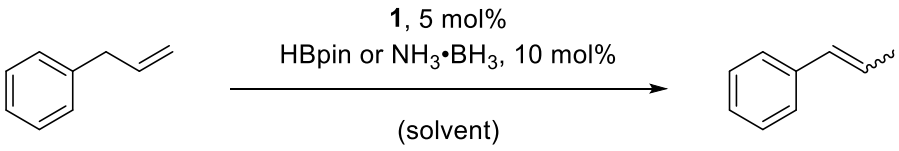

Entry	Solvent	Additive	Conditions	Conversion /% (*Trans* : *Cis* selectivity)
1	C_6D_6	HBpin	16 hr, 60 °C	93 (7.6 : 1)
2	C_6D_6	$NH_3{\cdot}BH_3$	16 hr, 60 °C	99 (25 : 1)
3	CD_3CN	HBpin	16 hr, 60 °C	-
4	CD_3CN	$NH_3{\cdot}BH_3$	16 hr, 60 °C	18 (27 : 1)
5	CD_2Cl_2	HBpin	16 hr, 30°C	-
6	CD_2Cl_2	$NH_3{\cdot}BH_3$	16 hr, 30°C	-
7	CD_2Cl_2	$NH_3{\cdot}BH_3$	16 hr, 60°C	-

Conditions : 600 µL solvent, 0.5 mmol allylbenzene, 0.025 mmol (5 mol%) **1**. Conversion determined by ^{1}H NMR spectroscopy. For Entry 7, suitable blast protection was employed.

As can be seen, when using either acetonitrile-d_3 or dichloromethane-d_2 reactivity is much reduced, and when it does proceed reaction selectivity is very similar to what is observed in benzene-d_6. The most reasonable explanation for this is that acetonitrile is coordinating enough to inhibit catalytic activity, and dichloromethane is similarly inhibiting activity either through coordination or by halogen exchange to form an iron chloride species, as has been previously reported. [31]

Variation of pre-catalyst

As discussed in the introduction, one of the merits of β-diketiminate ligands are their ease of tuneability for both steric and electronic properties. In isomerisation catalysis, the thermodynamic differences between isomer energies are often very small, thus by tweaking the properties of the ligand, it may be possible to significantly alter selectivity. The two most straightforward routes to do this are by modifying the side groups and their functionalities, or the substituents on the backbone of the ligand. In the standard catalyst **1**, the side group is 2,6-diisopropyl aniline and the backbone has two methyl functionalities.

Altering the side group is typically a matter of preparing an alternative, bulky, aniline and adding it to the backbone through a condensation reaction. Complexes **25** and **26** were prepared in this manner. Functionalising the backbone complicates ligand synthesis as the standard double condensation reaction is no longer straightforward; synthesis of **27** required an alternative route. Finally, salen complex **28** was also prepared. This is structurally very different from the β-diketiminate complexes (Figure 16), and provides some insight into the ligand and oxidation state dependence of the reaction. Preparation of complexes **1** and **25**–**28**, including the required proligands, are detailed in Section 7.1. These compounds were compared against $FeCl_2$, a simple iron salt and the precursor for the β-diketiminate complexes, under the previously optimised reaction conditions (Table 4).

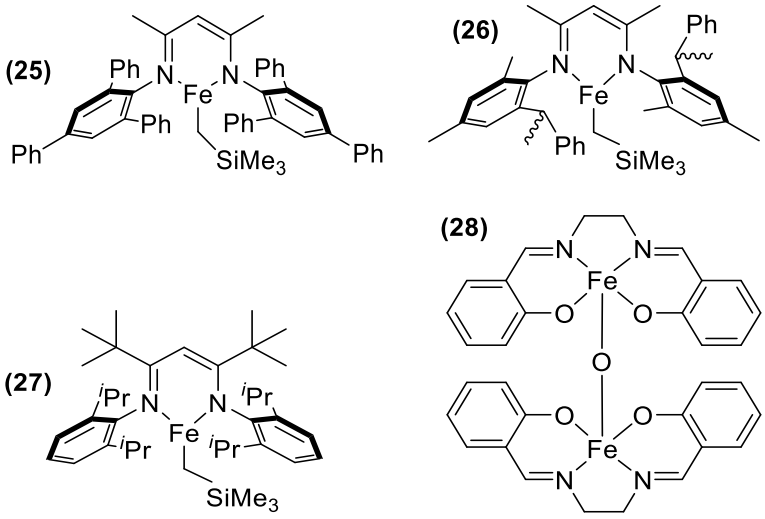

Figure 16 – Further iron complexes utilised as pre-catalysts.

Table 4 – Variation of pre-catalyst for allylbenzene isomerisation.

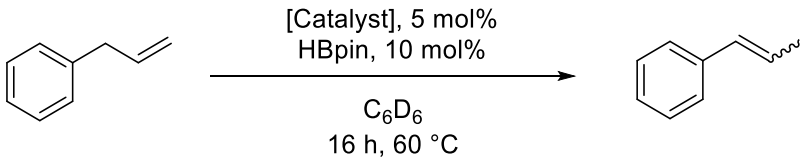

Entry	Catalyst	Conversion / % (*Trans* : *Cis* selectivity)
1	**1**	93 (7.6 : 1)
2	**25**	92 (5.8 : 1)
3	**26**	93 (6.3 : 1)
4	**27**	83 (4.2 : 1)
5	**28**	-
6	$FeCl_2$	-

Conditions: 0.5 mmol of allylbenzene, 600 µL of solvent. Entry 5 was performed in CD_3CN. Conversion monitored by ^1H NMR spectroscopy.

There is relatively little effect on yield and selectivity when changing the side group on the ligands — conversions are practically identical, and selectivity is only slightly altered (Entries 1-3). When modifying the backbone of the ligand a more significant effect can be observed – conversion is reduced, and the selectivity is significantly altered (Entries 1 vs. 4) – although there is still a strong preference for the *trans* product. Comparing reactivity between **27** and the similar cobalt complex **7** show that the metal centre also has a significant effect on both conversion and *cis-trans* selectivity (Scheme 66).

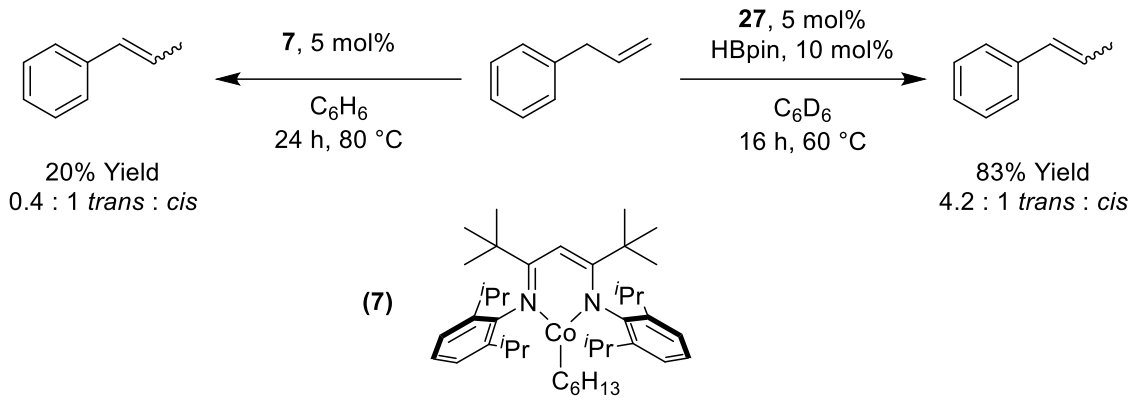

Scheme 66 – Cobalt complex **7** has the same β-diketiminate ligand as **27** - it has previously been reported to show differing *cis-trans* selectivity and conversion for the isomerisation of allylbenzene by Holland. [101] Note that this reaction does not require a hydride source.

The μ-oxo bridged salen complex **28** has no conversion under these reaction conditions – it is either unable to activate in the same manner as the β-diketiminate complexes, or cannot perform the isomerisation transformation once activated. The crucial role of the ligand is again highlighted in the reaction with $FeCl_2$; no conversion is observed. Given the relatively small changes in selectivity and conversion observed with the more challenging to prepare β-diketiminate complexes, it was determined to pursue using catalyst **1** in further studies.

2.3 Synthetic Scope of Reaction

Reactivity with functionalised allylbenzenes

The above studies enabled an optimised set of conditions for catalysis to be developed, and the range of substrates that it was possible to isomerise under these conditions was investigated. The initial focus was on allylbenzyl-like substrates. A range of these are commercially available, and many have applications in fragrances or can be further functionalised to yield useful compounds (an example of this is through ozonolysis, see Section 2.10). Reactivity was probed using both pinacolborane and ammonia borane to see if there were any different outcomes depending on the hydride source, and when conversion occurred substrates were isolated and fully characterised (see Section 7.2 for full procedure and assignments). A summary of outcomes is shown in Table 5.

Table 5 – Testing of allylbenzene-based substrates in isomerisation.

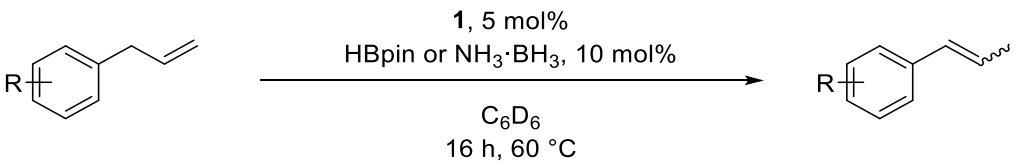

Entry	Substrate	HBpin Conversion / % (Trans : Cis Selectivity)	$NH_3{\cdot}BH_3$ Conversion / % Isolated / % (Trans : Cis Selectivity)	Product Number in Experimental
1	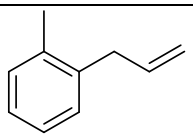	48 (8 : 1)	78 58 (12 : 1)	**29**
2	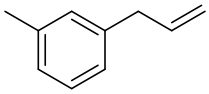	52 (9 : 1)	90 65 (18 : 1)	**30**
3	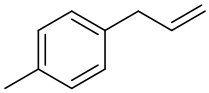	87 (10 : 1)	90 68 (24 : 1)	**31**
4	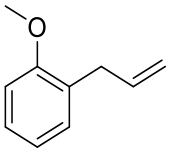	67 (4 : 1)	91 69 (7.2 : 1)	**32**
5	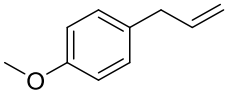	46 (6 : 1)	92 62 (9.4 : 1)	**33**
6	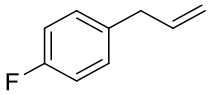	50 [a] (2.5 : 1)	70 [a] 41 (3 : 1)	**34**
7	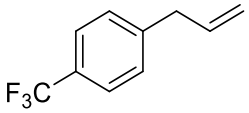	40 [a] (2 : 1)	58 [a] 39 (2.5 : 1)	**35**
8	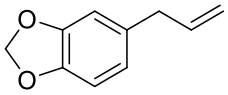	52 (5 : 1)	97 65 (11 : 1)	**36**
9	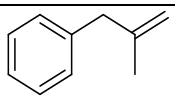	-	-	-
10	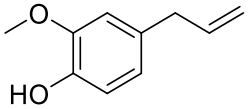	-	-	-

11	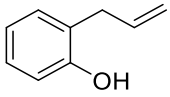	-	Hydrogenation observed only (5%)	-
12	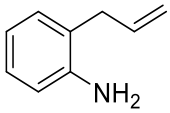	-	Hydrogenation observed only (7%)	-

Conditions : 0.5 mmol substrate, 600 µL C_6D_6 [a] 24 h, 80°C. Spectroscopic conversion determined by ^1H NMR spectroscopy.

A reasonable range of substrates can be isomerised with high yields in most cases, using both pinacolborane and ammonia borane, although ammonia borane gave higher conversions in all cases. Because of the higher conversion, these reactions were worked up and an isolated yield determined (the procedure is described in Section 7.2). Isolated yields are significantly lower, primarily as the volatile and oily nature of the catalysis products leads to material loss in the work-up. A small amount (typically 6-8%) of the substrate was also converted to the hydrogenated product when using ammonia borane.

Based on spectroscopic conversion using ammonia borane, some trends can be rationalised by using the electronic properties of the substrate. Methyl-substituted allylbenzenes are similar to allylbenzene (although the *ortho*-substituted substrate yields poorer conversion) (Entries 1–3). Using electron rich substrates also gives high conversions (Entries 4–5, 8). Electron poor substrates gave considerably lower conversions and required more demanding conditions (Entries 6–7). Some interpretation of this effect is given in Section 2.8.

Whilst most of the substrates tested proved amenable to isomerisation, a few substrates failed to give reasonable conversions, notably substrates containing alcohols and amines. (2-Methyl-2-propenyl)benzene and eugenol do not react when using either ammonia borane or pinacolborane (Entry 10). Reactions with 2-allyl phenol or 2-allyl amine result in some hydrogenation (5-7% conversion, products identified through previous reports [218]) when using ammonia borane, and no reaction at the double bond is observed when using pinacolborane (Entries 11 & 12).

In all cases where conversion is observed, the *E* product is the major product. The selectivity has some significant variation, both between substrates and when using pinacolborane or ammonia borane, and similar substrates have similar selectivities (for example, 3-methyl compared to 4-methyl). Strongly electron-withdrawing substrates such as 4-fluoroalllybenzene and 4-trifluoromethylallylbenzene gave the lowest *cis*-*trans* selectivities and conversions. Virtually all functionalised substrates have lower conversion with pinacolborane whilst ammonia borane remains high in many cases.

A final modification of the allylbenzene motif was using 4-phenyl-1-butene, which has an additional alkyl carbon compared to allylbenzene. Under raised temperature, reactions using 4-phenyl-1-butene did lead to appreciably high conversions (Scheme 67). While it is relatively easy to distinguish the 4-phenyl-2-butene and 4-phenyl-3-butene regioisomers through ^1H NMR spectroscopy, the selectivity between the respective *cis*-*trans* stereoisomers proved difficult to determine.

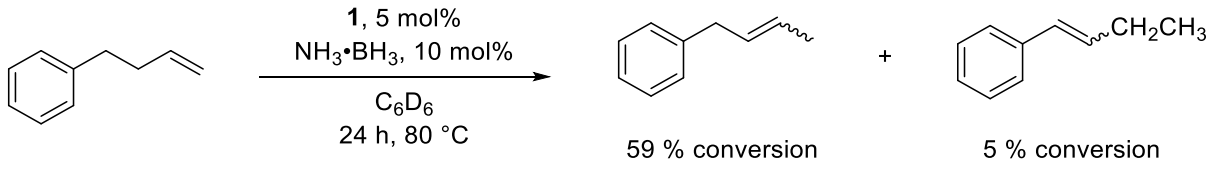

Scheme 67 – Isomerisation of 4-phenyl-1-butene.

The 4-phenyl-3-butene product is the most thermodynamically favoured owing to conjugation, whilst the 4-phenyl-2-butene is more accessible as the transformation is more straightforward (the 'chain walking' distance is less). The 4-phenyl-2-butene isomers are formed as the major product. The most likely rationalisation for this is that each chain-walking step is a distinct process, and the 4-phenyl-2-butene initially formed is more challenging to react and isomerise further, leading to (mostly) termination at this step. This is still interesting, as it confirms that isomerisation can be performed where there is not a significant enthalpic driving force towards forming conjugated systems, even though conditions are not as mild. Because of this, a series of alternative alkenes were investigated for catalytic potential.

Applying reactivity to terpenes

Terpenes are an extremely diverse range of unsaturated organic molecules, which can be isolated from plants or synthetically prepared. [222] Because of their diversity and their (potentially) sustainable sources, they are being pursued as a feedstock for a large variety of chemicals. However, there are still considerable challenges in both clean extraction and selective reaction of key terpenes. The majority of terpenes are unsaturated in some way, so several common terpenes were tested in reactivity. It was quickly determined that raised temperatures were required to achieve high conversions.

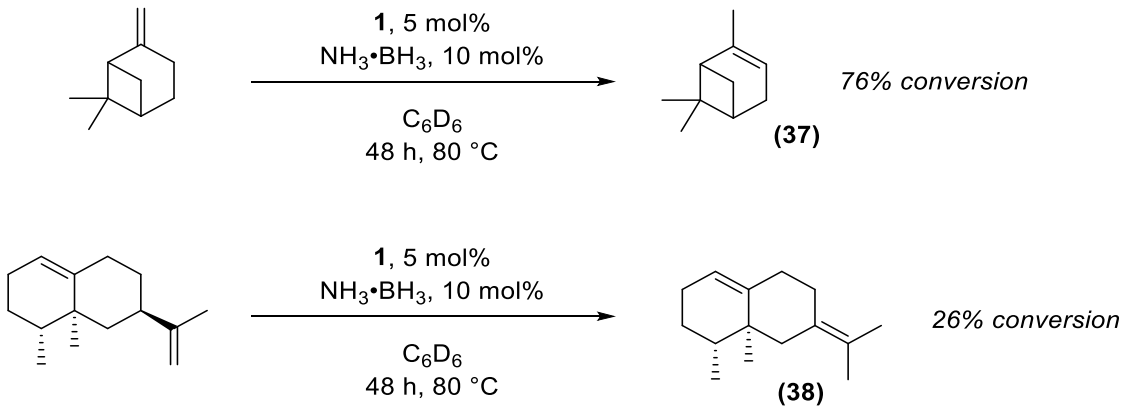

Scheme 68 – Reactivity observed with β-pinene (top) and valencene (bottom).

Both β-pinene and valencene have more substituted isomers that can be relatively easily accessed by chain walking isomerisation, (Scheme 68) which perhaps explains why modest conversion is observed in these cases. For valencene, the isomerised product **38** has a highly substituted alkene which is the probable reason for lower conversion in this case.

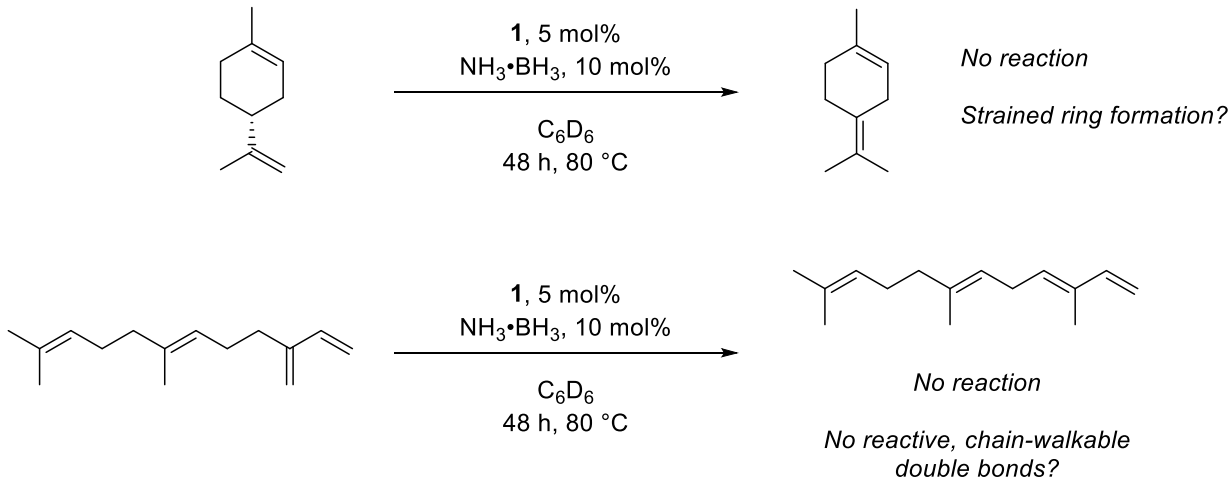

Scheme 69 – No reactivity was observed with limonene (top) or β-farnesene (bottom).

Alternative terpenes did not exhibit reactivity. Whilst limonene also can in theory isomerise to a more substituted structure, this results in a compound containing a very strained six-membered ring, dissuading its formation (Scheme 69). β-farnesene has several double bonds, although only one is terminal and can chain walk easily, and again no reaction is observed. Like (2-methyl)-2-propenylbenzene this is terminally disubstituted, which results in being probably too sterically challenged to activate.

Although reactivity with some terpenes was observed, it appears to be generally limited to terminal double bond functionalities where there is an obvious 'chain-walked' product possible.

Applying reactivity to hexenes

As stated previously, allylbenzene and certain terpenes are relatively amenable to isomerisation compared to most alkenes, as the more conjugated and substituted products they can form give a relatively large thermodynamic driving force. Alkenes that are considered relatively inactive, such as linear olefins, do not have this advantage — stability is determined by substitution only and the energy differences between isomers is comparatively small. Nevertheless, some catalytic systems do perform isomerisation of olefins selectively, as discussed in Section 1.3.

Each linear isomer of hexene was tested in isomerisation chemistry to determine if they were amenable to the catalysis and what selectivity would be observed. Apart from the terminal peaks, the ^{1}H NMR alkenyl peaks of hexene isomers are broadly similar so it was impossible to discern between them. Inverse gated ^{13}C NMR spectroscopy was instead used as a quantitative method (Figure 17). To attain quantitative $^{13}C\{^{1}H\}$ NMR spectra the time between scans was lengthened to 60 seconds (*i.e.* far greater than T_1), and the number of scans was increased to 512. The resulting experiment gave self-consistent data that could be integrated to an acceptable degree of precision, an example spectrum is shown in Figure 17. The peaks can be determined by comparison with the individual isomers, all of which are commercially available and can be used as references.

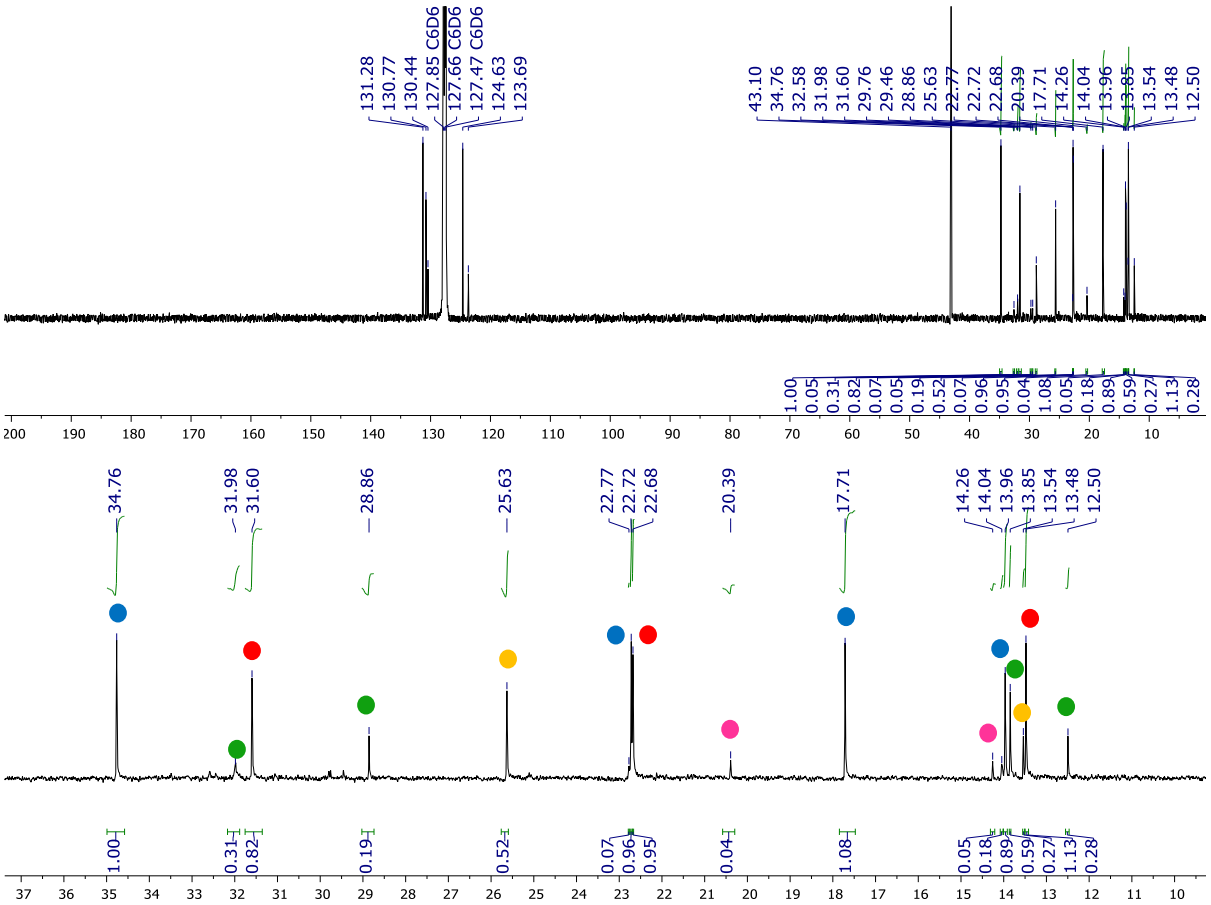

Figure 17 – An example $^{13}C\{^{1}H\}$ NMR plot run under the conditions stated above (126 MHz, C_6D_6), with a focus on the δ = 10-40 ppm region, showing the sp^3 carbons assigned. Peaks relating to 1-hexene are denoted with **red** ●, trans-2-hexene with **blue** ●, cis-2-hexene with **green** ●, trans-3-hexene with **orange** ●, cis-3-hexene with **pink** ●. Peaks were assigned by comparison to the individual isomers.

Under the standard reaction conditions (16 h, 60 °C), conversion was very poor. However, it was determined that under more demanding conditions, conversion can be improved considerably. As predicted, a wide range of isomers were formed; results are shown in Table 6.

Table 6 – Isomerisation of hexenes. The unreacted starting materials are italicised in the table.

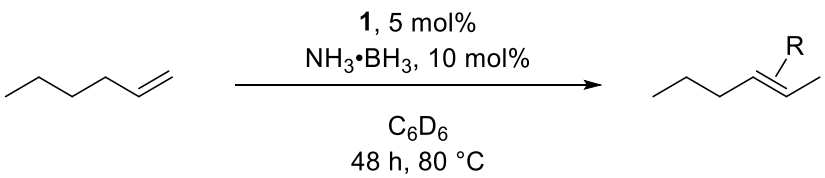

Substrate ↓	Conversion / %				
	1-Hexene	***Trans*-2-Hexene**	***Cis*-2-Hexene**	***Trans*-3-Hexene**	***Cis*-3-Hexene**
1-Hexene	*31*	42	10	15	2
Trans-2-Hexene	33	*37*	12	16	2
Cis-2-Hexene	44	9	*33*	13	1
Trans-3-Hexene	54	13	15	*14*	4
Cis-3-Hexene	44	28	7	17	*3*

Conditions: 0.5 mmol substrate, 600 µL C_6D_6, reaction stirred. Conversions determined by inverse-gated ^{13}C NMR spectroscopy as discussed above.

In all cases there is reasonably high conversion of the starting isomer into a range of other products. In general, 1-hexene and *trans*-2-hexene are the most favoured products, and *cis*-3-hexene the least favoured by a considerable degree. Whilst *trans*-3-hexene is the most thermodynamically favoured isomer, the highly substituted nature of it appears to limit its yield. The observation that the majority of conversions are similar regardless of the starting isomer suggest some form of thermodynamic equilibrium may be approached under these conditions, although even after 48 hours it appears it has not been fully reached.

To summarise this section, it is clear that the catalytic system tolerates substrates other than allylbenzene, although there are clear trends and limits to the catalysis. Functionalised allylbenzene-like substrates were generally converted with high yields and strong Z selectivity, similar to other previously reported systems (a broader comparison is discussed at the end of the chapter), although there is limited tolerance for some functional groups including amines and alcohols. Terpene substrates proved less amenable to isomerisation and appear very dependent on the structure of both the starting material and potential isomeric product. Finally, linear alkenes do give reasonable conversion at high temperature although there is a lack of regiocontrol as well as stereocontrol.

2.4 Proposing a Redox-Neutral Reaction Mechanism

The next two sections of this chapter deal with proposing a mechanism and catalytic cycle for this reaction from our initial observations, and seeking further validation or confutation. Given the competitiveness of isomerisation against hydroboration and transfer hydrogenation when **1** is used as a catalyst, it was initially thought that the mechanism for all three processes were directly related, most likely that they all proceed through an Fe(II) hydride-mediated mechanism. The nature of this hydride is discussed further in Section 2.6, but for now it was proposed to exist as the

monomeric species **39**. This was postulated to form from the pre-catalyst through a sigma-bond metathesis step to (in the case of HBpin) generate Me_3SiCH_2Bpin as a side product. This reaction has been previously investigated, and the borane adduct has been detected in mass spectrometry from the reaction of **1** and pinacolborane. [217] Ammonia borane is likely to generate dehydrogenated products, owing to the propensity of ammonia borane to react as such. Well defined dehydrogenated ammonia borane derivatives have been reported by Schneider using iron catalysts; [223] in this study ^{11}B NMR monitoring of the reaction yielded broad and complex signals. Neither ammonia borane or its derivatives are particularly soluble in the reaction mixture, and it is likely that this process is more complex and less easy to study. As a consequence, initial focus was on the reaction with pinacolborane.

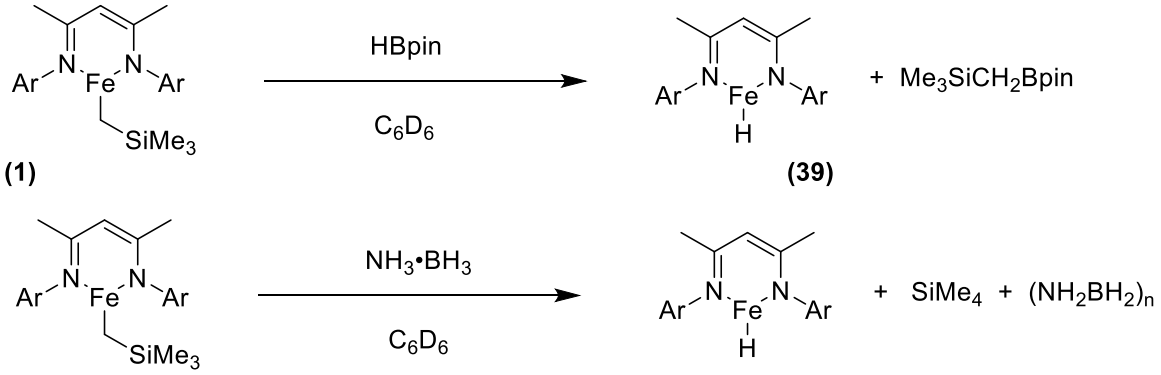

Scheme 70 – Proposed formation of an iron(II) hydride from pre-catalyst **1** using either pinacolborane or ammonia borane. For pinacolborane this generates a borane-tetramethylsilane adduct, whereas for ammonia borane tetramethylsilane is released along with oligomeric ammonia borane derivatives.

There are two principle pathways for catalytic isomerisation — an allyl route, where the reaction proceeds *via* an anionic allyl species, or alkyl, where instead the reaction proceeds through an alkyl iron-carbon intermediate **40**. These pathways can be thought of in terms of binding (the allyl route proceeds through an η^3 complex, the alkyl route through an η^1 complex), or in terms of hybridisation (an allyl intermediate is sp^2, an alkyl is sp^3). In both cases, it should be noted that the models can be viewed as extremes against a range of mechanistic behaviour, rather than distinct alternatives. An alkyl mechanism using the iron hydride previously discussed is shown in Scheme 71, and an allyl mechanism is shown in Scheme 72 — the oxidation states of all iron catalytic species are identified in the latter, whilst in the former it remains iron(II) throughout.

In the case of the allyl mechanism, it is reasonable to postulate that the iron hydride can add in the alternate regioselectivity to form the terminal alkyl iron complex **41** — this would appear the least sterically demanding outcome, and would lead to the terminal anti-Markovnikov product in a hydroboration process. **41** cannot easily react further in an isomerisation process beyond a concerted shift to form the active iron alkyl species, or simply eliminating to regenerate the substrate and iron hydride, so it may either act as an intermediary step or as a reversible cul-de-sac in terms of the catalytic cycle. Presumably the β-hydride elimination proceeds through species **42**, where the alkene is bound to the iron centre, before disassociating as free product. In the computational studies in Section 2.8, **42** can be shown to exist as a stable species rather than immediately disassociating ligand.

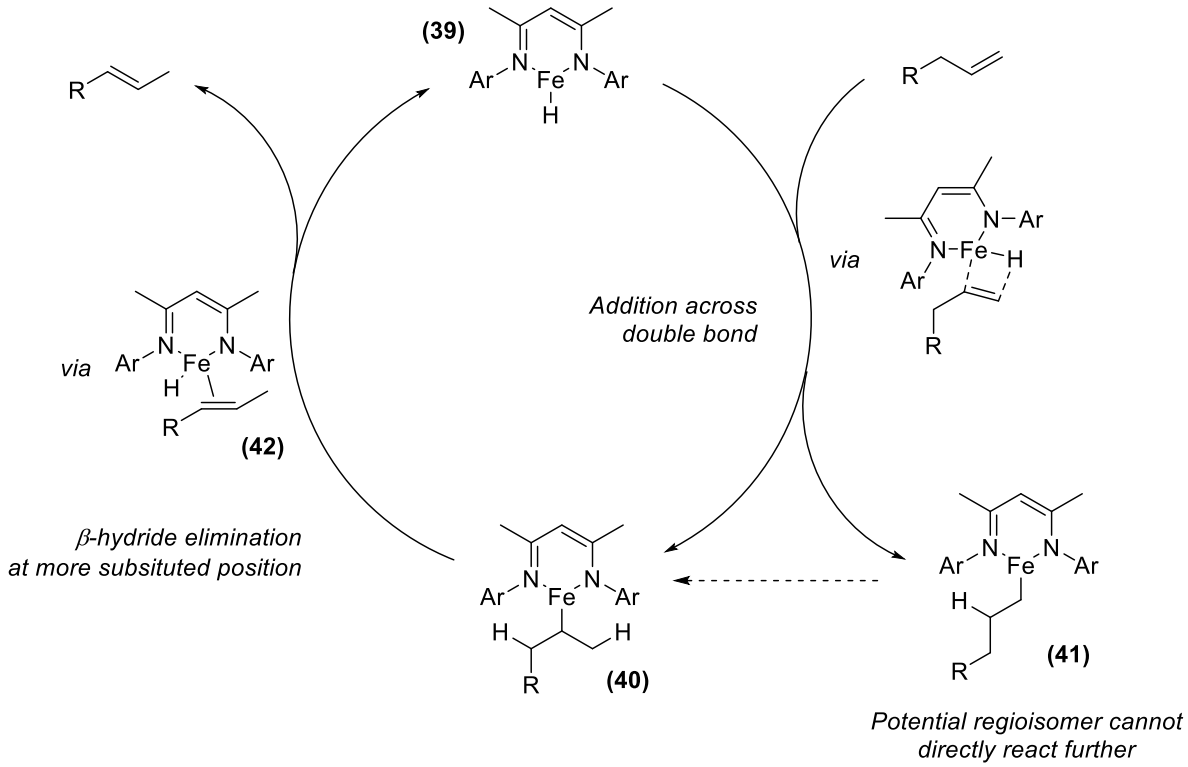

Scheme 71 – An alkyl mechanism for isomerisation proceeding through Fe(II) hydride **39**. This cycle is redox-neutral and proton transfer is intermolecular, proceeding through the alkyl iron intermediate **40**.

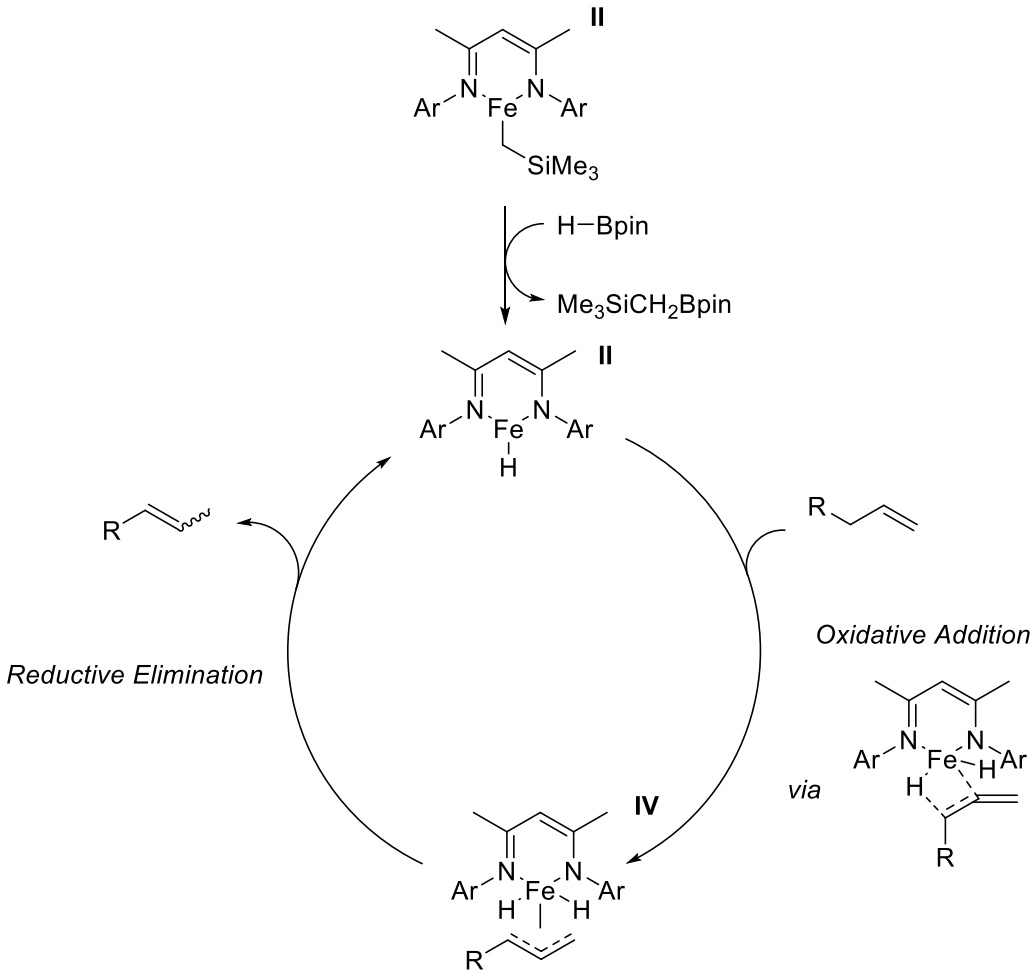

Scheme 72 – An allyl mechanism for isomerisation proceeding through an Fe(II) hydride. This reaction involves a two-electron oxidation/reduction pathway, and proton transfer can be either intermolecular or intramolecular depending on the specific proton eliminated.

Both routes have consequences on the nature of the reaction. An alkyl reaction must have intermolecular proton transfer, as the new C–H bond formed is the initial step. A reaction proceeding through an allyl intermediate is in contrast generally intramolecular, as the initial step is a C–H bond breaking, followed by a subsequent C–H bond formation, although this would be complicated if the initial catalytic species was a metal hydride. This difference is further investigated in the deuteration studies in Section 2.5.

In transition metal catalysis, the allyl route requires an oxidative addition step when breaking the C–H bond, and a consequent reductive step when generating the new C–H bond, whereas the alkyl route is a redox neutral procedure, with steps primarily being σ-bond metathesis. When starting with the Fe(II) hydride species above, formal two electron oxidation seems unlikely for a number of reasons. While high-oxidation species of iron are not unknown (even Fe(VI) species have been reported and characterised [224]), they are generally high-valent and require strongly electron-withdrawing ligands, rather than the low-valent bulky ligands used in these complexes. Secondly, the structure of the Fe(IV) species shown in Scheme 72 is unusual as the iron centre is penta-substituted — this is partly mitigated as two of the ligands are hydrides, but it still represents an unusual bulk and conformation for the metal centre to adopt in these conditions. Thirdly,

performing a two-electron oxidation of an Fe(II) centre typically requires either external energy (such as photolysis [225]), a stoichiometric oxidizing agent, or unusual environments about the metal centre. [226] Because the redox process as shown in Scheme 72 was considered unlikely to occur, the initial postulated mechanism was an alkyl route, as proposed in Scheme 71.

Some initial simple experiments were undertaken to confirm some of the underlying assumptions of both the catalytic cycles above (these additionally apply to those proposed in Section 2.8). Iron nanoparticles are potent in a range of catalytic reactions, and it is important to demonstrate that they are not playing an active role in this catalytic cycle. [227] The standard 'mercury-drop' test for nanoparticles does not always generate the correct result with iron species; [228] as an alternative a relatively simple test to discern between heterogeneous nanoparticle-catalysed processes and well-defined homogeneous complex-based systems has been developed by Morris. [229] Addition of a sub-catalytic amount of trimethylphosphine should halt all catalytic activity with a nanoparticle system, as the number of active sites is considerably less than the number of metal centres present, and there would be enough trimethylphosphine to bind to every site. In contrast, in a metal complex-mediated system the number of active sites should be (in theory) equal to the number of metal centres, so reactivity should be perturbed but not fully quenched owing to 'free' sites still remaining.

In the cases of using both pinacolborane and ammonia borane as additives, conversion is lowered significantly under the conditions in Scheme 73, but still observed. It was therefore determined that the reaction is not nanoparticle mediated.

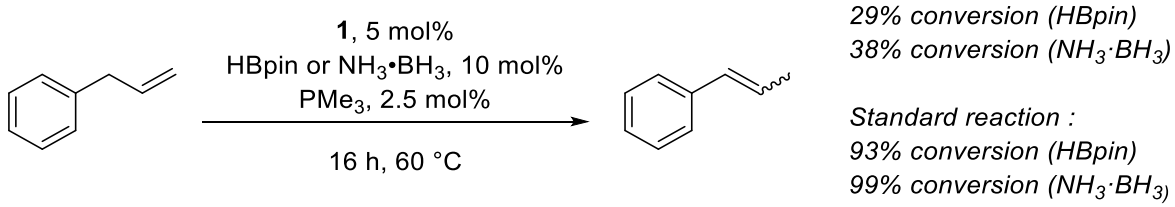

Scheme 73 – Test for nanoparticles. As conversion is still observed, it was concluded the reaction is not nanoparticle catalysed.

A radical clock reaction was also performed. The reaction was run with standard conditions and monitored, so after 4 hours it had reached 28% conversion. (Chloromethyl)cyclopropane was then added and conversion monitored intermittently against a standard reaction. Although conversion was lower in the reaction with (chloromethyl)cyclopropane, it was not inhibited at any point (Scheme 74). It is likely that the trap reacts in some form with the iron centre (for example, halide abstraction to form an iron chloride) but not directly reacting with radicals. The ring-opened product, 1-butene, that would form from radical trapping was not observed at any point in the reaction. This would appear to rule out a radical-mediated mechanism. Further details of both these experiments are given in Section 7.2.

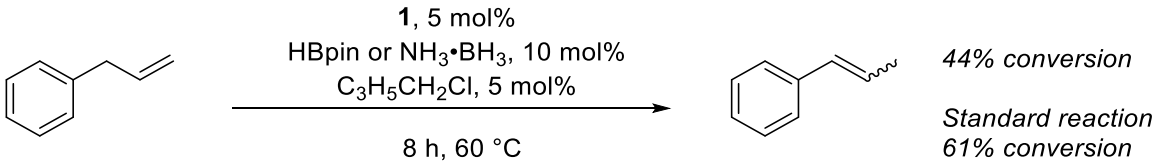

Scheme 74 – Although there was some alteration to reaction rate, the trapping agent (chloromethyl)cyclopropane was not observed to cyclise or fully halt reactivity, ruling out a radical mediated process.

2.5 Studying Catalytic Isomerisation with Deuteration Studies

Given that the isomerisation reaction is fundamentally a proton transfer, it was anticipated that isotopic experiments would be able to provide further insight into the mechanism, and either confirm or disprove the hypothesised Fe(II)-hydride alkyl reaction pathway.

The simplest way from a synthetic perspective to introduce deuterium into the catalytic process is by using deuterated, rather than protiated hydride sources. Preparation of deuterated ammonia borane proved difficult as the ND_3 fragment could neither be prepared or obtained; as an alternative deuterated dimethylamine boranes ($Me_2ND{\cdot}BH_3$ and $Me_2NH{\cdot}BD_3$) and deuterated pinacolborane (DBpin) could be prepared with a high isotopic purity – details of their preparation are given in Section 7.1.

The low loadings of the hydride sources mean a stoichiometric H/D exchange of the substrate would not be possible, regardless of mechanism. What would be expected when using a metal hydride would be a small amount of D-incorporation in the product, arising from the initially formed iron-deuteride adding across a substrate double bond, and subsequently eliminating to form an isotopically labelled molecule. This process then forms an iron hydride which can perform fully protic transformations on subsequent turnovers (Scheme 75).

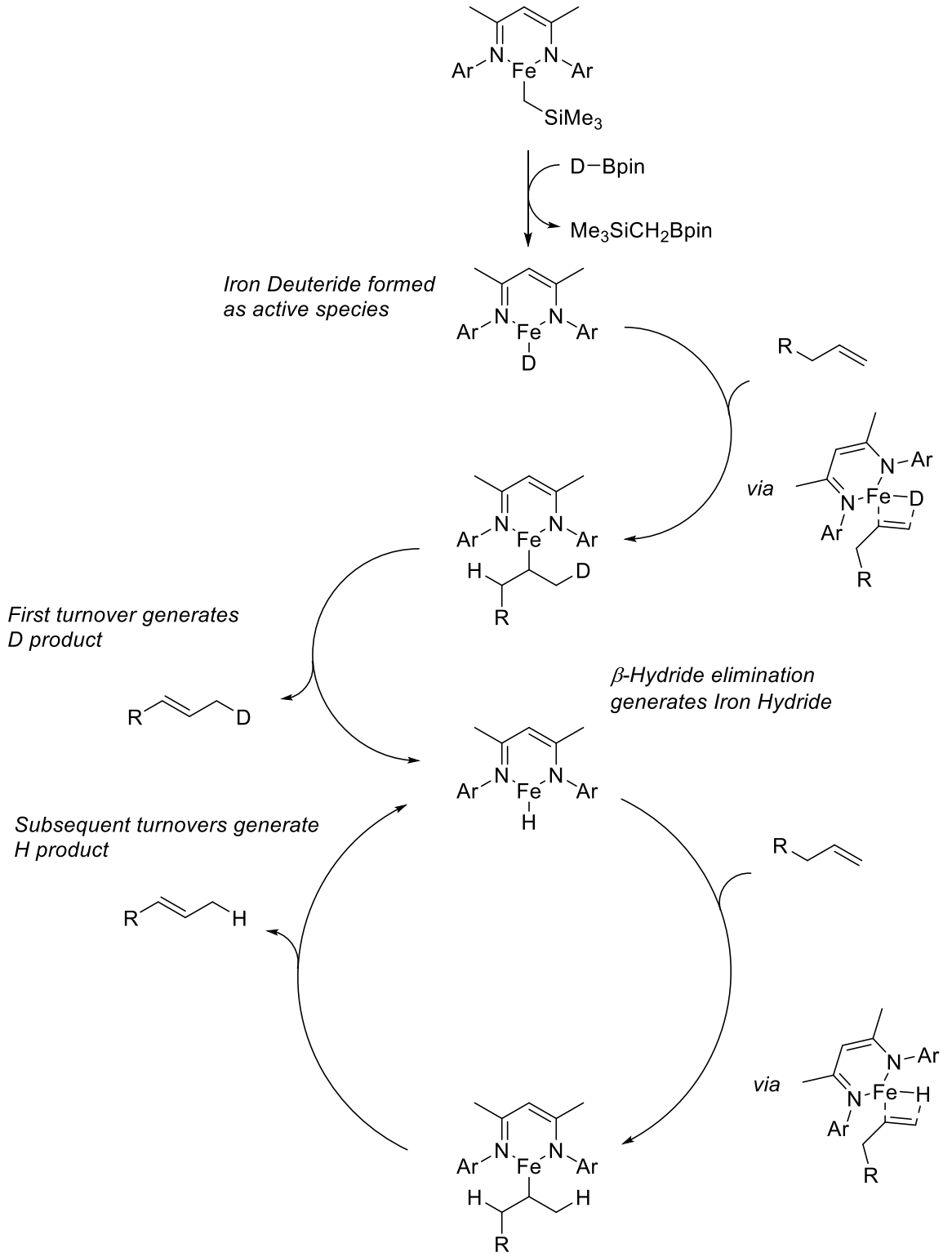

Scheme 75 – When using d-labelled additives (in this case DBpin), product generated from the first turnover should have deuterium incorporation, whereas from subsequent turnovers it should be fully protiated.

DBpin, $Me_2ND{\cdot}BH_3$ and $Me_2NH{\cdot}BD_3$ were each tested in turn under standard reaction conditions (Scheme 76). The resulting isomerised products were then analysed by ^1H and ^2H NMR spectroscopy to observe if any D-incorporation had occurred.

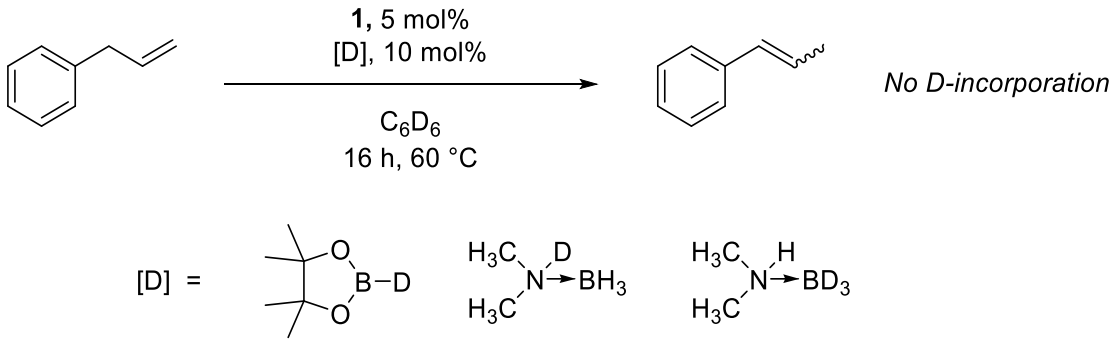

Scheme 76 – Use of deuterated hydride sources in catalysis.

In all cases, the product appears to be fully protiated; there is no apparent transfer of deuterium from the additive to the product. This is unexpected if the reaction proceeds through the hydride alkyl mechanism, as shown in Scheme 75. Possible explanations may be that only a small amount of catalyst is actually active and the TON is very high, thereby the first turnover product is not noticeable in the NMR spectrum, or that the product can undergo H/D exchange in some form. For the small amount of hydrogenated product formed in the dimethylamine borane reactions, some D-incorporation is observed, although it appears neither iso- nor regioselective to a specific site or product.

More information can be gained from isotopic labelling of the substrate. The protons primarily involved in the reaction are on the α-position relative to the aryl ring in allylbenzene (the terminally substituted allylbenzene is prepared for separate deuteration studies in Section 2.8). Isotopically labelling these internal positions proceeds through initially performing H/D exchange on phenylacetic acid, then sequential reduction to an alcohol and oxidation to an aldehyde, followed by a Wittig reaction to form the terminal alkene (outlined in Scheme 77, full experimental details and assignment of intermediate products are given in Section 7.2). Care must be taken with the final step, as *n*-butyl lithium is a strong enough base to catalyse isomerisation of the newly formed product, so the reaction needs a precise stoichiometry of substrate, Wittig salt and base to proceed cleanly towards the terminal alkene. A small amount of ethylbenzene was generated in the reaction and isolated with the product, which was formed in 90% d-isotopic purity. The α-protons are now only residual, and the remaining alkenyl NMR signals appear as complex multiplets.

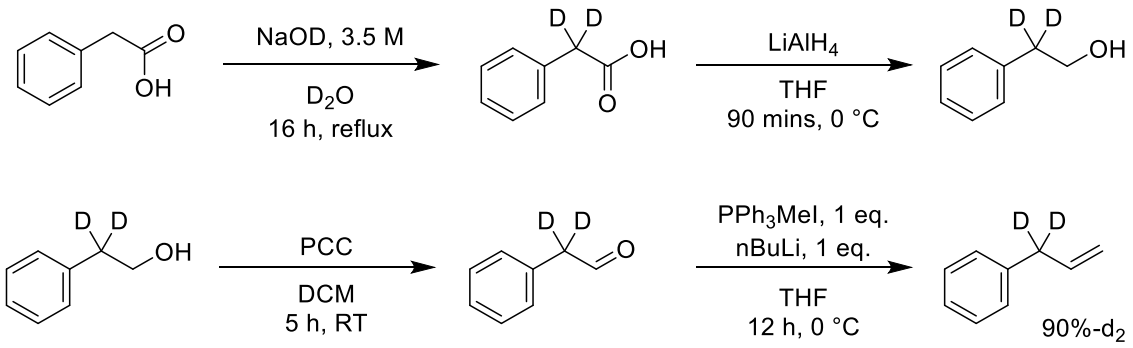

Scheme 77 – Synthesis of 1,1-d_2-allylbenzene. Full experimental details, and assignment of the intermediates and product are given in Section 7.2.

The d-labelled substrate was then reacted with catalyst in the presence of both pinacolborane and amine borane (Scheme 78). In both cases the product could be identified relatively cleanly as the 1,3-d_2 product (of both the *cis* and *trans* isomers) formed with 90% d-incorporation.

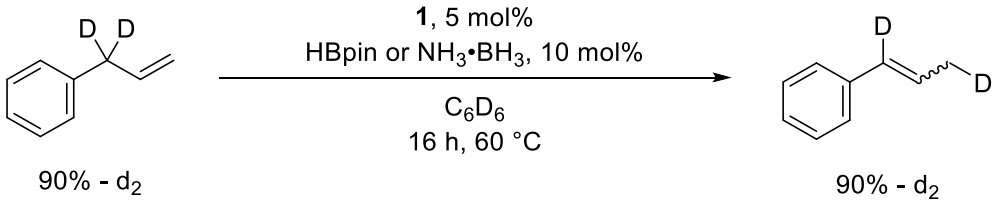

Scheme 78 – Isomerisation of 1,1-d_2-allylbenzene yields the more substituted product with no loss of deuterium in the presence of protiated hydride sources.

This study is a corollary of the previous study — namely there is no observable proton transfer between the additive and the substrate (if this were the case, the terminal position would be protioenriched compared to the alpha position, owing to the initial protic iron hydride addition (Scheme 79). In the event, both have equal isotopic incorporation). Furthermore, it demonstrates that the proton transfer is relatively well-defined in both cases, rather than proceeding through 1,2 hydride shift. This would appear to rule out an alternative hydrogen atom transfer (HAT) pathway, which proceeds through radical tautomerisation and would further appear to rule out **41** formed as an intermediate to **40**, as we would expect some scrambling across the double bond to account for the required rearrangement. If **41** does form, it can only be as a termination pathway or selectively eliminate back to the iron hydride and substrate.

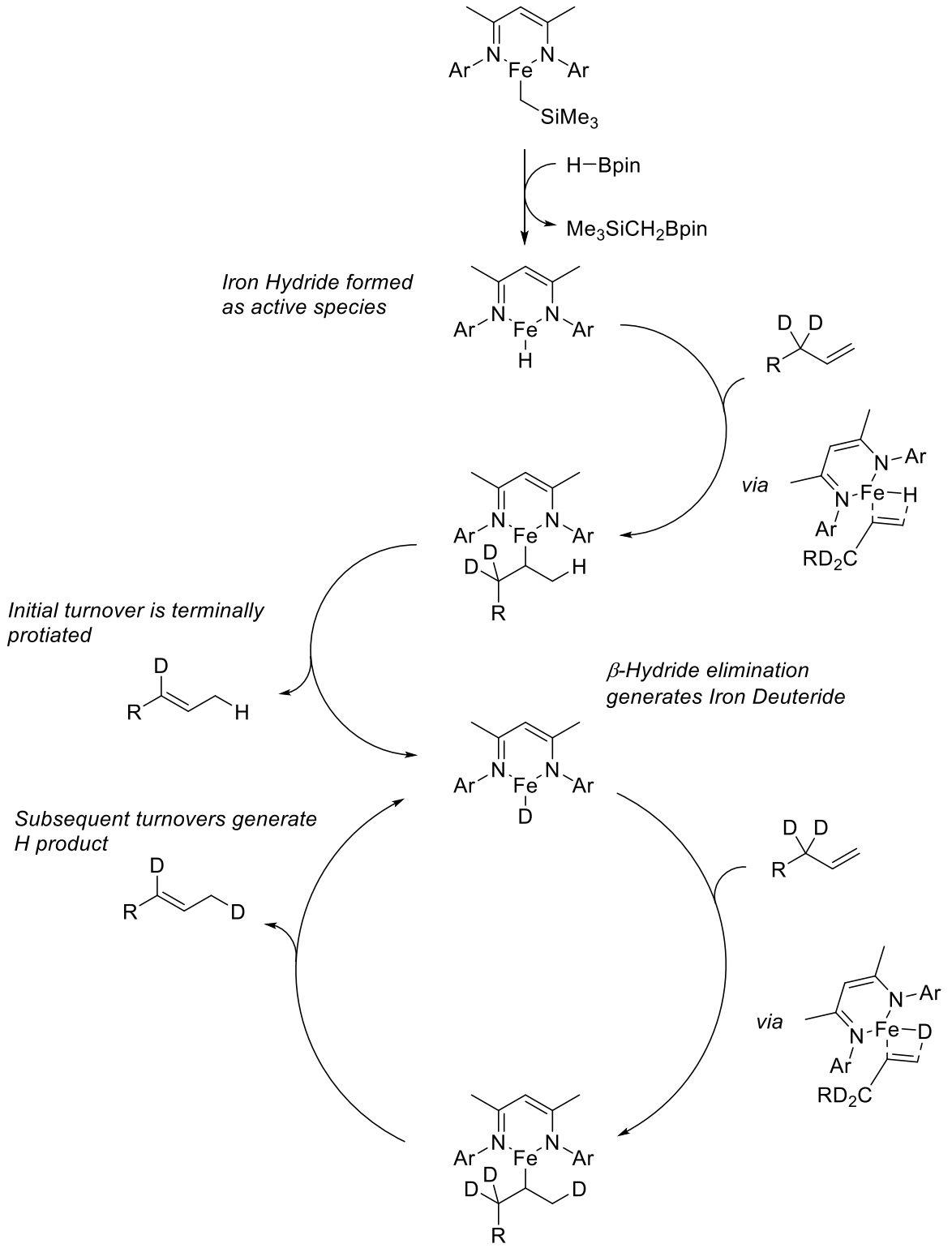

Scheme 79 – Through a hydride mechanism, the first turnover should lead to some protic incorporation on the terminal position. In the event, no incorporation is observed.

A scrambling experiment can also be performed, between two distinct substrates, one protic and one deuterated. If proton transfer is intermolecular, then both products will have a mixture of isotopes in their products, as a mixture of iron hydride and iron deuteride will be generated *in situ* (as per the above experiments, exchange from the additive appears to be negligible or non-

existent). 2-allylanisole was used as a protic reagent — it offers similar conversion over the same timescale as allylbenzene, and the alkenyl peaks are distinct enough to distinguish between products (Scheme 80). Using this experiment to determine the nature of proton transfer has been performed in a similar manner by Findlater [106] and Koh. [230]

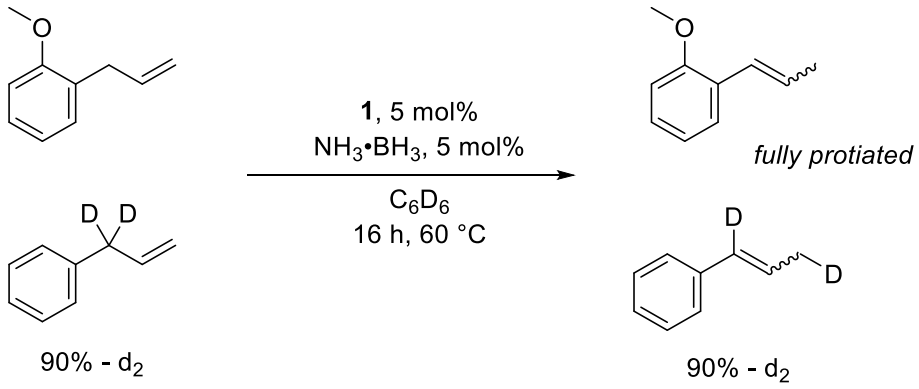

Scheme 80 – Isotope crossover experiment using both a protiated and a deuterated substrate. Under these conditions both products isoselectivity is preserved, rather than seeing H/D crossover. This further calls into doubt the role of an iron hydride in the mechanism.

Both products can be isolated, and the alkenyl shifts are distinctive enough to distinguish between them. No D-incorporation was observed, which indicates there is no H/D crossover, and consequently that proton transfer is intramolecular, rather than intermolecular. This clearly conflicts with the previously postulated cycle, where proton transfer must be intermolecular due to the regenerating Fe(II) hydride. The d-substrate is isolated as per the outcome in Scheme 78 with isoretention.

Intramolecular proton transfer in isomerisation is indicative of an allyl-type mechanism, [231] which was previously considered unfeasible owing to the Fe(II)/Fe(IV) redox cycle. However, the current proposition relies on the assumption that the active species is an Fe(II) hydride.

2.6 Using Iron(II) Hydrides and Hydrogen in Catalysis

The key intermediate in the initially proposed mechanism is the Fe(II) hydride **39**. This has been previously isolated and studied. [232] Of particular importance is its relationship with the dimeric species **43**. **39** has not been isolated crystallographically in its monomeric form, and instead the iron(II) hydride dimer **43** is isolated. It appears that in solution there is an equilibrium of the two structures which freely interconvert, with the monomeric hydride acting as the active species in further catalysis or synthetic steps, even when **43** is used as a starting reagent (Scheme 81). **43** can be independently prepared as detailed in Section 7.1, and used as an alternative pre-catalyst to **1**, for example, in dehydrocoupling chemistry. [46] The effectiveness of **43** as a pre-catalyst without an additional hydride source should support or disprove the role of **39** and further hydride derivatives in catalysis.

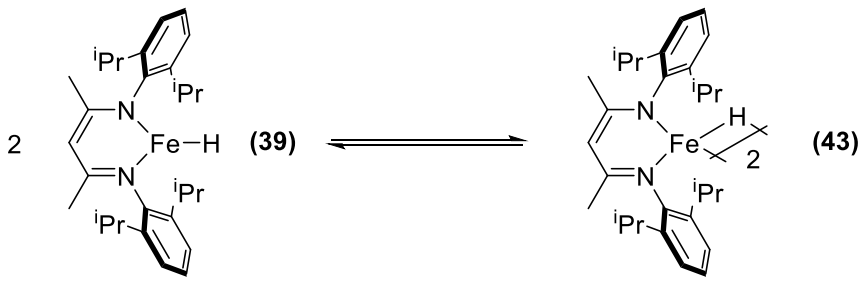

Scheme 81 – The proposed iron(II) hydride **39** has been shown to exist in equilibrium with, and crystallise out as, the dimeric species **43**. **43** can be independently prepared and used in catalysis, although it appears **39** is the active species in these processes.

On assuming the above equilibrium and the catalytic cycle shown in Scheme 71 to be correct, reactivity should proceed without a hydride source when using **43** as a pre-catalyst, as the role of the hydride source is solely to generate an Fe(II) hydride. In actuality, when using the hydride dimer in catalysis conversion is considerably less than the comparable **1** and HBpin (or **1** and ammonia borane) reactions (Table 7). Even under conditions more demanding than those of the catalytic process, conversion is still poor. Note that as to gain the most direct comparison, **43** was used in 2.5 mol% rather than 5 mol% as it contains two metal centres.

Table 7 – Comparison of reactivity of iron hydride species **43** against standard reaction conditions.

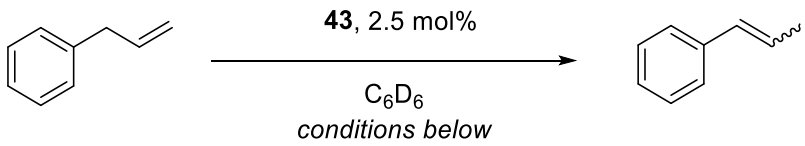

Catalyst (and Additive)	Conditions	Conversion (%)
43, 2.5 mol%	2 hours, 60 °C	*trace*
	16 hours, 60 °C	10
	24 hours, 80 °C	34
1, 5 mol% HBpin, 10 mol%	2 hours, 60 °C	29
	16 hours, 60 °C	93

Conditions : 0.5 mmol substrate, 600 µL solvent. Conversion determined by ^{1}H NMR spectroscopy.

We can further investigate the role of iron hydride species by performing the reaction under a hydrogen atmosphere. This could enable alternative iron hydride species to form through reaction with the pre-catalyst. This was performed at ambient pressures, as under high pressures the some substrate can be hydrogenated with **1**, [218] and it is clear the standard reaction is not highly pressurised. A minor signal of hydrogen forming is visible in the ^{1}H NMR spectrum of the standard reaction with ammonia borane, most likely arising from dehydrogenation, whereas it is not with pinacolborane. Both **1** and **43** were tested (Table 8). Full experimental detail is given in Section 7.2.

Table 8 – Testing complexes **1** and **43** for catalytic competency under a hydrogen atmosphere.

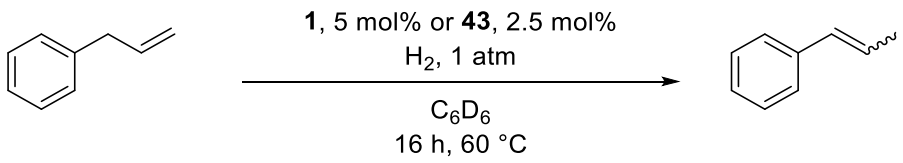

Catalyst	Isomerisation Conversion / %	Hydrogenation Conversion / %
1	-	-
43	7	9

Conditions : 0.5 mmol substrate, 600 µL solvent. Conversion determined by ^{1}H NMR spectroscopy.

When using **1** the outcome is straightforward — no reactivity occurs, identical to the reaction when performed under an argon atmosphere. Indeed, wide sweep NMR indicates that **1** remains intact under these conditions, and does not appear to react with hydrogen at all. When using **43** isomerisation is similar to the study in Table 7, and a small amount of hydrogenation (yielding propylbenzene) is also observed.

The studies with the hydride complex, coupled with the deuteration studies appear to disprove an iron(II) hydride mechanism for this catalytic process, as proton transfer clearly proceeds through an alternative pathway (as shown by deuteration experiments in Section 2.5) and the proposed iron hydride is not catalytically competent enough (*vide supra*). In Section 2.9 density functional theory studies further indicate that the transformation is not feasible. The sum total of this evidence is enough for us to rule out the initially proposed iron(II) hydride alkyl mechanism.

The departure from this form of chemistry is interesting, as it contrasts to the hydroboration and hydrogenation transformations that this study was initially built on. This is rationalised to an extent in Section 2.9. Because of this, it is necessary to further probe the reaction to propose and determine an alternative pathway for this catalysis.

2.7 Identification and Study of Iron(I) Species in Catalysis

Electron Paramagnetic Resonance (EPR) studies

Because of their ability to contain stable unpaired electrons, transition metal complexes are well-suited to studies utilising electron paramagnetic resonance spectroscopy (EPR spectroscopy, sometimes also termed electron spin resonance or ESR spectroscopy). EPR is considerably more sensitive than NMR spectroscopy, and consequently samples are analysed at a comparatively low concentration. Furthermore, metal-centred radicals can generally relax rapidly, so signals obtained at room temperature are typically too broad and weak to be fully observed. To circumvent this, analysis was taken using diluted aliquots that were cooled to 77 K — full experimental details are given in Section 7.2.

The intensity and shape of a peak is determined by a variety of factors, the three of which that are most significant are the g factor, the hyperfine coupling (if any) and the anisotropy of the system. The g factor is dependent on the electronic structure of the radical centre, whereas the latter two

factors are dependent on the molecular structure. The value of g can also strongly indicate whether a radical is metal or ligand centred. [233]

In a further comparison with NMR spectroscopy, EPR is most diagnostic when the spin of the system being analysed is S = ½. High spin-state transition metal centres frequently generate broad EPR peaks, and other charge/spin combinations lead to very weak or undetectable transitions (Additionally a fully paired metal centre where S = 0 is EPR silent). As detailed in the introduction, previous studies of these iron complexes have indicated they typically form high spin (S > ½) species. Even in cases where high-spin metal centres are present, EPR has proved useful in proving or disproving the presence of intermediates and pathways in catalysis, and recent studies by Peters, [234] Neidig [235] and Ge [236] highlight this.

When a solution of **1** is evaluated in a spectrometer, two relatively weak peaks are observed (Figure 18). High spin iron(II) centres are generally EPR silent [237] ; the signal is instead consistent with an Fe(III) complex present. A high spin Fe(III) centre has S = 5/2, and simulations of the free centre are consistent with the signals observed (simulation parameters are detailed in Section 7.2). The most reasonable source of this is an impurity in the starting pre-catalyst, either from an incomplete salt metathesis in the synthesis or slow oxidation of the material. In the presence of allylbenzene these increase in intensity slightly; again this appears to be small and probably arises from advantageous moisture present in the reaction environment.

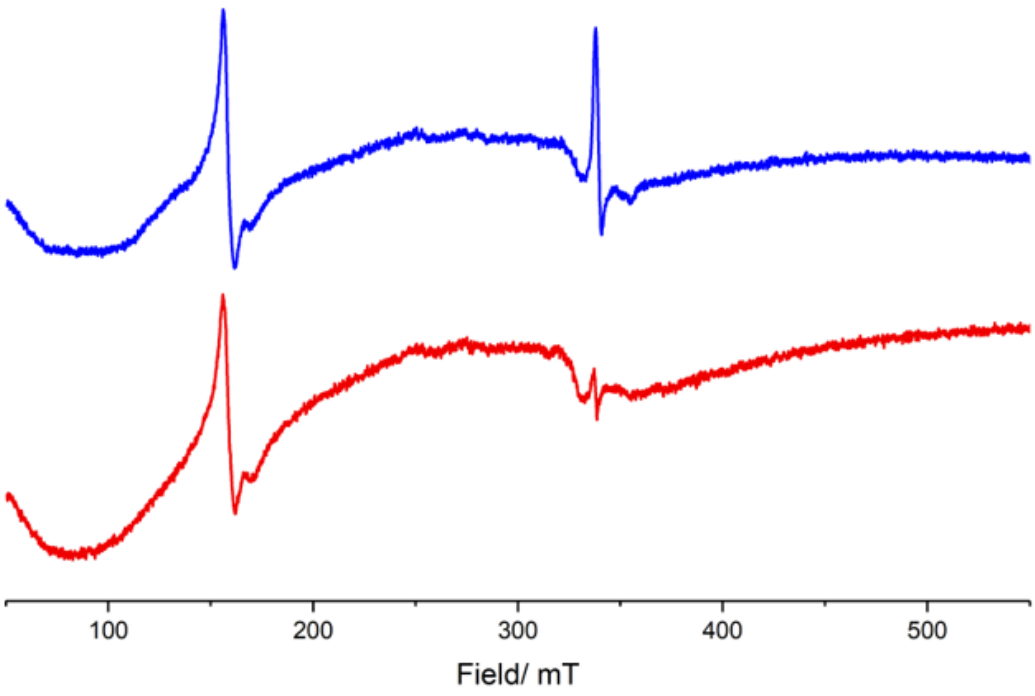

Figure 18 – EPR Spectra (CW X-band, 140 K) of **1** (**red**) and a mixture of **1** and allylbenzene (**blue**). Only some weak signals indicating Fe(III) environments are observed for a solution of **1**, which are slightly increased in relative intensity when allylbenzene is added.

Upon addition of pinacolborane there is a significant change to the EPR spectrum (Figure 19). The signal at 340 mT is overlaid by signals of considerably stronger intensity, and the signal at 160 mT is barely visible relative to the size of these. These consist of a very broad signal overlaying much of the observed spectrum, as well as a sharper, asymmetric signal at 300-350 mT.

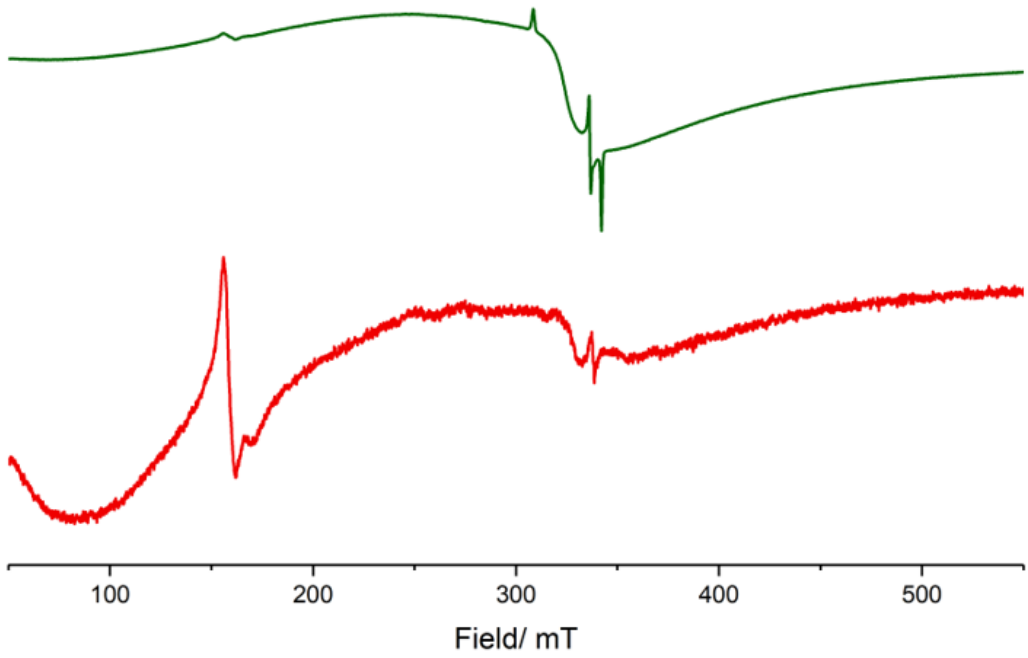

Figure 19 – EPR Spectra (CW X-band, 140 K) of **1** (**red**) and a mixture of 1 and pinacolborane (**green**, **1**:HBpin ratio of 1:2, as per isomerisation reaction conditions). The two signals are not to the same y axis scale.

The broad signal is effectively featureless, which limits extractable information and structural determination. In contrast the additional signals indicate a new, well defined environment is also forming, and this was analysed further (*vide infra*). There is no observable change in EPR data when 20 equivalents of allylbenzene are added to this mixture.

A further experiment was performed where conditions were approximated to hydroboration conditions — namely 20 equivalents of pinacolborane relative to iron centre. Compared to the isomerisation conditions the sharper signals are effectively subsumed, and the dominant signal is broad and featureless (Figure 20). This would appear to indicate that the two reactions have alternative metal environments, and provides a starting point to determining the reasons behind their divergent reaction pathways.

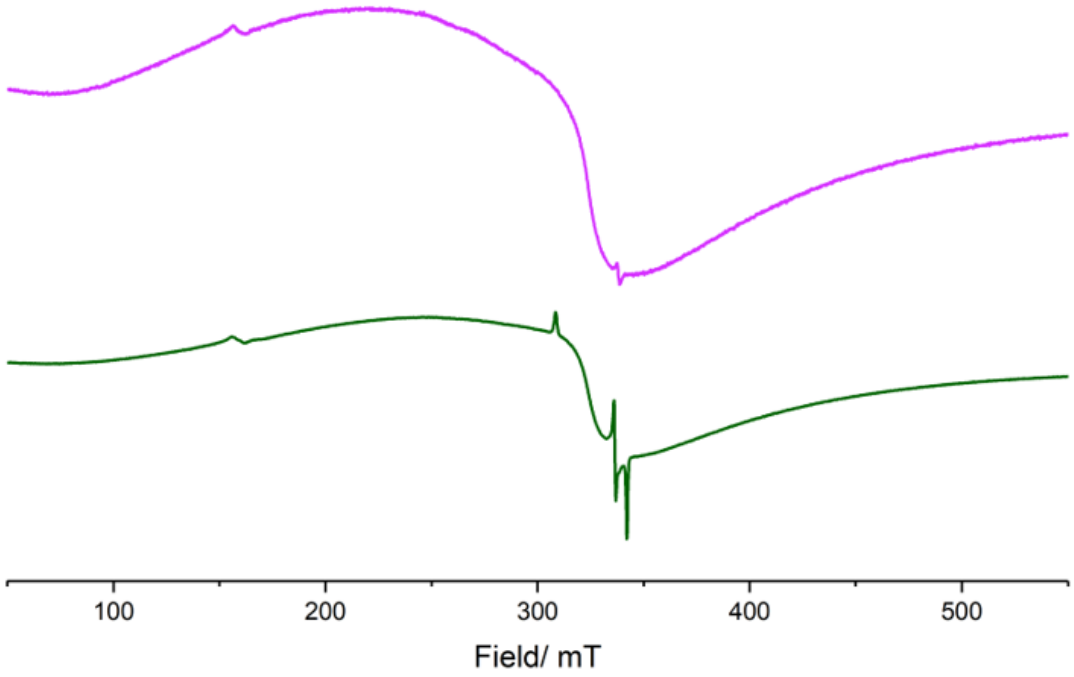

Figure 20 – EPR Spectra (CW X-Band, 140 K) of **1**, 2 equivalents of HBpin and 20 equivalents of allylbenzene (**green**) and **1**, 20 equivalents of HBpin and 20 equivalents of allylbenzene (**purple**). These are representative of the ratios of the reagents in catalytic isomerisation and hydroboration respectively.

The above observations were also repeated for 2 equivalents of ammonia borane, with a similar outcome. Data for 20 equivalents of ammonia borane was not cleanly determined, likely as the amount of (insoluble) ammonia borane present adversely affected measurement.

The well-defined signal observed from the reaction of **1** with both pinacolborane and ammonia borane was investigated further. Comparison with previous reports indicate a marked similarity of the observed sharp signals to those previously reported for complex **44** (Figure 21). This is an iron(I) species rather than iron(II), and exists in a d^7 low spin state (S = ½). This makes it considerably more amenable to EPR study. The sharp signals can be extracted for the above spectra and compared to signals simulated through EPR-Density Functional Theory (*Extraction, simulation and subsequent analysis performed by Dr Emma Richards, Cardiff University*) (Figure 22).

(44)

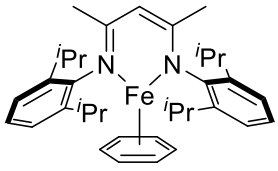

Figure 21 – EPR data was compared to previous reports and simulations of **44**, an Fe(I) complex.

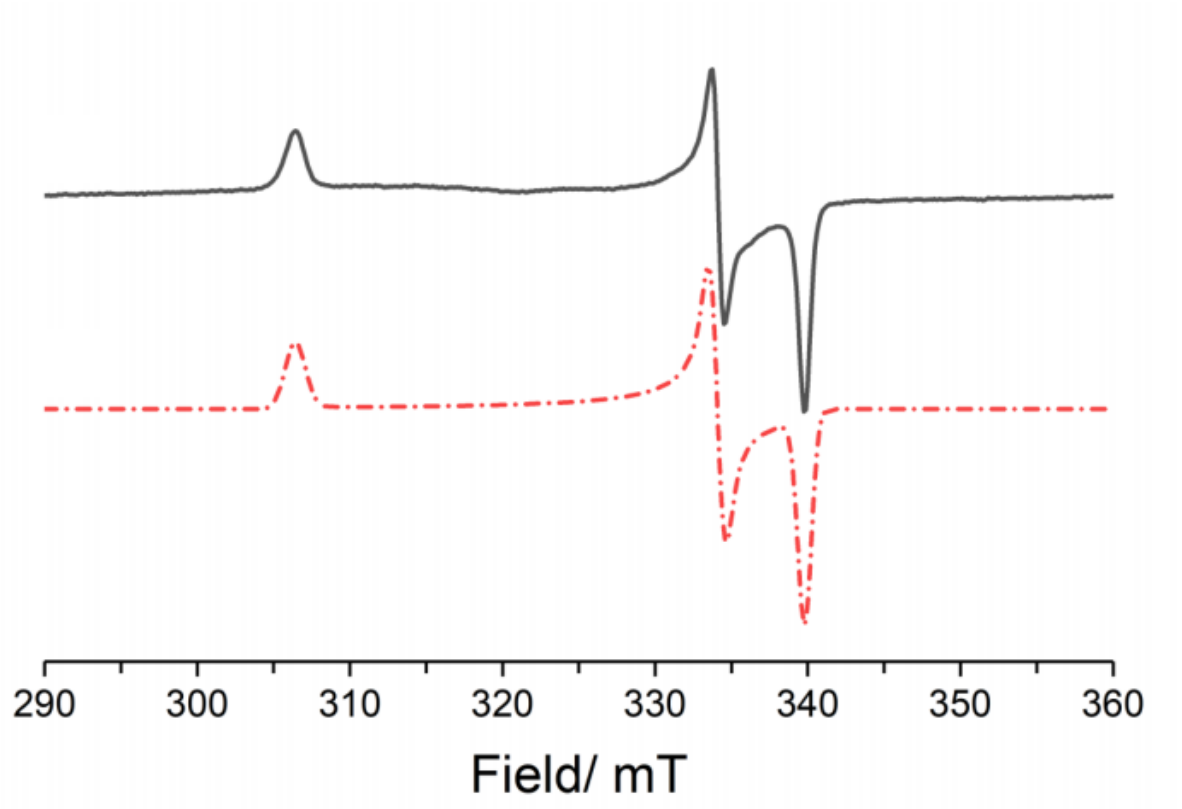

Figure 22 – Comparison of observed signal with other signals subtracted (**black**) and simulation of EPR signal of **44** (**red**). The similarity appears to confirm the formation of **44** *in situ* in the reaction.

The similarity of the observed signals compared to the simulated spectra of **44** give clear credence to the formation of **44** *in situ*. Further information on the electronic structure of **44** can be gleaned from extracting g bands and further EPR-DFT studies. It is clear that the structure is rhombic, leading to three g values being calculated. This indicates the unpaired electron is based primarily in the d_{z2} orbital. This is consistent with a basic crystal field analysis of a relatively flat, asymmetric trigonal planar complex, where we would expect the d_{xy}, d_{yz} and d_{xz} to be relatively low in energy (and fully occupied); the d_{x2-y2} to be very high in energy and the d_{z2} to be reasonably high in energy, leading to it being the SOMO — this is further confirmed with ORCA analysis. Furthermore, the spin density appears to be localised on the metal centre rather than shared between the metal centre and ligand, and no hyperfine coupling with nuclei (such as protons on the ligand) are observed. Further details on EPR calculations are given in experimental Section 7.2.

Table 9 – Comparison of g values determined from both experimental data from the reaction and theoretical analysis of complex **44**.

	g_1	g_2	g_3	g_{iso}
Experimental	1.984	2.018	2.200	2.067
Theoretical	1.979	2.015	2.128	2.041

EPR analysis gives clear indication that additional oxidation states of iron are forming in the reaction, with strong indications that one of these species is the iron(I) β-diketiminate species **44**, which appears to form from the reduction of **1** through some form of one-electron reduction

process. Elaboration on this process is given in Section 2.8, but before this two further studies were performed to further investigate the redox activity of **1** in this reaction.

Evans method analysis

At various points in Chapters 1 and 2, the paramagnetic nature of iron compounds is discussed, and furthermore that β-diketiminate iron complexes generally exist in high spin states. The spin state a metal complex exists in can be predicted to an accurate degree computationally, or determined through analytical methods such as a Gouy balance, but one of the most straightforward approaches is through application of Evans method. [238] **1** has previously been reported to be high spin, which for an iron(II) species equates to S=2 and a large μ_{obs} value. The consumption of **1** and formation of the low spin (S=½) iron (I) species **44** in the reaction should lead to a change in the magnetic moment of the solution. Thus, the magnetic moment of both the pre-catalyst and the reaction mixture was analysed using Evans method.

The difference in ^{1}H chemical shift between the residual C_6D_5H in the solvent (C_6D_6) and an internal capillary of C_6D_6 was measured. This is both dependent on the nature of the metal complex and the concentration in solution — as shown in Figure 23, the shift moves significantly upon varying concentration.

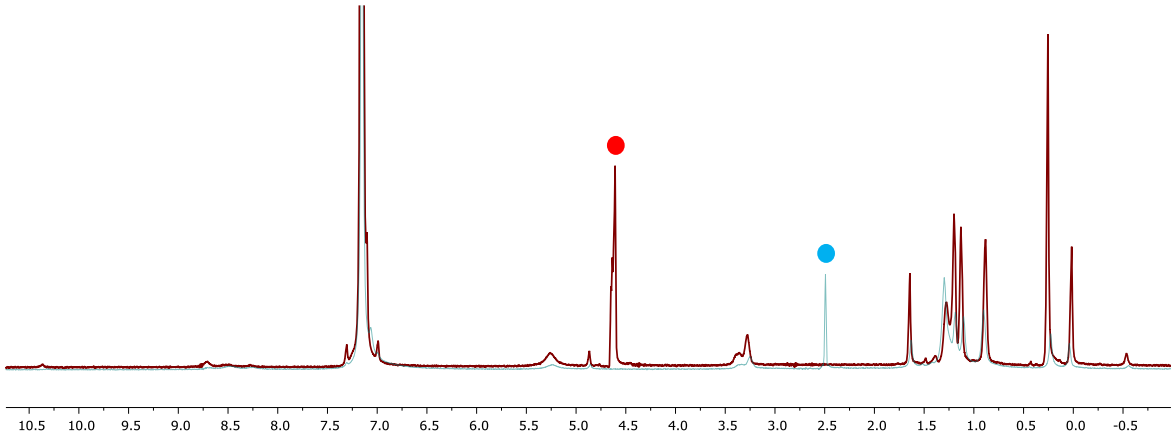

Figure 23 – Stacked spectra of different concentrations of **1** in C_6D_6 with an insert of C_6D_6. The shifted solvent peak is observed at 4.62 ppm in a solution of **1** at a concentration of 4.45×10^{-2} moldm^{-3} (●) and 2.49 ppm in a solution of concentration of 8.02×10^{-2} moldm^{-3} (●). This shows both the shifting observed with paramagnetic species and the concentration dependence.

The resulting shift in the experiment can be used to calculate the magnetic moment, and at either concentration the μ_{obs} can be determined as 5.73 Bohr Magnetons. This is within the expected range of Fe(II) high spin complexes, and very similar to the observed measurement for similar complexes reported by Hessen (Figure 24). [31]

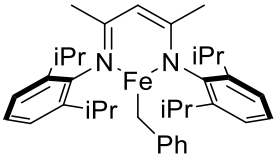

Hessen, 2005 5.6 B.M.

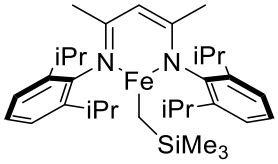

This study : 5.73 B.M.

Figure 24 – The μ_{obs} calculated for complex **1** is similar to isoelectronic complexes previously reported by Hessen.

1 was reacted with ammonia borane as per reaction conditions. The reaction solvent was removed under reduced pressure and the remaining precipitate was also analysed through Evans method. The diamagnetic parameters were kept the same — this potentially adds a level of error to the measurements but has a relatively minor effect on the calculation. In this case the μ_{obs} is significantly lower, at 5.07 Bohr Magnetons. Addition of pinacolborane to **1** also decreases μ_{obs}, although not to as great an extent. **44** has previously been isolated by Holland, and determined to have a μ_{obs} of 2.5 B.M., which is in the range expected for low-spin iron(I) species. [239]

The change in magnetic susceptibility of the solution relative to the pre-catalyst further confirms to us that some spin or oxidation state change is happening over the course of the reaction. As μ_{obs} is still relatively large compared to values normally seen for low-spin iron(I) species it suggests that either only a portion of **1** undergoes reduction to low spin complexes, or that there are additional high spin species forming.

Cyclic Voltammetry studies into reductive activation

EPR spectroscopy and Evans methods analysis above have indicated that our initial Fe(II) complex is being reduced to an Fe(I) species in the course of the reaction. In an effort to demonstrate that reduction of **1** was feasible, we performed cyclic voltammetry studies on the complex.

The need to maintain oxygen- and moisture-free conditions as well as examine relatively low potentials limits the range of solutions that can be used for these experiments. For example, while **1** is soluble in acetonitrile, when observing low potentials any metal-based signals are dwarfed by solvent effects. Furthermore, as most reference electrodes (*e.g.* potassium chloride) are aqueous based, it is necessary to use a pseudo-reference electrode (in this case, silver wire) and reference peaks to an observed signal (in this case, ferrocene oxidation). After some experimentation it was determined that THF with a suitable electrolyte gives a reasonably broad range and good solubility of the complex — full experimental details are given in Section 7.2.

Initial studies were conducted at 1 mM concentration, and a scan rate of 10 mVs^{-1}. As can be seen, there is a strong oxidation event observed at 1.2 V, this is close to the solvent oxidation potential. More pertinently, there are two events at lower potentials, although under initial conditions they appeared too weak to fully interpret. Increasing the concentration of **1** to 5 mM, as well as variation of the scan rate, gives an improved measurement (Figure 25). By addition of ferrocene, the two peaks can be assigned potentials relative to the Fc/Fc^{+} oxidation potential (Figure 26 & Figure 27). Beyond this there is a steady drop in the baseline, this is again likely solvent effects.

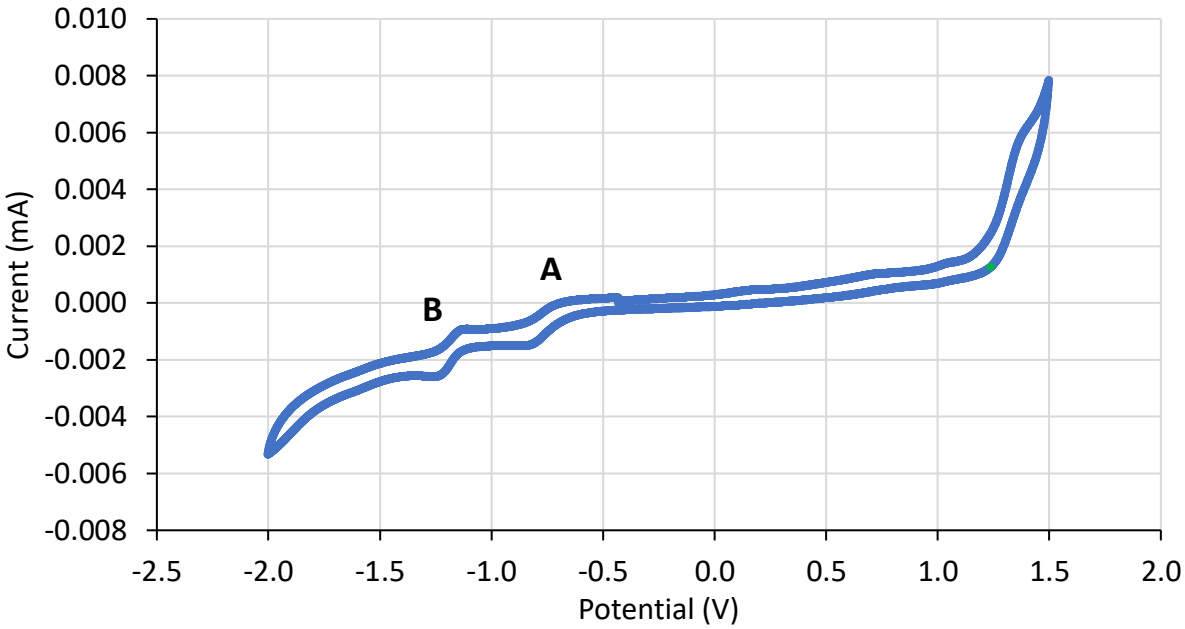

Figure 25 – Cyclic Voltammogram of **1** (5 mM, 0.1 M tBu_4NPF_6, in THF, 10 mVs^{-1} scan rate) — two distinctive steps can be observed at low potentials and are identified as **A** and **B** (silver wire used as pseudo-reference, although the potential is not directly referenced).

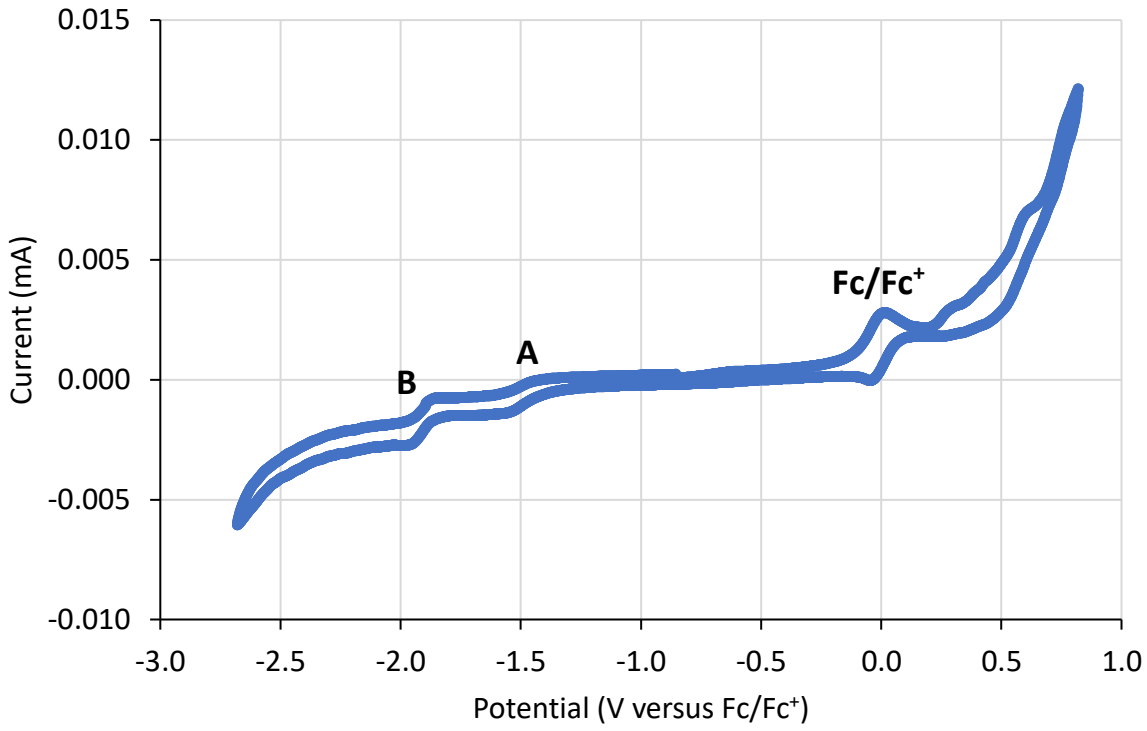

Figure 26 – Cyclic Voltammogram of **1** (5 mM, 0.1 M tBu_4NPF_6, in THF, 10 mVs^{-1} scan rate) with ferrocene. The distinctive Fc/Fc^+ oxidation step can be used as a reference peak.

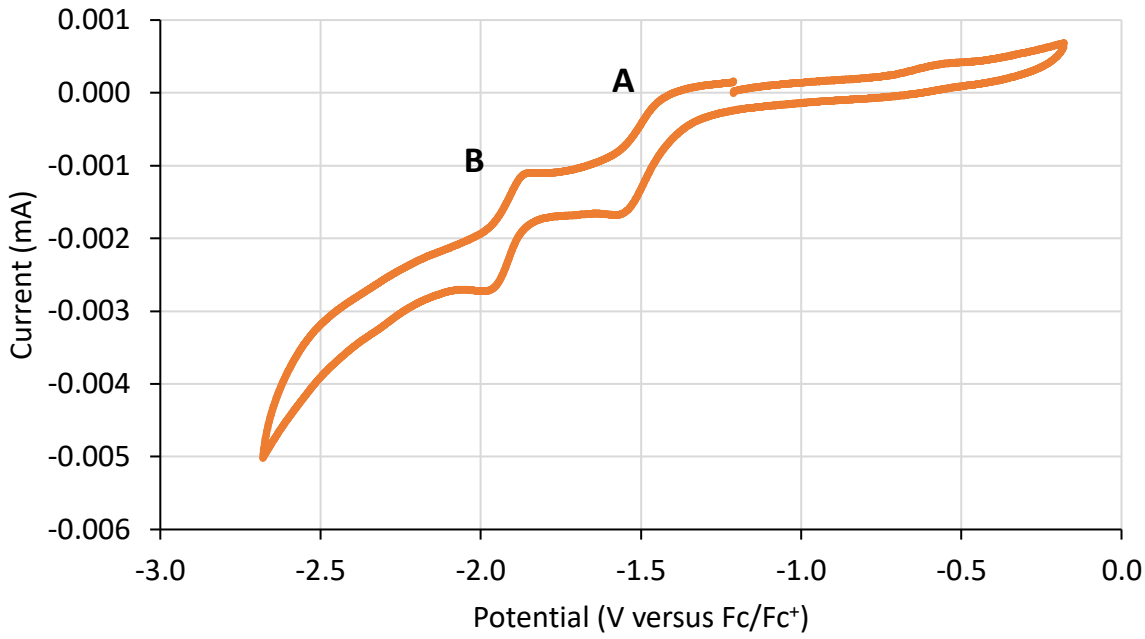

Figure 27 – Focused sweep on the region containing peaks **A** and **B** (Same conditions as Figure 26).

Table 10 – Determined potentials of **A** and **B** relative to ferrocene oxidation.

Peak	Potential (V vs. Fc/Fc^+)
A	−1.48
B	−1.92

Peak **A** was assigned as the Fe(II)/Fe(I) reduction step. At −1.48 V vs. Fc/Fc^+, the reduction appears to be chemically feasible with pinacolborane and ammonia borane. The oxidation potential of ammonia borane has previously been reported as +1.62 V, [240] although its poor solubility meant it could not be determined in the conditions used in the above studies — other studies report similar values. [241, 242] An oxidation potential for pinacolborane was neither determined nor has been previously reported; assuming it is similar to ammonia borane this would confirm the reduction step **A** should be feasible with either reagent. The outgoing reduction step is better defined than the reverse oxidation step — this could indicate a partial lack of reversibility of the process, or as an effect from the second step. Peak **B** is at a considerably lower potential (−1.92 V vs. Fc/Fc^+) — this could potentially arise from a second metal-based reduction (Fe(I)/Fe(0)), or a ligand-based reduction. Given the relative symmetry and therefore reversibility of the process, it was assigned to be some form of ligand reduction rather than a step that would readily degrade the metal centre. Regardless, it is postulated that the second reduction is not chemically attainable with the additives used in this catalysis, and does not play a role in the catalytic cycle.

The relatively amenable potential observed indicates to us that the reduction of our Fe(II) complex to an Fe(I) species is feasible under the catalytic reaction conditions, and adds further weight to the hypothesis that the reaction goes *via* a Fe(I) catalyst rather than an Fe(II) species. Using reduction as the method to access the active cycle, a new mechanism for the reaction can be proposed.

2.8 A Redox-Active Catalytic Cycle - Further Mechanistic Studies and Proposals

Investigations in Sections 2.5 through 2.7 provided a range of information about the catalytic cycle, with the three most important conclusions being:

- Proton transfer is intramolecular with respect to the substrate.
- A significant amount of Fe(I) species, as well as some Fe(III) species are formed *in situ* with both pinacolborane and ammonia borane; these signals are more intense in the latter.
- The reaction does not proceed through an Fe(II) hydride.

Because of this, the catalytic cycles in Section 2.4 are incorrect on two counts — the pre-catalyst does not activate in the manner proposed (Fe(II) hydride formation), and the resulting catalytic cycle does not occur as such. In this section new activation and catalytic mechanisms are proposed that better fit with the observed data. As the activation step and the catalytic cycle are distinct processes, they are evaluated in turn.

Activation of pre-catalyst : Formation of an Fe(I) species

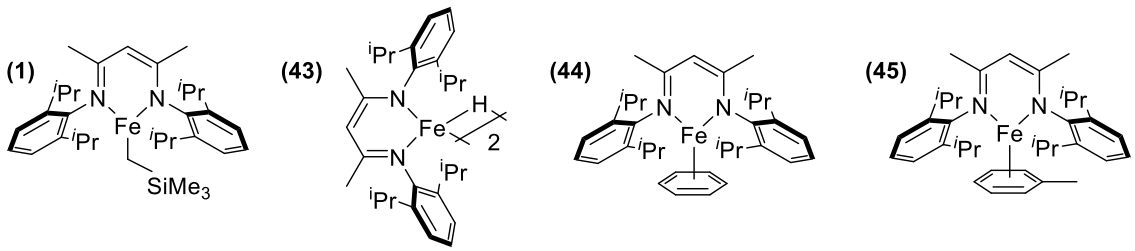

Figure 28 – Principal species relevant to the discussion below.

To add to the complexity, the reactions of pinacolborane and ammonia borane are distinct enough to warrant separate discussion, beginning with pinacolborane. The room temperature combination of **1** and a large excess of pinacolborane leads to paramagnetic signals that are indicative of iron hydride **43** forming, as well as diamagnetic NMR signals suggesting Me_3SiCH_2Bpin forming. This observation led to the (incorrect) proposition that this alone was enough to activate the catalyst. When pinacolborane is added in a 2:1 excess, the hydride signals are much weaker and signals belonging to **1** predominate, both initially at room temperature and post heating. ^{1}H NMR data for **44** has not been reported in benzene-d_6, but if it is similar to **45** (discussed below) the signals exist primarily in δ = 0–10 ppm range, where a range of poorly defined signals are present (both in the observed ^{1}H NMR spectra and in literature reports).

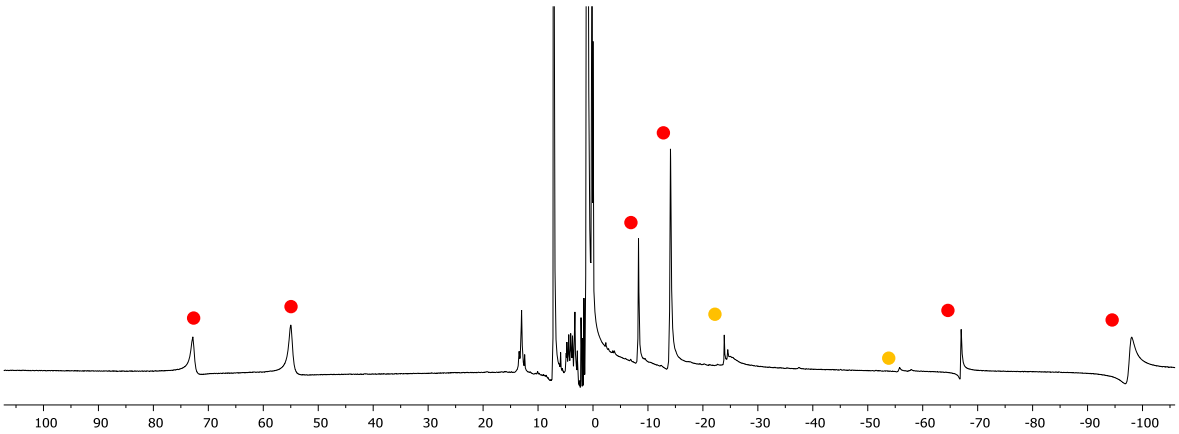

Figure 29 – NMR of a 1:2 mixture of **1** and HBpin. Primarily unreacted **1** is observed (signals identified with **red** ●), while a small number of signals related to **43** can also be seen (identified with **yellow** ●) (500 MHz, C_6D_6).

Addition of substrate leads to new signals forming over time (Figure 30). The substrate (and product) peaks dwarf any signals in the diamagnetic region, and some new signals are observed in the paramagnetic region. These shifts are more in common with iron-alkyl complexes, [243, 244] and we believe these are instead termination pathways rather than any catalytically competent species (the new species formed are <1% of the amount of allylbenzene present).

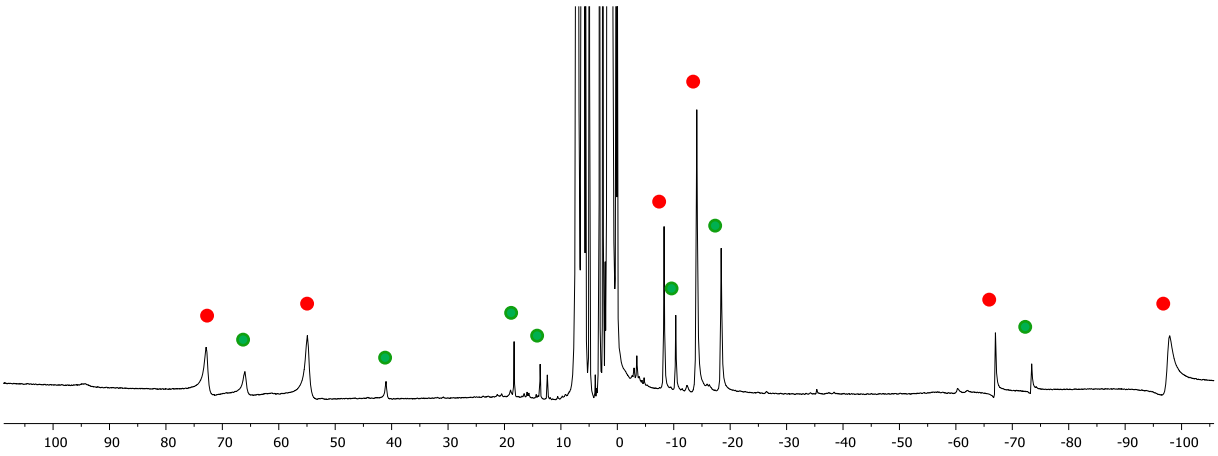

Figure 30 – NMR spectra (± 100 ppm, 500 MHz, C_6D_6) of the reaction of **1**, HBpin and substrate (1:2:20 equivalents). The new peaks formed (**green** ●) are similar to previously reported alkyl complexes, and it is proposed these are side reactions rather than active catalytic species.

Two alternative activation pathways are proposed. Firstly, it is proposed that at high temperatures the iron hydride reacts further to disproportionate into species in both the (I) and (III) oxidation state. No reaction of **43** (or consequent catalysis) occurs without a further hydride source even at high temperature, hence pinacolborane performs some role in catalysing or being consumed as part of this second activation step. The iron(III) hydride **46** has not been reported before and probably does not exist in its drawn form, and it likely reacts further to form additional iron(III) species. Alternatively, the formation of **44** is distinct from primary catalyst activation, which proceeds in a relatively direct method through reduction with pinacolborane. The proposal shown in Scheme 82 does this through an effective oxidation of the pinacolborane proton from the −1 to

+1 oxidation state, and a reduction of both the iron and boron centres. While a chemically balanced process, it is difficult to postulate a clean mechanistic pathway for such a reaction.

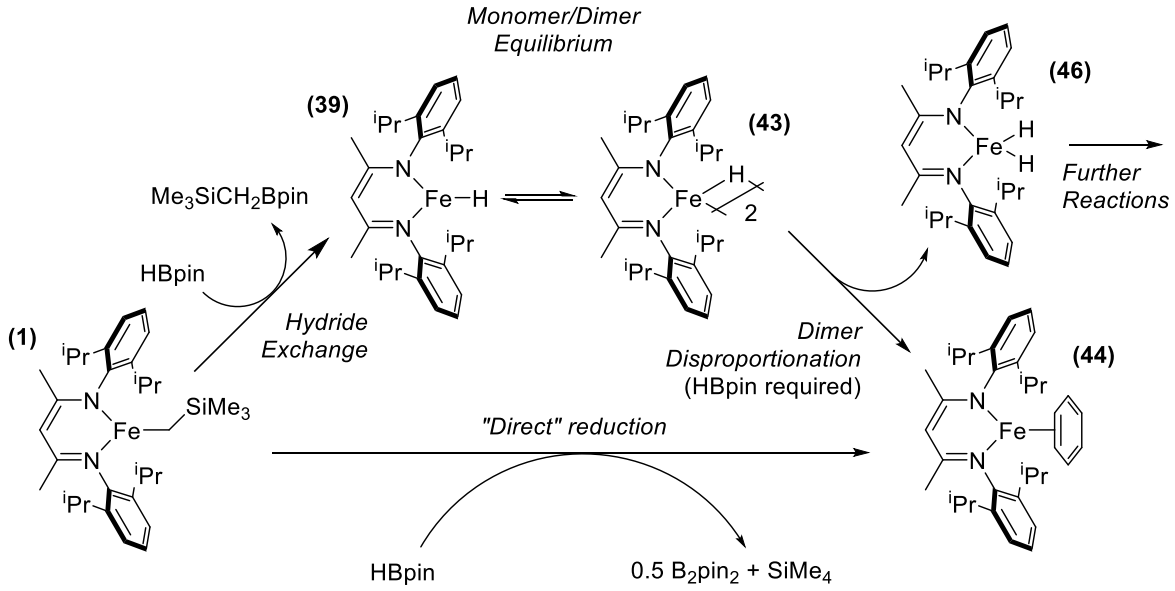

Scheme 82 – Proposed activation of **1** to form **44**, proceeding through a hydride or through a more direct manner. In both cases the steps are likely to be more complex than shown.

43 has previously been reported by Holland to undergo (redox-neutral) cleavage with trialkyl boron compounds to form iron-boron bridged hydrides and alkyl species (Scheme 83). [245] If pinacolborane was expected to behave in the same way, formation of **39** (although it could easily reform the dimer) and an iron-boron bridged hydride would be predicted, or alternatively a pinacolborane fragment would add across and bridge the iron centre. The bridging species could then be a potential intermediate towards a further, complex disproportionation process. Equally, in many reactions pinacolborane shows divergent reactivity compared to trialkyl boron compounds so an alternative pathway may occur.

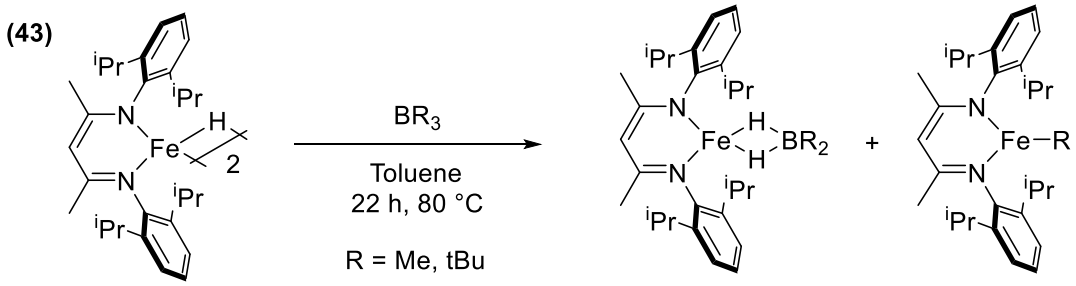

Scheme 83 – Previously reported reaction of **43** with boron compounds. With pinacolborane, **39** would be generated in the simplest reaction in lieu of an iron alkyl species, however if B-O cleavage instead occurs a bridged iron species would instead form.

It is difficult to distinguish the specific steps of this activation. The clearest evidence comes from using **43** and pinacolborane in catalysis — conversion is very similar to **1** and pinacolborane. Given **43** forms in the initial reaction between **1** and pinacolborane, this process should, therefore, occur under reaction conditions, although this does not mean a non-hydride path does not occur simultaneously.

The ammonia borane activation has similar proposals. Again, **43** is observed (in a small amount) by ^{1}H NMR spectroscopy from the reaction of **1** and ammonia borane, although in this case the near paramagnetic region is a veritable forest of peaks (Figure 31). The scheme below assumes the amidic proton is exchanged to generate tetramethylsilane, whilst the boron hydride is oxidised to dihydrogen, although this is more to simplify electronics than through experimental observation. It seems that activation with ammonia borane is poorly defined and proceeds through and generates a mix of metallic and amine borane-derived species.

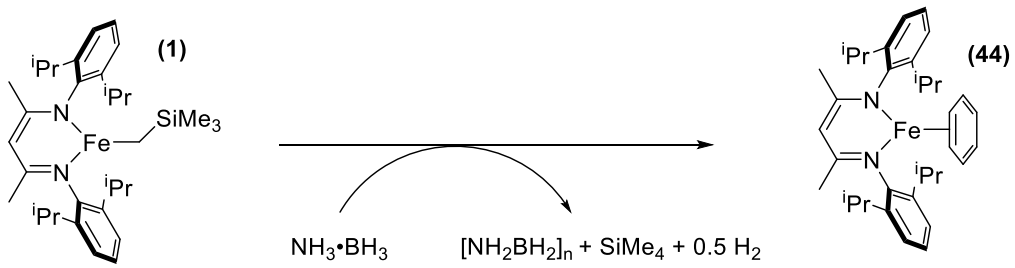

Scheme 84 – Postulated generation of an Fe(I) species by reaction with ammonia borane. Given the complexity of the ^{1}H NMR spectrum, it is likely that there are either parallel reactions going on or this is a simplified representation of the true nature of the reaction.

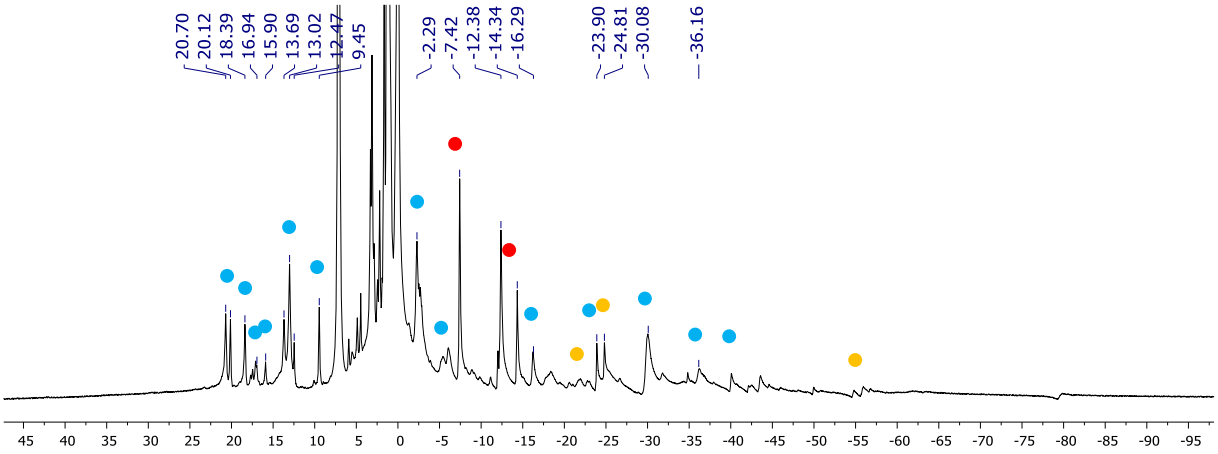

Figure 31 – Between +25 ppm and −85 ppm, a wide range of new peaks are observed in the ^{1}H NMR paramagnetic region from the reaction of **1** and ammonia borane. Signals belonging to **1** are identified with **red** ●, **43** are identified with **orange** ●, and major new signals are identified with **blue** ●, although a range of smaller signals can also be seen. This suggests the reaction generates a range of new organometallic species (500 MHz, C_6D_6).

In both the steps above, **44** is shown stabilised by a benzene ring. This is a matter of simplicity, and it is merely expected that this is initially formed owing to the greater concentration of solvent above anything else. Consequences for the EPR data of multiple ligands are elaborated on in the catalytic cycle discussion. Exchange between benzene and alternative stabilising ligands should be relatively facile, for example binding with substrate as shown in Figure 32. Binding studies performed by Holland have shown that styrene has (in an η^2 conformation with the terminal double bond) a considerably stronger binding energy than benzene (in an η^6 interaction) – presuming allylbenzene behaves similarly, it is likely to exchange with and displace benzene over time, forming species **47**. [246]

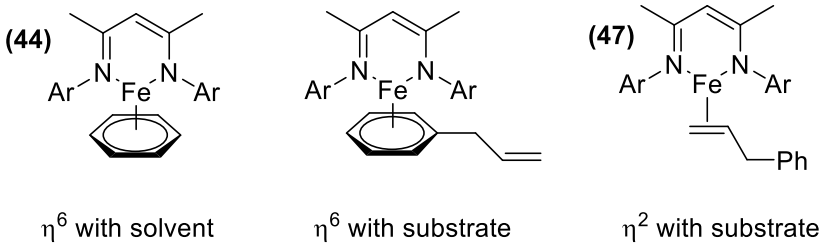

Figure 32 – The Fe(I) centre can be stabilised by interacting with solvent or substrate in a range of coordination environments.

Although it is clear that an iron(I) species is forming from the reaction of **1** and pinacolborane or ammonia borane, it appears formation (similar to many other one electron reduction processes) is complex and a range of activation pathways appear possible.

An iron(I)/(III) catalytic cycle

The allyl mechanism shown in Scheme 72 was previously ruled out, amongst other reasons, as an iron(II)/(IV) oxidative addition step as part of the catalytic cycle did not appear likely. On the other hand, two electron oxidation of an Fe(I) species, such as **44**, to form an iron(III) species appears considerably more feasible. Two-electron oxidation of iron species in catalysis is relatively uncommon compared to single electron processes, although work by Chirik and others have emphasised that the correct ligands and conditions can readily enable it. [247] Unlike iron(IV) species, compounds with iron(III) centres are ubiquitous with a wide range of ligands and environments, and can be more readily reacted with in catalytic roles.

The proposed catalytic cycle is shown in Scheme 85. Initially **44** exchanges ligand either by exchanging a molecule of solvent for substrate, or else by altering the binding of allylbenzene from η^6 to η^2, forming a η^2 metal-alkene complex (as shown in Figure 32). Unlike the activation of **1**, formation of **47** is likely to be straightforward and facile. It is also likely that this exchange exists in a form of equilibrium. From here, the iron centre formally adds across a β-hydride to form the allyl complex **48**. **48** is an iron(III) complex with both allyl and hydride ligands.

Reductive elimination can now occur, in one of two manners. Elimination at the more substituted position merely regenerates **47**, but if the new C–H bond is formed on the terminal position then complex **49** is formed. This is a second metal alkene complex, although importantly now the more substituted isomer is bound as a ligand. Through ligand exchange the isomerised product is released as a free molecule and **47** is regenerated (again, this is likely some form of reversible equilibrium). The *cis-trans* selectivity appears to be governed at the point of oxidative addition, as it appears unlikely that **48** can readily undergo the required interconversion between the two binding conformers that lead to the subsequent products. This is in turn determined by the conformation of **47** at the point oxidative addition is initiated.

Unlike the initially proposed iron(II) alkyl mechanism, this is consistent with the three key findings from the initial mechanistic work. Firstly, proton transfer in this reaction is solely intramolecular, undergoing a 1,3-hydride shift over the course of the reaction. Secondly, the iron(I) species formed from the reaction of pinacolborane (or ammonia borane) with the pre-catalyst has an active role in the reaction. Thirdly, the iron(II) hydride, although we cannot rule it out being part of the catalyst activation, is not an active species on the catalytic cycle.

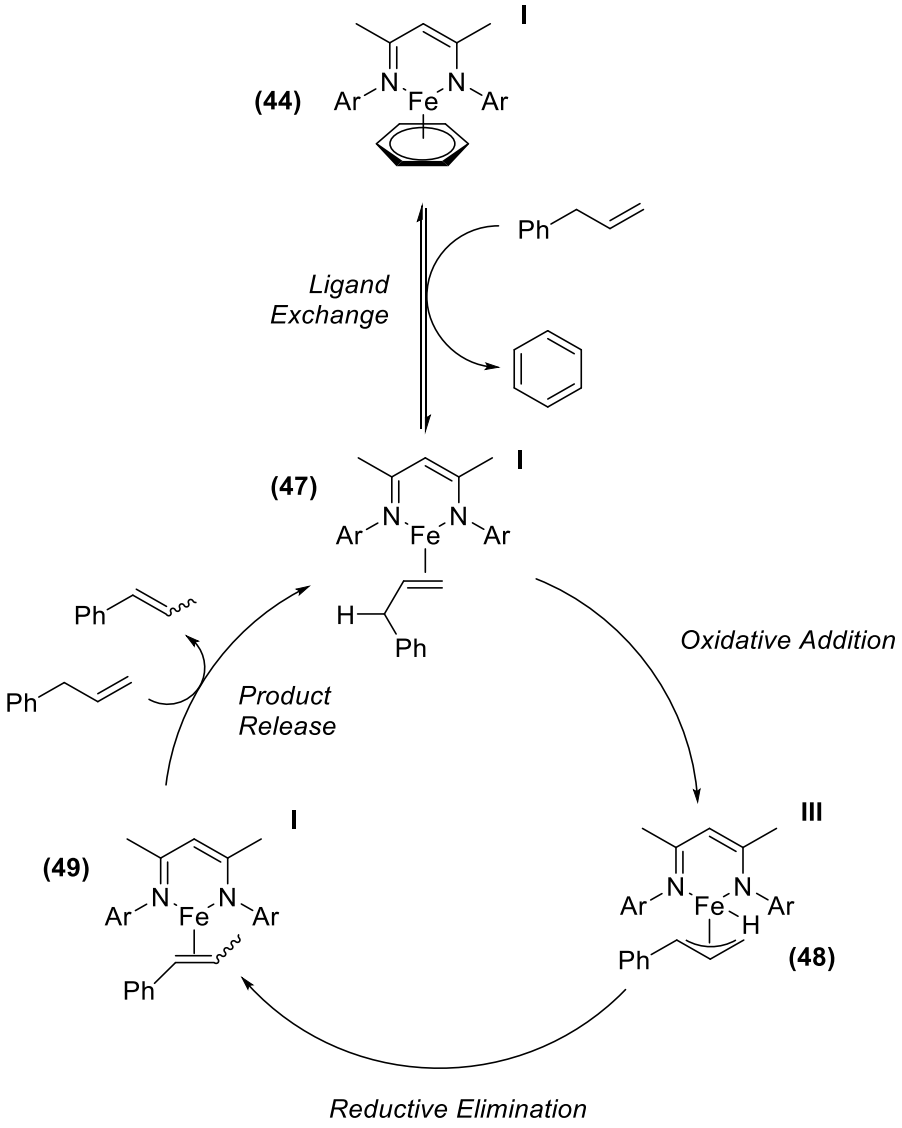

Scheme 85 – Proposed catalytic cycle proceeding from **44**. The transformation of allylbenzene to trans-β-methylstyrene is shown.

Further experiments were then performed to evaluate the mechanism as shown in Scheme 85. As **47** and **49** are Fe(I) species, and likely low spin, it raises the question of why they are not observed in EPR analysis when catalyst, pinacolborane and substrate are combined. As shown in Table 11, the calculated g values suggest that all three would generate essentially identical signals — the electron environment is centred strongly on the iron centre (as discussed in the EPR studies) and appears little affected by the auxiliary aryl/alkenyl ligand. Alternatively, it could be postulated that the majority of Fe(I) environments exists as **44**, so this dominates the EPR spectrum.

Table 11 – DFT-EPR predicted g values for the intermediates in the catalytic cycle. The similarities suggest all three signals are practically identical, or just that **44** is by far the most abundant S= 1/2 iron centre present. Experimental detail is in Section 7.2.

Structure	g_1	g_2	g_3
44	1.979	2.015	2.128
47	2.010	2.089	2.254
49	1.979	2.094	2.221

44 has previously been prepared independently of the reaction, through preparation of the analogous Fe(I) dinitrogen compound and subsequent displacement of dinitrogen with benzene. [239] In practice, repeating the literature method shown in did not result in preparation of the desired compound, and it is not entirely clear what the reaction generated. Furthermore, these species are inactive on their own in catalysis. Further details on the method for this reaction, including preparation and characterisation of the iron-lithium chloride adduct, are detailed in Section 7.1.

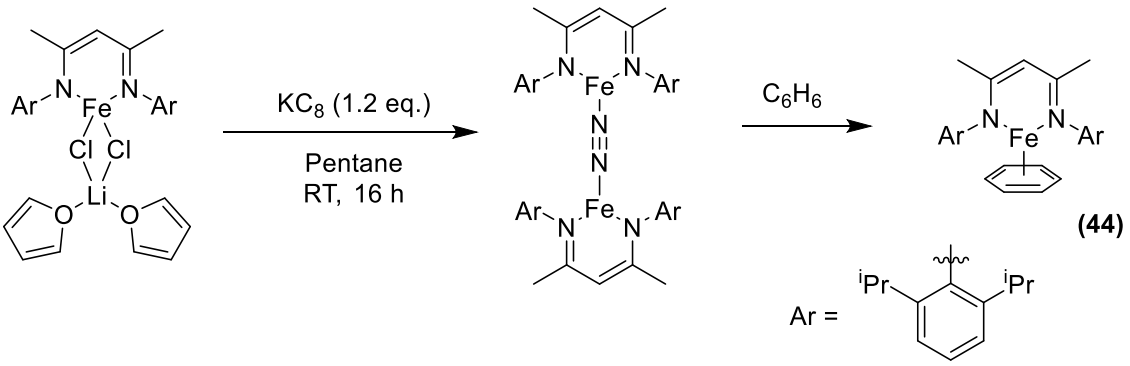

Scheme 86 – Attempted preparation of **44** from a literature procedure, however **44** was not isolated. Further details on the preparation and outcome are in Section 7.1.

As an alternative, **45** was prepared using the method reported by Scheer to greater success. [248] This differs from **44** only in that toluene is bound, rather than benzene, to the metal centre, although it is prepared in an alternative manner initially from the proligand (Scheme 87, further details and characterisation in Section 7.1). It was assumed the ligand exchange to form **47** from **45** was similar to when using **44**, and consequently the following steps on the catalytic cycle are the same.

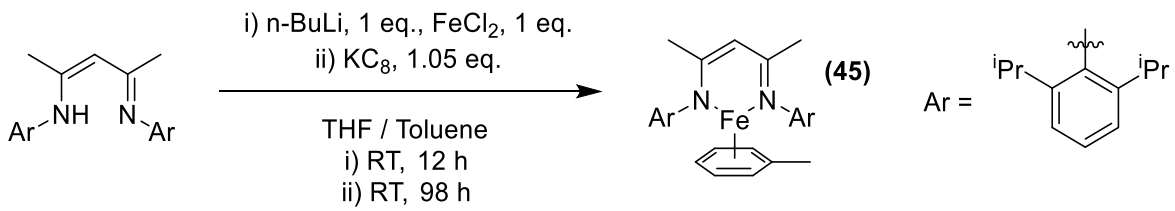

Scheme 87 – Preparation of iron(I)-tolyl species **45**, using the preparation reported by Scheer. [248]

45 can be used in catalysis, and proceeds without a further hydride source, contrasting to **43**. Indeed, the conversion and selectivity are very similar to those observed with **1** and pinacolborane.

It is a reasonable assumption to make that **45** can form **47** under reaction conditions as easily as **44** can, therefore this outcome goes some way to confirming the reaction proceeds through an iron(I) intermediate.

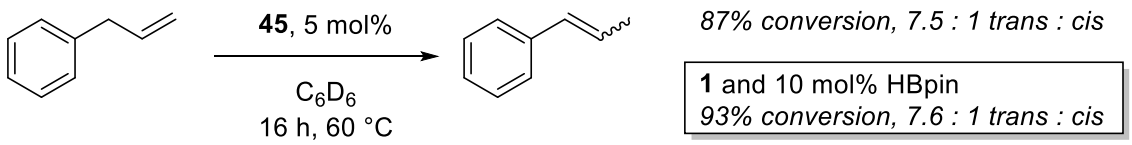

Scheme 88 – Iron(I) compound **45** is active in catalysis without a hydride source, and proceeds with reactivity and conversion similar to that observed in the standard reaction (with pinacolborane).

Further confirmation of the catalytic reaction could have been done through isolation of metal species crystallographically. Despite attempting this using a wide range of solvents and conditions (and attempts), none of the on-cycle species could be crystallised out from the reaction mixture. If **1** and ammonia borane are reacted in a 1:2 ratio and the residue is dissolved in pentane, **50** can be isolated as small dark crystals (*XRD analysis performed by Dr Nathan Coles, University of Bath*).

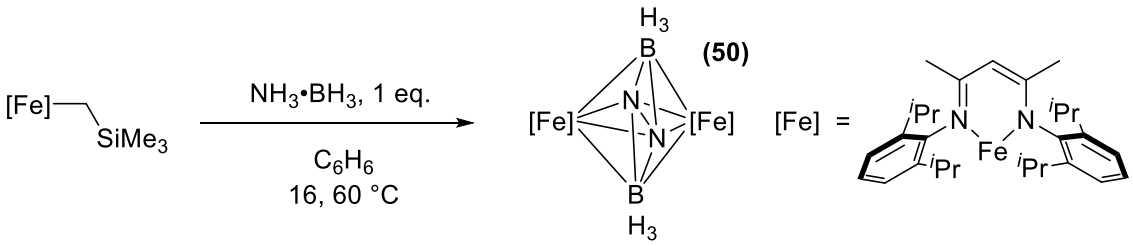

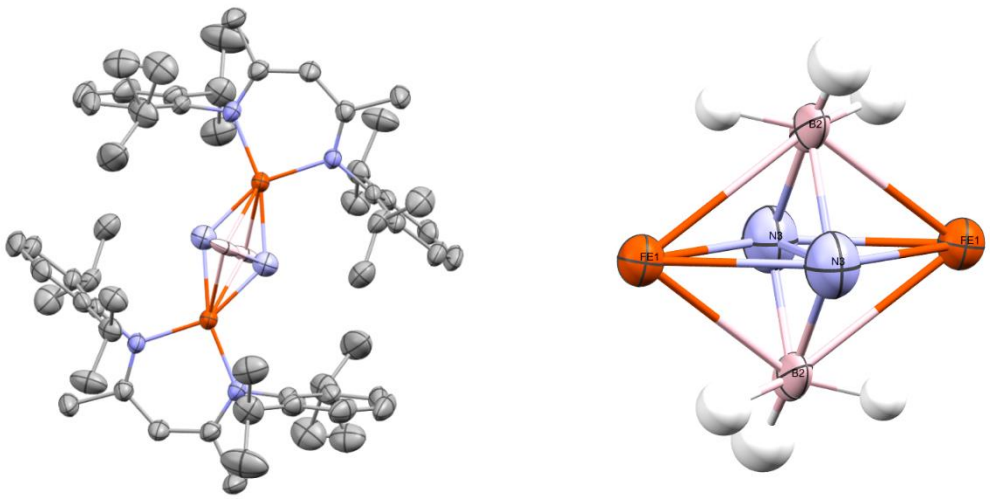

Figure 33 – Stoichiometric reaction of **1** and ammonia borane yields **50**, a dimeric iron complex bridged by boron and nitrogen centres. These could be isolated crystallographically (left, closer view of bridging atoms on right). Although distinguishing between boron and nitrogen environments was not entirely clear cut, it appears to contain BH_3 and N centres. Under this assignment observed bond lengths are (Å) : Fe1-N2 2.441(3); B2-N3 1.865(7); B1-B1 1.792(9); Fe1-N3 2.002(2). Note that the structure was not fully refined (R_1 = 5.3%, I/σ = 42.9)

The similarity of boron and nitrogen mean that the specific positions of boron and nitrogen centres could not be determined in complete confidence - the above structure, where the Fe–N bond length

is shorter than Fe–B bond length, appears to be the most likely. The most straightforward oxidation state determination suggests both iron centres exist in the (III) oxidation state. **50** does not give clear NMR data, and isomerisation catalysis does not proceed with **50** alone.

It is proposed that **50** is a termination step away from the catalytic cycle rather than an active species in catalysis, owing to its inactivity and the difficulty in postulating its role as an active species. A potential pathway to its formation is given in Scheme 89, where **43** reacts with dehydrocoupled ammonia borane derivatives, generating hydrogen and an initially bridged species with can further tautomerise to **50**. Formation from **44** is equally possible, where it would initially dehydrocouple ammonia borane to access the higher oxidation state. For pinacolborane no analogous termination products were isolated, and it is difficult to propose what structure they might take.

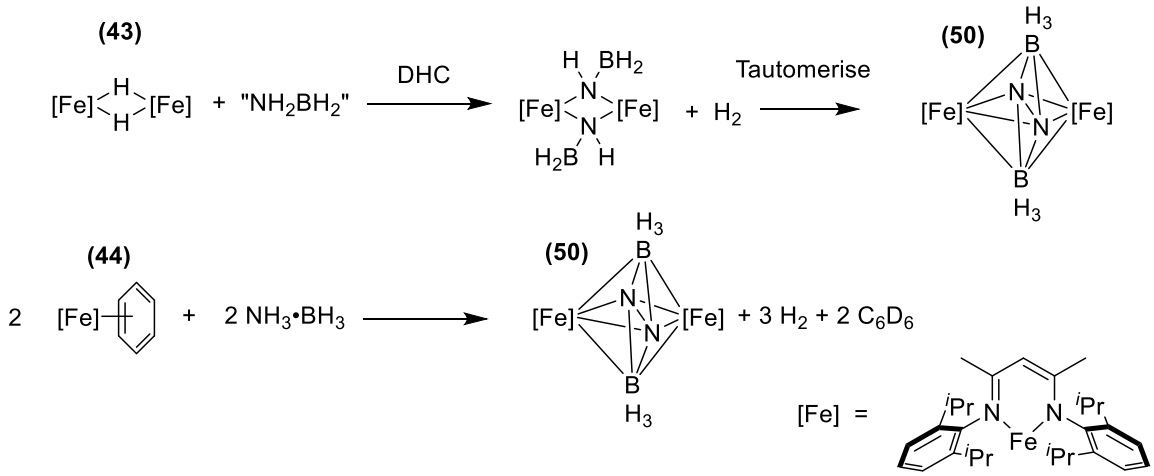

Scheme 89 – Proposed formation of **50** from **43** through an oxidative reaction with dehydrocoupled ammonia borane and subsequent tautomerisation. Reaction of **44** and ammonia borane is a plausible alternative method of formation.

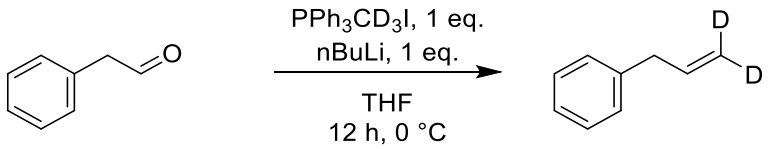

Figure 34 – The terminally deuterated substrate 3,3-d_2-allylbenzene was prepared as above, and used to determine a secondary kinetic isotope effect.

One final deuteration study was the investigation of a kinetic isotope effect (KIE) in the reaction. This would hopefully provide an insight into what kind of form the rate-determining step takes in the reaction — in particular whether it is the oxidative addition of **47** or the reductive elimination of **48**. The deuterated substrate in Section 2.5 did not give consistent KIE data compared to protiated allylbenzene, potentially owing to impurities present from the synthesis (in terms of other compounds in the reaction, rather than isotopic purity). As an alternative strategy, 3,3-d_2 allylbenzene was synthesised — this could be done in a higher yield and purity compared to the 1,1-d_2 isotopologue from phenylacetaldehyde and a deuterated Wittig reagent (see Section 7.2 for details and characterisation).

From this, a secondary KIE could be obtained. A significant KIE would be expected if the terminal carbon experienced a change in hybridisation during the rate-determining step (as occurs the in the reductive elimination step); conversely the KIE should be very close to 1 if this is not the case (as in the oxidative addition). Examples of this experiment's use for previous redox active cycles where C–H bonds are activated by metals include work by Jones, [249] Parkin [250] and Puddephatt. [251]

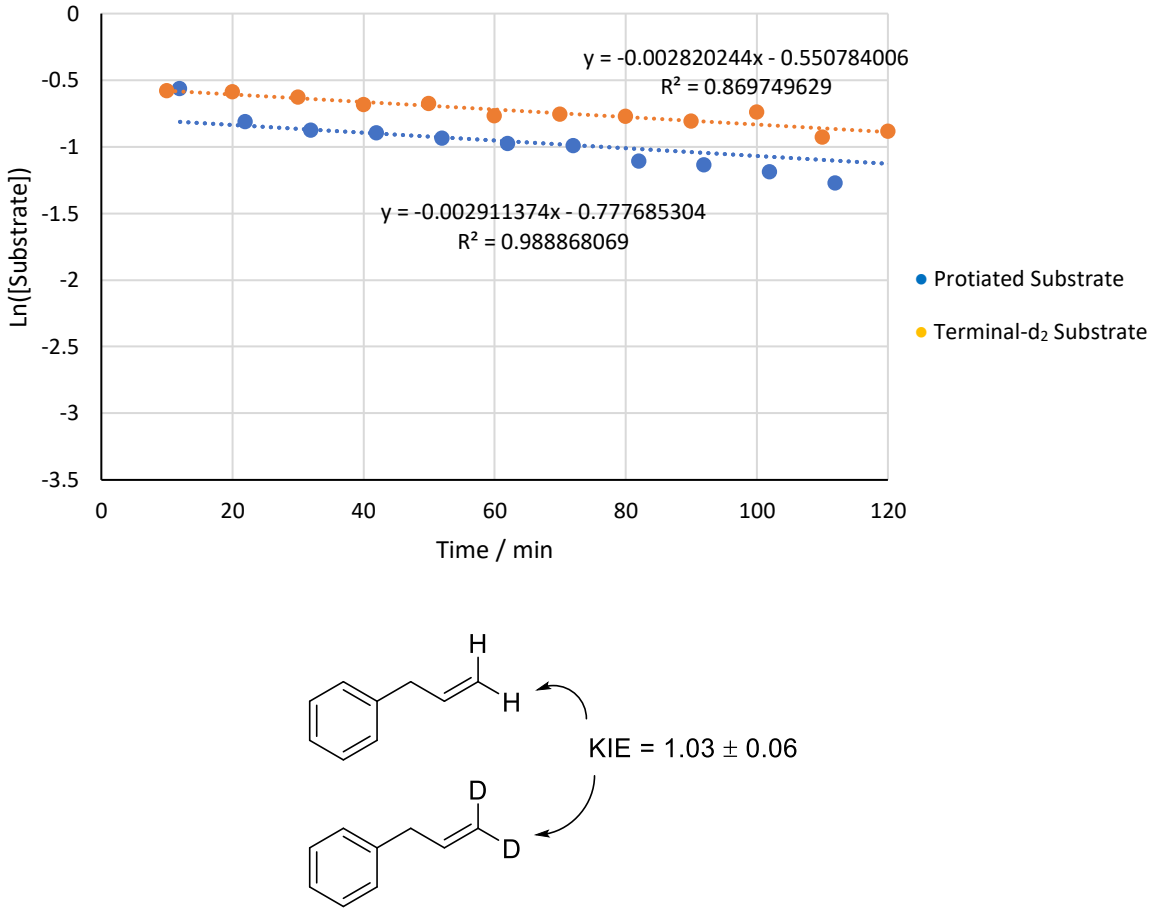

Figure 35 – Secondary KIE experiments. Comparison of initial rate of reaction between terminally protiated and deuterated products gives a KIE of 1.03 ± 0.06, for the context of the reaction mechanism this is effectively 1.

By comparing initial rates of reaction (up to approximately 20% conversion) between the 3,3-d_2-allylbenzene and the fully protic equivalent, a KIE of 1.03 ± 0.06 can be determined. Even by secondary KIE levels, this is very close to 1, indicating the rates of reaction are broadly similar. This implies that the rate-determining step is the oxidative addition to form the alkyl intermediate, rather than the reductive elimination to generate the product — this is revisited in Section 2.9.

The above proposals support the redox active mechanism, and we can account for some further observations to align with our mechanistic proposals. We can rationalise substrate performance by both electronic factors, as more electron-rich substrates can more easily undergo addition across a C–H bond, as well as steric factors, as terminal alkenes can more readily access the metal centre in the correct conformation.

In terms of the iron hydride, the poor reactivity could be rationalised by a slow dehydrogenative pathway, where the active species is generated by the elimination of H_2 figure (Scheme 90).

Although some studies of cobalt have indicated that Co(II) species play a role in a primarily Co(I)/(III) mediated process, for example by Tonzetich, [252] the inertness of the Fe(II) species and ease that the Fe(I)-tolyl species performs catalysis independently appears to fully rule the Fe(II) hydride out from any catalytic role.

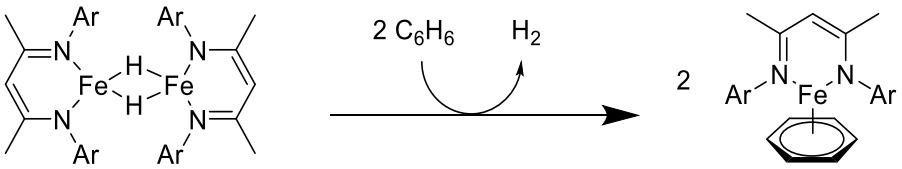

Scheme 90 – Potential reduction of the Fe(II) hydride *via* elimination of dihydrogen, proceeding without an external hydride source. Given the low catalytic turnover of the hydride, this reaction is likely to be slow with a low conversion.

The one aspect of the reaction that the above mechanism does not fully rationalise is the difference in regioselectivity between using pinacolborane and ammonia borane (and alternate hydride sources). For this, two potential explanations are proposed. One is that the differing kinetics in both activation processes result in different amounts of each intermediate species, and in the case of ammonia borane this leads to the *trans*-species forming in a greater quantity. The second proposal is that, for ammonia borane the complex NMR observed (Figure 31) suggests multiple iron species are formed, and there may be alternative *trans* selective catalytic pathways possible in the reaction mixture. Given that the selectivity of **45** is similar to the reaction of **1** and pinacolborane, rather than ammonia borane, it appears that activation with pinacolborane leads to solely the proposed activation and mechanistic pathway.

2.9 Theoretical Studies into Catalytic Alkene Isomerisation

To support our synthetic and spectroscopic observations and to study the reaction further, computational studies were performed on the catalytic process (*Calculations were run and analysed by Derek J Durand, Fey Group, University of Bristol*). The level of theory and additional data and specifications are given in Section 7.2; this section discusses the outcome and ramifications. Initially, as in the synthetic approach, it was proposed that the reaction proceeded in a redox-neutral manner through an Fe(II) hydride. The key species in Scheme 91 were optimised and the transition steps between them studied. **42** was determined to be a real species rather than a transition towards **39** (*i.e.* the more-substituted species is bound after β-hydride elimination before being eliminated as product), although the barrier to dissociation is small.

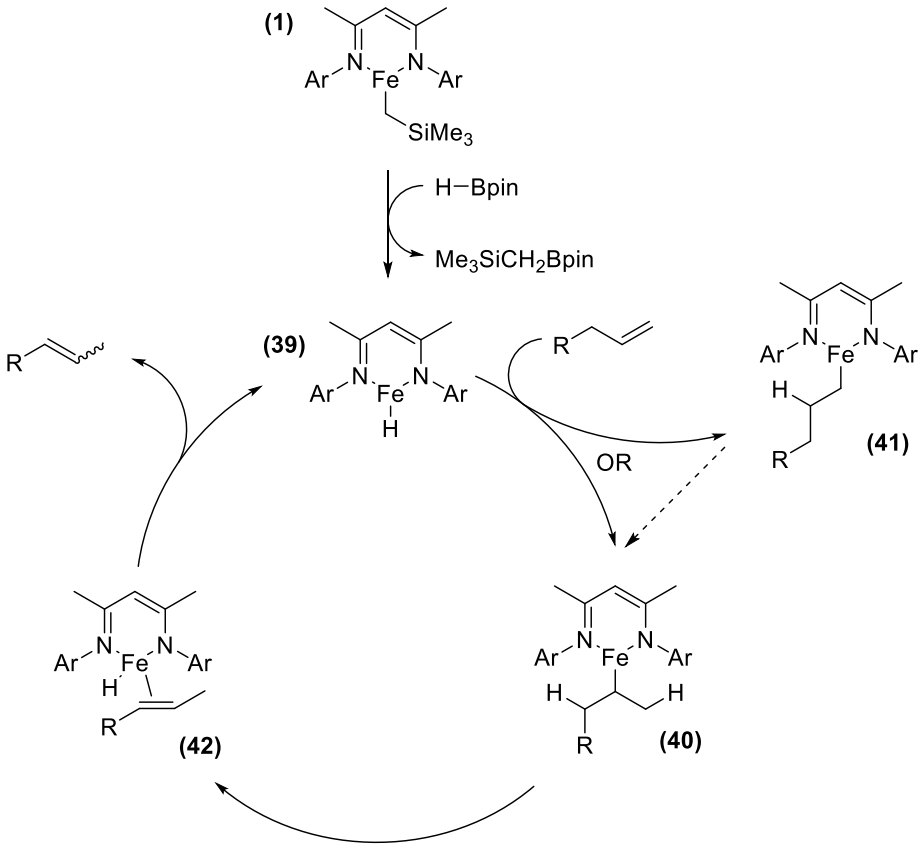

Scheme 91 – The alkyl mechanism initially studied with density functional theory.

Previous studies have shown that Fe(II) β-diketiminate complexes typically exist in a high spin quintet state, and this was shown by Evans analysis of **1**. In this case, all 3d orbitals are occupied (at least partially, Figure 36). The general order of orbital energies is also known [253], although the dz^2 and dyz orbitals in particular are extremely close in energy. Holland has shown that for particular processes, particularly when the metal centre moves to a more tetrahedral-like structure, the intermediate (triplet) state becomes closer in energy to the quintet state, and can sometimes be the most stable state. This is particularly important for β-hydride elimination, as the vacant d orbital in the triplet state can be donated into from a C–H bond as part of the elimination process. [254] Because of this, both the triplet and quintet energies were determined across the transformations, as was the singlet state (which is rarely encountered for these complexes) for completeness. Initially a *trans*-selective path was studied.

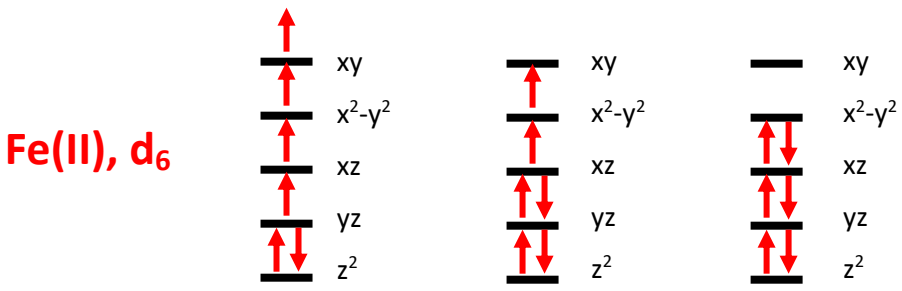

Figure 36 – A d_6 Fe(II) centre can adopt quintet (S=2), triplet (S=1), or singlet (S=0) spin states, as shown in the simple diagrams above. The d orbitals are assigned based on previous studies — [253] note the above diagram should not be taken as indicative of their relative differences in energy.

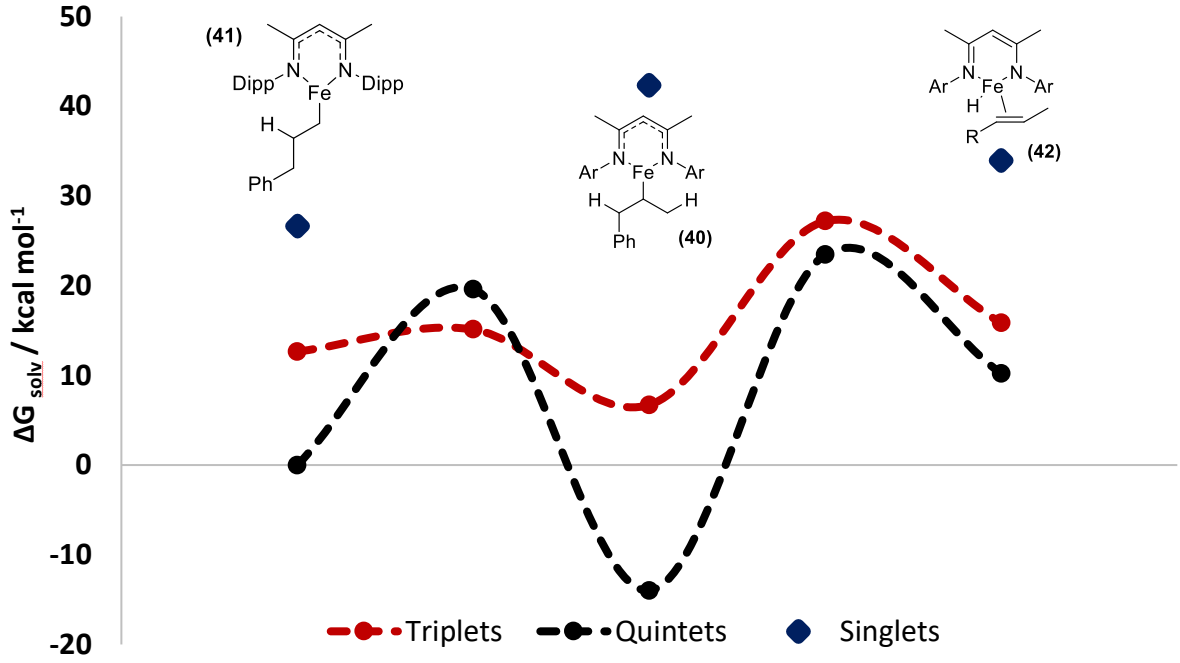

Figure 37 – Predicted energies and transition state energies of for the iron(II) alkyl mechanism (*trans* selective). The singlet surface is high in energy for all states. The quintet state of **40** is in an energy well of considerable depth, and this appears to halt further reactivity.

Formation of the iron hydride **39** from the reaction of **1** and pinacolborane was determined to be feasible under the conditions stated, which is consistent with the ^{1}H NMR spectra observed for this process (see Section 2.8). It also appears feasible for **39** to interconvert with the dimeric hydride **43**. However, no pathway proceeding directly from **43** could be determined, and it appears that only **39** is capable of further reactivity.

The insertion step to form **40** was calculated to be feasible for both the quintet (an activation barrier of 19.6 kcal mol^{-1}) and triplet (2.5 kcal mol^{-1}) states of **16**, although the triplet state of **39** is higher in energy (+ 12.6 kcal mol^{-1} relative to the quintet state). For both spin states the transformation is exergonic. The singlet state of **39** is considerably higher in energy (+26.7 kcal mol^{-1} relative to the quintet) and the insertion step is endergonic (+ 29.6 kcal mol^{-1}) — the transition state could not be determined. Regardless, it is pretty clear the reaction does not proceed on a singlet surface.

The previously discussed 1,2-shift from **41** to **40** appears feasible, should it occur at all. It is possible that this occurs through a spin crossover, as the triplet transition state is significantly lower than the quintet transition state (14.5 kcal mol^{-1} vs. 19.6 kcal mol^{-1}), although crossing points were not investigated further for this transformation.

Of greater interest is the subsequent β-hydride elimination step to eliminate the *trans* product. The lowest energy state for **40** is the quintet, and it exists in a relatively deep energy well, which seems to further decrease the likeliness of **41** forming at all, as it is considerably less thermodynamically favoured. The consequences of this are that the barrier to reforming **42** through elimination to form the *trans* product is rather high in the quintet state (37.4 kcal mol^{-1}), which seems thermodynamically unfeasible through Eyring-Polanyi analysis. The triplet state has a relatively high transition state energy, but the barrier to activation is significantly lower (20.1 kcal mol^{-1}) owing to the higher energy of the triplet state at **40**. Despite this, reaction progression along the triplet state

appears impossible, as the barrier for spin interconversion at **40** is too low and it will quickly adopt the quintet state. As the catalytic cycle cannot close, this shows the iron hydride mechanism cannot occur because the β-hydride elimination step is not feasible.

In the alkyl-mechanism proposed and studied by Turculet & Stradiotto for isomerisation-hydroboration, the alignment of the hydrides with respect to the substrate is important in allowing the reaction to proceed. [123] In this study, altering the conformation (by proceeding through a rotation of **40**) does not lead to the elimination step becoming feasible.

This offers some rationalisation on why isomerisation is observed as an underlying process in both hydroboration and transfer hydrogenation, but not in isomerisation alone through an alkyl Fe(II)-based mechanism. In both hydroboration and transfer hydrogenation, protonation of the iron centre is by an external source rather than through an intermolecular process, and the barrier of this has been shown to be considerably lower than the one determined above. [218] This avoids the reaction getting 'stuck' in an energy minimum and allows the process to be catalytic.

As was determined in Sections 2.5 and 2.6, the iron(II) hydride mechanism was further disproved through synthetic and isotopic studies, and the alternative allyl mechanism shown in Scheme 85 was proposed. This was also studied through DFT.

Iron(I) species have two potential spin states (doublet and quartet), while in the iron(III) oxidation state three potential spins states (doublet, quartet and sextet, all shown in Figure 38) can be adopted. The below orbital assignment is based on the same non-uniform trigonal planar structure observed for **1**, although given the coordination environment varies along the catalytic cycle it is possible the energy order is altered.

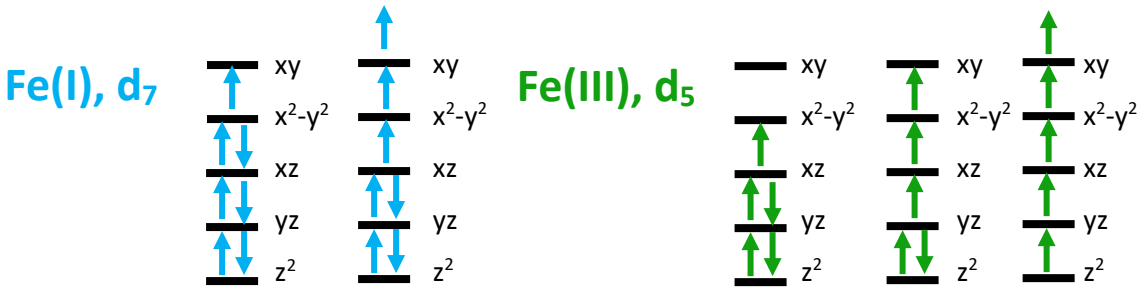

Figure 38 – The doublet and quartet states are possible for iron(I) centres, and the sextet state is further available for iron(III) species.

As **44** has been shown to experimentally to exist in the S = ½ (doublet) state, and the electronic structure of **47** has been shown to be very similar to **44**, we would predict **47** also exists in the lower spin state. However, DFT studies indicate that the quartet state is actually the more stable by 20.4 kcal mol^{-1}. Because of this, the mechanism was examined in starting from both the doublet and quartet states starting with the *trans*-forming reaction.

The oxidative addition process to form **48** is the most crucial step of the reaction as this initiates the redox process and (presuming *cis-trans* interconversion does not occur) determines the stereoselectivity of the product. **47** must initially adopt a conformation slightly higher in energy than the lowest state to be able to have the correct alignment to react, although the energy barrier

for this is low (0.3 kcal mol^{-1} to form the pre-*trans* doublet state, 0.4 kcal mol^{-1} to form the pre-*trans* quartet state). The regioselectivity is evaluated by investigating formation of the *cis* isomer below, but initially the spin selectivity was investigated. For the quartet the barrier to form the *trans* selective intermediate is exceptionally high (45.0 kcal mol^{-1}), whilst from the doublet it appears to be the more reasonable barrier of 25.7 kcal mol^{-1}. A simple molecular orbital approach rationalises this again, as there is no vacant d orbital for the C-H bond to interact in to in the quartet state, whereas the doublet state has an empty 3d orbital to serve as the LUMO. Furthermore, if the iron(I) species crossed readily to the quartet state, we would expect additional EPR signals or a change of the observed signal over time; this is not the case. The most reasonable conclusion to us is that the spin interconversion barrier of **47** from the doublet to quartet is too high, and the reaction instead remains on the doublet surface allowing catalysis to proceed. This was observed in similar circumstances by Smith. [255]

From the doublet *trans*-selective species **48** the reductive elimination has a relatively small activation barrier (2.7 kcal mol^{-1}) to generate the trans **49** species (Figure 39). The overall reaction of allylbenzene to trans-β-methylstyrene has a net exothermic energy of −4.6 kcal mol^{-1}, providing the driving force to allow the reaction to proceed to high yield.

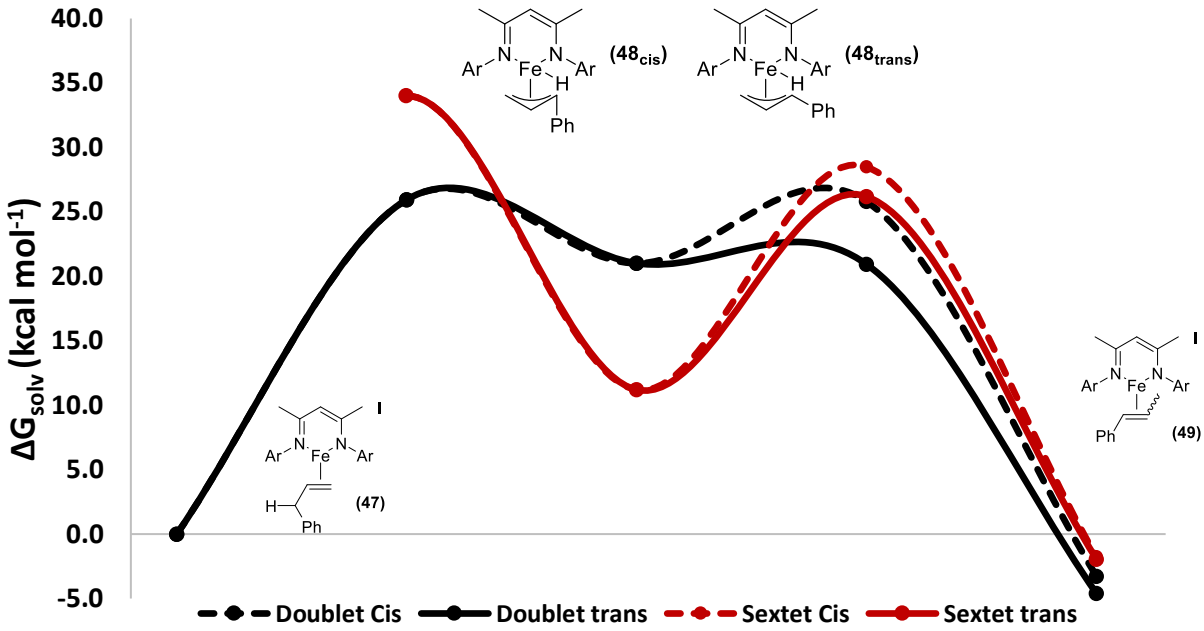

Figure 39 – Reaction profile for the allyl mechanism. Energies are taken relative to **47**$_{trans}$ for the trans cycle and **47**$_{cis}$ for the cis cycle (doublet spin state). For **48** the sextet state is considerably lower in energy than the doublet surface (for both structures), suggesting a spin crossover could occur as part of catalysis.

This confirms that the doublet surface provides a feasible pathway across the reaction profile. The quartet state appears to not be capable of performing the oxidative addition for the *trans* product, so can be ruled out as participating in catalysis despite its lower initial energy. The reaction cannot wholly take place on a sextet surface as neither **47** nor **49** can form a sextet state. **48** can form a sextet state, and it is 3.1 kcal mol^{-1} lower in energy than the doublet state, which raises the potential that the spin crossover occurs. Unlike the quartet state for **47**, it appears that the sextet state for **48** could react further in a second spin crossover event to revert to the doublet state of **49** (Figure

40). Despite some efforts, the minimal energy crossing points (MECPs) for the doublet-sextet crossover could not be determined for structures about the proposed transition state steps.

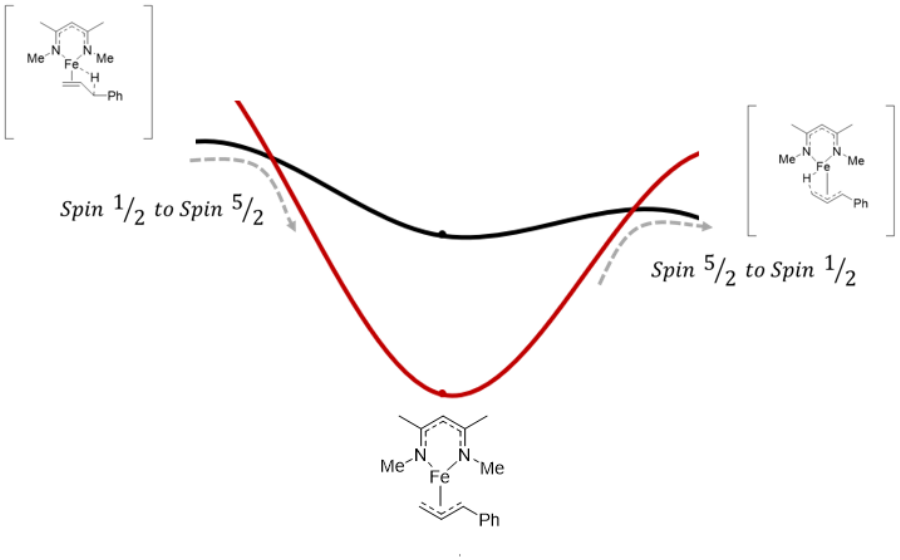

Figure 40 – Potential spin crossover events from doublet to sextet and the reverse about the formation of **48**. This is feasible for both the *trans* and *cis* selective pathways.

To investigate whether **48** can undergo spin interconversion, vertical excitation energies were calculated for **48** and associated transition states, both from doublet to sextet and the reverse process. In both cases, the energy barriers to interconversion are very low (< 0.1 kcalmol^{-1}) so spin interconversion should be facile. This does not confirm that spin interconversion takes place as part of the catalytic cycle, and it may be the sextet exists as a form of resting state before subsequent spin interconversion and then reductive elimination as two distinct processes. It should also be noted that depending on the functional used the difference in energies of the doublet and sextet vary – for example modelling with a BP86 functional for both predicts the doublet to be the lower in energy. A table of varying functionals, as well as an alternate basis set and their outcomes on the relative energies of the spin states is given in Section 7.2. For the purposes of this cycle, we cannot rule out a sextet formation at **48**, but we have no definitive evidence of the reaction proceeding along the sextet surface, and it remains equally feasible for the reaction to proceed solely in a doublet manner.

The parallel mechanism generating the *cis* product can also be calculated. **47** must be in an alternate conformation leading to the alternate C-H bond being activated. This is overall 2.4 kcal mol^{-1} higher in energy than the trans formation, so it is less favourable but still reasonably accessible, although the determined value is close to the lower limit of Density Functional Theory's chemical accuracy. The oxidative addition step in itself is extremely close in energy terms to the *trans*-forming process, leading to their overlap in Figure 39. Reductive elimination of the *cis* product also requires a slightly higher activation barrier. This explains both the *trans* preference for the catalytic cycle, as well as why some *cis* product is still observed. The *cis* oxidative addition transition state could not be determined in either the quartet or sextet spin state.

Table 12 – The catalytic pathway to the trans product has lower energy activation barriers as well as a greater overall reaction driving force. However, the cis product is still accessible across the mechanistic cycle, hence its formation to some degree. Note that the oxidative addition steps listed here include the energy required to form the correct conformer of **47**.

Selectivity	Activation Barriers ($\Delta G^{\ddagger}$) / kcal mol^{-1}		Overall Reaction / kcal mol^{-1}
	Oxidative Addition	Reductive Elimination	
Trans	25.7	2.6	−4.6
Cis	28.1	4.8	−3.3

The DFT studies above reinforce our previous synthetic proposals. Firstly, catalysis with the iron(II) hydride **39** which was ruled out experimentally was shown to be thermodynamically unfeasible, in particular with respect to the required β-hydride elimination step. Secondly, a cycle beginning with **44** does appear to be feasible, proceed through a redox-active allyl pathway, and to be able to rationalise the *trans* preference of the reaction. Although we cannot fully confirm the spin state of the entire process, a solely doublet surface is feasible but a spin conversion to the sextet state in the iron(III) species is also possible — the quartet state does not appear to be involved. Thirdly, the oxidative addition appears to be rate determining rather than reductive elimination owing to the considerably higher activation barrier, consistent with KIE studies.

2.10 Applications of Iron-Catalysed Double Bond Isomerisation

Ozonolysis of alkenes

While most alkene functionalisations involve addition reactions over the carbon-carbon double bond, there are more unusual processes where the carbon-carbon double bond is instead selectively cleaved, the most utilised of which is ozonolysis. Ozonolysis is considered a green route towards the synthesis of carbonyls, owing to the flexibility of required substrates and the relatively clean synthesis of ozone compared to most oxidizing agents, although it has some unique challenges on large scales. [256] To apply our isomerisation chemistry further, we opted to perform a further oxidation process to enable the synthesis of piperonal. Piperonal is commonly used as a cherry or vanilla flavouring in foods and fragrances, even being used in ice cream. [257]

Synthesis of aldehydes *via* ozonolysis of alkenes represents a clean, atom efficient and relatively green reaction pathway. Direct ozonolysis from isosafrole is not ideal, as it is more challenging to prepare and more expensive than safrole, and as such routes starting from safrole are more desirable. Most reported routes from safrole require large excesses of base [258] or more toxic metals [259] to achieve this transformation, either as a two-step isomerisation-oxidation process or with one-pot methodologies.

By performing isomerisation of safrole under our general reaction conditions, followed by an ozonolysis procedure with a reductive workup (Scheme 92), we were able to obtain piperonal is a reasonable yield. Because of the nature of the ozonolysis reaction, both *E* and *Z*-isosafrole are converted into the same product. Although there is some room for further reaction optimisation, this demonstrates an appreciably facile route for the synthesis of piperonal.

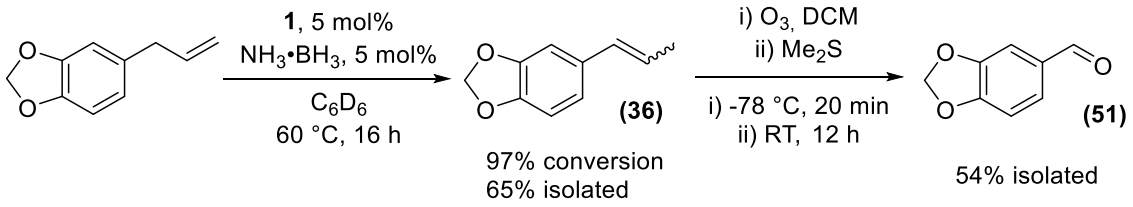

Scheme 92 – Synthesis of piperonal from safrole using our reported isomerisation catalysis and ozonolysis.

Sequential isomerisation-hydroboration studies

As discussed, hydroboration is relatively unusual in terms of addition reactions owing to its anti-Markovnikov regioselectivity. Whilst in many cases this is desirable, it also increases the challenge of synthesising more substituted organoboranes. Given that **1** has been previously reported as an effective hydroboration catalyst, and has in this chapter been shown to be adept at double bond isomerisation, it seems plausible that both transformations can be performed in a 'one-pot' reaction.

To do this, allylbenzene was isomerised under the standard reaction conditions, and after 16 hr a full equivalent of pinacolborane was added to the reaction. The $^{11}B\{^{1}H\}$ signal for the anticipated internal hydroboration product is practically indiscernible from the terminal product (δ = 36.6 vs 37.0 ppm), so observation of the methyl and alkyl peaks in the ^{1}H NMR was used to determine conversion.

In the 'one-pot' conditions detailed in Scheme 93, conversion is poor, and a significant amount of the terminally-hydroborated product is still isolated. This poor yield is likely explained as a significant amount of the metal has been reduced to Fe(I), whereas the hydroboration proceeds through Fe(II) centres. **1** is already relatively poor as a catalyst for the hydroboration of internal alkenes as previously reported, [217] so this reduction in activity has a major effect on conversion.

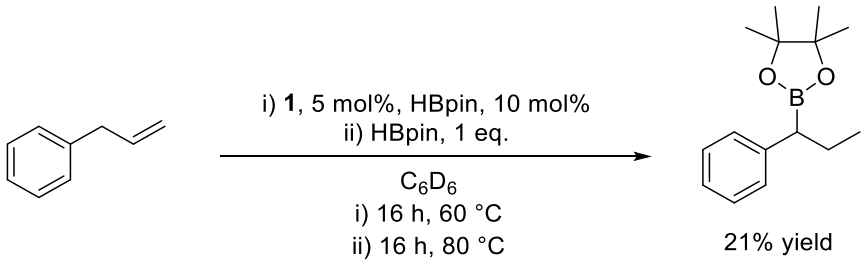

Scheme 93 – "One-pot" synthesis of a more substituted hydroboration product

A subsequent two-step synthesis shows that if the isomerisation product is isolated, then reacted in the presence of fresh catalyst, the conversion is as would be expected (Scheme 94). A further improvement can be attained by using **26** instead of **1** in the second step, which is considerably more adept at the hydroboration of internal alkenes.

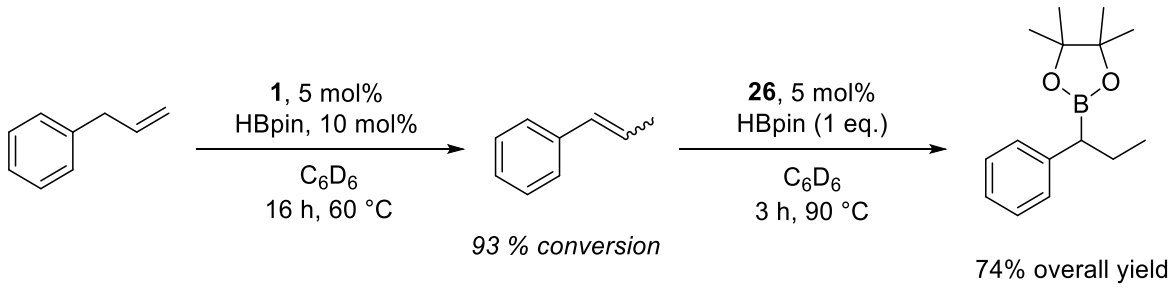

Scheme 94 – Two step synthesis of more substituted hydroboration product leads to a considerably higher yield.

By further utilising ozonolysis and hydrofunctionalisation on top of isomerisation chemistry we can generate compounds that are functionalised at initially saturated carbon centres. However, it appears **1** is ill-suited to performing the latter in a one-pot strategy.

2.11 Conclusions from Chapter 2

The reported synthetic study and investigations provide clear differences in catalytic performance and mechanism compared to previous reports. Activation of a pre-catalyst through the use of the hydridic reagents reported herein is a relatively uncommon process, and the reported reduction of the iron centre as opposed to σ-bond metathesis or other redox neutral methods is highly unusual, as it contrary to previous behaviour reported with **1** previously and in similar catalytic systems discussed in the introduction.

In terms of catalytic performance, there are clear limits on both functional group tolerance and the conditions required; some of the palladium systems discussed in the introduction (particularly the work from Danishefsky, Lindhardt and Skrydstrup) are considerably more tolerant and perform catalysis at lower loading and more facile conditions. [81] When compared to other catalytic systems using iron or cobalt, some studies have similar conditions and functional group tolerance (for example, the report by Findlater [106]), whereas others proceed over lower temperatures and shorter timescales (for example, the report by Xia [107]), although the system investigated does have some activity for simple linear alkenes, which is not commonly reported. The cis-trans selectivity of the reaction is predominantly trans selective – this is in common with the majority of previous studies. Modulation of the ligand did not have a major effect on selectivity and conversion, contrasting to the cobalt-based studies of Holland and Xia. [52]

A key difference, and what makes this study particularly noteworthy in the field, is the difference in mechanistic pathway between previously reported first-row catalysed studies and this one. Previous mechanistic studies into these reactions generally propose an alkyl mechanism, whereas in this study an allyl mechanism has been proposed and studied. This involves a two-electron oxidation/reduction process which is common for heavier transition metals but highly unusual for iron, and demonstrates that iron can behave like a heavier metal with the correct ligand environment and catalytic demands. Demonstration of ‘palladium-like’ behaviour in iron is desirable and indicates that further catalytic transformations that are generally limited to precious metals may be applicable to iron under the correct conditions.

Chapter 3 – Iron-catalysed Polymerisation of Arylallenes

As discussed in the introduction, allenes exhibit both analogous and divergent reactivity compared to alkenes. Given the range of reactions that iron catalysts can perform on alkenes (as reviewed and shown in Chapters 1 & 2), it seems likely that iron catalysts can perform corresponding transformations with allenes. In this chapter, the polymerisation of allenes catalysed by iron complexes is investigated. Furthermore, some investigations into forming dimeric and related species are also studied.

This chapter has been adapted and accepted for publication as *Polymerization of Allenes by Using an Iron(II) β-Diketiminate Pre-Catalyst to Generate High Mn Polymers* C. R. Woof, D. J. Durand, R. L. Webster, Chem. Eur. J., **2021**, 27, 12335

3.1 Preparation of Phenylallene and Reactions with Iron Complexes

Relatively few allenes are commercially available, so most compounds containing allenes require synthesis prior to use. There are well developed routes to many allene sub-structures that proceed relatively cleanly and from cheap starting materials. In this study, an adaptation of the Doering-Moore-Skattebøl reaction was used to synthesise a range of allenes. This was initially developed in 1958 by Doering and LaFlamme, with significant improvement from Moore and subsequently Skattebøl. Partly because of this sequential modification, and partly because of the range of substitutes it is amenable to, the range of conditions is vast. In all cases the underlying reaction pathway is formation of a gem-dibromocyclopropane, followed by a subsequent Skattebøl rearrangement to generate the consequent allene. Example reagents and the generally accepted mechanism are shown in Scheme 95.

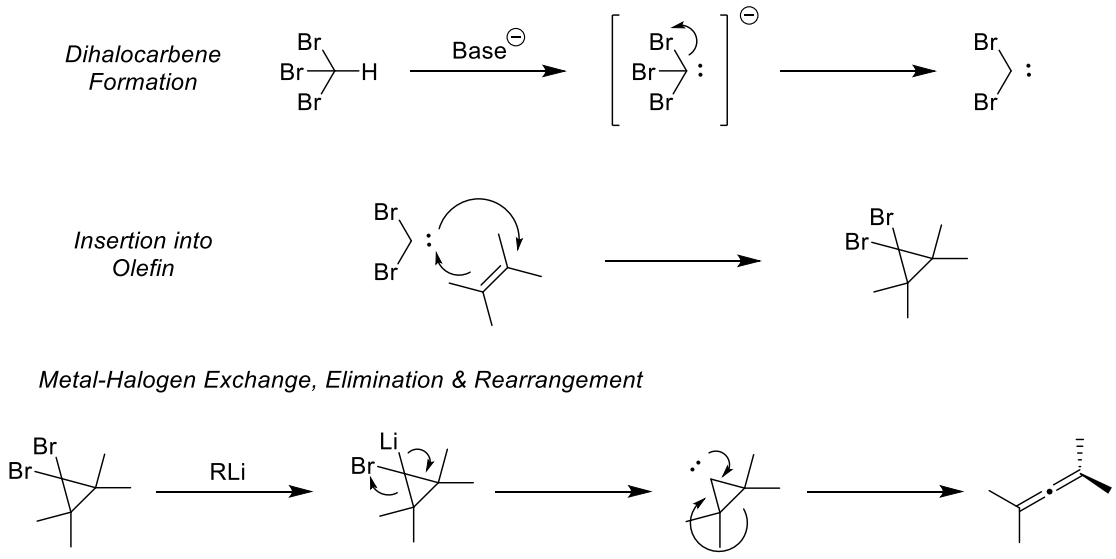

Scheme 95 – Generalised Doering-Moore-Skattebøl synthesis of allenes, and the accepted mechanistic pathway.

When using styrene as substrate, phenylallene **52**, is synthesised as the product. The conditions used for this are given in Scheme 96. This preparation was adapted from the procedure reported by Buono, [260] and can generate phenylallene on the gram scale cleanly and effectively, as well as functionalised derivatives. A wide range of styrene derivatives are commercially available or can be synthesised from the corresponding aldehydes, so this preparation can be used to synthesise a wide range of allenes.

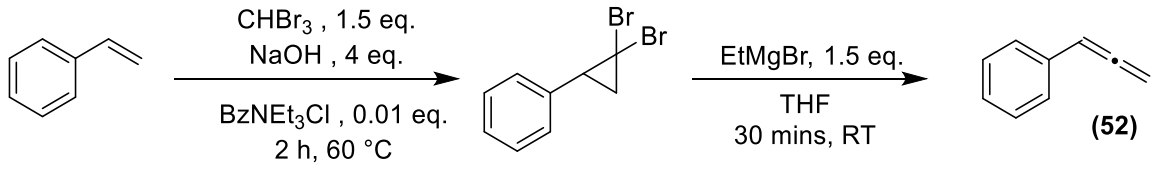

Scheme 96 – Synthesis of arylallenes used in this study.

Phenylallene has distinctive ^{1}H NMR signals at δ = 6.17 and 5.17 ppm, corresponding to the allenyl protons; the aryl peaks are less well-defined. Consequently it is relatively easy to monitor conversion and reaction of the allenyl group with an NMR internal standard. It was initially hoped that some form of isomerisation could be performed, as in the case of alkenes. Rather than alkene-alkene isomerisation, an allene-alkyne step was instead targeted. There are relatively few cases of this transformation being performed. The internal alkyne is more stable than the allene so the transformation can be performed catalytically, a notable recent report is from Tsurugi and Mashima using **53**, [261] and it has also been reported as an intermediate step in other catalytic transformations. [262] The terminal alkyne is less stable so generally requires further reagents, for example the use of cuprates as reported by Fleming (Scheme 97). [263]

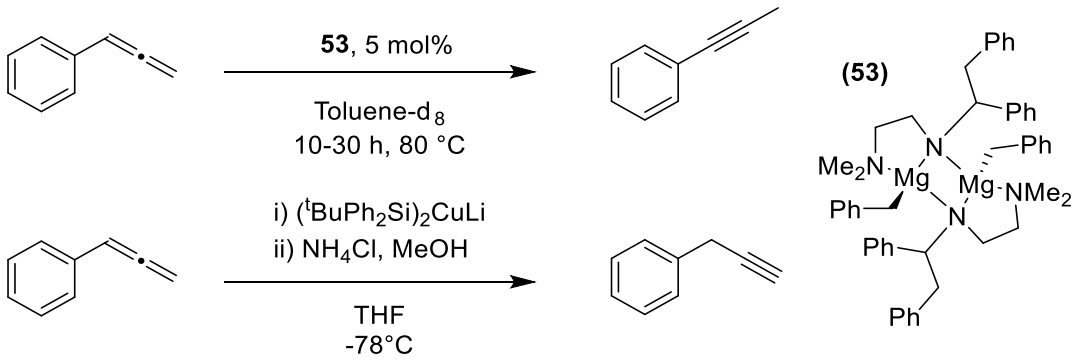

Scheme 97 – Previously reported isomerisation of phenylallene to alkynes.

Reacting iron catalyst **1** with phenylallene does not lead to any significant change to the ^{1}H NMR signals associated with phenylallene, nor any new signals forming in the diamagnetic region (δ = 0–10 ppm). Over time (and with heating), new signals are observed to form in the paramagnetic region; these are small compared to the catalyst after 1 hour of heating, but after one week of heating do increase in intensity when compared to the pre-catalyst. It is postulated that, similar to the reaction with allylbenzene in Chapter 2, phenylallene undergoes slow σ-insertion across the iron-carbon bond, but this does not lead to further catalytic activity. Quantitatively comparing these peaks to the starting material shows that only a small fraction of a percent of the substrate is

undergoing this reaction, and as in isomerisation chemistry these complexes are considered to be catalytically inactive. These species could not be isolated crystallographically despite attempts to do so.

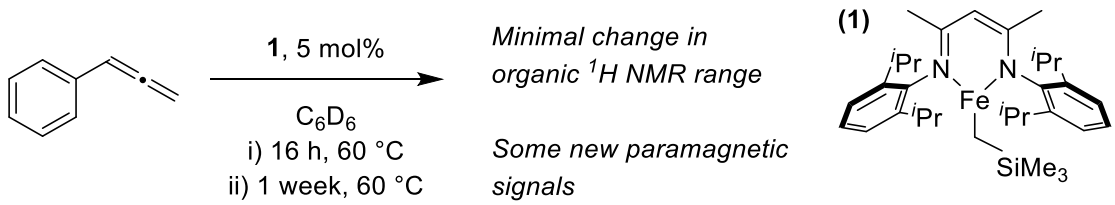

Scheme 98 – Reaction of phenylallene in a catalytic amount of **1** does not lead to any organic transformation, although some change to the paramagnetic NMR is observed.

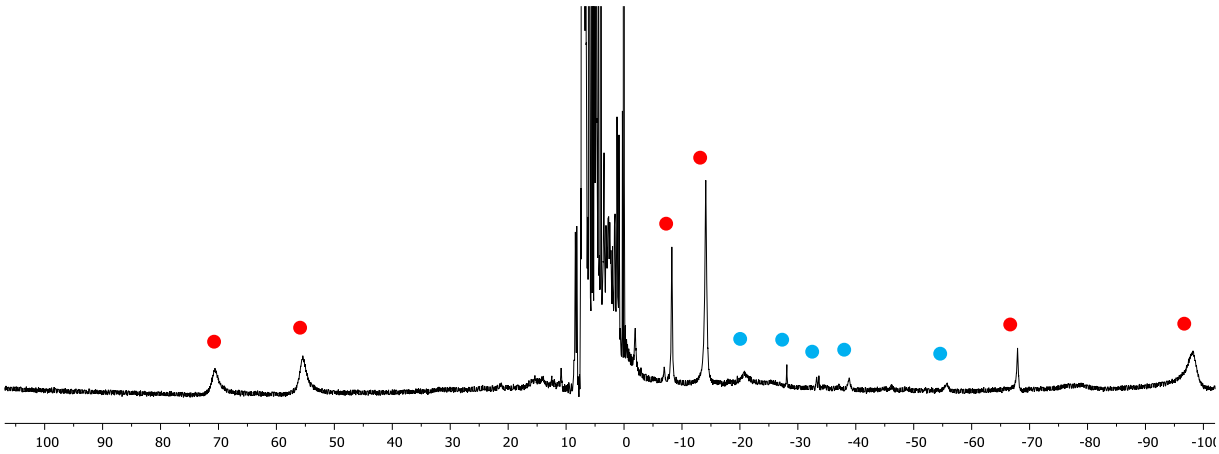

Figure 41 – Wide sweep NMR of the reaction shown in Scheme 98 after 1 hour. The paramagnetic region primarily comprises signals that can be assigned to **1**, identified by **red** ●, with a small number of new signals in the δ = −20 to −60 ppm range identified with **blue** ● (500 MHz, C_6D_6).

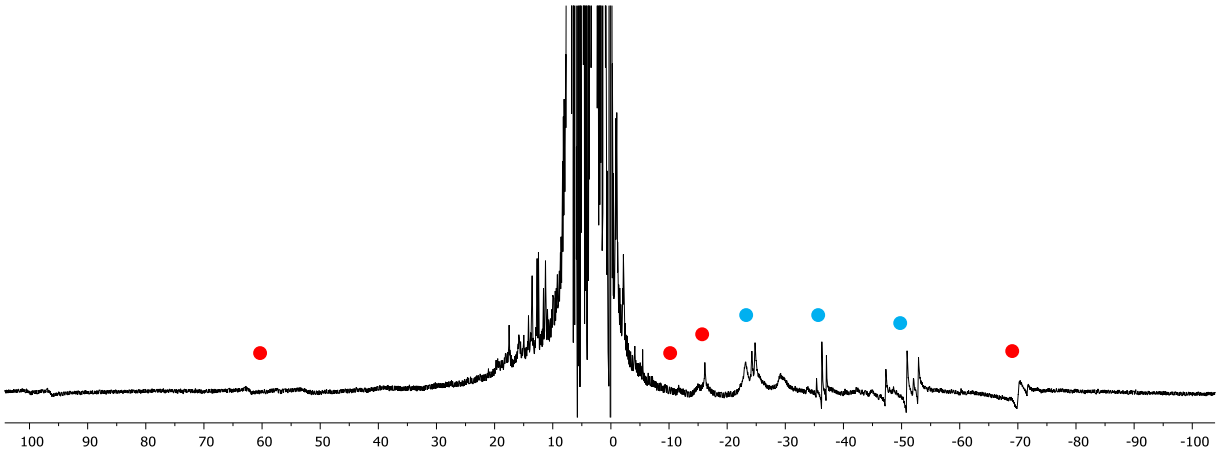

Figure 42 – After one week of heating, the signals for **1** are considerably weaker and the newer signals considerably stronger and more complex (500 MHz, C_6D_6).

Just as the isomerisation chemistry requires an additional hydride source to proceed when using **1**, it was proposed that an additional reagent was also required to perform catalysis with phenylallene. When ammonia borane is added to the reaction, there is significant consumption of the starting ^{1}H

NMR peaks of phenylallene. The internal alkyne isomer would be expected to have a terminal methyl signal at around δ = 1.7–2.0 ppm, but this is not observed, and neither is the spectra consistent with the terminal alkyne. Instead, a sharp signal at δ = 6.17 ppm is observed as well as three peaks at δ = 3.42–3.72 ppm. These peaks on first instance appear to be a triplet, however this is not the case — the peaks do not integrate as a conventional splitting pattern, are not spaced equally apart and the two end peaks are not equal in intensity (from left to right the ratio is approximately 0.6 : 1 : 0.65, in Figure 43 they are shown integrated relative to the signal at δ = 6.17 ppm). Several other smaller signals are also formed.

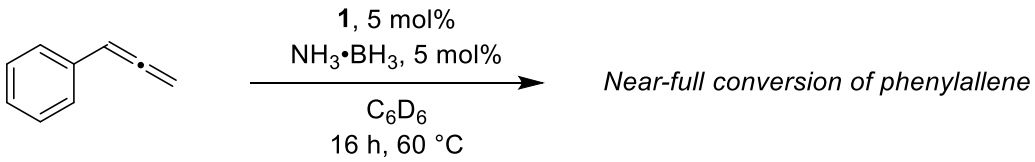

Scheme 99 – Adding a catalytic amount of ammonia borane to the reaction leads to near-complete conversion of phenylallene.

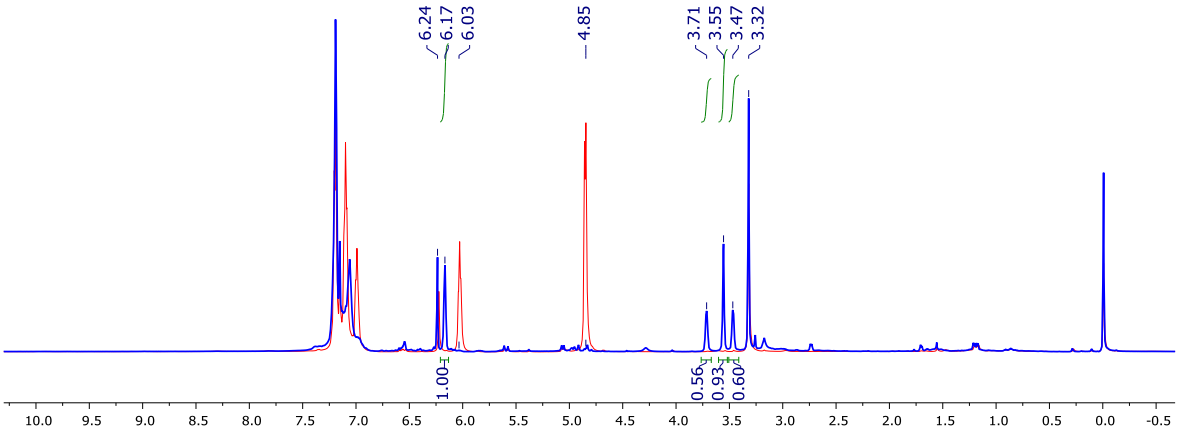

Figure 43 – Stacked NMR showing the reaction shown after 15 minutes (**red**) and 16 hours (**blue**). The initial phenylallene peaks at δ = 6.03 and 4.85 ppm are completely consumed, and new signals are formed. The signals at δ = 6.22 and 3.32 ppm are 1,3,5-trimethoxybenzene, used as an internal standard (500 MHz, C_6D_6).

Upon working up, a brown solid is formed that is insoluble in pentane and other non-polar solvents but soluble in THF. This can be isolated from the metal residue by passing through silica using THF as the eluent (full experimental details are given in Section 7.3).

Through further analysis of the isolated product (*vide infra*), it was determined that phenylallene is being polymerised in this reaction to form poly(phenylallene). Polymers containing allenes are relatively unusual; a summary of recent and notable reports are given in Section 1.4. Because of the unusual nature of this process, both the polymer and the reaction undergone to produce it were investigated further.

3.2 NMR Studies of Poly(phenylallene)

As mentioned in Section 1.4, there are two potential polymeric products possible from the polymerisation of monosubstituted allenes – the (2,3)-structure, sometimes referred to as the terminal isomer, and the (1,2)-structure, sometimes referred to as the internal isomer. These arise

depending on which of the double bonds is added over in the polymerisation process, with nomenclature assigning the carbons C_1 through C_3 in accordance with their distance from the functional group (Figure 44). The ^{1}H and ^{13}C NMR data for the (2,3)-structure has been previously reported (see citations in Section 7.3), but to our knowledge NMR assignment of the (1,2)-structure has not been reported previously.

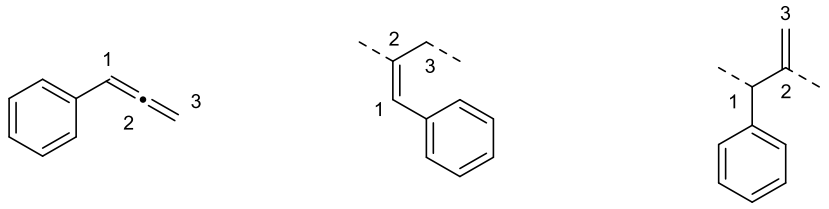

Phenylallene (2,3)-polymer (1,2)-polymer

Figure 44 – Numerical assignment of the allenic positions, which in turn describes the two polymeric structures depending on whether the activation occurs across the terminal (2,3) or internal (1,2) double bond. This nomenclature is used in this chapter and in Section 7.3 when assigning structures.

The main signals observed in the reaction are consistent with the (2,3)-structure forming. The *H*C_1 proton appears as a well-defined singlet, while the *H*C_3 protons are responsible for the three singlets observed in the δ = 3.47–3.71 ppm range. The (2,3)-structure has no formal tacticity as there are no chiral centres present, and further discussion on this NMR pattern is discussed below. The (1,2)-structure can also be identified, although it constitutes less than 15% of the overall polymer. In the latter case, C_1 is a chiral centre meaning that a range of tacticities are possible. The terminal alkene also induces complexity into the structure, and two distinct signals are observed for the terminal *H*C_3 environment. ^{1}H NMR spectral data and assignments are shown in Figure 45.

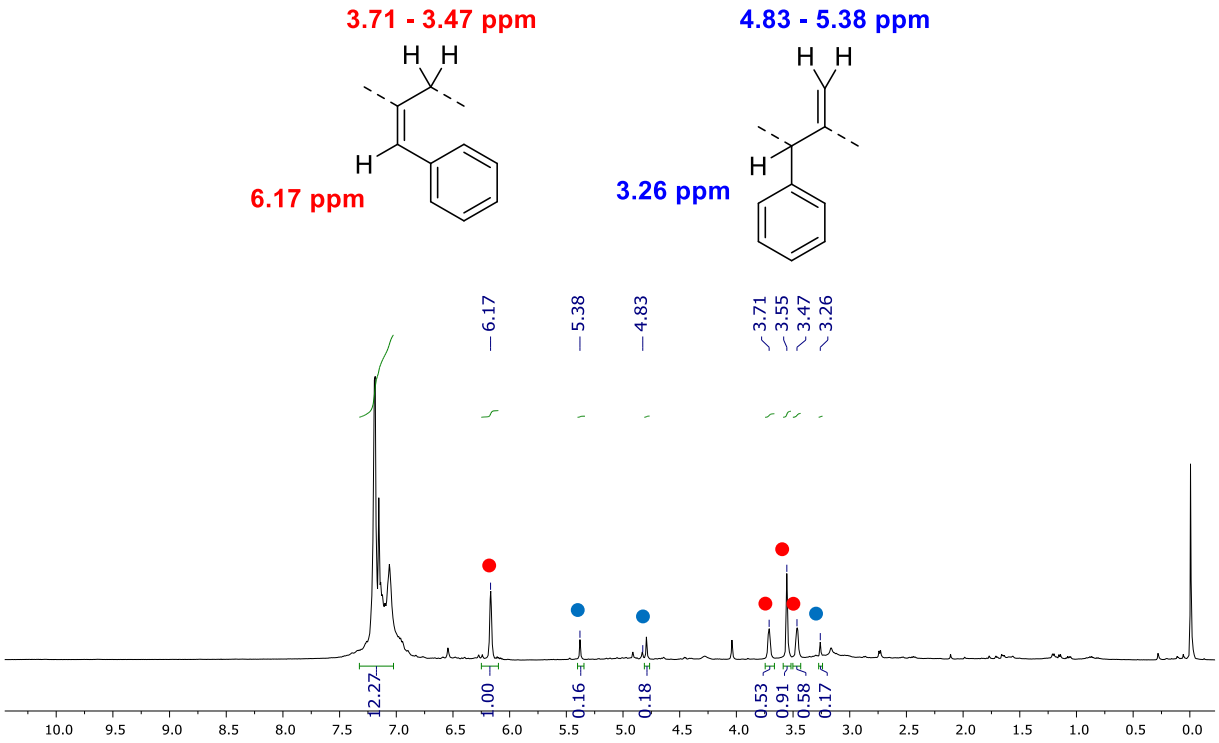

Figure 45 – ^{1}H NMR spectrum of the polymer (500 MHz, C_6D_6), and the NMR assignments of the respective structural isomers. The major (2,3)-polymer signals are denoted with ●, whilst the minor (1,2)-polymer signals are denoted with ●.

The $^{13}C\{^{1}H\}$ NMR can also be assigned. HSQC and HMBC NMR can be used to determine the assignment using the proton signals. For the (2,3)-structure there is again a clear triple splitting with each C_3 signal correlating with a distinct *H*C_3 signal. There are also three signals for both the C_1 and C_2 environments; their differences in chemical shift are considerably smaller. Each C_2 centre can again be correlated with a distinct *H*C_3 signal, while the C_1 signals are too close to each other in terms of chemical shift to determine specific correlation (Table 13). For the (1,2)-structure there is more than one signal for each position, and in this case for all three carbons the difference is reasonably large. This again highlights the more complex spatial arrangements possible for this structure. The aromatic ^{13}C NMR signals can also be assigned for the (2,3)-structure through HMBC NMR; for the (1,2)-structure these correlations are too weak to determine them fully. The non-aromatic chemical shifts, along with the NMR spectra are shown in Figure 46; full structural assignment is detailed in Section 7.3.

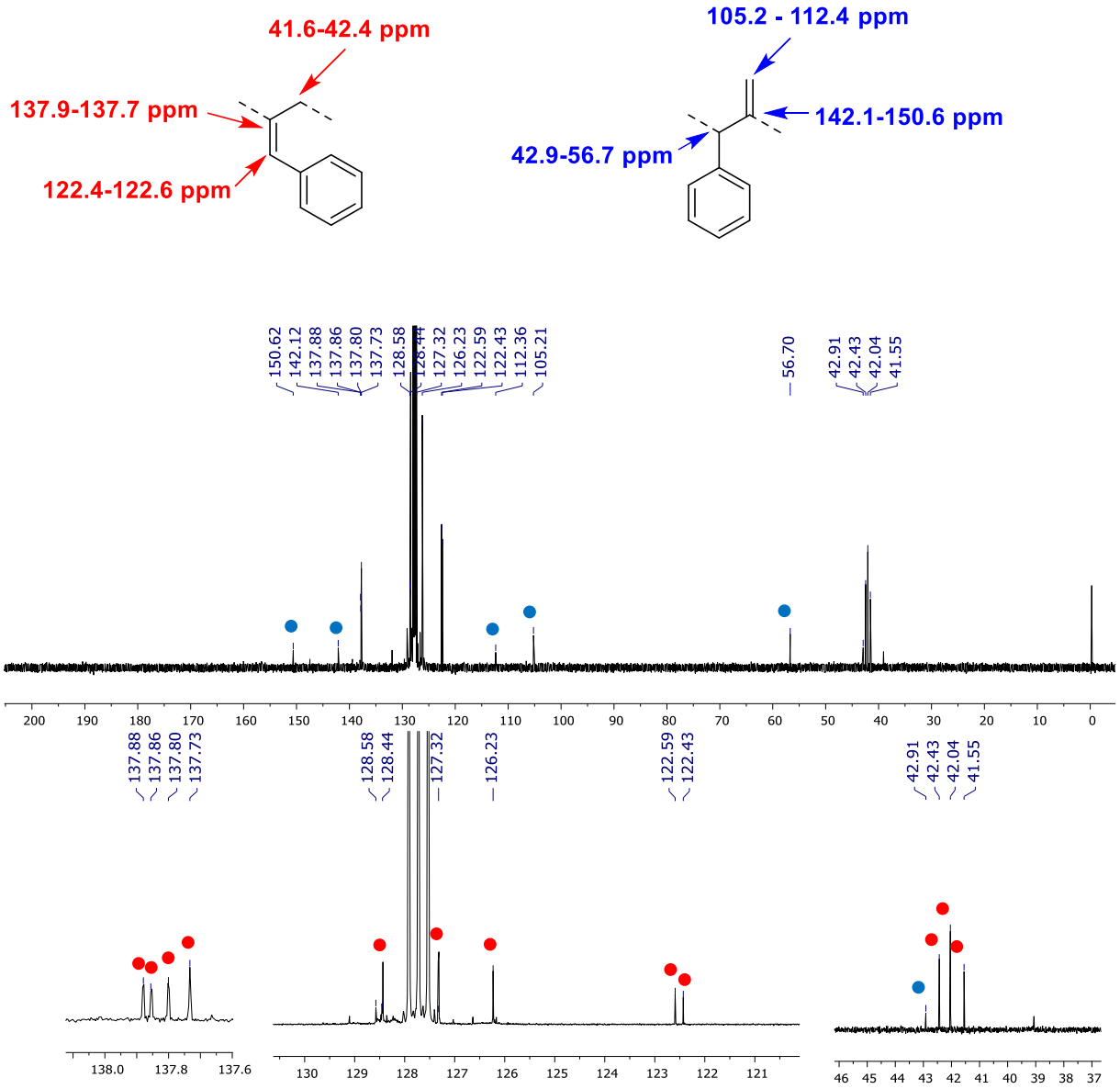

Figure 46 – ^{13}C assignments for the non-aromatic carbons in both structures, and the $^{13}C\{^{1}H\}$ NMR (126 MHz, C_6D_6). The major (2,3)-polymer signals are denoted with **red** ●, whilst the minor (1,2)-polymer signals are denoted with **blue** ●.

Table 13 – Summary of HSQC correlations between *H*C_3 and C_3 and HMBC correlations between *H*C_3 and C_2.

Nuclei	^{1}H δ / ppm	$^{13}C\{^{1}H\}$ δ / ppm
HC_3 / C_3	3.72	41.5
	3.56	42.0
	3.47	42.4
HC_3 / C_2	3.72	137.7
	3.56	137.8
	3.47	137.9

NMR spectroscopy clearly shows the reaction is selective towards the (2,3)-structure, with a small amount of (1,2)-structure forming. In light of this, several of the reaction schemes in this chapter

have the (2,3)-structure drawn as the only reaction product — this is not an indication that these reactions are fully regioselective towards this structure but merely to simplify the schemes.

In previous reports of (2,3)-poly(phenylallene), only one alkyl ^{1}H environment is observed on the main chain, however as shown above under these conditions three distinct signals are observed, along with distinct and correlating $^{13}C\{^{1}H\}$ NMR signals. This infers there are three distinct proton environments on the polymer formed in this reaction, which could arise from certain diads or more complex conformational structures.

Some simple NMR experiments provide some insight into this. Firstly, the ^{1}H signals themselves do not strongly correlate with each other through either COSY or NOESY NMR experiments. This implies that the environments occur in distinct regions, rather than adjacent to each other. Presumably this arises from three different conformations of the polymer in the solution phase. By performing variable temperature (VT) NMR experiments, it can be shown that these conformations neither interconvert nor coalesce at high temperatures in solution (up to 80°C). This implies these conformations have high energy barriers to interconvert.

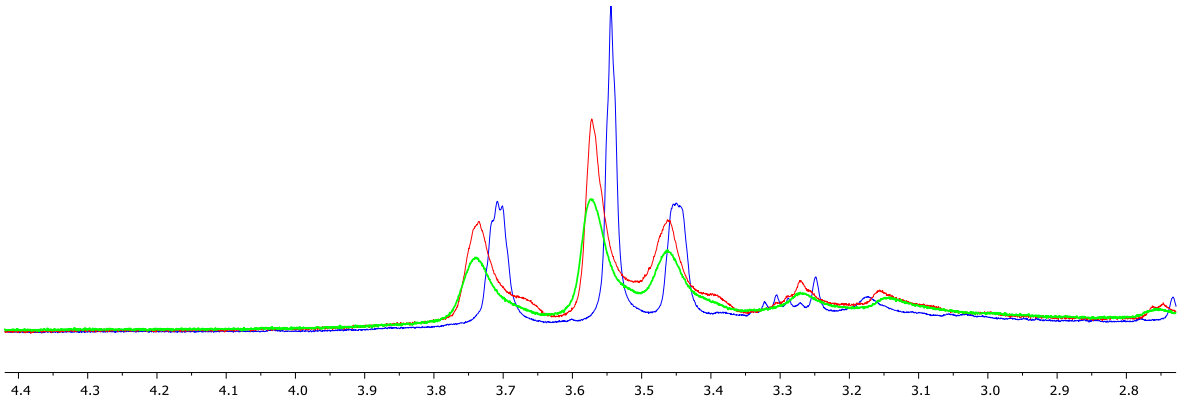

Figure 47 – The alkyl signals of the polymer shown at room temperature (**blue**), 60 °C (**red**) and 80 °C (**green**) (all 400 MHz, C_6D_6). Although there is some broadening and very minor shifting, there are still three distinct environments present even at raised temperatures.

The polymer was also heated in the solid state under an inert atmosphere to 200 °C then cooled and redissolved in solution, with no effect on the NMR. Heating above this temperature leads to product degradation. Further thermal studies in the solid state are discussed in Section 3.3.

In an effort to get a greater understanding of the conformations, further NMR studies were undertaken. NOESY NMR shows, as stated, that the alkyl peaks do not correlate, and beyond this relatively little information can be obtained from the spectra. NOESY NMR relies on the nuclear Overhauser effect (NOE) to identify protons adjacent to each other. While this effect is difficult to fully quantify in terms of distance, [264] it was hoped that differing correlations between the alkyl chain protons and other environments would give an indication of the structure. To study this further, selective 1D NOE NMR experiments were performed. This involves exciting one signal at a time and observing the effects on other signals. A positive signal is observed for the excited environment and negative (or, in some cases, weak positive and negative) signals for correlating protons; all other environments are silent.

The excitation width is sufficiently narrow to excite each of the three observed peaks in turn (^{1}H 500 MHz, C_6D_6, δ = 3.71, 3.55, 3.46 ppm respectively) and observe their respective NOE correlations. As in 2D NOESY, none of the peaks correlate with each other.

The central signal (δ = 3.55 ppm) is the simplest spectrum, in that there is no real correlation with any other environment (Figure 48). The remaining two signals do exhibit some correlation with both the alkenyl proton and the aryl region (Figure 49).

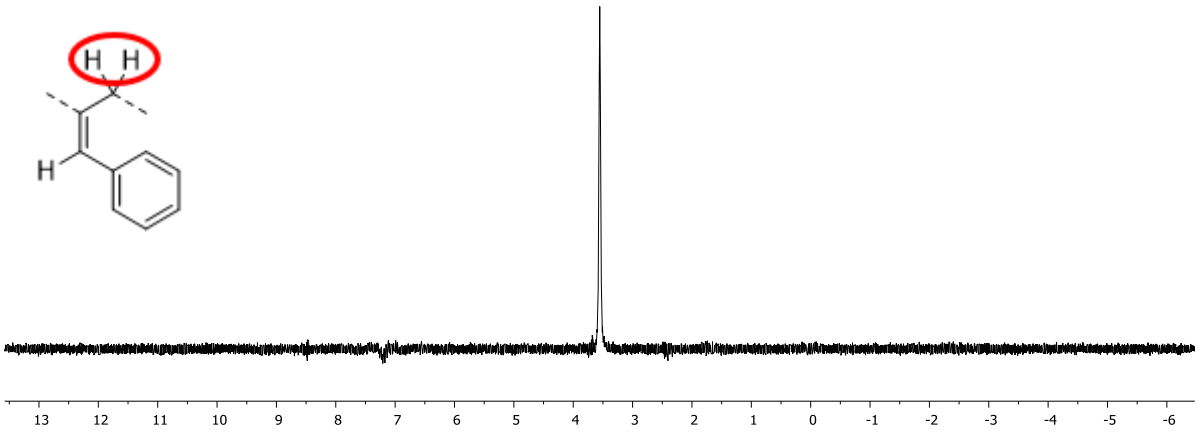

Figure 48 – NOE excitation of the central signal (δ = 3.55 ppm, protons circled) leads to no negative peaks, indicating no correlation with any other proton environment.

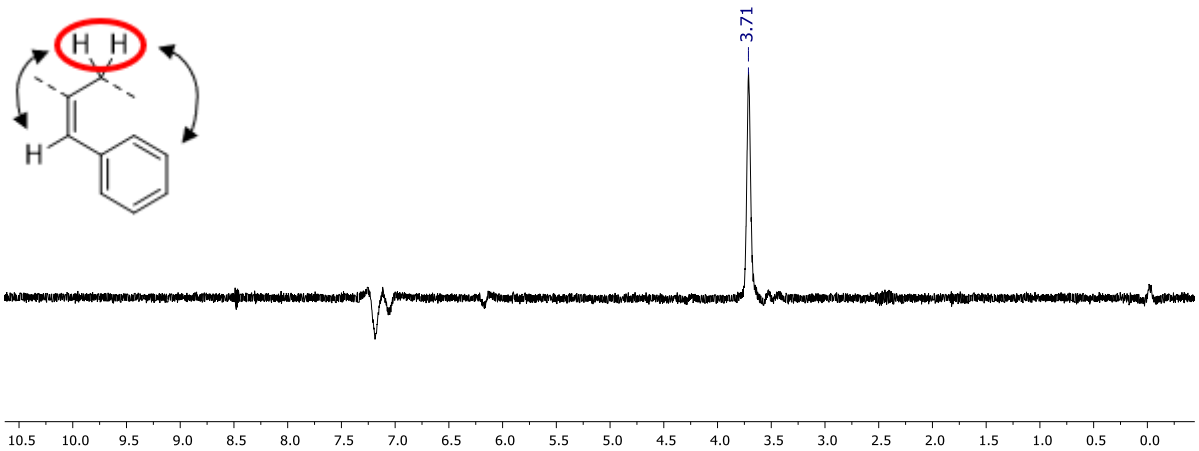

Figure 49 – NOE excitation of the downfield signal (δ = 3.71 ppm) shows some interaction with both the aryl (δ = 7.30-7.01 ppm) and alkenyl (δ = 5.97 ppm) environments. A similar outcome is found when the third signal (δ = 3.47 ppm) is analysed.

The difference is NOE signals and further NMR observations would appear to confirm that the range of signals observed arise from distinct polymer conformations in the solution state. However, NMR analysis alone is insufficient to propose what form these structures take.

To study this further, density functional theory studies were undertaken on seven-membered oligomeric structures, to observe what conformations are feasible and their relative energies (*Calculations performed by Derek J Durand, Fey Group, University of Bristol*), full experimental details are given in Section 7.3. Conformational searching yielded four unique structures – both computed and planar structures are shown below.

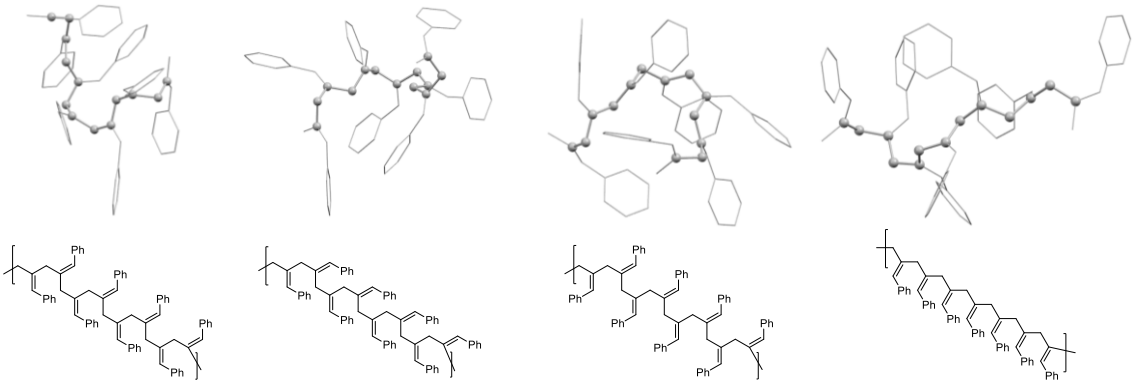

A 0.0 kcal mol^{-1} **B** 2.7 kcal mol^{-1} **C** 6.5 kcal mol^{-1} **D** 8.9 kcal mol^{-1}

Figure 50 – Modelling oligomeric structures yielded four potential conformations **A**-**D** – their energies relative to structure **A** are also shown.

As **A** is the most stable conformation, we would expect the most intense signal to belong to structure **A** (δ = 3.55 ppm). Given that two further environments are formed, it is likely these are **B** and **C**. From thermodynamics alone, **B** should form in a much greater amount compared to **C** as it is more stable (3.8 kcal mol^{-1}), although in the event they are formed in approximately equal quantities. Given only three structures are observed, it is likely that **D**, being the least stable conformer, does not form.

Modelling of population distribution indicate that occupations do not vary significantly as temperature is increased, which is consistent with the observations from the variable temperature experiments (full details in Section 7.3).

The variation in conformations contrasts to previous reports where no such difference is reported. To the best of our knowledge, no previous investigations into conformational studies have been undertaken, so previous studies are either very selective towards a single structure, or instead generate an unordered form leading to a single proton environment.

3.3 Optimisation and Structural Analysis of Polymer

NMR spectroscopy gives some insight into polymer structure, although this does not give much insight on the length of the polymer. In theory the end groups of the polymer should be identifiable in the ^{1}H NMR spectrum, and this can in turn lead to a determination of chain length; these could not be identified. This is likely because the long length of the polymer leads to the end group signals being drowned out by chain signals.

Non-NMR-based studies were undertaken to further study the nature of the polymer. Firstly, efforts were undertaken to determine the length and dispersity of the prepared polymer. Gel permeation chromatography (GPC) offers a measure of polymer size, which through analysis can determine the

key metrics of polymer length – the number average molecular weight, M_n, the weight average molecular weight, M_w, and the dispersity index, Đ.

A prepared sample of the polymer gives a relatively broad peak from GPC analysis, along with a small amount of large molecular weight material that was beyond the calibration analysis (>250 kDa). Under the conditions stated in Scheme 100, the calculated M_n is 159 kDa, with a Đ of 1.76 (Further details of the methodology are given in Section 7.3). By knowing the molecular weight of the monomer (116 $gmol^{-1}$) the degree of polymerisation (DP) can be determined to be 1370 units on average. This is considerably longer than the polymerisation reported by Endo [139] or Cui [144].

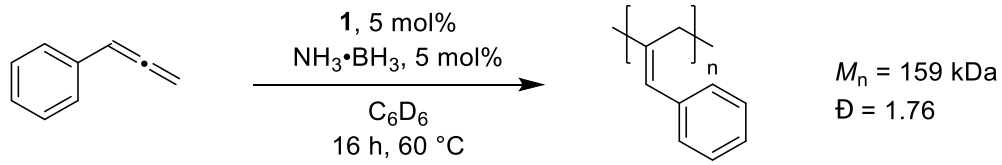

Scheme 100 – Under the initially studied conditions, polymers of high molecular weight but broad polydispersity were produced.

Using both conversion (determined by NMR spectroscopy) and polymer length (determined by GPC), efforts were undertaken to optimise the reaction, so as to generate long polymers as monodisperse as possible with high yields. Upon altering both temperature and catalyst loading, it is clear that the reaction proceeds at room temperature and at lower loadings (Table 14) than the initial conditions, without significant penalty to the conversion or polymer length.

Table 14 – Variation of catalyst loading and temperature studies.

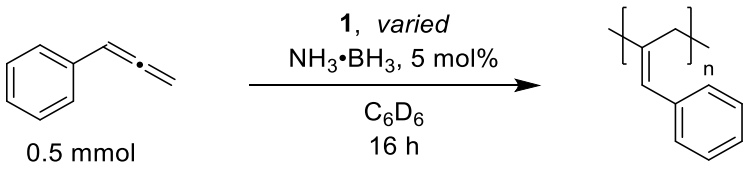

Entry	Catalyst Loading	Temperature / °C	Conversion / %	M_n / kDa	Đ
1	5 mol %	60 °C	97	159	1.76
2	5 mol %	RT	95	181	1.22
3	1 mol %	60 °C	94	162	1.81
4	1 mol %	80 °C	90 [a]	121	1.85
5	1 mol %	RT	93	189	1.19
6	20 mol %	RT	96	n/d	n/d

600 µL solvent used. Conversions determined by ^{1}H NMR spectroscopy, M_n and PDI through GPC. Structural data could not be determined for Entry 6 [a] 90% polymer, 6% alternative products (*vide infra*).

Varying the temperature whilst maintaining the catalyst loading (Entries 1 & 2) appears to increase M_n while decreasing polydispersity, with only a slight decrease in conversion. Furthermore, comparing reactions at different catalyst loadings but the same conditions otherwise show that catalyst loading has only a very minor effect on conversion, M_n and polydispersity (Entry 1 vs Entry 3 and Entry 2 vs Entry 5).

When the reaction is run at 80 °C, conversion of phenylallene remains high but unlike at lower temperatures a significant amount (6%) of an alternative, non-polymeric product is formed (Entry 4). Elucidation of the structure of this product, as well as attempts to prepare it selectively, are discussed in Section 3.6. Finally, when catalyst loading is greatly increased (Entry 6) conversion is essentially unchanged, although determining properties through GPC proved difficult. Through triple-detection analysis the determined M_n and M_w values are 1074 and 1204 kDa respectively - this is considerably beyond the resolution of the GPC column used (250 kDa) and as such these values should not be interpreted quantitatively. NMR spectroscopy indicates that the same mix of (1,2)- and (2,3)-structures are forming under these conditions.

As polymerisation reactions are generally sensitive to concentration in terms of polymer conversion and size, the amount of solvent was also varied (from the initial 0.6 mL), as well as performing the reaction in a stirred vessel as opposed to a J-Young NMR tube (Table 15).

Table 15 – Variation of solvent amount studies.

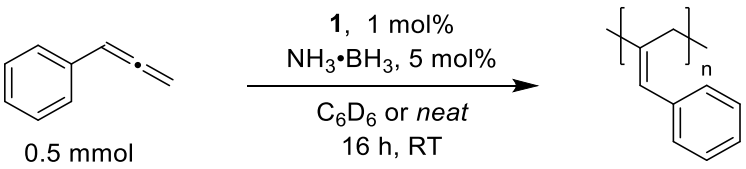

Entry	Amount of solvent (and alterations)	Conversion / %	M_n / kDa	PDI
1	0.6 mL	93	189	1.19
2	0.1 mL	92	n/d	n/d
3	*Neat*	71	12.6	1.75
4	0.6 mL, stirring	91	83.9	1.38
5	3 mL, 2.5 mmol substrate [a]	61 [a]	181	1.17

Conversions determined by ^{1}H NMR spectroscopy, M_n and PDI by GPC [a] Catalyst and ammonia borane loadings were kept at 5 mol% / 1 mol% with respect to phenylallene, isolated yield reported rather than spectroscopic conversion.

Concentrating the reaction mixture (Entry 2 vs Entry 1) leads to similar outcomes observed with 14 Entry 6, namely that conversion remains high, but the polymer cannot be analysed accurately through GPC (with triple detection analysis yielding values of M_n = 481 kDa and M_w = 732 kDa respectively). When all solvent is removed conversion and polymer length are significantly reduced (Entry 3). This can be interpreted that, as in isomerisation, the solvent plays a role in catalyst activation, leading to poorer activity without it. The effect of stirring is comparatively minor, and polymer length is lowered and dispersity increased compared to the non-agitated reaction (Entry

4). Finally, if the reaction is scaled up but concentration kept constant, the properties of the polymer remain broadly unchanged (Entry 5).

The conditions for the polymerisation of phenylallene contrast to when *rac*-lactide is used as a monomer. In this case, at room temperature conversion is minimal and raised temperatures are required to achieve comparable conversions. The polylactide produced is lower in molecular weight and similar to the previous reports of lactide polymerisation by Gibson (M_n = 37.5 kDa, Đ = 1.12) using similar complexes as discussed in Section 1.2. [32] Performing the reaction under neat conditions and raised temperature results in a further increase in polymer length (M_n = 25.7 kDa, Đ = 1.09). This is similar in length and conversion to previous reports using iron complexes, although the conditions are less facile. [265, 266]

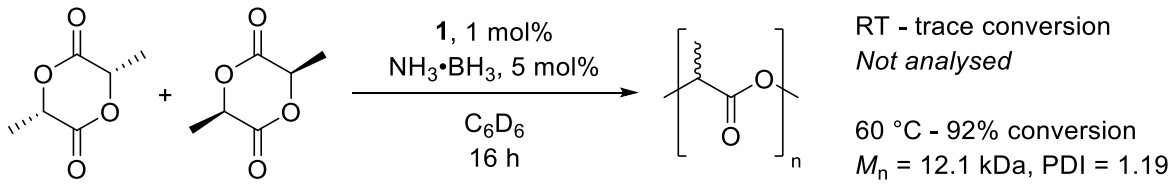

Scheme 101 – Using the same catalytic system for the polymerisation of *rac*-lactide generates high conversions, but only at a raised temperature.

A final principal variation of reaction was modification of the hydride source. In the isomerisation studies in Section 2.2, there are some differences in conversion and selectivity depending on the reagent used, and it was investigated if there was a similar effect in this reaction (Table 16).

Table 16 – Variation of hydride source for phenylallene polymerisation.

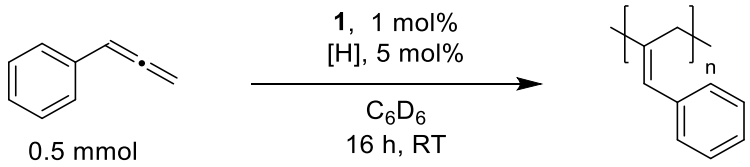

Entry	[H]	Conversion / %	M_n / kDa	PDI	(2,3) : (1,2) Structure
1	$NH_3{\cdot}BH_3$	93	189	1.19	6.5 : 1
2	HBpin	91	152	1.36	5.4 : 1
3	HBpin (1 eq.)	82 [a]	53	1.14	7.8 : 1
4	$Me_2NH{\cdot}BH_3$	89	10.5	6.19	5.1 : 1
5	$HSi(OEt)_3$	92	62	1.18	5.9 : 1

600 µL solvent used. Conversion and isomer ratio determined by ^{1}H NMR, M_n and PDI by GPC [a] 7% conversion to the hydroborated products also observed.

In terms of conversion alone, there is very little difference in any of the hydride sources, and the change in selectivity between structures is relatively minor. The exception to this is when a full stoichiometric equivalent of pinacolborane is used, where conversion and polymer length are noticeably lower. A small amount of the hydroborated allene is observed — further investigations into hydrofunctionalisation of allenes are detailed in Chapter 4 — although this is a minor product compared to polymerisation. At 5 mol% loading, ammonia borane and pinacolborane give polymers

of similar properties, whereas triethoxysilane and dimethylamine borane give polymers of shorter molecular weight. Dimethylamine borane gives exceptionally short and disperse polymers, and efforts to try and rationalise this are given in the mechanistic studies in Section 3.5.

From these studies the most optimal conditions for this polymerisation process can be determined, as shown in Scheme 102. Under these conditions, further structural analysis was undertaken (*vide infra*) as well as expanding the scope of polymerisation (see Section 3.4).

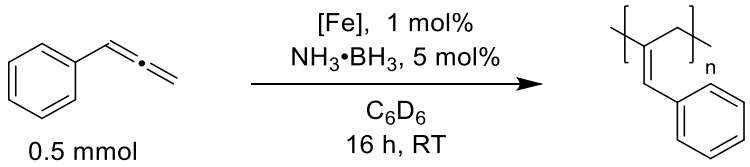

Scheme 102 – Optimised reaction conditions for the polymerisation of phenylallene.

Further polymer structural analysis

The macromolecular nature of polymers means that their physical properties, as well as the chemical properties, are important indicators of their behaviour and nature. The size of the polymers in this study has already been assessed through GPC; this section details other characterisation studies, particularly those involving the polymer in the solid state.

In the standard experimental setup, where the THF eluent is simply removed under reduced pressure, a sticky brown solid is obtained. If the polymer is dissolved in the minimum amount of benzene and dried methanol is added dropwise, the polymer is observed to precipitate as a pale brown solid out of solution. Following decanting of solution, a further wash with methanol then drying, the resulting solid is not sticky, although it is less readily soluble in non-polar solvents. This method reduces the isolated yield of the polymer from 82% to 61%.

Some simple studies of the polymers visual and thermal properties can be undertaken by using a combination of a microscope camera and a hot stage (Full details of this is given in Section 7.3). Looking at the precipitated polymer under a microscope shows that it has a non-crystalline but defined structure, with irregularly shaped particles of a range of sizes (Figure 51). Upon heating, using a hot-stage setup, there is a clear transition to a more ill-defined phase above 65 °C (Figure 52). As temperature and time continue, the solid undergoes a visual transition whilst remaining a solid, indicating it has transitioned into a viscous or rubbery state (Figure 53). This step appears to be reversible. Upon further heating a significant colour change is observed, this is irreversible and is likely chemical decomposition of the polymer (Figure 54).

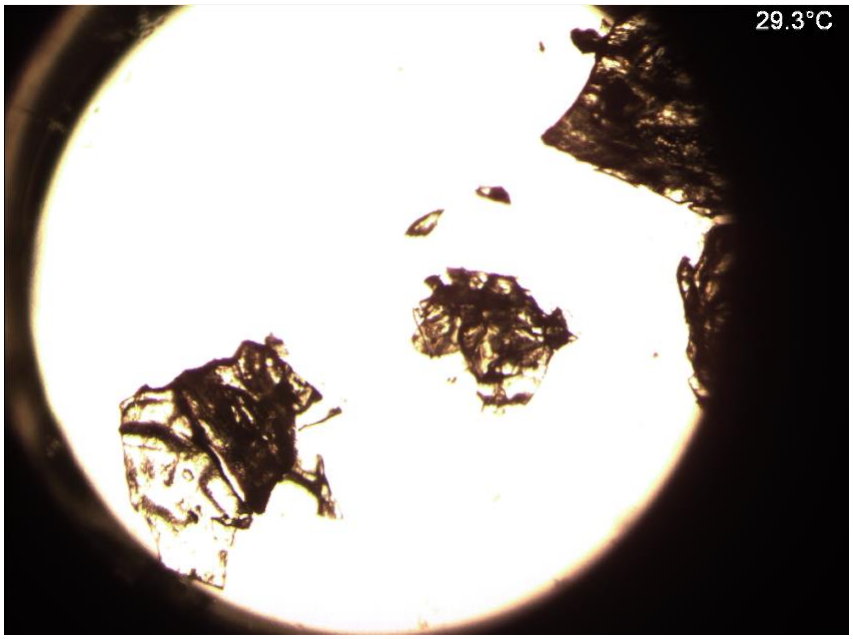

Figure 51 – Microscope images of the precipitated polymer product at close to room temperature. The solid exists as a wide range of particle sizes that are irregular in shape.

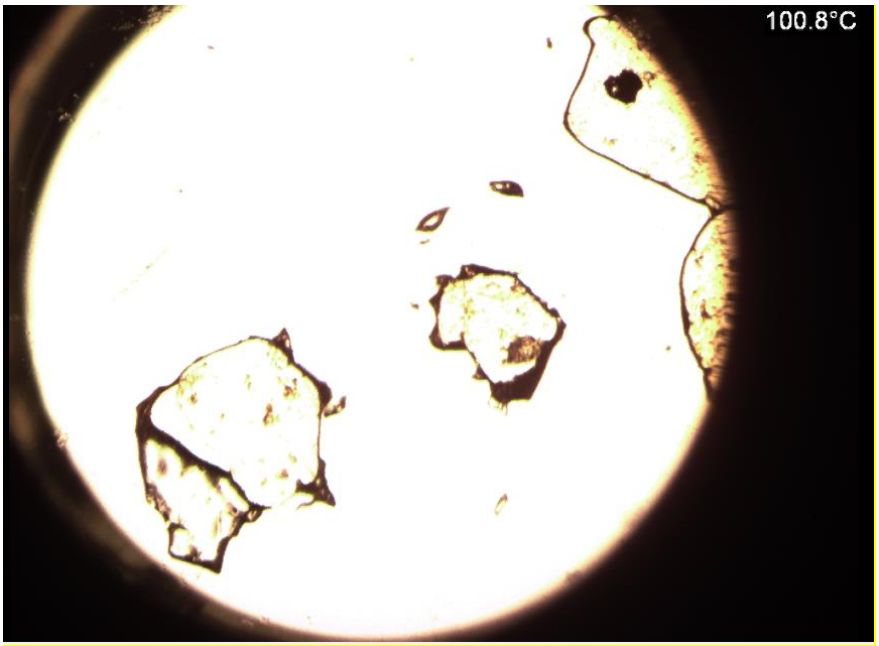

Figure 52 – Upon ramped heating the polymer begins to visually change above 65 °C to have less defined surfaces and structure.

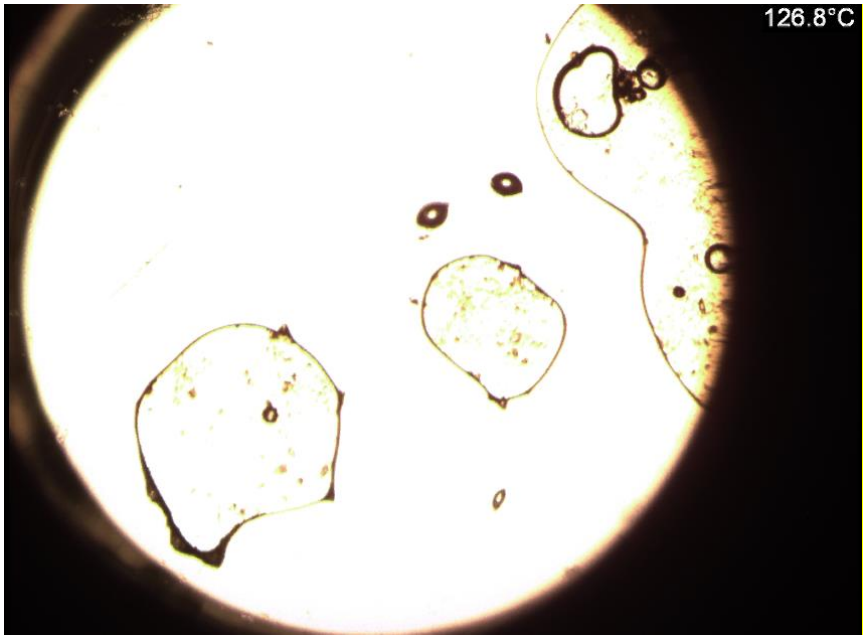

Figure 53 – In the high temperature phase, the polymer begins to flow and spread out over the surface, demonstrating its viscous nature.

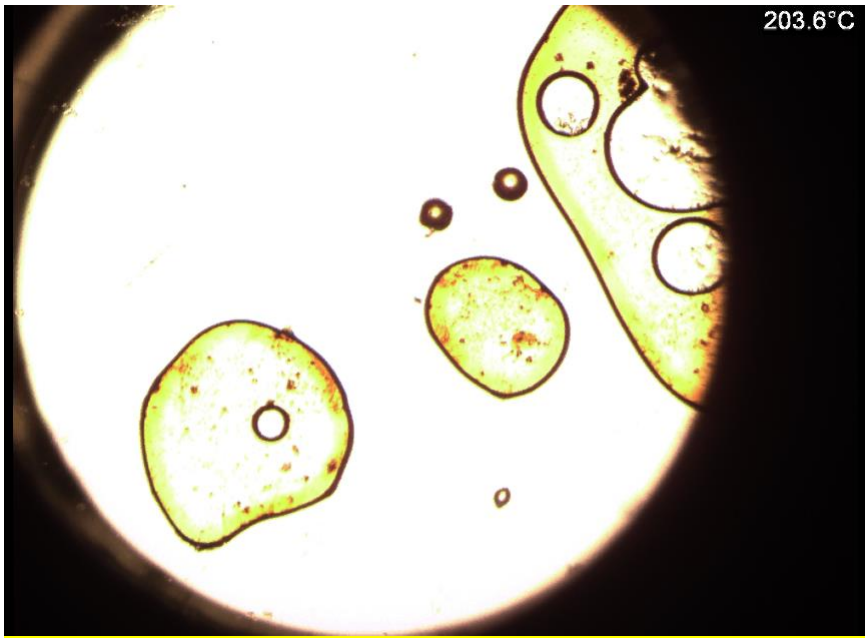

Figure 54 – At temperatures around and over 200 °C, the polymer steadily undergoes a colour change to a much darker solid that does not revert upon cooling. Note that the false colour of the microscope suggests it is dark yellow; in reality the solid is dark brown.

The visible observations are consistent with the polymer undergoing a glass transition from a brittle to a rubbery solid state, which decomposes at high temperatures. This is common for many amorphous solids, especially polymers.

The temperature at which these two forms transition is the glass transition temperature, T_g. T_g can be determined through visual techniques as above — the point at which the transition begins to be observed upon heating in this case is 65 °C. A far more informative and accurate technique for determining this value, as well as other thermal properties, is through the use of Differential

Scanning Calorimetry (DSC). DSC measures and monitors temperature and heat flow of a sample against a standard to quantify physical and chemical changes over a range of temperatures. As DSC is conducted in a carefully controlled environment, and relies on thermal events, rather than visual ones, it can typically determine and characterise events to a highly accurate degree.

Furthermore, DSC can unambiguously distinguish between a glass transition and a melting transition, owing to the differing thermodynamics. A glassy transition is not an enthalpic process (and hence heat flow is unaffected), but the change in heat capacity across the transition leads to a change in the baseline of the trace. In contrast, melting is normally a strongly endothermic process, and as such generates a major peak in the DSC trace.

Poly(phenylallene) formed under the optimised reaction conditions was subjected to DSC analysis. The sample was heated from 25 °C to 200 °C, then cooled back to 25 °C, then ramped again (full details of DSC equipment and setup are in Section 7.3). The trace for the second ramping cycle is shown in Figure 55.

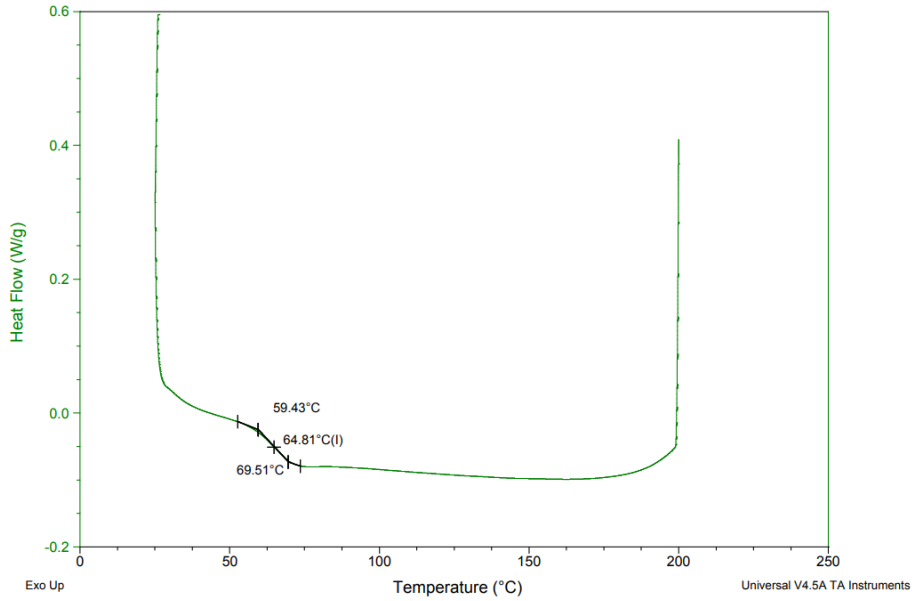

Figure 55 – DSC trace of poly(phenylallene). Run conditions: 25°C to 250 °C at 10 °C/min under nitrogen flow. The T_g transition is determined at 64.8 °C. Full DSC setup is described in Section 7.3.

The visible transition of structure is replicated in the baseline shift that has been identified between 59.4 °C and 69.5 °C. This is indicative of a glass transition as opposed to a significant enthalpic process such as melting, as although the baseline has changed there is not a defined peak. Beyond this there is little of note, and there is a clear absence of further events such as melting or crystallisation. DSC traces are repeated for the substrates detailed in Section 3.4 and display similar T_g events, although the determined temperature does vary.

Upon heating up to 225 °C, a strongly exothermic event is observed at 205 °C upwards. This is likely the aforementioned decomposition visually observed on the hot stage. Repeating the analysis after this does not lead to any thermal events, reinforcing the indication that the polymer has broken down. If heating is kept below 200 °C the analysis is generally repeatable (*i.e.* the third heating sequence produces a similar trace to the second).

To gain a greater understanding of the form of the polymer solid, wide-angle X-ray scattering (WAXS, also referred to as wide-angle X-ray diffraction, WAXD) was performed (*experiments performed and analysed by Dr Adam Squires, University of Bath*). This should provide some insight into the structure of the polymer, in particular whether it is ordered or amorphous. An ordered, crystalline structure would be expected to generate significant Bragg peaks. A small sample of polymer was heated to above T_g and then stretched out into a long fibre and cooled, in an effort to induce 2D orientation about the structure. This was then subject to analysis (Figure 56).

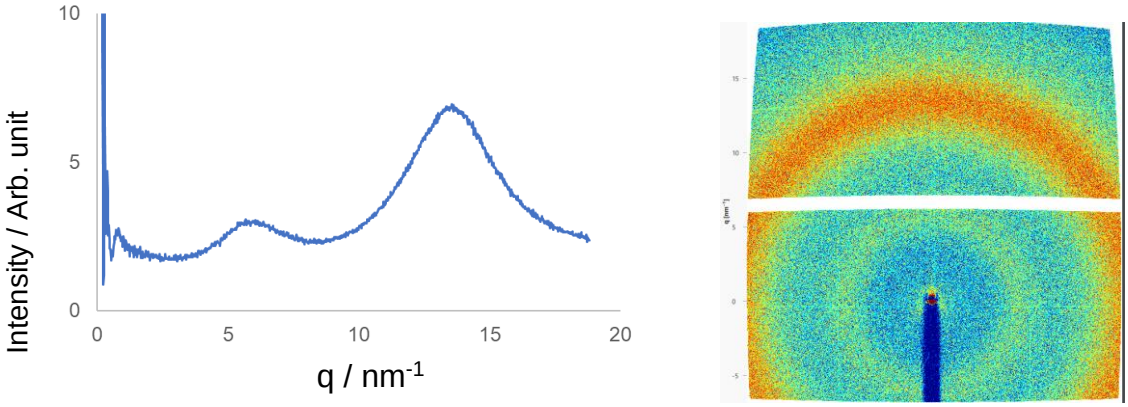

Figure 56 – WAXS analysis generates no Bragg peaks or orientation, indicating the solid polymer is amorphous in structure. Two intense rings are observed — the raw data is shown on the right and a 1D normalised graph on the left.

From the data (full experimental setup detailed in Section 7.3), no Bragg peaks were observed, and there appear to be no specific orientation in the fibre sample. This confirms the polymer is amorphous, which would be expected given that a range of conformers are proposed to exist as per NMR and DFT studies in Section 3.2. Two broad rings of reasonable intensity are observed at q values of approximately 5 and 13 nm^{-1}, with the latter being more intense. Converting these into d-spacings gives real space distances of approximately 12.5 and 5 Å respectively. These signals could not be directly correlated to any structural property or behaviour, although they have similarities with previously reported data for amorphous comb polymers by Fujimori. [267] It appears it may arise from some form of π-stacking or interaction between chains.

To further study the structure of the polymer, in particular to try and observe any end groups, matrix-assisted laser desorption/ionisation (MALDI) analysis was performed. MALDI is a soft ionisation technique that ionises large molecules — in a polymer it can produce ions of a repeating molecular weight, leading to determination of both the repeating mass unit and the residual mass, which can be used to determine chemical structure. The polymer lengths produced in this reaction (under standard conditions) are beyond the detection limits of the spectrometer. To surmount this, methanol was added to the reaction after 5 minutes, with the aim of quenching all reactivity very rapidly at this point. The resulting polymer length was determined to be 10.5 kDa (through GPC analysis), within the range of suitability for MALDI analysis. A range of matrixes and conditions were tested before a suitable setup was found (details in Section 7.3); fragments were generally limited to 1000–3500 m/z range (Figure 57). Below this a range of signals (some associated with the matrix,

other assignable) without a repeating pattern were observed, at higher m/z values no signals were observed.

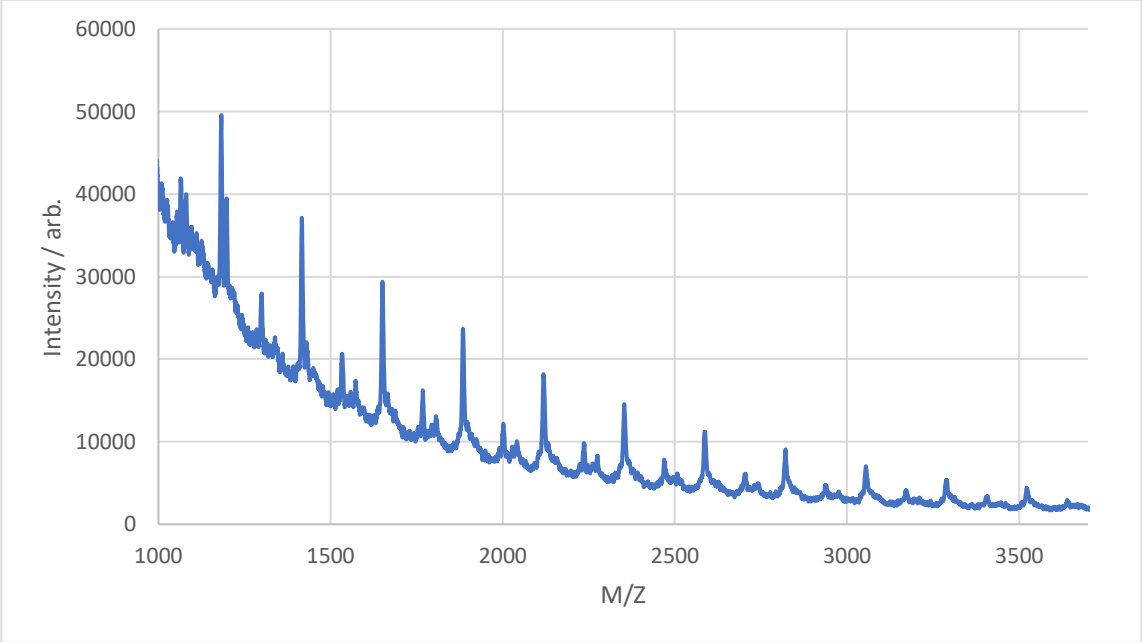

Figure 57 – MALDI spectra (1000–3500 m/z) of quenched polymer. As discussed below, the repeating unit is consistent with poly(phenylallene) and the M/Z values used to postulate end groups. A list of detected and assigned peaks is given in Section 7.3.

The mass units have a repeating distance of 117 m/z, assuming singly charged fragments this supports a repeating unit weight of 117 Da, consistent with the weight of the monomer and indicating the fragments are reasonably well-defined. The residual mass of the polymer chain can be determined through analysis to be 140.01 Da. It is proposed that this is a sodium adduct, leaving a 117.02 Da organic residue. This is proposed to be end groups of PhCHCCH– and H–, or that the smaller chain lengths cyclise as a termination step – the structures for the fragment at 1416.7 m/z is shown in Figure 58. Considering the mechanistic proposals in Section 3.5 (*vide infra*), the former seems most likely.

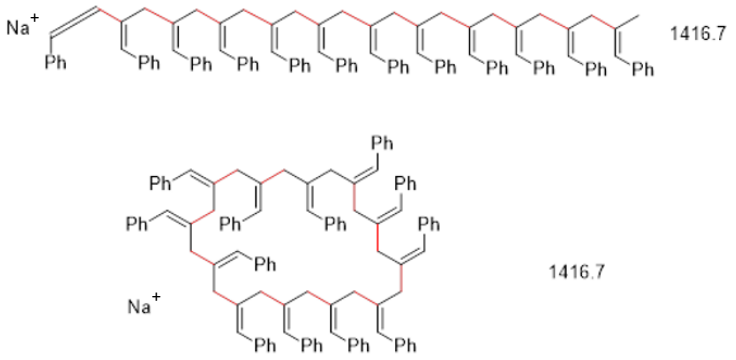

Figure 58 – The observed fragments were proposed to arise from short chain polymer fragments with an allene and proton end groups, or through small, cyclised structures. The former structure is consistent with the mechanistic proposals in Section 3.5. Note that the structures shown are not meant to represent conformations, and it is unlikely the fragment is 'all-syn' in structure.

3.4 Preparation and Analysis of Functionalised Poly(phenylallenes)

Efforts were undertaken to apply this polymerisation chemistry to a range of other allenes, as relatively few previously reported polymerisation studies probe reactivity on substrates beyond phenylallene. Allenes **54-59** were prepared through the standard methodology outlined in Section 3.1, and full NMR assignment and Mass Spectrometry analysis for all allenes (as well as the dibromocyclopropyl intermediates prepared as an intermediate) are given in Section 7.3. These were tested in polymerisation. In all entries, the (2,3)-structure is the major product formed, the structure of this, along with conversion and additional properties determined from NMR, GPC and DSC are shown in Table 17.

Table 17 – Variation of allene used in polymerisation, with conversion and key polymer properties detailed.

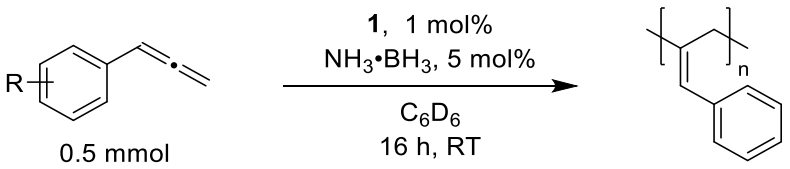

Entry	Major isomer	Conversion (%)	$\mathbf{P_{2,3}}$: $\mathbf{P_{1,2}}$	M_n (kDa)	PDI	*DP*	T_g (°C)
1	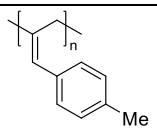 **P54$_{2,3}$**	94	8 : 1	229	1.63	1760	86.4
2	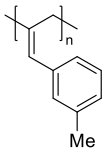 **P55$_{2,3}$**	96	7 : 1	72	1.17	550	63.0
3	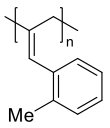 **P56$_{2,3}$**	91	5 : 1	185	1.62	1420	75.4
4	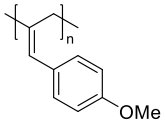 **P57$_{2,3}$**	98	11 : 1	174	2.05	1190	81.6
5[a]	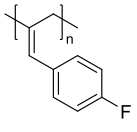 **P58$_{2,3}$**	77	13 : 1	53	1.12	400	57.0

6[a]	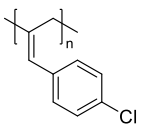 **P59$_{2,3}$**	74	6 : 1	166	1.67	1110	97.1

600 µL solvent used. Conversion and structural ration determined by ^{1}H NMR spectroscopy. M_n, PDI and *DP* determined by GPC. T_g determined by DSC. [a] 5 mol% catalyst used.

For methyl and methoxy-substituted phenylallenes, conversions remain high (Entries 1-4), although there are significant differences in both polymer length and (2,3) : (1,2) polymer regioselectivity. There are clear relationships between growing polymer length, increased polydispersity and raised T_g. The meta-methyl substituted substrate in particular gives shorter polymer lengths, suggesting a significantly reduced rate of propagation compared to terminating or side-steps. The ortho- and para-methyl substituted substrates are close to non-substituted phenylallene in their properties.

When switching to halo-substituted substrates, conversion is very poor under standard conditions, and it is necessary to raise catalyst loading to achieve reasonable yields of polymer. Even under these conditions, 4-fluorophenylallene generates shorter polymers with a lower conversion than the other substrates.

In all cases the (2,3)-polymer is by far preferred over the (1,2)-structure. Furthermore, the same triple splitting observed for polyphenylallene (*vide supra*) is also observed for all the substrates. The para-functionalised polymers were previously reported by Cui, albeit in considerably lower M_n. [144] The meta-methyl substituted polymer has been proposed to form by Barrett [145], while the ortho-polymer has not previously been reported. For the (2,3)-structures, a more thorough ^{1}H and ^{13}C{^{1}H} NMR structural determination than has previously been reported is given in Section 7.3. The (1,2)-structures are more challenging to assign, particularly in cases where the amount of polymer formed is low, and HMBC correlations are too weak to determine. These, along with all other structural data is given in the aforementioned experimental section.

Two non-aryl allenic substrates were also tested for performance. Cyclohexylallene and methoxyallene are both commercially available, and both have been reported to undergo living polymerisation in some conditions. [268, 269] Under the standard reaction conditions neither undergoes any transformation. At raised temperatures cyclohexylallene remains inert whereas methoxyallene slowly degrades to ill-defined products (Figure 59). It should be noted that in the presence of **1** but not a hydride source, cyclohexylallene undergoes a small amount of insertion, similar to phenylallene. To study alternative aryl substituents napthylallene was prepared. This forms oligomeric products under reaction conditions even if **1** is not present, and clean conversion to well-defined polymeric products could not be attained.

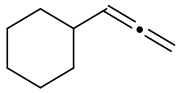

Cyclohexylallene
Inert at RT and 60 °C

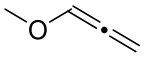

Methoxyallene
Inert at RT, degrades at 60 °C

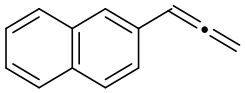

Napthylallene
Ill-defined reactions (with or without catalyst) at RT

Figure 59 – Outcomes with alternative substrates. Aside from temperature, conditions are the same as Scheme 102. Note that raised catalyst loading does not have an effect on the outcomes.

For arylallenes, the nature of substitution clearly has some effect on the properties of the resulting polymer, although a range of substituted polymers can be formed in reasonably high (2,3)-regioselectivity. However, this reactivity cannot be applied to non-aryl substrates.

3.5 Mechanistic Studies into Phenylallene Polymerisation

The same synthetic experiments used in Chapter 2 to investigate the mechanism can also be applied to the catalysis discussed in this chapter. Firstly, we can evaluate whether the reaction is nanoparticle mediated through a PMe_3 poisoning experiment (Scheme 103). Again, reactivity is slower but not fully inhibited, indicating the reaction is homogeneous rather than nanoparticle-based (the reaction was performed at 5 mol% catalyst loading so a sub-catalytic amount of PMe_3 could be accurately added).

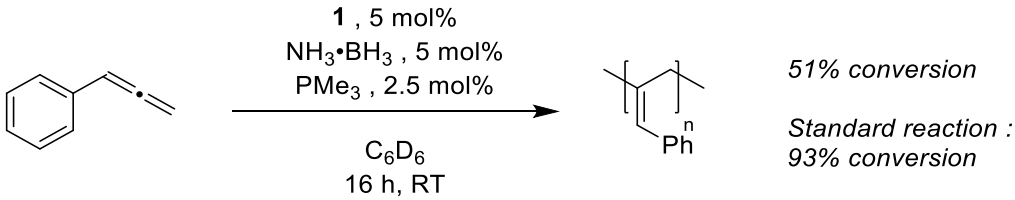

Scheme 103 – Test for nanoparticles, as investigated for isomerisation in Section 2.4. As reactivity is not fully quenched it appears the reaction is not nanoparticle mediated.

We can also employ the use of a radical clock to gain further insight into the mechanism. The reaction was setup as per standard reaction conditions and run for four hours. Following this (chloromethyl)cyclopropane **60** was added and the reaction was allowed to proceed further. Conversion over 16 hours appeared practically unaltered (91% as opposed to 93% without radical clock, Scheme 104). Distillation of volatiles away from the catalyst/polymer shows that only a small amount of the cyclic clock is opened into 1-butene (less than 10%). This appears to discount a radical-mediated mechanism, similar to the outcome in Chapter 2.

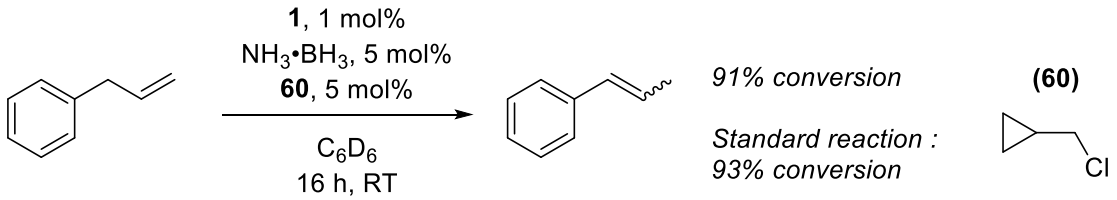

Scheme 104 – Adding radical trapping reagents has minimal effect on reactivity, and only a small amount of the ring-opened product is observed. This appears to rule out a radical-mediated mechanism, similar to the experimental findings in Section 2.4.

Deuteration Studies

Attempts were made to observe the selectivity of the reaction by use of deuterium-labelling. This was done to determine if there is any H/D exchange between the amine borane or alternative hydride source into the polymeric product, and to observe if there is any H/D scrambling from the monomer to polymer. From a synthetic standpoint the simplest alteration is to use the previously synthesised deuterated amine boranes $Me_2ND{\cdot}BH_3$ and $Me_2NH{\cdot}BD_3$ as co-catalysts (Scheme 105). As using $Me_2NH{\cdot}BH_3$ leads to a high conversion but considerably shorter polymer lengths than other reagents such as HBpin or $NH_3{\cdot}BH_3$, observation of any end groups should be easier with these.

Scheme 105 – Use of deuterated amine boranes in catalysis. Using these has no observable effect on the properties of the polymer.

Under these conditions, no observable change is noted in the reaction mixture ^1H or ^2H NMR spectra or the isolated polymeric product. This is similar to the lack of incorporation observed when deuterated amine boranes are used in isomerisation catalysis in Chapter 2. An important caveat is that incorporation would only be expected on the end groups, so D-incorporation may just be too minor to be observable.

A deuterated substrate can also be synthesised, and this study should be more conclusive than the previous deuteration study as the whole polymer chain should see a change in NMR signals. Styrene-β-β-d_2 can be prepared relative straightforwardly, and from this the standard preparation can be adapted; the products themselves can be compared to the isotopically labelled substrates prepared by Murphy to confirm their structures (Scheme 106). [270] Yields were lower than the analogous protic substrate (see Section 7.3). The CD_2 functionality is isotopically preserved in the synthesis, which can be rationalised by the mechanism in Scheme 95.

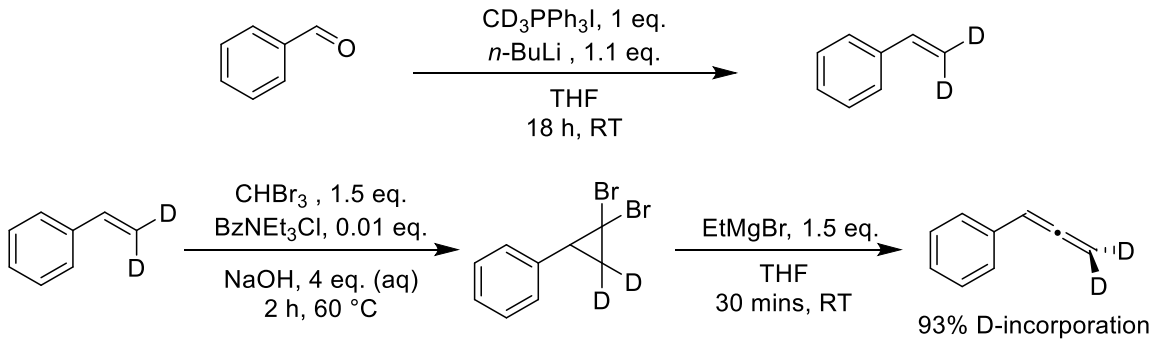

Scheme 106 – Synthesis of styrene-β,β-d_2 and phenylallene-3,3-d_2.

The resulting allene was then used in catalysis. There does not appear to be any interconversion between the *H*C_1 and *D*C_3 positions (no ^{2}H NMR signal is observed for the former and only residual ^{1}H NMR signals are observed for the latter; the D-incorporation on the product is the same as the starting material, Scheme 107). The ^{2}H NMR spectrum still shows the *D*C_3 signal as three distinct environments.

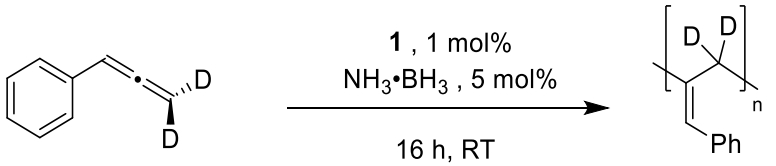

Scheme 107 – Using phenylallene-3,3-d_2 produces a polymer with deuteration solely on the main chain.

Use of metal hydrides and hydrogen in catalysis

Just as in the case of the isomerisation chemistry, the iron(II) hydride dimer **43** can be independently synthesised and used in catalysis to demonstrate its activity without a further hydride source. Similar to when using **1** without a further hydride source, only a small amount of conversion (<5%) is observed under standard reaction conditions (16 h, RT), unless a further hydride source is added (Scheme 108).

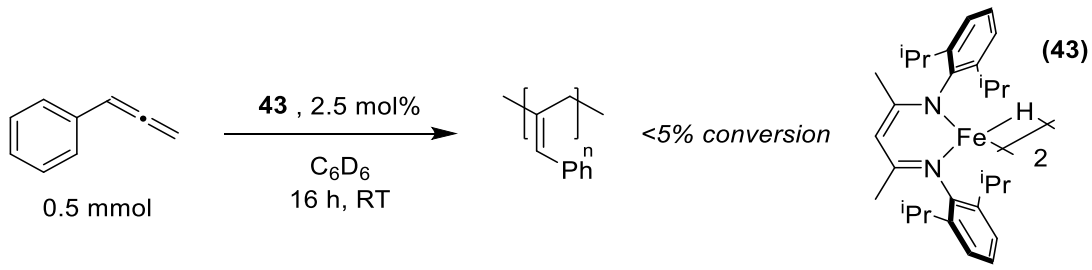

Scheme 108 – Iron hydride **43** is not active as a catalyst without further reagents, similar to the outcome observed with isomerisation catalysis in Chapter 2.

Performing the reaction with **1** or **43** under an atmosphere of hydrogen instead of a hydride source also leads to conversion identical to when performed under an argon atmosphere (Scheme 109). These observations are similar to the experimental outcomes in Chapter 2, and suggest that a similar mechanistic process is occurring here.

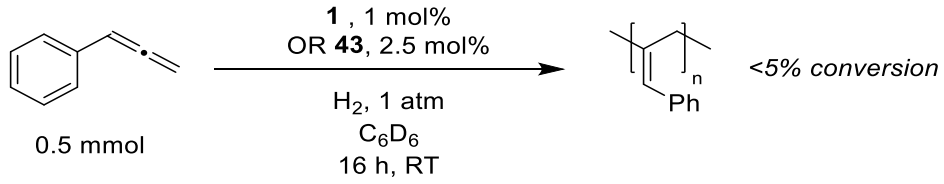

Scheme 109 – Performing the reaction under a hydrogen atmosphere, but without a further hydride source does not alter reactivity when compared to running the reaction under an inert atmosphere, again similar to the outcome in Chapter 2.

Proposing an Fe(I) mechanism

As in Chapter 2, it is instead proposed that the initial pre-catalyst is reduced to an iron(I) species, specifically the iron-benzene complex **44** (Scheme 110). This seems reasonable as the reaction conditions are similar to the isomerisation conditions, and the outcomes when using iron(II) hydrides are inert for both reactions.

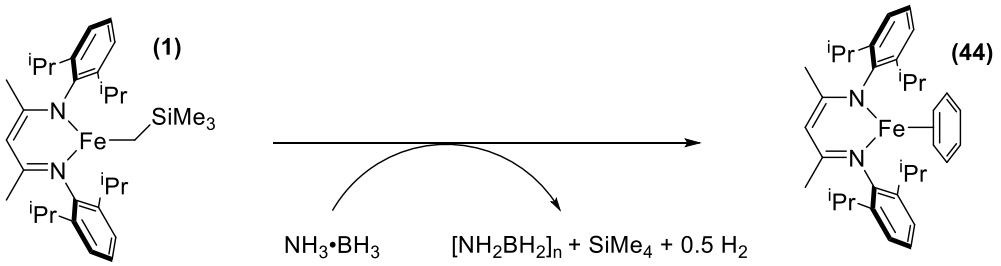

Scheme 110 – It is proposed that the pre-catalyst **1** is reduced to the iron(I) complex **44** through the reaction with ammonia borane. The activation path proposed in Chapter 2, where ammonia borane is dehydrogenated, is shown.

The solvent stabilised Fe(I) species **45** can again be utilised in catalysis to confirm this hypothesis. This is active in catalysis, and produces a polymer of similar M_n weight and at a similar conversion when compared to the standard reaction conditions (Scheme 111). Furthermore, the (2,3):(1,2) structure ratio is very similar to the standard reaction (6.0 : 1).

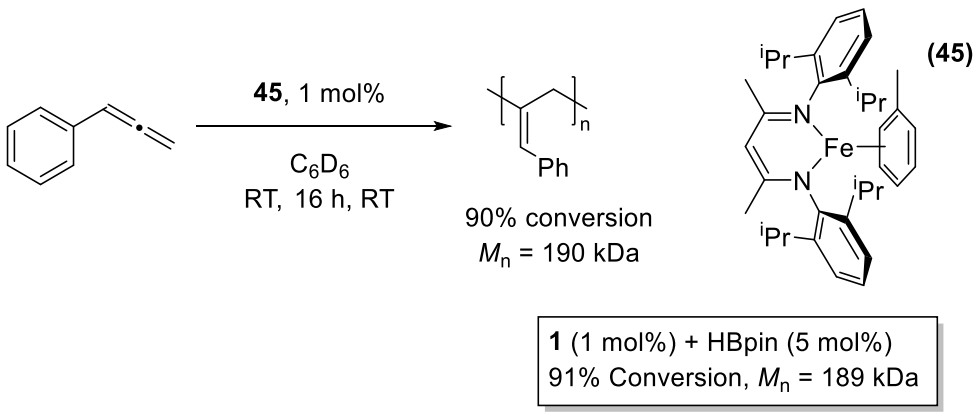

Scheme 111 – Using the Fe(I) tolyl species **45** in the reaction alone generates polymers with conversion and properties similar to standard reaction conditions.

NMR analysis of the reaction mixture shows a wide range of signals, very similar to the reaction of ammonia borane and **1** in Section 2.8, and no purported intermediates could be identified. As in

the isomerisation chemistry in Chapter 2, a significant amount of **1** remains unreacted even at the conclusion of the reaction. When using dimethylamine borane, the ^{1}H NMR spectrum shows that primarily complex **61** is forming, which has previously been identified in dehydrocoupling studies. [47] The poor reactivity of dimethylamine borane may be rationalised as it readily forms **61** (and undergoes further dehydrocoupling) compared to ammonia borane, which does not dehydrocouple effectively under these conditions.

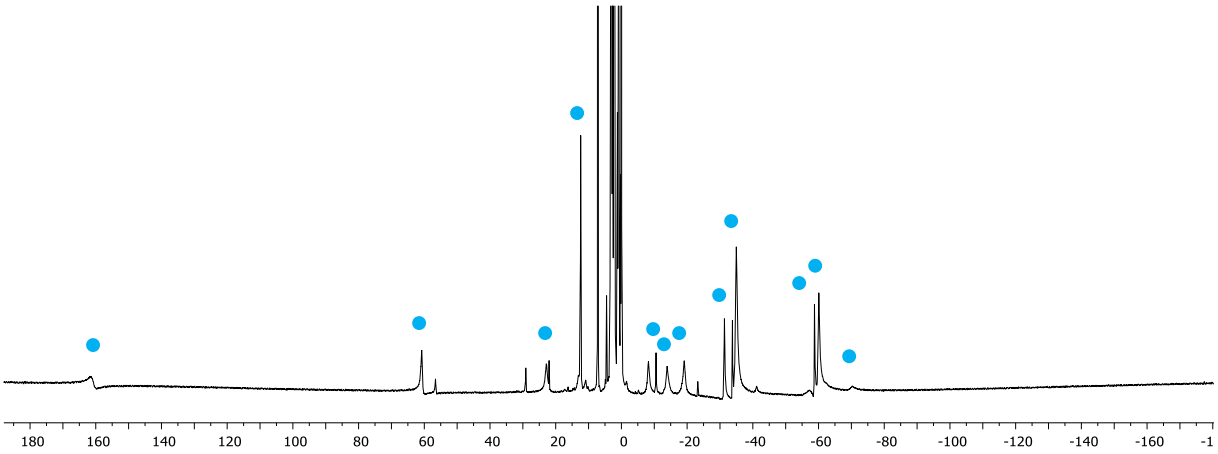

(61)

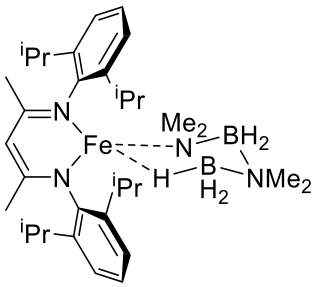

Figure 60 – In contrast to reactions with ammonia borane, where a range of signals are formed in the paramagnetic range, reactions with dimethylamine borane show signals primarily belonging to **61**, identified with **blue** ●. This rationalises the poor relatively poor yield and polymer weights observed when dimethylamine borane is used as a hydride source.

A catalytic cycle can be proposed starting with **44**. It seems feasible that through ligand exchange **44** converts into the Fe(I) allene complex **62** with relative ease. From here, it is proposed that oxidative addition occurs across a terminal C–H bond to form Fe(III) species **63**. This has some precedent with first row transition metals [271] — a particularly pertinent example with iron has been reported by Ackermann [272] — and has similarities to the mechanism proposed in Chapter 2. **63** has axial chirality depending on which terminal proton is activated but with no formal stereogenic centre, although this merely determines conformation about the end group rather than the overall chain. From here the iron centre remains in the Fe(III) oxidation state. A second molecule of allene can add over the iron-carbon bond to form a new complex **64** with an sp^3 alpha carbon as opposed to an sp^2 centre. Further additions then continue an essentially identical manner, increasing polymer length stepwise. The proposed initial and subsequent steps are shown in Figure 61.

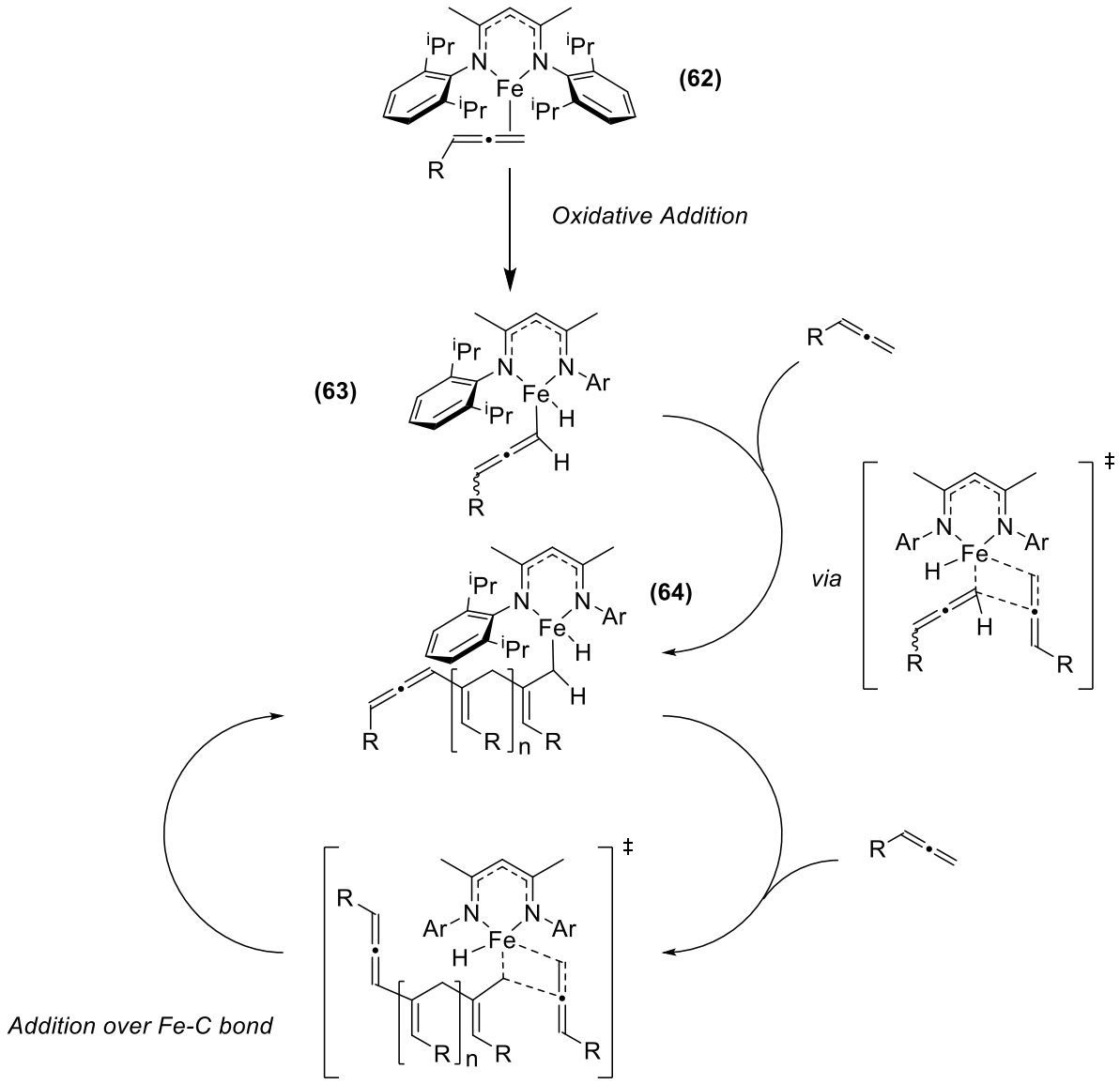

Figure 61 – Proposed catalytic cycle for polymerisation.

The polymer can be terminated in one of two obvious ways. First, reductive elimination of **64** and ligand exchange with solvent can reform **44** and eliminate the polymer. Alternatively, through quenching of the reaction with methanol as in Section 3.3, the O–H bond adds across the iron-carbon bond, releasing polymer and an inert iron complex. In this process a black precipitate is observed, and it is likely that any iron species produced in this way readily decomposes further. Through either process the resulting polymer is consistent with the ions observed in MALDI analysis.

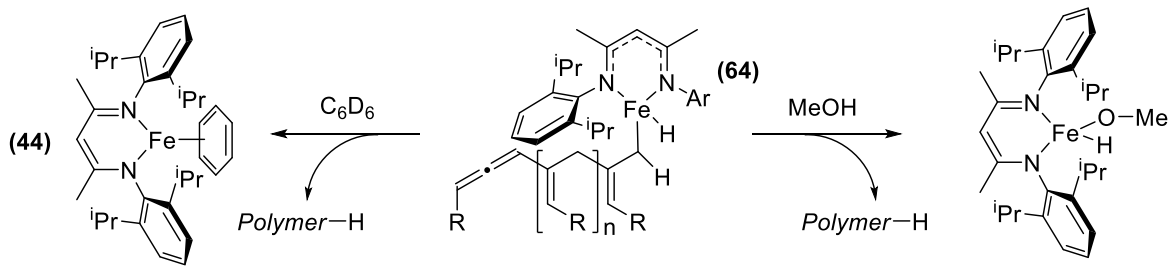

Scheme 112 – Polymer growth can be terminated either by inherent reductive elimination or addition of a quenching reagent such as methanol. The Fe(III) alkoxide/hydride as drawn is very likely to react and decompose further.

The long chain length and high *DP* indicate only a small amount of iron centres are active in the reaction, and the propagation process is reasonably facile compared to initiation. However, the high polydispersity suggests that the balance between initiation, propagation and termination steps in terms of rate is complex. The cycle as above does not explain the differing conformations observed in the polymer; these are proposed to arise from the conformational arrangement about the active site, with minor changes in the conformation of the main polymer change with respect to the iron centre leading to changes in conformation.

3.6 [2+2] Cycloaddition of Allenes using Iron Catalysts

As stated previously, there is a secondary product observed in the catalytic polymerisation of phenylallene, which can be isolated as a white solid that is (unlike the polymer) soluble in non-polar solvents. NMR and mass spectrometry analysis show that this is a dimeric structure. There are *E* and *Z*-isomers present which can be distinguished by NMR spectroscopy, as the cyclobutane protons have distinct chemical shifts. Upon increasing catalyst loading the yield with respect to the dimer can be increased to 27%, and full characterisation of both $\mathbf{65}_{\mathbf{trans}}$ and $\mathbf{65}_{\mathbf{cis}}$ (Scheme 113). At room temperature, no dimer is observed to form.

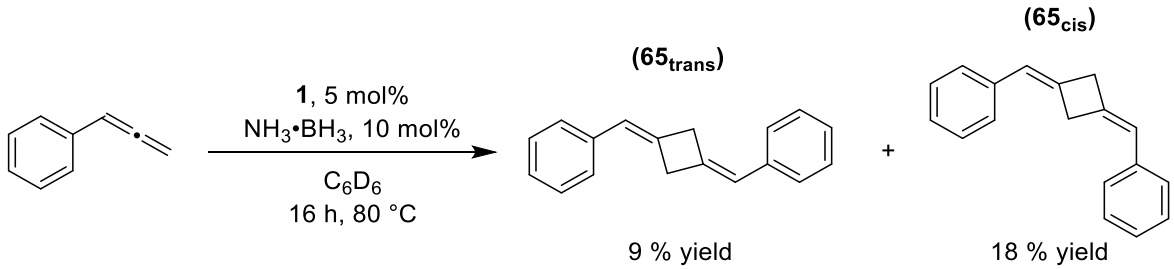

Scheme 113 – [2+2] cycloaddition of allenes generates cis : trans cyclobutane structures in a 2 : 1 selectivity.

This form of [2+2] cycloaddition is exceptionally unusual. In general, forming 4 membered carbon rings through opening double bonds is disfavoured owing to the steric strain generated. Allenes are more amenable to this process than alkenes; for example, heating of phenylallene at high temperature generates cyclobutane structures, although this process is neither facile nor clean. Furthermore, in thermal dimerisation the 1,2-structure is the dominant product as opposed to the 1,3-structure formed in this process (Scheme 114).

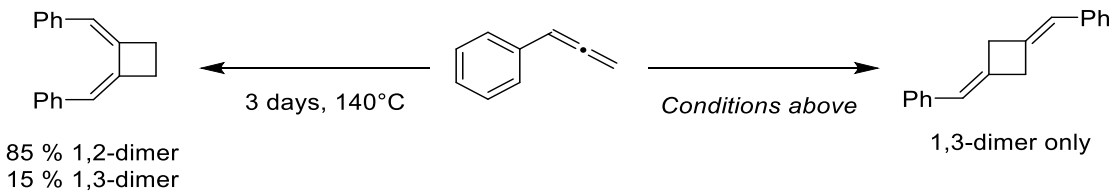

Scheme 114 – Comparison of thermal dimerisation of allenes, where the major product is the 1,2-substituted ring, and the reaction above, where 1,3-subsituted rings are the only structure observed. *E-Z* selectivity about the double bond is not considered.

Thermal dimerisation was first identified by Verdol in 1955, [273] and although some synthetic uses have been reported, [274] the poor selectivity and the need to separate products from a range of isomers and oligomers limit its usefulness.

Cyclobutanes are interesting due to their strained structure, which presents opportunity for further reactions, and in the case of having two sp_2 carbons in the cycle the strain is increased considerably. The 1,3-dimethylenecyclobutane also has some curious electronic properties. If two of the central C–H bonds are homolytically cleaved, a C_6H_6 structure is formed (Scheme 115). This is termed a non-Kekulé structure, as it has 6 π electrons but is clearly not aromatic. [275]

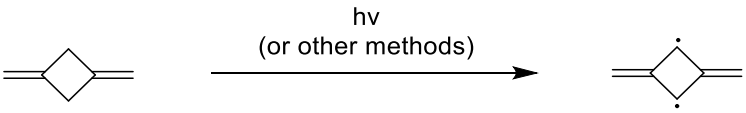

Scheme 115 – Radical cleavage of a 1,3-dimethylenecyclobutane fragment generates a non-Kekulé structure, containing a non-aromatic structure with six π electrons and six carbon centres. The unusual spin properties of the fragment have potential applications in organic electronics.

This molecule can be isolated in an argon matrix, and studies indicate it exists in a triplet spin state, which is very unusual for an organic molecule. [276] Dougherty has speculated that these molecules may be used to develop magnetic materials with solely organic components. [277] By substituting this fragment with aromatic rings, the radical system can potentially be stabilised further, but to investigate this further, practical methods of synthesising the required dimer are needed.

Synthesis of functionalised 1,3-dimethylenecyclobutane structures is challenging and limited. Huenig developed an elimination-based pathway from more accessible cyclobutane rings, [278] whilst Braverman has reported a dimerisation of allenic sulfones which forms a substituted 1,3-ring in addition to an acyclic dimer (Scheme 116). [279]

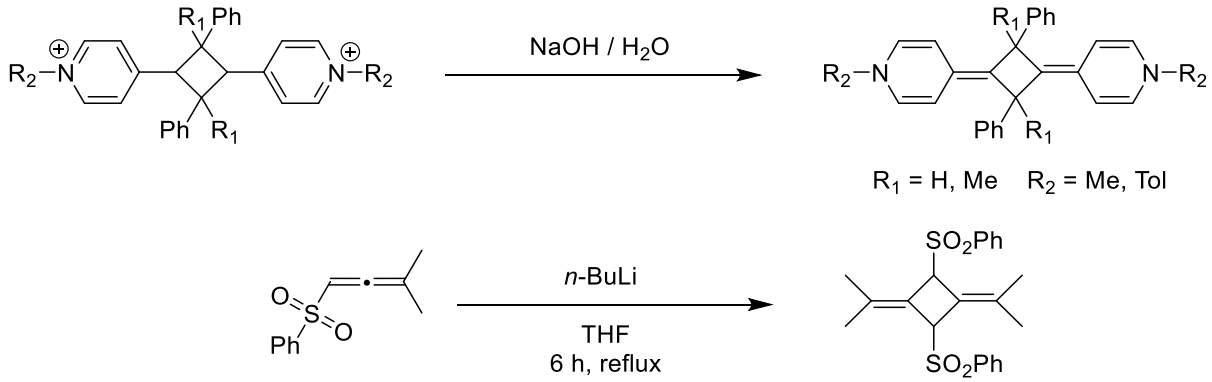

Scheme 116 – Synthetic routes to 1,3-dimethylenecyclobutane systems include base mediated elimination as reported by Huenig, [278] and dimerisation of allenic sulfones reported by Braverman. [279]

The only route to synthesis of the compounds isolated in this study is by Dixneuf. [280] Starting with an allenylboronate, the ring formation is performed by a ruthenium complex. The aryl substituents are subsequently added through a Suzuki-like coupling with an aryl iodide. Intriguingly, if phenylallene is prepared and reacted with the bulky ruthenium catalyst showed in scheme, the 1,2-substituted cyclobutane system shown is formed as opposed to any 1,3-products (Scheme 117).

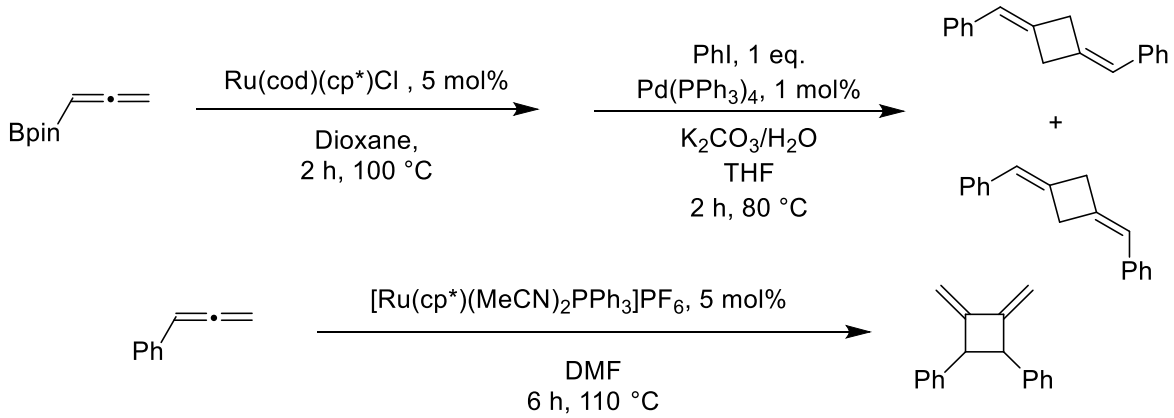

Scheme 117 – Dixneuf reported synthesis of the phenyl substituted 1,3-dimethylcyclobutane ring using sequential ruthenium and palladium-catalysed reactions. Note that treating phenylallene with bulky ruthenium catalysts generates more substituted 1,2-subsituted products only. [280]

These systems serve to highlight that 1,3-cyclobutane rings of this type are challenging to form. Because of this, a range of further studies were undertaken to try and optimise the formation of the dimer over the polymer and glean further understanding of the reaction.

Optimisation of dimerisation reaction

Efforts were undertaken to increase the conversion of the dimer at expense of the polymer. Initially, the pre-catalysts tested in Chapter 2 were tested in this reaction and the dimer conversion and selectivity were observed (Table 18). **28** is insoluble in benzene so acetonitrile-d_3 was used as an alternative solvent.

Table 18 – Variation of catalyst and its effect on dimer conversion.

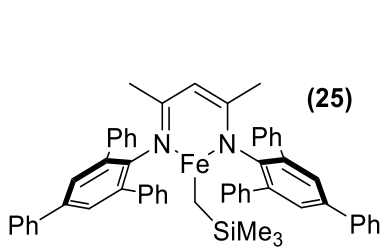

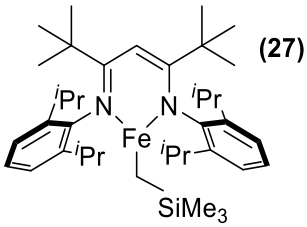

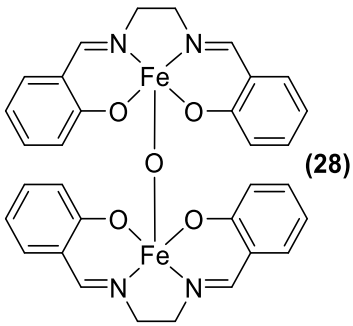

Catalyst	Dimer Isolated Yield / %	*Trans* : *Cis* Selectivity
1	27	1 : 2.0
25	15	1 : 1.9
27	13	1 : 1.4
28 [a]	-	-
$FeCl_2$	-	-
none	-	-

Conditions : 0.5 mmol phenylallene, 5 mol% catalyst, 10 mol% $NH_3{\cdot}BH_3$, 600 µL C_6D_6, 16 h, 80 °C. Selectivity determined by ^1H NMR spectroscopy [a] 1 mol% catalyst, 600 µL MeCN-d_3 used as solvent.

Using alternative β-diketiminate complexes **25** and **27** resulted in the same selectivity in the product, although conversion is less than when using **1** (Entries 1-3). **28** and $FeCl_2$ were inactive under these conditions — using **28** did result in some polymerisation occurring, although conversion was low, and the polymeric products could not be easily characterised. In all cases where dimerisation is involved, it is still the minor product compared to polymerisation. Without a metal species no conversion is observed, showing it is clearly not simply a thermal process. Given **1** is most effective in producing the dimer, it was used in further studies.

Replacing ammonia borane with an alternative reagent has some effect on the properties of the polymers produced, so it was expected to somewhat affect the amount and selectivity of dimer product formed. As in the isomerisation and polymerisation chemistry a range of reagents were tested under the conditions displayed in Table 19.

Table 19 – Effect of hydride source on dimer conversion and selectivity.

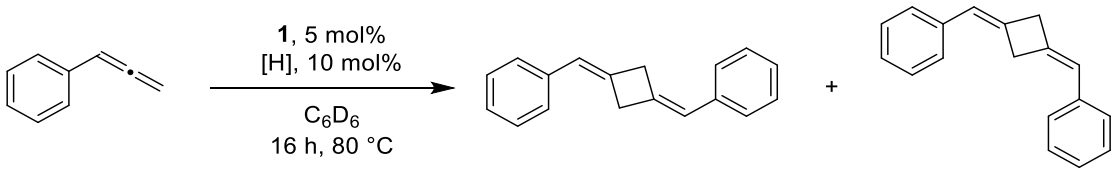

Entry	[H]	Dimer Isolated Yield / %	*Trans* : *Cis* Selectivity
1	$NH_3{\cdot}BH_3$	27	1 : 2.0
2	HBpin	13	1 : 3.0
3	H_3SiPh	19	1 : 2.5
4	$Me_2NH{\cdot}BH_3$	25	1 : 2.0
5	$KHBEt_3$	-	-
6	None	-	-

600 µL solvent used. Conversion and selectivity determined by ^{1}H NMR spectroscopy.

Selectivity is not particularly affected by hydride source, with all the ratios lying between 2:1 and 3:1 *cis* : *trans*. All the hydride sources that lead to phenylallene polymerisation can generate the dimer to some extent (Entries 1-4), although ammonia borane results in the highest conversion. Use of alternative reducing agents did not lead to any reactivity (Entry 5), and **1** is not capable of dimerisation without a hydride source (Entry 6).

Finally, temperature and other conditions were varied from the conditions in Table 20 to see if selectivity could be improved any further. Given that the polymerisation varies greatly when experimental conditions are varied, it was expected that dimerisation would too.

Table 20 – Variation of reaction conditions and effects on dimer conversion and selectivity.

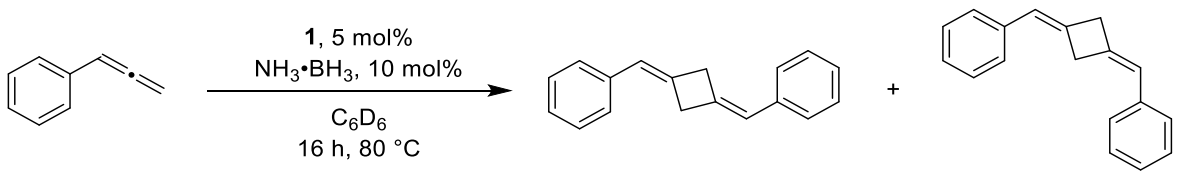

Entry	Variation from Conditions in	Dimer Isolated Yield / %	*Trans* : *Cis* Selectivity
1	16 h, 60 °C	16	1 : 2.0
2	16 h, RT	*trace*	-
3	3 mL C_6D_6 instead of 600 µL C_6D_6	17	1 : 1.7
4	1 equivalent DMAP added	25	1 : 2.0
5	MeCN-d_3 instead of C_6D_6	-	-
6	1 h, 80 °C	13	1 : 1.8

600 µL solvent used, unless stated otherwise. Conversion determined by ^{1}H NMR spectroscopy.

Upon lowering the temperature, the conversion to the dimer rapidly decreases (Entries 1-2), and at room temperature the only products observed are those related to the polymerisation reaction. Dilution has a minor negative effect on dimer formation over the time of the reaction (Entry 3).

In order to inhibit polymerisation, it was hoped that addition of DMAP (4-dimethylaminopyridine) would alter reactivity. DMAP is strongly nucleophilic, so it should bind strongly to iron catalysts and displace polymeric chains. In practice, it appears to have an insignificant effect on both catalytic activity and selectivity (simultaneous polymer formation also remains high, Entry 4). Contrastingly, using a strongly coordinating solvent, in this case acetonitrile, completely inhibits all catalysis (Entry 5). Halting the reaction before full conversion reveals that the *cis*-*trans* selectivity does not vary greatly over the course of the reaction (similar to the isomerisation chemistry in Chapter 2, Entry 6).

A final alteration to the experimental setup was through use of a syringe pump to add the reagent slowly. This should reduce the concentration of phenylallene in the reaction mixture, which was also performed in more dilute conditions (Table 21, experimental setup detailed in Section 7.3).

Table 21 – Syringe pump experiments, with the standard condition outcomes shown as a comparison.

Entry	Catalyst Loading	Volume / mL	Temp / Time	Isolated Yield / %
Standard Conditions	5%	0.6	80 °C, 16 h	27
1	5%	6	80 °C, 16 h	28
2	1%	6	80 °C, 16 h	7
3	5%	6	RT, 16 h	-
4	1%	6	RT, 16 h	-

Conditions : **1** used as catalyst, 10 mol% $NH_3{\cdot}BH_3$. Conversion determined by ^1H NMR spectroscopy.

Using the same catalyst loading, time and temperature results in conversion being very similar to the standard (non-syringe pump) experiments (Entry 1). Reducing catalyst loading leads to a reduction in dimer conversion (7%) (Entry 2). Performing the reaction at room temperature leads to no dimerised products being isolated (Entries 3&4).

Despite the various alterations above, none of the conditions or alternative reagents lead to a reaction system where dimerisation is favoured over polymerisation, and the maximum dimer conversion has not exceeded 30%.

Given that both reactions involve the activation of the terminal double bond, and require both the iron catalyst and ammonia borane (or an alternative hydrogen source) to proceed there is some indication that both dimerisation and polymerisation reactions follow similar mechanistic pathways — as discussed above, the polymerisation reaction is proposed to proceed through an Fe(I) mechanism. As both reactions are observed simultaneously, mechanistic probing is difficult, although the reaction proceeds when PMe_3 is added, and when a radical trap is used. Using deuterated amine boranes does not result in any d-incorporation observed on the products, and the iron hydride dimer **43** does not perform dimerisation in itself.

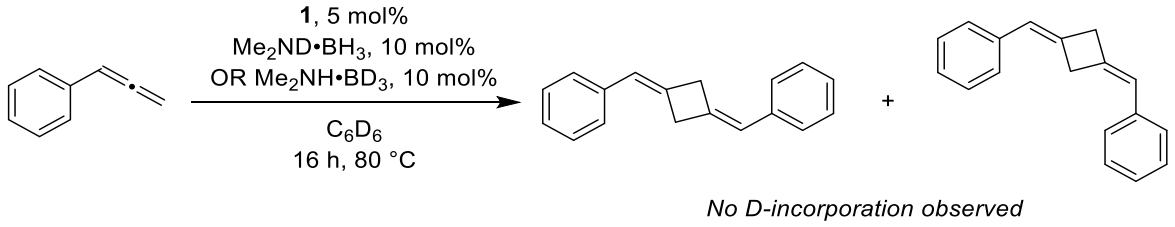

Scheme 118 – Using deuterated amine boranes does not result in any observable d-incorporation on the dimeric products.

Assuming the reaction is Fe(I)-based, the most likely proposition is the allene displacing the solvent and binding in an η^2 fashion to form **62**, as in polymerisation. The simplest mechanistic proposal involves the bound allene then performing a [2+2] cycloaddition — presumably this proceeds as one of the bonds is being activated by the metal centre. The metal centre shifts binding to the unreacted alkene as part of this transformation, and the product molecule is displaced by a further molecule of allene. This mechanism does not fully rationalise why the 1,3-product is formed readily over the thermal 1,2-product, although presumably the mode of metal-allene binding directs it towards this product. Unlike with polymerisation, the proposed catalytic cycle is not redox-active (apart from catalyst activation) and instead proceeds only in the Fe(I) oxidation state (Scheme 119).

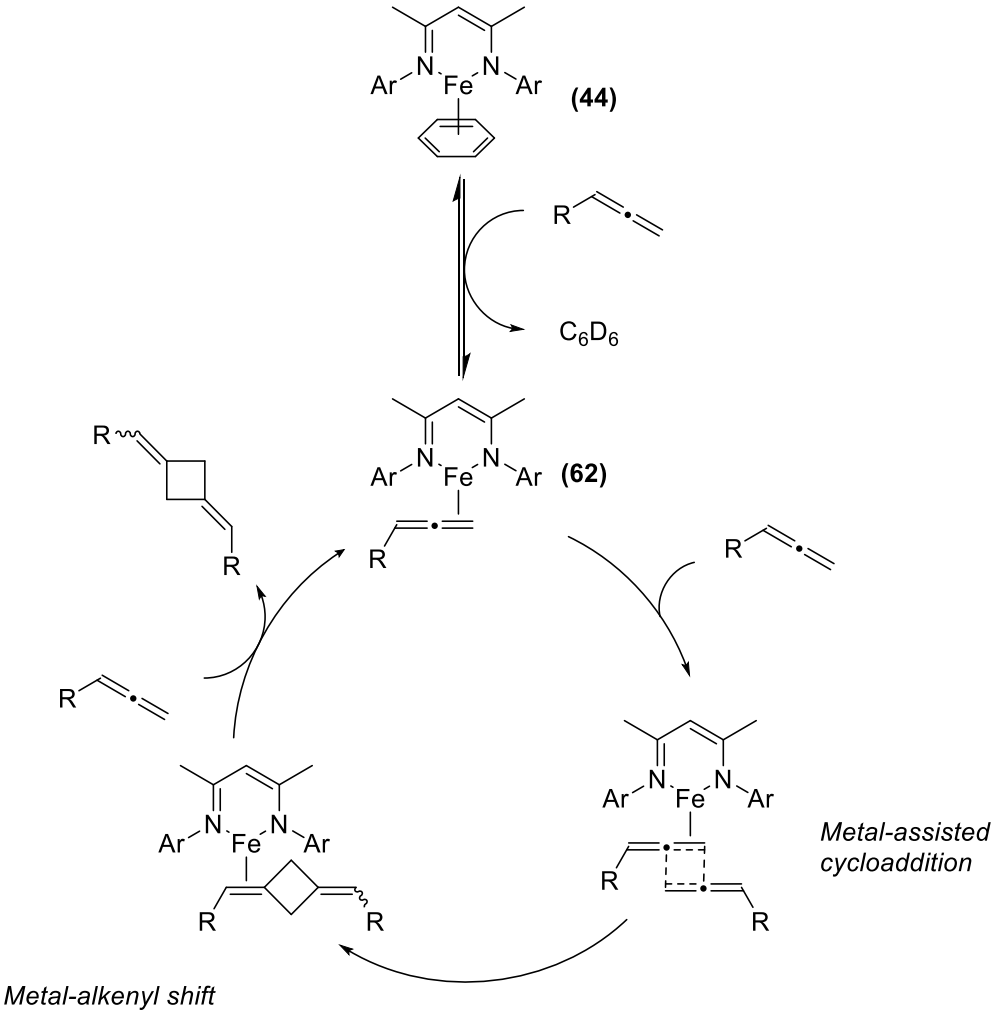

Scheme 119 – Proposed catalytic cycle for allene dimerisation.

Forming the 1,3-dimerisation product from terminal allenes is exceptionally unusual, especially with a very high selectivity over the 1,2-dimer product. However, the amenability of polymerisation of phenylallene using this catalytic system clearly limits the specific conversion towards the dimeric product, and it is likely alternative catalytic systems are required to achieve high selectivities and conversion towards the desired product.

3.7 [2+2] Heterocoupling of Allenes with Alkynes

Concurrently with our own investigations of allene polymerisation and dimerisation, Yoshikai reported a cobalt-catalysed intermolecular [2+2] cycloaddition between alkynes and allenes. This proceeds with a cobalt salt, proligand and indium metal as a reducing agent (Scheme 120). [281]

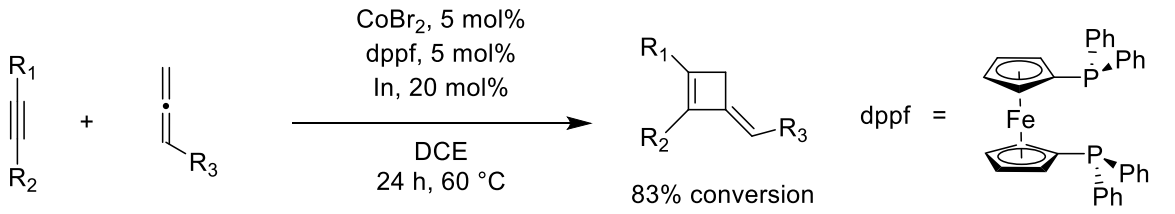

Scheme 120 – Intermolecular [2+2] cycloaddition between alkynes and allenes reported by Yoshikai. [281]

A full cycle is not proposed, although the general pathway is suggested to be a one electron reduction to a Co(I) species, which is then amenable to oxidatively cyclise the two coupling partners; the ring is then formed by reductive elimination.

Studies were undertaken to see if similar reactivity could be observed using the iron pre-catalyst and co-reagents used in this study. Cyclohexylallene is reported as an amenable substrate, and using this was also hoped to prevent the substrate from polymerising. Phenylallene was also tested, the conditions are shown in Scheme 121.

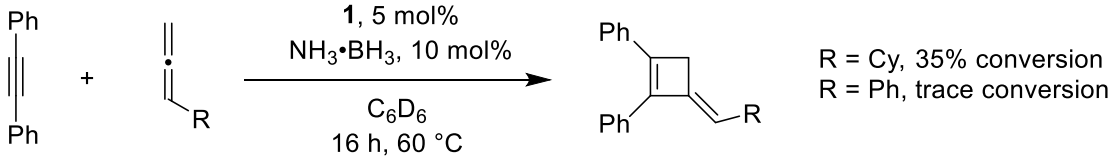

Scheme 121 – Reactions of cyclohexylallene and phenylallene with diphenylacetylene in the presence of an iron pre-catalyst and ammonia borane.

The reaction with cyclohexylallene is clean, with no homocoupled structures observed, although the overall yield is reasonably low compared to the literature study (83% for the same substrates). When using phenylallene the outcome of the reaction contains a mixture of polymer, alkyne-allene product and additional peaks that could not be easily assigned, and the conversion could not be determined with accuracy.

Catalysing [2+2] cycloadditions of this form using the iron catalysts seems to be challenging with phenylallene and derivatives, owing to the amenability of polymerisation and an alternative reaction pathway. While alternative substrates that do not undergo polymerisation do selectively undergo this reaction, they are not as potent or active as previously reported examples.

3.8 Conclusions from Chapter 3

Polymerisation of allenes is a relatively unstudied field, and this study investigates both the catalytic process and the properties of the produced polymers. The catalysis reported herein is facile and at a low loading compared to previous, serendipitous observations with Grubbs catalyst and similar complexes. Compared to the previous reported rare-earth metal catalysis by Cui, the polymers prepared herein are considerably longer, with only a small increase in polydispersity. While the reported f-block catalysis is strongly (2,3)-selective, which in turn leads to a well-defined melting point, this catalysis produces a significant amount of (1,2)-structure. This has enabled the (1,2)-conformation to be further studied by NMR, but no clear melting points could be determined in this study. Finally, compared to previous living polymerisation reports, again the polymer length and dispersity is increased, and there are clear mechanistic differences between both studies. Throughout this study we have used GPC and DSC to compare directly to previous reports, as well as using techniques not previously reported, such as MALDI, to examine structure further.

The unusual NMR signals about the alkyl chain have not, to our knowledge, been previously observed or studied for these polymers. Our own conclusion was that there are a range of conformational blocks which lead to varying chemical shifts based on the ^{1}H and ^{13}C NMR signals and Density Functional Theory modelling. However, it is likely that alternative analytical methods would be able to probe these structures more deeply and gain a better of understanding of how and why they occur.

The [2+2] dimerization of phenylallene into a 1,3-cyclobutane product is a rare transformation, with only one example of direct previous precedent (*vide supra*). The study reported herein achieves this reaction in one step from phenylallene, but there is a clear limit to conversion to the dimeric species, which hinders further probing of reactivity and using the product in further reactions. This process likely requires significant changes in reaction setup to achieve high and scalable conversions, but the report herein is still exceptionally unusual as a demonstration of reactivity.

Chapter 4 – Iron-Catalysed Hydrophosphination of Allenes

In Chapters 1 and 2, it was shown that iron pre-catalysts can form a broad range of carbon-heteroatom bonds using alkene substrates through hydrofunctionalisation. Furthermore, in Chapter 3 it has been shown that the same iron catalysts can functionalise allene substrates effectively. In this chapter these two aspects are combined; iron complexes are used to catalytically hydrophosphinate allene substrates to create a new C–P bond, and the scope and mechanism of this process are investigated.

4.1 Iron-catalysed C–X Bond Forming Reactions with Allenes (X = B, Si, N, P)

The preliminary work to the isomerisation studies in Chapter 2 involved the reported hydroboration of alkenes using iron(II) β-diketiminate pre-catalysts, primarily **1**. [217] This would appear to be readily applicable to allenes, as various hydroboration studies are reported (as reviewed in Section 1.5). However, as seen in Chapter 3, using a catalytic amount of pinacolborane catalysed polymerisation rather than any hydroboration. If the amount of pinacolborane is increased to one equivalent, a mixture of the hydroboration and polymerisation products are observed, although there is a strong preference for the polymer (Scheme 122). The ^{1}H NMR spectrum is complex, and it appears a range of isomers of the hydroborated product are formed.

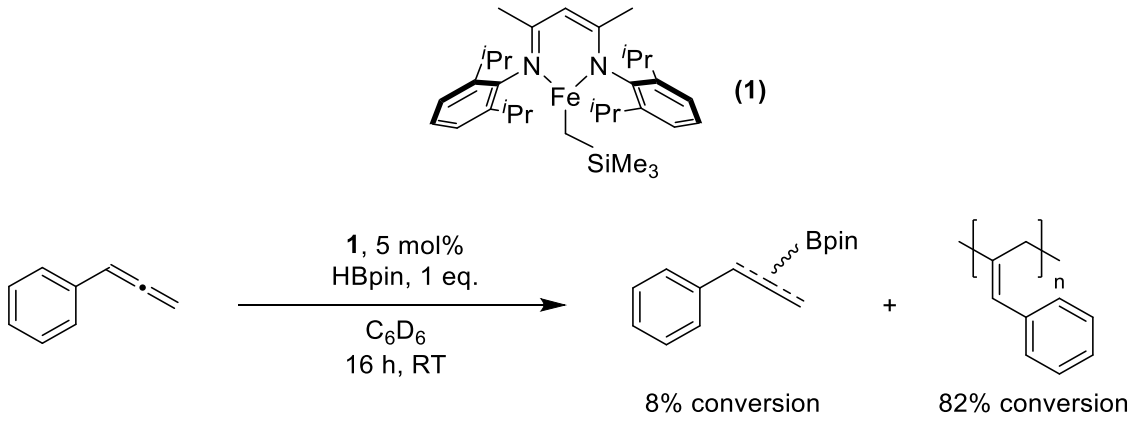

Scheme 122 – Attempted hydroboration of phenylallene. The majority of product formed is polymer, and the hydroborated products appear to be in a range of regio- and stereoisomers. Conversion determined by *in situ* ^{1}H NMR spectroscopy.

Similarly, we can use triethoxysilane, which was also shown to enable polymerisation when used in a sub-stoichiometric loading. When one full equivalent is used the conversion to polymerisation is still high, but no signals that can be easily attributed to the hydrosilylated products were observed (Scheme 123).

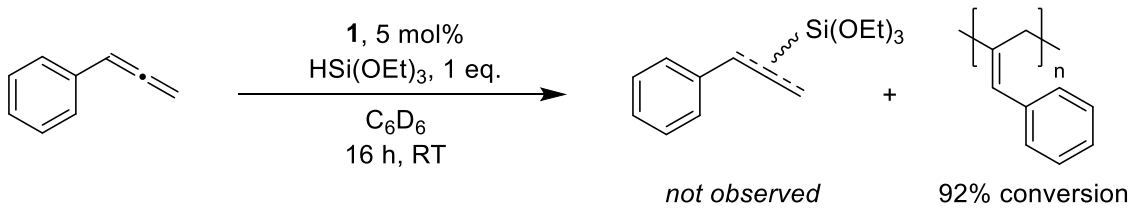

Scheme 123 – Attempted hydrosilylation of phenylallene. In this case, no hydrosilylated product is observed to form. Conversion determined by *in situ* ^{1}H NMR spectroscopy.

In Chapters 2 and 3, we have proposed that HBpin and alternate hydride sources reduce the Fe(II) species **1** to an Fe(I) species, which is then able to readily perform isomerisation or polymerisation reactions. The facile conditions and thermodynamic favourability of polymerisation mean that if this route is possible, it will be favoured over alternative (hydrofunctionalisation) reactions. Hydrosilylation of alkenes does not occur under similar reaction conditions with **1** as the catalyst; this may be entirely unfeasible, regardless of competing processes.

Alternatively, if a more electron-withdrawing heteroatom is used (such as nitrogen or phosphorus), the hydrogen becomes more protic in character than hydridic. Because of this, it appears less likely that the reagent would react with the catalyst and reduce it to Fe(I) species, and instead form an iron-amido or iron-phosphido intermediate (Figure 62). These are proposed in previously reported hydroamination and hydrophosphination reactions discussed in Section 1.5.

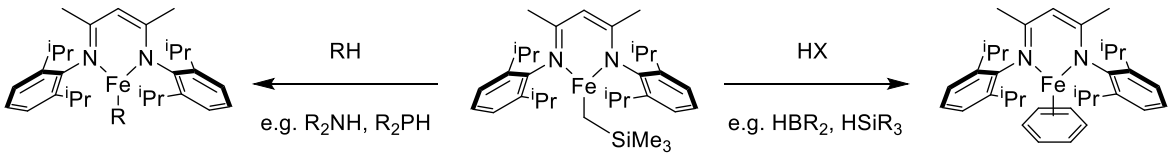

Figure 62 – By using protic rather than hydridic reagents, it was hypothesised that **1** could be activated to form Fe(II) species readily capable of performing hydrofunctionalisation reactions, rather than solvent-stabilised Fe(I) species capable of performing competing processes.

Nitrogen has an extremely diverse range of potential substrates, for this study benzylamine and aniline were tested, owing to their relative ease to dry, distil and handle. Disappointingly, these did not yield any conversion (Scheme 124). This is perhaps to be expected, as intermolecular hydroamination or alkenes has proved exceptionally challenging to perform with first row transition metals such as iron. [40] NMR studies indicate the pre-catalyst remains intact during the reaction, indicating that neither benzylamine or aniline are capable of facilitating catalysis, and the yield of polymeric products produced is similar to running the reaction without a hydride source as in Section 3.1.

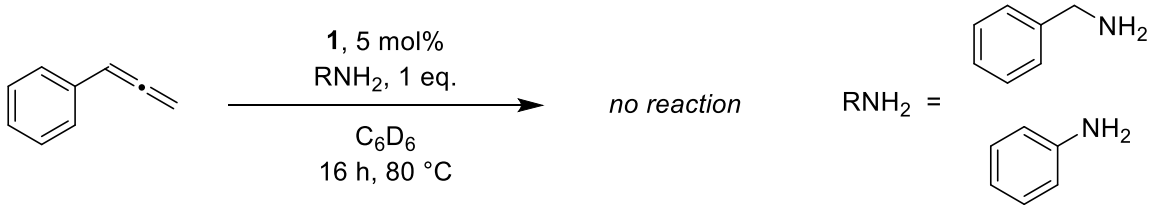

Scheme 124 – Attempted hydroamination of phenylallene with both benzylamine and aniline leads to no conversion to hydroaminated products.

In contrast to hydroamination, hydrophosphination has previously been reported with a range of iron catalysts, some examples are shown in Scheme 125. Gaumont initially showed that simple iron halide salts can catalyse hydrophosphination, but in these cases a very large loading is required. [282] Lower loadings and more facile conditions have subsequently been reported by Webster [45, 283] and Kays. [284] This includes **1**, although the conditions are not as facile compared to pre-catalysts such as **66** and **28** (shown below).

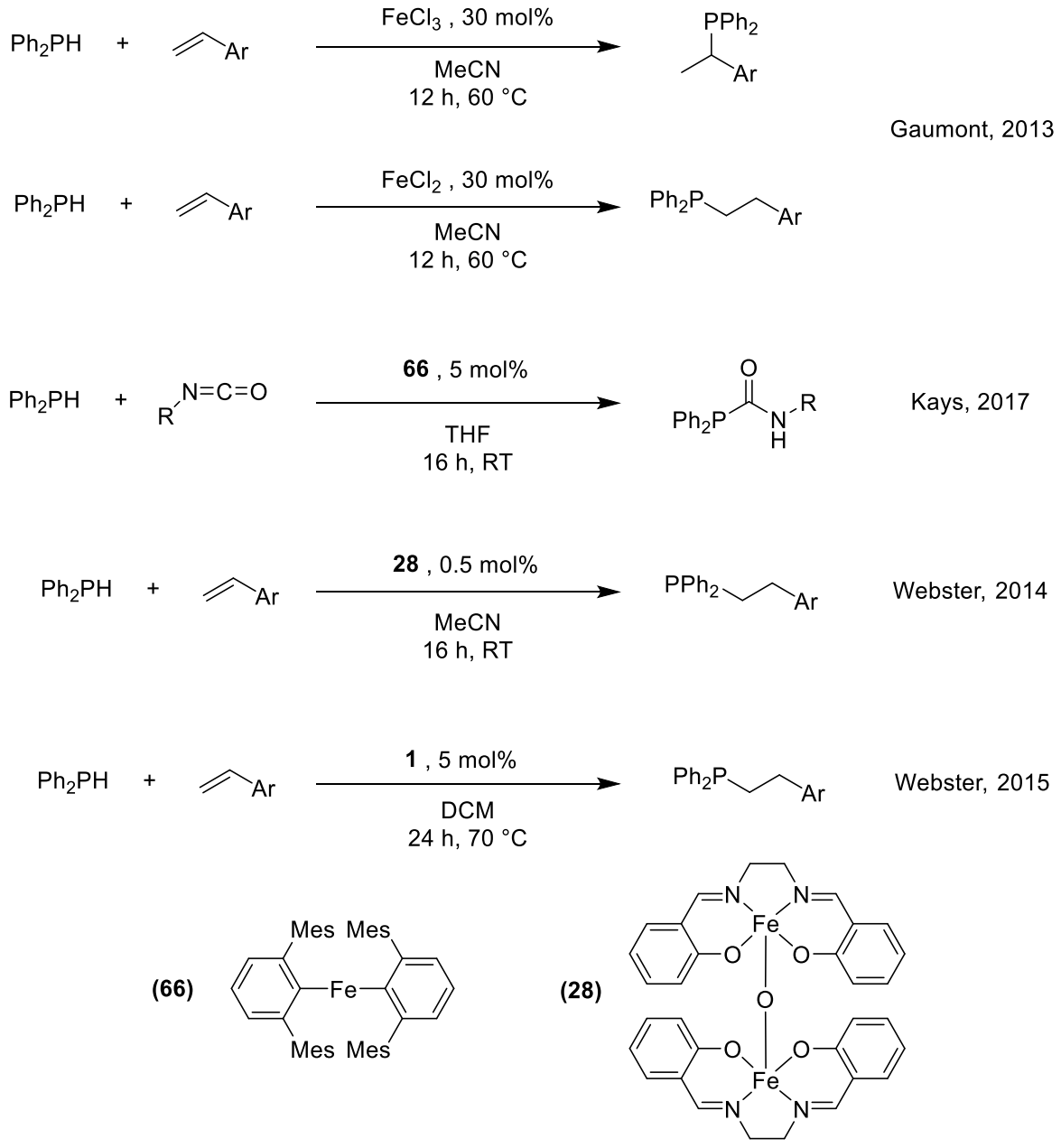

Scheme 125 – Previous examples of iron-catalysed hydrophosphination of alkenes and other unsaturated compounds

Because of this, it seemed that hydrophosphination of allenes should be achievable even if hydroamination has been shown not to be, as activation of **1** with diphenylphosphine has already been shown to be feasible. As discussed in Section 1.5, there are various reaction involving allenes as substrates to form new C–P bonds, despite this there are very few methods that use simple

phosphines or are applicable to a broad range of allenes. In particular, diphenylphosphine is an affordable phosphorus reagent that is relatively easy to handle, furthermore when added across alkenes and alkynes the products are normally stable enough to be worked up and characterised in air. Ligands with an 'RPPh$_2$' structure are also extremely common in both organometallic synthesis and catalysis, so products formed from hydrophosphination with diphenylphosphine have potential applications in these fields. [285, 286]

An initial reaction was prepared using the conditions shown in Scheme 126. As there are two potential double bonds to add over, initially two equivalents of diphenylphosphine were reacted with phenylallene to see if there was a preference in the reaction for forming monofunctionalised products, difunctionalised products or a mixture of both. The use of phosphorus reagents means that ^{31}P NMR spectroscopy can be used as a rapid and informative method to monitor the reaction. As well as unreacted diphenylphosphine, the dehydrocoupled product Ph_4P_2 is observed, as well as four new signals, labelled A through D, although D is only formed in a very small amount (Figure 63). ^{1}H NMR spectroscopy indicates that the amount of polymer forming is minor compared to the attempted hydroboration and hydrosilylation reactions, whilst a range of new signals are observed in both the alkenyl and alkyl regions. This shows that hydrophosphination is occurring under these conditions.

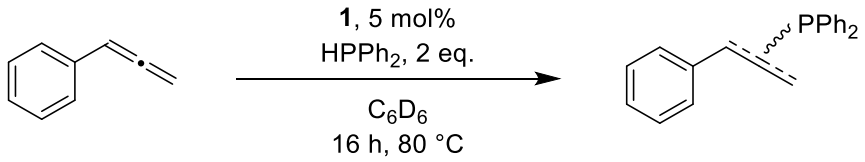

Scheme 126 – Attempted hydrophosphination of phenylallene.

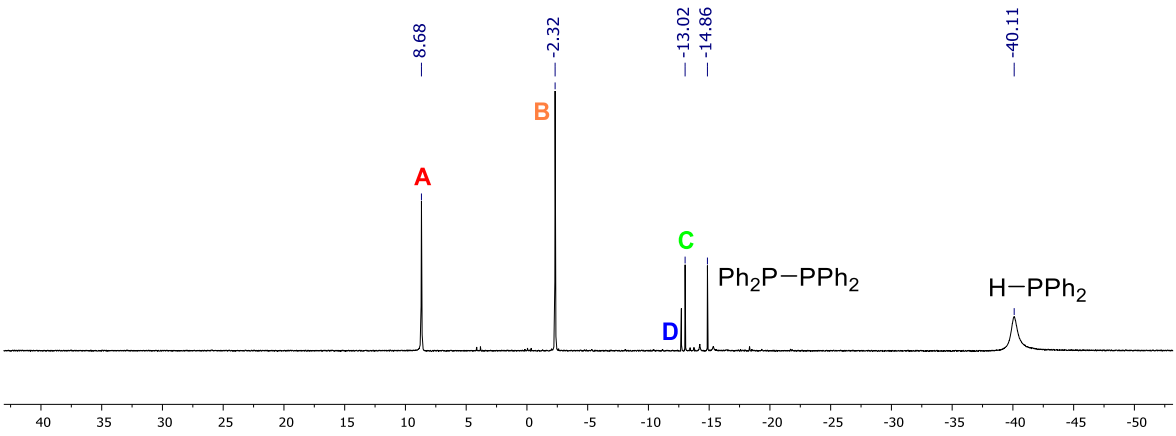

Figure 63 – ^{31}P{^{1}H} NMR spectra of the reaction shown in Scheme 126 (202 MHz, C_6D_6). As well as the starting diphenylphosphine and some dehydrocoupled product, four new signals (labelled **A**, **B**, **C** and **D**) are observed to form.

4.2 Studying Hydrophosphination Products through NMR Spectroscopy

As stated in introduction Section 1.5, the cumulated nature of allenes mean a range of regio and stereoisomers are possible in hydrofunctionalisation reactions, which helps explain why four distinct new signals appear. The three major signals A-C can be compared to the previously reported products characterised by Mitchell. [175] All three peaks are reasonably close to the three reported

isomers (**67**-**69**) shown in table. **69** is a regioisomer of both **67** and **68**, which are *E*/*Z* stereoisomers of each other.

Table 22 – The three new phosphorus signals compared to the chemical shifts and structures reported by Mitchell. Although there are some minor differences in chemical shift they compare reasonably well (202 MHz, C_6D_6).

Signal	Observed δ / ppm	Reported δ / ppm	Structure
A	8.7	6.7	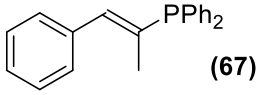 **(67)**
B	−2.4	−4.1	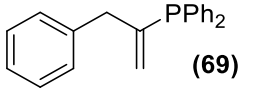 **(69)**
C	−13.0	−14.9	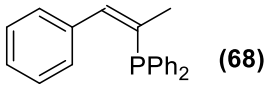 **(68)**

To our knowledge, Mitchell's radical preparation is the only reported synthesis of these compounds using an allenic substrate. However, structures **67** and **68** can alternatively be prepared from the hydrophosphination of 1-phenyl-1-propyne, while **69** cannot without proceeding through a complex reaction path (Figure 64). Moreover, this reaction has been reported with a range of catalysts, including Webster, [287] Cui, [288] Alonso [289] and Mulvey. [290] By performing this reaction, we can affirmatively assign **67** and **68** as specific structures, and **69** by process of elimination.

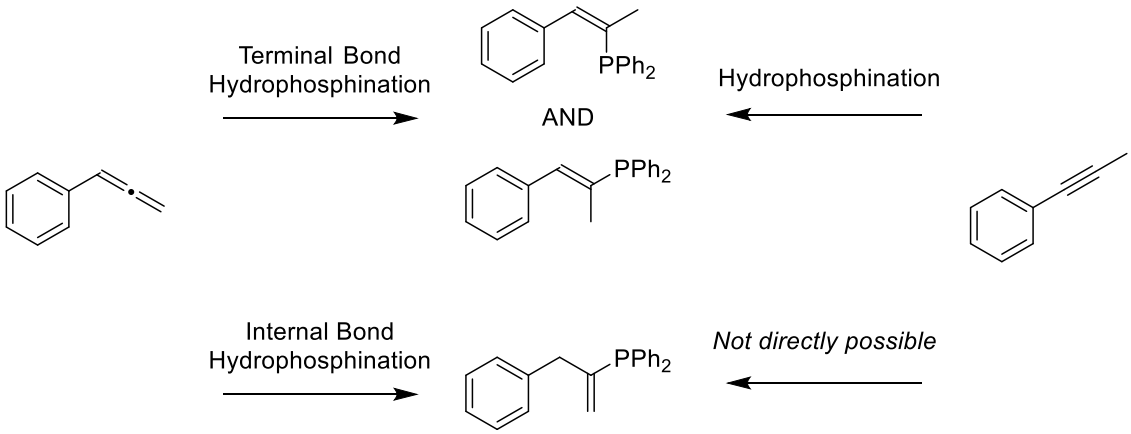

Figure 64 – Hydrophosphination of 1-phenyl-1-propyne yields only the internal hydrophosphination products, meaning these structures can be confirmed synthetically. Formation of the internal product would only be possible through a more complex rearrangement.

Whilst there are some minor differences in chemical shift, the *Z*-isomer is reported as being between δ = 8.7–9.5 ppm and the *E* isomer between δ = −12.3–−13.4 ppm in each of these studies. This is opposite to the earlier assignment by Mitchell and a minority of previous reports, [291] despite this the greater number of studies assign them in this conformation and it relates better to the ^{1}H NMR assignment (*vide infra*). The internal product **69** is unequivocally identifiable with signal B. All three observed products, their ^{31}P chemical shifts and terminology used in the rest of this chapter are given in Figure 65.

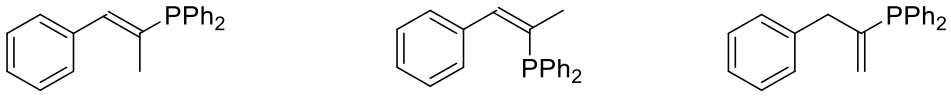

67 Terminal *E*
^{31}P δ = -13.0 ppm

68 Terminal *Z*
^{31}P δ = 8.7 ppm

69 Internal
^{31}P δ = -2.4 ppm

Figure 65 – The structures, naming convention and ^{31}P chemical shift (500 MHz, C_6D_6) of the hydrophosphinated products observed in this study.

Signal D is formed in a comparatively small amount (<1%), and is neither reported in previous reports nor formed from the hydrophosphination of 1-phenyl-1-propyne. It is likely an alternative regioisomer, with the C–P bond forming at either the 1 or 3 positions. Given the greater reactivity of the terminal bond it is proposed to be the latter (Figure 66).

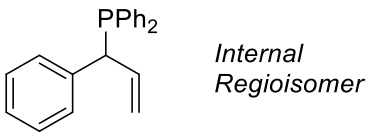

Internal Regioisomer

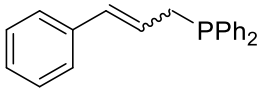

Terminal Regioisomer
Likely **D**
^{31}P δ = -12.4 ppm

Figure 66 – The minor signal **D** is likely the terminally functionalised product with alternate regioselectivity.

The products can be isolated from the reaction mixture by standard column chromatography, although the R_f values are so similar that all three products co-elute (see Section 7.4 for further discussion on this). A wide range of NMR experiments are available for organophosphorus compounds owing to the presence of ^{1}H, ^{13}C and ^{31}P nuclei and because of this it is possible to fully assign ^{1}H and ^{31}P signals for the isomeric mixture. The ^{1}H spectrum of the three isomers is shown in Figure 67, with the peaks identified with the respective isomers.

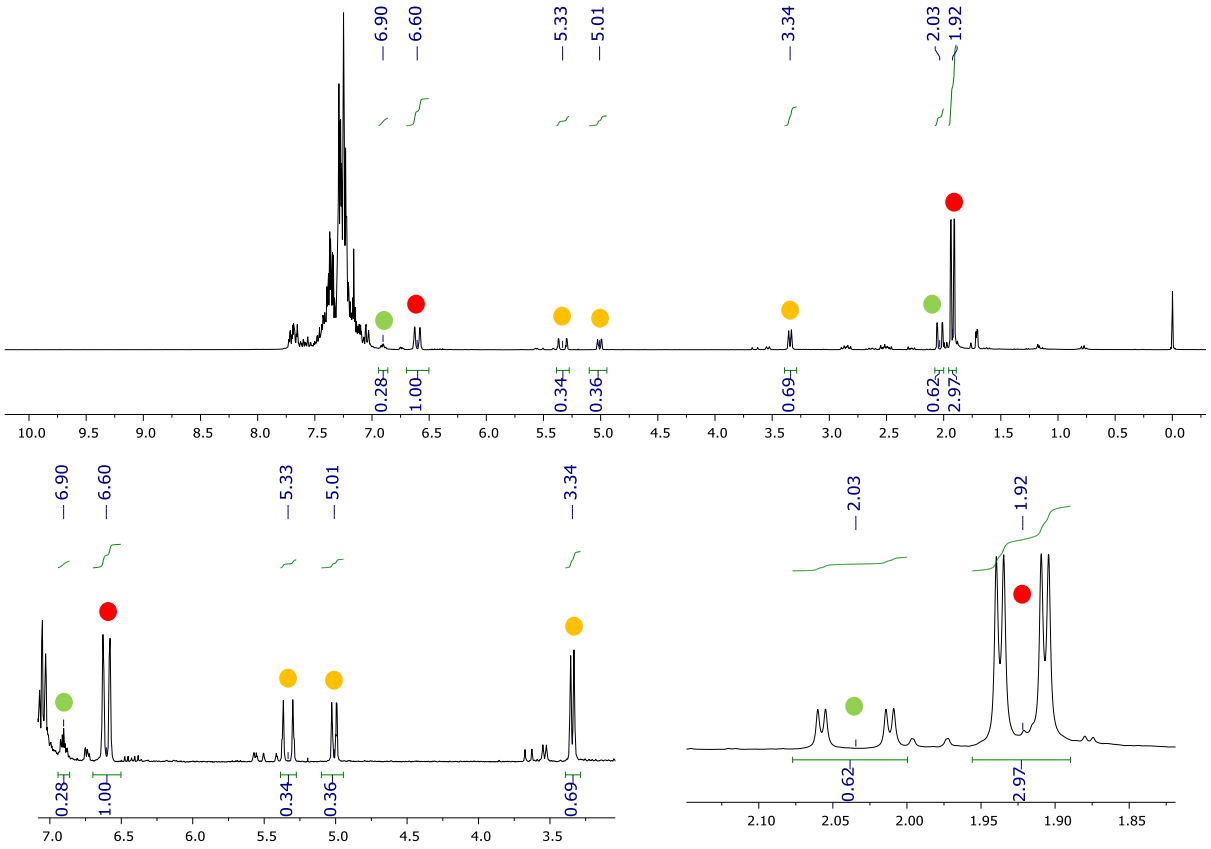

Figure 67 – ^{1}H NMR (500 MHz, $CDCl_3$) of the three hydrophosphinated products. Signals belonging to the terminal *Z* product **68** are identified with **red** ●, signals belonging to the terminal *E* product **67** are identified with **green** ●, and signals belonging to the internal product **69** are identified with **yellow** ●.

P–H *J* couplings are observed in both ^{31}P and ^{1}H NMR, and these support the structure of each isomer. The *Z*-isomer is the most straightforward as the coupling is clear in the α-proton, the methyl protons and the P-centre. The *E*-isomer is reported to have a $^{3}J_{PH}$ coupling across the double bond of 9.1 Hz; experimentally both the α-proton and the phosphorus signal appear as complex multiplets and precise coupling values cannot be determined from them (when using some of the functionalised arylallenes tested in Section 4.4, the coupling of the *E* isomer is well-defined enough to determine a $^{3}J_{PH}$ coupling value of similar frequency). The well-defined methyl signal does allow the remaining to *J* values to be determined. All determined *J* values are reasonably consistent with literature data, [290] and the values observed support the structure of both isomers.

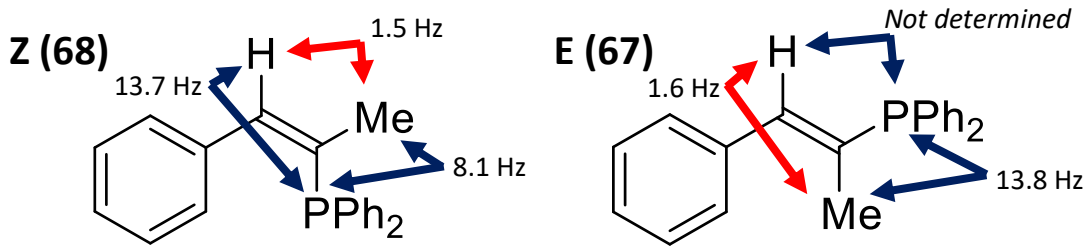

Figure 68 – Observed *J* coupling values between the phosphorus and non-aryl protons (**blue**) and between non-aryl protons (**red**) for the terminal *Z* and *E*-isomers (500 MHz for ^{1}H, 202 MHz for ^{31}P, both C_6D_6).

The internal product has very different non-aryl NMR shifts to the terminal products (Figure 69), and as it cannot be prepared from the alkyne, literature characterisation is limited. Determining all coupling values is slightly complicated by the closeness in *J* values between the geminal but inequivalent protons labelled H_A and H_B and their respective coupling with the α-protons; this leads to a splitting pattern very similar to a doublet of quartets ('dq'). With careful measurement the coupling values of the actual doublet of triplets of doublets ('dtd') pattern can be obtained. The α-protons would be expected to have a doublet of doublet of doublet ('ddd') splitting, in practise they are observed as a broad doublet consistent with the $^3J_{PH}$ coupling frequency. Finally, the assignment of H_A and H_B can be determined by the relative strength of coupling to the phosphorus centre ($^3J_{HAP} > {}^3J_{HBP}$, as per the Karplus relationship) and that H_A has weak NOESY correlation with the aryl region, whereas H_B does not.

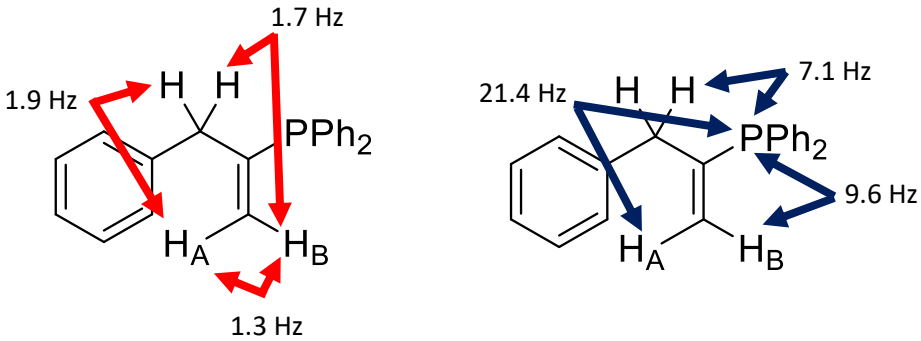

Figure 69 – Observed *J* coupling values for the internal product **69**. P-H coupling values are in **blue** and H-H coupling values are in **red** (500 MHz for ^{1}H, 202 MHz for ^{31}P, both C_6D_6).

In terms of $^{13}C\{^1H\}$ NMR, the three compounds have a mixture of easily identifiable and more difficult to ascertain signals. The P*Ph*$_2$ groups are essentially identical in each isomer in terms of $^{13}C\{^1H\}$ chemical shift, and as such appear as single or overlaying doublets (coupling to the phosphorus) despite arising from three different molecules. Furthermore, the C_{META} and C_{PARA} environments on the phenyl ring are difficult to determine, owing to the broad and overlapping aryl ^{1}H signals and their distance from any useful handle signals to correlate with. C_{ORTHO} and C_{IPSO} can be determined for each isomer using HMBC experiments, correlating to the alpha proton (or protons) in each case. Finally, the formerly allenic carbon bound to the phosphorus centre does not generate an observable signal — no peak with the correct HMBC correlation could be determined for each isomer, and no signal with the predicted large $^1J_{PC}$ coupling was observed. $^{13}C\{^1H\}$ data, along with mass spectrometry and FTIR data are detailed in Section 7.4.

4.3 Variation and Optimisation of Reaction

Because the three hydrophosphination products each have distinct peaks in ^{31}P NMR spectrum, as well as in ^{1}H NMR (*vide supra*), the former can be used as a quick and straightforward tool to determine reaction conversion. Although regular ^{31}P NMR experiments cannot be quantified accurately, inverse gated setups can be used to determine a reasonable quantitative result. By adding a known amount of triphenylphosphine to the reaction as an internal standard a concentration, and therefore amount of each product can be determined.

Some variations of reaction conditions were performed to see what effect they had on selectivity and yield. This was done partly to maximise conversion of the starting materials in the most facile conditions, partly to observe if the regio- and stereoselectivity between the three products could be altered, and party to see if any doubly hydrophosphinated products could be formed. Initially temperature and other reaction conditions were altered (Table 23).

Table 23 – Variation of reaction conditions.

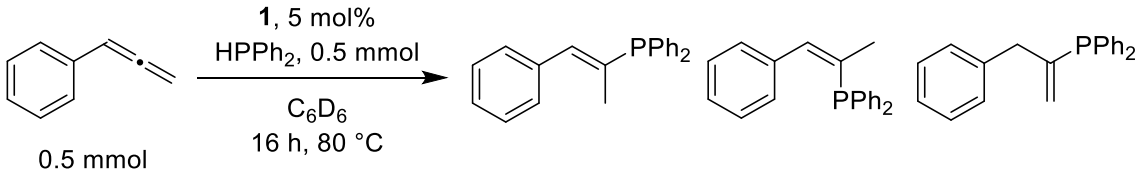

Entry	Deviation from Standard Conditions Above	Conversion / %				
		All HP	Terminal *E*	Terminal *Z*	Internal	Ph_4P_2
1	None	45	5	32	8	46
2	RT instead of 80 °C	23	3	14	6	17
3	60 °C instead of 80 °C	32	4	21	7	24
4	No stirring (NMR tube)	25	2	19	4	34
5	CD_2Cl_2 instead of C_6D_6	61	5	42	14	16

600 µL solvent used. Conversion determined by in situ inverse gated ^{31}P NMR (202 MHz). "All HP" refers to total conversion to hydrophosphinated products.

The initially observed reaction has an overall conversion to the hydrophosphinated products of 45 %, and a similar level of conversion towards dehydrocoupling (46 %, Entry 1). Lowering the temperature decreases conversion of both (Entries 2 & 3), although it slightly increases chemoselectivity of hydrophosphination against dehydrocoupling (32% hydrophosphinated vs. 24% dehydrocoupled at 60 °C, 23% vs. 17% at RT). Stirring has an important role in conversion, and performing the reaction in a J-Young NMR tube as opposed to a stirred Schlenk flask reduces conversion (Entry 4). Previous reports have indicated that changing the solvent has a significant effect on chemoselectivity in some hydrophosphination reactions [45], and there is a reasonable increase in chemoselectivity towards the hydrophosphinated products (61% vs. 45%), although overall conversion is actually decreased (Entry 5). In all cases, the ratio between compounds is reasonably constant, with the terminal *Z*-isomer being formed in the greatest conversion and the terminal *E* the least.

While overall conversion at 80 °C is reasonably high (91% of $HPPh_2$ in C_6D_6), the poor chemoselectivity means conversion to hydrophosphination is disappointingly low. Given that under these conditions a considerable amount of the starting allene is left unreacted, it was hypothesised that varying the concentration in some way may improve conversion. The reaction was run with different amounts of each substrate (Table 24).

Table 24 – Variation of reagent volumes and catalysts.

Entry	Deviation from Table 23	Conversion / %				
		All HP	Terminal *E*	Terminal *Z*	Internal	Ph_4P_2
1	None	45	5	32	8	46
2	0.6 mmol $HPPh_2$	52	6	36	10	-
3	1.0 mmol $HPPh_2$	68	6	44	18	-
4	0.6 mmol Phenylallene	82	8	51	23	2
5	1.0 mmol Phenylallene	82	7	52	23	2
6	As Entry 4, and **28** as catalyst	16	2	8	6	75
7	As Entry 4, and **27** as a catalyst	66	6	43	17	2
8	As Entry 4, and $FeCl_2$ as catalyst	4	trace	4	trace	3
9	As Entry 4, no catalyst	trace	trace	trace	trace	4

Conditions as per the scheme in Table 23. In Entry 6, acetonitrile-d_3 was used in place of benzene-d_6. Conversion determined by inverse gated ^{31}P NMR spectroscopy with respect to the limiting reagent. "All HP" refers to total conversion to hydrophosphinated products.

(27)

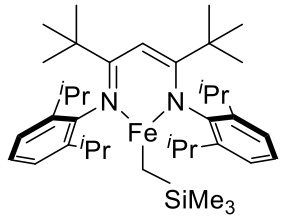

(28)

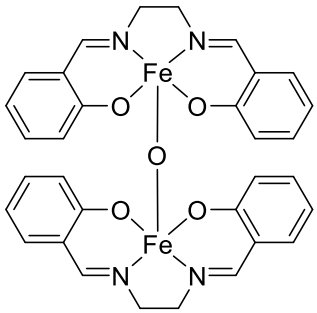

Initially the amount of diphenylphosphine was increased, as more of this converted in the reaction when compared to the allene. By doing this the conversion of the allene was slightly increased with a small excess (52%, versus 45% under equimolar conditions), and further with one full additional equivalent (68%, Entries 2 & 3). Note that conversion was determined by ^1H NMR with respect to the limiting reagent, phenylallene, but from ^{31}P NMR it is clear a large amount of Ph_4P_2 is additionally forming. Hence, although the conversion with respect to phenylallene is improving, with respect to diphenylphosphine it is even lower than at one equivalent (34%). Furthermore, no doubly hydrophosphinated products are observed to form, even though the stoichiometry of the reaction would allow them to.

The reaction was run instead with phenylallene in slight excess (Entry 4). In this case there is a large increase in chemoselectivity towards hydrophosphination (82% hydrophosphination vs. 2% dehydrocoupling), with the effect of preparing the hydrophosphinated products in a reasonably high yield. A small amount of allene polymer is formed in these conditions (approximately 10% of the starting material), and a reasonable amount of it is left unreacted (approximately 20%, note as phenylallene is in excess the conversion with respect to phenylallene is 68%) , along with some

unreacted diphenylphosphine. Increasing the amount of phenylallene further does not have an effect on the reaction conversion, merely increasing the amount of both unreacted and polymerised phenylallene. Some discussion on why the reaction outcome is dependent on the amount of reactant is given in Section 4.6.

A final set of optimisation studies were undertaken by varying the catalyst present. Switching to the salen complex **28**, even under the most optimal conditions for the β-diketiminate complex **1** nearly totally flips chemoselectivity from 82% hydrophosphination to 75% dehydrocoupling (Entry 6). The bulky complex **27** does not exhibit such drastic change, and instead results in a reduced conversion to hydrophosphination (66%) and a very slight change in ratio of products formed in preference of the internal product (Entry 7). Finally, the two reagents only react in trace amounts with a 5 mol% loading of $FeCl_2$ or without any catalyst (Entries 8-9).

If the optimised conditions are applied to 1-phenyl-1-propyne, the substrates respective activity and selectivity can be compared (Scheme 127). Using the alkyne leads to a lower conversion (73% vs. 84%) and conversion to hydrophosphination (69% vs. 82%), although selectivity towards the *Z* isomer is greatly improved (67% *Z* isomer **68**, 2 % *E* isomer **67**) – as discussed previously, the internal product cannot readily be formed. Using phenylallene, therefore, generates a higher yield in a like-for-like comparison, and an alternative regioselectivity.

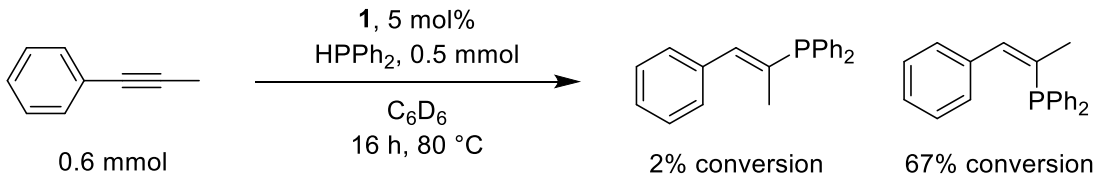

Scheme 127 – Hydrophosphination of 1-phenyl-1-propyne is leads to lower conversion than when using phenylallene, although the reaction is considerably more *Z*-selective.

4.4 Synthetic Scope – Variation of Allene

With optimised conditions in hand, the range of substrates tested was expanded. A range of derivatives of phenylallene can be synthesised as they were in Chapter 3. This represents an a more straightforward preparation than synthesis of 1-phenyl-1-propene derivatives, which typically require palladium cross-coupling processes. [292] Furthermore several commercially available allenes were also tested in catalysis. Many of the resultant products have not been reported previously, hence this methodology provides an opportunity to make novel phosphorus(III) compounds. A summary of outcomes is presented in Table 25.

Substrates **54**–**59** were utilised in polymerisation catalysis, and their synthesis and spectroscopic data is provided in Section 7.3. Substrates **70** and **71** were only used in hydrophosphination; their synthesis and spectroscopic data is provided in Section 7.4. Cyclohexylallene and methoxyallene are commercially available.

Table 25 – Variation of allenes in catalysis

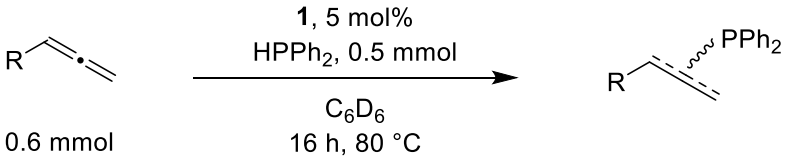

Entry	Substrate	Conversion / %				Compound Numbers in Experimental (*E*, *Z*, Internal)
		Overall	Terminal *E*	Terminal *Z*	Internal	
1	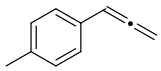 **54**	81	6	48	27	**72, 73, 74**
2	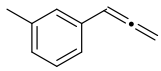 **55**	75	12	52	11	**75, 76, 77**
3	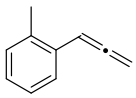 **56**	74	6	60	8	**78, 79, 80**
4	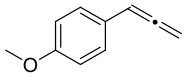 **57**	86	15	60	11	**81, 82, 83**
5	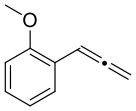 **70**	91	10	60	21	**84, 85, 86**
6	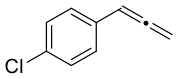 **59**	77	6	70	1	**87, 88, 89**
7	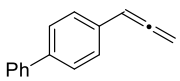 **71**	60	6	40	14	**90, 91, 92**
8	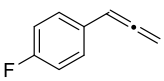 **58**	59	4	54	1	**93, 94, 95**
9	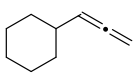	46[a]	6	32	2	**96, 97, 98** (other isomers **99**)

10	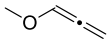	34[b]	20	12	-	**100, 101** (no internal isomer observed)

600 µL solvent used. Substrates in entries 1-8 were prepared as per the experimental details listed above. Conversion determined by *in situ* inverse gated ^{31}P NMR spectroscopy.

For arylallenes, the difference in ^{31}P chemical shift between each substrate are relatively minor. For example, looking at the terminal *Z* products, the ^{31}P chemical shift for **68** is 8.7 ppm, for **94** it is 8.3 ppm, and for **82** it is 10.0 ppm. Proton chemical shifts are also generally similar in chemical shift and coupling frequencies.

For all arylallene substrates the reaction is predominantly terminal *Z* selective, typically with around 75% regioselectivity towards this isomer. Nevertheless, there is some terminal *E* and internal product observed in each reaction, although for the 4-chloro- and 4-fluoro- substrates the amount of internally substituted product formed is very low. Overall conversion for methyl-substituted substrates is similar to non-substituted phenylallene (Entries 1–3), whilst for methoxy substituted substrates there is a slight improvement in conversion (Entries 4-5). The remaining substrates have conversions that are lower, especially for the 4-fluoro substrate (Entries 6–8). In all cases a small amount of Ph_4P_2 is observed, for the poorer converting substrates this is increased. Entries 1–8 generate compounds that were previously unreported; data for all observed products is reported in Section 7.4.

The majority of the compounds are stable enough in air to be isolated through standard column chromatography procedure. The exceptions are methoxy-based compounds **82-86**, as well as the cyclohexyl and methoxyallene compounds, which rapidly degrade in air; these are instead isolated through a silica plug in an argon atmosphere.

The non-aryl allenic substrates exhibit differences in their behaviour. Their NMR data is, predictably, less similar to the arylallenes. The ^{31}P NMR of the cyclohexylallene reaction clearly shows that five, rather than three products are forming (Figure 70). These consist of the terminal *E*, terminal *Z* and internal products, and furthermore the regioisomeric alternative *E* and *Z*-products where the new P–H bond is formed on the terminal carbon atom, similar to the **D** environment in the initial studies (**99**, Figure 71). The complexity of the product mixture, along with the paucity of literature reports mean it was not possible to determine which signals belonged to which specific isomer – their ^{1}H NMR signals also overlay (see experimental section).

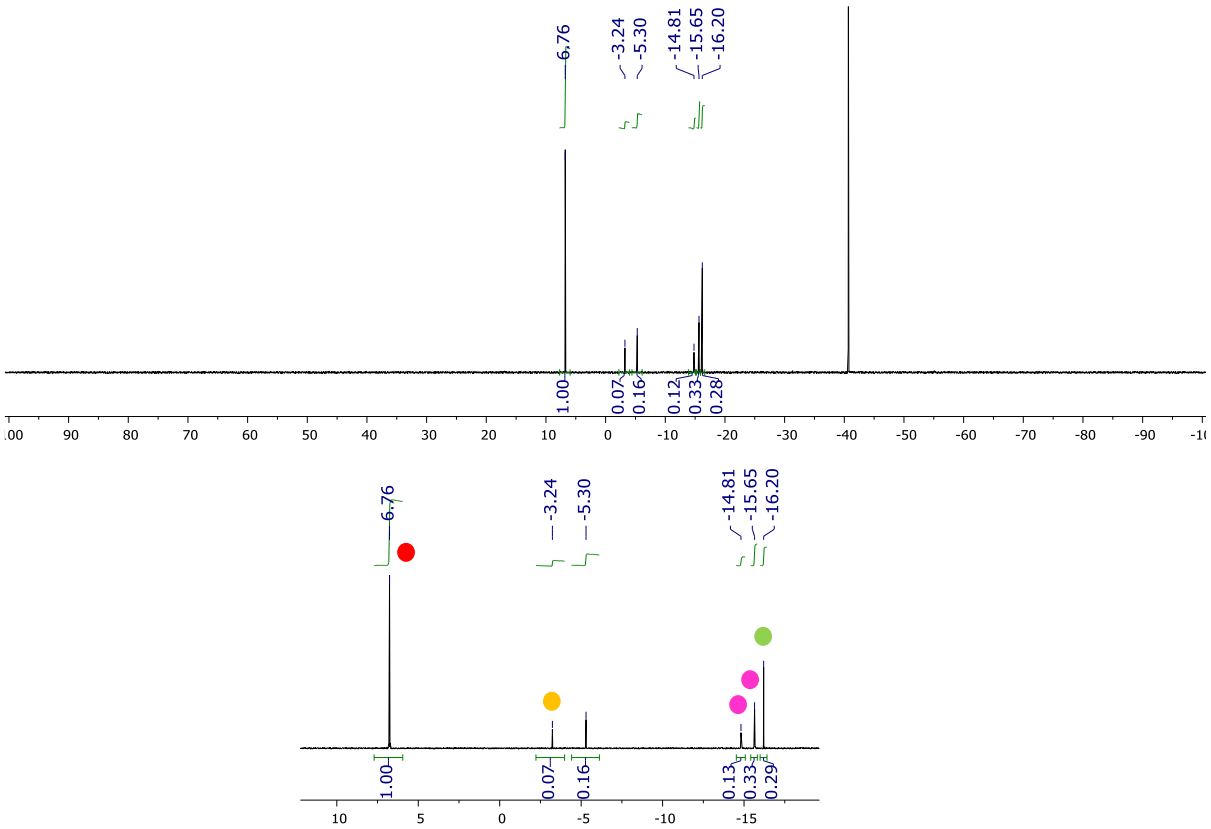

Figure 70 – In situ inverse gated ^{31}P NMR of the reaction of diphenylphosphine and cyclohexylallene. The three regioisomers formed in the reactions with arylallenes are again formed here (Terminal *Z* denoted with **red**, terminal *E* with **green**, internal with **orange**) along with two further new signals (**pink**) which were assigned to the structures below. PPh_3 used as internal standard (δ = 5.3 ppm), unreacted $HPPh_2$ observed at δ = −40.0 ppm (202 MHz, C_6D_6).

(99)

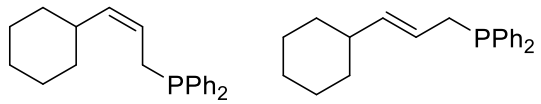

Alternate Terminal Products
$^{31}P\{^1H\}$ δ = -14.8, -15.6 ppm
(Specific assignment not determined)

Figure 71 – The two further regioisomers observed in the reaction with cyclohexylallene and their chemical shifts (202 MHz, C_6D_6).

In the case of methoxyallene, only the standard terminal products were observed and there is no clear indication of the internal product forming to any degree (^{31}P NMR shown in Figure 72). Conversion is again low, but heating methoxyallene over the reaction period indicates that it degrades at 80 °C, which is affecting conversion rather than inertness to react. There are also two signals that appear as doublets in the $^{31}P\{^1H\}$ NMR spectrum with J_{PP} values of 25.4 Hz — it is likely this is a double hydrophosphination product, forming in 2% conversion. Comparing to coupling values of other diphosphine compounds it is likely this is a $^3J_{PP}$ coupling. [293] The ^1H NMR spectra could not be fully assigned, but the signals observed as consistent with the structure shown in Figure 73 forming (A 2,3-double hydrophosphination as opposed to a 1,2 or 1,3).

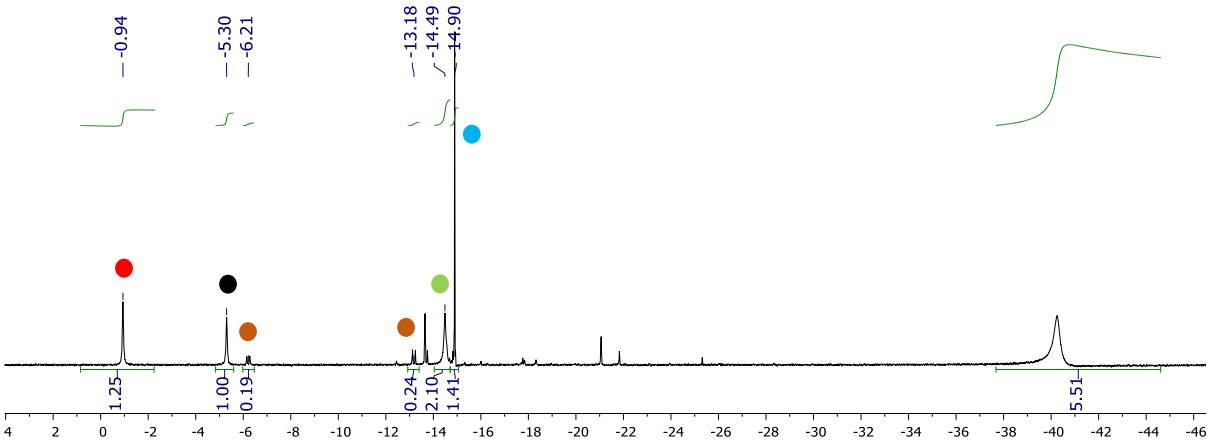

Figure 72 *In situ* inverse gated ^{31}P NMR of the reaction with methoxyallene. In addition to the Terminal *Z*, Terminal *E*, Dehydrocoupled and PPh_3 reference signals (**red**, **green**, **blue** and **black** respectively), two minor signals (**brown**) show a small amount of double hydrophosphination is occurring (202 MHz, C_6D_6), as well as some other minor unidentified products.

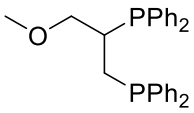

$^{31}P\{^{1}H\}$ δ = -6.2 (^{3}J = 25.4 Hz), -13.2 ppm (^{3}J = 25.4 Hz)

Figure 73 – Proposed structure of double hydrophosphination product.

The range of allenes that react is somewhat broader than those that are amenable to polymerisation, as non-aryl allenes have been shown to hydrophosphinate under the same conditions as aryl ones. Although in all cases the mono-hydrophosphinated product is formed, there is still a mixture of structural isomers in all cases when reacting with diphenylphosphine.

4.5 Synthetic Scope – Variation of Phosphine

Using alternative phosphorus reagents can diversify the range of compounds available in this catalysis. Dicyclohexylphosphine is commercially available, and ligands with a $RPCy_2$ structure have found applications in a vast range of catalytic transformations, a recent example is shown by Hartwig for rhodium-catalysed hydroamination. [294] The P–H bond of dicyclohexylphosphine is considered more challenging to activate than that of diphenylphosphine owing to the move away from aryl functional groups.

Under the same conditions, with phenylallene as the substrate, conversion is considerably reduced when switching from diphenylphosphine to dicyclohexylphosphine, with overall conversion being 8% compared to 82% (Scheme 128). The reaction products have not been previously reported, but by reacting dicyclohexylphosphine with 1-phenyl-1-propyne and comparing the products the internal regioisomer **104** can be identified (again, the reaction with 1-phenyl-1-propyne is lower in conversion compared to phenylallene). Given the strong stereoselectivity of the previous substrates to the *Z*-isomer over the *E*-isomer, it appears reasonable to assume that of the two remaining peaks, the one formed in greater abundance is the *Z*-isomer **103** and the other peak is the *E*-isomer **102**.

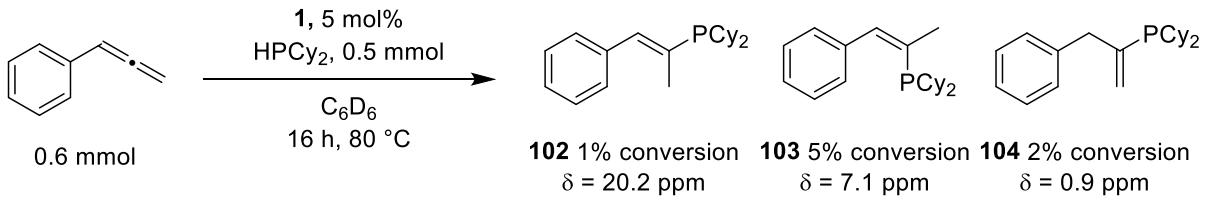

Scheme 128 – Hydrophosphination of phenylallene with dicyclohexylphosphine yields the three regioisomeric products observed in reactions with diphenylphosphine, although the conversion is much lower under the same reaction conditions. $^{31}P\{^{1}H\}$ NMR chemical shift for each product is also shown (202 MHz, C_6D_6).

We can also utilise primary phosphines as reagents, which can be generalised as RPH_2. These substrates can complicate regioselectivity, as they have the potential to singly or doubly hydrophosphinate an unsaturated bond. Waterman [295] and Yao [296] have previously reported the hydrophosphination of 1-phenyl-1-propene with phenylphosphine using zirconium catalysts, as well as characterised the resulting *E* and *Z*-products, although only in the former have the isomers been formally distinguished. Under standard reaction conditions the conversion of phenylphosphine is reasonably high, the outcome of this reaction is shown in Scheme 129.

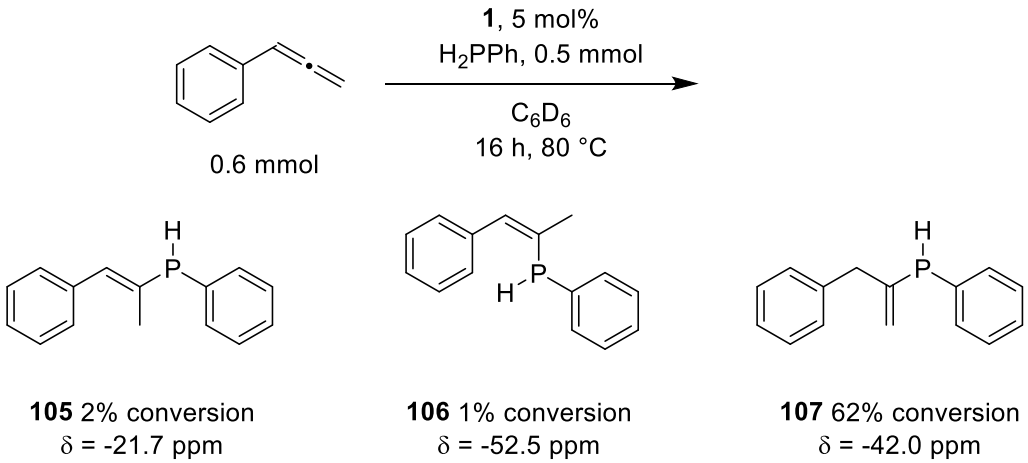

Scheme 129 – Hydrophosphination of phenylallene with phenylphosphine. A small amount of the terminal *E* and *Z*-isomers are formed, but the reaction is strongly regioselective towards the internal product – $^{31}P\{^{1}H\}$ NMR chemical shift is shown for each product (202 MHz, C_6D_6)

The chemical shifts of the products are significantly more upfield than the any of the previous hydrophosphination products. This arises as all the products are still secondary phosphines leading to much greater shielding, and large $^{1}J_{PH}$ values (between 210 and 220 Hz) can be observed for each product in both the ^{31}P and ^{1}H NMR spectra. As **105** and **106** are both known compounds, their structural data can be easily elucidated from the product mixture. Perhaps surprisingly, **107** is by far the dominant reaction product, and the reaction is far more regioselective than any other encountered in this study. Although **107** is not previously reported or characterised, the abundance in which it is formed mean assignment is conclusive enough to ascertain the structure (See Section 7.4).

As phenylphosphine is a primary phosphine (and the products secondary), it is in theory possible for the product to further react to form a tertiary P-centre through further hydrophosphination or dehydrocoupling, in the event none are observed. It is equally possible for phenylphosphine to react

twice with phenylallene to form a diphosphine with two "PHPh" functionalities; again this is not observed. A small amount of phenylphosphine (2%) dehydrocouples to form Ph_5P_5 under these conditions, whilst the remaining phenylallene is polymerised into polyphenylallene.

Doubling the equivalents of phenylphosphine (*i.e.* 1 mmol H_2PPh and 0.6 mmol phenylallene, other conditions unaltered) does not have a significant effect on the reaction — relative conversion to the hydrophosphinated products is 66% compared to 65% above. Running the reaction in two equivalents of phenylallene (*i.e.* 0.5 mmol H_2PPh) likewise does not have a meaningful effect on the reaction conversion or outcome.

When using cyclohexylphosphine, no reaction occurs at all. This may be predicted, both from the analogous decrease of reactivity from diphenyl- to dicyclohexylphosphine, as well as the previously reported differences in reactivity of phenylphosphine and cyclohexylphosphine (where the latter is much more challenging as a hydrophosphination substrate). [297]

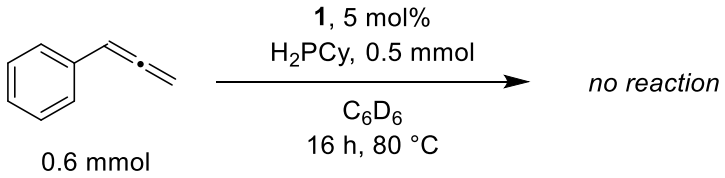

Scheme 130 – Attempted hydrophosphination of phenylallene with cyclohexylphosphine. No reactivity was observed.

These reactions show that the phosphine reagent can be altered in this catalysis without entirely inhibiting reaction, although conversion is much poorer when using non-phenyl substituted reagents, highlighting the importance of the functional groups around phosphorus relative to reactivity.

4.6 Mechanistic Studies into Catalytic Allene Hydrophosphination

Previous mechanistic studies have been undertaken with this catalytic system and both alkenes and alkynes. In both cases, the productive catalytic pathway is proposed to involve the formation of an iron(II) phosphido complex, which can then coordinate over an unsaturated bond and undergo elimination through protonolysis. The mechanism for alkyne hydrophosphination is shown in Scheme 131 — this provides a useful starting point and comparison for studies into allene hydrophosphination.

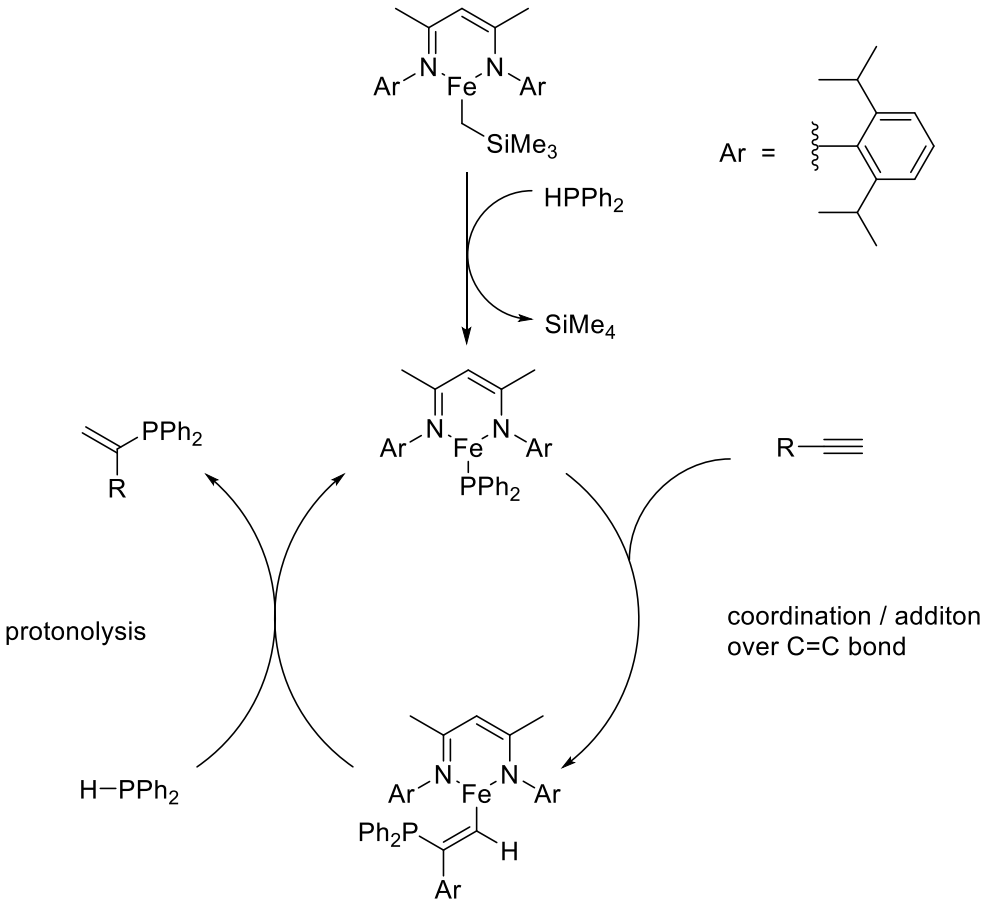

Scheme 131 – Mechanistic proposal for terminal alkyne hydrophosphination with diphenylphosphine and **1** as a catalyst as previously proposed by Webster. [298]

As in Chapters 2 and 3, some simple mechanistic experiments were performed. A sub-stoichiometric amount of PMe_3 does not fully inhibit reactivity, ruling out a nanoparticle role. A radical trap experiment did also not affect reaction conversion, and furthermore the (chloromethyl)cyclopropane could be recovered, unreacted, through trap-to-trap distillation. These experiments are discussed in greater detail in Chapters 2 and 3, as well as the experimental section.

A further trapping experiment can be performed to investigate whether the reaction proceeds through a 'free' phosphorus nucleophile rather than a metal catalytic species. A stoichiometric equivalent of benzaldehyde reaction was added to the reaction, with the expectation that this is more amenable to nucleophilic attack that the allenic substrate (Scheme 132). This outcome has previously been observed for outer-sphere based hydrophosphination catalysis, where a formal P-nucleophile is formed, which subsequently attacks the carbonyl rather than react with an alkenyl substrate. This can be observed both from the aldehyde proton ^{1}H NMR signal decreasing in intensity, and new phosphorus environments being observed in the ^{31}P NMR spectrum. [166] In this reaction, the presence of benzaldehyde does not perturb reactivity significantly, and it can be observed, unreacted, at the conclusion of the reaction. No new phosphorus environments are observed to form in ^{31}P NMR, which appears rule out this process.

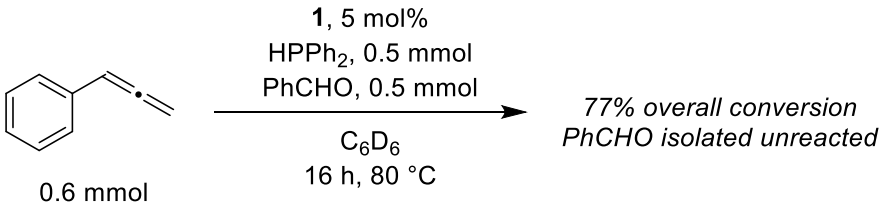

Scheme 132 – Addition of benzaldehyde to the reaction does not significantly affect conversion or selectivity, and the unreacted benzaldehyde can be isolated at the end of the reaction. This observation appears to rule out a nucleophilic phosphorus-based mechanism.

The deuterated analogue of diphenylphosphine, $DPPh_2$, is relatively simple to prepare and was used to investigate the mechanism further. If a single product is initially formed but then isomerise to form the other two products, generating a mixture, then all the products would be deuterated at the same site (an analogous form of this rearrangement has previously been reported by Archibald [299]). Using $DPPh_2$ generates three deuterophosphinated products in the predicted manner, with a single D–P function added across the double bond (Scheme 133). The ^2H NMR shows three new environments have formed, and they can be further confirmed through changes in the splitting of the remaining protic peaks (the coupled and decoupled ^{31}P spectra become complex multiplets).

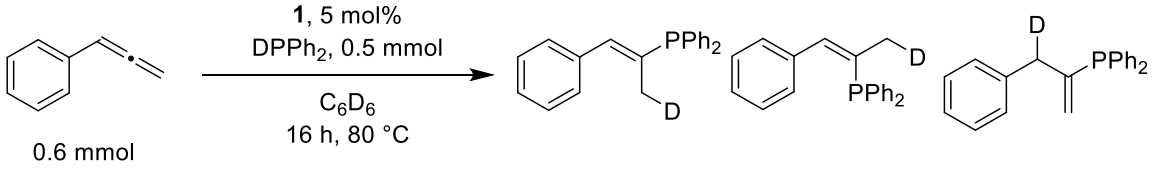

Scheme 133 – Reaction with $DPPh_2$. The selectively deuterated products of each of the previously observed products could be isolated.

The mechanistic postulations in both Chapters 2 and 3 involve the same reduction of the initial pre-catalyst through the use of a catalytic amount of a hydride source to form the solvent-stabilised iron(I) species **44**. The analogous iron(I) species **45** was used in both cases in catalysis, and the similar outcomes support its role as an active species. For the reported hydrophosphination it appears that **44** or similar compounds are not the active species in catalysis. This is because firstly, in the presence of **1** and a hydride source phenylallene readily polymerises rather than undergo hydrofunctionalisation, as can be seen in Sections 3.1 and 4.1. The high yields of the hydrophosphinated product in this reaction contrast to this and suggest this mode of reactivity is not accessible under these in conditions. Secondly, using **45** in catalysis under the same reaction conditions generates a complex, somewhat insoluble mixture of polymer and tetraphenyldiphosphine with only a small amount of hydrophosphinated products formed. It is still possible that a very small amount of Fe(I) complex forms, and this leads to the small amount of polymer formed, particularly in the reaction with phenylphosphine – this can be seen as a minor competing process rather than a crucial part of the mechanistic pathway.

Instead, we propose that **1** is interconverted into the same iron-phosphido complex proposed for alkyne hydrophosphination, **108**, releasing a molecule of $SiMe_4$ (Scheme 134). This step can be considered irreversible, which drives the reaction forward. As this activation is non-substrate dependent it appears a reasonable assumption that it is possible in this reaction as it for reactions with alkenes and alkynes.

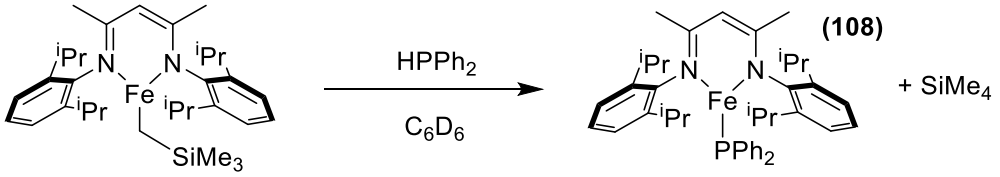

Scheme 134 – Formation of an iron-phosphido species **108** from the reaction of **1** and diphenylphosphine.

Isolating **108** crystallographically proved difficult, as a mixture of **1** and diphenylphosphine reacts readily to produce tetraphenyldiphosphine at high temperatures, and not at all at low temperature. Previous attempts through metathesis processes have also proved unsuccessful, and have been shown in many cases to perform alternative metathesis reactions. [300] Grubba and Stoian have previously reported formation of a solvent-stabilised analogue **109**. [301] This does not exist as in its monomeric form at raised temperature, and the formation of dimeric species **110** from the reaction of a primary alkyl phosphine suggests that **108** may also exist as a dimer to some extent (drawn as **111** in Figure 74). As in the case with the iron hydride in Section 2.6, it was proposed that it is possible for both the monomer and dimeric form exist to some extent in equilibrium, but the closed nature of **111** precludes the dimer itself from being actively involved in the catalytic process.

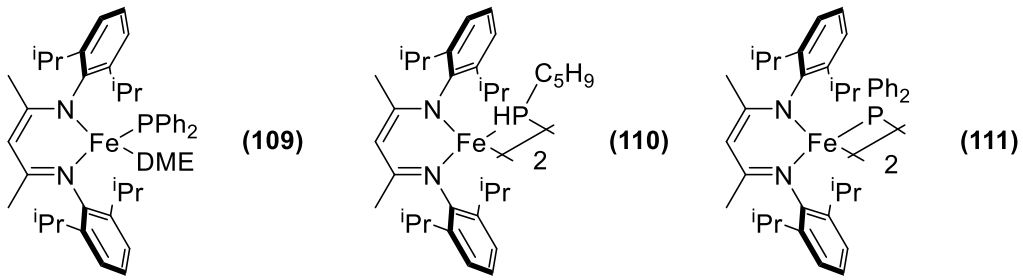

Figure 74 – A solvent-stabilised analogue of **108** has been prepared by Grubba and Stoian **109**, and the formation of dimeric species **110** from the reaction of **1** and linear primary phosphines suggest that a dimeric form of the iron-phosphido complex **111** may also be formed in the reaction.

From here it is proposed that **108** performs hydrophosphination through a mechanism broadly similar to the alkyne hydrophosphination pathway, a scheme showing the formation of the terminal *Z*-product is shown in Scheme 135.

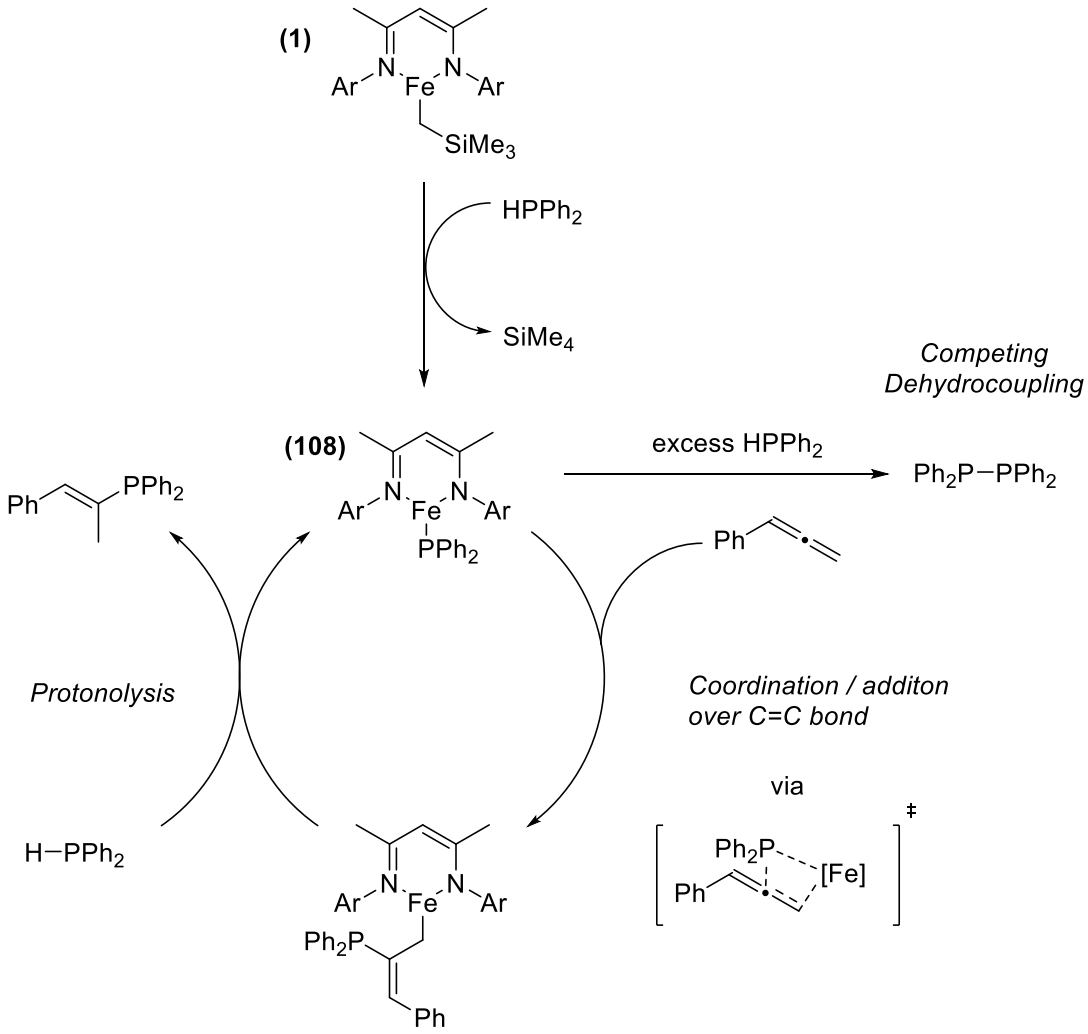

Scheme 135 – Proposed catalytic cycle for allene hydrophosphination (Terminal-*Z* hydrophosphination of phenylallene shown)

The iron-phosphorus bond is added over an unsaturated bond. The phosphorus atom forms on the β-position, although the route of attack and specific bond added over does vary and determines selectivity (*vide infra*). A second molecule of diphenylphosphine can then react, protonating and releasing the product and regenerating **108**.

It has been seen that running the reaction at equal stoichiometries leads to a significant amount of tetraphenyldiphosphine being produced, as opposed to running in an excess of allene where only a small amount of this is formed. Grubba and Stoian's findings with **109**, coupled with previous studies into phosphine dehydrocoupling with **1**, suggest that **108** should readily dehydrocouple diphenylphosphine in the presence of additional diphenylphosphine and the absence of alternative reaction pathways. Hence, the excess of allene is necessary to divert the reaction towards the addition pathway.

The poorer conversion of the electron withdrawing allenes (such as **58**) and the improved performance of electron rich substrates (such as **57**) suggest that the electrophilicity of the allene is important, with increasing electrophilicity yielding a more facile transformation.

In terms of the effect of phosphine reagents, the poor reactivity of dicyclohexylphosphine, but the absence of any tetracyclohexyldiphosphine forming suggest that both formation of the iron phosphide species and consequent reactivity are both reduced when the phenyl groups are replaced with cyclohexyl ones. Contrastingly, phenylphosphine has a similar reactivity to diphenylphosphine, and the improved regioselectivity towards the internal product can be rationalised by the reduced sterics of the phosphide complex (thereby making it easier to access and functionalise the internal double bond), or the variation in electronics around the phosphorus centre.

As proposed, the selectivity of the reaction, both regio- and stereo-, is determined by the conformation of the addition step across the double bond, forming intermediates with fixed products (Figure 75). Regioselectivity is determined by whether the internal or terminal double bond is activated. Given both regioisomers form it appears that the barriers to both are reasonably close in energy, and precise regioselectivity is determined by relatively small differences in sterics and electronics. It is interesting that phenylphosphine and diphenylphosphine exhibit very different regioselectivities, indicating that the sterics and electronics of both the phosphido intermediate and allene influence reactivity.

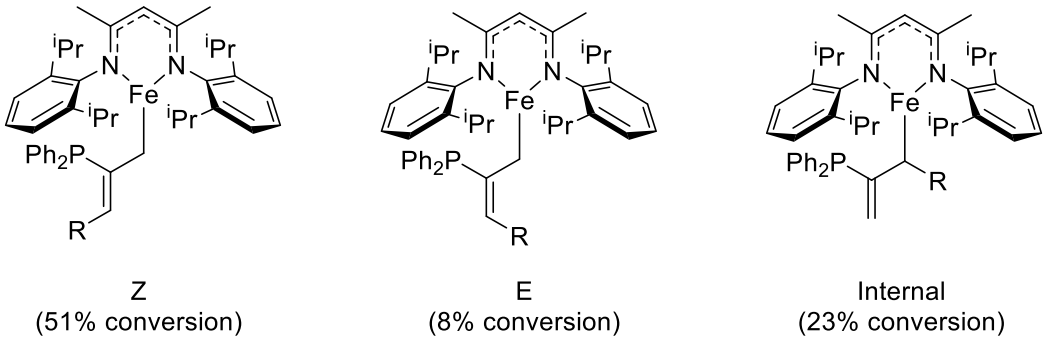

Figure 75 – The iron-alkyl intermediates that lead to the three observed products being formed. The conformation the iron phosphide adds across the allene determine which of these species is formed, and hence the resulting product.

The *E*-*Z* selectivity of the terminal isomers also warrants discussion. The *E*-isomer appears to be the more favoured product owing to the reduced sterics about the double bond, but in the reaction the *Z*-isomer forms in strong stereoselectivity. Again, we can compare this to the reactivity of the alkyne 1-phenyl-1-propyne. The majority of the methods of hydrophosphination of this substrate are *E* selective (although Cui's findings indicate some complexes are strongly *Z*-selective and Mulvey's produces both isomers in equal ratio). [287-290] However, as using **1** in hydrophosphination of 1-phenyl-1-propyne is strong *Z*-selective, this suggests that the structure of intermediate **108** is important in determining stereoselectivity.

4.7 Conclusions from Chapter 4

Allenes are emerging as valuable substrates in hydrofunctionalisation, but hydrophosphination reactions are little studied compared to alternative heteroatoms. The reaction developed in this chapter is considerably broader in scope and deeper in study than previous radical methods reported, and the use of diphenylphosphine leads to the direct preparation of P(III) products and

avoids the use of complex phosphorus reagents or multiple steps, compared to the majority of studies discussed in Section 1.5. The substrate scope for this process is tolerant to all allene substrates tested, and because of this novel compounds could be prepared and characterised. This contrasts favourably to both the scope for allenes in Chapter 3, and previous reports where substrates tested are often very limited. Higher conversions remain from aryl phosphine reagents and arylallenes, particularly those with electron-rich substituents, while some reagents (e.g. methoxyallene, cyclohexylphosphine) proved less amenable.

The stereo- and regioselectivity appears little affected by reaction optimisation, or through uses of alternative catalysts, with the three structural isomers forming in a roughly constant ratio. Improving the selectivity here likely requires further understanding of the addition step; Density Functional Theory studies would provide valuable insight into this process. This could also provide some further comparisons of allene versus previously reported alkyne hydrophosphination.

Chapter 5 – Iron-catalysed Diphosphine Formation from Phosphines and Chlorophosphines

In Chapter 4, a hydrophosphination reaction was reported and investigated, with the primary phosphorus reagent being diphenylphosphine, $HPPh_2$. In this catalytic process, a small amount of the dehydrocoupled product **112**, Ph_4P_2, is also observed, something that is common in a range of hydrophosphination processes. As referred to in Chapters 1 and 4, iron complex **1** can also be used to dehydrocouple phosphines in high conversions; a general reaction is shown in Scheme 136. [45] Some other catalysts capable of phosphine dehydrocoupling are discussed in Section 1.6.

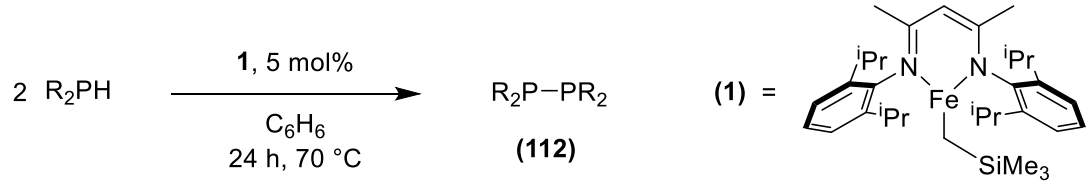

Scheme 136 – Previously reported dehydrocoupling of diphenylphosphine catalysed by **1**.

In this chapter, the study of an alternative P–P coupling process is investigated; that of coupling a phosphine with a chlorophosphine. The merits of this process, as well as some previous studies into it are reviewed in Section 1.6. Compared to dehydrocoupling, this process has some additional complexities, primarily as it is a heterocoupling of two distinct reagents rather than a homocoupling of a single species. This means that chemoselectivity is less easy to control, as there are competing homocoupling processes. Furthermore, phosphines are prone to exchange in solution with each other, so chlorophosphines can interconvert to phosphines and *vice versa*. The consequences of these processes competing has clear outcomes in Section 5.3.

5.1 Forming P–P bonds using Iron Catalysts from Phosphines and Chlorophosphines

Initial studies were undertaken using chlorodiphenylphosphine ($ClPPh_2$) and diphenylphosphine. Both are commercially available and relatively affordable phosphorus reagents, and their spectral data is well known. In this case, both homo- and heterocoupling in the reaction will generate the same compound, tetraphenyldiphosphine **112**, Ph_4P_2. This simplifies spectral data and product isolation, but does leave open some mechanistic specifics. These aspects are discussed further for non-symmetric couplings and in the mechanism discussion.

An initial reaction (Scheme 137) was performed using **1** as a pre-catalyst. ^{1}H NMR spectroscopy is not a very effective tool for reaction monitoring in this process as barring the P–H proton in diphenylphosphine, the remaining aryl signals are complex and overlap. Instead ^{31}P NMR techniques offer more conclusive and interpretable data.

The NMR data shows that some diphenylphosphine (δ = −40.6 ppm), and a large amount of chlorodiphenylphosphine (δ = 82.2 ppm) are left unreacted after 2 hours. Nevertheless, a new signal is formed at 15.3 ppm, this is consistent with the reported data for Ph_4P_2 (38% conversion).

Running the reaction for a further 14 hours shows an increase in conversion to Ph_4P_2 (44% conversion); beyond this timepoint any further conversion is negligible.

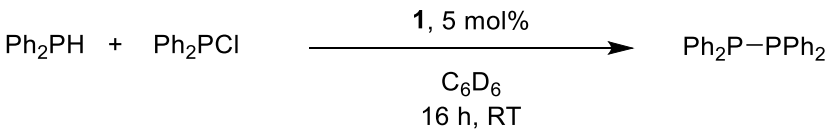

Scheme 137 – Initial reaction of diphenylphosphine and chlorodiphenylphosphine catalysed by **1.**

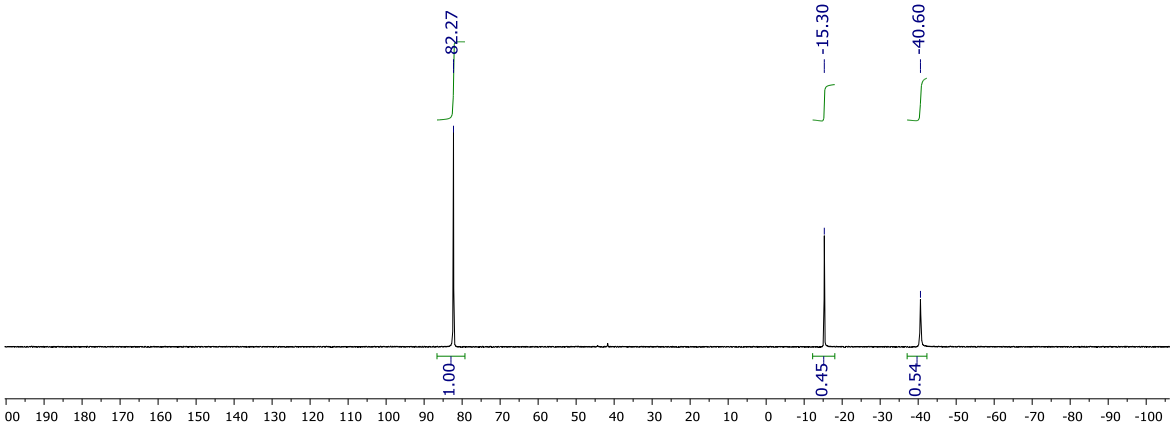

Figure 76 – Inverse gated ^{31}P NMR of the reaction after 2 hours. $ClPPh_2$ is observed at δ = 82.3 ppm, Ph_4P_2 at δ = -15.3 ppm and $HPPh_2$ at δ = -40.6 ppm. It initially appears that the diphenylphosphine is consumed and forms tetraphenyldiphosphine, but the chlorodiphenylphosphine remains unreacted.

From the NMR above the most immediate conclusion is that the dominant reaction occurring is the previously reported dehydrocoupling from diphenylphosphine to tetraphenyldiphosphine, with the chlorodiphenylphosphine remaining unreacted in the reaction. However, a comparison of the conditions in Scheme 136 and Scheme 137 show that here coupling is occurring in considerably more facile conditions, even if the conversion is slightly lower. Combining both diphenylphosphine and chlorodiphenylphosphine in the absence of an iron complex leads to very low conversion (4%). Evidently the reaction occurring in Scheme 137 is not a simple dehydrocoupling of two molecules of diphenylphosphine, and the iron complex has some role to play in the reaction.

5.2 Further Studies into Iron-Catalysed Phosphine Dehydrochlorination

Investigations were undertaken to see if any alternative iron catalysts were adept at forming Ph_4P_2 from diphenylphosphine and chlorodiphenylphosphine, and if they could attain higher conversions than **1** (44%). **1** and complex **28** were tested along with a range of iron salts. Ph_4P_2 precipitates as a thick solid in acetonitrile which hinders NMR monitoring, because of this an isolated yield was determined instead (Table 26).

Table 26 – Variation of catalyst experiments.

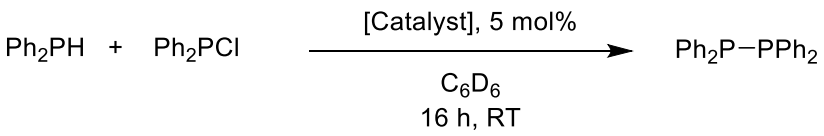

Catalyst	Conversion
None	4
1	44
28	33 [a]
$FeCl_2$	4
$FeCl_3$	7
$Fe(acac)_2$	41
$Fe(acac)_3$	57

Conditions : 0.5 mmol $ClPPh_2$, 0.5 mmol $HPPh_2$, 0.05 mmol catalyst, 600 µL solvent used. Conversion determined as an overall P-conversion using Inverse Gated ^{31}P NMR Spectroscopy. [a] 600 µl MeCN-d_3 used,

(28)

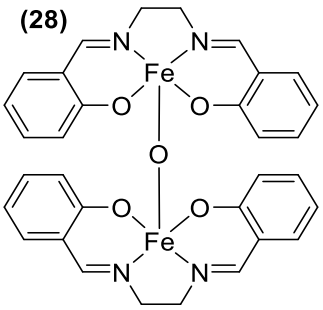

isolated yield of Ph_4P_2.

When both reagents are added to the reaction without a catalyst, there is a slow background reaction (4% after 16 hours, 7% after 5 days), with the chlorophosphine consumed at a greater rate than the phosphine indicating that there is a slow background coupling and exchange process ongoing (Entry 1). **28** is a slightly poorer catalyst than **1** in this reaction, although again, conversion is higher than simply dehydrocoupling diphenylphosphine under the same conditions (Entry 2). Unlike in the previous catalytic studies, simple iron salts did display some reactivity, although chloride salts proved essentially inactive (Entries 3–4). The metal acetylacetonate complexes $Fe(acac)_2$ and $Fe(acac)_3$ did however give reasonable conversions, and the latter is considerably higher in conversion than **1**.

The chloride salts are essentially insoluble in the reaction mixture, which may explain their lack of reactivity. The acetylacetonate complexes are readily soluble, and their proficiency indicates that the defining properties of β-diketiminate complexes (narrow active site, ligands with important steric effects etc.) appear to be less significant in determining reactivity in this process. $Fe(acac)_3$ is commercially available and is neither particularly toxic nor difficult to handle, so represents a better pre-catalyst choice over **1** for this reaction.

Unlike studies in previous chapters, conversion does not appear to be significantly affected by increasing the temperature, nor stirring of the reaction mixture. In previous chapters variation in

the amounts of reagent relative to each other has also had significant effects on chemoselectivity as well as conversion, and studies were undertaken to alter loadings in this reaction (Table 27).

Table 27 – Variation of substrate and catalyst loading studies.

Reagents and Amounts	Conversion to Ph_4P_2 / %
0.5 mmol $HPPh_2$, 0.05 mmol $ClPPh_2$, 0.025 mmol $Fe(acac)_3$	12
0.5 mmol $ClPPh_2$, 0.05 mmol $HPPh_2$, 0.025 mmol $Fe(acac)_3$	9
0.5 mmol $HPPh_2$, 0.5 mmol $ClPPh_2$, 0.005 mmol $Fe(acac)_3$	5

Conditions : 600 µL Benzene-d_6, 16 h, RT. Conversion is given as an overall P-conversion using Inverse Gated ^{31}P NMR Spectroscopy.

Adding a catalytic amount of chlorodiphenylphosphine against a full equivalent of diphenylphosphine, or vice versa, leads to low conversion, and it appears limited to an approximate equivalent of each reagent, although with the phosphine in excess conversion is slightly higher. A low loading of catalyst also perturbs reactivity significantly.

Although alternative iron complexes can be used, it is clear both reagents are required to perform coupling reactions, rather than using a sub-stoichiometric amount. This is examined further in Section 5.4, however for now the optimised conditions were taken forward for examining the scope of the reaction.

5.3 Synthetic Scope - Variation of Phosphine and Chlorophosphine

Formation of symmetric diphosphines

Efforts were undertaken to see if any other secondary phosphines and chlorophosphines can couple to each other in the presence of $Fe(acac)_3$. The first reactions tested yielded symmetrical products, and are shown in Table 28, along with the initially tested reaction of diphenylphosphine and chlorodiphenylphosphine.

Table 28 – Dehydrochlorination reactions yielding symmetrical diphosphines.

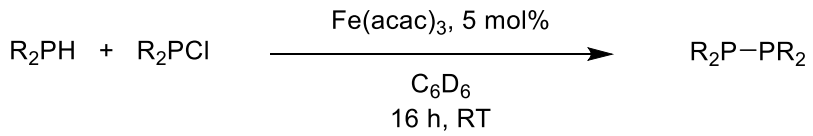

Entry	Phosphine	Chlorophosphine	Product	Conversion (%)
1	Ph_2PH	Ph_2PCl	Ph_4P_2 **112**	62
2	Cy_2PH	Cy_2PCl	Cy_4P_2 **113**	35
3	Cy_2PH	Cy_2PCl	Cy_4P_2	59 [a]
4	$(^tBu)_2PH$	$(^tBu)_2PCl$	$(^tBu)_4P_2$	0

Conditions: 0.5 mmol phosphine, 0.5 mmol chlorophosphine, 600 µL solvent. Spectroscopic conversions determined through inverse gated ^{31}P NMR with respect to chlorophosphine. [a] 2hr, 60°C

When using cyclohexyl-substituted reagents conversion is noticeably lower (Entry 2). Again more of the phosphine is consumed, however in this case there is a reasonable amount of both starting materials remaining. With heating, higher conversions are obtained, although again conversion

reaches a plateau (in this case 59%, Entry 3).The decrease in reactivity from phenyl- to cyclohexylphosphines has some similarity with the hydrophosphination catalysis discussed in Section 4.5. Di-*tert*-butyl substituted reagents were inert in reaction, and no $^{t}Bu_4P_2$ was observed to form (the $^{31}P\{^{1}H\}$ peak has been previously reported to be at δ = −40.6 ppm, [203] although in the event no new signals are observed, Entry 4).

Formation of asymmetric diphosphines

We can also utilise the phosphines and chlorophosphines above and couple them to reagents with different functionalities, potentially yielding asymmetric diphosphines. These give two distinct signals in the ^{31}P NMR spectrum. Owing to the chemical shift inequivalence a large $^{1}J_{PP}$ coupling is observed in asymmetric systems, typically around 210 Hz. A summary of outcomes is shown in Table 29.

Table 29 – Dehydrochlorination reactions yielding asymmetric diphosphines.

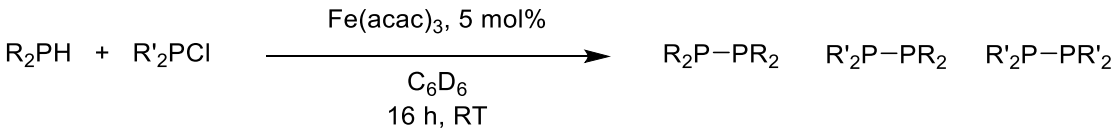

Entry	Phosphine	Chlorophosphine	Product	Conversion (%)	Selectivity
1	Ph_2PH	$(iPr)_2PCl$	Ph_4P_2	57 [a]	-
2	Cy_2PH	Ph_2PCl	Ph_4P_2	95	19 : 1
			Cy_2PPPh_2 **114**	5	
3	Ph_2PH	Cy_2PCl	Ph_4P_2	85	17 : 1
			Ph_2PPCy_2	5	
			Cy_4P_2	*trace*	
4	Cy_2PH	$(iPr)_2PCl$	Cy_4P_2	34	2.3 : 1
			$Cy_2PP(iPr)_2$ **115**	15	
5	$(tBu)_2PH$	Ph_2PCl	tBu_2PPPh_2 **116**	10 [a]	1.2 : 1
			Ph_4P_2	8 [a]	
6	$(tBu)_2PH$	$(iPr)_2PCl$	$(tBu)_2PP(iPr)_2$	*trace*	-
7	$(tBu)_2PH$	Cy_2PCl	-	-	-

Conditions : 0.5 mmol phosphine, 0.5 mmol chlorophosphine, 600 µL solvent. Spectroscopic conversions determined through inverse gated ^{31}P NMR with respect to chlorophosphine. [a] Conversion with respect to phosphine.

In the majority of reactions a mixture of hetero- and homocoupling is observed, and there does not appear to be a clear preference for hetero or homocoupling of substrates, all other things considered equal. This complicates determining the conversion, as some potential products only form from one of the reagents. From a practical perspective, one of the reagents is always observed in all of the products in each reaction, and this is the reagent used to determine a conversion (whether this is the phosphine or chlorophosphine is specified).

Entries 1–3 and 5 contain either diphenylphosphine or chlorodiphenylphosphine, and in these reactions there is a clear preference for forming Ph_4P_2. Comparing Entries 2 and 3, there is still some

effect on conversion depending on whether the starting "Ph_2P" fragment is a phosphine or a chlorophosphine, with a slightly higher conversion obtained when the arylchlorophosphine is used. In cases where forming Ph_4P_2 is not possible, a greater mixture of products is formed but conversion is lower, with some preference towards the Cy_4P_2 product (Entries 4,6,7). A minor ^{31}P signal consistent with iPr_4P_2 reported by Lake can also be seen in Entry 4, [302] although it is too weak to be accurately quantified and assigned. Reactions using di-*tert*-butylphosphine result in low conversions, even when Ph_4P_2 can be formed (Entries 5-7). The ^{31}P and ^{1}H NMR chemical shifts of all the identified products are assigned in Section 7.5.

The range of asymmetric phosphines possible to prepare is limited by the preference of forming Ph_4P_2 in the reaction, which occurs rapidly even when it is formally a homocoupling process. It is unlikely that this occurs as a formal dehydrocoupling or dechlorocoupling, as we would expect significant changes in reaction outcome depending on if the starting material is diphenylphosphine or chlorodiphenylphosphine. Instead, it is proposed that phosphorus exchange is facile under the reaction conditions. Further discussion on this process is given in the next section.

The scope was expanded to silane compounds, although it appears they do not react in conditions which work well for analogous phosphines. This in both the case of preferentially forming a coupled aryl product (when then the aryl reagent is triphenylsilane), or formation of Ph_4P_2 where it is possible, when triphenylsilane and chlorodiphenylphosphine are reacted together (Scheme 138). The latter is a clear indication that no reactivity at all occurs under these conditions, and can be repeated with methylphenylsilane, diphenylsilane and poly(methylhydrosiloxane) with the same outcome.

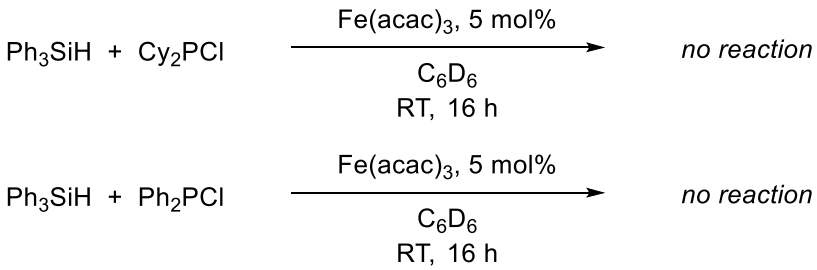

Scheme 138 – No reaction is observed when a secondary phosphine is replaced by a tertiary silane.

Reaction with primary phosphines

Dehydrocoupling of primary phosphines has also been reported on numerous occasions, with recent examples including carbene-mediated processes by Radius, [303] and alkali metal-catalysed dehydrocoupling by Manners. [304] These can dimerise, or more commonly form oligomeric species that cyclise into rings.

Under the same reaction conditions, phenylphosphine and dichlorophenylphosphine react to form the five-membered phosphine species pentaphenylcyclopentaphosphine, or Ph_5P_5 **117**. This has previously been isolated crystallographically to show it adopts an 'envelope' structure analogous to a cyclopentane ring. The phosphorus environments are not equivalent in this structure, and rather than a single sharp peak a broader range of signals are observed in the $\delta = -2\text{–}-5$ ppm range in the ^{31}P NMR spectrum. The analogous cyclohexyl reagents can be used to prepare tetracyclohexyltetraphosphine **118**, which adopts a rigid four membered ring, leading to a single,

well-defined ^{31}P NMR peak at δ = −66.7 ppm. In both cases, the ring size is consistent to what is generally reported for the dehydrocoupling of phenylphosphine and cyclohexylphosphine.

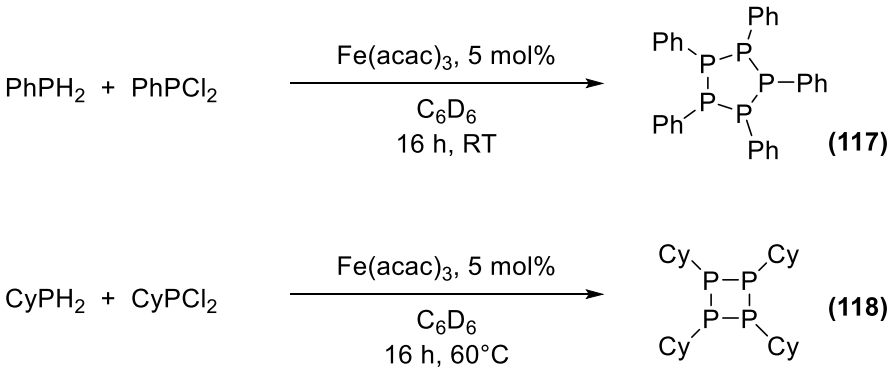

Scheme 139 – Formation of phenylphosphine and cyclohexylphosphine rings using primary phosphines and chlorophosphines.

The conversions for both are higher than for the comparative secondary couplings (91% for phenyl, 85% for cyclohexyl with heating). As would be expected from the secondary coupling, when cyclo- and phenyl-substituted reagents are mixed the formation of the phenylphosphine product is strongly favoured, and no cyclohexylphosphine rings are observed to form — a summary of all primary phosphine reactions is shown in Table 30.

Table 30 – Dehydrochlorination of primary phosphines and chlorophosphines

Entry	Phosphine	Chlorophosphine	Product	Conversion / %
1	$PhPH_2$	$PhPCl_2$	Ph_5P_5	91
2	$CyPH_2$	$CyPCl_2$	Cy_4P_4	85 [a]
3	$CyPH_2$	$PhPCl_2$	Ph_5P_5	47
4	$PhPH_2$	$CyPCl_2$	Ph_5P_5	39

Conditions – 0.5 mmol phosphine, 0.5 mmol chlorophosphine, 0.025 mmol $Fe(acac)_3$, 600 µL benzene-d_6, 16 h, RT. Conversion is given as an overall P-conversion using Inverse Gated ^{31}P NMR Spectroscopy [a] 16 h, 60 °C.

Without a catalyst the background reaction for Entry 1 is noticeable under these conditions (approx. 15%), and has been reported by Seichter to proceed to high yields under reflux conditions. [305] However, addition of catalyst is still necessary to achieve high yields under these conditions. Of note is that in Entry 3 almost all the chlorophosphine (94%) is cyclised, and this would appear to offer an effective route to cyclisation of chlorophosphines through the reaction with sacrificial cyclohexylphosphine. The reverse process with dichlorocyclohexylphosphine is less efficient (78%, Entry 4).

5.4 Mechanistic Studies into Iron-Catalysed Phosphine Dehydrochlorination

Probing the reactivity of this process is considerably different to the previous mechanistic studies in Chapters 2–4. The catalyst used, rather than a well-defined complex with a ligand environment that strongly governed reactivity, is instead a simpler iron complex with a less well-defined ligand environment. This raises questions about the precise form of the iron centre in catalysis.

Furthermore, the reaction selectivity appears strongly dependent on the functional groups on phosphorus centres as well as, secondarily, whether the compound is a phosphine or a chlorophosphine. The difference between homo- and heterocoupled products appear relatively minor. Finally, it appears that the phosphorus environments are exchanging under reaction conditions, explaining the formation of certain reaction products.

Several direct observations highlight the divergence of reactivity observed in this process to earlier studies. In Chapter 2, the visible colour change is relatively slight and slow over time, and this effect is even less in Chapter 3 and 4. In this reaction, we observe a very rapid and defined colour change upon addition of both phosphorus reagents, from the dark red associated with the pre-catalyst to a pale yellow colour (Figure 77). The colour change, both in terms of colour and intensity, suggests a significant alteration of the environment about the metal centre.

Of further note is the observation that a small amount of orange oil precipitates out over the course of the reaction (this can be suspended into solution by agitation but the effect on colour is slight). Ph_4P_2 is readily soluble in benzene at the concentration it is formed in in this reaction, as are both starting materials. Removing the solvent leaves behind an off-white solid, from which Ph_4P_2 can be purified from by passing through a silica plug. If decanted, the orange layer can be reduced to a sticky precipitate under vacuum.

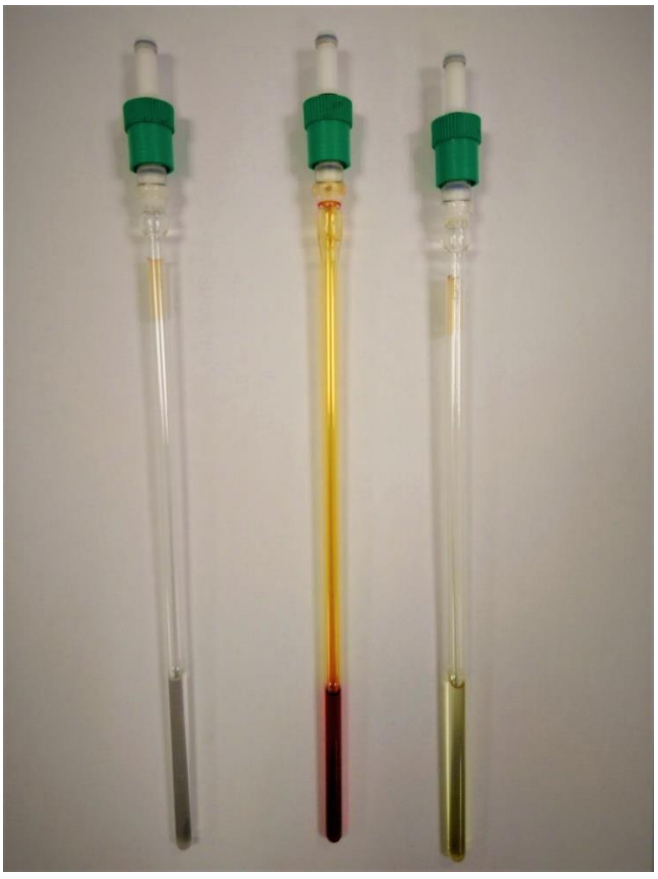

Figure 77 – Comparison of $HPPh_2$ and $ClPPh_2$ in a solution of benzene (colourless), a solution of $Fe(acac)_3$ (0.25 mmol) in benzene (dark red), and the reaction mixture (pale yellow, with a pale orange oil precipitate)

The reaction between Ph_2PH and Ph_2PCl is initially rapid before plateauing at a point well below full conversion of the starting materials. Only 11% more conversion is observed between 2 and 16 hours (46% vs. 57%). This is very different from reaction profiles of previous reactions.

No significant reaction is observed between the reaction of Ph_2PH and $Fe(acac)_3$ or Ph_2PCl and $Fe(acac)_3$. This is unlike the previous catalytic processes which either involve an additional reagent that reacts with the pre-catalyst, or one of the reagents can be identified with some confidence as playing a role in initial catalyst activation. Furthermore, the reaction does not appear dependent on order of addition, and the $Fe(acac)_3/Ph_2PH$ or $Fe(acac)_3/Ph_2PCl$ solutions can be left for an extended period of time before addition of the second reagent with no real consequences on reactivity.

Phosphorus exchange is already discussed in the introduction. From looking at the NMR spectra it is clear exchange occurs with relative ease. For example, in the reaction between chlorodiphenylphosphine and dicyclohexylphosphine both diphenylphosphine and chlorodicyclohexylphosphine are observed to form *in situ* (Figure 78). The reagents themselves do not exchange as rapidly without addition of the catalyst, although it is not clear whether the exchange is metal-facilitated or accelerated by the HCl produced in the reaction.

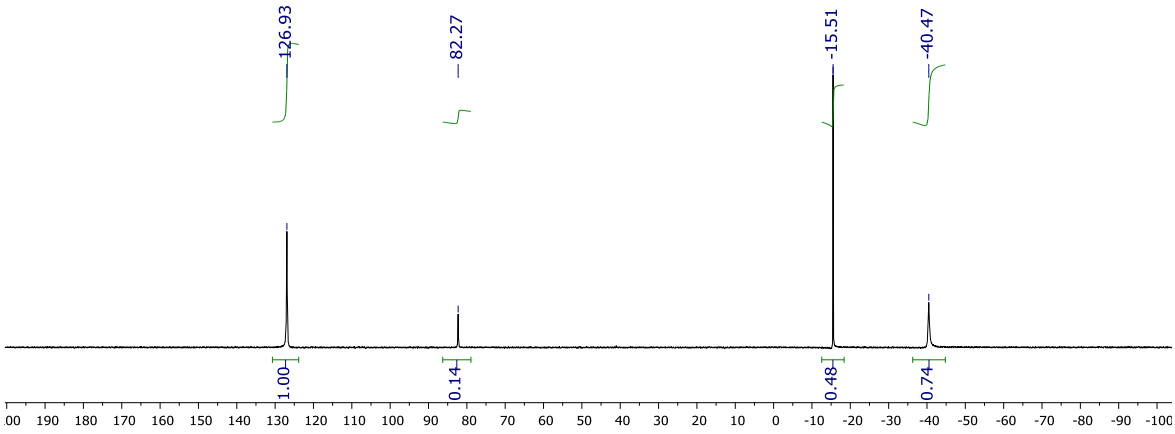

Figure 78 – Inverse gated ^{31}P NMR (202 MHz, C_6D_6, unreferenced) of the reaction of chlorodiphenylphosphine and dicyclohexylphosphine (Table 29, Entry 2) after two hours shows the formation of both diphenylphosphine (δ = -40.5 ppm) and chlorodicyclohexylphosphine (δ = 126.8 ppm) *in situ*. Also observed is Ph_4P_2 (δ = -15.5 ppm); dicyclohexylphosphine is completely consumed.

The significant change in colour suggests that there is a change in the electronic properties of the iron centre, and because of this EPR spectroscopy was again used to investigate the reaction. $Fe(acac)_3$ is a high-spin Fe(III) centre with five unpaired electrons. Much like the high-spin species investigated in Chapter 2, this leads to a broad, complex peak, although effective g-values can still be ascertained (g'_{eff} = 8.9, 4.7, 3.28). The signal g'eff = 4.7 in particular corresponds to a high-spin iron species in a strong crystal field with low symmetry, very much what would be expected for $Fe(acac)_3$.

Adding either diphenylphosphine or chlorodiphenylphosphine does not appear to affect the EPR data in any way, which is consistent in the observation that neither appears to react with the complex alone. However, when reacting both a significant change does occur (Figure 79). The initial signals are reduced in intensity, although a small amount remains, but a new signal emerges. This

is considerably more symmetric, although still broad, axial resonance with $g_{\perp} \approx 2.07$ and $g_{||} \approx 1.93$. This signal was assigned as a low-spin Fe(III) state (S = ½).

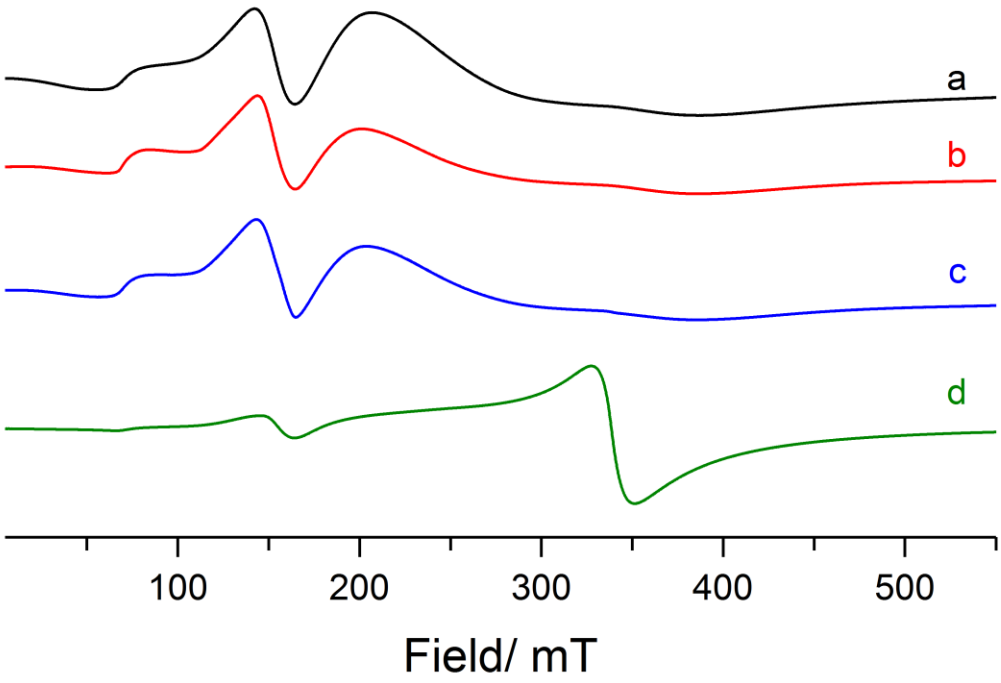

Figure 79 – EPR data for studies into dehydrochlorination (CW X-Band, 140 K). The spectrum for $Fe(acac)_3$ is shown (**a, black**), and it appears little changed when either diphenylphosphine (**b, red**) or chlorodiphenylphosphine (**c, blue**) is added. However, adding both leads to a marked change in the spectra (**d, green**).

Over the course of the reaction a spin conversion clearly occurs from high to low spin. Given the oxidation state does not change, it cannot be a direct substitution of acac ligands for phosphines without forming highly unusual species (furthermore if this happened, some binding of phosphine and chlorophosphine would be expected to the iron centre when these are reacted alone).

Addition of $Fe(acac)_3$ and Ph_4P_2 together does not lead to an observable colour change, and it does not lead to a change in EPR spectra with respect to the starting complex or new ^{31}P NMR signals forming. Because of this, it seems likely the new species is not solely a phosphine-ligated iron centre.

To explore the reactivity of hydrogen chloride, investigations were performed to determine if the reaction is acid-catalysed or -assisted. HCl was prepared in situ and bubbled through different combinations of reagents and catalyst (Table 31, setup described in Section 7.5).

Table 31 – HCl addition experiments. Full experimental details and conditions for the setup are given in Section 7.5.

Entry	Reagents	Outcome
1	$HPPh_2$ only	No reaction
2	$ClPPh_2$ only	No reaction
3	$HPPh_2$ & $Fe(acac)_3$ (0.05 eq.)	No reaction
4	$HPPh_2$ & $ClPPh_2$	18% conversion

In itself, HCl does not appear to homocouple diphenylphosphine or chlorodiphenylphosphine (Entries 1–2). Furthermore, it does not appear to promote dehydrocoupling of diphenylphosphine in the presence of an iron centre, indicating although it may facilitate exchange it is not an active participant in it (In this case through a direct reaction to form chlorodiphenylphosphine and hydrogen, Entry 3). If both reagents are combined, however, the reaction does proceed, although conversion is lower than in the standard reaction conditions (Entry 4). The amount of HCl bubbled through in the setup was not quantified, so it is difficult to conclude why conversion is lower in this case.

If a radical trap is added quickly (2–3 minutes) after the reaction initiates, conversion is significantly reduced and the ring-opened product, 1-butene, can be isolated from the reaction mixture through trap-to-trap distillation (Scheme 140). This appears to indicate the reaction is radical mediated, again a departure from the observations in Chapters 2 through 4. Adding TEMPO to the reaction does not lead to the formation of any TEMPO-phosphorus adducts that can be observed in EPR or cleanly isolated synthetically — only TEMPO is observed in the EPR spectrum. Furthermore, reaction of diphenylphosphine and chlorodiphenylphosphine with a catalytic amount of TEMPO does not lead to a clean formation of Ph_4P_2, instead producing a mixture of phosphorus environments.

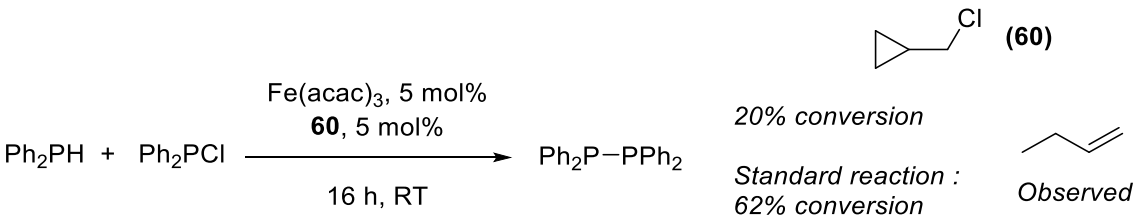

Scheme 140 – Addition of (chloromethyl)cyclopropane after the reaction initially begins leads to a significant reduction in conversion and observation of the ring-opened product forming.

The mechanistic outcomes are very different from the investigations in Chapters 2, 3 and 4. The role of the iron centre cannot even be clearly defined as a catalyst in this reaction, and it is difficult to propose a catalytic cycle that rationalises all the observations. A proposed role for the iron catalyst is to sequester the produced HCl from the coupling reaction, which may account for the precipitate and low spin compounds observed. This is consistent with the experimental observations, as the catalyst does not react with either of the compounds *per se*. Removing the HCl from the solution phase allows the reaction to proceed further in accordance with Le Chatelier's principle, on the assumption that the coupling exists in some form of equilibrium. However, the relatively low loading of the catalyst means that it must either sequester several equivalents of HCl

per iron centre, or not remove all from the reaction. The acetylacetonate ligands are likely displaced and protonated from this, and would likely also form part of the oily precipitate owing to their insolubility in benzene.

From this hypothesis, as well as our other observations, we can propose an overall reaction scheme. A small amount of the phosphine and chlorophosphine couple to generate HCl – this could arise from the background process, although the speed of it indicates to us it is metal mediated in some way. In either case the resulting HCl produced (or $Fe(acac)_3$) initiates further net dehydrochlorination, although H/Cl exchange is also widespread, with a strong preference for forming aryl diphosphine products and leaving non-aryl secondary phosphine and/or chlorophosphines uncoupled. The iron centres react with and sequester some of the produced acid, forming a low spin-state mixture which precipitates out of the reaction. Eventually the majority of the iron is consumed, the amount of HCl is increased and the reaction reaches a level of equilibrium (Scheme 141). The same mechanism applies for the primary phosphine reactions reported, and the higher conversion likely arises from an equilibrium positioned further towards the coupled products more (this seems reasonable owing to the higher reactivity of the primary phosphines).

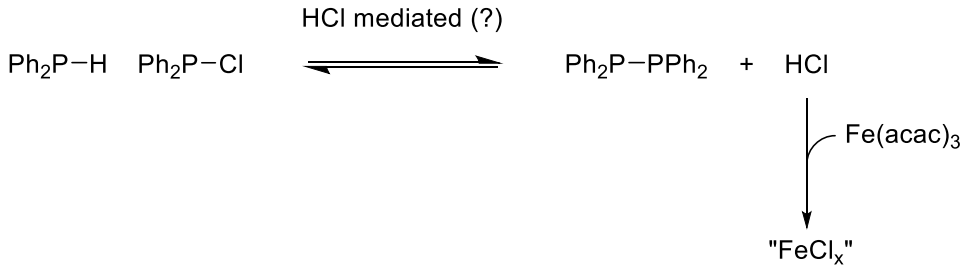

Scheme 141 – Proposed reaction process. The phosphine and chlorophosphine react to generate HCl and the coupled product, in a process presumably promoted by HCl. Excess HCl is sequestered by the iron complex to form iron (III) chloride adducts, allowing the equilibrium to proceed further.

We would not expect an iron-chloride species to adopt a low spin state, as halides are classic examples of weak field ligands which would promote high-spin metal centres. This suggests that the iron product is more complex than simple salts or has additional species ligated to it.

For phosphines and chlorophosphines with distinct R groups, the H/Cl exchange becomes more important. In the case when one of the reagents is aryl, the formation of tetraphenyldiphosphine is dominant (Scheme 142). This likely arises from the greater reactivity of aryl phosphines (as seen in other dehydrocoupling studies in Section 1.6) or the formation of a relatively strong P–P diphosphine bond driving the reaction forward.

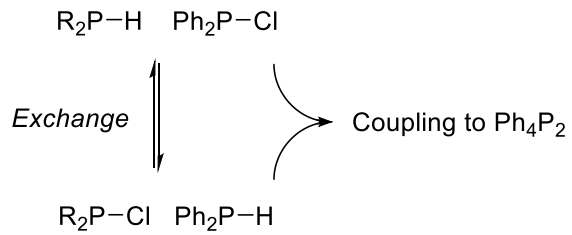

Scheme 142 – Where the phosphine and chlorophosphine have differing functionalities, they exchange to form the corresponding chlorophosphine and phosphine compounds. When diphenylphopshine or chlorodiphenylphosphine is present, tetraphenyldiphosphane is the dominant product formed, leaving the non-aryl phosphines uncoupled.

The pre-coupling exchange is the key factor in determining preference for the formation of the products, and the cause of both homo- and heterocoupled products forming. For primary phosphines the general mechanism is similar, however the actual formation of the closed ring is likely to be a complex phenomenon owing to the number of phosphorus centres required to form one product molecule. Given that no singly coupled phosphorus intermediates (*e.g.* of a RHPPClR structure) are observed and the ring size is very selective it is likely to be a rapid, complex process to ring formation.

5.5 Conclusions from Chapter 5

The work in this Chapter is very different from the previous studies, both in terms of the reaction itself and the approaches to understand it further. Reactions of phosphines and chlorophosphines are little studied, and approaches to coupling them are generally limited to stoichiometric base-mediated methods.

The dehydrocoupling of diphenylphosphine to tetraphenyldiphosphine has been reported for a range of catalysts, and high conversion and reasonably facile conditions have been reported — the dehydrochlorination reaction to form tetraphenyldiphosphine is very rapid but suffers from a relatively low overall conversion (for reasons elaborated on in Section 5.4). When using alternative phosphines and chlorophosphines the main challenge in selectivity, in particular preparing non-tetraaryldiphosphine products. For secondary phosphines, this limits the scope of reactivity compared to previous non-catalytic methods. For primary phosphines the reported yields are higher and compare favourably to previously reported dehydrocoupling approaches. The greater structural diversity possible with ringed structures as opposed to dimers also indicate that many more compounds can be prepared through this approach; this is further discussed in Chapter 6.

Mechanistically it is clear that the reaction, in contrast to previous dehydrocoupling work, is rapid and complex, and unlikely to proceed through well-defined metal phosphide compounds as proposed in Chapter 4 and previous dehydrocoupling studies. Instead, a radical mechanism is suggested, and the iron complex performs the unusual role of sequestering the released HCl from the reaction. This uncommon form of reactivity could certainly be investigated further to both maximise conversion and study the use of alternative metal compounds and salts.

Chapter 6 – General Conclusions and Future Work

In Chapter 2 it was shown that by varying reaction conditions from previously reported hydroboration and transfer hydrogenation catalysis, the catalytic isomerisation of alkenes can be performed with a β-diketiminate iron pre-catalyst and a catalytic amount of pinacolborane. Through further experimental variation optimised reaction conditions could be determined, with high conversions being achieved for the isomerisation of allylbenzene using both pinacolborane and alterative reagents including ammonia borane. This reactivity could then be applied to functionalised allylbenzenes, terpenes and linear alkenes with a range of outcomes. The reaction is predominantly *E* selective with a small amount of the *Z*-product formed.

An initial reaction mechanism was proposed involving formation of an iron(II) hydride species and subsequent addition and β-hydride elimination through an alkyl-type mechanism, which has mechanistic similarities to both the previous hydrogenation and hydroboration studies and literature reports with alternative iron pre-catalysts. Through deuteration experiments and independent preparation of the purported active species, it was shown that catalysis cannot proceed through this pathway. EPR spectroscopy indicated that iron(I) species are forming under reaction conditions, and an alternative catalytic cycle proceeding through a redox-active allyl mechanism was proposed. This is consistent with both the deuteration studies and the activity of an analogous iron(I) complex in catalysis, and further experimental studies support this mechanistic pathway. Density functional theory studies also support this mechanism while showing the alkyl pathway is not feasible, and it appears that it is plausible for the reaction to proceed on a fully low-spin surface or undergo a spin-crossover event. It was then shown isomerisation can be used in conjunction with other synthetic steps to prepare new compounds.

While iron(II) β-diketiminate complexes have been investigated for a range of catalytic behaviour, very little study has been undertaken into iron(I) species, particularly in redox active catalytic cycles. This opens the potential for new catalytic transformations beginning from iron(I) species such as **44** or **45**. The accessibility of the iron(I)/(III) redox cycle means reactions common with palladium(0)/(II) redox cycles could be attempted. For example, a Negishi coupling may be feasible using **45**, which typically requires a further reducing agent with iron pre-catalysts, proceeding through oxidation of the aryl bromide to form an Fe(III) species (Scheme 143). As well as not requiring exogenous reagents, this would be an unusual example of a well-defined iron complex performing cross-coupling reactions.

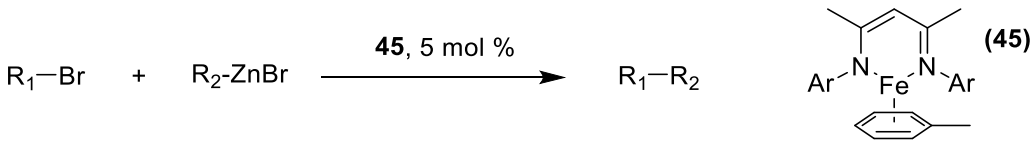

Scheme 143 – Low oxidation state complex may be a viable as a catalyst for the Negishi coupling without further reducing agents required.

Although all evidence indicates that the reduction step is direct and feasible, further studies into the step are needed to fully determine what reagents can reduce the iron centre in a well-defined manner. Traditional reducing agents, such as group 1 metals, could potentially form complex metal adducts but would likely react with more of the pre-catalyst than pinacolborane or ammonia

borane. A broad study of various reducing agents could lead to cheaper or more effective reagents being employed. Also to be investigated further is the differences in selectivity between ammonia borane and pinacolborane. Given the range of signals forming in the reaction with the former, it is likely there is some further complexity when using ammonia borane that is not fully determined herein.

In Chapter 3 attempts to apply isomerisation catalysis from alkenes to allenes instead resulting in the serendipitous discovery that β-diketiminate iron complexes can polymerise arylallenes. Through reaction optimisation it was shown that polymerisation proceeds with a further additive, low catalyst loading and at room temperature. From ^{1}H NMR spectroscopy studies, it appears the polymer has a more complex conformational environment than previous reports, and these conformers were further investigated with density functional theory. Material characterisation of the polymer also yielded further structural information. A range of polymers could be synthesised and analysed. Mechanistic experiments once again ruled out the reaction proceeding through an iron(II) hydride species, and an alternative reaction mechanism arising from oxidative addition of an iron(I) species was proposed.

Although the mechanistic postulation is generally consistent with observations, it does not fully rationalise the range of conformers observed, nor how and why the less stable conformations are readily formed. It seems reasonable that this could be controlled through further ligand alteration, although it would likely be at the expense of catalyst activity. Furthermore the polymeric products themselves could be investigated in more detail for potential applications. It is likely that through co-polymerisation with alternative monomers, variation of molecular weight and through variation of the workup procedure the material properties of the polymer could be altered.

It appears likely that other cumulenes would polymerise effectively to generate similar polymers. Diphenylketene does not polymerise effectively in the presence of **1**, although it seems reasonable to propose that alternative catalysts could generate polymers as shown in Scheme 144, which would be an unusual polyacetal derivative. This reactivity could also be applied to other unusual, conjugated compounds, such as carbodiimides and ethenimines. Further functionalisation of the double bond would also be desirable, to add functional groups to the repeating unit, or to add crosslinking between chains.

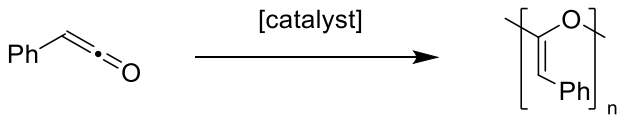

Scheme 144 – Polymerisation of ketenes would generate polyacetals similar to polyallenes but with a C–O repeating unit on the main chain. Phenylketene is not stable, but diphenylketene and various other ketenes are and could be utilised as monomers in a similar manner to phenylallene.

Dimerisation of phenylallene was also observed under some reaction conditions, and this was investigated further, although achieving high yields still remained challenging. The most effective way of generating higher yields would be development of a methodology where polymerisation is not as rapid as observed in this study. It is difficult to rationalise what modulation would be required to achieve this, and it likely a broad range of experimental variation would be necessary. These

dimeric species could be investigated further through double homolytic cleavage to form the non-Kekulé structures discussed in Section 3.6. Alternatively, selective addition reactions across the double bond could be employed to yield more complex molecules (Scheme 145).

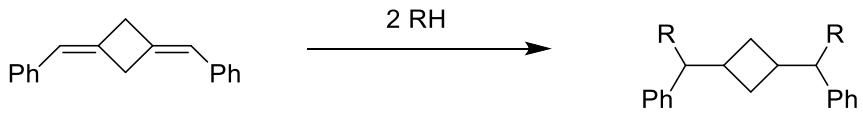

Scheme 145 – Adding across the alkene bond can lead to the linear cyclobutane structures. The unusual distance between the R groups in this structure may have application in ligand design.

Hydrofunctionalisation of allenes was attempted in Chapter 4, although attempts at catalytic hydroboration and hydrosilylation instead yielded polymerisation. Hydroamination did not proceed with the reagents and conditions tested, but hydrophosphination was observed with simple phosphorus reagents using iron complexes. Through NMR studies, along with comparison to previous reports, it is clear that three isomeric products were being formed, and their structures can be determined. Although conversion from reacting equimolar amounts of both reagents is low, by varying the concentrations, amongst other conditions, high conversion to the hydrophosphinated products can be achieved, and reactivity applied to a range of allenes and phosphines. From the substrate scope a range of new phosphorus compounds can be prepared, although they are formed as mixtures of isomers.

Mechanistically this reaction is different from those previously encountered as the iron centre is proposed to remain in the iron(II) oxidation state, forming an iron-phosphido intermediate and subsequent addition across the allene and protonolysis. This does not fully rationalise the selectivity between the *E*, *Z* and internal isomers – further theoretical studies into the selectivity would likely support or disprove the overall mechanism. Ideally from this some understanding on how to alter and control selectivity to a greater extent could be gained.

The produced phosphines could be investigated for their potential as monodentate ligands in catalysis, and the methoxy-functionalised products may even bind in a bidentate manner. The unreacted double bond could also be functionalised further. In a similar fashion, the secondary phosphine products arising from hydrophosphination with phenylphosphine could be further hydrophosphinated to form tertiary products. Neither of these reactions are observed under standard reaction conditions, so it is likely alternative catalysts or more forcing reagents and conditions would be required to achieve this.

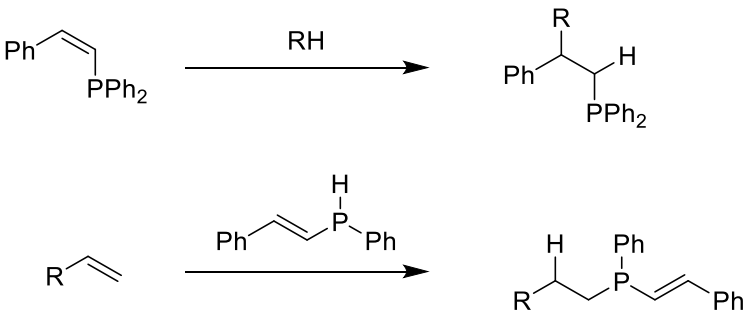

Scheme 146 – Further reaction of the catalysis products (either through double bonds or remaining P-H bonds) would lead to increased structural diversity.

Although the hydroamination of phenylallene was not successful herein, performing this reaction with an iron catalyst would be highly desirable. To achieve this different ligands/complexes may be required, or instead using alternate, more reactive nitrogen sources may prove successful. It would be interesting to see how the products and selectivity of hydrophosphination compares to any products observed in hydroamination.

Finally in Chapter 5, it was observed that the coupling of chlorodiphenylphosphine and diphenylphosphine can occur in the presence of an iron catalyst under more facile conditions than the dehydrocoupling of diphenylphosphine. While β-diketiminate complexes are adept at this transformation, using simple iron complexes such as $Fe(acac)_3$ as a pre-catalyst leads to higher conversions. When using phosphines and chlorophosphines with different functional groups a mixture of homo- and heterocoupled products are observed. Primary phosphines and chlorophosphines can also be coupled to form polyphosphine rings. There is a clear preference for forming Ph_4P_2 dimers (with secondary substrates) or Ph_5P_5 rings (with primary substrates) when at least one of the reagents has aryl substituents (either the phosphine or the chlorophosphine). When aryl reagents are not present a mixture of products if formed, although conversions are generally lower. Unlike the previous studies, the mechanism appears more ill-defined. It appears likely that phosphorus exchange occurs readily under the reaction conditions. It is also not entirely clear whether the iron acts as a catalyst in the general metal-mediated manner or instead abstracts HCl from the reaction mixture, thereby allowing the reaction to proceed further.

Deeper reaction study and monitoring would provide further insight into the transformation, although the speed of the reaction and the complexity of the reaction pathway mean this would not be straightforward to do. The applications of diphosphines as reagents and ligands has been touched upon in Section 1.7, but the applications of the polyphosphine rings are less explored. By applying the reactivity of this system to functionalised chlorophosphines, it appears possible to prepare a range of polyphosphines and develop and apply their chemistry further (Scheme 147). The relatively non-specific nature of the catalyst in this transformation also leads to the open question that other compounds other than iron complexes could potentially be used in the process, and the effects of using other compounds in catalytic loadings could be investigated.

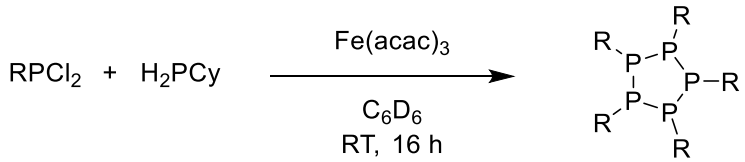

Scheme 147 – When using cyclohexylphosphine only the chlorophosphine is cyclised. By using these conditions a range of polyphosphines could be selectively prepared.

Chapter 7 – Experimental Section

7.1 Experimental Data Pertinent to Multiple Chapters

General experimental considerations

The majority of reagents used in these studies were purchased from Sigma-Aldrich and Acros. Notable exceptions include pentane and bromoform (Fisher). Substrates used in catalysis were dried with calcium hydride and distilled prior to use (when liquid).

For the isomerised products in Chapter 2, mass spectrometry data was performed and analysed by the EPSRC UK National Mass Spectrometry Facility at Swansea University. All other mass spectrometry data was performed on an Agilent 6545 Q-Tof LC/MS Spectrometer as part of the Material and Chemical Characterisation (MC^2) Facility at the University of Bath. CHN analysis was performed by Elemental Microanalysis Ltd, Okehampton, UK. Unless noted, all analysis was undertaken using equipment in the Department of Chemistry and MC^2 facility at the University of Bath.

NMR was performed on 300, 400 and 500 MHz Bruker and Agilent model spectrometers. ^{1}H and $^{13}C\{^{1}H\}$ NMR spectra were referenced to residual solvent signals, heteronuclear NMR to standard references or as stated. FTIR data was collected on a PerkinElmer Spectrum 100 FT-IR Spectrometer. More specialised equipment details are given in the relevant sub-section.

Solvents were dried using standard sodium and benzophenone protocol, and distilled prior to use ('wet' solvents were used without further purification) and stored under a nitrogen atmosphere. Methanol was instead dried by refluxing with crushed 3 Å molecular sieves for 2 hours under a nitrogen atmosphere before being distilled and stored under a nitrogen atmosphere with fresh 3 Å molecular sieves. Preparations described as being performed under an inert atmosphere or in a glovebox were performed using standard Schlenk and glovebox techniques unless explicitly stated.

In Chapters 2 and 5, all assigned compounds are previously known, and previous reports are cited (and are consistent with assignments stated). In Chapter 3, the majority of the polymeric products are known but full spectral data has, to our knowledge, not been reported to the level detailed herein. In Chapter 4, hydrophosphinated products that have been previously reported are again cited and are consistent with assignments stated.

Notes on NMR assignments

In most compounds, carbon environments are labelled 1, 2, 3… and these positions are identified in the assignment text as C_1, C_2, C_3… . Protons are identified by the carbon they are bonded to (*e.g.* HC_1), or to the heteroatom they are bonded to or immediately adjacent to (*e.g.* HN, $Si(CH_3)_3$), with the proton in question italicised. In some simple compounds where there is less ambiguity on position, the carbon environments are not numbered and the general chemical formula is written and the atom in question is italicised (*e.g.* CH_3CH_2OH or $Si(CH_3)_4$) – for aryl carbons, IUPAC nomenclature on position is used (*e.g.* C_{ORTHO}).

All $^{13}C\{^1H\}$ NMR signals are singlets unless stated. For paramagnetic species (such as iron pre-catalysts), all ^1H NMR signals are (typically broad) singlets unless stated.

Synthesis of reagents pertinent to multiple chapters - metal complexes and proligands

Synthesis of $FeCl_2(THF)_{1.5}$

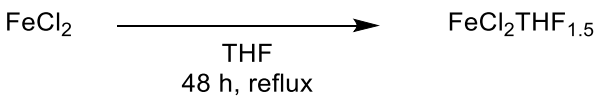

The THF adduct of Fe(II) chloride was prepared using a Soxhlet extractor. $FeCl_2$ (anhydrous, 10 g) was loaded into the thimble of the extractor under a dry nitrogen atmosphere. 200 mL of dry THF was added to the condenser, and the setup was refluxed for 48 hours. Upon cooling the solution was subject to reduced pressure and the desired THF adduct was precipitated as pale orange solid (5.88 g, 32% yield).

Synthesis of ((2,6-diisopropylphenyl)imino)pent-2-en-2-yl-2,6-diisopropylaniline

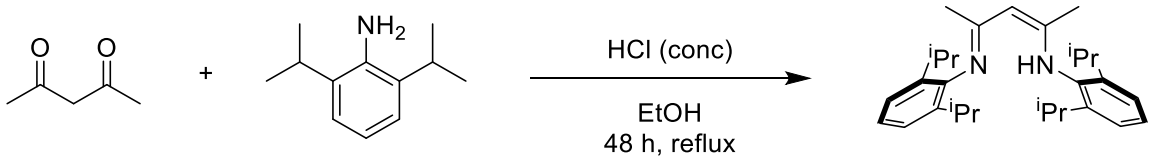

The synthesis of this proligand was initially reported by Feldman; [306] the synthesis below is as previously reported by Webster. [45] In a two-neck 500 mL round-bottomed flask 2,4-pentanedione (6.68 g, 0.067 mol) was mixed with 300 mL of ethanol and 2,6-diisopropylaniline (28.67 g, 0.162 mol). To the mixture was added 7.5 mL of 12 M hydrochloric acid and the solution was refluxed with vigorous stirring for 3 days. The resulting slurry was then allowed to cool to room temperature and filtered. The filtered solid was dried under reduced pressure, and the filtrate was evaporated on a rotary evaporator. The dried mass was combined with the filtrate residue and the mixture was refluxed in 250 mL hexane at 80 °C for 1 h. The mixture was then cooled and filtered. Next the solid residue was treated with 300 mL of a saturated aqueous solution of sodium carbonate and 500 mL of dichloromethane (DCM). The slurry was stirred until the solid dissolved. Stirring was then ceased giving a yellowish organic solution and a pale-yellow aqueous layer. The organic layer was separated using a separatory funnel and then dried over magnesium sulfate. The solution was filtered and dried under reduced pressure to yield an off-white solid that upon washing with 50 mL of cold methanol (−20 °C) yields the desired proligand as a white powder (21.7 g, 77% yield).

NMR Data

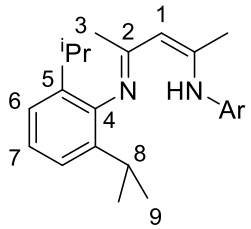

^1H (500 MHz, $CDCl_3$) δ 12.11 (N*H*, s , 1H), 7.11 (*H*C_6/*H*C_7, m, 6H), 4.85 (*H*C_1, s, 1H), 3.11 (*H*C_8, hep, ^3J = 6.9 Hz, 4H), 1.71 (*H*C_3, s, 6H), 1.21 (*H*C_9, d, ^3J = 6.9 Hz, 12H), 1.11 (*H*C_9, d, ^3J = 6.9 Hz, 12H)

$^{13}C\{^{1}H\}$ (126 MHz, $CDCl_3$) δ 161.1 (C_2), 142.4 (C_4), 140.1 (C_5), 125.0 (C_7), 123.1 (C_6), 93.1 (C_1), 28.2 (C_8), 24.2 (C_9), 23.2 (C_9), 20.7 (C_3)

Data is concordant with previous literature. [306]

Synthesis of 1

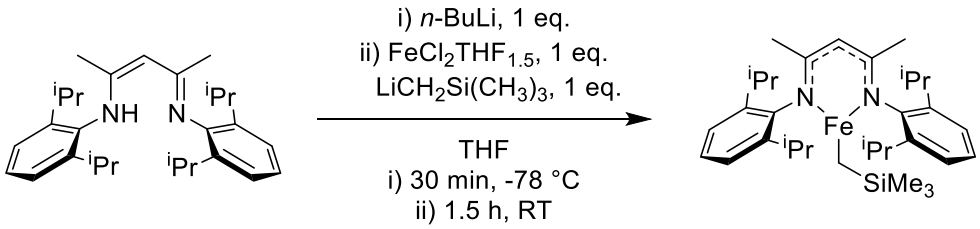

The proligand ((2,6-diisopropylphenyl)imino)pent-2-en-2-yl-2,6-diisopropylaniline (1.75 g, 4.18 mmol) was dissolved in 20 mL dry THF under an inert atmosphere and cooled to −78 °C. *n*-Butyl lithium (solution in hexane, 2.25 mL, 4.18 mmol) was added to the reaction mixture dropwise, and the solution was allowed to warm to room temperature and stirred for 30 minutes. Following this, $FeCl_2(THF)_{1.5}$ (982 mg, 4.28 mmol) was added under an argon atmosphere, and the solution was stirred for a further 45 minutes. $LiCH_2Si(CH_3)_3$ (394 mg, 4.18 mmol) was then added, and the solution was stirred for a further 45 minutes, by which time it had turned a dark red colour. The solvent was removed *in vacuo* and the residue was dissolved in 25 mL dry pentane three times, each time removing the pentane *in vacuo* to remove any residual THF. The product was purified by dissolving in the minimum amount of pentane and passing through a pad of Celite under a nitrogen or argon atmosphere. Following this, the elution was concentrated and cooled overnight in a freezer to afford **1** as yellow crystals (1.28 g, 58% yield).

NMR Data

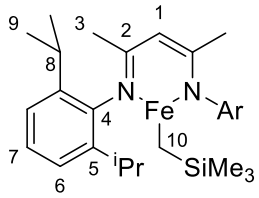

^{1}H (500 MHz, C_6D_6) δ 111.8 (HC_1, 1H), 72.8 (HC_3, 6H), 55.0 ($Si(CH_3)_3$, 9H), −8.3 (HC_6, 4H), −14.2 (HC_9, 12H), −67.0 (HC_7, 2H), −97.7 (HC_9, 12H), −124.6 (HC_8, 4H), −149.5 (HC_{10}, 2H)

Data is concordant with previous literature. Full characterisation, including crystallographic data, has previously been reported. [45]

Synthesis of *N*-pivaloyl-2,6-diisopropylanilide

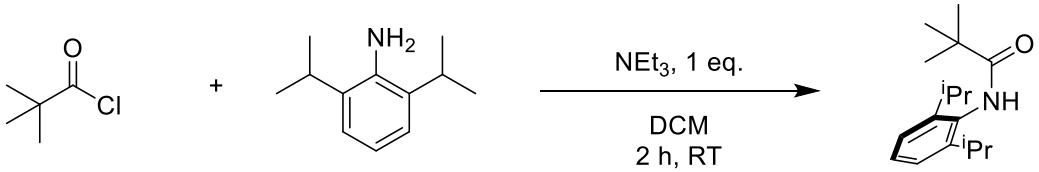

This synthesis is adapted from the reported preparation, and was performed on a tenth of the scale. [307] 2,6-Diisopropylaniline (9.75 g, 0.055 mol), triethylamine (7 mL, 0.05 mol) and

dichloromethane (25 mL) were combined in a three-necked round-bottom flask under air. A solution of pivaloyl chloride (6.2 mL, 0.05 mol) in dichloromethane (20 mL) was added dropwise over the course of 2 hours, with the mixture undergoing vigorous stirring. The mixture was then stirred for an additional 30 min, cooled in an ice bath and a fluffy white solid was isolated by filtration. The solid was washed with diethyl ether (3 × 20 mL) and then with copious amounts of water (4 × 30 mL). The solid was dried under vacuum for several hours to yield the product as a white solid (11.7 g, 90% yield).

Synthesis of *N*-(2,6-diisopropylphenyl)pivalimidoyl chloride

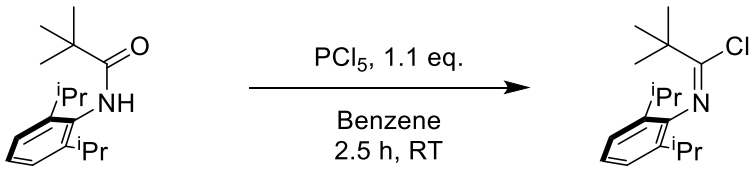

This synthesis is adapted from the reported preparation, and was performed on approximately a tenth of the scale. [307] *N*-pivaloyl-2,6-diisopropylanilide (10.5 g, 0.04 mol) was dissolved in 100 mL benzene in a three-necked round bottom flask and purged with nitrogen gas. A bubbler was attached with saturated sodium carbonate solution to neutralise HCl produced in the reaction. PCl_5 (9.4 g, 0.044 mmol, 1.1 eq.) was added in small chunks over 90 minutes, with care taken to keep the flask open to air for the shortest time possible. The solution was then stirred for a further hour. Following this, a distillation setup was placed on the flask, and the solvent and $POCl_3$ side-product were removed by gentle heating under ambient pressure. The crude product was then transferred into a Schlenk flask and distilled under a vacuum with heating, yielding a colourless oil (8.95 g, 80% yield).

Synthesis of *N*-(2,6-diisopropylphenyl)-3,3-dimethylbutan-2-imine

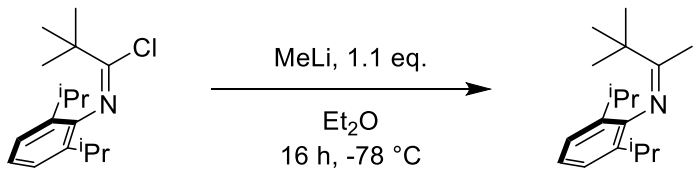

The synthesis is adapted from the reported preparation, and was performed on a tenth of the scale. [307] *N*-(2,6-diisopropylphenyl)pivalimidoyl chloride (4.53 g, 16 mmol) was dissolved in 20 mL dry diethyl ether in a flame-dried Schlenk flask, and cooled to −78 °C while stirring. Methyl lithium (11 mL, 17.6 mmol, 1.6 M in diethyl ether, 1.1 eq.) was added slowly over the course of 30 minutes. The mixture was allowed to warm to room temperature and stirred for 12 hours. The reaction was then quenched carefully by adding small portions of ice. 15 mL of deionised water was added to the reaction, and the organic layer was extracted and washed twice more with deionised water. The organic layer was dried with magnesium sulfate, the solvent removed under reduced pressure and the crude product then transferred into a Schlenk flask and distilled under vacuum with heating, yielding a colourless oil (3.43 g, 82% yield).

Synthesis of 2,2,6,6-tetramethyl-3,5-Bis(2,6-diisopropylphenylimido)heptane

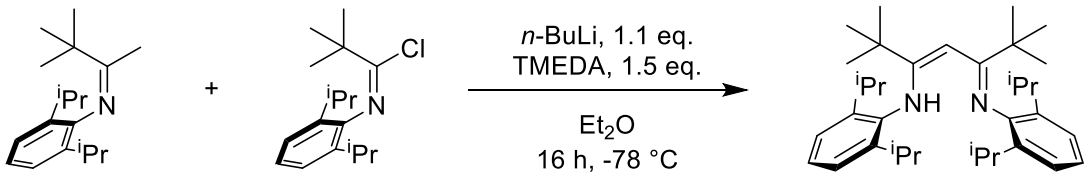

The synthesis is adapted from the reported preparation, and was performed on approximately a tenth of the scale. [307] *N*-(2,6-diisopropylphenyl)-3,3-dimethylbutan-2-imine (3.24 g, 12 mmol) was dissolved in 25 mL dry diethyl ether in a flame-dried Schlenk flask, and dry TMEDA (2.67 mL, 17.3 mmol, 1.5 eq.) was added. The solution was cooled to −78 °C while stirring and *n*-butyl lithium (5.3 mL, 2.5 M in hexanes, 13.2 mmol, 1.1 eq.) was slowly added over the course of 15 minutes. The reaction was then allowed to warm to room temperature and stirred for 16 hours, at which point it was cooled to −78 °C again and a solution of *N*-(2,6-diisopropylphenyl)pivalimidoyl chloride (3.36 g, 12 mmol) in 5 ml dry diethyl ether was added dropwise. The mixture was then allowed to warm to room temperature and stirred for a further 18 hours. Following this, it was refluxed for a further 2 hours under a nitrogen atmosphere, then cooled and quenched with a small amount of ice, then distilled water (20 mL). The organic layer was extracted, washed twice more with 20 mL deionised water, dried with magnesium sulfate and the solvent removed under reduced pressure. The crude product was dissolved in 40 mL of hot hexanes and slowly cooled to precipitate out as a white solid (5.13 g, 85% yield).

Synthesis of 27

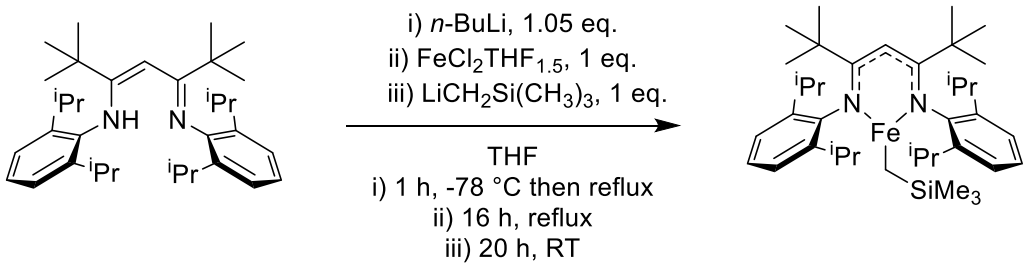

The proligand 2,2,6,6-tetramethyl-3,5-bis(2,6-diisopropylphenylimido)heptane (1.0 g, 2 mmol) was dissolved in 5 mL dry THF and cooled to −78 °C. *n*-Butyl lithium (1.6 M in hexanes, 1.38 mL, 2.1 mmol, 1.05 eq.) was added dropwise and the solution was sealed and heated at 70 °C for three hours. Volatiles were then removed under reduced pressure and the yellow precipitate was dissolved in 5 mL dry toluene. $FeCl_2THF_{1.5}$ (468 mg, 2 mmol, 1 eq.) was added and the solution refluxed for 16 hours. The solution was passed through a cannula filter and the solvent removed — the resulting precipitate was dissolved in 5 mL dry THF. $LiCH_2Si(CH_3)_3$ (188 mg, 2 mmol) was added, and the solution stirred for a further 20 hours. The solvent was removed, and the mixture was dissolved in pentane and passed through a second cannula filter. Complex **27** could then be crystallised from a concentrated solution of pentane (342 mg, 26% yield).

The peaks in the ^{1}H NMR could not be straightforwardly assigned to specific environments on the metal complex.

NMR Data

^{1}H (500 MHz, C_6D_6) δ 123.5, 71.4, 43.5, −5.1, −26.5, −99.3, −109.3, −131.8

CHN — Theoretical (%): 72.64 (C), 10.00 (H), 4.34 (N) Found (%): 72.24 (C), 9.97 (H), 4.58 (N)

Synthesis of 2,4,6-Triphenylaniline

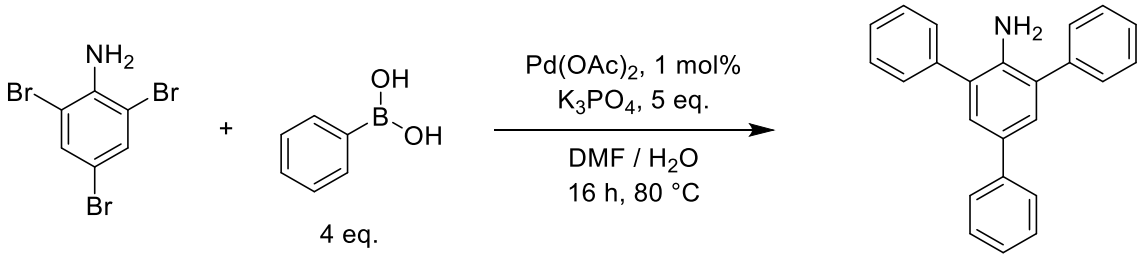

This synthesis was adapted from the literature procedure reported by Liu. [308] To a 250 mL round-bottom flask was added 2,4,6-trisbromoaniline (3.3 g, 10 mmol), phenyl boronic acid (4.9 g, 40 mmol, 4 eq.), potassium phosphate tribasic (11.5 g, 50 mmol, 5 eq.) and palladium(II) acetate (23 mg, 0.01 eq.). These were dissolved in a mixture of DMF (100 mL) and water (32 mL), and the reaction was heated at 80 °C for 16 hours. 150 mL brine was added following this, and the crude product was extracted with ethyl acetate (3 x 50 mL). The organic extracts were dried with magnesium sulphate and the solvent removed under reduced pressure. The product was then purified with column chromatography on silica gel using a ramped eluent of 125 : 1 petroleum ether 40-60 : ethyl acetate to 80 : 1 petroleum ether 40-60 : ethyl acetate, yielding an off-white powder (2.8 g, 87% yield).

NMR Data

^{1}H (500 MHz, $CDCl_3$) δ 7.62-7.56 (m, 6H), 7.51-7.48 (m, 4H), 7.42 (s, 2H), 7.41-7.37 (m, 4H), 7.29-7.26 (m, 1H), 3.92 (br. s, 2H, NH_2)

$^{13}C\{^{1}H\}$ (126 MHz, $CDCl_3$) δ 141.0, 140.5, 139.8, 131.2, 129.5, 129.1, 128.8, 128.5, 128.4, 127.6, 126.6, 126.5

Data concordant with previous literature. [308]

Synthesis of 2,4-Bis(2,4,6-triphenylphenylimido)pentane

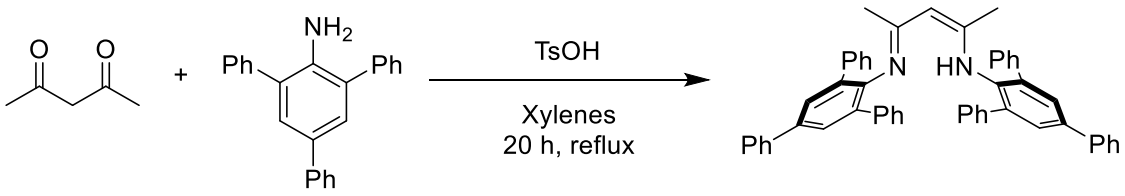

This synthesis was adapted from the procedure reported by Holland. [309] 2,4,6-triphenylaniline (1.6 g, 5 mmol), *para*-toluenesulfonic acid monohydrate (0.48 g, 2.5 mmol) and 2,4-pentanedione (0.26 mL, 2.5 mmol) were dissolved in 35 mL xylenes in a round-bottom flask. The flask was purged with nitrogen and the reaction was refluxed at 170 °C for 20 hours using a Dean-Stark condenser. After this time, 30 mL of saturated Na_2CO_3 solution and 30 mL of DCM were added and stirred vigorously for 30 mins. The organic layer was separated and washed with brine (30 mL x 2), then dried over $MgSO_4$. The solution was concentrated to 15 mL and approximately 10 mL of methanol was slowly added. Unlike in the literature report, crystallisation did not occur, so the solvents were removed, and the crude product was washed with MeOH and dried *in vacuo*. The product was isolated as a yellow powder (2.8 g, 78 % yield).

The triphenyl substituents were not fully assigned by $^{13}C\{^1H\}$ NMR; the peaks relating to them are denoted as (aryl) in the assignment below. *Ipso* carbons could be identified as such through DEPT-135 NMR, although not their specific positions, these are denoted as C_{IPSO} in the assignment below.

NMR Data

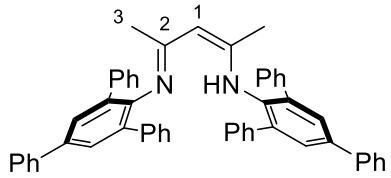

^1H (300 MHz, $CDCl_3$) δ 12.17 (N*H*, s, 1H), 7.71−7.08 (ar, m, 34H), 4.12 (*H*C_1, s, 1H), 1.23 (*H*C_3, s, 6H)

$^{13}C\{^1H\}$ (75 MHz, $CDCl_3$) δ 160.0 (C_2), 140.9 (C_{IPSO}), 140.6 (C_{IPSO}), 140.2 (C_{IPSO}), 137.3 (C_{IPSO}), 136.7 (C_{IPSO}), 129.4 (aryl), 128.9 (aryl), 128.4 (aryl), 128.2 (aryl), 127.2 (aryl), 126.9 (aryl), 126.8 (aryl), 96.6 (C_1), 21.2 (C_3)

Data is concordant with previous literature. [309]

Synthesis of 25

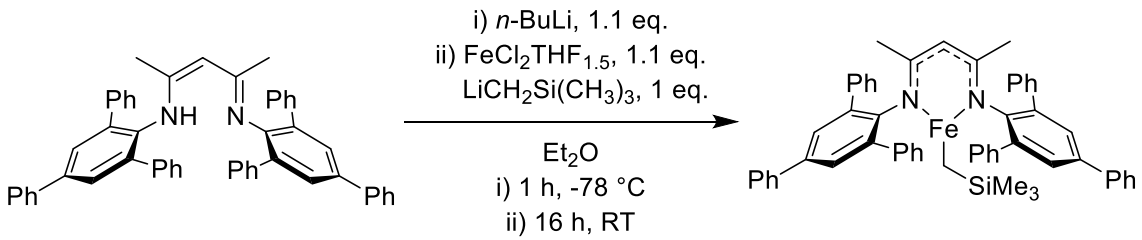

2,4-Bis(2,4,6-triphenylphenylimido)pentane (707 mg, 1.0 mmol) was dissolved in 10 mL dry diethyl ether and cooled under a nitrogen atmosphere to -78 °C. *n*-Butyl lithium (1.6 M solution in hexane, 0.66 mL, 1.1 mmol, 1.1 eq.) was added dropwise and the solution was allowed to warm and stirred for 1 hour. $FeCl_2THF_{1.5}$ (242 mg, 1.1 mmol, 1.1 eq.) was then added, and the reaction was stirred for a further 16 hours. A solution of $LiCH_2Si(CH_3)_3$ (104 mg dissolved in 5 ml diethyl ether, 1.1 mmol, 1.1 eq.) was then added dropwise, and the solution was stirred for another hour. Following this, the solvent was removed under reduced pressure, and the crude product dissolved in toluene and passed through a celite pad under an argon atmosphere. Removing the solvent yielded **25**; crystals suitable for XRD analysis were obtained by crystallisation from a toluene/pentane mixture at – 20 °C (678 mg, 80% yield).

The peaks in the ^{1}H NMR could not be straightforwardly assigned to specific environments on the metal complex.

NMR Data

^{1}H (300 MHz, C_6D_6) δ 50.9, 41.7, 12.6, 3.95, −4.1, −5.6, −15.1, −17.4, −18.1, −66.7

CHN — Theoretical (%): 80.64 (C), 6.17 (H), 3.30 (N) Found (%): 79.50 (C), 6.14 (H), 3.39 (N)

Synthesis of 2,4-dimethyl-6-(1-phenylethyl)aniline

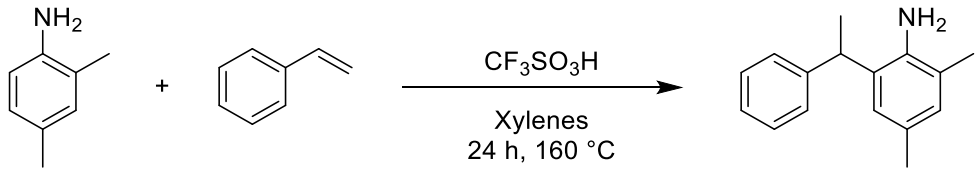

To a J-Young-tap Schlenk was added xylenes (25 mL), styrene (20 mL, 0.175 mol, 1.44 eq.) and trifluoromethanesulfonic acid (3 mL). 2,4-dimethylaniline (15 mL, 0.12 mol) was added, and the flask was sealed and heated at 160 °C for 24 hours. The flash was then allowed to cool, and xylenes removed under reduced pressure to leave a stodgy dark red residue. This was then washed with NaOH (1 M aqueous solution) twice and extracted with ethyl acetate, and the organic phases were combined. The solvent was removed under reduced pressure to leave a viscous red solution. The product was purified by column chromatography (95:5 petroleum ether 40-60 : ethyl acetate) to produce a cream/pink-coloured powdery solid.

An alternative workup was also developed, proceeding *via* the triflate salt. Following the cooling of the flask, xylenes were removed under reduced pressure and a few drops of dichloromethane were added so the residue flowed relatively freely. The residue was then dissolved in petroleum ether and passed through a Büchner filter, depositing a butterscotch-colour solid. The crude salt was washed twice with petroleum ether. Following this, the salt was deprotonated with NaOH (2 M aqueous solution) twice and extracted with DCM. The resulting organic layers were combined; solvent was removed under reduced pressure to leave an off-white solid (7.5 g, 28% yield).

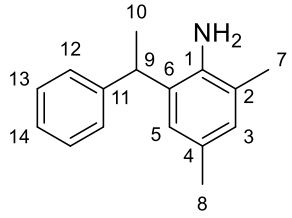

NMR Data

^{1}H (500 MHz, $CDCl_3$) δ 7.14-6.95 (aryl, m, 7H) 3.95 (*H*C$_9$, q, ^{3}J = 7.2 Hz, 1H) 2.9 (N*H*$_2$, s, 2H) 2.23 (*H*C$_8$, s, 3H), 1.78 (*H*C$_7$, s, 3H), 1.47 (*H*C$_{10}$, d, ^{3}J = 7.2 Hz, 3H)

^{13}C{^{1}H} (126 MHz, $CDCl_3$) δ 146.3 (C_{11}), 140.4 (C_1), 129.3 (aryl), 128.9 (aryl), 128.6 (C_{13}), 127.9 (C_{12}), 126.3 (aryl), 126.0 (aryl), 125.8 (aryl), 122.2 (C_2), 40.3 (C_9), 21.7 (C_{10}), 20.6 (C_8), 17.3 (C_7)

Data concordant with previous literature. [310]

Synthesis of *sec*-phenylethyl β-diketimine proligand (for 26)

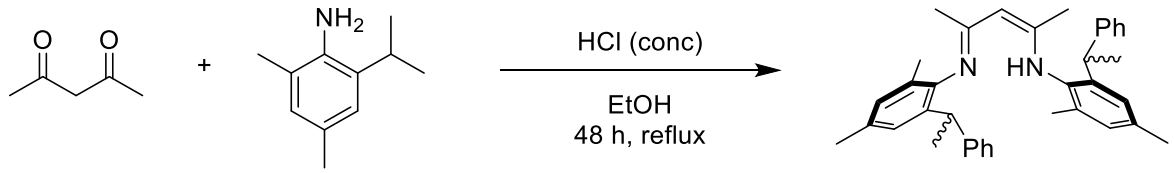

This synthesis has been previously reported by Webster. [217] To a 100 mL round-bottom flask was added 2,4-dimethyl-6-(1-phenylethyl)aniline (4 g, 17.75 mmol, 2.24 eq.), 2,4-pentanedione (0.81 mL, 7.92 mmol, 1 eq.) and 32 mL ethanol. HCl (30 wt%, 0.65 mL) was added and a reflux condenser attached; the solution was then heated to 90 °C for 48 hours then 95 °C for a further 16 hours. Ethanol and liberated water were removed by distillation by heating at 120 °C for 4 hours. The residue was dissolved in dichloromethane, washed with saturated sodium carbonate solution (3 x 50 mL), dried with magnesium sulfate and the solvent removed under reduced pressure. The product was purified by alumina column chromatography using 100% petroleum ether, yielding a foamy white solid (2.11 g, 52% yield).

As the product contains a mixture of diastersteroisomers the ^{1}H NMR spectrum is particularly complex, however full assignment is possible and has previously been reported. [217]

Synthesis of 26

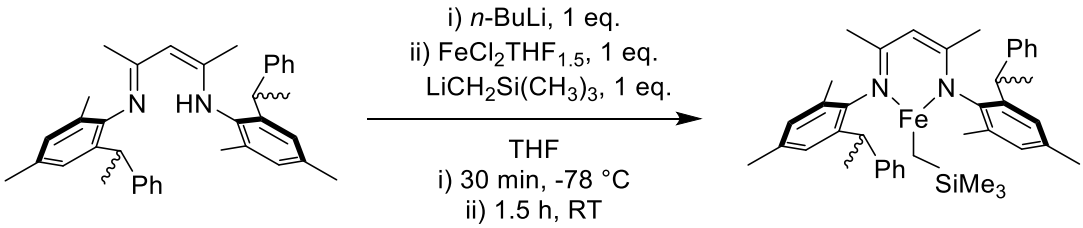

The required proligand (2.06 g, 4.18 mmol) was dissolved in 20 mL dry THF and cooled to −78 °C under a nitrogen atmosphere. *n*-Butyl lithium (solution in hexanes, 2.25 mL, 4.18 mmol, 1 eq.) was added dropwise, and the solution was allowed to warm to room temperature and stirred for 30 minutes. Following this, $FeCl_2{\cdot}THF_{1.5}$ (982 mg, 4.18 mmol) was added, and the solution was stirred for a further 45 minutes. $LiCH_2Si(CH_3)_3$ (394 mg, 4.18 mmol) was then added, and the solution stirred for a further 45 minutes, by which time the solution has turned a dark reddish-brown colour. The solvent was removed *in vacuo* and the residue washed thrice with pentane (15-20 mL) to remove any residual THF, each time removing the pentane *in vacuo*. The residue was then redissolved in pentane and passed through a pad of celite under a nitrogen atmosphere. **26** could be isolated through crystallisation from concentration of the eluted solution (1.93 g, 73% yield).

Synthesis of 2,2'-Ethylenebis(nitrilomethylidene)diphenol

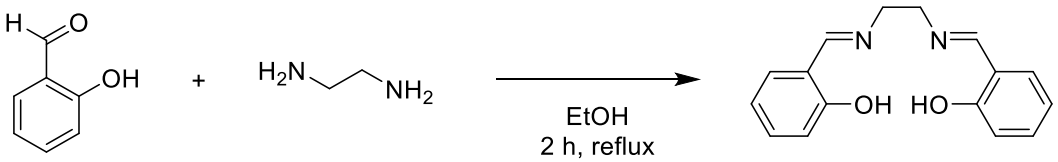

As previously reported, [311] to a 100 mL round bottom flask was added salicylaldehyde (2.44 g, 20 mmol, 2 eq.), ethylenediamine (0.60 g, 10 mmol, 1 eq.) and 45 mL ethanol. The solution was refluxed for 2 hours, then cooled to −20 °C. The precipitated yellow solid was filtered off, washed with cold ethanol and dried under vacuum to yield the desired proligand as a yellow crystalline solid (2.47 g, 92% yield).

NMR Data

^{1}H (500 MHz, $CDCl_3$) δ 13.19 (ArO*H*, s, 2H), 8.36 (ArC*H*N, s, 2H), 7.31-6.84 (ar, m, 8H), 3.95 (NCH_2CH_2N, s, 4H)

Data concordant with previous literature. [311]

Synthesis of 28

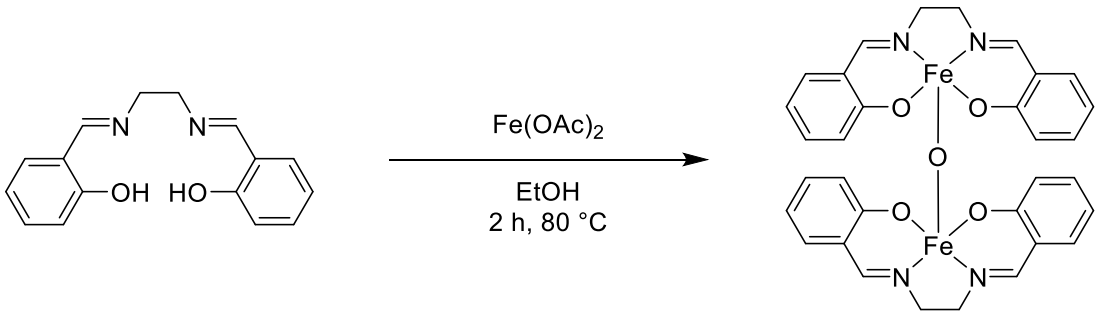

As previously reported, [311] Iron(II) acetate (0.95 g, 5.42 mmol, 1 eq.) was dissolved in 45 mL ethanol in a 250 mL round-bottom flask. To this was added 2,2'-Ethylenebis(nitrilomethylidene)diphenol (1.74 g, 6.50 mmol, 1.2 eq.) in 90 mL ethanol, and the mixture was stirred at 80 °C for 2 hours. The reaction mixture was cooled and filtered, and the precipitate washed with ethanol. Drying under a vacuum yielded **28** as a dark brown solid (1.88 g, 52% yield).

NMR Data

^{1}H (500 MHz, $CDCl_3$) δ 76.5, 47.3, 25.0, 20.5, 12.9, 10.1, 2.0, −66.2, −81.3

Full characterisation, including crystallographic data, has previously been reported. [311]

Synthesis of 43

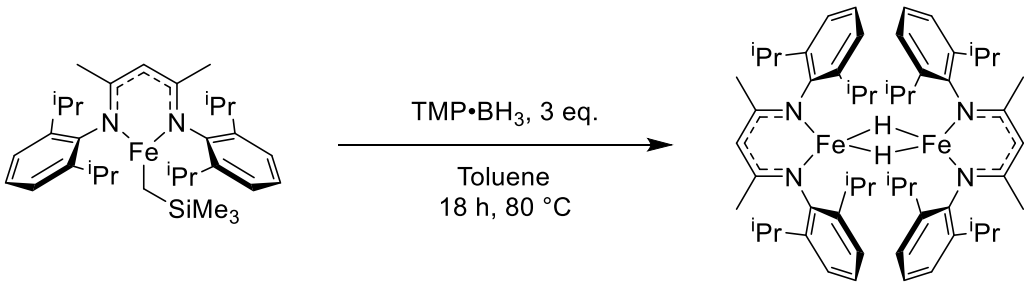

In a flame-dried Schlenk flask under an argon atmosphere, **1** (200 mg, 0.36 mmol) was dissolved in 1 mL dry toluene and TMP·BH_3 (124 mg, 1 mmol, 3 eq.) was added. The reaction was then stirred at 80 °C for 16 hours. The solvent was removed *in vacuo* and **43** was isolated through recrystallisation in pentane at −20 °C to yield a dark brown solid (203 mg, 60% yield).

NMR Data

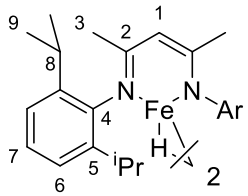

^{1}H (300 MHz, C_6D_6) δ 13.0 (*H*C_3 and *H*C_6), 7.0 (*H*C_9), −23.9 (*H*C_7), −25.9 (*H*C_9), −55.3 (*H*C_1) (*H*C_8 not observed)

Data is concordant with previous literature. [312] Full characterisation, including crystallographic data, has previously been reported. [46]

Synthesis of ((2,6-diisopropylphenyl)imino)pent-2-en-2-yl-2,6-diisopropylaniline lithium complex

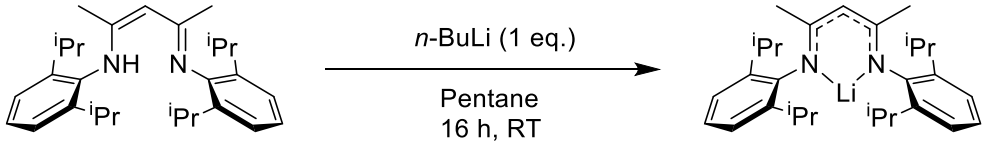

To a flame-dried Schlenk flask was added ((2,6-diisopropylphenyl)imino)pent-2-en-2-yl-2,6-diisopropylaniline (4.18 g, 10 mmol), which was dissolved in 20 mL pentane under a dry argon atmosphere, before being cooled to 0 °C. *n*-Butyl lithium (2.43 M in hexanes, 4.11 mL, 10 mmol) was added dropwise. The flask was allowed to warm to room temperature and stirred for 16 hours. The desired product could then be precipitated as a white solid from the solution at reduced temperatures. The solution was twice decanted and reduced in volume in order to obtain addition product (2.95 g, 70% yield).

NMR Data

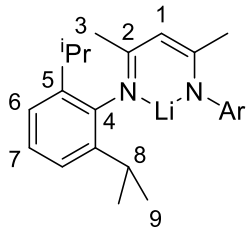

^{1}H (500 MHz, C_6D_6) δ 7.18-7.10 (ar, m, 6H), 4.84 (*H*C$_1$, s, 1H), 3.08 (*H*C$_8$, sep, ^{3}J = 6.8 Hz, 4H), 1.78 (*H*C$_3$, s, 6H), 1.16 & 1.13 (*H*C$_9$, d, ^{3}J = 6.9 Hz, 24H)

^{13}C{^{1}H} (126 MHz, C_6D_6) δ 164.1 (C_2), 149.3 (C_4), 140.8 (C_5), 128.4 (C_7), 123.4 (C_6), 93.1 (C_1), 28.3 (C_8), 24.2 & 24.1 (C_9), 23.4 (C_3)

^{7}Li (194 MHz, C_6D_6) δ 0.71 (s)

Data concordant with previous literature. [313]

Synthesis of ((2,6-diisopropylphenyl)imino)pent-2-en-2-yl-2,6-diisopropylaniline iron(II) chloride (with lithium-THF adduct)

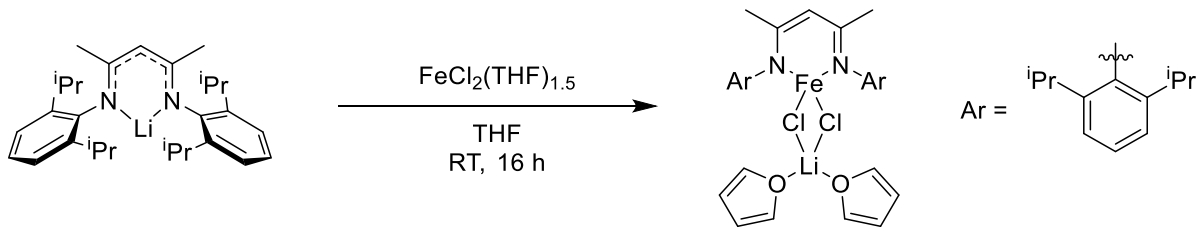

Synthesis of NACNACFe(μ-Cl_2)Li(THF)$_2$ directly from the required proligand has previously been reported by Webster, [45] the synthesis below is adapted from Holland [314] and provides a higher yielding route. The required lithium β-diketiminate complex (1.07 g, 2.5 mmol) was dissolved in 15 mL dry THF. To this solution was added $FeCl_2(THF)_{1.5}$ (0.57 g, 2.5 mmol) in small additions. The

resulting solution was stirred at room temperature overnight. The desired iron-lithium adduct could be isolated as a yellow solid by crystallisation from the solution at reduced temperatures (1.39 g, 81% yield).

NMR Data

As previously reported, the ^{1}H NMR spectrum of NACNACFe(μ-Cl_2)Li(THF)$_2$ in benzene-d_6 is more complex than expected, whilst in protic tetrahydrofuran the spectra considerably simpler.

^{1}H (300 MHz, C_6D_6) δ 16.49, 12.50, 8.72, 7.09, 3.32, 2.11, 1.67, 1.21, 0.93, 0.30, −18.06, −25.51, −38.44, −41.54, −46.12, −67.56

^{1}H (500 MHz, THF) δ 15.35, 7.03, −16.44, −42.76, −63.73

Although no melting point could be observed, the complex was observed to turn dark brown at around 300–320 °C indicating decomposition, consistent with previous reports. [314]

Synthesis of potassium graphite (KC_8)

This preparation was adapted from the procedure reported by Rabinovitz. [315] Graphite (2 g, 90–150 micrograde, Fluka) was added to a flame-dried J-Young tapped Schlenk flask, which was subsequently heated under vacuum with a heat gun for 1 hour to desorb any residual oxygen/moisture. In a glovebox under an argon atmosphere, potassium metal (0.82 g) was added in small chunks to the flask. The flask was then removed from the glovebox and placed in a silicone oil bath heated at 90 °C which was steadily raised to 200 °C, whilst maintaining vigorous stirring. After 45 minutes of vigorous stirring at 200 °C, KC_8 was obtained as bronze/golden powder in quantitative yield.

KC_8 was stored in a glovebox under an argon atmosphere, and all potentially flammable materials (latex gloves, weighing boats etc.) in contact with it were carefully quenched with an excess of isopropanol immediately upon exposure to air.

Attempted Synthesis of 44

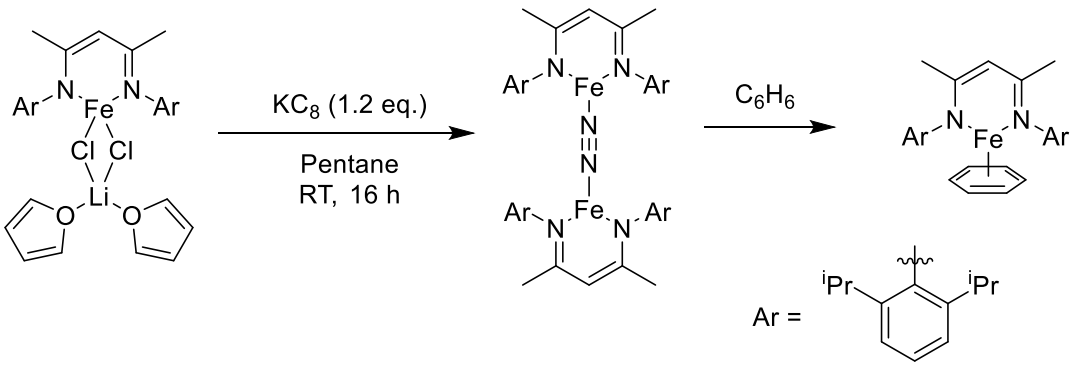

NACNACFe(μ-Cl_2)Li(THF)$_2$ (604 mg, 0.88 mmol) was added to a J-Young tapped Schlenk flask under an argon atmosphere and dry pentane (20 mL) was added, creating a dark brown slurry. To this was slowly added KC_8 (111 mg, 1.06 mmol, 1.2 eq.) under an argon atmosphere in a glove box. The sealed flask was then removed from the glovebox, exposed to a flow of dry nitrogen gas for thirty minutes, then sealed and stirred overnight at room temperature. The colour of solution changed from dark yellow to dark red and graphite was observed to precipitate as a black solid. The solution

was decanted *via* cannula filtration and reduced in volume and cooled, and a red solid was precipitated. The red solid was subsequently dissolved in dry protic benzene. NMR, Evans and UV-Vis data of the solid were, however, inconsistent with literature data of both the dinitrogen and benzene-coordinated complexes.

NMR Data (observed paramagnetic range signals)

^{1}H (500 MHz, C_6D_6) δ 12.60, −6.91, −20.63, −33.84, −39.11, −40.35, −41.78

Reported NMR Data for $(NACNACFe)_2N_2$ ($FeC_{58}H_{82}N_6$)

^{1}H (400 MHz, C_6D_{12}) 53, -19, −20, −98, −112, −123, −280

Reported NMR Data for NACNACFe-Benzene-μ_6 ($FeC_{35}H_{47}N_2$)

^{1}H (400 MHz, C_6D_{12}) 118, 11, −28, −42, −57, −158, −205

λ_{max} = 328 nm (Literature value for $FeC_{35}H_{47}N_2$ λ_{max} = 496 nm, for $FeC_{58}H_{82}N_6$ λ_{max} = 499 nm. *Note that both complexes also have reported peaks at 917 nm / 911 nm respectively; however these wavelengths are beyond the limit of detection for our instrument setup*)

μ_{obs} = 3.8 B.M. (assuming a $FeC_{35}H_{47}N_2$ molecular formula, literature μ_{obs} = 2.5 B.M.) or 5.1 B.M. (assuming an $FeC_{58}H_{82}N_6$ molecular formula, literature μ_{obs} = 7.9 B.M.)

Both reported species structural and spectroscopic data was obtained from literature reports. [239]

Synthesis of 45

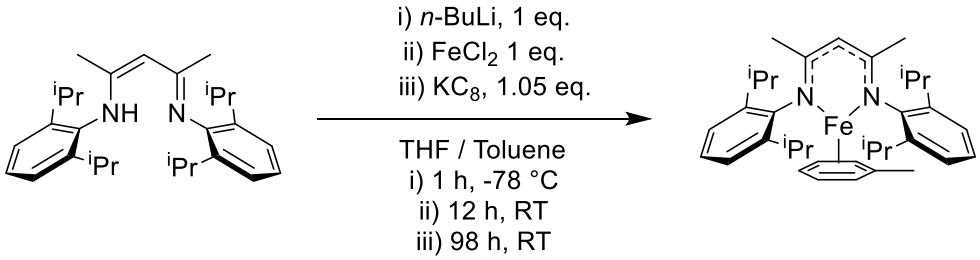

45 was prepared using the method reported by Scheer. [248] A slurry of ((2,6-diisopropylphenyl)imino)pent-2-en-2-yl-2,6-diisopropylaniline (6.68 g, 24.0 mmol) dissolved in 100 mL dry THF was cooled to −78 °C and *n*-butyl lithium (solution in hexanes, 15 mL, 24.0 mmol, 1 eq.) was added dropwise. The resulting clear red solution was stirred at room temperature for 1 hour. The solution was slowly transferred into a slurry of anhydrous $FeCl_2$ (3.04 g, (24.0 mmol) in 5 mL THF, forming an intense dark yellow solution, which was stirred at room temperature for 12 hours. After removal of solvent, the brownish solid was dissolved in 50 mL of toluene. The intense dark yellow solution was transferred into a slurry of 1.05 equivalents of potassium graphite in 10 mL toluene. The mixture was stirred at room temperature for 98 hours and a color change to olive green was observed. Remaining graphite and salts were removed *via* filtration of the olive-green solution over celite. The solvent was removed under reduced pressure and a dark green-brown solid was obtained. The solid was dissolved in 100 mL dry hexane and the solution was filtered over celite, with the desired dark green solid precipitating at −20°C under reduced pressure.

The ^{1}H NMR was found to be very broad in both toluene-d_8 and benzene-d_6 — the data below is reported in toluene-d_8 to prevent any toluene-benzene ligand exchange. No peaks were observed

in the far downfield region (δ = 512.9 ppm and 487.6 ppm) as reported, however other signals are consistent with previous reports. [248]

NMR Data

^{1}H (500 MHz, C_7D_8) δ 10.7 (3H), 7.60 (7H), 2.56 (3H), 1.73 (12H)

Synthesis of reagents pertinent to multiple chapters – further reagents & deuterated compounds

Synthesis of tetramethylpiperidine borane ($C_9H_{19}N{\cdot}BH_3$)

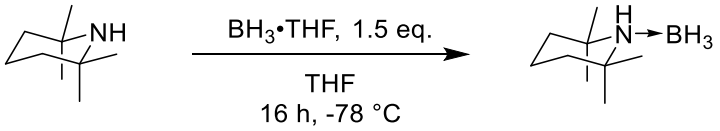

The synthesis was adapted from previous methodology. [218] Tetramethylpiperidine (TMP) (4 mmol, 565 µL) was placed in a flame-dried Schlenk flask under a nitrogen atmosphere. The vessel was then cooled to −78 °C and a solution of BH_3·THF in THF (1 M, 6 mmol, 6 mL) was added slowly dropwise, with stirring. The solution was then stirred at room temperature for a further 16 hours. The solvent and excess BH_3·THF were removed under vacuum, affording the product as a white solid.

NMR Data

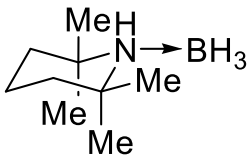

^{1}H (500 MHz, C_6D_6) δ 2.55-1.88 (N*H* and B*H*$_3$, 4H), 1.21 (equatorial *H*C_{PARA}, dt, $^{3}J_{eq\text{-}eq}$ = 13.7 Hz, $^{3}J_{eq\text{-}ax}$ = 3.3 Hz, 1H), 1.15 (Me, s, 12H), 1.05 (axial *H*C_{META}, dt, $^{3}J_{ax\text{-}ax}$ = 14.1 Hz, $^{3}J_{ax\text{-}eq}$ = 3.3 Hz, 2H), 0.88 (axial *H*C_{PARA}, dt, $^{3}J_{ax\text{-}ax}$ = 14.1 Hz, $^{3}J_{ax\text{-}eq}$ = 3.7 Hz, 1H), 0.68 (equatorial *H*C_{META}, td, $^{3}J_{eq\text{-}eq}$ = 13.7 Hz, $^{3}J_{eq\text{-}ax}$ = 3.7 Hz, 2H)

^{13}C{^{1}H} (126 MHz, C_6D_6) δ 40.2 (C_{META}), 33.4 (Methyl), 20.2 (C_{ORTHO}), 16.2 (C_{PARA})

^{11}B (160 MHz, C_6D_6) δ −20.7 (q, $^{1}J_{HB}$ = 99 Hz)

Data is concordant with previous literature. [47, 316]

Synthesis of aniline borane ($PhNH_2{\cdot}BH_3$)

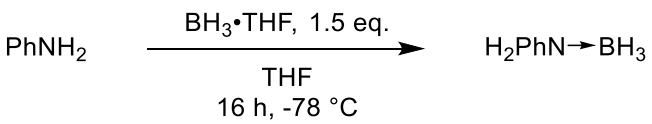

As reported by Manners, [317] but performed herein on a smaller scale, 0.50 mL of aniline (0.51 g, 5.5 mmol) was dissolved in 10 mL of dry tetrahydrofuran in a Schlenk flask under a nitrogen

atmosphere. The reaction mixture was cooled to −78 °C and 5 mL of BH_3·THF adduct (1.0 M in tetrahydrofuran, 5 mmol) was added to dropwise. The reaction was allowed to warm to room temperature and stirred for 16 hours. Solvent and remaining reagent were removed under reduced pressure to give a fluffy white solid, with a distinctive singlet in the $^{11}B\{^1H\}$ NMR at δ = −15.5 ppm.

Synthesis of Wittig Reagents (CH_3PPh_3I and CD_3PPh_3I)

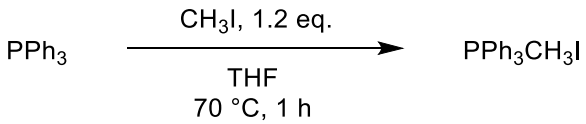

Triphenylphosphine (5.62 g, 21.4 mmol) was dissolved in 40 mL dry THF in a flame-dried Schlenk flask under a nitrogen atmosphere. Iodomethane (1.60 mL, 3.65 g, 25.7 mmol) was added dropwise, and the flask was then sealed and heated to 70 °C for 1 hour. A white precipitate was observed to form. The precipitate was filtered on a Buchner funnel and washed with xylenes. Vacuum drying for 1 hour yielded a white powder (8.68 g, 99% yield). Spectroscopic data was consistent with commercial material (Acros, 99%).

For the preparation of CD_3PPh_3I, an identical preparation was used with the exception of using iodomethane-d_3 (1.61 mL, 3.67 g, 25.7 mmol) in place of iodomethane. (8.67 g, 97% yield, 98% d-incorporation).

NMR Data (For CD_3PPh_3I)

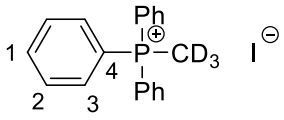

^1H (500 MHz, $CDCl_3$) δ 7.86-7.64 (ar, m, 15H)

$^{13}C\{^1H\}$ (126 MHz, $CDCl_3$) δ 135.4 (C_1, d, ^4J = 3.0 Hz), 133.5 (C_3, d, ^2J = 10.9 Hz), 130.6 (C_2, d, ^3J = 12.9 Hz), 119.0 (C_4, d, ^1J = 88.7 Hz), 25.8 (Me, br s)

^2H (77 MHz, $CDCl_3$) δ 3.21 (s)

$^{31}P\{^1H\}$ (202 MHz, $CDCl_3$) δ 22.5 (s)

Synthesis of d-pinacolborane (DBpin)

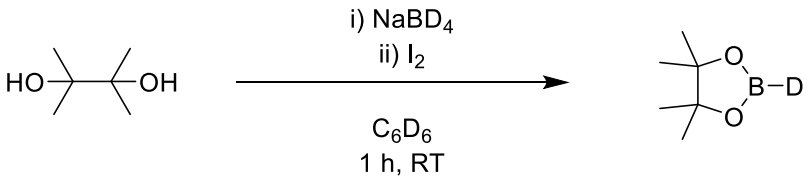

As previously reported, [218] $NaBD_4$ (0.5 g, 12.2 mmol, 3 eq.) was dissolved in 10 mL diglyme in a flame-dried Schlenk flask under an argon atmosphere. Pinacol (0.48 g, 4.08 mmol, 1 eq.) was dissolved in benzene-d_6 in a separate, flame-dried Schlenk flask and added dropwise to the first flask by means of a cannula. Following addition, a solution of iodine (1.55 g, 6.11 mmol, 1.5 eq.) in diglyme (6 mL) was added dropwise over the course of 45 minutes. A flow of argon was passed over

the solution to remove unreacted B_2D_6. The resulting DBpin was used as a solution and concentration determined by addition of an internal standard.

NMR Data

^{1}H (400 MHz, C_6D_6) δ 1.00 (s, C*H*$_3$, 9H)

^{11}B (128 MHz, C_6D_6) δ 27.2 (s)

Synthesis of dimethylamine-d borane ($(CH_3)_2ND{\cdot}BH_3$)

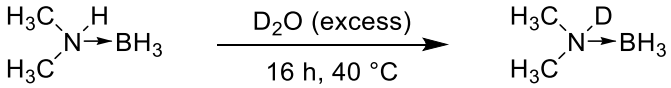

This synthesis was adapted from the method reported by Manners. [318] Dimethylamine-borane (300 mg, 5.1 mmol) was dissolved in 2.5 mL D_2O and stirred at 40°C for 16 hours. The product was extracted with DCM (3 × 5 mL) and the solvent removed under reduced pressure. The product was then purified *via* sublimation to yield a white solid (200 mg, 67% yield).

NMR Data

^{1}H{^{11}B} (300 MHz, $CDCl_3$) δ 2.53 ($(CH_3)_2ND{\cdot}BH_3$), 1.51 ($(CH_3)_2ND{\cdot}BH_3$, s, 3H)

^{13}C{^{1}H} (126 MHz, $CDCl_3$) δ 44.4

^{2}H (77 MHz, $CHCl_3$) δ 3.81 (s)

^{11}B (160 MHz, $CDCl_3$) δ −14.1 (q, ^1J = 19.6 Hz)

Data concordant with previous literature. [318]

Synthesis of dimethylamine borane-d_3 ($(CH_3)_2NH{\cdot}BD_3$)

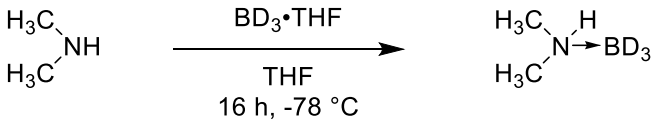

The synthesis used was adapted from the method reported by Manners. [318] Dimethylamine (2 M in THF, 2 mmol, 1 mL) was added to a Schlenk flask under a nitrogen atmosphere and cooled to −78 °C. $BD_3{\cdot}THF$ (1 M in THF, 2 mmol, 2 mL) was added dropwise whilst stirring, and the solution was allowed to warm and stirred for a further 16 hours. Solvent and volatiles were then removed under reduced pressure, and the crude product was washed with hexane (3 × 1 mL) and purified by sublimation, yielding a white solid (35 mg, 29% yield).

NMR Data

^{1}H (300 MHz, $CDCl_3$) δ 3.81 ($(CH_3)_2NHBD_3$, br s, 1H), 2.57 ($(CH_3)_2NHBD_3$, d, ^3J = 5.8 Hz, 6H)

^{13}C{^{1}H} (126 MHz, $CDCl_3$) δ 44.7

^{11}B (160 MHz, $CDCl_3$) δ -14.2 (br s)

Data concordant with previous literature. [318]

7.2 Experimental Data Pertinent to Chapter 2

General Considerations & Procedures

General Procedure for Isomerisation of Alkenes

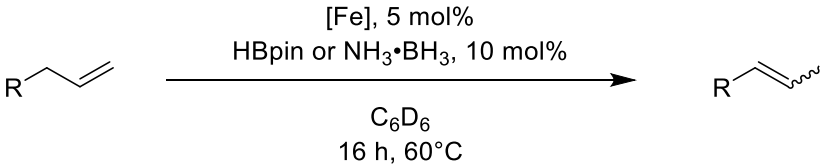

Experiments were performed under an argon atmosphere in an M-Braun glove box. The required iron pre-catalyst (0.025 mmol, 5 mol% relative to substrate) was dissolved in 600 µL dry deuterated benzene solvent and added to a J-Young tap NMR tube. To this was added pinacolborane (0.05 mmol, 7.2 µL) / ammonia borane (0.05 mmol, 1.6 mg) or alternative hydride source, followed by the substrate (0.5 mmol). The tube was sealed, and the reaction allowed to proceed for the time and temperature stated. The product was isolated by exposing the reaction to air, and carefully removing most of the solvent by passing nitrogen over the mixture, followed by filtration through a silica plug using pentane as the eluent. Pentane was removed by blowing nitrogen over the eluate, yielding the desired product.

For linear alkenes, reactions were performed in a J-Young Schlenk flask of approximately 20 mL volume, and the reaction was subject to stirring.

Synthesis of piperonal from isosafrole *via* ozonolysis

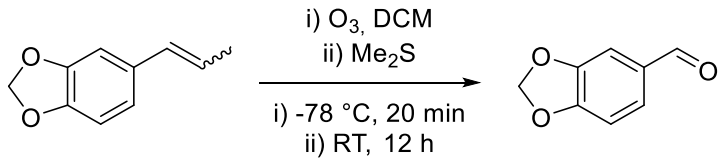

144 µL of isosafrole **36** (prepared from standard procedure on larger scale) was dissolved in approximately 4 mL dichloromethane in a 250 mL round-bottom flask, which was then cooled to −78 °C. Ozone (supplied from a Wallace & Tiernan Ozone generator at 230 V) was then bubbled through the reaction for 20 minutes, at which point the solution turned from colourless to dark blue. Following this, the reaction was bubbled through for 20 minutes with oxygen and 1 hour with nitrogen, at which point the reaction turned colourless again. Dimethyl sulphide (3.1 eq., 165.7 µL, 196 mg) was then added and the reaction was stirred at room temperature overnight. The solution was washed with saturated sodium carbonate solution, followed by saturated brine solution twice, and the solvent (and acetaldehyde side-product) then removed under reduced pressure to leave piperonal **51** as a white solid (81 mg, 54% yield).

Nanoparticle Test

This procedure was adapted from report by Morris. [229] Reactions were set up under standard conditions with trimethylphosphine (1.3 µL, 2.5 mol%, 0.5 equiv. with respect to catalyst) additionally added. In a nanoparticle-based system, the reaction would be expected to be fully quenched with a sub-stoichiometric amount of PMe_3 sufficient to bind to all active sites. In reactions

with both pinacolborane and ammonia borane conversion was reduced but still present under standard reaction conditions, indicating nanoparticles are not active in catalysis.

Blank Reactions

To a solution of allylbenzene (66.1 µL, 0.5 mmol) in 600 µL of C_6D_6 was added 1.6 mg (0.05 mmol, 0.1 eq) of ammonia borane. After heating at 80 °C for 48 hours, no reactivity was observed. The same outcome was observed when 7.2 µL (0.05 mmol, 0.1 eq) of HBpin was used in place of ammonia borane.

To a solution of 14 mg (0.025 mmol) of **1** in 600 µL of C_6D_6 was added 66.1 µL (0.5 mmol, 20 eq) of allylbenzene. After heating at 80 °C for 48 hours, no reactivity was observed.

Evans Method Setup

Measurements were performed on a Bruker 500 MHz NMR spectrometer at 298 K, in a J-Young NMR tube under an argon atmosphere with a sealed C_6D_6 capillary inserted. To 600 µL C_6D_6 was added the required solid (between 3-5 mg, accurately weighed). The magnetic susceptibility was determined by the difference in ^{1}H NMR chemical shift of the residual protic peaks of benzene-d_6 in the solution and the capillary using standard calculations and reported susceptibilities and diamagnetic contributions. The contribution values and equations were adapted from web.mit.edu/5.03/www/readings/magnetism/calculator.html

Kinetic Reactions

Experiments were set up as per standard reaction setup, with the addition of 1,3,5-trimethoxybenzene (15-20 mg, accurately weighed) to act as an internal standard. The sealed reaction vessel was monitored in a Bruker 400 MHz NMR Spectrometer, with measurements taken every 10 minutes at room temperature for two hours.

Test for activation of catalyst using H_2

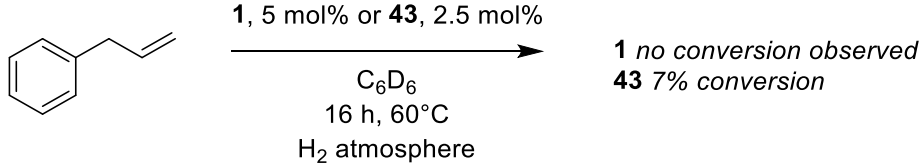

Allylbenzene (66.1 µL, 0.5 mmol) and **1** (14.0 mg, 0.025 mmol, 5 mol%) were added to 600 µL benzene-d_6 in a J-Young NMR tube under an argon atmosphere in a glovebox as per the standard reaction setup. The reaction vessel was then removed from the glovebox and the atmosphere removed by freeze-pump-thaw technique on a high-vacuum Schlenk line three times. The vessel was then filled with hydrogen gas (1 atmosphere pressure), sealed, and subject to standard reaction conditions (16 h, 60°C). Following this, no reactivity was observed. ^{1}H NMR only indicated allylbenzene present in the δ = 0–10 ppm region.

To further discount the role of iron hydrides in catalysis, the same experiment was repeated, with the exception of using the dimeric Fe(II) hydride **43** (11.8 mg, 0.0125 mmol, 2.5 mol%) in place of **1**. In this case, a small amount of isomerisation is observed (approx. 7%) which is similar to the same reaction under an argon atmosphere. There is also a small amount of conversion to the

hydrogenated product (approx. 9 %). The hydrogen setup has been reported in greater detail by Whittlesey. [319]

Radical Clock Test

We have previously reported this radical clock test for other catalytic reactions. [44] The reaction was prepared under normal reaction conditions using HBpin (10 mol%). The reaction was allowed to proceed for 4 hours at 60 °C, at which point conversion to product was observed to be partial (28%). (Chloromethyl)cyclopropane **60** (0.025 mmol, 4.6 µL) was then added to the reaction and heating was continued. Although reactivity was perturbed, catalysis still proceeded beyond addition of the radical trap, (after a further 4 hours 44% conversion) and the ring opened product expected from a radical system (1-butene) was not observed, only the initial (chloromethyl)cyclopropane.

Cyclic Voltammetry Experimental Setup

Cyclic voltammetry experiments were performed under an argon atmosphere using standard Schlenk techniques and a custom built three-necked Schlenk flask. To 25 mL of dry THF was added the required pre-catalyst (37 mg, 5 mM concentration) and tetrabutylammonium hexafluorophosphate (1.16 g, 0.1 M concentration). A standard three electrode setup was used (glassy carbon working electrode, platinum counter electrode and silver pseudo-reference electrode). Voltammograms were referenced to Fc/Fc^+ oxidation potential by addition of 1 mg ferrocene to the solution.

Experiments were performed by increasing potential from 0 V to the maximum potential, followed by decreasing to the minimum potential and subsequent raising it back to 0 V. The data shown has the oxidative sweep above the reduction sweep on the y axis.

Synthesis of Deuterated Substrates

Synthesis of 2,2-d_2-phenylacetic acid

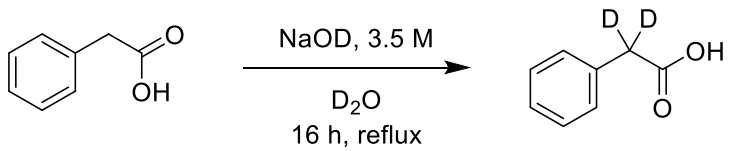

This synthesis was adapted from the procedure reported by Gao. [320] To a J-Young Schlenk flask under air was added 6.8 g (50 mmol) of phenylacetic acid and 20 mL of 3.5 M sodium deuteroxide solution in D_2O. The flask was sealed and heated to 100 °C overnight with stirring. After cooling, 20 mL of 4 M hydrochloric acid solution was used to neutralise the mixture. The crude product was extracted with dichloromethane (30 mL), dried with magnesium sulphate and the solvent was removed under reduced pressure. The process was then repeated with the crude product to give 2,2-d_2-phenylacetic acid with 97% deuterium incorporation (white solid, 98% yield, 6.72 g).

NMR Data

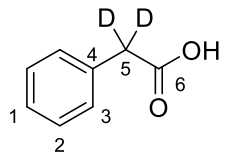

^{1}H (500 MHz, $CDCl_3$) 7.26-7.37 (ar, m, 5H)

$^{13}C\{^{1}H\}$ (126 MHz, $CDCl_3$) 178.4 (C_6), 133.3 (C_4), 129.5 (C_3), 128.8 (C_2), 127.5 (C_1), 40.7 (C_5)

^{2}H (77 MHz, $CHCl_3$) 3.72 (s)

FTMS (NSI) $[2M-2H+Na]^-$ 297.1046 (calc) 297.1045 (obs) $[2M-H]^-$ 275.1227 (calc) 275.1226 (obs)

Data is concordant with previous literature. [320]

Synthesis of 2,2-d_2-2-phenylethanol

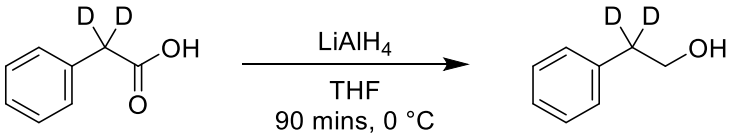

1.64 g of lithium aluminium hydride was suspended in 50 mL dry tetrahydrofuran and cooled to 0 °C. To this was added dropwise a solution of 2,2-d_2-phenylacetic acid (5 g, 36 mmol) in 40 mL dry tetrahydrofuran. The mixture was stirred for 90 minutes and quenched with 0.5 M hydrochloric acid. The mixture was then filtered and washed with ethyl acetate. The organic phase of the eluent was washed with both water and brine, dried with magnesium sulfate and concentrated under reduced pressure. The crude product was then purified with column chromatography (5:1 petroleum ether 40-60 : ethyl acetate). Careful rotary evaporation yielded the purified product containing some residual ethyl acetate (floral-smelling clear liquid 4.0 g, 90% yield).

NMR Data

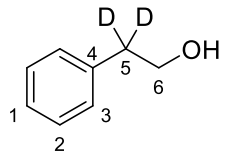

^{1}H (300 MHz, $CDCl_3$) 7.37-7.21 (ar, m, 5H), 3.86 ($PhCD_2CH_2OH$, br s, 2H), 1.51 ($PhCD_2CH_2OH$, s, 1H)

$^{13}C\{^{1}H\}$ (126 MHz, $CDCl_3$) 138.5 (C_4), 129.2 (C_2), 128.7 (C_3), 126.6 (C_1), 63.7 (C_6) (C_5 not observed)

^{2}H (77 MHz, $CDCl_3$) 2.86 (s)

Data is concordant with previous literature. [320]

Synthesis of 2,2-d_2-phenylacetaldehyde

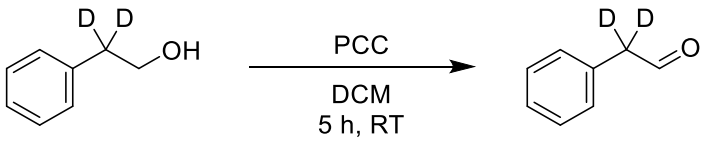

Pyridinium chlorochromate (1.6 g, 7.5 mmol) and dry silica gel (7.5 g) were mixed in 15 mL dichloromethane and 2,2-d_2-2-phenylethanol (0.62 g, 5 mmol) dissolved in 10 mL dichloromethane was added; the resultant mixture was stirred for 5 hours. Following this, the reaction was filtered through a silica plug and washed through with diethyl ether, and the solvent was removed to give the crude 2,2,-d_2-phenylacetaldehyde product (clear oil, 0.65 g, 97% yield).

NMR Data (crude product, ^{1}H assigned only)

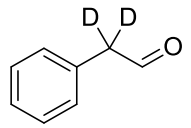

^{1}H (500 MHz, $CDCl_3$) 9.75 ($PhCD_2CHO$, s, 1H) 7.18–7.41 (ar, m, 5H)

MS [M-H] 121.0701 (theoretical) 121.0635 (obs)

Synthesis of 1,1-d_2-allylbenzene

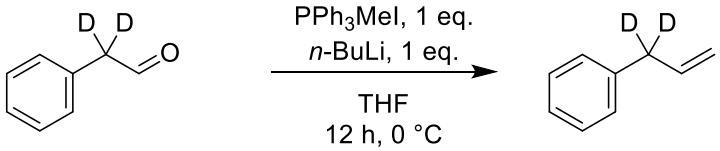

To a stirred solution of methyltriphenylphosphonium iodide (5.5 mmol, 2.22 g) in 10 mL dry THF was added *n*-butyl lithium solution (6 mmol, 1.54 M in hexanes, 3.89 mL) under a nitrogen atmosphere. The solution was cooled to 0 °C and crude phenyacetaldehyde-2-2-d_2 (566 µL, 0.61 g, 5 mmol) was added. The reaction was then allowed to warm to room temperature and stirred for 12 hours. The reaction was then quenched with 0.5 M HCl, and the product was extracted with diethyl ether and washed with water. The organic solution was concentrated to give a crude product, which was purified through column chromatography (9:1 pentane : ethyl acetate). Careful rotary evaporation yielded the deuterated substrate with a small amount of remaining ethyl acetate (clear yellow liquid, 0.49 g, 82% yield, 90% deuterium incorporation).

NMR Data

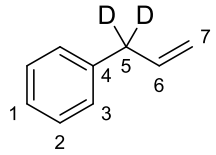

^{1}H (300 MHz, $CDCl_3$) 7.36–7.17 (ar, m, 5H) 5.97 ($PhCD_2CHCH_2$, m, 1H) 5.09 ($PhCD_2CHCH_2$, m, 2H)

$^{13}C\{^1H\}$ (126 MHz, $CDCl_3$) 137.4 (C_4), 128.6 (C_3), 128.4 (C_2), 126.0 (C_6), 125.8 (C_1), 115.7 (C_7), 16.2 (C_5)

^{2}H (77 MHz, $CHCl_3$) 3.36 (s)

TOF-MS [M-] 129.0908 (theoretical) 129.0918 (observed)

Data concordant with previous literature. [320]

Synthesis of 3,3-d_2-allylbenzene

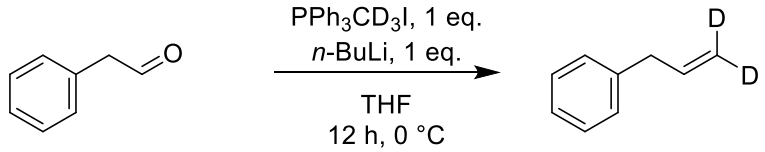

Methyltriphenylphosphonium iodide-d_3 (8 mmol, 3.25 g) was dissolved in 30 mL dry THF in a flame-dried J-Young Schlenk flask and cooled to −78 °C. To this solution, *n*-butyl lithium (8 mmol, 1.43 M in hexanes, 5.59 mL) was added dropwise, and the reaction was allowed to stir for 15 minutes before warming to room temperature. Following a further 30 minutes of stirring, the reaction was cooled again to −78 °C and phenylacetaldehyde (8 mmol, 961 mg, 890 µL) was added dropwise. After 20 minutes of stirring, the reaction was allowed to warm to room temperature and stirred for an additional 16 hours. The reaction was quenched by the addition of 10 mL deionised water (initially added dropwise), and the product was extracted with petroleum ether (2 × 20 mL). The organic layers were washed with brine, dried with magnesium sulphate, and concentrated under reduced pressure. The product was purified by column chromatography (using pentane as the eluent) and carefully concentrated *via* rotary evaporation to yield a colourless oil (26% yield, 250 mg, 82% d-incorporation).

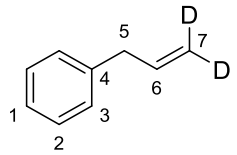

NMR Data

^{1}H (500 MHz, $CDCl_3$) 7.35–7.16 (ar, m, 5H), 5.92 ($PhCH_2CHCD_2$, m, 1H), 3.40 ($PhCH_2CHCD_2$, d, 2H, ^{3}J = 6.7 Hz)

^{13}C{^{1}H} (126 MHz, $CDCl_3$) 140.2 (C_4), 137.4 (C_6), 128.7 (C_3), 128.6 (C_2), 126.2 (C_1), 40.3 (C_5) (C_7 not observed)

^{2}H (77 MHz, $CDCl_3$) 5.13 (s)

TOF-MS [M+Na^+] 143.0840 (theoretical), 143.0824 (observed)

Data concordant with previous literature. [321]

Electron Paramagnetic Resonance (EPR) Studies

Preparation of samples and EPR spectrometer setup

Samples for EPR measurements were prepared under a nitrogen atmosphere in a glovebox. A solution of **1** was prepared by dissolving approximately 4 mg of **1** in 200 µL of dry benzene (in all cases, a further 10 µL of dry toluene was also added to improve the quality of the polycrystalline

glass formed in frozen solution, and thereby enhance the quality of the EPR spectra). The solutions were transferred to a J-Young EPR tube (Wilmad Labglass 727-LPV-250M) in the glove box and then cooled to 77 K before rapid transfer to the pre-cooled EPR cavity. The X-band CW EPR measurements were performed on a Bruker EMX spectrometer utilising an ER4119HS resonator, 100 kHz field modulation at 140 K.

EPR Density Functional Theory Studies

All EPR density functional theory (DFT) calculations were carried out with ORCA (version 4.1.0). [322] A combination of basis sets was used for calculation of the spin Hamiltonian EPR parameters, including CP for Fe, and def2-TZVP on C/H/N atoms, in conjunction with the B3LYP density functional and RIJCOSX approximation. [323-326]The grid sizes were set to Grid5 and "normal" SCF criteria (with Slow Convergence, maximum of 500 iterations). The spin–orbit mean field operator (SOMF(1X)) was used, and the origin for the g-tensor was taken at the centre of the electronic charge.

The observed EPR data, as well as the modelled data for **44**, **47** and **49** are shown the table below. All species were modelled in the low spin state. The anisotropy parameters are tabulated below this.

	g-values				**Euler angles/ rad**		
	g_1	g_2	g_3	g_{iso}	α	β	γ
1 + HBPin (Expt)	1.984	2.018	2.200	2.067	−1.900	1.490	0.669
44 (DFT)	1.979	2.015	2.128	2.041	−1.900	1.490	0.669
47 (DFT)	2.010	2.089	2.254	2.118	1.843	1.937	3.038
49 (DFT)	1.979	2.094	2.221	2.098	1.793	1.480	-3.095

	g-values				**Anisotropy parameters**			
	g_1	g_2	g_3	g_{iso}	$\Delta g_3 - g_1$	$\Delta g_3 - g_2$	$\Delta g_2 - g_1$	Δg_{rel}
1 + HBPin (Expt)	1.984	2.018	2.200	2.067	0.216	0.182	0.034	84.3
44 (DFT)	1.979	2.015	2.128	2.041	0.149	0.113	0.036	75.8
47 (DFT)	2.010	2.089	2.254	2.118	0.244	0.165	0.079	67.6
49 (DFT)	1.979	2.094	2.221	2.098	0.242	0.127	0.115	52.5

Density Functional Theory (DFT) Studies

Calculations of the Fe(I/III) catalytic cycle were carried out using the Jaguar software package [327] using the B3LYP density functional with Grimme's D3 dispersion correction (unless stated), with frequency calculations carried out at 298 K. [328-332] Fe was modelled using the triple-zeta Los Alamos effective core potential as implemented in Jaguar, with all other atoms modelled using the

6-31G* basis set. Implicit solvation was accounted for using a polarisable continuum model with benzene as the solvent. [333]

Studies into the Fe(II) alkyl mechanism

Grimme's D3 dispersion correction was not used, and frequency calculations were carried out at 333.15 K for the Fe(II) cycle to simulate experimental conditions and explore the temperature effect on the thermodynamic well for **40**. The energies for the intermediates on the catalytic cycle are shown below. **42** was found to optimise to a stable state rather than ejecting the substrate entirely and effectively forming **39**, and as such the β-hydride elimination is treated as the transformation of **40** to **42.**

	Relative ΔG_{solv}				
Species	**Quintet**	**$\Delta\Delta G_{solv}$**	**Triplet**	**$\Delta\Delta G_{solv}$**	**Singlet**
39	0.0		12.6		26.7
39 – 40 (TS)	19.6	19.6	15.1	2.5	
40	-14.0		6.7		56.3

The transition states for the singlet state could not be determined, although this is academic as the singlet state surface is considerably higher than the triplet or quintet surfaces across the hypothetical catalytic cycle.

Calculated free and potential energies for the insertion step (**39** to **40**) — all energies are in kcal mol^{-1}.

Calculated free and potential energies for optimised structures of catalytic species in the singlet spin state — all energies are in kcal mol^{-1}.

Species	**ΔE**	**ΔE_{solv}**	**ΔG_{solv} (333.15K)**
41	17.99	22.50	25.51
41 - 40 (TS)	-	-	-
40	29.37	33.88	41.07
40 - 42 (TS)	-	-	-
42	22.15	26.67	32.55

Calculated free and potential energies for optimised structures of catalytic species in the triplet spin state — all energies are in kcal mol^{-1}.

Species	**ΔE**	**ΔE_{solv}**	**ΔG_{solv} (333.15K)**
41	9.38	10.86	11.16
41 - 40 (TS)	9.34	13.86	14.45
40	-0.77	0.67	5.28
40 - 42 (TS)	19.10	23.62	25.40
42	11.10	12.53	14.39

Calculated free and potential energies for optimised structures of catalytic species in the quintet spin state — all energies are in kcal mol^{-1}.

Species	ΔE	ΔE_{solv}	ΔG_{solv} (333.15K)
41	0.00	0.00	0.00
41 - 40 (TS)	17.57	18.50	19.59
40	-18.68	-17.42	-13.98
40 - 42 (TS)	21.82	22.48	23.45
42	3.95	1.82	2.44

Studies into the Fe(I)/Fe(III) allyl mechanism

Both the *trans* and *cis*-product forming mechanisms were investigated. Both require a specific conformation about **47** which determines stereochemistry, these structures are identified as $\mathbf{47}_{trans}$ and $\mathbf{47}_{cis}$, although this should not be taken as a statement of formal stereochemistry about **47**. The lowest energy structure of **47** cannot undergo oxidative addition as neither β C–H bond is in a feasible position to interact, and is termed $\mathbf{47}_{neutral}$ in the tables below.

The sextet is only modelled for species where a sextet spin state is possible. The $\mathbf{47}_{cis}$ **-** $\mathbf{48}_{cis}$ **(TS)** transition state could only be determined for the doublet state. To obtain estimated values for the alternate spin states, the doublet optimised $\mathbf{47}_{cis}$ **-** $\mathbf{48}_{cis}$ **(TS)** structure was ran as a quartet and sextet spin state structure. The sextet transition states are unlikely to be real and/or not be spin-contaminated by the doublet spin configuration, as the sextet spin configuration is not possible for d^7 species that these transition states arise to/from.

Calculated free and potential energies for optimised species in the doublet spin configuration for the Fe(I/III) catalytic cycle — all energies are in kcal mol^{-1}.

Species	ΔE	ΔE_{solv}	ΔG_{solv} (298.15K)
$\mathbf{47}_{neutral}$	0.00	0.00	0.00
$\mathbf{47}_{trans}$	-0.37	-0.06	0.32
$\mathbf{47}_{trans}$ **-** $\mathbf{48}_{trans}$ **(TS)**	24.22	24.58	25.99
$\mathbf{48}_{trans}$	15.60	16.03	18.33
$\mathbf{48}_{trans}$ **-** $\mathbf{49}_{trans}$ **(TS)**	20.02	19.69	20.96
$\mathbf{49}_{trans}$	-5.88	-5.55	-4.63
$\mathbf{47}_{cis}$	-0.44	-0.74	1.39
$\mathbf{47}_{cis}$ **-** $\mathbf{48}_{cis}$ **(TS)**	29.43	29.40	29.44
$\mathbf{48}_{cis}$	17.47	17.95	21.04
$\mathbf{48}_{cis}$ **-** $\mathbf{49}_{cis}$ **(TS)**	25.22	25.64	25.84
$\mathbf{49}_{cis}$	-4.52	-4.39	-3.29

Calculated free and potential energies for optimised species in the quartet spin configuration for the Fe(I/III) catalytic cycle — all energies are in kcal mol^{-1}.

Species	ΔE	ΔE_{solv}	ΔG_{solv} (298.15K)
$47_{neutral}$	-20.37	-20.26	-20.37
47_{trans}	-20.80	-20.63	-18.71
47_{trans} - 48_{trans} (TS)	29.71	28.96	26.33
48_{trans}	4.16	4.46	3.04
48_{trans} - 49_{trans} (TS)	7.59	6.93	3.50
49_{trans}	-26.77	-26.32	-16.46
47_{cis}	-20.20	-19.71	-18.72
47_{cis} - 48_{cis} (TS)	*29.13*	*29.70*	-
48_{cis}	19.03	19.00	19.27
48_{cis} - 49_{cis} (TS)	14.50	12.54	10.41
49_{cis}	-23.20	-22.95	-1.95

Calculated free and potential energies for optimised species in the sextet spin configuration for the Fe (I/III) catalytic cycle – all energies are in kcal mol^{-1}.

Species	ΔE	ΔE_{solv}	ΔG_{solv} (298.15K)
47_{trans} - 48_{trans} (TS)	39.25	38.98	34.05
48_{trans}	18.99	18.62	15.24
48_{trans} - 49_{trans} (TS)	32.68	31.85	26.23
47_{cis} - 48_{cis} (TS)	*69.80*	*73.01*	-
48_{cis}	15.84	15.10	11.21
48_{cis} - 49_{cis} (TS)	32.94	33.08	28.53

Studies into spin state crossover in allyl mechanism

Owing the closeness of the spin state energies, the presence of spin crossover processes was investigated. As this is most likely to occur during oxidative addition (where a sextet state becomes possible), it was attempted to find minimum-energy crossing points (MECPs) in the region about **47_{trans} - 48_{trans} (TS)**. However, these failed to converge from multiple initial geometries.

Vertical excitation energies were performed on both transition state structures and **48** from the doublet to sextet spin state and from the sextet to doublet spin state. Vertical excitation energy is

defined as ΔE for sextet spin configuration at the optimised geometry for the doublet spin configuration and *vice versa* for sextet optimised geometry. As the structures for **47_{cis} - 48_{cis} (TS)** structures could not be determined in the quartet and sextet states, these were not evaluated.

Vertical excitation energies from doublet spin state.

Species	Doublet (Hartrees)	Sextet (Hartrees)	Vertical Excitation Energy (kcal mol^{-1})
47_{trans} - 48_{trans} (TS)	-1711.818856	-1711.740846	48.95
48_{trans}	-1711.832469	-1711.83242	0.03
48_{trans} - 49_{trans} (TS)	-1711.826656	-1711.78593	25.56
47_{cis} - 48_{cis} (TS)	-1711.811178	-1711.741678	43.61
48_{cis}	-1711.829418	-1711.77108	36.61
48_{cis} - 49_{cis} (TS)	-1711.81716	-1711.759504	36.18

Vertical excitation energies from sextet spin state.

Species	Sextet (Hartrees)	Doublet (Hartrees)	Vertical Excitation Energy (kcal mol^{-1})
47_{trans} - 48_{trans} (TS)	-1711.795903	-1711.81526	-12.15
48_{trans}	-1711.828351	-1711.82832	0.02
48_{trans} - 49_{trans} (TS)	-1711.807268	-1711.813527	-3.93
48_{cis}	-1711.833967	-1711.829265	2.95
48_{cis} - 49_{cis} (TS)	-1711.805309	-1711.81897	9.41

Variation of functional/basis set

The single point solvated energies of the species and transition states above were evaluated with different functionals. The geometries were determined with the B3LYP-D3/6-31G(d)/LACV3P* method. As the **47_{cis} - 48_{cis} (TS)** structures could not be determined in the quartet and sextet states, these were not evaluated.

Single point solvated potential energies of B3LYP-D3/6-31G(d)/LACV3P* geometries using different functionals for the doublet (S = ½) spin configuration.

	ΔE_{solv} (kcal mol^{-1})			
Species	**B3LYP-D3**	**BP86** [330, 331]	**PBE0** [332]	**PBE0-D3**
47$_{neutral}$	0.00	0.00	0.00	0.00
47$_{trans}$	-0.06	2.41	0.53	0.18
47$_{trans}$ - 48$_{trans}$ (TS)	24.58	21.46	25.72	23.65
48$_{trans}$	16.04	19.24	24.92	20.67
48$_{trans}$ - 49$_{trans}$ (TS)	19.69	20.31	25.15	21.96
49$_{trans}$	-5.55	1.77	-0.16	-3.16
47$_{cis}$	-0.74	4.91	1.60	-0.14
47$_{cis}$ - 48$_{cis}$ (TS)	29.40	23.47	30.14	29.25
		17.58	22.76	19.80
		23.24	27.89	25.40
49$_{cis}$	-4.39	0.97	-0.71	-3.77

Single point solvated potential energies of B3LYP-D3/6-31G(d)/LACV3P* geometries using different functionals for the quartet (S = 3/2) spin configuration.

	ΔE_{solv} (kcal mol^{-1})			
Species	**B3LYP-D3**	**BP86**	**PBE0**	**PBE0-D3**
47$_{neutral}$	-20.26	-11.73	-17.98	-17.27
47$_{trans}$	-20.63	-11.47	-26.71	-24.88
47$_{trans}$ - 48$_{trans}$ (TS)	28.96	34.69	35.82	33.76
48$_{trans}$	4.46	14.85	6.33	3.20
48$_{trans}$ - 49$_{trans}$ (TS)	6.93	16.40	14.25	11.07
49$_{trans}$	-26.32	-11.22	-23.39	-26.39
47$_{cis}$	-19.71	-5.95	-22.48	-23.46
47$_{cis}$ - 48$_{cis}$ (TS)	-	-	-	-
48$_{cis}$	19.00	30.66	33.46	30.51
48$_{cis}$ - 49$_{cis}$ (TS)	12.54	18.98	18.50	16.02
49$_{cis}$	-22.95	-10.31	-19.79	-22.46

Single point solvated potential energies of B3LYP-D3/6-31G(d)/LACV3P* geometries using different functionals for the sextet (S = 5/2) spin configuration.

	ΔE_{solv} (kcal mol^{-1})			
Species	**B3LYP-D3**	**BP86**	**PBE0**	**PBE0-D3**
47$_{trans}$ - 48$_{trans}$ (TS)	38.98	-10.00	65.04	62.97
48$_{trans}$	18.62	38.22	19.72	16.40
48$_{trans}$ - 49$_{trans}$ (TS)	31.85	-26.19	41.52	38.34
47$_{cis}$ - 48$_{cis}$ (TS)	-	-	-	-
48$_{cis}$	15.10	-35.52	49.72	46.77
48$_{cis}$ - 49$_{cis}$ (TS)	33.08	-11.18	55.46	52.97

The higher quality basis set, 6-311+G(d,p) was also used as a comparison. Single point solvated potential energies were calculated using the 6-311+G(d,p) basis set on geometries optimised using B3LYP-D3/6-31g(d)/LACV3P*.

	ΔE_{solv} (kcal mol^{-1})		
Species	**Doublet (S = ½) state**	**Quartet (S = 3/2) state**	**Sextet (S = 5/2) state**
47$_{neutral}$	0.00	-21.15	-
47$_{trans}$	0.54	-21.50	-
47$_{trans}$ - 48$_{trans}$ (TS)	24.35	27.76	54.35
48$_{trans}$	14.70	3.32	16.77
48$_{trans}$ - 49$_{trans}$ (TS)	18.12	5.76	37.60
49$_{trans}$	-2.42	-25.74	-
47$_{cis}$	0.27	-19.39	-
47$_{cis}$ - 48$_{cis}$ (TS)	28.67	-	-
48$_{cis}$	17.54	19.01	29.76
48$_{cis}$ - 49$_{cis}$ (TS)	24.44	11.09	51.68
49$_{cis}$	-2.03	-22.39	-

Assignment of Products

Reactions with ammonia borane were worked up and subject to full assignment. In the majority of cases the *cis* product was not formed in enough quantity to analyse (see Section 2.3); where it is it is also assigned below in turn with the *trans* product.

29 (*E*)-1-(2-Methylbenzyl)prop-1-ene

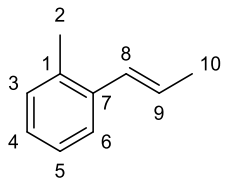

Obtained from standard procedure, 82% Spectroscopic Conversion, 58% Isolated, 38.3 mg.

^{1}H (500 MHz, $CDCl_3$) 7.44–7.09 (aromatic, m, 4H), 6.62 ($CH_3PhC\mathit{H}CHCH_3$, dq, 1H, ^{3}J = 15.6 Hz, ^{4}J = 1.8 Hz), 6.13 ($CH_3PhCHC\mathit{H}CH_3$, dq, 1H, ^{3}J = 15.6 Hz, ^{3}J = 6.6 Hz), 2.36 ($C\mathit{H_3}PhCHCHCH_3$, s, 3H), 1.93 ($CH_3PhCHCHC\mathit{H_3}$, dd, 3H, ^{3}J = 6.6 Hz, ^{4}J = 1.8 Hz)

$^{13}C\{^{1}H\}$ (126 MHz, $CDCl_3$) 137.2 (C_7), 134.9 (C_1), 130.9 (C_3), 130.2 (C_9), 129.0 (C_6), 127.1 (C_5), 126.8 (C_4) 123.6 (C_8), 55.3 (C_2), 18.9 (C_{10})

TOF-MS (EI+) [O] 148.0888 (calc) 148.0889 (obs)

Data concordant with previous literature. [109]

30 (*E*)-1-(3-Methylbenzyl)prop-1-ene

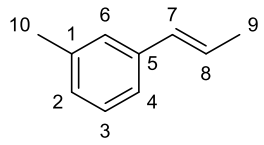

Obtained from standard procedure, 92% Spectroscopic Conversion, 65% Isolated, 43.0 mg.

^{1}H (500 MHz, $CDCl_3$) 7.10–7.25 (aromatic, m, 4H), 6.39 ($CH_3PhC\mathit{H}CHCH_3$, dq, 1H, ^{3}J = 15.7 Hz, ^{4}J = 1.7 Hz), 6.24 ($CH_3PhCHC\mathit{H}CH_3$, dq, 1H, ^{3}J = 15.7 Hz, ^{3}J = 6.6 Hz), 2.35 ($C\mathit{H_3}PhCHCHCH_3$, s, 3H), 1.89 ($CH_3PhCHCHCH_3$, dd, 3H, ^{3}J = 6.6 Hz, ^{4}J = 1.7 Hz)

^{13}C{^{1}H} (126 MHz, $CDCl_3$) 138.0 (C_5), 137.9 (C_1), 131.1 (C_7), 128.3 (C_6), 127.5 (C_3), 126.6 (C_2), 125.5 (C_8), 122.9 (C_4), 21.5 (C_{10}), 18.5 (C_9)

TOF-MS (EI+) [M] 132.0939 (calc) 132.0933 (obs)

Data concordant with previous literature. [334]

31 (*E*)-1-(4-Methylbenzyl)prop-1-ene

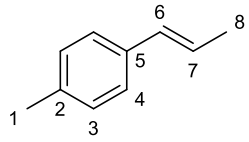

Obtained from standard procedure, 98% Spectroscopic Conversion, 72% Isolated, 47.6 mg.

^{1}H (300 MHz, $CDCl_3$) 7.01–7.18 (ar, m, 4H), 6.30 ($CH_3PhC\mathit{H}CHCH_3$, ^{3}J = 15.7 Hz, ^{4}J = 1.6 Hz, 1H), 6.11 ($CH_3PhCHC\mathit{H}CH_3$, dq, ^{3}J = 15.7 Hz, ^{3}J = 6.5 Hz, 1H), 2.25 ($C\mathit{H_3}PhCHCHCH_3$, s, 3H), 1.79 ($CH_3PhCHCHC\mathit{H_3}$, dd, ^{3}J = 6.5 Hz, ^{4}J = 1.6 Hz, 3H),

^{13}C{^{1}H} (126 MHz, $CDCl_3$) – 136.4 (C_2), 135.2 (C_5), 130.8 (C_6), 129.2 (C_3), 125.7 (C_4), 124.6 (C_7), 21.1 (C_1), 18.4 (C_8)

TOF-MS (ASAP+) [M-H] 131.0861 (calc) 131.0851 (obs)

Data concordant with previous literature. [109]

32 (*E*)-1-(2-Methoxybenzyl)prop-1-ene

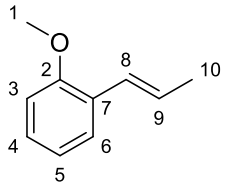

Obtained from standard procedure, 92% spectroscopic yield, 69% isolated product, 51.1 mg.

^{1}H (500 MHz, $CDCl_3$) 7.42–6.83 (ar, m, 4H), 6.73 ($CH_3OPhC\mathit{H}CHCH_3$, dq, ^{3}J = 15.9 Hz, ^{4}J = 1.8 Hz, 1H), 6.24 ($CH_3OPhCHC\mathit{H}CH_3$, dq, ^{3}J = 15.9 Hz, ^{3}J = 6.6 Hz, 1H), 3.85 ($C\mathit{H_3}OPhCHCHCH_3$, s, 3H), 1.91 ($CH_3OPhCHCHC\mathit{H_3}$, dd, ^{3}J = 6.6 Hz, ^{4}J = 1.8 Hz, 3H)

$^{13}C\{^{1}H\}$ (126 MHz, $CDCl_3$) 156.2 (C_2), 127.8 (C_4), 127.0 (C_7), 126.5 (C_9), 126.4 (C_6), 125.6 (C_8), 120.6 (C_5), 110.7 (C_3), 55.4 (C_1), 18.9 (C_{10})

TOF-MS (ASAP+) [M+O+H] 165.0916 (calc) 165.0909+ (obs)

Data concordant with previous literature. [109]

33 (E)-1-(4-Methoxybenzyl)prop-1-ene ((*E*)-Anethole)

Obtained from standard procedure, 98% spectroscopic yield, 62% isolated, 45.9 mg.

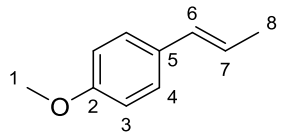

^{1}H (500 MHz, $CDCl_3$) 7.11 (HC_4, d, ^{3}J = 8.6 Hz), 6.84 (HC_3, d, ^{3}J = 8.6 Hz), 6.42 ($CH_3OPhCHCHCH_3$, dq, ^{3}J = 15.8 Hz, ^{4}J = 1.7 Hz, 1H), 6.17 ($CH_3OPhCHCHCH_3$, dq, ^{3}J = 15.8 Hz, ^{3}J = 6.6 Hz, 1H) 3.86 ($CH_3OPhCHCHCH_3$, s, 3H), 1.93 ($CH_3OPhCHCHCH_3$, dd, ^{3}J = 6.6 Hz, ^{4}J = 1.7 Hz, 3H)

$^{13}C\{^{1}H\}$ (126 MHz, $CDCl_3$) 158.6 (C_2), 130.8 (C_5), 130.4 (C_6), 126.9 (C_4), 123.5 (C_7), 113.9 (C_3), 55.2 (C_1), 18.4 (C_8)

TOF-MS (ASAP+) [M+H] 149.0966 (calc) 149.1058 (obs)

Data concordant with previous literature. [107]

34 (*E*)-1-(4-Fluorophenyl)prop-1-ene

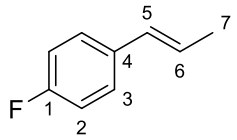

Obtained from modified procedure, 70% spectroscopic yield, 41% isolated product, 28.0 mg.

^{1}H (500 MHz, $CDCl_3$) 7.25–7.31 (ar, m, 2H), 7.01-6.95 (ar, m, 2H), 6.37 ($FPhCHCHCH_3$, dq, ^{3}J = 15.7 Hz, ^{4}J = 1.8 Hz, 1H), 6.15 ($FPhCHCHCH_3$, dq, ^{3}J = 15.7 Hz, ^{3}J = 6.6 Hz, 1H), 1.88 ($FPhCHCHCH_3$, dd, ^{3}J = 6.6 Hz, ^{4}J = 1.8 Hz, 3H)

$^{13}C\{^{1}H\}$ (126 MHz, $CDCl_3$) 161.8 (C_1, d, ^{1}J = 245.5 Hz) , 134.1 (C_4, d, ^{4}J = 3.3 Hz), 129.8 (C_6), 127.2 (C_3, d, ^{3}J = 7.7 Hz), 125.4 (C_5, d, ^{5}J = 1.9 Hz), 115.2 (C_2, d, ^{2}J = 21.4 Hz) 18.4 (C_7)

^{19}F (470 MHz, $CDCl_3$) -116.0 (s)

TOF-MS (ASAP+) [M-H] 135.0610 (calc) 135.0607 (obs)

The minor product (*Z*)-1-(4-Fluorophenyl)prop-1-ene was also observed in the ^{19}F NMR and ^{1}H NMR.

^{1}H (500 MHz, $CDCl_3$) 7.20–6.92 (m, 4H) 5.95 (m, 1H), 5.78 (dq ^{3}J = 11.5 Hz, ^{4}J = 7.1 Hz, 1H), 1.62 (m, 3H)

^{19}F (470 MHz, $CDCl_3$) -118.2 (s)

Data concordant with previous literature. [109]

35 (*E*)-1-(4-Trifluorophenyl)prop-1-ene

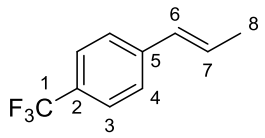

Obtained from modified procedure, 58% spectroscopic yield, 39% isolated product, 36.3 mg.

^{1}H (500 MHz, $CDCl_3$), 7.62–7.36 (ar, m, 4H), 6.43 ($CF_3PhCHCHCH_3$, dq, ^{3}J = 15.8 Hz, ^{4}J = 1.5 Hz, 1H) 6.35 ($CF_3PhCHCHCH_3$, dq, ^{3}J = 15.8 Hz, ^{3}J = 6.4 Hz, 1H), 1.92 ($CF_3PhCHCHCH_3$, dd, ^{3}J = 6.4 Hz, ^{4}J = 1.4 Hz, 3H)

^{13}C{^{1}H} (126 MHz, $CDCl_3$) 141.3 (C_2), 129.9 (C_5), 128.9 (C_6), 128.6 (C_7), 125.9 (C_4), 125.4 (C_3), 123.2 (C_1) 18.5 (C_8)

^{19}F (470 MHz, $CDCl_3$) -62.4 (s)

TOF-MS (ASAP+) [M] 186.0656 (calc) 186.0653 (obs) [M-H] 185.0578 (calc) 185.0575 (obs)

The minor product (*Z*)-1-(4-Trifluorophenyl)prop-1-ene was also observed ^{19}F NMR and ^{1}H NMR.

^{1}H (500 MHz, $CDCl_3$) 7.60–7.25 (m, 4H), 6.00-5.87 (m, 2H), 1.53 (s, 3H)

^{19}F (470 MHz, $CDCl_3$) -62.3 (s)

Data concordant with previous literature. [335]

36 Isosafrole

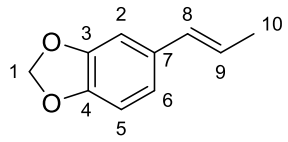

Obtained from standard procedure, 97% spectroscopic yield, 65% isolated, 52.7 mg.

^{1}H (500 MHz, $CDCl_3$) 6.89–6.74 (ar, m, 3H) 6.32 ($PhCHCHCH_3$, ^{3}J = 14.4 Hz, ^{4}J = 1.2 Hz, 1H), 6.08 ($PhCHCHCH_3$, dq, ^{3}J = 14.4 Hz, ^{3}J = 6.6 Hz, 1H), 5.92 (OCH_2O, d, ^{4}J = 1.2 Hz, 2H), 1.86 ($PhCHCHCH_3$, dd, ^{3}J = 7.5 Hz, ^{4}J = 1.2 Hz, 3H)

^{13}C{^{1}H} (126 MHz, $CDCl_3$) 147.8 (C_3), 145.7 (C_4), 132.9 (C_7), 130.9 (C_8), 124.3 (C_9), 120.4 (C_6), 108.3 (C_5), 105.7 (C_2), 101.0 (C_1), 18.7 (C_{10})

Data concordant with previous literature. [336]

37 Pinene

Pinene conversion determined by comparison of ^{1}H NMR peaks of starting material and product as shown below.

4.79 - 4.87 ppm

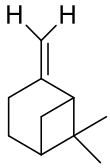

5.30 ppm

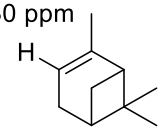

38 Naphthalene,1,2,3,5,6,7,8,8a-octahydro-1,8a-dimethyl-7-(1-methylethylidene)- (1R,8aS)

Conversion from valencene was determined by comparison of ^{1}H NMR peaks of starting material and product as shown below.

5.33 ppm

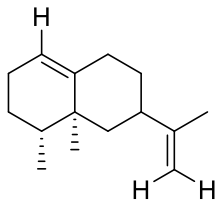

4.65-4.71 ppm

5.30 ppm

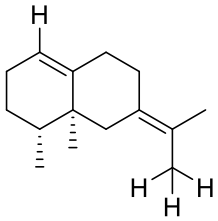

1.72 ppm

51 Piperonal (Prepared from isosafrole *via* ozonolysis)

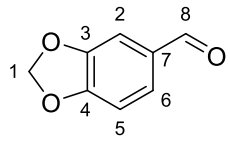

Isolated as white solid (81 mg, 54% yield).

^{1}H (500 MHz, $CDCl_3$) 9.82 (PhC*H*O, s, 1H) 7.42 (*H*C_6, dd, ^{3}J = 7.9 Hz, ^{4}J = 1.6 Hz, 1H), 7.34 (*H*C_2, d, ^{4}J = 1.6 Hz, 1H), 6.94 (*H*C_5, d, ^{3}J = 7.9 Hz), 6.08 (OCH_2O, s, 2H)

^{13}C{^{1}H} (126 MHz, $CDCl_3$) 190.4 (C_8), 153.3 (C_4), 148.9 (C_3), 132.1 (C_7), 128.8 (C_6), 108.5 (C_5), 107.1 (C_2), 102.3 (C_1)

TOF-MS [M+H] 151.0389 (calc) 151.0387 (obs)

Data concordant with previous literature. [337]

7.3 Experimental Data Pertinent to Chapter 3

General Considerations & Procedures

General Procedure for Polymerisation of Allenes

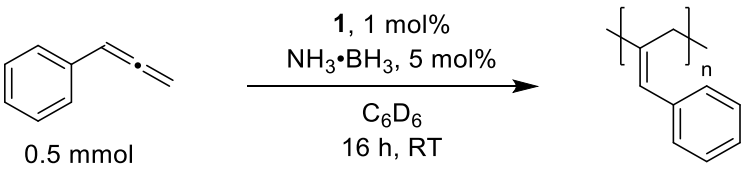

Experiments were performed under an argon atmosphere in an M-Braun glove box. The required pre-catalyst **1** (2.8 mg, 0.005 mmol, 1 mol%) and ammonia borane or alternative additive (5 mol%) were accurately weighed out and dissolved in dry deuterated benzene (600 µL) in a J-Young tap NMR tube. To this was added the required monomer (0.5 mmol), and the tube was sealed for the time and conditions reported.

To isolate the polymer, the solvent was removed from the reaction under reduced pressure. The residue was dissolved in approximately 2 mL of dry THF and, under an argon atmosphere, passed through a plug of approximately 1 cm of silica and 1 cm of celite. The resulting solution was dried under reduced pressure, yielding the polymer as a sticky brown solid.

For the scaled-up reaction, a J-Young tapped Schlenk flask was instead used as a vessel, and the residue was dissolved in approximately 10 mL of dry THF for purification.

For preparation of samples for DSC and WAXD analysis, the isolated polymer was redissolved in the minimum amount of benzene at room temperature. Dry methanol was added to the stirred solution dropwise, until precipitation of polymer was observed. The solution was decanted, the solid washed with methanol a second time, then dried under reduced pressure. This yielded an amorphous pale brown solid.

Analysis Techniques and Methods

Molecular weights and polydispersity were determined through Size Exclusion Chromatography, using an Agilent 1260 Infinity Gel Permeation Chromatography (GPC) instrument equipped with a PLgel 5 µm MIXED-D column (300 x 7.5 mm) at 1 µL min^{-1} flow rate at 35 °C. Samples were dissolved in GPC-grade THF at a concentration of 1 mg mL^{-1}. Molecular sizes and other data were determined through in-built Triple Detection analysis using Light Scattering measurement. Differential Scanning Calorimetry (DSC) analysis was conducted using a TA Instruments DSC Q20 Instrument. The samples were ramped from 25 °C to 200 °C at 10 °C min^{-1}, then cooled back down to 25 °C at the same rate. A second heating cycle at the same rate was then performed for purposes of analysis.

Variable temperature NMR (VT-NMR) experiments were performed on a Bruker 400 MHz NMR spectrometer equipped with variable temperature apparatus. The isolated polymer (approx. 20 mg) was dissolved in 600 µl C_6D_6 and heated to 60 °C and then to 80 °C. Although the peaks belonging to the HC_3 positions broaden as the temperature is raised, they do not appear to interconvert or converge at raised temperature (see spectra in Section 3.2).

WAXS experiments were performed on an Anton Paar SAXSpoint instrument with wavelength 0.154 nm, and sample-detector distance 119 mm. Visual heating experiments were performed on a Mettler Toledo FP82HT Hot Stage, and observed with a microscope camera as it was ramped from 25 °C to 200 °C.

Matrix-assisted laser-desorption time-of-flight (MALDI-ToF) analysis was performed using a Bruker Autoflex speed instrument using a DCTB matrix (*trans*-2-[3-(4-tertbutylphenyl)-2-methyl-2-propenylidene]malononitrile) in a 5 : 1 mixture of matrix : polymer (both dissolved and prepared as 10 mg / mL solutions in THF). The equipment was operated in a linear acquisition mode using POS voltage polarity. Addition of a salt to the mixture (sodium triflate in THF, 1 equivalent relative to polymer) did not enhance the data.

Summary of MALDI peaks observed.

m/z	Time (arb)	Intens.	SN	Res.	Area	Rel. Intens.	FWHM
1009.119	21973.98	41172.000	3.555	131.143	81832.583	0.830	7.695
1065.348	22556.79	41713.000	3.831	189.463	52822.430	0.841	5.623
1182.494	23723.56	49581.461	10.008	224.182	124571.286	1.000	5.275
1299.581	24833.26	27985.000	3.148	224.696	38789.094	0.564	5.784
1416.600	25893.40	37132.000	9.622	252.285	124698.186	0.749	5.615
1533.614	26910.54	20660.000	3.183	216.054	41715.767	0.417	7.098
1650.891	27891.70	29385.000	9.140	266.149	130399.629	0.593	6.203
1768.111	28838.14	16231.000	3.384	327.153	35322.843	0.327	5.405
1884.755	29749.26	23618.000	8.593	298.995	129314.730	0.476	6.304
2118.921	31496.90	18189.000	7.384	283.094	118577.979	0.367	7.485
2353.199	33151.10	14554.000	6.587	289.998	113645.497	0.294	8.115
2587.007	34721.73	11197.000	5.699	311.302	96319.795	0.226	8.310
2821.237	36225.47	9074.000	4.945	330.467	74028.665	0.183	8.537
3054.910	37664.62	7031.000	4.129	308.015	62368.426	0.142	9.918
3289.027	39052.27	5355.535	3.190	351.508	45290.432	0.108	9.357

General Procedure for Dimerisation of Allenes

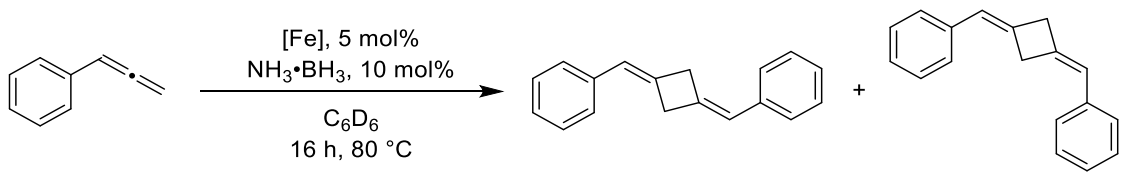

The reaction was setup as per the standard procedure, with the exception of varied reaction conditions and increased catalyst and ammonia borane loading. Following the specified time and temperature, the solvent was removed under reduced pressure. The residue was dissolved in pentane and the dimer isolated by passing through a silica plug. The pentane was removed by passing the eluted solution under a flow of nitrogen, yielding the product **65** as a white precipitate.

For the syringe pump experiments, a Cole-Parmer Syringe Pump was used, with an addition rate of 20 μL min^{-1}.

Nanoparticle Test

The procedure was adapted from Morris. [229] Reactions were set up under standard conditions but additionally trimethylphosphine (1.3 µL, 2.5 mol%, 0.5 equiv. with respect to catalyst) was added. Reaction was observed to be reduced, but not fully, indicating the active catalyst in the reaction was not nanoparticle-based.

Radical Trap Test

The reaction was initially prepared as standard, and reacted for 2 hours, where conversion was determined by NMR. Under an argon atmosphere (chloromethyl)cyclopropane (1.2 µL, 0.0125 mmol, 2.5 mol%) was added to the reaction. After a further 14 hours conversion was determined to be 91% (under standard conditions, 93%). Distillation of the reaction mixture away from catalyst/polymer indicates that the majority of the radical clock remains as starting material, with only a small (<10 %) decyclised to form 1-butene, indicating to us that it is not halting reactivity by reacting with radical species.

Blank Reactions

Phenylallene (0.5 mmol, 67.4 µL) and **1** (0.025 mmol, 5 mol%, 14 mg) were dissolved in 600 µL C_6D_6. After 16 hours, 3% conversion to ill-defined polymeric products was observed. Conversion did not significantly increase further with heating.

Phenylallene (0.5 mmol, 67.4 µL) and ammonia borane (0.05 mmol, 10 mol%, 6 mg) were dissolved in 600 µl C_6D_6. The reaction was heated to 60 °C for 48 hours — no conversion was observed.

Reactions under a Hydrogen atmopshere

The reactions were prepared using the same setup as described in Section 7.2.

Synthesis of Allenes & Precursors

Synthesis of gem dibromocyclopropanes

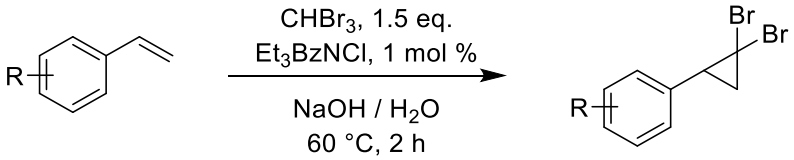

This reaction was performed under air. Sodium hydroxide (3.2 g, 80 mmol, 4 eq.) was dissolved in 3 mL of deionised water and allowed to cool to room temperature. To this was added the required styrene (20 mmol), bromoform (2.6 mL, 30 mmol, 1.5 eq.) and benzyl triethylammonium chloride (50 mg, 0.2 mmol, 0.01 eq.). The reaction was stirred at 60 °C for 2 hours, and then quenched by addition of 20 mL of water. The product was extracted with dichloromethane (3 x 50 mL), washed with brine (50 mL) and dried with magnesium sulphate. Volatiles were then removed under reduced pressure. The product was then purified by silica gel chromatography using 100% petroleum ether 40-60 as the eluent, except for **57'**, where 4:96 Ethyl Acetate : Petroleum Ether was used.

Synthesis of allenes

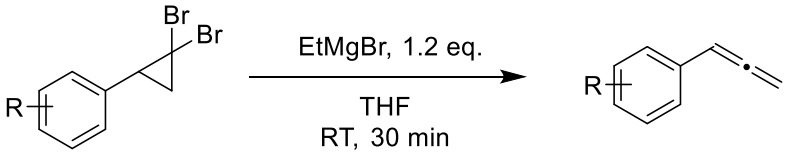

This reaction was performed under a nitrogen atmosphere using standard Schlenk techniques. The required dibromocyclopropane (10 mmol) was added to 20 mL of dry THF and cooled to 0 °C. To this, ethylmagnesium bromide (3.0 M in diethyl ether, 4 mL, 12 mmol, 1.2 equiv) was added dropwise, and the reaction was allowed to warm to room temperature. The reaction was cooled to 0 °C and quenched after 30 minutes through careful addition of deionised water (2 mL). 15 mL of 1 M hydrochloric acid was added to the reaction, and the product was extracted with petroleum ether (2 x 10 mL). The organic layers were combined, dried with magnesium sulphate and the solvent removed under reduced pressure. In most cases the product was found to be pure, however if needed further purification was undertaken by silica gel chromatography using 100% pentane as the eluent. The product was then dried with calcium hydride, distilled, degassed, and then stored in a freezer under an argon atmosphere.

Synthesis of Deuterated Phenylallene

Synthesis and characterisation of CD_3PPh_3I is detailed in Section 7.1.

Synthesis of Styrene-β,β-d_2

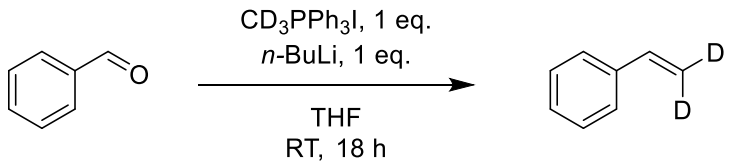

Methyltriphenylphosphonium iodide-d_3 (4.87 g, 12 mmol) was dissolved in 30 mL of dry THF in a Schlenk flask under an argon atmosphere. The solution was cooled to −78 °C and *n*-butyl lithium solution (1.43 M in hexanes, 8.4 mL, 12 mmol, 1 eq) was added dropwise. After 15 minutes, the solution was allowed to warm to room temperature, and stirred for an additional thirty minutes. The solution was then cooled again and benzaldehyde (1.21 mL, 12 mmol, 1 eq) was added dropwise. After 20 minutes the reaction was allowed to warm to room temperature, and stirred for a further 18 hours. The reaction was then quenched by addition of 1 M HCl solution. The crude product was extracted with petroleum ether (2 × 25 mL), dried with magnesium sulfate and the solvent removed under reduced pressure. The product was purified by silica column chromatography using 100% pentane and the solvent was removed under reduced pressure yielding a colourless oil (479 mg, 38% yield).

Synthesis of (2,2-dibromocyclopropyl-3,3-d_2)benzene

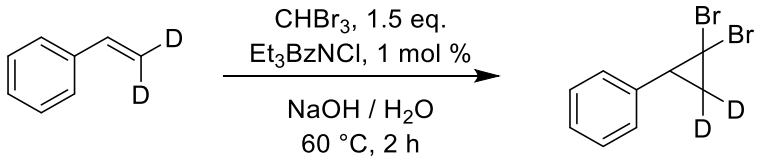

This reaction was performed under air. Sodium hydroxide (0.64 g, 16 mmol, 4 eq.) was dissolved in 0.6 mL of deionised water and allowed to cool to room temperature. To this was added styrene-β,β-d_2 (423 mg, 4 mmol), bromoform (0.52 mL, 6 mmol, 1.5 eq.) and benzyl triethylammonium chloride (10 mg, 0.04 mmol, 0.01 eq.). The reaction was stirred at 60 °C for 2 hours, and then quenched by addition of 20 mL of water. The product was extracted with dichloromethane (3 x 20 mL), washed with brine (50 mL) and dried with magnesium sulphate. Volatiles were then removed under reduced pressure. The product was then purified by silica gel chromatography using 100% petroleum ether 40-60 as the eluent, yielding a clear oil (242 mg, 22% yield).

NMR

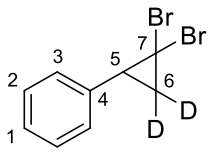

^{1}H (500 MHz, $CDCl_3$) δ 7.39–7.27 (ar, m, 5H) 2.95 (*H*C_5, br s, 1H)

^{13}C{^{1}H} (126 MHz, $CDCl_3$) δ 136.4 (C_4), 129.3 (C_3), 128.7 (C_1), 128.0 (C_2), 36.1 (C_5), 28.7 (C_7) (C_6 not observed)

^{2}H (77 MHz, $CDCl_3$) δ 2.06 (d, ^{3}J = 8.9 Hz)

Synthesis of 3,3-d_2-phenylallene

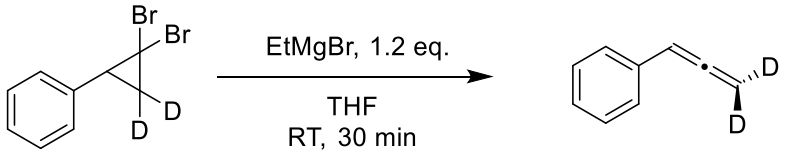

This reaction was performed under a nitrogen atmosphere using standard Schlenk techniques. (2,2-dibromocyclopropyl-3,3-d_2)benzene (278 mg, 1 mmol) was added to 10 mL of dry THF and cooled to 0 °C. To this, ethylmagnesium bromide (3.0 M in diethyl ether, 0.5 mL, 1.5 mmol, 1.5 equiv) was added dropwise, and the reaction was allowed to warm to room temperature. The reaction was cooled to 0 °C and quenched after 30 minutes through careful addition of deionised water (2 mL). 1 M hydrochloric acid (10 mL) was added to the reaction, and the product was extracted with petroleum ether (2 x 10 mL). The organic layers were combined, dried with magnesium sulphate and the solvent removed under reduced pressure, leaving a clear oil (114 mg, 84% yield, 93% D-incorporation).

NMR Data

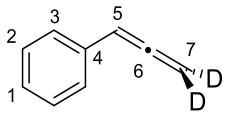

^{1}H (500 MHz, C_6D_6) δ 7.26–6.93 (ar, m, 5H), 6.05 (*H*C_5, s, 1H)

^{13}C{^{1}H} (126 MHz, C_6D_6) δ 210.2 (C_6), 134.3 (C_3), 128.9 (C_2), 127.2 (C_1), 127.1 (C_3), 94.6 (C_5), 78.5 (m, C_7)

^{2}H (77 MHz, C_6D_6) δ 4.84 (s)

Use of 3,3-d$_2$-phenylallene in catalysis

Conditions and workup used were identical to the protic substrate.

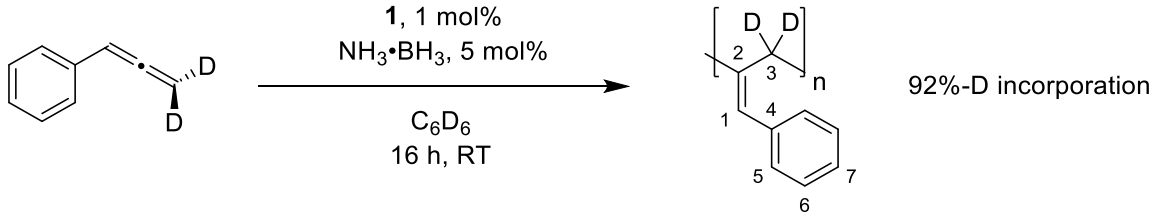

NMR Data for Polymer

^{1}H (500 MHz, C_6D_6) δ 7.29–7.01 (ar, m, 5H), 6.24 (*H*C_1, s, 1H), 3.67/3.57/3.52 (residual protic *H*C_3, three m)

^{13}C{^{1}H} (126 MHz, C_6D_6) δ 138.3 (C_4), 138.2 (C_2), 128.8 (C_7), 127.7 (C_5), 126.6 (C_6), 123.0 (C_1), (C_3 not observed)

^{2}H (77 MHz, C_6D_6) δ 3.70/3.54/3.45 (all s)

Density Functional Theory Studies

A seven-unit chain of poly(phenylallene) was modelled computationally. A conformational search was performed with PCM10 using the standard MMFF94 forcefield, with a minimum of 500 conformers screened and a maximum of 20 duplicates or 1000 conformers screened. Four species (**A**–**D**) featuring repeating units were identified as unique stereoisomers, as well as one atactic isomer.

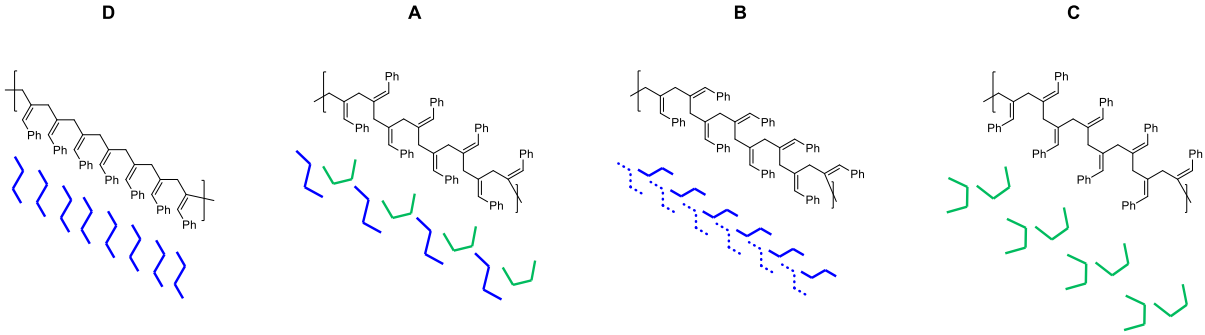

Density functional theory optimisations of these structures were performed using Jaguar 8.5 and the standard B3LYP hybrid density functional with Grimme's D3 dispersion correction. Atoms were modelled using the standard Pople basis set 6-31G(d), solvation was modelled using a polar continuum model with the solvent as benzene, and frequency calculations were carried out at 298.15 K to confirm species were intermediates, with additional thermochemistry corrections calculated at 323.15, 358.15 and 373.15 K to model the effect of reaction temperature on the relative populations of the different species. Convergence criteria were set to five times the standard for Jaguar, as no material changes in optimised geometry were observed when using the more computationally expensive criteria for test calculations. All calculations were run with the standard medium-fine grid density in Jaguar.

Single point potential energies (s.p.e's) were then calculated with the 6-311+G(d,p) basis set using the optimised geometries and the same DFT approach. A trial optimisation of Conformer B using the B3LYP-D3/6-311+g(d,p) theory level revealed no notable structural changes to that observed using 6-31G(d).

Calculated relative free energies used for Maxwell-Boltzmann population distributions. All energies reported in kcal mol^{-1}.

Species	Relative ΔG (6-31G* 298K)	(s.p.e + ΔG Correction @ 298.15 K)	(s.p.e + ΔG Correction @ 323.15 K)	(s.p.e + ΔG Correction @ 358.15 K)	(s.p.e + ΔG Correction @ 373.15 K)
A	0.00	0.00	0.00	0.00	0.00
B	2.73	1.76	1.95	2.14	2.33
C	6.49	5.82	5.84	5.87	5.90
D	8.88	6.46	6.54	6.63	6.73
Atactic	6.12	4.43	4.77	5.13	5.49

Population distributions calculated using the Maxwell-Boltzmann distribution.

Species	% Population 298.15 K	% Population 323.15 K	% Population 358.15 K	% Population 373.15 K
A	95.09	95.32	95.16	95.16
B	4.85	4.61	4.73	4.09
C	0.01	0.01	0.02	0.03
D	0.00	0.00	0.01	0.01
Atactic	0.05	0.06	0.07	0.06

Characterisation of Allenes & Precursors

52' (2,2-Dibromocyclopropyl)benzene

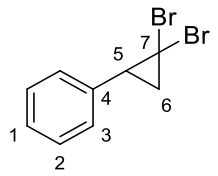

Obtained from standard procedure, 60% isolated yield (3.32 g), colourless liquid.

^{1}H (500 MHz, $CDCl_3$) δ 7.42–7.25 (ar, m, 5H), 2.99 (*H*C_5, dd, ^{3}J = 10.5 Hz, ^{3}J = 8.1 Hz, 1H), 2.16 (*H*C_6, dd, ^{3}J = 10.5 Hz, ^{2}J = 7.7 Hz, 1H), 2.05 (*H*C_6, dd, ^{3}J = 8.1 Hz, ^{2}J = 7.7 Hz, 1H)

^{13}C{^{1}H} (126 MHz, $CDCl_3$) δ 136.1 (C_4), 129.0 (C_3), 128.4 (C_1), 127.7 (C_2), 36.1 (C_5), 28.6 (C_7), 27.4 (C_6)

TOF-MS [M+H] 273.8978 (theoretical) 273.8993 (observed)

Data concordant with previous literature. [260]

52 Phenylallene

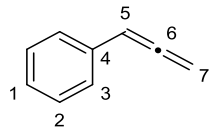

Obtained from standard procedure, 81% isolated yield (0.94 g), colourless liquid.

^{1}H (500 MHz, $CDCl_3$) δ 7.34–7.17 (ar, m, 5H), 6.17 (*H*C_5, t, ^{4}J = 6.8 Hz, 1H), 5.15 (*H*C_7, d, ^{4}J = 6.8 Hz, 2H)

^{13}C{^{1}H} (126 MHz, $CDCl_3$) δ 209.9 (C_6), 134.0 (C_4), 128.7 (C_2), 127.0 (C_1), 126.8 (C_3), 94.1 (C_5), 78.9 (C_7)

TOF-MS [M+H] 116.0626 (theoretical) 116.0728 (observed)

Data concordant with previous literature. [260]

54' 1-(2,2-Dibromocyclopropyl)-4-methylbenzene

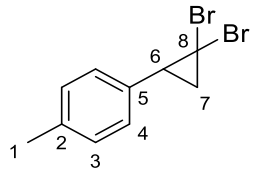

Obtained from standard procedure, 46% isolated yield (2.65 g), colourless liquid.

^{1}H (500 MHz, $CDCl_3$) δ 7.19–7.12 (ar, m, 4H), 2.92 (*H*C_6, dd, ^{3}J = 10.5 Hz, ^{3}J = 8.3 Hz, 1H), 2.35 (*H*C_1, s, 3H), 2.12 (*H*C_7, dd, ^{3}J = 10.5 Hz, ^{2}J = 7.7 Hz, 1H), 2.01 (*H*C_7, dd, ^{3}J = 8.3 Hz, ^{2}J = 7.7 Hz, 1H)

^{13}C{^{1}H} (126 MHz, $CDCl_3$) δ 137.5 (C_5), 133.1 (C_2), 129.2 (C_3), 128.9 (C_4), 35.8 (C_6), 29.0 (C_8), 27.3 (C_7), 21.4 (C_1)

TOF-MS [M+H] 287.9149 (theoretical), 287.9142 (observed)

Data concordant with previous literature. [260]

54 4-Methylphenylallene

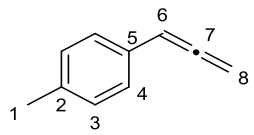

Obtained from standard procedure, 92% yield (1.20 g), colourless oil.

^{1}H (500 MHz, $CDCl_3$) δ 7.20 (*H*C_4, d, ^{3}J = 7.9 Hz, 2H), 7.12 (*H*C_3, d, ^{3}J = 7.9 Hz, 2H), 6.14 (*H*C_6, t, ^{4}J = 6.8 Hz, 1H), 5.13 (*H*C_8, d, ^{4}J = 6.8 Hz, 2H), 2.33 (*H*C_1, s, 3H)

^{13}C{^{1}H} (126 MHz, $CDCl_3$) δ 209.8 (C_7), 136.8 (C_2), 131.0 (C_5), 129.5 (C_3), 129.4 (C_4), 126.7 (C_3), 93.9 (C_6), 78.8 (C_8), 21.3 (C_1)

TOF-MS [M+H] 130.0783 (theoretical), 130.0763 (observed)

Data concordant with previous literature. [260]

55' 1-(2,2-Dibromocyclopropyl)-3-methylbenzene

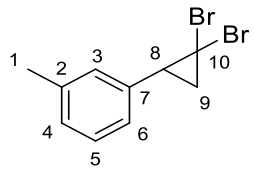

Obtained from standard procedure, 52% yield (3.01 g), colourless oil.

^{1}H (500 MHz, $CDCl_3$) δ 7.43–7.02 (ar, m, 4H), 2.94 (*H*C_8, dd, ^{3}J = 10.5 Hz, ^{3}J = 8.4 Hz, 1H), 2.38 (*H*C_1, s, 3H), 2.12 (*H*C_9, dd, ^{3}J = 10.5 Hz, ^{2}J = 7.7 Hz, 1H), 2.01 (*H*C_9, dd, ^{3}J = 8.4 Hz, ^{2}J = 7.7 Hz, 1H)

^{13}C{^{1}H} (126 MHz, $CDCl_3$) δ 137.5 (C_7), 133.1 (C_2), 129.3 (C_3), 129.2 (C_5), 128.9 (C_4), 126.3 (C_6), 35.8 (C_8), 29.0 (C_{10}), 27.3 (C_9), 21.4 (C_1)

TOF-MS [M+H] 287.9195 (theoretical), 287.9149 (observed)

Data concordant with previous literature. [270]

55 3-Methylphenylallene

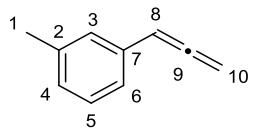

Obtained from standard procedure, 73% yield (0.95 g), colourless oil.

^{1}H (500 MHz, $CDCl_3$) δ 7.34–7.17 (ar, m, 4H), 6.14 (*H*C_8, t, ^{4}J = 6.8 Hz, 1H), 5.13 (*H*C_{10}, d, ^{4}J = 6.8 Hz, 2H) 2.34 (*H*C_1, s, 3H)

$^{13}C\{^{1}H\}$ (126 MHz, $CDCl_3$) δ 209.8 (C_9), 136.8 (C_2), 131.0 (C_7), 129.5 (C_4), 129.4 (C_5), 126.7 (C_3), 126.3 (C_6), 93.9 (C_8), 78.8 (C_{10}), 21.3 (C_1)

Data concordant with previous literature. [270]

56' 1-(2,2-Dibromocyclopropyl)-2-methylbenzene

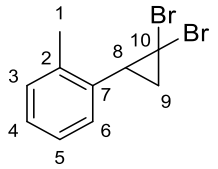

Obtained from standard procedure, 62 % yield (3.60 g), colourless oil.

^{1}H (500 MHz, $CDCl_3$) δ 7.29–7.23 (*H*C_3/*H*C_6, m, 2H), 7.17 (*H*C_5, m, 1H) 6.98 (*H*C_4, m, 1H), 2.83 (*H*C_8, dd, ^{3}J = 10.4 Hz, ^{3}J = 8.4 Hz, 1H), 2.50 (*H*C_1, s, 3H), 2.15 (*H*C_9, dd, 1H, ^{3}J = 10.4 Hz, ^{2}J = 7.7 Hz), 2.05 (*H*C_9, dd, 1H, ^{3}J = 8.4 Hz, ^{2}J = 7.7 Hz)

$^{13}C\{^{1}H\}$ (126 MHz, $CDCl_3$) δ 139.3 (C_7), 135.6 (C_2), 130.0 (C_3), 127.9 (C_6), 127.8 (C_4), 126.0 (C_5), 35.5 (C_8), 28.5 (C_{10}), 27.0 (C_9), 20.3 (C_1)

TOF-MS [M+H] 287.9149 (theoretical) 287.9028 (observed)

Data concordant with previous literature. [260]

56 2-Methylphenylallene

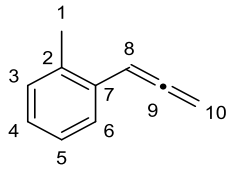

Obtained from standard procedure, 81% yield (1.05 g), pale yellow oil.

^{1}H (500 MHz, $CDCl_3$) δ 7.39 (*H*C_6, m, 1H), 7.19–7.08 (*H*C_3/*H*C_4/*H*C_5, m, 3H), 6.35 (*H*C_8, t, 1H, ^{4}J = 6.8 Hz), 5.11 (*H*C_{10}, d, 2H, ^{4}J = 6.8 Hz), 2.36 (*H*C_1, s, 3H)

$^{13}C\{^{1}H\}$ (126 MHz, $CDCl_3$) δ 210.6 (C_9), 135.0 (C_7), 132.3 (C_2), 130.6 (C_4), 127.3 (C_6), 127.0 (C_3), 126.3 (C_5), 91.3 (C_8), 78.1 (C_{10}), 20.0 (C_1)

TOF-MS [M+H] 130.0783 (theoretical) 130.0755 (observed)

Data concordant with previous literature. [260]

57' 1-(2,2-Dibromocyclopropyl)-4-methoxybenzene

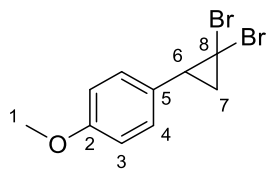

Obtained from standard procedure, 32% yield (1.98 g), colourless oil.

^{1}H (500 MHz, $CDCl_3$) δ 7.17 (*H*C_4, d, ^{3}J = 8.7 Hz, 2H), 6.89 (*H*C_3, d, ^{3}J = 8.7 Hz, 2H), 3.81 (*H*C_1, s, 3H), 2.89 (*H*C_6, dd, ^{3}J = 10.6 Hz, ^{3}J = 8.2 Hz, 1H), 2.11 (*H*C_7, ^{3}J = 10.6 Hz, ^{2}J = 7.7 Hz, 1H), 1.95 (*H*C_7, ^{3}J = 8.2 Hz, ^{2}J = 7.7 Hz, 1H)

^{13}C{^{1}H} (126 MHz, $CDCl_3$) δ 159.1 (C_2), 130.1 (C_4), 128.3 (C_5), 113.8 (C_3), 55.4 (C_1), 35.5 (C_6), 29.4 (C_8), 27.5 (C_7)

TOF-MS [M+H] 304.9098 (theoretical) 304.9223 (observed)

Data concordant with previous literature. [260]

57 4-Methoxyphenylallene

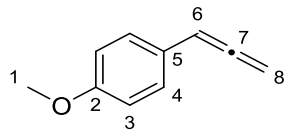

Obtained from standard procedure, 76% yield (0.98 g), pale yellow oil.

^{1}H (500 MHz, $CDCl_3$) δ 7.24 (*H*C_4, d, 2H, ^{3}J = 8.7 Hz), 6.86 (*H*C_3, d, 2H, ^{3}J = 8.7 Hz) 6.13 (*H*C_6, t, ^{4}J = 6.8 Hz, 1H), 5.12 (*H*C_8, d, ^{4}J = 6.8 Hz, 2H), 3.80 (*H*C_1, s, 3H)

^{13}C{^{1}H} (126 MHz, $CDCl_3$) δ 209.5 (C_7), 158.9 (C_2), 127.9 (C_4), 126.3 (C_5), 114.3 (C_3), 93.5 (C_6), 78.9 (C_8), 55.4 (C_1)

TOF-MS [M+H] 147.0732 (theoretical) 147.0805 (observed)

Data concordant with previous literature. [260]

58' 1-(2,2-Dibromocyclopropyl)-4-fluorobenzene

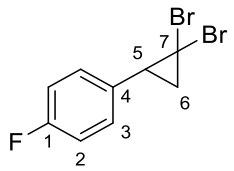

Obtained from standard procedure, 29% yield (1.71 g), colourless oil.

^{1}H (500 MHz, $CDCl_3$) δ 7.26–7.19 (*H*C_3, m, 2H), 7.09–7.01 (*H*C_2, t, 2H, ^{3}J = 8.7 Hz), 2.92 (*H*C_5, ^{3}J = 10.5 Hz, ^{3}J = 8.3 Hz), 2.14 (*H*C_6, dd, 1H, ^{3}J = 10.5 Hz, ^{2}J = 7.8 Hz), 1.96 (*H*C_6, dd, 1H, ^{3}J = 8.3 Hz, ^{2}J = 7.8 Hz)

^{13}C{^{1}H} (126 MHz, $CDCl_3$) δ 162.3 (C_1, d, ^{1}J = 246.6 Hz), 132.0 (C_4, d, ^{4}J = 3.2 Hz), 130.7 (C_3, d, ^{3}J = 8.2 Hz), 115.4 (C_2, d, ^{2}J = 21.7 Hz), 35.3 (C_5), 28.3 (C_7), 27.6 (C_6)

^{19}F{^{1}H} (470 MHz, $CDCl_3$) δ −114.4 (s)

TOF-MS [M-H] 291.8899 (theoretical), 291.8990 (observed)

Data concordant with previous literature. [270]

58 4-Fluorophenylallene

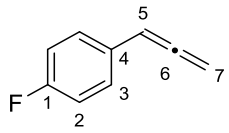

Obtained from standard procedure, 63% yield (0.85 g), colourless oil.

^{1}H (500 MHz, $CDCl_3$) δ 7.24–7.19 (*H*C_3, m, 2H), 6.99–6.92 (*H*C_2, t, ^{3}J = 8.7 Hz, 2H), 6.09 (*H*C_5, t, ^{4}J = 6.8 Hz, 1H), 5.10 (*H*C_7, d, ^{4}J = 6.8 Hz, 2H)

^{13}C{^{1}H} (126 MHz, $CDCl_3$) δ 209.7 (C_6), 162.0 (C_1, d, ^{1}J = 246.0 Hz), 130.0 (C_4, d, ^{4}J = 3.3 Hz), 128.2 (C_3, d, ^{3}J = 8.1 Hz), 115.7 (C_2, d, ^{2}J = 2.9 Hz), 93.2 (C_5), 79.2 (C_7)

^{19}F{^{1}H} (470 MHz, $CDCl_3$) δ −115.6 (s)

TOF-MS [M+H] 134.0532 (theoretical), 134.0527 (observed)

Data concordant with previous literature. [270]

59' 1-(2,2-Dibromocyclopropyl)-4-chlorobenzene

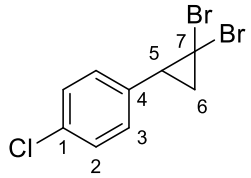

Obtained from standard procedure, 41% yield (2.55 g), colourless oil.

^{1}H (500 MHz, $CDCl_3$) δ 7.33 (*H*C_3, d, ^{3}J = 8.5 Hz, 2H), 7.19 (*H*C_2, d, ^{3}J = 8.5 Hz, 2H), 2.91 (*H*C_5, dd, ^{3}J = 10.5 Hz, ^{3}J = 8.2 Hz, 1H), 2.15 (*H*C_6, dd, ^{3}J = 10.5 Hz, ^{2}J = 7.8 Hz, 1H), 1.97 (*H*C_6, dd, ^{3}J = 8.2 Hz, ^{2}J = 7.8 Hz, 1H)

^{13}C{^{1}H} (126 MHz, $CDCl_3$) δ 134.7 (C_4), 133.7 (C_1), 130.4 (C_2), 128.7 (C_3), 35.5 (C_5), 27.9 (C_7), 27.6 (C_6)

TOF-MS [M+H] 307.8603 (theoretical) 307.8632 (observed)

Data concordant with previous literature. [270]

59 4-Chlorophenylallene

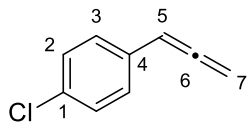

Obtained from standard procedure, 61% yield (0.92 g), colourless oil.

^{1}H (500 MHz, $CDCl_3$) δ 7.27 (ar, d, ^{3}J = 8.6 Hz, 2H), 7.22 (ar, d, ^{3}J = 8.6 Hz, 2H), 6.12 (*H*C_5, t, ^{4}J = 6.8 Hz, 1H), 5.16 (*H*C_7, d, ^{4}J = 6.8 Hz, 2H)

^{13}C{^{1}H} (126 MHz, $CDCl_3$) δ 210.0 (C_6), 132.6 (C_4), 132.6 (C_1), 128.9 (C_2), 128.0 (C_3), 93.3 (C_5), 79.3 (C_7)

TOF-MS [M+H] 150.0236 (theoretical) 150.0306 (observed)

Data concordant with previous literature. [270]

Characterisation of Polymers

P52 Polyphenylallene

93% spectroscopic conversion, 6.5 : 1 (2,3) : (1,2) conformation, 82% isolated product (48 mg, brown solid).

P52$_{2,3}$ Isomer

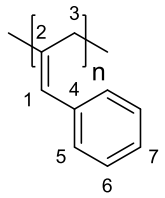

^{1}H (500 MHz, C_6D_6) δ 7.29–7.01 (ar, m, 5H) 5.97 (*H*C_1, s, 1H), 3.71/3.55/3.47 (*H*C_3, three s, 2H, 0.5/0.9/0.6 signal intensity ratio)

^{13}C{^{1}H} (126 MHz, C_6D_6) δ 137.9 (C_4), 137.9/137.8/137.7 (C_2), 128.4 (C_7), 127.3 (C_5), 126.2 (C_6), 122.6/122.4 (C_1) 42.4/42.0/41.6 (C_3)

P52$_{1,2}$ Isomer

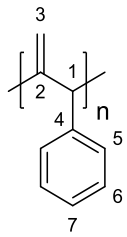

^{1}H (500 MHz, C_6D_6) δ 7.29–7.01 (ar, m, 5H), 4.83/5.38 (*H*C_3, two s, 2H, 1:1 signal intensity ratio), 3.26 (*H*C_1, s, 1H),

^{13}C{^{1}H} (126 MHz, C_6D_6) δ 56.7/42.9 (C_1), 105.2/112.4 (C_3), 150.6/142.1 (C_2) (aryl signals could not be determined)

P54 Poly(4-methylphenyl)allene

94% spectroscopic conversion, 6.5 : 1 (2,3) : (1,2) conformation, 79% isolated product (51 mg, brown solid).

P54$_{2,3}$ Isomer

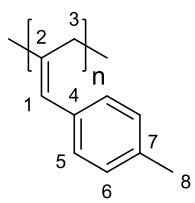

^{1}H (500 MHz, C_6D_6) δ 7.26–6.93 (ar, m, 4H), 6.22 (*H*C_1, s, 1H), 3.81/3.62/3.52 (*H*C_3, three s, 2H, 0.5/1/0.5 signal intensity), 2.15 (*H*C_8, s, 3H)

^{13}C{^{1}H} (126 MHz, C_6D_6) δ 137.1 (C_7), 136.0 (C_2), 135.5 (C_4), 129.5 (C_6), 127.7 (C_5), 122.8/122.7 (C_1), 42.7/42.3/41.9 (C_3), 21.2 (C_8)

P54$_{1,2}$ Isomer

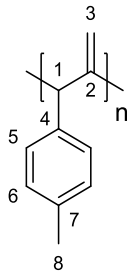

^{1}H (500 MHz, C_6D_6) δ 7.26–6.93 (ar, m, 4H), 4.96/5.40 (*H*C_3, two s, 2H, 1:1 signal intensity ratio), 4.11 (*H*C_1, s, 1H), 2.08 (*H*C_8, s, 3H)

^{13}C{^{1}H} (126 MHz, C_6D_6) δ 142.8 (C_2), 137.3 (C_7), 111.8 (C_3), 30.3 (C_1), 21.2 (C_8) (remaining aryl peaks not determined)

P55 Poly(3-methylphenyl)allene

96% conversion, 7:1 (2,3) : (1,2) conformation, 80% isolated product (58 mg, brown oil).

P55$_{2,3}$ Isomer

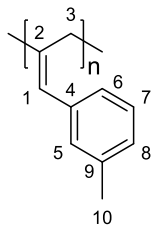

^{1}H (500 MHz, C_6D_6) δ 7.21–6.98 (ar, m, 4H), 6.22 (*H*C_1, m 1H), 3.83/3.62/3.52 (*H*C_3, three s, 2H, 0.5/0.9/0.5 signal intensity ratio), 2.15 (*H*C_{10}, s, 3H)

^{13}C{^{1}H} (126 MHz, C_6D_6) δ 138.2/138.1/138.0 (C_4), 138.0 (C_9), 137.8 (C_2), 128.7 (aryl), 128.6 (aryl), 127.4 (C_5), 124.7/124.8 (aryl), 122.9/123.1 (C_1), 41.9/42.5/42.8 (C_3), 21.6 (C_{10})

Although the signals at δ = 128.7 ppm, 128.6 ppm and 124.7/125.8 ppm respectively could be identified as aryl carbons, they could not be definitively assigned to the specific positions of C_6, C_7 and C_8.

P55$_{1,2}$ Isomer

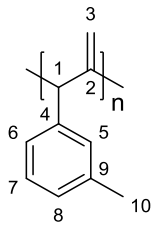

^{1}H (500 MHz, C_6D_6) δ 7.21–6.98 (ar, m, 4H), 4.99/4.89 (*H*C$_3$, two s, 2H, 1:1 signal intensity ratio) , 3.30 (*H*C$_1$, s, 1H), 2.19 (*H*C$_{10}$, s, 3H)

^{13}C{^{1}H} (126 MHz, C_6D_6) δ 148.0 (C_4), 140.1 (C_9), 136.4 (C_2), 112.6 (C_3), 28.4 (C_1), 21.6 (C_{10}) (remaining aryl signals not determined)

P56 Poly(2-methylphenyl)allene

91% conversion, 5 : 1 (2,3) : (1,2) conformation, 82% isolated product (52 mg, brown oil).

P56$_{2,3}$ Isomer

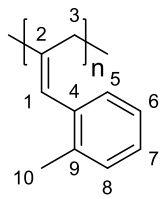

^{1}H (500 MHz, C_6D_6) δ 7.21–6.98 (ar, m, 4H), 6.41 (*H*C$_1$, m, 1H), 3.67/3.53/3.51 (*H*C$_3$, m, 2H, 0.5/0.8/0.6 signal intensity ratio), 2.17 (*H*C$_{10}$, s, 3H)

^{13}C{^{1}H} (126 MHz, C_6D_6) δ 141.3 (C_4), 138.2/138.3 (C_2), 136.4/136.6 (C_9), 130.6 (C_8), 127.3 (aryl), 126.8 (aryl), 126.2 (aryl), 120.3/120.1 (C_1), 42.5/41.9/41.2 (C_3), 20.0 (C_{10})

Although the signals at δ = 127.3 ppm, 126.8 ppm and 126.2 ppm respectively could be identified as aryl carbons, they could not be affirmatively assigned to the specific positions of C_5, C_6 and C_7. (C_8 was identified through strong HMBC coupling with *H*C$_{10}$)

P56$_{1,2}$ Isomer

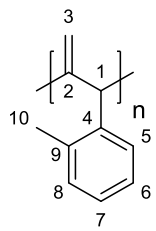

^{1}H (500 MHz, C_6D_6) δ 6.90–7.41 (ar, m, 4H), 4.85-5.11 (*H*C$_3$, m, 2H), 2.98 (*H*C$_1$, m, 1H), 2.19 (*H*C$_{10}$, s, 3H)

^{13}C{^{1}H} (126 MHz, C_6D_6) δ 161.5 (C_2), 142.8 (C_4), 136.6 (C_9), 125.9 (aryl) 123.6 (aryl), 94.3 (C_3), 28.7 (C_1), 20.8 (C_{10}) (Remaining aryl signals not determined, the signals for C_9 for each isomer are also partially overlayed)

P57 Poly(4-methoxyphenyl)allene

98% conversion, 11 : 1 (2,3) : (1,2) conformation, 92% isolated product (64 mg, brown solid).

P57$_{2,3}$ Isomer

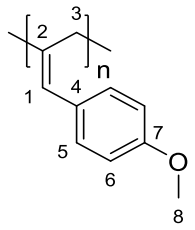

^{1}H (500 MHz, C_6D_6) δ 7.18 (*H*C$_5$, m, 2H) 6.80 (*H*C$_6$, m, 2H), 6.22 (*H*C$_1$, s, 1H), 3.80/3.66/3.57 (*H*C$_3$, 3 s, 2H, 1/0.5/1 signal intensity ratio), 3.36 (*H*C$_8$, s, 3H)

^{13}C{^{1}H} (126 MHz, C_6D_6) δ 158.7 (C_7), 135.9 (C_2), 131.1 (C_5), 128.8 (C_4), 122.4 (C_1), 114.3 (C_6), 54.9 (C_8), 42.6/42.4/41.6 (C_3)

P57$_{1,2}$ Isomer

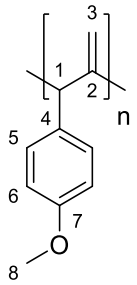

^{1}H (500 MHz, C_6D_6) δ 7.31–6.70 (aryl, m, 4H) 5.44/4.97/4.88 (*H*C$_3$, 3 s, 2H, 1/2/2 signal intensity ratio), 3.29 (*H*C$_8$) (*H*C$_1$ is obscured by (2,3) polymer methoxy group and chain peaks)

^{13}C{^{1}H} (126 MHz, C_6D_6) δ 159.5 (C_7), 148.4 (C_2), 135.7 (C_4), 130.4/130.1 (C_3), 54.8 (C_8) (Remaining aryl and C_1 peaks not determined)

P58 Poly(4-fluorophenyl)allene

77% spectroscopic conversion, 13 : 1 (2,3) : (1,2) conformation, 62% isolated product (42 mg, brown solid).

P58$_{2,3}$ Isomer

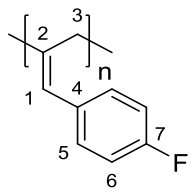

^{1}H (500 MHz, C_6D_6) δ 7.03–6.62 (ar, m, 4H), 6.03 (*H*C$_1$, m, 1H), 3.58/3.49/3.41 (*H*C$_3$, m, 2H, 0.5:0.5:1 signal intensity ratio)

$^{13}C\{^{1}H\}$ (126 MHz, C_6D_6) δ 161.9 (C_7, d, ^{1}J = 245.8 Hz), 137.4/137.3/137.3 (C_2, three s), 130.4 (C_4, s), 129.1 (C_5, d, ^{3}J = 7.4 Hz), 121.8/121.6 (C_1, two s), 115.7 (C_6, d, ^{2}J = 21.4 Hz), 42.5/42.0/41.3 (C_3, three s)

$^{19}F\{^{1}H\}$ (470 MHz, C_6D_6) -115.5 (s)

P58$_{1,2}$ Isomer

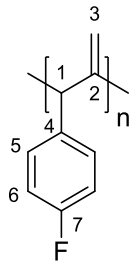

^{1}H (500 MHz, C_6D_6) δ 7.03–6.62 (ar, m, 4H), 4.89-4.71 (*H*C_3, m, 2H), 4.47 (*H*C_1, m, 1H)

$^{19}F\{^{1}H\}$ (470 MHz, C_6D_6) δ -114.5 (s)

The yield of the (1,2) polymer is considerably reduced for this substrate, and as such $^{13}C\{^{1}H\}$ NMR signals were too weak to yield conclusive assignment.

P59 Poly(4-chlorophenyl)allene

74% spectroscopic conversion, 6 : 1 (2,3) : (1,2) conformation, 61% isolated product (45 mg, brown solid).

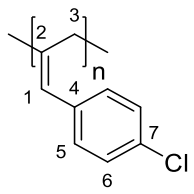

P59$_{2,3}$ Isomer

^{1}H (500 MHz, C_6D_6) δ 7.18 (*H*C_5, m, 2H), 6.87 (*H*C_6, m, 2H), 6.17 (*H*C_1, s, 1H), 3.43/3.34 (*H*C_3, two s, 2H, 0.5/1.5 signal intensity ratio)

$^{13}C\{^{1}H\}$ (126 MHz, C_6D_6) δ 138.7/138.5 (C_2), 136.4 (C_4), 132.4 (C_7), 129.0 (C_5), 128.8 (C_6), 121.8/121.6 (C_1), 42.7/42.1/41.5 (C_3)

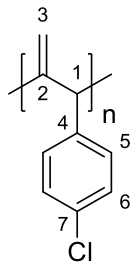

P59$_{1,2}$ Isomer

^{1}H (500 MHz, C_6D_6) δ 7.23–6.75 (ar, m, 4H), 4.89/4.84 (*H*C$_3$, two s, 2H, 1:1 signal intensity ratio), 4.47 (*H*C$_1$, s, 1H)

^{13}C{^{1}H} (126 MHz, C_6D_6) δ 142.8 (C_2), 94.3 (C_3), 20.8 (C_1) (aromatic peaks not determined)

NMR Characterisation of Dimeric Species

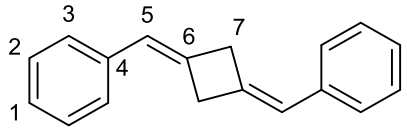

65 - *Trans* Isomer

^{1}H (500 MHz, $CDCl_3$) δ 7.36–7.15 (ar, m, 10H), 6.33 (*H*C$_5$, t, ^{4}J = 2.5 Hz, 2H) , 3.87 (*H*C$_7$, t, ^{4}J = 2.5 Hz, 4H)

^{13}C{^{1}H} (126 MHz, $CDCl_3$) δ 138.3 (C_6), 137.8 (C_4), 128.6 (C_2), 127.3 (C_3), 126.4 (C_1), 122.3 (C_5), 42.5 (C_7)

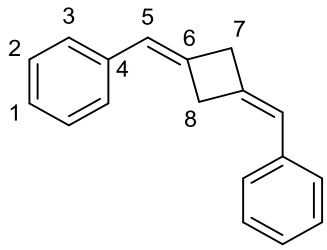

65 - *Cis* Isomer

The ^{1}H and ^{13}C{^{1}H} signals are distinct for *H*C$_7$/*H*C$_8$ and C$_7$/C$_8$, and were determined as the *J* coupling value between *H*C$_8$ and *H*C$_5$ is larger than between *H*C$_7$ and *H*C$_5$.

^{1}H (500 MHz, $CDCl_3$) δ 7.36–7.15 (ar, m, 10H), 6.30 (*H*C$_5$, dd, ^{4}J = 2.9 Hz, ^{4}J = 2.0 Hz, 2H), 4.01 (*H*C$_8$, dd, ^{4}J = 5.9 Hz, ^{4}J = 2.9 Hz, 2H), 3.71 (*H*C$_7$, dd, ^{4}J = 5.9 Hz, ^{4}J = 2.0 Hz, 2H)

^{13}C{^{1}H} (126 MHz, $CDCl_3$) δ 138.2 (C_6), 137.8 (C_4), 128.6 (C_2), 127.3 (C_3), 126.4 (C_1), 122.5 (C_5), 42.8 (C_7), 42.0 (C_8)

7.4 Experimental Data Pertinent to Chapter 4

Synthesis and Characterisation of allenes unique to Chapter 4

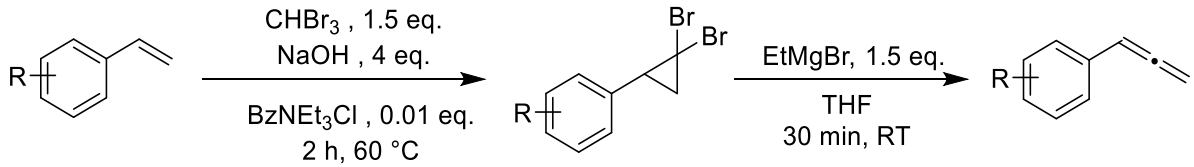

Allenes were prepared through the route above, described in greater detail in Section 7.3. For the synthesis of dibromocyclopropyl compound **70'**, 96:4 Pet Ether 40-60 : Ethyl Acetate was used in as the eluent for column chromatography. **71** is a solid, and was dried under vacuum on a Schlenk line for 1 hour rather than distilled as in the standard preparation.

Structural Data

70' 1-(2,2-Dibromocyclopropyl)-2-methoxybenzene

Obtained from standard procedure (except as noted above), 34% yield, colourless oil.

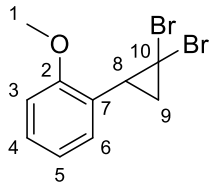

^{1}H (500 MHz, $CDCl_3$) δ 7.31 (*H*C_4, m, 1H), 6.98–6.90 (*H*C_3/*H*C_5/*H*C_6, m, 3H), 3.95 (*H*C_1, s, 3H), 2.97 (*H*C_8, dd, ^{3}J = 10.4 Hz, ^{3}J = 8.6 Hz, 1H), 2.09 (*H*C_9, dd, ^{3}J = 10.4 Hz, ^{2}J = 7.6 Hz, 1H), 1.97 (*H*C_9, dd, ^{3}J = 8.6 Hz, ^{2}J = 7.6 Hz, 1H)

^{13}C{^{1}H} (126 MHz, $CDCl_3$) δ 159.4 (C_2), 129.0 (C_4), 128.6 (C_6), 125.7 (C_7), 120.3 (C_5), 110.6 (C_3), 56.0 (C_1), 32.3 (C_8), 29.1 (C_{10}), 26.9 (C_9)

TOF-MS [M+Na] 328.8975 (theoretical) 328.9067 (observed)

Data concordant with previous literature [270]

70 2-Methoxyphenylallene

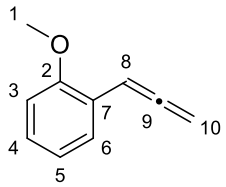

Obtained from standard procedure, 79% yield, colourless oil.

^{1}H (500 MHz, $CDCl_3$) δ 7.40 (*H*C_6, dd, ^{3}J = 7.6 Hz, ^{4}J = 1.7 Hz, 1H)), 7.18 (*H*C_5, m, 1H)), 6.93 (*H*C_4, m, 1H), 6.86 (*H*C_3, dd, ^{3}J = 8.2 Hz, ^{4}J = 1.1 Hz, 1H), 6.57 (*H*C_8, t, ^{4}J = 6.9 Hz, 1H), 5.11 (*H*C_{10}, d, ^{4}J = 6.9 Hz, 2H), 3.84 (*H*C_1, s, 3H)

$^{13}C\{^{1}H\}$ (126 MHz, $CDCl_3$) δ 210.3 (C_9), 156.0 (C_2), 128.1 (C_5), 127.9 (C_6), 122.5 (C_7), 120.9 (C_4), 111.1 (C_3), 87.9 (C_8), 78.1 (C_{10}), 55.7 (C_1)

TOF-MS [M+Na] 169.0600 (theoretical) 169.0764 (observed)

Data concordant with previous literature [270]

71' 4-(2,2-Dibromocyclopropyl)-1,1'-biphenyl

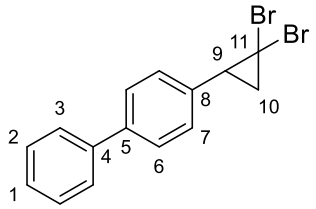

Obtained from standard procedure, 67% yield, white solid.

The precise assignment of C_3 and C_7 could not be determined.

^{1}H (500 MHz, $CDCl_3$) δ 7.67–7.57 (*H*C_3 & *H*C_7, m, 4H), 7.46 (*H*C_2, m, 2H), 7.38–7.31 (*H*C_1 & *H*C_6, m, 3H), 3.01 (*H*C_9, dd, ^{3}J = 10.4 Hz, ^{3}J = 8.4 Hz, 1H), 2.18 (*H*C_{10}, dd, ^{3}J = 10.4 Hz, ^{2}J = 7.6 Hz, 1H), 2.06 (*H*C_{10}, dd, ^{3}J = 8.4 Hz, ^{2}J = 7.6 Hz, 1H)

$^{13}C\{^{1}H\}$ (126 MHz, $CDCl_3$) δ 140.6 (C_4), 140.5 (C_5), 135.0 (C_8), 129.3 (C_6), 128.8 (C_2), 127.4 (C_1), 127.1 (C_3/C_7), 127.0 (C_3/C_7), 35.7 (C_9), 28.5 (C_{11}), 27.4 (C_{10})

TOF-MS [M+Na] 349.9306 (theoretical) 349.9291 (observed)

Data concordant with previous literature. [270]

71 (4-Phenyl)phenylallene

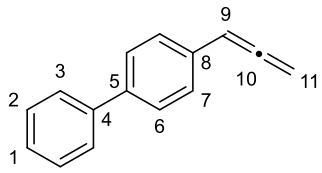

Obtained from standard procedure (except as noted above), 72% yield, white solid.

^{1}H (500 MHz, $CDCl_3$) δ 7.60 (*H*C_3, m, 2H), 7.55 (*H*C_6, d, ^{3}J = 8.3 Hz, 2H), 7.44 (*H*C_2, m, 2H), 7.38 (*H*C_7, d, ^{3}J = 8.3 Hz, 2H), 7.35 (*H*C_1, m, 1H), 6.21 (*H*C_9, t, ^{4}J = 6.7 Hz, 1H), 5.19 (*H*C_{11}, d, ^{4}J = 6.7 Hz, 2H)

$^{13}C\{^{1}H\}$ (126 MHz, $CDCl_3$) δ 210.2 (C_{10}), 141.0 (C_4), 139.9 (C_5), 133.1 (C_8), 128.9 (C_2), 127.5 (C_6), 127.4 (C_1), 127.2 (C_7), 127.1 (C_3), 93.8 (C_9), 79.0 (C_{11})

TOF-MS [M+H] 192.0939 (theoretical) 192.0953 (observed)

Data concordant with previous literature. [270]

General considerations and procedures

General Reaction Procedure

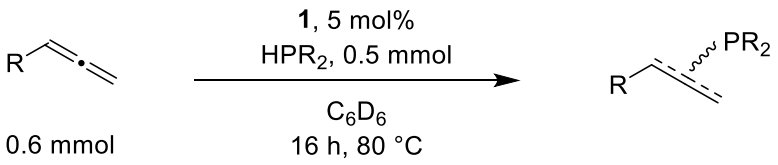

0.6 mmol

Experiments were performed under an argon atmosphere in an M-Braun glove box. To a flame dried J-Young ampoule of approximately 20 mL volume was added **1** (14 mg, 0.025 mmol, 5 mol%) and triphenylphosphine (approximately 10 mg, accurately weighed) dissolved in 600 µL benzene-d_6. To this was added the required allene (0.6 mmol) and phosphine (0.5 mmol). The ampoule was then sealed and heated, with stirring, for the times and conditions reported.

A spectroscopic conversion was determined by decanting the reaction mixture into a J-Young NMR tube at the end of the reaction and determining conversion by inverse-gated ^{31}P NMR spectroscopy using PPh_3 as an internal standard. In a minority of optimisation experiments phenylallene was the limiting reagent — in these cases 1,3,5-trimethoxybenzene (approximately 8 mg, accurately weighed) was added in lieu of triphenylphosphine and conversion was determined by ^{1}H NMR spectroscopy. Solvent was then removed from the reaction, and the hydrophosphination products were isolated through column chromatography (silica gel, 4:1 Petroleum Ether 40-60 : DCM eluent) under air. For the majority of products this workup yields the phosphine products, although a small amount of the phosphine oxides were observed in ^{31}P and ^{1}H NMR spectroscopy. Some reactions generated products that oxidise rapidly in air — these were isolated from the catalyst by means of a silica plug under an argon atmosphere using 100% pentane as the eluent. These are noted in the characterisation of products section and Section 4.4.

Test for P-nucleophiles

To test if the reaction proceeded through a phosphorus nucleophile, benzaldehyde (0.5 mmol, 50.8 µL) was added to the reaction using phenylallene and diphenylphosphine as substrates under the standard reaction procedure. The hydrophosphinated products were formed as usual, and no new phosphorus compounds were observed in inverse gated ^{31}P NMR spectroscopy.

Radical Trap Test

To test for radicals a radical trap was used. The catalytic reaction using phenylallene and diphenylphosphine as substrates was allowed to proceed for 4 hours, after which a reasonable amount of conversion (24%) had occurred. To the reaction was added (chloromethyl)cyclopropane (0.025 mmol, 2.3 µL, 1 eq. relative to **1**) and the reaction was allowed to proceed for a further 12 hours. After that point conversion was the same as the reaction without (chloromethyl)cyclopropane after 16 hours, and the (chloromethyl)cyclopropane can be isolated, unreacted, from the reaction mixture using trap to trap distillation. This outcome would appear to rule out the presence of radicals in the reaction.

Nanoparticle Test

To test for nanoparticles a procedure was adapted from Morris. [229] Reactions were set up under standard conditions but additionally trimethylphosphine (1.3 µL, 2.5 mol%, 0.5 equiv. with respect to catalyst) was added. Reaction conversion was observed to be reduced (32% conversion to hydrophosphinated products), but not fully quenched, indicating the active catalyst in the reaction was not nanoparticle-based.

Preparation of $DPPh_2$ and Deuteration Studies

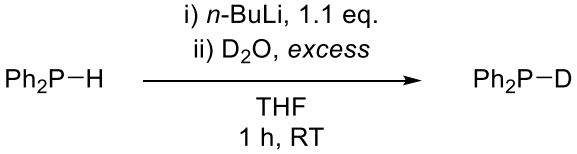

$DPPh_2$ was prepared as previously reported by Hilt. [102] Diphenylphosphine (5 mmol, 1.0 eq.) was dissolved in 5 mL dry THF and cooled to 0 °C. *n*-Butyl lithium (5.5 mmol, 1.1 eq.) was then added dropwise. After stirring for 1 h at room temperature, deuterium oxide (0.2 mL, degassed) was added, and after a further 10 minutes stirring anhydrous magnesium sulfate were added. The solution of $DPPh_2$ was decanted *via* cannula filtration and the solvent was removed *in vacuo*. Diphenylphosphine-d_1 (95%-d) was obtained in quantitative yield as colourless oil.

The reaction was performed and worked up as per the standard method (*vide supra*).

TOF-MS [M+H] 304.1360 (theoretical), 304.1366 (observed)

Terminal *E* Product (**67-d**)

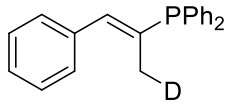

$^{31}P\{^{1}H\}$ (162 MHz, $CDCl_3$) δ −13.3 (br s)

^{31}P (162 MHz, $CDCl_3$) δ −13.3 (m)

^{1}H (500 MHz, $CDCl_3$) δ 7.11–7.56 (ar, m, 15H), 6.90 (PhC*H*C(CH_2D)PPh_2, dt, ^{3}J = 7.5 Hz, ^{4}J = 1.2 Hz, 1H), 2.13 (PhCHC(C*H*$_2$D)PPh_2, m, 2H)

$^{13}C\{^{1}H\}$ (126 MHz, $CDCl_3$) δ 142.9 (Ph*C*HC(CH_2D)PPh_2, d, ^{2}J = 29.2 Hz), 136.1 (C_{IPSO}, d, ^{3}J = 14.0 Hz), 129.6 (C_{ORTHO}, s), 15.1 (PhCHC(*C*H_2D)PPh_2, m)

^{2}H (77 MHz, $CDCl_3$) δ 2.04 (s)

Terminal *Z* Product (**68-d**)

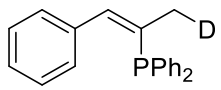

$^{31}P\{^{1}H\}$ (162 MHz, $CDCl_3$) δ 8.4 (br s)

^{31}P (162 MHz, $CDCl_3$) δ 8.4 (dt, ^{3}J = 13.8 Hz, ^{3}J = 8.8 Hz)

^{1}H (500 MHz, $CDCl_3$) δ 7.11–7.56 (ar, m, 15H), 6.72 (PhC*H*C(CH_2D)PPh_2, dt, ^{3}J = 13.8 Hz, ^{4}J = 1.6 Hz, 1H), 1.92 (PhCHC(C*H*$_2$D)PPh_2, br d, ^{3}J = 8.8 Hz, 2H)

^{13}C{^{1}H} (126 MHz, $CDCl_3$) δ 139.2 (Ph*C*HC(CH_2D)PPh_2, d, ^{2}J = 28.5 Hz), 136.3 (C_{IPSO}, d, ^{3}J = 11.8 Hz), 129.5 (C_{ORTHO}, s) 17.9 (PhCHC(*C*H_2D)PPh_2, m)

^{2}H (77 MHz, $CDCl_3$) δ 1.84 (s)

Internal Product (**69-d**)

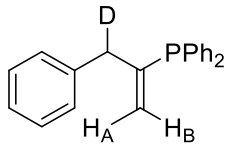

^{31}P{^{1}H} (162 MHz, $CDCl_3$) δ −2.3 (br s)

^{31}P (162 MHz, $CDCl_3$) δ −2.3 (m)

^{1}H (500 MHz, $CDCl_3$) δ 7.11–7.56 (ar, m, 15H), 5.45 (H_A, ddd, ^{3}J = 21.4 Hz, ^{4}J = 1.9 Hz, ^{2}J = 1.3 Hz, 1H), 5.13 (H_B, ddd, ^{3}J = 9.7 Hz, ^{4}J = 1.4 Hz, ^{2}J = 1.3 Hz, 1H) 3.34 (PhC*H*DC(CH_2)PPh_2, br d, ^{3}J = 8.0 Hz, 1H)

^{13}C{^{1}H} (126 MHz, $CDCl_3$) δ 148.3 (C_{IPSO}, d, ^{3}J = 17.3 Hz), 129.8 (C_{ORTHO}, s), 125.0 (PhCHDC(*C*H_2)PPh_2, d, ^{2}J = 13.1 Hz), 41.9 (Ph*C*HDC(CH_2)PPh_2, m)

^{2}H (77 MHz, $CDCl_3$) δ 3.46 (s)

Assignment of Products

As the products are isolated as a mixture of the (normally) three structural isomers, analysis of the mixture of the isomers (R_f, Mass Spec, FTIR data) is given first, followed by compound-specific NMR assignment.

For the *E*-isomer products for the reactions with arylallenes, the PhC*H*C(CH_3)PPh_2 is in the aromatic region, and not observed as a well-defined peak in the ^{1}H NMR spectrum. The chemical shift was determined by the HSQC correlation with the Ph*C*HC(CH_3)PPh_2 centre. For **87**, **90** and **93** this correlation is well-defined enough to determine a $^{3}J_{PH}$ coupling value. For non-aryl allenes, the signal is clearly observable in the ^{1}H NMR spectrum.

For the internal isomer products, H_A and H_B (as shown in the product structures) can be distinguished as H_A exhibits weak NOESY correlation with the aromatic protons, whereas H_B does not, and the *J* coupling value between H_A and the P centre ($^{3}J_{HAP}$) is considerably greater than $^{3}J_{HBP}$.

Reaction with Phenylallene (52)

84% conversion of starting material (2% dehydrocoupling, 82% hydrophosphination), 63 % isolated yield of hydrophosphinated products, clear oil. All three isomers co-elute with R_f = 0.35 (1 : 4 DCM : Petroleum Ether 40-60 eluent, silica gel column).

TOF-MS [M+H] 302.1224 (theoretical), 302.1261 (observed)

FTIR-ATR υ (cm^{-1}): 3073, 3025, 1584, 1478, 1434, 1374

67 Terminal *E* Product (8% Conversion)

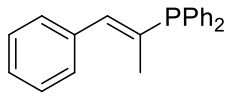

$^{31}P\{^{1}H\}$ (202 MHz, $CDCl_3$) δ −13.3 (s)

^{31}P (162 MHz, $CDCl_3$) δ −13.3 (m)

^{1}H (500 MHz, $CDCl_3$) δ 7.11–7.56 (ar, m, 15H), 7.29 (PhC*H*C(CH_3)PPh_2, m, 1H), 2.03 (PhCHC(C*H*$_3$)PPh_2, ^{3}J = 13.8 Hz, ^{4}J = 1.5 Hz)

$^{13}C\{^{1}H\}$ (126 MHz, $CDCl_3$) δ 143.3 (Ph*C*HC(CH_3)PPh_2, d, ^{2}J = 29.2 Hz), 136.2 (C_{IPSO}, d, ^{3}J = 14.0 Hz), 129.0 (C_{ORTHO}, s), 15.2 (PhCHC(*C*H_3)PPh_2, d, ^{2}J = 10.9 Hz)

68 Terminal *Z* Product (51% Conversion)

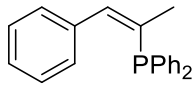

$^{31}P\{^{1}H\}$ (202 MHz, $CDCl_3$) δ 8.4 (s)

^{31}P (162 MHz, $CDCl_3$) δ 8.4 (dq, ^{3}J = 13.7 Hz, ^{3}J = 8.1 Hz)

^{1}H (500 MHz, $CDCl_3$) δ 7.11–7.56 (ar, m, 15H), 6.60 (PhC*H*C(CH_3)PPh_2, dq, 1H, ^{3}J = 13.7 Hz, ^{4}J = 1.6 Hz), 1.92 (PhCHC(C*H*$_3$)PPh_2, dd, 3H, ^{3}J = 8.1 Hz, ^{4}J = 1.6 Hz)

$^{13}C\{^{1}H\}$ (126 MHz, $CDCl_3$) δ 139.2 (Ph*C*HC(CH_3)PPh_2, d, ^{2}J = 28.6 Hz), 136.3 (C_{IPSO}, d, ^{3}J = 11.6 Hz), 129.1 (C_{ORTHO}, s) 18.1 (PhCHC(*C*H_3)PPh_2, d, ^{2}J = 17.1 Hz)

69 Internal Product (23% Conversion)

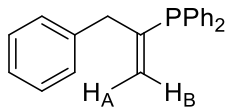

$^{31}P\{^{1}H\}$ (202 MHz, $CDCl_3$) δ −2.2 (s)

^{31}P (162 MHz, $CDCl_3$) δ −2.2 (ddt, ^{3}J = 21.4 Hz, ^{3}J = 9.6 Hz, ^{3}J = 7.1 Hz)

^{1}H (500 MHz, $CDCl_3$) δ 7.11–7.56 (ar, m, 15H), 5.33 (H_A, dtd, ^{3}J = 21.4 Hz, ^{4}J = 1.9 Hz, ^{2}J = 1.3 Hz, 1H), 5.01 (H_B, dtd, ^{3}J = 9.6 Hz, ^{4}J = 1.7 Hz, ^{2}J = 1.3 Hz, 1H) 3.34 (PhC*H*$_2$C(CH_2)PPh_2, br d, ^{3}J = 7.1 Hz, 2H)

$^{13}C\{^{1}H\}$ (126 MHz, $CDCl_3$) δ 148.3 (C_{IPSO}, d, ^{3}J = 17.2 Hz), 129.5 (C_{ORTHO}, s), 125.0 (PhCH_2C(*C*H_2)PPh_2, d, ^{2}J = 13.1 Hz), 42.1 (Ph*C*H_2C(CH_2)PPh_2, d, ^{2}J = 22.7 Hz)

Data for **67** and **68** is concordant with previous reports. [288] Data for **69** is concordant with previous reports. [175]

Reaction with 4-Methylphenylallene (54)

83% conversion of starting material (2% dehydrocoupling, 81% hydrophosphination), 69% isolated yield of hydrophosphinated products, clear oil. All three isomers co-elute with R_f = 0.30 (1:4 DCM : Petroleum Ether 40-60 eluent, silica gel column).

TOF-MS [M+H] 316.1381 (theoretical) 316.1380 (observed)

FTIR-ATR υ (cm^{-1}): 3052, 2974, 2906, 1564, 1478, 1432, 1312

72 Terminal E product (12% conversion)

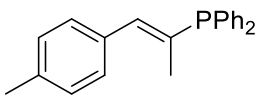

$^{31}P\{^{1}H\}$ (202 MHz, $CDCl_3$) δ −13.3 (s)

^{31}P (162 MHz, $CDCl_3$) δ −13.3 (m)

^{1}H (500 MHz, $CDCl_3$) δ 7.52–7.01 (ar, m, 14H), 7.20 ($CH_3ArCHC(CH_3)PPh_2$, m, 1H), 2.38 ($CH_3ArCHC(CH_3)PPh_2$, s, 3H), 2.14 ($CH_3ArCHC(CH_3)PPh_2$, dd, ^{3}J = 13.8 Hz, ^{4}J = 1.5 Hz, 3H)

$^{13}C\{^{1}H\}$ (126 MHz, $CDCl_3$) δ 143.3 ($CH_3ArCHC(CH_3)PPh_2$, d, ^{2}J = 29.3 Hz), 138.6 (C_{PARA}, s), 135.6 (C_{IPSO}, d, ^{3}J = 11.0 Hz), 129.7 (C_{ORTHO}, s), 21.4 ($CH_3ArCHC(CH_3)PPh_2$, s), 15.3 ($CH_3ArCHC(CH_3)PPh_2$, d, ^{2}J = 11.0 Hz)

73 Terminal Z product (52% conversion)

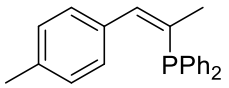

$^{31}P\{^{1}H\}$ (202 MHz, $CDCl_3$) δ 9.0 (s)

^{31}P (162 MHz, $CDCl_3$) δ 9.0 (dq, ^{3}J = 14.3 Hz, ^{3}J = 8.8 Hz)

^{1}H (500 MHz, $CDCl_3$) δ 7.52–7.01 (ar, m, 14H), 6.72 ($CH_3ArCHC(CH_3)PPh_2$, dq, ^{3}J = 14.3 Hz, ^{4}J = 1.5 Hz, 1H), 2.36 ($CH_3ArCHC(CH_3)PPh_2$, s, 3H), 2.02 ($CH_3ArCHC(CH_3)PPh_2$, dd, ^{3}J = 8.8 Hz, ^{4}J = 1.5 Hz, 3H)

$^{13}C\{^{1}H\}$ (126 MHz, $CDCl_3$) δ 139.4 ($CH_3ArCHC(CH_3)PPh_2$, d, ^{2}J = 30.0 Hz), 137.0 (C_{PARA}, s) 135.6 (C_{IPSO}, d, ^{3}J = 11.0 Hz), 129.6 (C_{ORTHO}, s), 21.3 ($CH_3ArCHC(CH_3)PPh_2$, s), 18.1 ($CH_3ArCHC(CH_3)PPh_2$, d, ^{2}J = 15.8 Hz)

74 Internal Product (11% conversion)

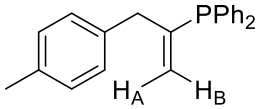

$^{31}P\{^{1}H\}$ (202 MHz, $CDCl_3$) δ −2.5 (s)

^{31}P (162 MHz, $CDCl_3$) δ −2.5 (ddt, ^{3}J = 21.5 Hz, ^{3}J = 9.5 Hz, ^{3}J = 7.2 Hz)

^{1}H (500 MHz, $CDCl_3$) δ 7.52–7.01 (ar, m, 14H), 5.45 (H_A, dtd, ^{3}J = 21.5 Hz, ^{4}J = 1.9 Hz, ^{2}J = 1.3 Hz, 1H), 5.15 (H_B, dtd, ^{3}J = 9.5 Hz, ^{4}J = 1.5 Hz, ^{2}J = 1.3 Hz, 1H), 3.41 ($CH_3ArCH_2C(CH_2)PPh_2$, br d, ^{3}J = 7.2 Hz, 2H), 2.33 ($CH_3ArCH_2C(CH_2)PPh_2$, s, 3H)

$^{13}C\{^{1}H\}$ (126 MHz, $CDCl_3$) δ 148.5 (C_{IPSO}, d, ^{3}J = 17.2 Hz), 135.8 (C_{PARA}, s), 134.1 (C_{ORTHO}, s), 124.7 ($CH_3ArCH_2C(CH_2)PPh_2$, d, ^{2}J = 12.9 Hz), 41.7 ($CH_3ArCH_2C(CH_2)PPh_2$, d, ^{2}J = 22.9 Hz), 21.2 ($CH_3ArCH_2C(CH_2)PPh_2$, s)

Reaction with 3-Methylphenylallene (55)

77% conversion of starting material (2% dehydrocoupling, 75% hydrophosphination), 63% isolated yield of hydrophosphinated products, clear oil. All three isomers co-elute with R_f = 0.30 (1:4 DCM : Petroleum Ether 40-60 eluent, silica gel column)

TOF-MS [M+H] 316.1381 (theoretical) 316.1380 (observed)

FTIR-ATR υ (cm^{-1}): 3052, 2915, 1584, 1479, 1434, 1308

Note : In NMR assignments below, C_{ORTHO} refers to the para-methyl position (The ortho-methyl C_{ORTHO} position could not be assigned for these products)

75 Terminal *E* product (12% conversion)

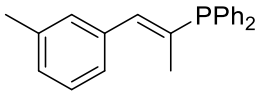

$^{31}P\{^{1}H\}$ (162 MHz, $CDCl_3$) δ −13.1 (s)

^{31}P (162 MHz, $CDCl_3$) δ −13.1 (m)

^{1}H (400 MHz, $CDCl_3$) δ 7.52–7.01 (ar, m, 14H), 7.32 ($CH_3ArCHC(CH_3)PPh_2$, m, 1H), 2.29 ($CH_3ArCHC(CH_3)PPh_2$, s, 3H), 2.05 ($CH_3ArCHC(CH_3)PPh_2$, dd, ^{3}J = 13.8 Hz, ^{4}J = 1.6 Hz, 3H)

$^{13}C\{^{1}H\}$ (100 MHz, $CDCl_3$) δ 143.3 ($CH_3ArCHC(CH_3)PPh_2$, d, ^{2}J = 29.4 Hz), 137.1 (C_{IPSO}, d, ^{3}J = 11.6 Hz), 128.8 (C_{ORTHO}, s), 21.6 ($CH_3ArCHC(CH_3)PPh_2$, s), 15.2 ($CH_3ArCHC(CH_3)PPh_2$, d, ^{2}J = 11.3 Hz)

76 Terminal *Z* product (52% conversion)

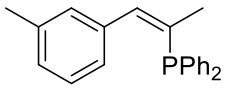

$^{31}P\{^{1}H\}$ (162 MHz, $CDCl_3$) δ 8.4 (s)

^{31}P (162 MHz, $CDCl_3$) δ 8.4 (dq, ^{3}J = 13.8 Hz, ^{3}J = 9.0 Hz)

^{1}H (400 MHz, $CDCl_3$) δ 7.52–7.01 (ar, m, 14H), 6.60 ($CH_3ArCHC(CH_3)PPh_2$, dq, ^{3}J = 13.8 Hz, ^{4}J = 1.6 Hz, 1H), 2.27 ($CH_3ArCHC(CH_3)PPh_2$, s, 3H), 1.93 ($CH_3ArCHC(CH_3)PPh_2$, dd, ^{3}J = 9.0 Hz, ^{4}J = 1.6 Hz, 3H)

$^{13}C\{^{1}H\}$ (100 MHz, $CDCl_3$) δ 139.4 ($CH_3ArCHC(CH_3)PPh_2$, d, ^{2}J = 28.5 Hz), 137.3 (C_{IPSO}, d, ^{3}J = 10.9 Hz), 128.8 (C_{ORTHO}, s), 21.6 ($CH_3ArCHC(CH_3)PPh_2$, s), 18.1 ($CH_3ArCHC(CH_3)PPh_2$, d, ^{2}J = 17.1 Hz)

77 Internal Product (11% conversion)

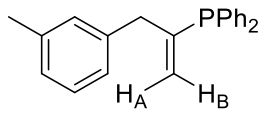

$^{31}P\{^{1}H\}$ (162 MHz, $CDCl_3$) δ −2.2 (s)

^{31}P (162 MHz, $CDCl_3$) δ −2.2 (ddt, ^{3}J = 21.5 Hz, ^{3}J = 9.6 Hz, ^{3}J = 7.1 Hz)

^{1}H (400 MHz, $CDCl_3$) δ 7.52–7.01 (ar, m 14H), 5.37 (H_A, dtd, ^{3}J = 21.5 Hz, ^{4}J = 1.9 Hz, ^{2}J = 1.3 Hz, 1H), 5.15 (H_B, dtd, ^{3}J = 9.6 Hz, ^{4}J = 1.9 Hz, ^{2}J = 1.3 Hz, 1H), 3.43 ($CH_3ArCH_2C(CH_2)PPh_2$, br d, ^{3}J = 7.1 Hz, 2H), 2.24 ($CH_3ArCH_2C(CH_2)PPh_2$, s, 3H)

$^{13}C\{^{1}H\}$ (100 MHz, $CDCl_3$) δ 148.3 (C_{IPSO}, d, ^{3}J = 17.3 Hz), 137.9 (C_{ORTHO}, s), 124.9 ($CH_3ArCH_2C(CH_2)PPh_2$, d, ^{2}J = 13.5 Hz), 42.0 ($CH_3ArCH_2C(CH_2)PPh_2$, d, ^{2}J = 24.4 Hz), 21.5 ($CH_3ArCH_2C(CH_2)PPh_2$, s)

Reaction with 2-Methylphenylallene (56)

76% conversion of starting material (2% dehydrocoupling, 74% hydrophosphination), 61% isolated yield of hydrophosphinated products, clear oil. All three isomers co-elute with R_f = 0.30 (20% DCM : 80% Petroleum Ether 40-60 eluent, silica gel column).

TOF-MS [M+H] 316.1381 (theoretical) 316.1372 (observed)

FTIR-ATR υ (cm^{-1}): 3054, 3016, 2910, 1479, 1457, 1434, 1182, 1117

Note : In NMR assignments below, C_{ORTHO} refers to the meta-methyl position (The ipso-methyl C_{ORTHO} position could not be assigned for these products)

78 Terminal *E* product (6% conversion)

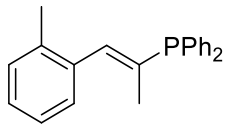

$^{31}P\{^{1}H\}$ (202 MHz, $CDCl_3$) δ −14.0 (s)

^{31}P (162 MHz, $CDCl_3$) δ −14.0 (m)

^{1}H (500 MHz, $CDCl_3$) δ 7.63–7.12 (ar, m, 14H), 7.22 ($CH_3ArCHC(CH_3)PPh_2$, m, 1H), 2.21 ($CH_3ArCHC(CH_3)PPh_2$, s, 3H), 2.02 ($CH_3ArCHC(CH_3)PPh_2$, dd, ^{3}J = 13.3 Hz, ^{4}J = 3.6 Hz, 3H)

$^{13}C\{^{1}H\}$ (126 MHz, $CDCl_3$) δ 143.0 ($CH_3ArCHC(CH_3)PPh_2$, d, ^{2}J = 32.9 Hz), 137.0 (C_{IPSO}, d, ^{3}J = 11.3 Hz), 128.9 (C_{ORTHO}, s), 19.9 ($CH_3ArCHC(CH_3)PPh_2$, s), 14.6 ($CH_3ArCHC(CH_3)PPh_2$, d, ^{2}J = 10.9 Hz)

79 Terminal *Z* product (60% conversion)

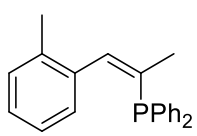

$^{31}P\{^{1}H\}$ (202 MHz, $CDCl_3$) δ 5.8 (s)

^{31}P (162 MHz, $CDCl_3$) δ 5.8 (dq, ^3J = 13.4 Hz, ^3J = 9.3 Hz)

^{1}H (500 MHz, $CDCl_3$) δ 7.63–7.12 (ar, m, 14H), 6.70 ($CH_3ArCHC(CH_3)PPh_2$, dq, ^3J = 13.4 Hz, ^4J = 4.1 Hz, 1H), 2.21 ($CH_3ArCHC(CH_3)PPh_2$, s, 3H), 1.88 ($CH_3ArCHC(CH_3)PPh_2$, dd, ^3J = 9.3 Hz, ^4J = 4.1 Hz, 3H)

^{13}C{^{1}H} (126 MHz, $CDCl_3$) δ 138.6 ($CH_3ArCHC(CH_3)PPh_2$, d, ^2J = 26.2 Hz), 136.3 (C_{IPSO}, d, ^3J = 11.5 Hz), 128.9 (C_{ORTHO}, s), 20.0 ($CH_3ArCHC(CH_3)PPh_2$, s), 17.6 ($CH_3ArCHC(CH_3)PPh_2$, d, ^2J = 17.7 Hz)

80 Internal Product (8% conversion)

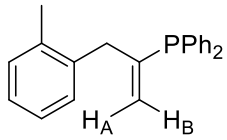

^{31}P{^{1}H} (202 MHz, $CDCl_3$) δ −1.1 (s)

^{31}P (162 MHz, $CDCl_3$) δ −1.1 (m)

^{1}H (500 MHz, $CDCl_3$) δ 7.63–7.12 (ar, m, 14H), 5.23 (H_A, dtd, ^3J = 22.6 Hz, ^4J = 4.1 Hz, ^2J = 1.9 Hz, 1H), 5.15 (H_B, dtd, ^3J = 9.6 Hz, ^4J = 4.6 Hz, ^2J = 1.9 Hz, 1H), 3.43 ($CH_3ArCH_2C(CH_2)PPh_2$, m, 2H), 2.19 ($CH_3ArCH_2C(CH_2)PPh_2$, s, 3H)

^{13}C{^{1}H} (126 MHz, $CDCl_3$) δ 147.0 (C_{IPSO}, d, ^3J = 18.5 Hz), 130.5 (C_{ORTHO}, s), 124.4 ($CH_3ArCH_2C(CH_2)PPh_2$, d, ^2J = 14.3 Hz), 39.5 ($CH_3ArCH_2C(CH_2)PPh_2$, d, ^2J = 22.9 Hz), 19.6 ($CH_3ArCH_2C(CH_2)PPh_2$, s)

Reaction with 4-Methoxyphenylallene

93% conversion of starting material (7% dehydrocoupling, 86% hydrophosphination), 62% isolated yield of hydrophosphinated products, clear oil. The hydrophosphinated products rapidly decompose in air, so were isolated by passing the reaction mixture through silica with 100% pentane under a dry argon atmosphere.

TOF-MS [M-H] 332.1330 (theoretical) 332.1338 (observed)

FTIR-ATR υ (cm^{-1}): 3059, 2961, 2832, 1658, 1508, 1437, 1247, 1175, 1035

81 Terminal *E* Product (15% Conversion)

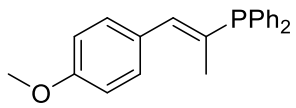

^{31}P{^{1}H} (162 MHz, C_6D_6) δ −12.8 (s)

^{31}P (162 MHz, C_6D_6) δ −12.8 (m)

^{1}H (500 MHz, C_6D_6) δ 7.56–6.62 (ar, m, 14H), 6.96 ($CH_3OArCHC(CH_3)PPh_2$, m, 1H), 3.35 ($CH_3OArCHC(CH_3)PPh_2$, s, 3H), 2.31 ($CH_3OArCHC(CH_3)PPh_2$, m, 3H)

^{13}C{^{1}H} (126 MHz, C6D6) δ 158.8 (C_{PARA}, s), 143.5 ($CH_3OArCHC(CH_3)PPh_2$, d, ^2J = 29.3 Hz), 136.5 (C_{IPSO}, d, ^3J = 12.3 Hz), 130.8 (C_{ORTHO}, s), 54.7 ($CH_3OArCHC(CH_3)PPh_2$, s), 14.3 ($CH_3OArCHC(CH_3)PPh_2$, m)

82 Terminal *Z* Product (60% Conversion)

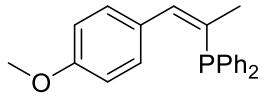

$^{31}P\{^{1}H\}$ (162 MHz, C_6D_6) δ 10.0 (s)

^{31}P (162 MHz, C_6D_6) δ 10.0 (dq, ^{3}J = 14.0 Hz, ^{3}J = 8.2 Hz)

^{1}H (500 MHz, C_6D_6) δ 7.56–6.62 (ar, m, 14H), 6.75 ($CH_3OArCHC(CH_3)PPh_2$, br d, ^{3}J = 14.0 Hz, 1H), 3.31 ($CH_3OArCHC(CH_3)PPh_2$, s, 3H) 2.08 ($CH_3OArCHC(CH_3)PPh_2$, dd, ^{3}J = 8.2 Hz, ^{4}J = 1.5 Hz, 3H)

$^{13}C\{^{1}H\}$ (126 MHz, C_6D_6) δ 159.3 (C_{PARA}, s), 139.9 ($CH_3OArCHC(CH_3)PPh_2$, d, ^{2}J = 32.9 Hz), 137.5 (C_{IPSO}, d, ^{3}J = 13.4 Hz), 130.9 (C_{ORTHO}, s) 54.8 ($CH_3OArCHC(CH_3)PPh_2$, s), 18.1 ($CH_3OArCHC(CH_3)PPh_2$, d, ^{2}J = 14.5 Hz)

83 Internal Product (11% Conversion)

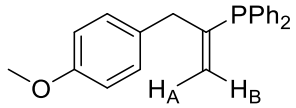

$^{31}P\{^{1}H\}$ (202 MHz, C_6D_6) δ −2.6 (s)

^{31}P (162 MHz, C_6D_6) δ −2.6 (ddt, ^{3}J = 21.0 Hz, ^{3}J = 9.6 Hz, ^{3}J = 7.0 Hz)

^{1}H (500 MHz, C_6D_6) δ 7.56–6.62 (ar, m, 14H), 5.31 (H_A, dtd, ^{3}J = 21.0 Hz, ^{4}J = 1.5 Hz, ^{2}J = 1.3 Hz, 1H), 5.09 (H_B, dtd, ^{3}J = 10.9 Hz, ^{4}J = 1.3 Hz, ^{2}J = 1.3 Hz, 1H) 3.48 ($CH_3OArCH_2C(CH_2)PPh_2$, br d, ^{3}J = 7.0 Hz, 2H), 3.31 ($CH_3OArCH_2C(CH_2)PPh_2$, s, 3H)

$^{13}C\{^{1}H\}$ (126 MHz, C_6D_6) δ 160.0 (C_{PARA}, s), 149.6 (C_{IPSO}, d, ^{3}J = 18.7 Hz), 129.5 (C_{ORTHO}, s), 124.6 ($CH_3OArCH_2C(CH_2)PPh_2$, d, ^{3}J = 13.3 Hz), 54.8 ($CH_3OArCH_2C(CH_2)PPh_2$, s), 41.7 ($CH_3OArCH_2C(CH_2)PPh_2$, d, ^{2}J = 22.8 Hz)

Reaction with 2-Methoxyphenylallene (70)

93% conversion of starting material (2% dehydrocoupling, 91% hydrophosphination), 59% isolated yield of hydrophosphinated products, clear oil. The hydrophosphinated products rapidly decompose in air, so were isolated by passing the reaction mixture through silica with 100% pentane under a dry argon atmosphere.

TOF-MS [M-H] 332.1330 (theoretical) 332.1326 (observed)

FTIR-ATR υ (cm^{-1}): 3051, 2695, 2284, 1480, 1435, 1245, 1197, 1122, 1026

Note : In NMR assignments below, C_{ORTHO} refers to the ipso-methoxy position (The meta-methoxy C_{ORTHO} position could not be assigned for these products)

84 Terminal *E* product (10% conversion)

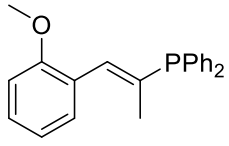

$^{31}P\{^{1}H\}$ (162 MHz, $CDCl_3$) δ −12.8 (s)

^{31}P (162 MHz, $CDCl_3$) δ −12.8 (m)

^{1}H (400 MHz, $CDCl_3$) δ 7.52–6.88 (ar, m, 14H), 7.07 ($CH_3OPhCHC(CH_3)PPh_2$, m, 1H), 2.38 ($CH_3OPhCHC(CH_3)PPh_2$, s, 3H), 2.14 ($CH_3OPhCHC(CH_3)PPh_2$, dd, ^{3}J = 13.8 Hz, ^{4}J = 1.5 Hz, 3H)

$^{13}C\{^{1}H\}$ (126 MHz, $CDCl_3$) δ 158.0 (C_{ORTHO}, s), 148.1 ($CH_3OArCHC(CH_3)PPh_2$, d, ^{2}J = 18.9 Hz), 136.9 (C_{IPSO}, d, ^{3}J = 12.4 Hz), 55.0 ($CH_3OArCHC(CH_3)PPh_2$, s), 14.7 ($CH_3OArCHC(CH_3)PPh_2$, m)

85 Terminal *Z* product (60% conversion)

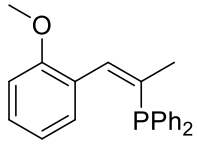

$^{31}P\{^{1}H\}$ (162 MHz, C_6D_6) δ 8.0 (s)

^{31}P (162 MHz, C_6D_6) δ 8.0 (dq, ^{3}J = 15.1 Hz, ^{3}J = 8.1 Hz)

^{1}H (400 MHz, C_6D_6) δ 7.52–6.88 (ar, m, 14H), 6.94 ($CH_3OArCHC(CH_3)PPh_2$, dq, ^{3}J = 15.1 Hz, ^{4}J = 1.5 Hz, 1H), 3.37 ($CH_3OArCHC(CH_3)PPh_2$, s, 3H), 2.07 ($CH_3OArCHC(CH_3)PPh_2$, dd, ^{3}J = 8.1 Hz, ^{4}J = 1.5 Hz, 3H)

$^{13}C\{^{1}H\}$ (126 MHz, C_6D_6) δ 157.8 (C_{ORTHO}, s), 142.8 ($CH_3OArCHC(CH_3)PPh_2$, m), 137.6 (C_{IPSO}, d, ^{3}J = 13.4 Hz), 55.0 ($CH_3OArCHC(CH_3)PPh_2$, s), 17.8 ($CH_3OArCHC(CH_3)PPh_2$, d, ^{2}J = 13.9 Hz)

86 Internal Product (21% conversion)

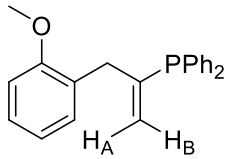

$^{31}P\{^{1}H\}$ (162 MHz, $CDCl_3$) δ −1.2 (s)

^{31}P (162 MHz, $CDCl_3$) δ −1.2 (m)

^{1}H (400 MHz, $CDCl_3$) δ 7.52–6.88 (ar, m 14H), 5.55 (H_A, dtd, ^{3}J = 23.0 Hz, ^{4}J = 2.2 Hz, ^{2}J = 1.3 Hz, 1H), 5.41 (H_B, dtd, ^{3}J = 10.3 Hz, ^{4}J = 1.7 Hz, ^{2}J = 1.3 Hz, 1H), 3.76 ($CH_3OArCH_2C(CH_2)PPh_2$, br d, ^{3}J = 5.9 Hz, 2H), 3.31 ($CH_3OArCH_2C(CH_2)PPh_2$, s, 3H)

$^{13}C\{^{1}H\}$ (126 MHz, $CDCl_3$) δ 161.5 (C_{ORTHO}, s), 124.5 ($CH_3OArCH_2C(CH_2)PPh_2$, d, ^{2}J = 15.7 Hz), 54.8 ($CH_3OArCH_2C(CH_2)PPh_2$, s), 36.6 ($CH_3OArCH_2C(CH_2)PPh_2$, d, ^{2}J = 22.2 Hz)

Reaction with 4-Chlorophenylallene (59)

95% conversion of starting material (18% dehydrocoupling, 77% hydrophosphination), 62% isolated yield of hydrophosphinated products, clear oil. All three isomers co-elute with R_f = 0.41 (1:4 DCM : Petroleum Ether 40-60 eluent, silica gel).

TOF-MS [M+H] 337.0906 (theoretical) 337.0913 (observed)

FTIR-ATR υ (cm^{-1}): 3055, 2963, 2873, 2219, 1590, 1489, 1436, 1403, 1258

87 Terminal *E* product (6% conversion)

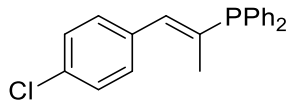

$^{31}P\{^{1}H\}$ (161 MHz, $CDCl_3$) δ −13.4 (s)

^{31}P (161 MHz, $CDCl_3$) δ −13.4 (m)

^{1}H (400 MHz, $CDCl_3$) δ 7.76–7.02 (ar, m, 14H), 7.12 (ClArC*H*C(CH_3)PPh_2, br d, ^{3}J = 6.9 Hz, 1H), 2.01 (ClArCHC(C*H*$_3$)PPh_2, dd, ^{3}J = 13.8 Hz, ^{4}J = 1.5 Hz, 3H)

$^{13}C\{^{1}H\}$ (100 MHz, $CDCl_3$) δ 141.4 (ClAr*C*HC(CH_3)PPh_2, d, ^{2}J = 10.9 Hz), 136.2 (C_{IPSO}, d, ^{3}J = 11.8 Hz), 130.7 (C_{ORTHO}, s) 15.3 (ClArCHC(*C*H_3)PPh_2, d, ^{2}J = 10.8 Hz)

88 Terminal *Z* product (70% conversion)

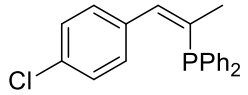

$^{31}P\{^{1}H\}$ (161 MHz, $CDCl_3$) δ 8.1 (s)

^{31}P (161 MHz, $CDCl_3$) δ 8.1 (dq, ^{3}J = 13.0 Hz, ^{3}J = 9.2 Hz)

^{1}H (400 MHz, $CDCl_3$) δ 7.76–7.02 (ar, m, 14H), 6.50 (ClArC*H*C(CH_3)PPh_2, dq, ^{3}J = 13.0 Hz, ^{4}J = 1.6 Hz, 1H), 1.89 (ClArCHC(C*H*$_3$)PPh_2, dd, ^{3}J = 9.2 Hz, ^{4}J = 1.6 Hz, 3H)

$^{13}C\{^{1}H\}$ (100 MHz, $CDCl_3$) δ 137.5 (ClAr*C*HC(CH_3)PPh_2, d, ^{2}J = 27.3 Hz), 136.0 (C_{IPSO}, d, ^{3}J = 11.6 Hz), 130.3 (C_{ORTHO}, s) 18.1 (ClArCHC(*C*H_3)PPh_2, d, ^{2}J = 17.8 Hz)

89 Internal Product (1% conversion)

The internal product is only observed in a small amount, so $^{13}C\{^{1}H\}$ and ^{31}P (^{1}H coupled) signals and coupling constants were not able to be determined.

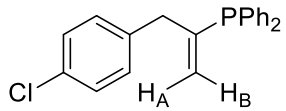

$^{31}P\{^{1}H\}$ (202 MHz, $CDCl_3$) δ −2.6 (s)

^{1}H (500 MHz, $CDCl_3$) δ 7.76–7.02 (ar, m, 14H), 5.44 (H_A, m, 1H), 4.89 (H_B, m, 1H) 3.32 (ClArC*H*$_2$C(CH_2)PPh_2, br d, ^{3}J = 7.2 Hz, 2H)

Reaction with (4-Phenyl)phenylallene (71)

61% conversion of starting material (1% dehydrocoupling, 60% hydrophosphination), 32% isolated yield of hydrophosphinated products, oily yellow solid. All three isomers co-elute with R_f = 0.41 (1:4 DCM : Petroleum Ether 40-60 eluent, silica gel).

TOF-MS [M-H] 378.1537 (theoretical) 378.1550 (observed)

FTIR-ATR υ (cm^{-1}): 2923, 2857, 1605, 1511, 1485, 1437, 1270, 1170, 1118

90 Terminal *E* Product (6% Conversion)

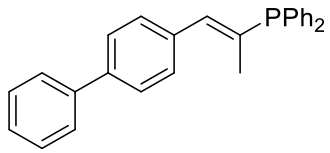

$^{31}P\{^{1}H\}$ (162 MHz, C_6D_6) δ −13.1 (s)

^{31}P (162 MHz, C_6D_6) δ −13.1 (m)

^{1}H (500 MHz, C_6D_6) δ 7.80–6.76 (ar, m, 19H), 6.98 ((Ph)ArC*H*C(CH_3)PPh_2, br d, ^{3}J = 8.5 Hz, 1H), 2.07 ((Ph)ArCHC(C*H*$_3$)PPh_2, m, 3H)

$^{13}C\{^{1}H\}$ (126 MHz, C6D6) δ 142.9 ((Ph)Ar*C*HC(CH_3)PPh_2, d, ^{2}J = 25.2 Hz), 15.8 ((Ph)ArCHC(*C*H_3)PPh_2, m)

91 Terminal *Z* Product (40% Conversion)

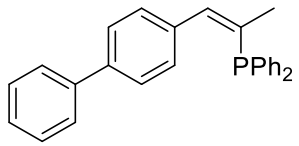

$^{31}P\{^{1}H\}$ (162 MHz, $CDCl_3$) δ 8.8 (s)

^{31}P (162 MHz, $CDCl_3$) δ 8.8 (dq, ^{3}J = 13.4 Hz, ^{3}J = 9.0 Hz)

^{1}H (400 MHz, $CDCl_3$) δ 7.80–6.76 (ar, m, 19H), 6.60 ((Ph)ArC*H*C(CH_3)PPh_2, dq, 1H, ^{3}J = 13.4 Hz, ^{4}J = 1.6 Hz, 1H), 1.96 ((Ph)ArCHC(C*H*$_3$)PPh_2, dd, ^{3}J = 9.0 Hz, ^{4}J = 1.6 Hz, 3H)

$^{13}C\{^{1}H\}$ (126 MHz, C_6D_6) δ 141.6 ((Ph)Ar*C*HC(CH_3)PPh_2, d, ^{2}J = 29.2 Hz), 138.6 (C_{IPSO}, d, ^{3}J = 16.4 Hz), 18.7 ((Ph)ArCHC(*C*H_3)PPh_2, d, ^{2}J = 13.6 Hz)

92 Internal Product (14% Conversion)

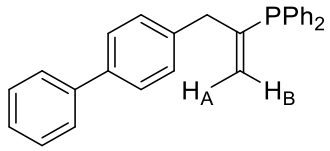

$^{31}P\{^{1}H\}$ (202 MHz, C_6D_6) δ −2.3 (s)

^{31}P (162 MHz, C_6D_6) δ −2.3 (m)

^{1}H (500 MHz, C_6D_6) δ 7.56–6.62 (ar, m, 19H), 5.40 (H_A, br d, ^{3}J = 21.4 Hz, 1H), 5.09 (H_B, br d, ^{3}J = 9.4 Hz, ^{4}J = 1.3 Hz, ^{2}J = 1.3 Hz, 1H), 3.38 ((Ph)ArC*H*$_2$C(CH_2)PPh_2, d, ^{3}J = 7.4 Hz, 2H)

$^{13}C\{^{1}H\}$ (126 MHz, C_6D_6) δ 121.0 ((Ph)ArCH_2C(*C*H_2)PPh_2, d, ^{3}J = 13.3 Hz), 41.8 ((Ph)Ar*C*H_2C(CH_2)PPh_2, m)

Reaction with 4-Fluorophenylallene (58)

94 % conversion of starting material (35% dehydrocoupling, 59% hydrophosphination), 46 % isolated yield of hydrophosphinated products. All three isomers co-elute with R_f = 0.37 (1:4 DCM : Petroleum Ether (40-60) eluent, silica gel).

TOF-MS [M+H] 316.1381 (theoretical) 316.1380 (observed)

FTIR-ATR υ (cm^{-1}): 3013, 2910, 1600, 1505, 1479, 1432, 1224

93 Terminal *E* product (4% conversion)

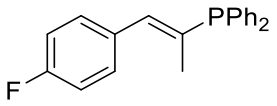

$^{31}P\{^{1}H\}$ (161 MHz, $CDCl_3$) δ −13.6 (s)

^{31}P (161 MHz, $CDCl_3$) δ −13.6 (m)

^{1}H (400 MHz, $CDCl_3$) δ 7.71–6.84 (ar, m, 14H), 6.97 (FAr*CH*C(CH_3)PPh_2, br d, ^{3}J = 9.0 Hz, 1H), 2.00 (FArCHC(C*H*$_3$)PPh_2, dd, ^{3}J = 13.8 Hz, ^{4}J = 1.6 Hz, 3H)

$^{13}C\{^{1}H\}$ (100 MHz, $CDCl_3$) δ 160.2 (C_{PARA}, d, ^{1}J = 238.0 Hz), 147.4 (FAr*C*HC(CH_3)PPh_2, d, ^{2}J = 32.7 Hz), 130.3 (C_{ORTHO}, d, ^{3}J = 9.1 Hz) 14.6 (FArCHC(*C*H_3)PPh_2, d, ^{2}J = 17.3 Hz)

$^{19}F\{^{1}H\}$ (376 MHz, $CDCl_3$) δ −115.8 (s)

^{19}F (376 MHz, $CDCl_3$) δ −115.8 (tt, ^{3}J = 9.7 Hz, ^{4}J = 4.5 Hz)

94 Terminal *Z* product (54% conversion)

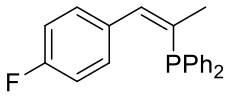

$^{31}P\{^{1}H\}$ (161 MHz, $CDCl_3$) δ 8.3 (s)

^{31}P (161 MHz, $CDCl_3$) δ 8.3 (dq, ^{3}J = 13.6 Hz, ^{3}J = 9.0 Hz)

^{1}H (400 MHz, $CDCl_3$) δ 7.71–6.84 (ar, m, 14H), 6.54 (FAr*CH*C(CH_3)PPh_2, dq, ^{3}J = 13.6 Hz, ^{4}J = 1.6 Hz, 1H), 1.89 (FArCHC(C*H*$_3$)PPh_2, dd, ^{3}J = 9.0 Hz, ^{4}J = 1.6 Hz, 3H)

$^{13}C\{^{1}H\}$ (100 MHz, $CDCl_3$) δ 160.6 (C_{PARA}, d, ^{1}J = 247.0 Hz), 136.7 (FAr*C*HC(CH_3)PPh_2, d, ^{2}J = 28.7 Hz), 136.2 (C_{IPSO}, d, ^{3}J = 10.8 Hz), 131.0 (C_{ORTHO}, d, ^{3}J = 9.6 Hz) 16.8 (FArCHC(*C*H_3)PPh_2, d, ^{2}J = 16.9 Hz)

$^{19}F\{^{1}H\}$ (376 MHz, $CDCl_3$) δ −114.6 (s)

^{19}F (376 MHz, $CDCl_3$) δ −114.6 (tt, ^{3}J = 9.2 Hz, ^{4}J = 4.6 Hz)

95 Internal Product (1% conversion)

The internal product is only observed in a small amount, so $^{13}C\{^{1}H\}$ and ^{31}P (^{1}H coupled) signals and coupling constants were not able to be determined.

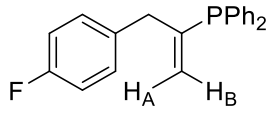

$^{31}P\{^{1}H\}$ (202 MHz, $CDCl_3$) δ −2.7 (s)

^{1}H (500 MHz, $CDCl_3$) δ 7.71–6.84 (ar, m, 14H), 5.34 (H_A, d, ^{3}J = 21.3 Hz, 1H), 5.01 (H_B, d, ^{3}J = 9.4 Hz, 1H) 3.34 (FArCH_2C(CH_2)PPh_2, br d, ^{3}J = 7.2 Hz, 2H)

$^{19}F\{^{1}H\}$ (376 MHz, $CDCl_3$) δ −112.2 (s)

^{19}F (376 MHz, $CDCl_3$) δ −112.2 (tt, ^{3}J = 9.4 Hz, ^{4}J = 4.7 Hz)

Reaction with cyclohexylallene

46% conversion of starting material (no dehydrocoupling observed), 36% isolated yield of hydrophosphinated products, clear oil. The hydrophosphinated products rapidly decompose in air, so were isolated by passing the reaction mixture through silica with 100% pentane under a dry argon atmosphere.

TOF-MS [M+H] 308.1694 (theoretical), 308.1673 (observed)

FTIR-ATR υ (cm^{-1}): 2921, 2849, 1479, 1436, 1197, 1123

96 Terminal *E* Product (6% Conversion)

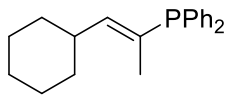

$^{31}P\{^{1}H\}$ (202 MHz, $CDCl_3$) δ −16.2 (s)

^{31}P (162 MHz, $CDCl_3$) δ −16.2 (m)

^{1}H (500 MHz, $CDCl_3$) δ 7.60–6.93 (ar, m, 10H), 5.47 (CyCHC(CH_3)PPh_2, dq, ^{3}J = 5.7 Hz, ^{4}J = 1.3 Hz), 2.85 (PhCHC(CH_3)PPh_2, ^{3}J = 7.2 Hz, ^{4}J = 1.3 Hz, 3H), 1.81–0.90 (cy, m, 11H)

$^{13}C\{^{1}H\}$ (126 MHz, $CDCl_3$) δ 123.6 (CyCHC(CH_3)PPh_2, m), 26.1 (CyCHC($C$$H_3$)$PPh_2$, m)

97 Terminal *Z* Product (32% Conversion)

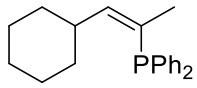

$^{31}P\{^{1}H\}$ (202 MHz, C_6D_6) δ 6.7 (s)

^{31}P (202 MHz, C_6D_6) δ 6.7 (dq, ^{3}J = 17.9 Hz, ^{3}J = 7.3 Hz)

^{1}H (400 MHz, C_6D_6) δ 7.60–6.93 (ar, m, 10H), 5.58 (CyCHC(CH_3)PPh_2, dq, ^{3}J = 17.9 Hz, ^{4}J = 1.4 Hz, 1H), 2.77 (CyCHC(CH_3)PPh_2, dq, ^{3}J = 7.3 Hz, ^{4}J = 1.4 Hz, 3H), 1.81–0.90 (cy, m, 11H)

$^{13}C\{^{1}H\}$ (100 MHz, C_6D_6) δ 122.1 (CyCHC(CH_3)PPh_2, m), 32.8 (CyCHC($C$$H_3$)$PPh_2$, m)

98 Internal Product (2% Conversion)

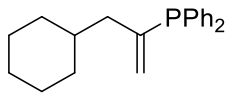

Unlike in other structures, the terminal alkene protons (H_A and H_B) appear as one complex signal as opposed to two well-defined signals.

$^{31}P\{^{1}H\}$ (202 MHz, $CDCl_3$) δ −3.2 (s)

^{31}P (162 MHz, $CDCl_3$) δ −3.2 (m)

^{1}H (500 MHz, $CDCl_3$) δ 7.60–6.93 (ar, m, 10H), 4.71 ($CyCH_2C(CH_2)PPh_2$, m, 2H) 2.18 ($CyCH_2C(CH_2)PPh_2$, m, 2H), 1.81–0.90 (cy, m, 11H)

$^{13}C\{^{1}H\}$ (126 MHz, $CDCl_3$) δ 41.2 ($CyCH_2C(CH_2)PPh_2$, m)

99 Terminal (Alternate Regioselectivity) Products (6% Conversion)

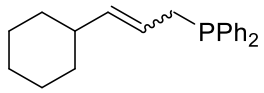

$^{31}P\{^{1}H\}$ (202 MHz, $CDCl_3$) δ −14.8 (s), −15.6 (s)

^{31}P (162 MHz, $CDCl_3$) δ –14.8 (m), −15.6 (m)

^{1}H (500 MHz, $CDCl_3$) δ 7.60–6.93 (ar, m, 10H), 6.16–5.99 ($CyCHCHCH_2PPh_2$ & $CyCHCHCH_2PPh_2$, m, 2H), 3.32 ($CyCHCHCH_2PPh_2$, m, 2H), 1.81–0.90 (cy, m, 11H)

$^{13}C\{^{1}H\}$ (126 MHz, $CDCl_3$) δ 151.7–149.5 (($CyCHCHCH_2PPh_2$ & $CyCHCHCH_2PPh_2$, m), 28.7 ($PhCHCHCH_2PPh_2$, m)

Reaction with methoxyallene

47% conversion of starting material (13% dehydrocoupling, 34% hydrophosphination). The hydrophosphinated products are not stable in air so could not be isolated through standard column chromatography. Note than unlike the other products formed with diphenylphosphine, these products could not be purified by passing through a silica plug.

TOF-MS [M+H] 257.1089 (theoretical), 257.1094 (observed)

FTIR-ATR υ (cm^{-1}): 3052, 2930, 2279, 1630, 1479, 1434, 1219, 1120

100 Terminal *E* Product (20% Conversion)

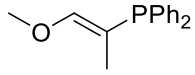

$^{31}P\{^{1}H\}$ (202 MHz, C_6D_6) δ −14.5 (s)

^{1}H (500 MHz, C_6D_6) δ 7.60–6.89 (ar, m, 10H), 6.51 ($CH_3OCHC(CH_3)PPh_2$, d, ^{3}J = 10.4 Hz, 1H), 3.08 ($CH_3OCHC(CH_3)PPh_2$, s, 3H) 1.13 ($CH_3OCHC(CH_3)PPh_2$, d, ^{3}J = 6.9 Hz, 3H)

$^{13}C\{^{1}H\}$ (126 MHz, C_6D_6) δ 157.0 ($CH_3OCHC(CH_3)PPh_2$, d, ^{2}J = 77.6 Hz), 59.0 ($CH_3OCHC(CH_3)PPh_2$, s) 20.7 ($PhCHC(CH_3)PPh_2$, d, ^{2}J = 30.9 Hz)

101 Terminal *Z* Product (12% Conversion)

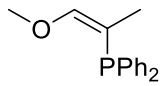

$^{31}P\{^{1}H\}$ (202 MHz, C_6D_6) δ −0.9 (s)

^{1}H (500 MHz, C_6D_6) δ 7.60–6.89 (ar, m, 10H), 6.18 ($CH_3OCHC(CH_3)PPh_2$, d, ^{3}J = 14.9 Hz, 1H), 3.00 ($CH_3OCHC(CH_3)PPh_2$, s, 3H) 1.18 ($CH_3OCHC(CH_3)PPh_2$, d, ^{3}J = 6.8 Hz, 3H)

$^{13}C\{^{1}H\}$ (126 MHz, C_6D_6) δ 149.4 ($CH_3OCHC(CH_3)PPh_2$, d, ^{2}J = 10.4 Hz), 59.5 ($CH_3OCHC(CH_3)PPh_2$, s) 24.3 ($CH_3CHC(CH_3)PPh_2$, d, ^{2}J = 13.2 Hz)

Reaction with dicyclohexylphosphine

8% conversion of starting material (no dehydrocoupling, 8% hydrophosphination). The hydrophosphinated products oxidize in air and are not readily soluble in pentane, the products were instead isolated with dichloromethane as the solvent in a silica plug under an argon atmosphere.

TOF-MS [M+H] 314.2163 (theoretical), 314.2165 (observed)

FTIR-ATR υ (cm^{-1}): 2920, 2848, 2260, 1556, 1446, 1326, 1291, 1178

The low conversion of products and abundance of starting material meant that the ^{13}C NMR could not be assigned.

102 Terminal *E* Product (1% Conversion)

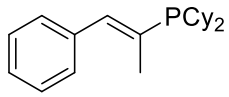

$^{31}P\{^{1}H\}$ (162 MHz, $CDCl_3$) δ 20.2 (s)

^{31}P (162 MHz, $CDCl_3$) δ 20.2 (m)

^{1}H (500 MHz, $CDCl_3$) δ 7.55–6.60 (ar, m, 5H), 6.75 ($PhCHC(CH_3)PCy_2$, m, 1H), 2.07 ($PhCHC(CH_3)PPh_2$, m, 3H), 1.90–0.92 (cy, m, 22H)

103 Terminal *Z* Product (5% Conversion)

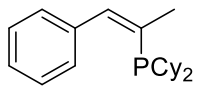

$^{31}P\{^{1}H\}$ (162 MHz, $CDCl_3$) δ 7.1 (s)

^{31}P (162 MHz, $CDCl_3$) δ 7.1 (m)

^{1}H (500 MHz, $CDCl_3$) δ 7.55–6.60 (ar, m, 5H), 6.33 ($PhCHC(CH_3)PCy_2$, m, 1H), 1.91 ($PhCHC(CH_3)PPh_2$, m, 3H), 1.90–0.92 (cy, m, 22H)

104 Internal Product (2% Conversion)

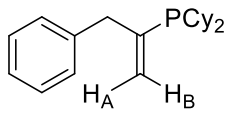

$^{31}P\{^{1}H\}$ (162 MHz, $CDCl_3$) δ −0.9 (s)

^{31}P (162 MHz, $CDCl_3$) δ −0.9 (m)

^{1}H (500 MHz, $CDCl_3$) δ 7.55–6.60 (ar, m, 5H), 5.55 (H_B, d, ^{3}J = 12.6 Hz, 1H), 5.33 (H_A, d, ^{3}J = 29.2 Hz, 1H), 3.28 (PhC*H*$_2$C(CH_2)PCy_2, d, ^{3}J = 17.2 Hz, 2H), 1.90–0.92 (cy, m, 22H)

$^{13}C\{^{1}H\}$ (126 MHz, $CDCl_3$) δ 146.5 (C_{IPSO}, d, ^{3}J = 18.7 Hz), 129.5 (C_{ORTHO}, s), 126.0 ($PhCH_2C(CH_2)PHPh$, d, ^{2}J = 29.0 Hz), 43.9 ($PhCH_2C(CH_2)PPh_2$, d, ^{2}J = 6.6 Hz)

Reaction with phenylphosphine

66% conversion of starting material (2% dehydrocoupling, 64% hydrophosphination), 51% isolated yield of hydrophosphinated products, clear oil. The hydrophosphinated products rapidly decompose in air, so were isolated by passing the reaction mixture through silica with 100% pentane under a dry argon atmosphere.

TOF-MS [M+H] 227.0983 (theoretical), 227.0988 (observed)

FTIR-ATR υ (cm^{-1}): 3026, 2959, 2321, 1709, 1599, 1494, 1437, 1189, 1112

105 Terminal *E* Product (2% Conversion)

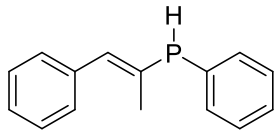

$^{31}P\{^{1}H\}$ (162 MHz, C_6D_6) δ −21.7 (s)

^{31}P (162 MHz, C_6D_6) δ −21.7 (br d, ^{1}J = 212.4 Hz)

^{1}H (500 MHz, C_6D_6) δ 7.44–6.91 (ar, m, 10H), 6.82 (PhC*H*C(CH_3)PHPh, br d, ^{3}J = 7.7 Hz, 1H), 4.94 (PhCHC(CH_3)P*H*Ph, d, ^{1}J = 212.4 Hz, 1H), 1.88 (PhCHC(C*H*$_3$)PPh_2, ^{3}J = 6.2 Hz, ^{4}J = 1.5 Hz, 3H)

106 Terminal *Z* Product (1% Conversion)

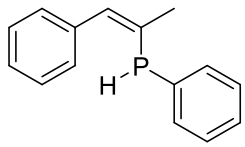

$^{31}P\{^{1}H\}$ (162 MHz, C_6D_6) δ −52.5 (s)

^{31}P (162 MHz, C_6D_6) δ −52.5 (m)

^{1}H (500 MHz, C_6D_6) δ 7.44–6.91 (ar, m, 10H), 6.78 (PhC*H*C(CH_3)PHPh, m, 1H) 4.87 (PhCHC(CH_3)P*H*Ph, d, ^{1}J = 218.2 Hz, 1H), 1.85 (PhCHC(C*H*$_3$)PPh_2, dd, ^{3}J = 4.9 Hz, ^{4}J = 1.6 Hz, 3H)

107 Internal Product (61% Conversion)

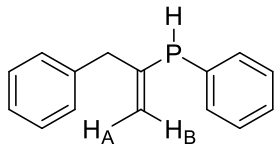

$^{31}P\{^{1}H\}$ (162 MHz, C_6D_6) δ −42.0 (s)

^{31}P (162 MHz, C_6D_6) δ −42.0 (ddm, ^{1}J = 214.4 Hz, ^{3}J = 30.5 Hz)

^{1}H (500 MHz, C_6D_6) δ 7.44–6.91 (ar, m, 10H), 5.47 (H_B, dtdd, ^{3}J = 13.4 Hz, ^{4}J = 2.7 Hz, ^{2}J = 1.3 Hz, ^{4}J = 0.9 Hz, 1H), 5.28 (H_A, dtd, ^{3}J = 30.5 Hz, ^{4}J = 1.9 Hz, ^{2}J = 1.3 Hz, 1H), 4.64 ($PhCH_2C(CH_2)PHPh$, dd, ^{1}J = 214.4 Hz, ^{4}J = 0.9 Hz, 1H), 3.31 ($PhCH_2C(CH_2)PPh_2$, br d, ^{3}J = 13.5 Hz, 2H)

$^{13}C\{^{1}H\}$ (126 MHz, C_6D_6) δ 146.5 (C_{IPSO}, d, ^{3}J = 18.7 Hz), 129.5 (C_{ORTHO}, s), 126.0 ($PhCH_2C(CH_2)PHPh$, d, ^{2}J = 29.0 Hz), 43.9 ($PhCH_2C(CH_2)PPh_2$, d, ^{2}J = 6.6 Hz)

Data for **105** and **106** is concordant with previous reports. [164]

7.5 Experimental Data Pertinent to Chapter 5

General Reaction Procedure

Experiments were performed under an argon atmosphere in an M-Braun glovebox. $Fe(acac)_3$ (8.8 mg, 0.025 mmol, 5 mol%) or alternative iron complex was dissolved in 600 µL C_6D_6 and added to a J-Young NMR tube. The required phosphine (0.5 mmol) and chlorophosphine (0.5 mmol) were then added. The reaction was sealed and allowed to react for the time reported. Conversion was determined through inverse-gated ^{31}P NMR spectroscopy (16 scans).

To work up the products, the solvent was removed under reduced pressure and the resulting precipitate dissolved in eluent and passed through a silica plug. For secondary phosphine products, pentane was used as the eluent, for primary phosphine products dichloromethane was used. The solvent was removed under reduced pressure and product(s) dissolved in 600 µL benzene-d_6 for NMR characterisation.

Test for reaction with HCl

The reactions were prepared with 1.5 mmol of substrate(s) and 0.15 mmol of catalyst (when used) in 2.5 mL dry benzene. The reaction was performed in a Schlenk flask under a nitrogen atmosphere on a Schlenk line.

To a 100 mL two necked round bottom flask was added approximately 10 g of anhydrous calcium chloride. The flask was connected to a 'T' adapter with a dropping funnel and PVC tubing attached. HCl (30 wt% in water) was added to the dropping funnel and added dropwise to the flask. At the point effervescence was first observed a steady nitrogen flow was applied through the second flask neck, and the PVC tube opened to allow gas to bubble through (*via* an attached glass pipette) the reaction flask. Bubbling was allowed to proceed for approximately 15 minutes, after which the

reaction flask was sealed and allowed to proceed for 16 hours before analysis. The residue in the round-bottom flask was carefully quenched with copious amounts of water.

Radical Clock Test

The reaction was prepared as per the standard reaction (with diphenylphosphine and chlorodiphenylphosphine as substrates), and after two minutes (chloromethyl)cyclopropane (0.025 mmol, 4.6 µL) was added. The reaction was left for a further 16 hours, following which conversion was determined. Volatiles were then isolated through trap-to-trap distillation under reduced pressure, from which 1-butene was identified through ^{1}H NMR.

TEMPO Reaction

In place of a catalyst, (2,2,6,6-tetramethylpiperidin-1-yl)oxyl (TEMPO, 0.05 mmol, 0.1 eq., 7.8 mg) was added to the reaction, which was run for 16 hours at room temperature. ^{31}P NMR showed some new phosphorus species along with both starting materials but poor conversion to Ph_4P_2. EPR analysis of the reaction mixture (same setup as below) did not indicate any radicals that could be identified as phosphorus based.

EPR Studies

Samples for EPR measurements were prepared under a nitrogen atmosphere in a glovebox. 2.9 mg of $Fe(acac)_3$ was dissolved in 200 µL benzene and 10 µL toluene. The solutions were transferred to a J-Young EPR tube (Wilmad Labglass 727-LPV-250M) in the glove box and then cooled to 77 K before rapid transfer to the pre-cooled EPR cavity. The X-band CW EPR measurements were performed on a Bruker EMX spectrometer utilising an ER4119HS resonator, 100 kHz field modulation at 140 K. For reactions with phosphines, 0.16 mmol of the desired phosphine was further added to the EPR tube.

Product Characterisation

112 Tetraphenyldiphosphane (Ph_4P_2)

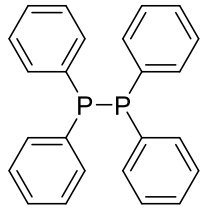

$^{31}P\{^{1}H\}$ (202 MHz) δ −14.9 (s)

$^{13}C\{^{1}H\}$ (126 MHz) δ 136.2 (C_{ORTHO}, t, ^{2}J = 5.3 Hz), 134.44 (C_{IPSO}, t, ^{1}J = 12.9 Hz), 130.02 (C_{PARA}, s), 128.18 (C_{META}, t, ^{3}J = 3.3 Hz)

^{1}H (500 MHz) δ 7.63–7.69 (m, 8H), 7.02–7.08 (m, 12H)

Data concordant with previous literature. [338]

113 Tetracyclohexyldiphosphane (Cy_4P_2)

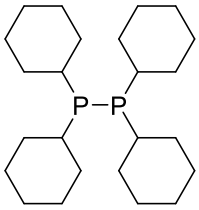

$^{31}P\{^1H\}$ (202 MHz, C_6D_6) δ -21.0 (s)

^1H (500 MHz, C_6D_6) δ 2.05–0.90 (m, 44H)

Data concordant with previous literature. [203]

114 1,1-dicyclohexyl-2,2-diphenyldiphosphane (Cy_2PPPh_2)

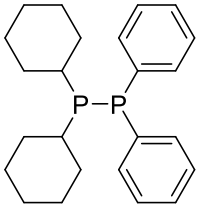

$^{31}P\{^1H\}$ (202 MHz, C_6D_6) δ −6.3 (*P*Cy_2, d, ^1J = 220 Hz), −28.2 (*P*Ph_2, d, ^1J = 220 Hz)

^1H (500 MHz, C_6D_6) δ 7.92–7.03 (ar, m, 10H), 2.24–0.87 (cy, m, 22H)

Data concordant with previous literature. [203]

115 1,1-diisoproypl,2,2-dicyclohexyldiphosphane (iPr_2PPCy_2)

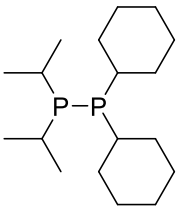

$^{31}P\{^1H\}$ (202 MHz, C_6D_6) δ 21.1 (*P*iPr_2, d, ^1J = 262 Hz), −2.8 (*P*Cy_2, d, ^1J = 262 Hz)

^1H (500 MHz, C_6D_6) δ 2.16–0.90 (m, 36 H)

Data comparable to tBu_2PPCy_2 as previously reported. [203]

116 1,1-ditertbutyl-2,2-diphenyldiphosphane (tBu_2PPPh_2)

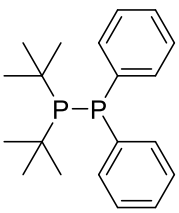

$^{31}P\{^1H\}$ (202 MHz, C_6D_6) δ 32.8 (*P*tBu_2, d, ^2J = 238 Hz), −24.2 (*P*Ph_2, d, ^2J = 238 Hz)

^1H (500 MHz, C_6D_6) δ 7.96–7.01 (ar, m, 10H), 1.13 (C(C*H*$_3$)$_3$, d, ^3J = 9.8 Hz, 18H)

Data concordant with previous literature. [203]

117 Pentaphenylcyclopentaphosphine (Ph_5P_5)

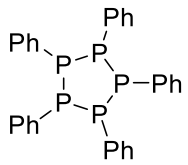

$^{31}P\{^1H\}$ (202 MHz, C_6D_6) δ −2.4–−4.9 (m)

^1H (500 MHz, C_6D_6) δ 7.90–6.52 (ar, m, 25H)

Data concordant with previous literature. [304]

118 Tetracyclohexylcyclotetraphosphine (Cy_4P_4)

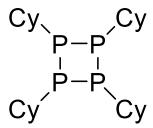

$^{31}P\{^1H\}$ (202 MHz, C_6D_6) δ −66.7 (s)

^1H (500 MHz, C_6D_6) δ 1.89–0.72 (cy, m, 44H)

Data concordant with previous literature. [304]

Chapter 8 – References

1. Media, N. *All Nobel Prizes in Chemistry*. 2021 5th May 2021]; Available from: https://www.nobelprize.org/prizes/lists/all-nobel-prizes-in-chemistry.
2. Twilton, J., et al., *The merger of transition metal and photocatalysis.* Nature Reviews Chemistry, 2017. **1**(7): p. 0052.
3. Hall, M. *The five most expensive metals and where they are mined*. Mining Technology 2020.
4. Tchounwou, P.B., et al., *Heavy Metal Toxicity and the Environment*, in *Molecular, Clinical and Environmental Toxicology: Volume 3: Environmental Toxicology*, A. Luch, Editor. 2012, Springer Basel: Basel. p. 133-164.
5. *ICH guideline Q3D (R1) on elemental impurities* E.M. Agency, Editor. 2019: The Netherlands.
6. Haynes, W.R., *CRC Handbook of Chemistry and Physics, 97th Edition (CRC Handbook of Chemistry & Physics)*. 97 ed. 2016: CRC Press.
7. Emsley, J., *Nature's Building Blocks: An A-Z Guide to the Elements*. 2011, New York: Oxford University Press.
8. Balaraman, E., et al., *Iron-catalyzed dehydrogenation reactions and their applications in sustainable energy and catalysis.* Catalysis Science & Technology, 2017. **7**(15): p. 3177-3195.
9. Cernak, T., et al., *The medicinal chemist's toolbox for late stage functionalization of drug-like molecules.* Chemical Society Reviews, 2016. **45**(3): p. 546-576.
10. Rana, S., et al., *Organic synthesis with the most abundant transition metal–iron: from rust to multitasking catalysts.* Chemical Society Reviews, 2021. **50**(1): p. 243-472.
11. Mako, T.L. and J.A. Byers, *Recent advances in iron-catalysed cross coupling reactions and their mechanistic underpinning.* Inorganic Chemistry Frontiers, 2016. **3**(6): p. 766-790.
12. Morris, R.H., *Asymmetric hydrogenation, transfer hydrogenation and hydrosilylation of ketones catalyzed by iron complexes.* Chemical Society Reviews, 2009. **38**(8): p. 2282-2291.
13. Ni, C., et al., *Reaction of a sterically encumbered iron(i) aryl/arene with organoazides: formation of an iron(v) bis(imide).* Chemical Communications, 2008(45): p. 6045-6047.
14. Ni, C., et al., *Univalent transition metal complexes of arenes stabilized by a bulky terphenyl ligand: differences in the stability of Cr(i), Mn(i) or Fe(i) complexes.* Chemical Communications, 2008(8): p. 1014-1016.
15. Fürstner, A., *Iron Catalysis in Organic Synthesis: A Critical Assessment of What It Takes To Make This Base Metal a Multitasking Champion.* ACS Central Science, 2016. **2**(11): p. 778-789.
16. Alonso, P.J. and J.I. Martínez, *Magnetic properties of a Kramers doublet. An univocal bridge between experimental results and theoretical predictions.* Journal of Magnetic Resonance, 2015. **255**: p. 1-14.
17. Wolford, N.J., A. Radovic, and M.L. Neidig, *C-Term magnetic circular dichroism (MCD) spectroscopy in paramagnetic transition metal and f-element organometallic chemistry.* Dalton Transactions, 2021. **50**(2): p. 416-428.
18. Nasu, S., *General Introduction to Mössbauer Spectroscopy*, in *Mössbauer Spectroscopy: Tutorial Book*, Y. Yoshida and G. Langouche, Editors. 2013, Springer Berlin Heidelberg: Berlin, Heidelberg. p. 1-22.
19. Daifuku, S.L., et al., *A Combined Mössbauer, Magnetic Circular Dichroism, and Density Functional Theory Approach for Iron Cross-Coupling Catalysis: Electronic Structure, In Situ Formation, and Reactivity of Iron-Mesityl-Bisphosphines.* Journal of the American Chemical Society, 2014. **136**(25): p. 9132-9143.

20. Loup, J., et al., *Mössbauer and mass spectrometry support for iron(ii) catalysts in enantioselective C–H activation.* Dalton Transactions, 2019. **48**(16): p. 5135-5139.
21. Chen, W.-T., et al., *Theoretical Analysis of Fe K-Edge XANES on Iron Pentacarbonyl.* ACS Omega, 2020. **5**(10): p. 4991-5000.
22. Chang, Q., et al., *XAFS Studies of Fe−SiO2 Fischer-Tropsch Catalyst During Activation in CO, H2, and Synthesis Gas.* ChemCatChem, 2019. **11**(8): p. 2206-2216.
23. Sears, J.D., P.G.N. Neate, and M.L. Neidig, *Intermediates and Mechanism in Iron-Catalyzed Cross-Coupling.* Journal of the American Chemical Society, 2018. **140**(38): p. 11872-11883.
24. *Metal Complexes of Schiff Bases and β-Ketoamines*, in *Progress in Inorganic Chemistry*. p. 83-214.
25. Tsai, Y.-C., *The chemistry of univalent metal β-diketiminates.* Coordination Chemistry Reviews, 2012. **256**(5): p. 722-758.
26. Sgro, M.J. and D.W. Stephan, *Non-innocent reactivity of bis-phosphinimine pincer ligands in palladium complexes.* Dalton Transactions, 2011. **40**(11): p. 2419-2421.
27. Camp, C. and J. Arnold, *On the non-innocence of "Nacnacs": ligand-based reactivity in β-diketiminate supported coordination compounds.* Dalton Transactions, 2016. **45**(37): p. 14462-14498.
28. Roddick, D.M., et al., *Coordinatively unsaturated tris(trimethylsilyl)silyl complexes of chromium, manganese, and iron.* Journal of the American Chemical Society, 1987. **109**(3): p. 945-946.
29. Bhutto, S.M. and P.L. Holland, *Dinitrogen Activation and Functionalization Using β-Diketiminate Iron Complexes.* European Journal of Inorganic Chemistry, 2019. **2019**(14): p. 1861-1869.
30. Holland, P.L., et al., *Electronically Unsaturated Three-Coordinate Chloride and Methyl Complexes of Iron, Cobalt, and Nickel.* Journal of the American Chemical Society, 2002. **124**(48): p. 14416-14424.
31. Sciarone, T.J.J., A. Meetsma, and B. Hessen, *Neutral and cationic Fe(II) β-diketiminate complexes.* Inorganica Chimica Acta, 2006. **359**(6): p. 1815-1825.
32. Gibson, V.C., et al., *A well-defined iron(ii) alkoxide initiator for the controlled polymerisation of lactide.* J. Chem. Soc.{,} Dalton Trans., 2002(23): p. 4321-4322.
33. McWilliams, S.F., et al., *Effects of N2 Binding Mode on Iron-Based Functionalization of Dinitrogen to Form an Iron(III) Hydrazido Complex.* Journal of the American Chemical Society, 2018. **140**(27): p. 8586-8598.
34. Bar, A.K., et al., *Coupling of Nitric Oxide and Release of Nitrous Oxide from Rare-Earth-Dinitrosyliron Complexes.* Journal of the American Chemical Society, 2020. **142**(9): p. 4104-4107.
35. Tan, G., et al., *The Charge Transfer Approach to Heavier Main-Group Element Radicals in Transition-Metal Complexes.* Angewandte Chemie International Edition, 2017. **56**(41): p. 12741-12745.
36. Beaumier, E.P., et al., *Modern applications of low-valent early transition metals in synthesis and catalysis.* Nature Reviews Chemistry, 2019. **3**(1): p. 15-34.
37. Biyikal, M., et al., *β-Diketiminate Zinc Complexes for the Hydroamination of Alkynes.* European Journal of Inorganic Chemistry, 2010. **2010**(7): p. 1070-1081.
38. Casey, K.C., J.K. Appiah, and J.R. Robinson, *Low-Symmetry β-Diketimine Aryloxide Rare-Earth Complexes: Flexible, Reactive, and Selective.* Inorganic Chemistry, 2020. **59**(20): p. 14827-14837.
39. Vela, J., et al., *Synthesis and Reactivity of Low-Coordinate Iron(II) Fluoride Complexes and Their Use in the Catalytic Hydrodefluorination of Fluorocarbons.* Journal of the American Chemical Society, 2005. **127**(21): p. 7857-7870.

40. Colonna, P., et al., *Alkene Hydroamination via Earth-Abundant Transition Metal (Iron, Cobalt, Copper and Zinc) Catalysis: A Mechanistic Overview.* Advanced Synthesis & Catalysis, 2020. **362**(8): p. 1550-1563.
41. Bernoud, E., et al., *Well-Defined Four-Coordinate Iron(II) Complexes For Intramolecular Hydroamination of Primary Aliphatic Alkenylamines.* Angewandte Chemie International Edition, 2014. **53**(19): p. 4930-4934.
42. Lepori, C., R. Guillot, and J. Hannedouche, *C1-symmetric β-Diketiminatoiron(II) Complexes for Hydroamination of Primary Alkenylamines.* Advanced Synthesis & Catalysis, 2019. **361**(4): p. 714-719.
43. Lepori, C., et al., *Well-Defined β-Diketiminatocobalt(II) Complexes for Alkene Cyclohydroamination of Primary Amines.* ACS Catalysis, 2018. **8**(5): p. 4446-4451.
44. Espinal-Viguri, M., et al., *Hydrophosphination of Unactivated Alkenes and Alkynes Using Iron(II): Catalysis and Mechanistic Insight.* ACS Catalysis, 2016. **6**(11): p. 7892-7897.
45. K, K.A., et al., *Facile, Catalytic Dehydrocoupling of Phosphines Using β-Diketiminate Iron(II) Complexes.* Chemistry – A European Journal. **21**(45): p. 15960-15963.
46. Gasperini, D., et al., *Seeking Heteroatom-Rich Compounds: Synthetic and Mechanistic Studies into Iron Catalyzed Dehydrocoupling of Silanes.* ACS Catalysis, 2020.
47. Coles, N.T., M.F. Mahon, and R.L. Webster, *Phosphine- and Amine-Borane Dehydrocoupling Using a Three-Coordinate Iron(II) β-Diketiminate Precatalyst.* Organometallics, 2017. **36**(11): p. 2262-2268.
48. McWilliams, S.F., et al., *Coupling dinitrogen and hydrocarbons through aryl migration.* Nature, 2020. **584**(7820): p. 221-226.
49. Crockett, M.P., et al., *Rational Design of an Iron-Based Catalyst for Suzuki–Miyaura Cross-Couplings Involving Heteroaromatic Boronic Esters and Tertiary Alkyl Electrophiles.* Angewandte Chemie International Edition, 2020. **59**(13): p. 5392-5397.
50. Ding, K., et al., *Coordination of N-methylpyrrolidone to iron(II).* Journal of Organometallic Chemistry, 2009. **694**(26): p. 4204-4208.
51. Cowley, R.E., et al., *Mechanism of Catalytic Nitrene Transfer Using Iron(I)–Isocyanide Complexes.* Organometallics, 2013. **32**(19): p. 5289-5298.
52. Kim, D., et al., *Highly Z-Selective Double Bond Transposition in Simple Alkenes and Allylarenes through a Spin-Accelerated Allyl Mechanism.* Journal of the American Chemical Society, 2021. **143**(8): p. 3070-3074.
53. Schröder, G., J.F.M. Oth, and R. Merényi, *Molecules Undergoing Fast, Reversible Valence-Bond Isomerization. (Molecules with Fluctuating Bonds).* Angewandte Chemie International Edition in English, 1965. **4**(9): p. 752-761.
54. Van Roosmalen, A.J. and J.C. Mol, *Active centers for the metathesis and isomerization of alkenes on tungsten-oxide/silica catalysts.* Journal of Catalysis, 1982. **78**(1): p. 17-23.
55. Grubbs, R.H., *The Olefin Metathesis Reaction*, in *Progress in Inorganic Chemistry*. 1978. p. 1-50.
56. Molloy, J.J., T. Morack, and R. Gilmour, *Positional and Geometrical Isomerisation of Alkenes: The Pinnacle of Atom Economy.* Angewandte Chemie International Edition, 2019. **58**(39): p. 13654-13664.
57. Prosser, T.J., *The Rearrangement of Allyl Ethers to Propenyl Ethers.* Journal of the American Chemical Society, 1961. **83**(7): p. 1701-1704.
58. Cram, D.J. and R.T. Uyeda, *Electrophilic Substitution at Saturated Carbon. XXII. Intramolecular Hydrogen Transfer Reactions in Base-Catalyzed Allylic Rearrangements.* Journal of the American Chemical Society, 1964. **86**(24): p. 5466-5477.
59. Hartung, C.G., et al., *A Base-Catalyzed Domino-Isomerization–Hydroamination Reaction—A New Synthetic Route to Amphetamines.* Tetrahedron, 2000. **56**(29): p. 5157-5162.

60. Saha, A. and D. Nasipuri, *A stereoselective synthesis of (±)-veadeiroic acid and (±)-veadeirol - two novel diterpenes with cleistanthane skeleton.* Tetrahedron Letters, 1991. **32**(27): p. 3213-3214.
61. Larionov, E., H. Li, and C. Mazet, *Well-defined transition metal hydrides in catalytic isomerizations.* Chemical Communications, 2014. **50**(69): p. 9816-9826.
62. Sen, A. and T.W. Lai, *Mechanism of palladium(II)-catalyzed carbon-carbon double bond isomerization in olefins.* Inorganic Chemistry, 1984. **23**(20): p. 3257-3258.
63. Capaldo, L., L.L. Quadri, and D. Ravelli, *Photocatalytic hydrogen atom transfer: the philosopher's stone for late-stage functionalization?* Green Chemistry, 2020. **22**(11): p. 3376-3396.
64. Shevick, S.L., et al., *Catalytic hydrogen atom transfer to alkenes: a roadmap for metal hydrides and radicals.* Chemical Science, 2020. **11**(46): p. 12401-12422.
65. Jolly, P.W., F.G.A. Stone, and K. Mackenzie, *1190. Chemistry of the metal carbonyls. Part XXXII. Isomerisation of allyl compounds and the dimerisation of norbornadiene.* Journal of the Chemical Society (Resumed), 1965(0): p. 6416-6420.
66. Bright, A., et al., *Products formed from rhodium trichloride trihydrate and allyl alcohol or diallyl ether; the crystal and molecular structure of [Rh2Cl4(C6H11O)2],CH3OH.* Journal of the Chemical Society D: Chemical Communications, 1971(13): p. 712-713.
67. Baudry, D., M. Ephritikhine, and H. Felkin, *Isomerisation of allyl ethers catalysed by the cationic iridium complex [Ir(cyclo-octa-1,5-diene)(PMePh2)2]PF6. A highly stereoselective route to trans-propenyl ethers.* Journal of the Chemical Society, Chemical Communications, 1978(16): p. 694-695.
68. Yamamoto, Y., R. Fujikawa, and N. Miyaura, *Stereoselective Isomerization of Unsymmetrical Diallyl Ethers to Allyl (E)-Vinyl Ethers by a Cationic Iridium Catalyst.* Synthetic Communications, 2000. **30**(13): p. 2383-2391.
69. Massad, I. and I. Marek, *Alkene Isomerization through Allylmetals as a Strategic Tool in Stereoselective Synthesis.* ACS Catalysis, 2020. **10**(10): p. 5793-5804.
70. Donohoe, T.J., T.J.C. O'Riordan, and C.P. Rosa, *Ruthenium-Catalyzed Isomerization of Terminal Olefins: Applications to Synthesis.* Angewandte Chemie International Edition, 2009. **48**(6): p. 1014-1017.
71. Huang, R.-Z., et al., *Rhodium-Catalyzed Enantioconvergent Isomerization of Homoallylic and Bishomoallylic Secondary Alcohols.* Journal of the American Chemical Society, 2018. **140**(44): p. 14647-14654.
72. Negishi, E.-c., *Palladium-Catalyzed Isomerization of Alkenes, Alkynes, and Related Compounds Without Skeletal Rearrangements*, in *Handbook of Organopalladium Chemistry for Organic Synthesis*. p. 2783-2788.
73. Davies, N.R., *Palladium-catalysed Olefine Isomerization.* Nature, 1964. **201**(4918): p. 490-491.
74. Fan, J., et al., *Palladium catalyzed isomerization of alkenes: a pronounced influence of an o-phenol hydroxyl group.* Organic & Biomolecular Chemistry, 2009. **7**(15): p. 3168-3172.
75. Kocen, A.L., et al., *Alkene Isomerization by "Sandwich" Diimine-Palladium Catalysts.* Organometallics, 2017. **36**(4): p. 787-790.
76. Kocen, A.L., M. Brookhart, and O. Daugulis, *Palladium-catalysed alkene chain-running isomerization.* Chemical Communications, 2017. **53**(72): p. 10010-10013.
77. Guo, C. and X. Lu, *A facile and stereoselective synthesis of dienediones and 6-oxo-2,4-dienoic esters.* Tetrahedron Letters, 1992. **33**(25): p. 3659-3662.
78. Danishefsky, S., et al., *An approach to the synthesis of the naphthyridinomycin alkaloids: The synthesis of two subunits.* Tetrahedron Letters, 1984. **25**(38): p. 4199-4202.
79. Danishefsky, S.J., et al., *Total synthesis of quinocarcinol methyl ester.* Journal of the American Chemical Society, 1985. **107**(5): p. 1421-1423.

80. Danishefsky, S., B.J. Uang, and G. Quallich, *Total synthesis of vineomycin B2 aglycon.* Journal of the American Chemical Society, 1984. **106**(8): p. 2453-2455.
81. Gauthier, D., et al., *In Situ Generated Bulky Palladium Hydride Complexes as Catalysts for the Efficient Isomerization of Olefins. Selective Transformation of Terminal Alkenes to 2-Alkenes.* Journal of the American Chemical Society, 2010. **132**(23): p. 7998-8009.
82. Hanna, S., T.W. Butcher, and J.F. Hartwig, *Contra-thermodynamic Olefin Isomerization by Chain-Walking Hydrofunctionalization and Formal Retro-hydrofunctionalization.* Organic Letters, 2019. **21**(17): p. 7129-7133.
83. Masarwa, A., et al., *Merging allylic carbon–hydrogen and selective carbon–carbon bond activation.* Nature, 2014. **505**(7482): p. 199-203.
84. Nelson, S.G., C.J. Bungard, and K. Wang, *Catalyzed Olefin Isomerization Leading to Highly Stereoselective Claisen Rearrangements of Aliphatic Allyl Vinyl Ethers.* Journal of the American Chemical Society, 2003. **125**(43): p. 13000-13001.
85. Sommer, H., T. Weissbrod, and I. Marek, *A Tandem Iridium-Catalyzed "Chain-Walking"/Cope Rearrangement Sequence.* ACS Catalysis, 2019. **9**(3): p. 2400-2406.
86. Shimizu, H., et al., *Rhodium-Catalyzed Reaction of 1-Alkenylboronates with Aldehydes Leading to Allylation Products.* Angewandte Chemie International Edition, 2011. **50**(48): p. 11465-11469.
87. Grotjahn, D.B., et al., *Extensive Isomerization of Alkenes Using a Bifunctional Catalyst: An Alkene Zipper.* Journal of the American Chemical Society, 2007. **129**(31): p. 9592-9593.
88. Reihlen, H., et al., *Über Carbonyle und Nitrosyle. IV.* Justus Liebigs Annalen der Chemie, 1930. **482**(1): p. 161-182.
89. Pearson, A.J., *Tricarbonyl(diene)iron complexes: synthetically useful properties.* Accounts of Chemical Research, 1980. **13**(12): p. 463-469.
90. Frankel, E.N., E.A. Emken, and V.L. Davison, *Isomerization of unsaturated fatty esters by iron pentacarbonyl. Preparation of iron tricarbonyl complexes of polyunsaturated fats.* Journal of the American Oil Chemists Society, 1966. **43**(5): p. 307-311.
91. Fleckner, H., F.W. Grevels, and D. Hess, *Tricarbonylbis(.eta.2-cis-cyclooctene)iron: photochemical synthesis of a versatile tricarbonyliron source for olefin isomerization and preparative applications.* Journal of the American Chemical Society, 1984. **106**(7): p. 2027-2032.
92. Rodriquez, J., P. Brun, and B. Waegell, *Synthesis of substituted iron carbonyl conjugated dienyl complexes from 4-vinylcyclohexenes under kinetic or-thermodynamic control.* Tetrahedron Letters, 1986. **27**(7): p. 835-836.
93. Cherkaoui, H., M. Soufiaoui, and R. Grée, *From allylic alcohols to saturated carbonyls using Fe(CO)5 as catalyst: scope and limitation studies and preparation of two perfume components.* Tetrahedron, 2001. **57**(12): p. 2379-2383.
94. Branchadell, V., C. Crévisy, and R. Grée, *Theoretical Study on the Mechanism of Iron Carbonyls Mediated Isomerization of Allylic Alcohols to Saturated Carbonyls.* Chemistry – A European Journal, 2003. **9**(9): p. 2062-2067.
95. Sawyer, K.R., et al., *Mechanism for Iron-Catalyzed Alkene Isomerization in Solution.* Organometallics, 2008. **27**(17): p. 4370-4379.
96. Casey, C.P. and C.R. Cyr, *Iron carbonyl catalyzed isomerization of 3-ethyl-1-pentene. Multiple olefin isomerizations via a .pi.-allyl metal hydride intermediate.* Journal of the American Chemical Society, 1973. **95**(7): p. 2248-2253.
97. Crivello, J.V. and S. Kong, *Efficient Isomerization of Allyl Ethers and Related Compounds Using Pentacarbonyliron.* The Journal of Organic Chemistry, 1998. **63**(19): p. 6745-6748.
98. Sergeyev, S. and M. Hesse, *A New Convenient Method for the Preparation of Enamides from N-Allylamides.* Synlett, 2002. **2002**(08): p. 1313-1317.

99. Chase, H.M., et al., *Combined 1H NMR and DFT study of the solvent effects on the iron pentacarbonyl-catalyzed photo-assisted isomerization of allyl alcohol.* Journal of Physical Organic Chemistry, 2013. **26**(4): p. 322-326.
100. Jennerjahn, R., et al., *Benign Catalysis with Iron: Unique Selectivity in Catalytic Isomerization Reactions of Olefins.* ChemSusChem, 2012. **5**(4): p. 734-739.
101. Chen, C., et al., *Z-Selective Alkene Isomerization by High-Spin Cobalt(II) Complexes.* Journal of the American Chemical Society, 2014. **136**(3): p. 945-955.
102. Schmidt, A., A.R. Nödling, and G. Hilt, *An Alternative Mechanism for the Cobalt-Catalyzed Isomerization of Terminal Alkenes to (Z)-2-Alkenes.* Angewandte Chemie International Edition, 2015. **54**(3): p. 801-804.
103. Crossley, S.W.M., F. Barabé, and R.A. Shenvi, *Simple, Chemoselective, Catalytic Olefin Isomerization.* Journal of the American Chemical Society, 2014. **136**(48): p. 16788-16791.
104. Li, G., et al., *Radical Isomerization and Cycloisomerization Initiated by H• Transfer.* Journal of the American Chemical Society, 2016. **138**(24): p. 7698-7704.
105. Liu, X., et al., *Cobalt-Catalyzed Regioselective Olefin Isomerization Under Kinetic Control.* Journal of the American Chemical Society, 2018. **140**(22): p. 6873-6882.
106. Zhang, S., et al., *Cobalt(II)-Catalyzed Stereoselective Olefin Isomerization: Facile Access to Acyclic Trisubstituted Alkenes.* Journal of the American Chemical Society, 2020. **142**(19): p. 8910-8917.
107. Liu, H., et al., *Cobalt-Catalyzed Z to E Isomerization of Alkenes: An Approach to (E)-β-Substituted Styrenes.* Organic Letters, 2020. **22**(3): p. 1193-1198.
108. Liu, H., et al., *Cobalt-Catalyzed E-Selective Isomerization of Alkenes with a Phosphine-Amido-Oxazoline Ligand.* ACS Omega, 2020. **5**(20): p. 11655-11670.
109. Mayer, M., A. Welther, and A. Jacobi von Wangelin, *Iron-Catalyzed Isomerizations of Olefins.* ChemCatChem, 2011. **3**(10): p. 1567-1571.
110. Fürstner, A., et al., *Preparation, Structure, and Reactivity of Nonstabilized Organoiron Compounds. Implications for Iron-Catalyzed Cross Coupling Reactions.* Journal of the American Chemical Society, 2008. **130**(27): p. 8773-8787.
111. Cahard, D., et al., *Iron(II) complexes are suitable catalysts for the isomerization of trifluoromethylated allylic alcohols. Synthesis of trifluoromethylated dihydrochalcones.* Journal of Fluorine Chemistry, 2013. **155**: p. 78-82.
112. Chong, T.S., S.T. Tan, and W.Y. Fan, *FTIR Studies of Iron–Carbonyl Intermediates in Allylic Alcohol Photoisomerization.* Chemistry – A European Journal, 2006. **12**(19): p. 5128-5133.
113. Xia, T., et al., *Isomerization of Allylic Alcohols to Ketones Catalyzed by Well-Defined Iron PNP Pincer Catalysts.* Chemistry – A European Journal, 2018. **24**(16): p. 4043-4049.
114. Latham, D.E., et al., *One-Pot Conversion of Allylic Alcohols to α-Methyl Ketones via Iron-Catalyzed Isomerization–Methylation.* Organic Letters, 2019. **21**(19): p. 7914-7918.
115. Werncke, C.G. and I. Müller, *The ambiguous behaviour of diphosphines towards the quasilinear iron(i) complex [Fe(N(SiMe3)2)2]− – between inertness, P–C bond cleavage and C–C double bond isomerisation.* Chemical Communications, 2020. **56**(15): p. 2268-2271.
116. Li, H., et al., *Iron-catalysed tandem isomerisation/hydrosilylation reaction of allylic alcohols with amines.* RSC Advances, 2014. **4**(49): p. 25892-25897.
117. Pereira, S. and M. Srebnik, *Transition Metal-Catalyzed Hydroboration of and CCl4 Addition to Alkenes.* Journal of the American Chemical Society, 1996. **118**(4): p. 909-910.
118. Lata, C.J. and C.M. Crudden, *Dramatic Effect of Lewis Acids on the Rhodium-Catalyzed Hydroboration of Olefins.* Journal of the American Chemical Society, 2010. **132**(1): p. 131-137.
119. Yamamoto, Y., et al., *Iridium-catalyzed hydroboration of alkenes with pinacolborane.* Tetrahedron, 2004. **60**(47): p. 10695-10700.

120. Edwards, D.R., C.M. Crudden, and K. Yam, *One-Pot Carbon Monoxide-Free Hydroformylation of Internal Olefins to Terminal Aldehydes.* Advanced Synthesis & Catalysis, 2005. **347**(1): p. 50-54.
121. Obligacion, J.V. and P.J. Chirik, *Bis(imino)pyridine Cobalt-Catalyzed Alkene Isomerization–Hydroboration: A Strategy for Remote Hydrofunctionalization with Terminal Selectivity.* Journal of the American Chemical Society, 2013. **135**(51): p. 19107-19110.
122. Ogawa, T., et al., *Cobalt- and Iron-Catalyzed Isomerization–Hydroboration of Branched Alkenes: Terminal Hydroboration with Pinacolborane and 1,3,2-Diazaborolanes.* Organometallics, 2017. **36**(2): p. 417-423.
123. Macaulay, C.M., et al., *Alkene Isomerization–Hydroboration Catalyzed by First-Row Transition-Metal (Mn, Fe, Co, and Ni) N-Phosphinoamidinate Complexes: Origin of Reactivity and Selectivity.* ACS Catalysis, 2018. **8**(11): p. 9907-9925.
124. Chen, X., et al., *Asymmetric remote C-H borylation of internal alkenes via alkene isomerization.* Nature Communications, 2018. **9**(1): p. 3939.
125. Yu, X., et al., *Site-selective alkene borylation enabled by synergistic hydrometallation and borometallation.* Nature Catalysis, 2020. **3**(7): p. 585-592.
126. Sandler, S.R., et al., *ALLENES.* Sourcebook of Advanced Organic Laboratory Preparations, 1992: p. 194-196.
127. Rivera-Fuentes, P. and F. Diederich, *Allenes in Molecular Materials.* Angewandte Chemie International Edition, 2012. **51**(12): p. 2818-2828.
128. Hoffmann-Röder, A. and N. Krause, *Synthesis and Properties of Allenic Natural Products and Pharmaceuticals.* Angewandte Chemie International Edition, 2004. **43**(10): p. 1196-1216.
129. Yu, S. and S. Ma, *How easy are the syntheses of allenes?* Chem. Commun., 2011. **47**(19): p. 5384-5418.
130. Liu, L., R.M. Ward, and J.M. Schomaker, *Mechanistic Aspects and Synthetic Applications of Radical Additions to Allenes.* Chemical Reviews, 2019. **119**(24): p. 12422-12490.
131. Li, W. and J. Zhang, *4.05 Addition of HX Reagents to Alkenes, Alkynes, and Allenes without Transition Metal.* Comprehensive Organic Synthesis II, 2014: p. 342-391.
132. Yu, Z.-X., et al., *Origins of Differences in Reactivities of Alkenes, Alkynes, and Allenes in [Rh(CO)2Cl]2-Catalyzed (5 + 2) Cycloaddition Reactions with Vinylcyclopropanes.* Journal of the American Chemical Society, 2008. **130**(8): p. 2378-2379.
133. Endo, T. and I. Tomita, *Novel polymerization methods for allene derivatives.* Progress in Polymer Science, 1997. **22**(3): p. 565-600.
134. Yu, Z.-P., et al., *Polyallene-block-polythiophene-block-polyallene Copolymers: One-Pot Synthesis, Helical Assembly, and Multiresponsiveness.* Macromolecules, 2016. **49**(4): p. 1180-1190.
135. Zhu, Y.-Y., et al., *Synthesis and Chiroptical Properties of Helical Polyallenes Bearing Chiral Amide Pendants.* Macromolecules, 2014. **47**(20): p. 7021-7029.
136. Baker Jr, W.P., *Polymerization of allene by organometallic initiation.* Journal of Polymer Science Part A: General Papers, 1963. **1**(2): p. 655-670.
137. Leland, J., J. Boucher, and K. Anderson, *Polymerization of phenylallene, α-methylphenylallene, and 1-(1,2-propadienyl)pyrrolidinone.* Journal of Polymer Science: Polymer Chemistry Edition, 1977. **15**(11): p. 2785-2788.
138. Yokozawa, T., N. Ito, and T. Endo, *Radical Polymerization Behavior of Phenylallene. Synthesis of Functional Polymer Containing Styryl Moiety on the Backbone.* Chemistry Letters, 1988. **17**(12): p. 1955-1958.
139. Takagi, K., I. Tomita, and T. Endo, *A Novel Living Coordination Polymerization of Phenylallene Derivatives by π-Allylnickel Catalyst.* Macromolecules, 1997. **30**(24): p. 7386-7390.

140. Yamauchi, A., et al., *Well-defined polymer microspheres formed by living dispersion polymerization: precisely functionalized crosslinked polymer microspheres from monomers possessing cumulated double bonds.* NPG Asia Materials, 2016. **8**(9): p. e307-e307.
141. Takagi, K., I. Tomita, and T. Endo, *Block copolymerization of alkoxyallenes with phenylallene by the living coordination system with π-allylnickel catalyst.* Polymer Bulletin, 1997. **39**(6): p. 685-692.
142. Nakagawa, K. and I. Tomita, *Synthesis of Poly(p-phenylene-vinylene) with Chiral Higher-Order Structure from Simple Monomers by Three-Component Coupling Polymerization.* Macromolecules, 2007. **40**(26): p. 9212-9216.
143. Suzuki, M., et al., *Ni-Catalyzed Living Coordination Polymerization of Allenes Having Si-Based Functional Groups.* Polymer Journal, 1999. **31**(11): p. 1021-1024.
144. Lin, F., et al., *Highly 2,3-Selective Polymerization of Phenylallene and Its Derivatives with Rare-Earth Metal Catalysts: From Amorphous to Crystalline Products.* Angewandte Chemie International Edition, 2017. **56**(46): p. 14653-14657.
145. Ahmed, M., et al., *Allene Cross-Metathesis: Synthesis of 1,3-Disubstituted Allenes.* Organic Letters, 2000. **2**(4): p. 551-553.
146. Choi, J.-C., et al., *Polymerization of arylallenes catalyzed by organo-rhodium(I) and -cobalt (I) complexes to give structurally regulated high-mass polymers.* Applied Organometallic Chemistry, 1997. **11**(12): p. 957-961.
147. Ma, S., *Electrophilic Addition and Cyclization Reactions of Allenes.* Accounts of Chemical Research, 2009. **42**(10): p. 1679-1688.
148. Huo, J., et al., *A minireview of hydroamination catalysis: alkene and alkyne substrate selective, metal complex design.* BMC Chemistry, 2019. **13**(1): p. 89-89.
149. Ayinla, R.O. and L.L. Schafer, *Intermolecular hydroamination of oxygen-substituted allenes. New routes for the synthesis of N,O-chelated zirconium and titanium amido complexes.* Dalton Transactions, 2011. **40**(30): p. 7769-7776.
150. Blieck, R., et al., *Copper-Catalyzed Hydroamination of Terminal Allenes.* Organic Letters, 2016. **18**(6): p. 1482-1485.
151. Alessandro Perego, L., et al., *Copper-Catalyzed Hydroamination of Allenes: from Mechanistic Understanding to Methodology Development.* ACS Catalysis, 2017. **7**(7): p. 4253-4264.
152. Cooke, M.L., K. Xu, and B. Breit, *Enantioselective Rhodium-Catalyzed Synthesis of Branched Allylic Amines by Intermolecular Hydroamination of Terminal Allenes.* Angewandte Chemie International Edition, 2012. **51**(43): p. 10876-10879.
153. C. Brown, H., R. Liotta, and G. W. Kramer, *Hydroboration. 51. Hydroboration of representative allenes with 9-borabicyclo[3.3.1]nonane. An exceptional directive effect providing a direct synthesis of B-allyl-9-borabicyclo[3.3.1]nonane derivatives.* Journal of the American Chemical Society, 1979. **101**(11): p. 2966-2970.
154. Devaprabhakara, D. and P.D. Gardner, *Hydroboration of Allenes.* Journal of the American Chemical Society, 1963. **85**(10): p. 1458-1460.
155. Kister, J., et al., *Stereoselective Synthesis of γ-Substituted (Z)-Allylic Boranes via Kinetically Controlled Hydroboration of Allenes with 10-TMS-9-borabicyclo[3.3.2]decane.* Journal of the American Chemical Society, 2009. **131**(40): p. 14174-14175.
156. Nagashima, Y., et al., *Stereodivergent Hydroboration of Allenes.* Chemistry – An Asian Journal, 2018. **13**(8): p. 1024-1028.
157. Semba, K., et al., *Highly Selective Copper-Catalyzed Hydroboration of Allenes and 1,3-Dienes.* Chemistry – A European Journal, 2013. **19**(22): p. 7125-7132.
158. Cai, Y., et al., *Access to Functionalized E-Allylsilanes and E-Alkenylsilanes through Visible-Light-Driven Radical Hydrosilylation of Mono- and Disubstituted Allenes.* Organic Letters, 2019. **21**(24): p. 9836-9840.

159. Wang, C., W.J. Teo, and S. Ge, *Access to stereodefined (Z)-allylsilanes and (Z)-allylic alcohols via cobalt-catalyzed regioselective hydrosilylation of allenes.* Nature Communications, 2017. **8**(1): p. 2258-2258.
160. Jiang, Y.-N., et al., *A conjugated microporous polymer as a recyclable heterogeneous ligand for highly efficient regioselective hydrosilylation of allenes.* Chem. Commun., 2020. **56**(10): p. 1597-1600.
161. Eto, M., *Functions of Phosphorus Moiety in Agrochemical Molecules.* Bioscience, Biotechnology, and Biochemistry, 1997. **61**(1): p. 1-11.
162. Yu, H., et al., *Development and Clinical Application of Phosphorus-Containing Drugs.* Medicine in Drug Discovery, 2020. **8**: p. 100063.
163. Pringle, P.G. and M.B. Smith, *Platinum(0)-catalysed hydrophosphination of acrylonitrile.* Journal of the Chemical Society, Chemical Communications, 1990(23): p. 1701-1702.
164. Bange, C.A. and R. Waterman, *Challenges in Catalytic Hydrophosphination.* Chemistry – A European Journal, 2016. **22**(36): p. 12598-12605.
165. Koshti, V., S. Gaikwad, and S.H. Chikkali, *Contemporary avenues in catalytic PH bond addition reaction: A case study of hydrophosphination.* Coordination Chemistry Reviews, 2014. **265**: p. 52-73.
166. Rosenberg, L., *Mechanisms of Metal-Catalyzed Hydrophosphination of Alkenes and Alkynes.* ACS Catalysis, 2013. **3**(12): p. 2845-2855.
167. Swamy, K.C.K., et al., *Reactivity of allenylphosphonates/allenylphosphine oxides – some new addition/cycloaddition and cyclization pathways.* Pure and Applied Chemistry, 2019. **91**(5).
168. Guo, H., et al., *Neighboring Group Participation of Phosphine Oxide Functionality in the Highly Regio- and Stereoselective Iodohydroxylation of 1,2-Allenylic Diphenyl Phosphine Oxides.* The Journal of Organic Chemistry, 2008. **73**(20): p. 7934-7938.
169. Bhuvan Kumar, N.N., et al., *Allenylphosphonates with a 1,3,2-dioxaphosphorinane ring: Synthesis, structures, stability and utility.* Journal of Chemical Sciences, 2009. **121**(1): p. 23-36.
170. Chakravarty, M. and K. C. Kumara Swamy, *Palladium-Catalyzed Coupling of Allenylphosphonates, Phenylallenes, and Allenyl Esters: Remarkable Salt Effect and Routes to Novel Benzofurans and Isocoumarins.* The Journal of Organic Chemistry, 2006. **71**(24): p. 9128-9138.
171. Srinivas, V., K.V. Sajna, and K.C. Kumara Swamy, *Zn(OTf)2 catalyzed addition–cyclization reaction of allenylphosphine oxides with propargyl alcohol-unexpected formation of 2,5-dimethylenetetrahydrofurans and 2-substituted furans.* Tetrahedron Letters, 2011. **52**(41): p. 5323-5326.
172. Eren, N.M., et al., *Synthesis, Structure, and Solution Studies of Lithiated Allylic Phosphines and Phosphine Oxides.* Organometallics, 2020. **39**(11): p. 2080-2090.
173. Bravo-Altamirano, K., Z. Huang, and J.-L. Montchamp, *Palladium-catalyzed phosphorus–carbon bond formation: cross-coupling reactions of alkyl phosphinates with aryl, heteroaryl, alkenyl, benzylic, and allylic halides and triflates.* Tetrahedron, 2005. **61**(26): p. 6315-6329.
174. Bravo-Altamirano, K. and J.-L. Montchamp, *Palladium-Catalyzed Dehydrative Allylation of Hypophosphorous Acid with Allylic Alcohols.* Organic Letters, 2006. **8**(18): p. 4169-4171.
175. Mitchell, T.N. and K. Heesche, *Preparation of vinylphosphines by means of free radical addition of diphenylphosphine to alkynes and allenes.* Journal of Organometallic Chemistry, 1991. **409**(1-2): p. 163-170.
176. Takaki, K., et al., *Intermolecular Hydrophosphination of Alkynes and Related Carbon−Carbon Multiple Bonds Catalyzed by Organoytterbiums.* The Journal of Organic Chemistry, 2003. **68**(17): p. 6554-6565.

177. Busacca, C.A., et al., *Ambient Temperature Hydrophosphination of Internal, Unactivated Alkynes and Allenyl Phosphineoxides with Phosphine Borane Complexes.* Organic Letters, 2009. **11**(24): p. 5594-5597.
178. Bravo-Altamirano, K., I. Abrunhosa-Thomas, and J.-L. Montchamp, *Palladium-Catalyzed Reactions of Hypophosphorous Compounds with Allenes, Dienes, and Allylic Electrophiles: Methodology for the Synthesis of Allylic H-Phosphinates.* The Journal of Organic Chemistry, 2008. **73**(6): p. 2292-2301.
179. Ribière, P., et al., *NiCl2-Catalyzed Hydrophosphinylation.* The Journal of Organic Chemistry, 2005. **70**(10): p. 4064-4072.
180. Zhao, C.-Q., L.-B. Han, and M. Tanaka, *Palladium-Catalyzed Hydrophosphorylation of Allenes Leading to Regio- and Stereoselective Formation of Allylphosphonates.* Organometallics, 2000. **19**(21): p. 4196-4198.
181. Huang, Y., et al., *Palladium Template Promoted Asymmetric Synthesis of 1,2-Diphosphines by Hydrophosphination of Functionalized Allenes.* Organometallics, 2010. **29**(3): p. 536-542.
182. Hu, S., et al., *Palladium-catalyzed C–P cross-coupling of allenic alcohols with H-phosphonates leading to 2-phosphinoyl-1,3-butadienes.* Chemical Communications, 2021. **57**(3): p. 339-342.
183. Amedjkouh, M., et al., *SYNTHESIS AND CYCLIZATION OF PHOSPHORYLATED β-ALLENIC AMINES.* Phosphorus, Sulfur, and Silicon and the Related Elements, 1997. **126**(1): p. 53-64.
184. Zhao, R., et al., *TfOH-Catalyzed Phosphinylation of 2,3-Allenols into γ-Ketophosphine Oxides.* The Journal of Organic Chemistry, 2020. **85**(12): p. 8185-8195.
185. Geeson, M.B. and C.C. Cummins, *Let's Make White Phosphorus Obsolete.* ACS Central Science, 2020.
186. Elmsley, J., *Nature's Building Blocks : An A-Z Guide to the Elements*. 2011: Oxford University Press.
187. Buonomo, J.A. and C.C. Aldrich, *Mitsunobu Reactions Catalytic in Phosphine and a Fully Catalytic System.* Angewandte Chemie International Edition, 2015. **54**(44): p. 13041-13044.
188. Methot, J.L. and W.R. Roush, *Nucleophilic Phosphine Organocatalysis.* Advanced Synthesis & Catalysis, 2004. **346**(9-10): p. 1035-1050.
189. Jordan, A., R.M. Denton, and H.F. Sneddon, *Development of a More Sustainable Appel Reaction.* ACS Sustainable Chemistry & Engineering, 2020. **8**(5): p. 2300-2309.
190. Fey, N., et al., *Development of a Ligand Knowledge Base, Part 1: Computational Descriptors for Phosphorus Donor Ligands.* Chemistry – A European Journal, 2006. **12**(1): p. 291-302.
191. Gorman, A.D., et al., *Phosphophosphidites Derived from BINOL.* European Journal of Inorganic Chemistry, 2019. **2019**(11-12): p. 1633-1639.
192. McFarlane, H.C.E. and W. McFarlane, *Intermolecular association of biphosphines.* J. Chem. Soc.{,} Chem. Commun., 1972. **0**: p. 1189-1190.
193. Harris, R.K., E.M. Norval, and M. Fild, *Nuclear magnetic resonance studies of scrambling reactions in solutions of tetra-alkyl- and tetra-aryl-diphosphanes.* J. Chem. Soc.{,} Dalton Trans., 1979. **0**: p. 826-831.
194. Molloy, A.D., G. Sánchez-Sanz, and D.G. Gilheany, *PP-Rotation, P-Inversion and Metathesis in Diphosphines Studied by DFT Calculations: Comments on Some Literature Conflicts.* Inorganics, 2016. **4**(4): p. 36.
195. Szynkiewicz, N., Ł. Ponikiewski, and R. Grubba, *Symmetrical and unsymmetrical diphosphanes with diversified alkyl, aryl, and amino substituents.* Dalton Transactions, 2018. **47**(47): p. 16885-16894.
196. Branfoot, C., et al., *Radical-initiated P,P-metathesis reactions of diphosphanes: evidence from experimental and computational studies.* Dalton Transactions, 2021.

197. Bohm, V.P.W. and M. Brookhart, *Dehydrocoupling of Phosphanes Catalyzed by a Rhodium(I) Complex.* Angewandte Chemie International Edition, 2001. **40**: p. 4694-4696.
198. D, M.J., et al., *Catalytic P□H Activation by Ti and Zr Catalysts.* Chemistry – A European Journal. **12**(34): p. 8696-8707.
199. Naseri, V., et al., *Stoichiometric and catalytic Sn-mediated dehydrocoupling of primary phosphines.* Chem. Commun., 2010. **46**(27): p. 5000-5002.
200. Pearce, K.G., et al., *Exploring the Reactivity of Donor-Stabilized Phosphenium Cations: Lewis Acid-Catalyzed Reduction of Chlorophosphanes by Silanes.* Inorganic Chemistry, 2018. **57**(18): p. 11530-11536.
201. Stéphanie S. Le Corre, M.B., Hélène Couthon-Gourvès, Jean-Pierre Haelters and Paul-Alain Jaffrès, *Atherton–Todd reaction: mechanism, scope and applications.* Beilstein J. Org. Chem., 2014. **10**: p. 1166-1196.
202. Cavell, R.G., C.M. Angelov, and D.A. Mazzuca, *Oxidative-Rearrangement Reactions of σ3, λ3 Dialkyl(Silylamino)Phosphines with Chlorophosphines; Formation of a P–P Bond Via a New Road to Phosphinophosphoranimines.* Phosphorus, Sulfur, and Silicon and the Related Elements, 1996. **109**(1-4): p. 625-628.
203. Dodds, D.L., et al., *Stereospecific Diphosphination of Activated Acetylenes: A General Route to Backbone-Functionalized, Chelating 1,2-Diphosphinoethenes.* Organometallics, 2006. **25**(25): p. 5937-5945.
204. Sato, A., H. Yorimitsu, and K. Oshima, *Synthesis of (E)-1,2-Diphosphanylethene Derivatives from Alkynes by Radical Addition of Tetraorganodiphosphane Generated In Situ.* Angewandte Chemie International Edition, 2005. **44**(11): p. 1694-1696.
205. Kawaguchi, S.-i., et al., *Photochemical behaviors of tetraphenyldiphosphine in the presence of alkynes.* Tetrahedron Letters, 2006. **47**(23): p. 3919-3922.
206. Okugawa, Y., K. Hirano, and M. Miura, *Brønsted Base Mediated Stereoselective Diphosphination of Terminal Alkynes with Diphosphanes.* Organic Letters, 2017. **19**(11): p. 2973-2976.
207. Otomura, N., K. Hirano, and M. Miura, *Diphosphination of 1,3-Dienes with Diphosphines under Visible-Light-Promoted Photoredox Catalysis.* Organic Letters, 2018. **20**(24): p. 7965-7968.
208. Poljanšek, I. and A. Šebenik, *Bulk polymerization of styrene and methyl methacrylate using tetraphenylbisphosphine as an initiator.* Macromolecular Chemistry and Physics, 1999. **200**(9): p. 2088-2099.
209. Sato, Y., et al., *Highly Selective Phosphinylphosphination of Alkenes with Tetraphenyldiphosphine Monoxide.* Angewandte Chemie International Edition, 2016. **55**(33): p. 9700-9703.
210. Franz, R., et al., *Chalcogen-Transfer Rearrangement: Exploring Inter- versus Intramolecular P–P Bond Activation.* Chemistry – A European Journal. **n/a**(n/a).
211. Issleib, K. and G. Schwager, *Beiträge zur Komplexchemie der Phosphine und Phosphinoxyde. IX. Schwermetallkomplexe des Tetracyclohexyldiphosphins.* Zeitschrift für anorganische und allgemeine Chemie, 1961. **311**(1-2): p. 83-91.
212. Coburger, P., et al., *Oxidative P–P Bond Addition to Cobalt(–I): Formation of a Low-Spin Cobalt(III) Phosphanido Complex.* Angewandte Chemie International Edition, 2017. **56**(50): p. 15871-15875.
213. Dierkes, P. and P. W. N. M. van Leeuwen, *The bite angle makes the difference: a practical ligand parameter for diphosphine ligands.* Journal of the Chemical Society, Dalton Transactions, 1999(10): p. 1519-1530.
214. Mansell, S.M., *Catalytic applications of small bite-angle diphosphorus ligands with single-atom linkers.* Dalton Transactions, 2017. **46**(44): p. 15157-15174.

215. Chen, X.-Y., et al., *FMPhos: Expanding the Catalytic Capacity of Small-Bite-Angle Bisphosphine Ligands in Regioselective Alkene Hydrofunctionalizations.* ACS Catalysis, 2020: p. 14349-14358.
216. Carter, A., et al., *High activity ethylene trimerisation catalysts based on diphosphine ligands.* Chemical Communications, 2002(8): p. 858-859.
217. Espinal-Viguri, M., C.R. Woof, and R.L. Webster, *Iron-Catalyzed Hydroboration: Unlocking Reactivity through Ligand Modulation.* Chemistry - A European Journal, 2016. **22**(33): p. 11605-11608.
218. Espinal-Viguri, M., et al., *Room Temperature Iron-Catalyzed Transfer Hydrogenation and Regioselective Deuteration of Carbon–Carbon Double Bonds.* Journal of the American Chemical Society, 2019. **141**(1): p. 572-582.
219. Linford-Wood, T.G., N.T. Coles, and R.L. Webster, *Room temperature iron catalyzed transfer hydrogenation using n-butanol and poly(methylhydrosiloxane).* Green Chemistry, 2021. **23**(7): p. 2703-2709.
220. Provis-Evans, C.B., E.A.C. Emanuelsson, and R.L. Webster, *Rapid Metal-Free Formation of Free Phosphines from Phosphine Oxides.* Advanced Synthesis & Catalysis, 2018. **360**(20): p. 3999-4004.
221. Melen, R.L., *Dehydrocoupling routes to element–element bonds catalysed by main group compounds.* Chemical Society Reviews, 2016. **45**(4): p. 775-788.
222. Seigler, D.S., *Introduction to Terpenes*, in *Plant Secondary Metabolism*. 1998, Springer US: Boston, MA. p. 312-323.
223. Glüer, A., et al., *Highly Active Iron Catalyst for Ammonia Borane Dehydrocoupling at Room Temperature.* ACS Catalysis, 2015. **5**(12): p. 7214-7217.
224. Chirik, P.J., *An FeVI Nitride: There Is Plenty of Room at the Top!* Angewandte Chemie International Edition, 2006. **45**(42): p. 6956-6959.
225. Herrero, C., et al., *Successive light-induced two electron transfers in a Ru–Fe supramolecular assembly: from Ru–Fe(ii)–OH2 to Ru–Fe(iv)–oxo.* Chemical Science, 2015. **6**(4): p. 2323-2327.
226. Ghosh, M., et al., *A μ-Phosphido Diiron Dumbbell in Multiple Oxidation States.* Angewandte Chemie International Edition, 2019. **58**(40): p. 14349-14356.
227. Lopez-Tejedor, D., R. Benavente, and J.M. Palomo, *Iron nanostructured catalysts: design and applications.* Catalysis Science & Technology, 2018. **8**(7): p. 1754-1776.
228. Bedford, R.B., et al., *Iron nanoparticles in the coupling of alkyl halides with aryl Grignard reagents.* Chem. Commun., 2006(13): p. 1398-1400.
229. Sonnenberg, J.F. and R.H. Morris, *Distinguishing homogeneous from nanoparticle asymmetric iron catalysis.* Catal. Sci. Technol., 2014. **4**(10): p. 3426-3438.
230. Yu, X., et al., *Iron-Catalyzed Tunable and Site-Selective Olefin Transposition.* Journal of the American Chemical Society, 2020. **142**(42): p. 18223-18230.
231. Hassam, M., et al., *Isomerization of Allylbenzenes.* Chemical Reviews, 2015. **115**(11): p. 5462-5569.
232. Smith, J.M., R.J. Lachicotte, and P.L. Holland, *NN Bond Cleavage by a Low-Coordinate Iron(II) Hydride Complex.* Journal of the American Chemical Society, 2003. **125**(51): p. 15752-15753.
233. Goswami, M., et al., *EPR Spectroscopy as a Tool in Homogeneous Catalysis Research.* Topics in Catalysis, 2015. **58**(12): p. 719-750.
234. Schild, D.J., et al., *Generating Potent C–H PCET Donors: Ligand-Induced Fe-to-Ring Proton Migration from a Cp*FeIII–H Complex Demonstrates a Promising Strategy.* Journal of the American Chemical Society, 2020. **142**(44): p. 18963-18970.
235. Neate, P.G.N., et al., *TMEDA in Iron-Catalyzed Hydromagnesiation: Formation of Iron(II)-Alkyl Species for Controlled Reduction to Alkene-Stabilized Iron(0).* Angewandte Chemie International Edition, 2020. **59**(39): p. 17070-17076.

236. Zhao, Y. and S. Ge, *Chromium-Catalyzed Selective Dimerization/Hydroboration of Allenes to Access Boryl-Functionalized Skipped (E,Z)-Dienes.* Angewandte Chemie International Edition, 2021. **60**(4): p. 2149-2154.
237. Mathies, G., et al., *High-frequency EPR study of the high-spin FeII complex Fe[(SPPh2)2N]2.* Journal of Magnetic Resonance, 2012. **224**: p. 94-100.
238. Piguet, C., *Paramagnetic Susceptibility by NMR: The "Solvent Correction" Removed for Large Paramagnetic Molecules.* Journal of Chemical Education, 1997. **74**(7): p. 815.
239. Smith, J.M., et al., *Studies of Low-Coordinate Iron Dinitrogen Complexes.* Journal of the American Chemical Society, 2006. **128**(3): p. 756-769.
240. Demirci, U.B., *Ammonia Borane: An Extensively Studied, Though Not Yet Implemented, Hydrogen Carrier.* Energies, 2020. **13**(12): p. 3071.
241. Faverio, C., et al., *Ammonia borane as a reducing agent in organic synthesis.* Organic & Biomolecular Chemistry, 2020.
242. Ghosh, S. and B.R. Jagirdar, *Synthesis and Mechanism of Formation of Metal Nanosponges and their Catalytic and Hydrogen Sorption Properties.* ChemistrySelect, 2018. **3**(25): p. 7184-7194.
243. Vela, J., et al., *Alkyl isomerisation in three-coordinate iron(ii) complexes.* Chemical Communications, 2002(23): p. 2886-2887.
244. Vela, J., et al., *Reversible Beta-Hydrogen Elimination of Three-Coordinate Iron(II) Alkyl Complexes: Mechanistic and Thermodynamic Studies.* Organometallics, 2004. **23**(22): p. 5226-5239.
245. Yu, Y., W.W. Brennessel, and P.L. Holland, *Borane B−C Bond Cleavage by a Low-Coordinate Iron Hydride Complex and N−N Bond Cleavage by the Hydridoborate Product.* Organometallics, 2007. **26**(13): p. 3217-3226.
246. Yu, Y., et al., *Binding Affinity of Alkynes and Alkenes to Low-Coordinate Iron.* Inorganic Chemistry, 2006. **45**(15): p. 5742-5751.
247. Arevalo, R. and P.J. Chirik, *Enabling Two-Electron Pathways with Iron and Cobalt: From Ligand Design to Catalytic Applications.* Journal of the American Chemical Society, 2019. **141**(23): p. 9106-9123.
248. Spitzer, F., et al., *Influence of the nacnac Ligand in Iron(I)-Mediated P4 Transformations.* Angewandte Chemie International Edition, 2016. **55**(13): p. 4340-4344.
249. Jones, W.D., *Isotope Effects in C−H Bond Activation Reactions by Transition Metals.* Accounts of Chemical Research, 2003. **36**(2): p. 140-146.
250. Churchill, D.G., et al., *Normal and Inverse Primary Kinetic Deuterium Isotope Effects for C−H Bond Reductive Elimination and Oxidative Addition Reactions of Molybdenocene and Tungstenocene Complexes: Evidence for Benzene σ-Complex Intermediates.* Journal of the American Chemical Society, 2003. **125**(5): p. 1403-1420.
251. Aseman, M.D., et al., *Secondary Kinetic Isotope Effects in Oxidative Addition of Benzyl Bromide to Dimethylplatinum(II) Complexes.* Organometallics, 2013. **32**(9): p. 2593-2598.
252. Hussah Alawisi, H.D.A., and Zachary J. Tonzetich, *Catalytic Hydrogenation of Alkenes and Alkynes by a Cobalt Pincer Complex: Evidence of Roles for Both Co(I) and Co(II).* Organometallics, 2021.
253. Holland, P.L., *Electronic Structure and Reactivity of Three-Coordinate Iron Complexes.* Accounts of Chemical Research, 2008. **41**(8): p. 905-914.
254. Bellows, S.M., T.R. Cundari, and P.L. Holland, *Spin Crossover during β-Hydride Elimination in High-Spin Iron(II)– and Cobalt(II)–Alkyl Complexes.* Organometallics, 2013. **32**(17): p. 4741-4751.
255. Lutz, S.A., et al., *Two-State Reactivity in Iron-Catalyzed Alkene Isomerization Confers σ-Base Resistance.* Journal of the American Chemical Society, 2020. **142**(36): p. 15527-15535.

256. G. Van Ornum, S., R. M. Champeau, and R. Pariza, *Ozonolysis Applications in Drug Synthesis.* Chemical Reviews, 2006. **106**(7): p. 2990-3001.
257. Sinha, A.K., U.K. Sharma, and N. Sharma, *A comprehensive review on vanilla flavor: Extraction, isolation and quantification of vanillin and others constituents.* International Journal of Food Sciences and Nutrition, 2008. **59**(4): p. 299-326.
258. Kümmerle, A.E., et al., *Studies towards the identification of putative bioactive conformation of potent vasodilator arylidene N-acylhydrazone derivatives.* European Journal of Medicinal Chemistry, 2009. **44**(10): p. 4004-4009.
259. Luu, T.X., et al., *Fast and Green Microwave-Assisted Conversion of Essential Oil Allylbenzenes into the Corresponding Aldehydes via Alkene Isomerization and Subsequent Potassium Permanganate Promoted Oxidative Alkene Group Cleavage.* Molecules, 2009. **14**(9): p. 3411-3424.
260. Clavier, H., et al., *Highly Selective Cobalt-Mediated [6 + 2] Cycloaddition of Cycloheptatriene and Allenes.* Organic Letters, 2011. **13**(2): p. 308-311.
261. Rochat, R., et al., *Organomagnesium-Catalyzed Isomerization of Terminal Alkynes to Allenes and Internal Alkynes.* Chemistry – A European Journal, 2015. **21**(22): p. 8112-8120.
262. Gao, L. and Z. Li, *Direct Synthesis of 1-Arylprop-1-ynes with Calcium Carbide as an Acetylene Source.* Synlett, 2019. **30**(13): p. 1580-1584.
263. Barbaro, A., et al., *The reaction of tert-butyldiphenylsilylcuprates with allenes.* Journal of the Chemical Society, Perkin Transactions 1, 1991(11): p. 2811-2816.
264. Jones, C.R., C.P. Butts, and J.N. Harvey, *Accuracy in determining interproton distances using Nuclear Overhauser Effect data from a flexible molecule.* Beilstein Journal of Organic Chemistry, 2011. **7**: p. 145-150.
265. Driscoll, O.J., et al., *Iron(III) Salalen Complexes for the Polymerisation of Lactide.* European Journal of Inorganic Chemistry, 2018. **2018**(47): p. 5129-5135.
266. Rittinghaus, R.D., et al., *New Kids in Lactide Polymerization: Highly Active and Robust Iron Guanidine Complexes as Superior Catalysts.* ChemSusChem, 2019. **12**(10): p. 2161-2165.
267. Fujimori, A., et al., *Highly Ordered and Stable Layered "Polymer Nanosheets" Constructed with Amorphous Side Chains and π–π Stacking of Functional Groups in Ternary Comb Copolymers.* The Journal of Physical Chemistry B, 2010. **114**(6): p. 2100-2110.
268. Endo, T., K. Takagi, and I. Tomita, *Design and synthesis of polymerizable cumulated double bond system. -Living coordination polymerization of alkylallenes by π-allylnickel catalyst.* Tetrahedron, 1997. **53**(45): p. 15187-15196.
269. Tomita, I., et al., *A Novel Living Coordination Polymerization of Methoxyallene by .pi.-Allylnickel Catalyst.* Macromolecules, 1994. **27**(15): p. 4413-4414.
270. Zhao, Z., L. Racicot, and G.K. Murphy, *Fluorinative Rearrangements of Substituted Phenylallenes Mediated by (Difluoroiodo)toluene: Synthesis of α-(Difluoromethyl)styrenes.* Angewandte Chemie International Edition, 2017. **56**(38): p. 11620-11623.
271. Xiang-Lei Han, P.-P.L., Qingjiang Li, *Recent advances of allenes in the first-row transition metals catalyzed C—H activation reactions.* Chin. Chem. Lett., 2019. **30**(8): p. 1495-1502.
272. Mo, J., et al., *1,4-Iron Migration for Expedient Allene Annulations through Iron-Catalyzed C–H/N–H/C–O/C–H Functionalizations.* Angewandte Chemie International Edition, 2018. **57**(26): p. 7719-7723.
273. Blomquist, A.T. and J.A. Verdol, *Thermal Dimerization of Allene to 1,2-Dimethylenecyclobutane1.* Journal of the American Chemical Society, 1956. **78**(1): p. 109-112.
274. Borden, W.T., et al., *Transannular photochemical ring closure of 1,2,5,6-tetramethylenecyclooctane as a synthetic route to small-ring propellanes.* The Journal of Organic Chemistry, 1975. **40**(17): p. 2438-2442.
275. Dowd, P. and Y.H. Paik, *Dimethylenecyclobutadiene.* Journal of the American Chemical Society, 1986. **108**(10): p. 2788-2790.

276. Snyder, G.J. and D.A. Dougherty, *2,4-Dimethylene-1,3-cyclobutanediyl, the non-Kekule isomer of benzene. Synthesis, EPR, and electronic spectroscopy.* Journal of the American Chemical Society, 1989. **111**(11): p. 3927-3942.
277. Dougherty, D.A., *Spin control in organic molecules.* Accounts of Chemical Research, 1991. **24**(3): p. 88-94.
278. Horner, M. and S. Huenig, *Bicyclo[1.1.0]butanes. A new synthetic route and valence isomerizations.* Journal of the American Chemical Society, 2002. **99**(18): p. 6120-6122.
279. Braverman, S., et al., *Synthetic applications of the carbanion walk mechanism: A novel and facile method for the preparation of 1,3-dimethylenecyclobutane and conjugated vinylallene derivatives.* Tetrahedron Letters, 1986.
280. Bustelo, E., et al., *An Opened Route to 1,3-Dimethylenecyclobutanes via Sequential Ruthenium-Catalyzed [2 + 2] Cycloaddition of Allenyl Boronate and Palladium Suzuki Coupling.* Journal of the American Chemical Society, 2005. **127**(33): p. 11582-11583.
281. Ding, W. and N. Yoshikai, *Cobalt-Catalyzed Intermolecular [2+2] Cycloaddition between Alkynes and Allenes.* Angewandte Chemie International Edition, 2019. **58**(8): p. 2500-2504.
282. Routaboul, L., et al., *Iron-salt-promoted highly regioselective α and β hydrophosphination of alkenyl arenes.* Chemistry, 2013. **19**(27): p. 8760-4.
283. Gallagher, K.J. and R.L. Webster, *Room temperature hydrophosphination using a simple iron salen pre-catalyst.* Chem. Commun., 2014. **50**(81): p. 12109-12111.
284. Sharpe, H.R., et al., *Iron(II)-Catalyzed Hydrophosphination of Isocyanates.* Angewandte Chemie International Edition, 2017. **56**(17): p. 4845-4848.
285. Kamer, P.C.J. and P.W.N.M. van Leeuwen, *Phosphorus(III) Ligands in Homogeneous Catalysis: Design and Synthesis*. 1st ed. 2012, Oxford, UK: John Wiley & Sons, Ltd.
286. Musina, E.I., A.S. Balueva, and A.A. Karasik, *Phosphines: preparation, reactivity and applications*, in *Organophosphorus Chemistry: Volume 48*. 2019, The Royal Society of Chemistry. p. 1-63.
287. Barrett, A.N., et al., *Hydrophosphination using [GeCl{N(SiMe3)2}3] as a pre-catalyst.* Chemical Communications, 2020. **56**(88): p. 13623-13626.
288. Hu, H. and C. Cui, *Synthesis of Calcium and Ytterbium Complexes Supported by a Tridentate Imino-Amidinate Ligand and Their Application in the Intermolecular Hydrophosphination of Alkenes and Alkynes.* Organometallics, 2012. **31**(3): p. 1208-1211.
289. Moglie, Y., et al., *Catalyst- and solvent-free hydrophosphination and multicomponent hydrothiophosphination of alkenes and alkynes.* Green Chemistry, 2016. **18**(18): p. 4896-4907.
290. Pollard, V.A., et al., *Lithium-Aluminate-Catalyzed Hydrophosphination Applications.* Angewandte Chemie International Edition, 2019. **58**(35): p. 12291-12296.
291. Blackaby, W.J.M., et al., *N-Heterocyclic Carbene Non-Innocence in the Catalytic Hydrophosphination of Alkynes.* ChemCatChem, 2019. **11**(7): p. 1893-1897.
292. Cabezas, J.A. and N. Ferllini, *Regiospecific Palladium-Catalyzed Cross-Coupling Reactions Using the Operational Equivalent of 1,3-Dilithiopropyne.* Synthesis, 2020. **52**(16): p. 2387-2394.
293. Coles, N.T., M.F. Mahon, and R.L. Webster, *1{,}1-Diphosphines and divinylphosphines via base catalyzed hydrophosphination.* Chem. Commun., 2018. **54**(74): p. 10443-10446.
294. Strom, A.E., D. Balcells, and J.F. Hartwig, *Synthetic and Computational Studies on the Rhodium-Catalyzed Hydroamination of Aminoalkenes.* ACS Catalysis, 2016. **6**(9): p. 5651-5665.
295. Bange, C.A. and R. Waterman, *Zirconium-Catalyzed Intermolecular Double Hydrophosphination of Alkynes with a Primary Phosphine.* ACS Catalysis, 2016. **6**(10): p. 6413-6416.

296. Zhang, Y., et al., *Hydrophosphination of alkenes and alkynes with primary phosphines catalyzed by zirconium complexes bearing aminophenolato ligands.* Dalton Transactions, 2018. **47**(27): p. 9090-9095.
297. Cibuzar, M.P., S.G. Dannenberg, and R. Waterman, *A Commercially Available Ruthenium Compound for Catalytic Hydrophosphination.* Israel Journal of Chemistry, 2020. **60**(3-4): p. 446-451.
298. K, K.A., et al., *Markovnikov versus anti-Markovnikov Hydrophosphination: Divergent Reactivity Using an Iron(II) β-Diketiminate Pre-Catalyst.* Chemistry – A European Journal. **23**(38): p. 9039-9043.
299. Aguiar, A.M. and T.G. Archibald, *The stereospecific addition of organophosphides to termimal alkynes.* Tetrahedron Letters, 1966. **7**(45): p. 5471-5475.
300. Kaniewska, K., et al., *Homoleptic mono-, di-, and tetra-iron complexes featuring phosphido ligands: a synthetic, structural, and spectroscopic study.* Dalton Transactions, 2020. **49**(29): p. 10091-10103.
301. Kaniewska, K., et al., *Syntheses, Structures and Reactivity of Terminal Phosphido Complexes of Iron(II) Supported by a β-Diketiminato Ligand.* European Journal of Inorganic Chemistry, 2018. **2018**(38): p. 4298-4308.
302. Beachley, O.T., et al., *Reactions of Neopentylindium(III) Derivatives with Isopropylphosphorus Compounds.* Organometallics, 2001. **20**(23): p. 4896-4902.
303. Schneider, H., D. Schmidt, and U. Radius, *The reductive P–P coupling of primary and secondary phosphines mediated by N-heterocyclic carbenes.* Chemical Communications, 2015. **51**(50): p. 10138-10141.
304. Wu, L., et al., *Homo- and heterodehydrocoupling of phosphines mediated by alkali metal catalysts.* Nature Communications, 2019. **10**(1): p. 2786.
305. Henderson, W.A., M. Epstein, and F.S. Seichter, *Some Aspects of the Chemistry of Cyclopolyphosphines.* Journal of the American Chemical Society, 1963. **85**(16): p. 2462-2466.
306. Feldman, J., et al., *Electrophilic Metal Precursors and a β-Diimine Ligand for Nickel(II)- and Palladium(II)-Catalyzed Ethylene Polymerization.* Organometallics, 1997. **16**(8): p. 1514-1516.
307. *Complexes of Bulky β-Diketiminate Ligands*. 2010, Wiley-Blackwell. p. 1-55.
308. Liu, C., et al., *Facile synthesis of mono-, bis- and tris-aryl-substituted aniline derivatives in aqueous DMF.* Arkivoc, 2012. **2012**(9): p. 62-62.
309. Cowley, R.E. and P.L. Holland, *Ligand Effects on Hydrogen Atom Transfer from Hydrocarbons to Three-Coordinate Iron Imides.* Inorganic Chemistry, 2012. **51**(15): p. 8352-8361.
310. Cherian, A.E., E.B. Lobkovsky, and G.W. Coates, *Chiral anilines: development of C2-symmetric{,} late-transition metal catalysts for isoselective 2-butene polymerization.* Chem. Commun., 2003(20): p. 2566-2567.
311. Provis-Evans, C.B., et al., *Regioselective Alkyne Cyclotrimerization with an In Situ-Generated [Fe(II)H(salen)]·Bpin Catalyst.* ACS Catalysis, 2020. **10**(17): p. 10157-10168.
312. Dugan, T.R., et al., *Synthesis, Spectroscopy, and Hydrogen/Deuterium Exchange in High-Spin Iron(II) Hydride Complexes.* Inorganic Chemistry, 2014. **53**(5): p. 2370-2380.
313. Kysliak, O., H. Görls, and R. Kretschmer, *Salt metathesis as an alternative approach to access aluminium(i) and gallium(i) β-diketiminates.* Dalton Transactions, 2020. **49**(19): p. 6377-6383.
314. Smith, J.M., R.J. Lachicotte, and P.L. Holland, *Tuning metal coordination number by ancillary ligand steric effects: synthesis of a three-coordinate iron() complex.* Chemical Communications, 2001(17): p. 1542-1543.

315. Weitz, I.S. and M. Rabinovitz, *The application of C8K for organic synthesis: reduction of substituted naphthalenes.* Journal of the Chemical Society, Perkin Transactions 1, 1993(1): p. 117-120.
316. Leitao, E.M. and I. Manners, *Rehydrogenation of Aminoboranes to Amine–Boranes Using H2O: Reaction Scope and Mechanism.* European Journal of Inorganic Chemistry, 2015. **2015**(13): p. 2199-2205.
317. Jaska, C.A., et al., *Transition Metal-Catalyzed Formation of Boron−Nitrogen Bonds: Catalytic Dehydrocoupling of Amine-Borane Adducts to Form Aminoboranes and Borazines.* Journal of the American Chemical Society, 2003. **125**(31): p. 9424-9434.
318. Sloan, M.E., et al., *Homogeneous Catalytic Dehydrocoupling/Dehydrogenation of Amine−Borane Adducts by Early Transition Metal, Group 4 Metallocene Complexes.* Journal of the American Chemical Society, 2010. **132**(11): p. 3831-3841.
319. Miloserdov, F.M., et al., *Zn-Promoted C–H Reductive Elimination and H2 Activation via a Dual Unsaturated Heterobimetallic Ru–Zn Intermediate.* Journal of the American Chemical Society, 2020. **142**(13): p. 6340-6349.
320. Wu, Q., et al., *Nickel-Catalyzed Allylic C(sp2)–H Activation: Stereoselective Allyl Isomerization and Regiospecific Allyl Arylation of Allylarenes.* European Journal of Organic Chemistry. **2016**(32): p. 5415-5422.
321. Spallek, M.J., et al., *Modular Palladium Bipyrazoles for the Isomerization of Allylbenzenes – Mechanistic Considerations and Insights into Catalyst Design and Activity, Role of Solvent, and Additive Effects.* Advanced Synthesis & Catalysis. **354**(8): p. 1466-1480.
322. Neese, F., *Software update: the ORCA program system, version 4.0.* WIREs Computational Molecular Science, 2018. **8**(1): p. e1327.
323. Stephens, P.J., et al., *Ab Initio Calculation of Vibrational Absorption and Circular Dichroism Spectra Using Density Functional Force Fields.* The Journal of Physical Chemistry, 1994. **98**(45): p. 11623-11627.
324. Vosko, S.H., L. Wilk, and M. Nusair, *Accurate spin-dependent electron liquid correlation energies for local spin density calculations: a critical analysis.* Canadian Journal of Physics, 1980. **58**(8): p. 1200-1211.
325. Becke, A.D., *Density-functional thermochemistry. III. The role of exact exchange.* The Journal of Chemical Physics, 1993. **98**(7): p. 5648-5652.
326. Lee, C., W. Yang, and R.G. Parr, *Development of the Colle-Salvetti correlation-energy formula into a functional of the electron density.* Physical Review B, 1988. **37**(2): p. 785-789.
327. Inc., S., *Jaguar, version 8.5*. 2014: New York, NY.
328. Grimme, S., et al., *A consistent and accurate ab initio parametrization of density functional dispersion correction (DFT-D) for the 94 elements H-Pu.* The Journal of Chemical Physics, 2010. **132**(15): p. 154104.
329. Perdew, J.P., *Density-functional approximation for the correlation energy of the inhomogeneous electron gas.* Physical Review B, 1986. **33**(12): p. 8822-8824.
330. Becke, A.D., *Density-functional exchange-energy approximation with correct asymptotic behavior.* Physical Review A, 1988. **38**(6): p. 3098-3100.
331. Goerigk, L. and S. Grimme, *A thorough benchmark of density functional methods for general main group thermochemistry, kinetics, and noncovalent interactions.* Physical Chemistry Chemical Physics, 2011. **13**(14): p. 6670-6688.
332. Miertuš, S., E. Scrocco, and J. Tomasi, *Electrostatic interaction of a solute with a continuum. A direct utilizaion of AB initio molecular potentials for the prevision of solvent effects.* Chemical Physics, 1981. **55**(1): p. 117-129.
333. Adamo, C. and V. Barone, *Toward reliable density functional methods without adjustable parameters: The PBE0 model.* The Journal of Chemical Physics, 1999. **110**(13): p. 6158-6170.

334. Zhu, N., J. Zhao, and H. Bao, *Iron catalyzed methylation and ethylation of vinyl arenes.* Chem. Sci., 2017. **8**(3): p. 2081-2085.
335. del Hoyo, A.M., A.G. Herraiz, and M.G. Suero, *A Stereoconvergent Cyclopropanation Reaction of Styrenes.* Angewandte Chemie International Edition. **56**(6): p. 1610-1613.
336. Jeon, J.-H., et al., *Contact and Fumigant Toxicities of 3-Methylphenol Isolated from Ostericum koreanum and Its Derivatives against House Dust Mites.* Journal of Agricultural and Food Chemistry, 2012. **60**(50): p. 12349-12354.
337. Strohmeier, G.A., et al., *Enzymatic One-Step Reduction of Carboxylates to Aldehydes with Cell-Free Regeneration of ATP and NADPH.* Chemistry – A European Journal, 2019. **25**(24): p. 6119-6123.
338. Dobrovetsky, R., K. Takeuchi, and D.W. Stephan, *Metal-free Lewis acid mediated dehydrocoupling of phosphines and concurrent hydrogenation.* Chem. Commun., 2015. **51**(12): p. 2396-2398.